Synthesis and Reactivity of the 2-Phosphaethynolate Anion and Phosphinecarboxamide

Andrew Jupp

Wadham College

University of Oxford

A thesis submitted for the degree of

Doctor of Philosophy

Hilary 2016

Abstract

Synthesis and Reactivity of the 2-Phosphaethynolate Anion and Phosphinecarboxamide

Andrew Jupp — Wadham College

DPhil Inorganic Chemistry — Hilary 2016

This thesis describes a novel synthesis of the 2-phosphaethynolate anion, $[PCO]^-$, via reaction of the $[P_7]^{3-}$ Zintl cluster with carbon monoxide. The ligand properties of this fundamental molecule have been probed and compared to common isoelectronic pseudohalides: cyanate and isocyanate. The first ambient-temperature synthesis of the heavier congener, $[PCS]^-$, is also reported, and studies show that this anion can act as an ambidentate ligand.

The cycloaddition chemistry of $[PCO]^-$ with heteroallenes afforded a range of novel anionic phosphorus-containing heterocycles. A collaborative study has shown that $[PCO]^-$ can act as a catalyst for the trimerisation of isocyanates, and potential intermediates in this catalytic cycle have been isolated.

By analogy with Wöhler's historic synthesis of urea, the reaction of $[PCO]^-$ with ammonium salts yields phosphinecarboxamide. This unprecedented molecule is a rare example of an air-stable "user-friendly" primary phosphine, and its structure and ability to coordinate to metal centres were explored. It was found that this species has similar σ donor and π acceptor properties to phosphine, PH_3.

This reactivity has been extended to incorporate *N*-functionalised phosphinecarboxamides with a range of different functional groups. The Brønsted acidity, *P*-functionalisation and oxidation chemistry of these species was subsequently investigated to afford a diverse family of carbamoyl-bearing phosphides, phosphines and phosphine oxides. Some of these species have great potential to become industrially relevant molecules in the future. Preliminary results showing the generality of the reaction of $[PCO]^-$ with other protic nucleophiles are additionally presented.

Acknowledgements

There are many people that have made my DPhil a hugely enjoyable and rewarding experience, and without whom this body of work would not have been possible. Firstly, I would like to thank my supervisor, Professor Jose Goicoechea, for his enthusiasm, ideas and encouragement, and his unerring ability to get the first (and usually subsequent) rounds of beers in the pub after a long week in the lab. I really have had a blast, so thank you. And to Professor Simon Aldridge, who really planted the seed of inquisitiveness and enjoyment of inorganic chemistry during my undergraduate studies.

I have been lucky enough to share a lab over the last few years with some truly excellent and diverse people, and I want to thank them all. Dr. Caroline Knapp kept a watchful eye over me when I first entered the lab and taught me the basics of Schlenk-line chemistry. Dr. Mark Irwin was always available for practical advice, be it chemistry, bike maintenance or computer-related issues. Dr. Rob Turbervill was the one who encouraged me, in his somewhat unorthodox manner, to think critically about my research and to become a competent practical chemist, and I am very grateful to him. I am less grateful to Rob and Mark for the amount of junk mail I receive regarding political parties and Mediterranean cruises, but it's nice to know that, although they've left the group, they still think of me from time to time! I would like to thank Dr. Gaby Espinoza-Quintero for being the coolest, most impromptu and downright kookiest person I have ever met; the lab has been a more sombre place since she finished. I have spent a disproportionate amount of time over the last few years chatting drivel with Jordan Waters, typically while staying late in the lab or over a couple of games of pool and some questionable food in the Uni Club. It has been an absolute pleasure, although he may have caused irreparable damage to my sanity. And a big thanks to our post-doc during my time in the lab, Dr. Thomas Robinson, for many useful

chats about chemistry, a shared enjoyment of crosswords, and for proof-reading this thesis in its entirety in a very short timeframe.

It has been immensely enjoyable to supervise and work with some really talented undergraduate students on a wide array of projects: Gemma Trott, Mike Geeson, James Holl, Jamie Windmill and Dave Gillott. I wish them all the best for the future, and in particular to Gemma and Mike for their continuing careers in chemistry; I'm sure we'll run into each other at conferences down the years and reminisce. Éleonore Payen de le Garanderie was a visiting student in the group and a lovely person to meet and work with.

Outside of the immediate group, I would like to thank Dr. Nick Rees for assistance with NMR spectroscopy, Colin Sparrow for mass spectrometry persistence, and Dr. Amber Thompson for crystallographic wisdom.

I need to thank my family. I don't tell them enough, but I am incredibly grateful for all their support and the sacrifices they have made over the years that have led me to where I am now; I could not have done it without them. And I'm sure they will be delighted that this chapter in my life is over, and now I can finally go and get a "proper job". Many close friends outside of chemistry have also helped keep me in touch with the real world over the last few years.

Lastly, this would certainly not have been possible without the friendship, humour, gentle nagging, tolerance, cynicism, love and unwavering encouragement of Becky Cross, and she deserves more plaudits than I know how to express with any degree of eloquence. So, to keep it simple and all-encompassing, thank you for everything.

Thank you all. On to the next adventure.

Abbreviations

18-crown-6	1,4,7,10,13,16-hexaoxacyclooctadecane
2,2,2-crypt	4,7,13,16,21,24-hexaoxa-1,10-diazabicyclo[8.8.8]hexacosane
Å	ångström
Ae	alkaline earth metal
amid	amidinate
An	actinide
Ar	aryl group
Ar^F	3,5-bis(trifluoromethyl)phenyl (3,5-$(CF_3)_2C_6H_3$)
au	atomic unit
av	average (mean)
BAPO	bis(acyl) phosphine oxide
BCPO	bis(carbamoyl) phosphine oxide
Bn	benzyl
CAAC	cyclic (alkyl)(amino)carbene
calc	calculated
CI	chemical ionisation
cm^{-1}	wavenumber
COD	1,5-cyclooctadiene
COSY	correlation spectroscopy
Cp	cyclopentadienyl or cyclopentadienide
Cp*	pentamethylcyclopentadienyl or pentamethylcyclopentadienide
CSD	Cambridge Structural Database
Cy	cyclohexyl
d	doublet
Da	Dalton
DBU	1,8-diazabicyclo[5.4.0]undec-7-ene
DCM	dichloromethane
DFT	density functional theory
Dipp	2,6-diisopropylphenyl (2,6-$^{i}Pr_2C_6H_3$)
DME	1,2-dimethoxyethane
DMF	*N*,*N*-dimethylformamide
ESI	electrospray ionisation
Et	ethyl

FG	functional group
FI	field ionisation
g	gram
GABA	gamma-aminobutyric acid
GOF	goodness-of-fit
h	Planck's constant
HOMO	highest occupied molecular orbital
Hz	hertz
^{i}Pr	isopropyl
IR	infrared
J	joule
J	coupling constant
k	rate constant
K	kelvin
K	transmission coefficient
K_B	Boltzmann constant
k_c	rate constant at coalescence temperature
KHMDS	potassium bis(trimethylsilyl)amide
kJ	kilojoule
LUMO	lowest unoccupied molecular orbital
m	multiplet
m	mass
Me	methyl
MeCN	acetonitrile
MERP	minimum energy reaction profile
Mes	mesityl (2,4,6-$Me_3C_6H_2$)
Mes*	supermesityl (2,4,6-$^{t}Bu_3C_6H_2$)
mg	milligram
mL	millilitre
mol	mole
MS	mass spectrometry
NHC	N-heterocyclic carbene
NMR	nuclear magnetic resonance
NPA	natural population analysis
NRT	natural resonance theory

OTf	triflate or trifluoromethanesulfonate (CF_3SO_3)
p-cymene	*para*-cymene, *para*-isopropyltoluene
Ph	phenyl
PI	photoiniator
ppm	parts per million
q	quartet
quint	quintet
R	gas constant
s	singlet
SOMO	singly occupied molecular orbital
t	triplet
^{t}Bu	*tert*-butyl
T	temperature
T_c	coalescence temperature
TEP	Tolman Electronic Parameter
THF	tetrahydrofuran
Tipp	2,4,6-triisopropylphenyl (2,4,6-^{i}Pr$_3$C$_6$H$_2$)
TMPTA	trimethylolpropane triacrylate
Tol	tolyl
UV	ultraviolet
2,6-Xylyl	2,6-dimethylphenyl (2,6-$Me_2C_6H_3$)
z	charge
γ	gyromagnetic ratio
δ	chemical shift
μL	microlitre
ν	vibrational frequency
°	degree
°C	degree Celsius

Library of numbered compounds

Chapter 2:

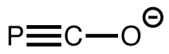

1

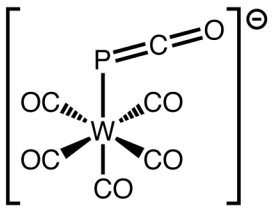

2

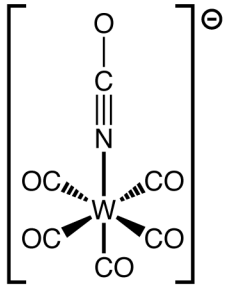

3

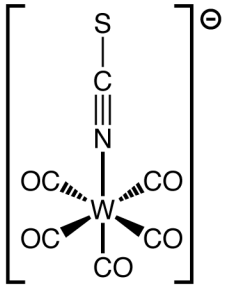

4

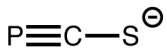

5

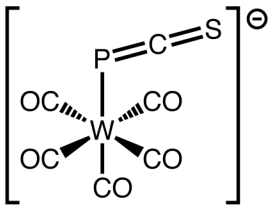

6a

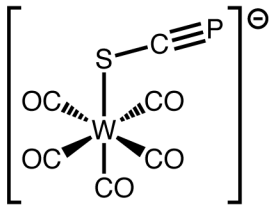

6b

Chapter 3:

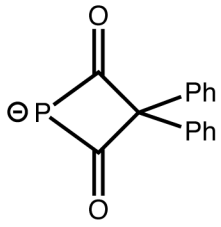

7

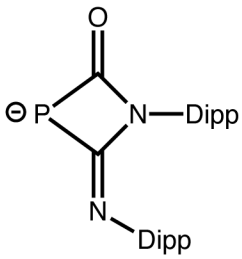

8

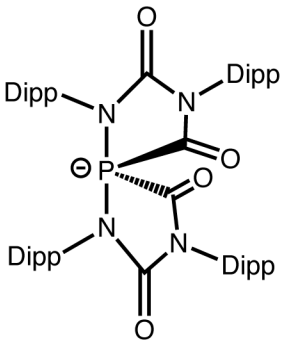

9

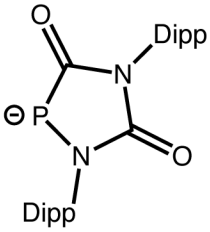

10

Chapter 4:

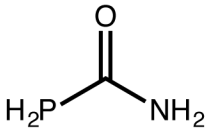

11

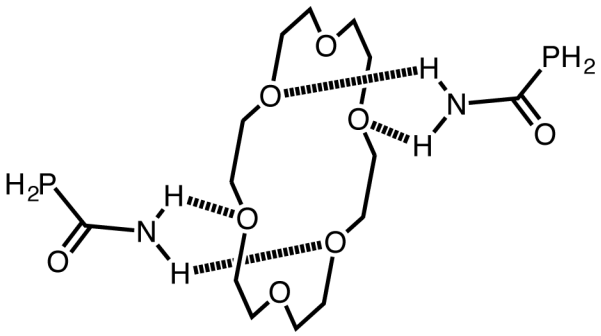

12

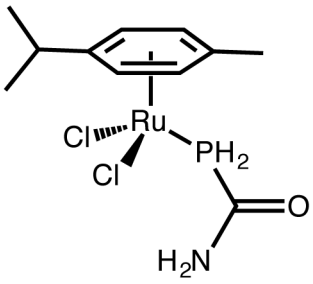

13

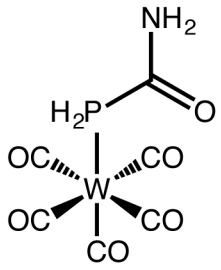

14

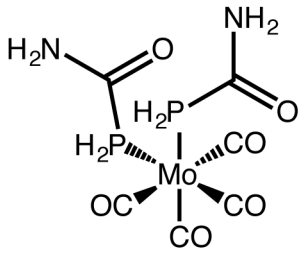

15

Chapter 5:

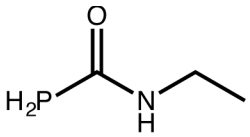

16

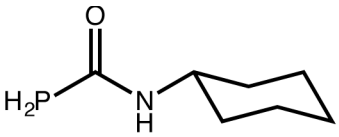

17

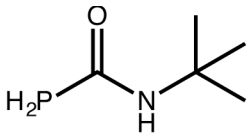

18

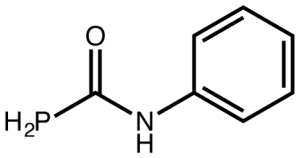

19

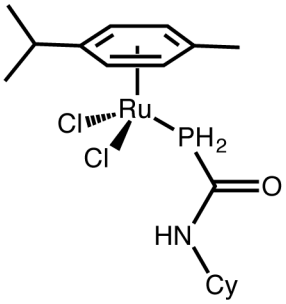

20

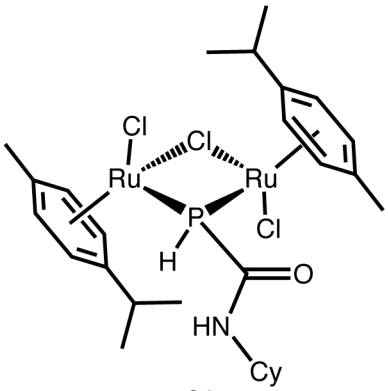

21

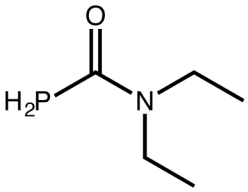

22

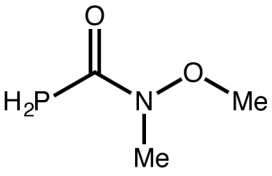

23

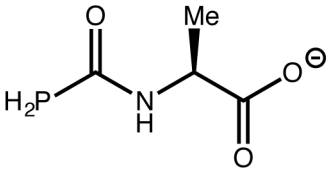

24

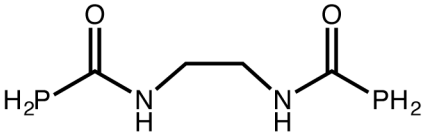

25

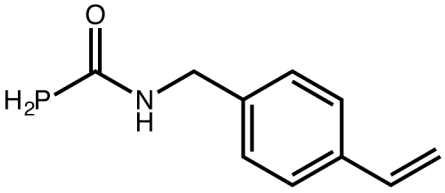

26

Chapter 6:

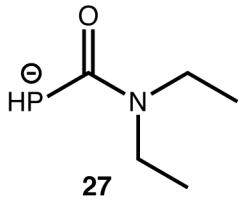

27

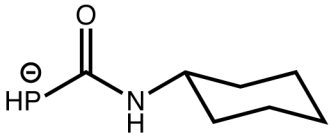

28

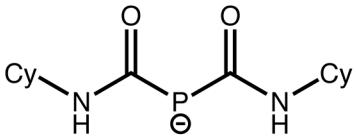

29

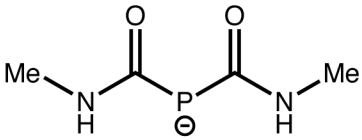

30

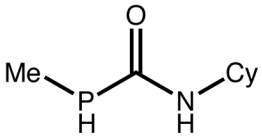

31

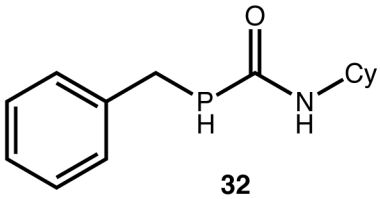

32

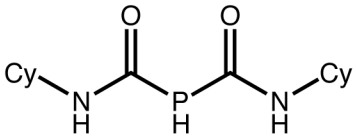

33

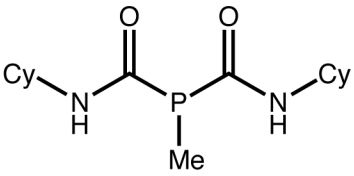

34

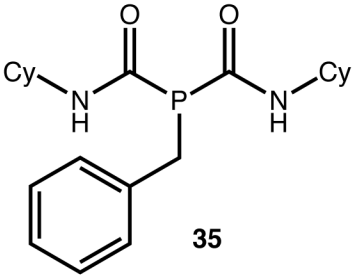

35

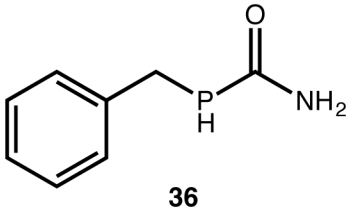

36

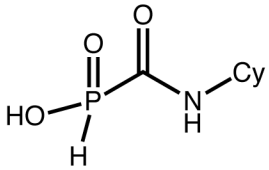

37

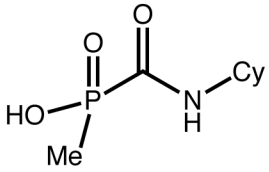

38

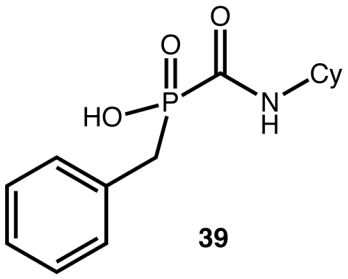

39

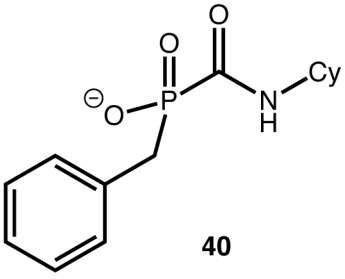

40

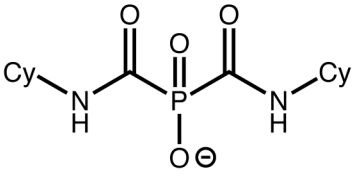

41

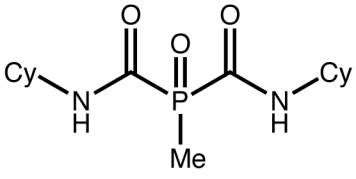

42

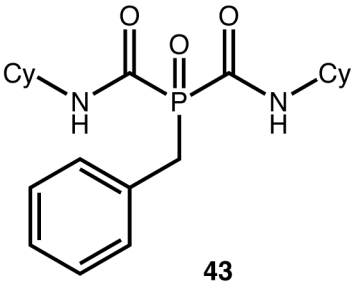

43

Chapter 7:

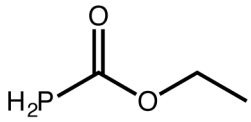

44

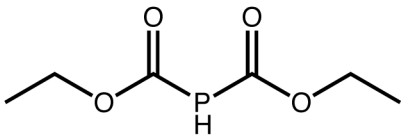

45

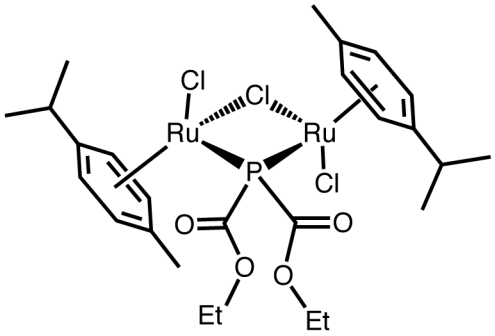

46

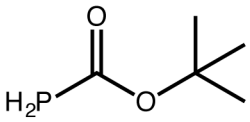

47

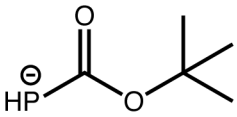

48

Contents

Chapter 1
Introduction

1.1 Phosphorus

The ubiquity of phosphorus-containing molecules in the world around us cannot be overstated. Phosphorus has wide-ranging applications in all areas of chemistry, and is an essential building block in every known form of life.[1,2] It was first discovered in 1669 by Hennig Brand, an alchemist from Hamburg, who heated the malodorous residues of urine with sand and coal in a quest for the "philosopher's stone".[3,4] The substance he isolated gave off a pale green glow, and he thus named it phosphorus, from the Greek for *light-bearer*.

Science and industry has progressed since this time, and urine is no longer the main chemical feedstock for elemental phosphorus. The industrial reduction of phosphate rock to white phosphorus currently exceeds half a million tons annually, which represents the major commercial phosphorus atom source for food production, speciality chemicals and pharmaceutical applications.[5] However, the global supply of phosphate rock is finite, and although there is debate over how quickly the supply is dwindling, many scientists predict that there will be severe shortages within the next century and the possibility of a phosphate-based economy as political tensions rise.[6,7] Ironically, due to mankind's heavy usage of phosphate-based fertilisers, there is also a real environmental problem of the presence of *too much* phosphorus in lakes and oceans, leading to algal blooms wreaking havoc on marine ecosystems.[8] These two dovetailing problems necessitate the use of efficient phosphorus recycling schemes, which are likely to involve the chemical or biological treatment of human and animal waste matter.[9] There is therefore a possibility, with a historical nod to the pioneering Brand, that urine could again become a major source of phosphorus in the future.

1.2 Phosphorus and nitrogen

Phosphorus and nitrogen are both in group 15 of the periodic table, and as such are valence isoelectronic. This leads to similarities between the elements and general trends in many different physical and chemical properties as the group is descended. However, there are typically stark differences between the first and second row elements of the p-block, which can be ascribed to strong changes in effective nuclear charge, ionisation energies and orbital size.[10] This is highlighted in the range of allotropy displayed by the pnictogens.

Elemental nitrogen exclusively forms a gaseous dimer with a N≡N triple bond under standard conditions, featuring one of the strongest bonds in chemistry (946 kJ mol^{-1}), and requires forcing conditions or enzymes for activation.[11–13] In contrast, phosphorus has four principal allotropes, all of which are solely σ bonded species. The most common is white phosphorus, which consists of discrete tetrahedral P_4 units. The inherent ring strain in this molecule (P–P–P angles approximately 60˚, P–P bond lengths approximately 2.21 Å) also makes it the most reactive.[14] Red phosphorus is formed by heating white phosphorus to 250 ˚C, and features an amorphous polymeric network of P_4 units linked by P–P bonds.[10] Further heating leads to violet, or Hittorf's phosphorus, which consists of a polymer of alternating [P_8] and [P_9] units linked by pairs of P atoms.[15] The most thermodynamically stable allotrope is black phosphorus, which is a layered structure of puckered six-membered rings, and is formed under high temperature and pressure.[16]

Diphosphorus, P_2, has been shown to exist in equilibrium with P_4, and can be obtained in appreciable concentrations at 1100 K at low pressures. Carbene-supported diphosphorus fragments have been published by the groups of both Robinson and Bertrand (an example is shown in Figure 1.6).[17,18] Elegant work from Cummins and co-workers has explored the solution-phase chemistry of this species with its mild generation from a niobium complex, directly from P_4, or more recently from a bis(anthracene) complex (shown in

Scheme 1.1).[19–21] This has allowed the subsequent trapping of the P_2 fragment with a range of dienes and its detection by molecular beam mass spectrometry.[22] The reaction of this fragment with azide affords the $[P_2N_3]^-$ anion, which is a rare example of a planar aromatic inorganic species (Scheme 1.1).[23]

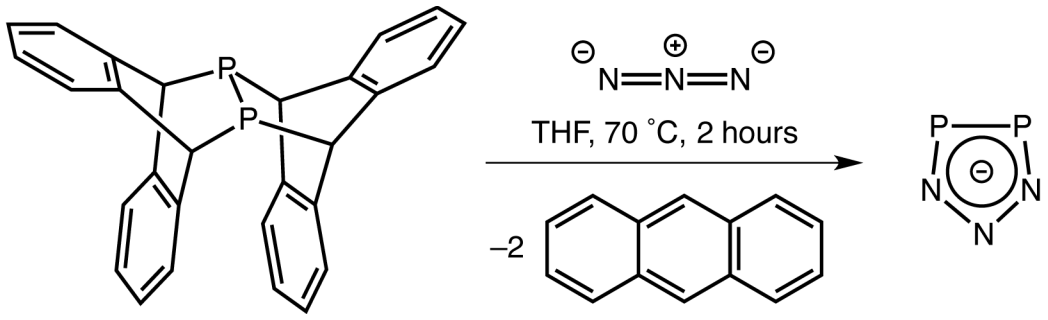

Scheme 1.1: Thermal generation and trapping of diphosphorus to yield the $[P_2N_3]^-$ ring.[23]

1.3 The double bond rule

Multiple bonds involving elements with a principal quantum number greater than two were once thought to be inaccessible under the tenets of the *double bond rule*.[24,25] This theory is borne out in the above allotropes, where the propensity for catenation of phosphorus illustrates its reluctance to form (p–p)π bonds, which can be attributed to the decreasing percentage overlap between p orbitals on descending the group (Table 1.1).

Table 1.1: Nitrogen and phosphorus bond strengths, in kJ mol^{-1}.[26]

	N	**P**
Single	161	209
Double	456	351
Triple	946	490

This theory, however, only takes bond strength into consideration. There are numerous examples that circumvent this by employing bulky ligands that both kinetically and thermodynamically stabilise double and even triple bonds of the heavier elements in the p-

block.[27,28] Over the last few decades, heavy main-group analogues of alkenes and alkynes have developed from academic curiosities towards useful reagents in organic synthesis,[29] polymer science,[30] and molecular electronics.[31]

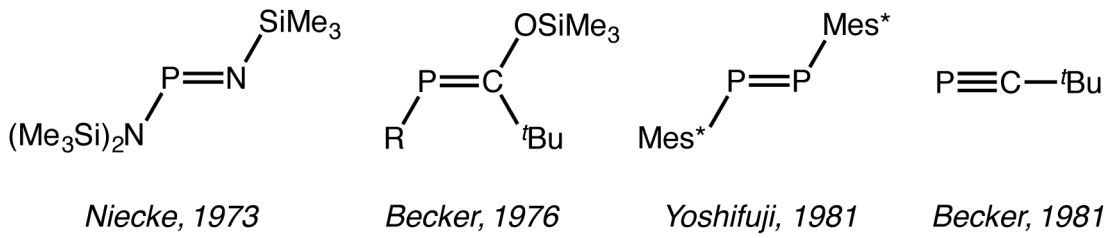

Figure 1.1: Early examples of phosphorus-containing analogues of imines, alkenes and alkynes.

The molecules in Figure 1.1 represent milestones in the preparation and isolation of unsaturated group 15 compounds. The first example of a multiple bond to phosphorus was Niecke's iminophosphane derivative, which contained a P=N double bond synthesised via a reductive elimination reaction.[32] The first isolable phosphaalkene, containing a P=C double bond, was synthesised by Becker in 1976,[33] and five years later the first species containing a P=P double bond, a diphosphene, was published by Yoshifuji.[34] Becker extended his work to synthesise the first stable compound featuring a P≡C triple bond (a phosphaalkyne) in 1981.[35] The impressive progress in this field is highlighted by the preparation of the first multiple bond between two bismuth atoms in a dibismuthene in 1997 by Tokitoh and Okazaki.[36] The synthesis, properties and subsequent chemistry of phosphaalkenes and phosphaalkynes will be explored in more detail later in the chapter.

1.4 Phosphorus as a "carbon copy"

Phosphorus is undeniably a multi-faceted element, and comparisons can be drawn to some of its neighbouring elements in the periodic table. There are clear similarities between certain compounds of phosphorus and those of the other pnictogens; for example, the binary hydrogen compounds of group 15, EH_3 (E = N–Bi), are all trigonal pyramidal with a lone

pair of electrons. Less obvious, perhaps, is the link to silicon when phosphorus is in a high coordination environment. For instance, the evidence of similar factors affecting the stereochemistry at Si and P during substitution reactions has led to the conclusion that similar S_N2-type mechanisms are in action,[37] although more recent theoretical calculations have demonstrated that there are subtle differences depending on the steric bulk around the phosphorus centre.[38] The most profound relationship, though, is between that of phosphorus and carbon, and this warrants further discussion.

1.4.1 The isolobal analogy

The principle of isolobality is a concept that has been exploited by chemists for several decades to help rationalise the structure and bonding of novel compounds, by relating seemingly unrelated fragments of molecules. The Nobel Laureate Roald Hoffmann described two fragments as isolobal "*...if the number, symmetry properties, approximate energy and shape of the frontier orbitals are similar – not identical, but similar*".[39,40] The last part makes it a particularly powerful concept, as there is no necessity for the fragments to be either isoelectronic or isostructural. It is, however, a relatively simple model, and it makes no predictions as to the kinetic or thermodynamic stability of a molecule derived from a stable isolobal analogue. For example, the conceptual dimerisation of methylene, CH_2, leads to the organic molecule ethylene, whereas dimerisation of the isolobal $Fe(CO)_4$ fragment yields the thermally unstable $[Fe_2(CO)_8]$.[39] Although originally used to relate transition metal moieties to known organic fragments, it has since been extended to the rest of the periodic table.[41] The analogy pertinent to this discussion is that of the methine fragment, C–H, and the phosphorus atom (Figure 1.2). This hints at the possibility of the replacement of CH with P in common organic compounds, at least on the basis of the similarity of their frontier orbitals.

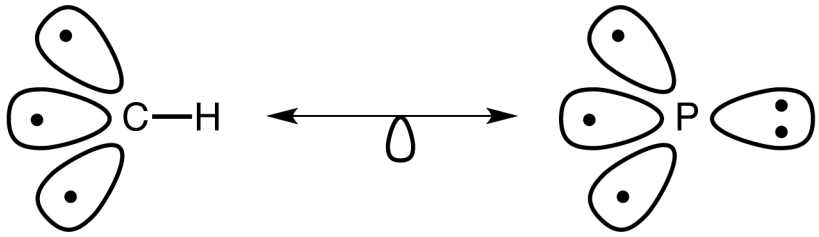

Figure 1.2: Isolobality of C–H and P fragments.

1.4.2 Phospha-organic chemistry

The parallels between phosphorus and carbon run deeper than simple isolobality; they are also related by the diagonal relationship, which is a well-documented phenomenon resulting from the competing factors of going across a period (from left to right) and of descending a group. The consequence is that the ability of phosphorus to accept or release electrons is somewhat similar to that of carbon, and thus the elements are chemically similar. Although the σ electronegativity of phosphorus is lower than that of carbon ($\chi_P = 2.19$, $\chi_C = 2.55$), the values of π electronegativity are almost identical, or possibly even higher for phosphorus.[42,43] This has led to some fascinating analogies between the chemistry of low-coordinate compounds of phosphorus and carbon (Figure 1.3), and the birth of a subfield of organophosphorus chemistry called "phospha-organic" chemistry.[44,45]

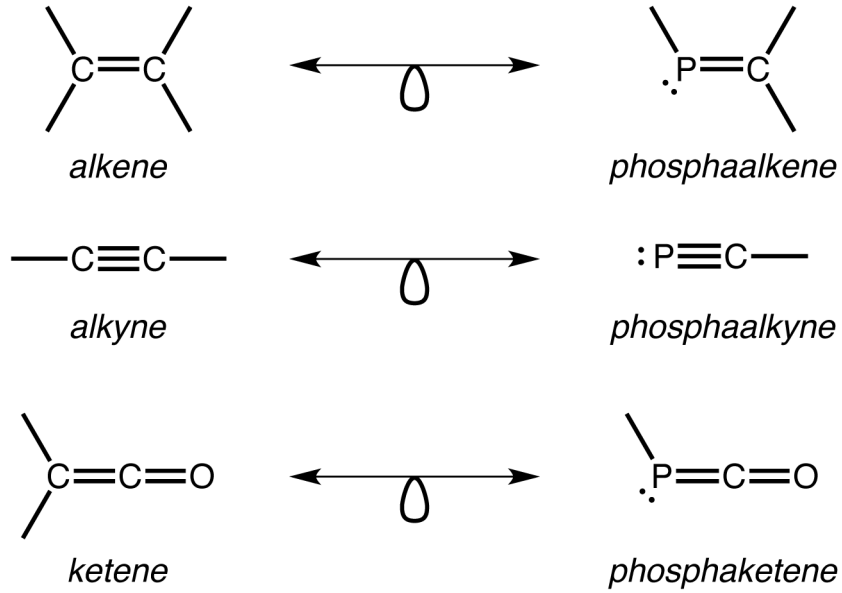

Figure 1.3: Low-coordinate carbon species and their phosphorus-containing analogues.

1.4.2.1 Phosphaalkenes

A widely studied exemplar of phospha-organic chemistry is the phosphaalkene. As the synthesis and reactivity of these compounds have been reviewed extensively,[45–49] only the most apposite cases will be discussed further. There are many different synthetic procedures for these species, and the two most general are depicted in Scheme 1.2. The first is Becker's original synthesis of the first isolable phosphaalkene (already depicted in Figure 1.1), and is important both historically and practically. Becker's phosphaalkene was synthesised by a 1,3-silyl migration driven by the oxophilicity of the silicon atom, which is now known as the Becker rearrangement.[33] This has been extended to form a series of related compounds by the reaction of bis(trimethylsilyl)phosphines with CO_2,[50] CS_2,[51] phosgene[52,53] and carbodiimides,[54] all driven by the desire for silicon to form bonds with oxygen, sulfur and nitrogen. The use of silylphosphines as synthons for low-coordinate phosphorus species will be a recurring theme in the subsequent sections. The second scheme is the 1,2-elimination of HX to yield a double bond, often stimulated by the presence of amine bases such as DBU (1,8-diazabicyclo[5.4.0]undec-7-ene).[55,56]

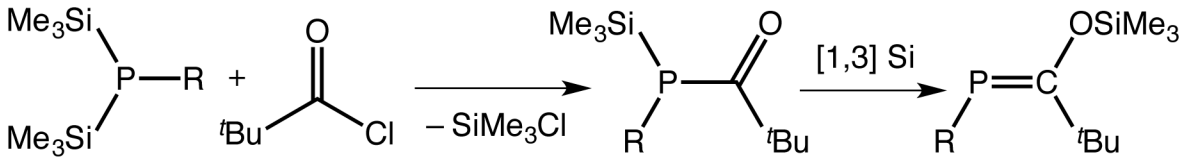

R = Me, Ph

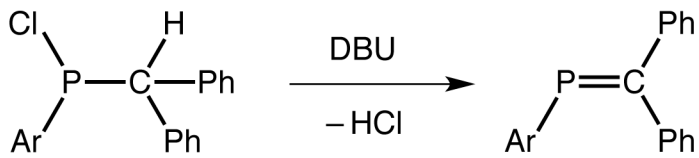

Ar = Mes, 2,6-Xylyl

Scheme 1.2: Becker's (above) and Bickelhaupt's (below) general synthetic procedures for stable and isolable phosphaalkenes.[33,56]

In line with the electronegativity data listed in the previous section, the π component of the double bond in the simplest member of this class of compounds, $HP{=}CH_2$, is essentially

apolar, whereas the σ component is highly polarised.[57] UV photoelectron spectroscopy on this molecule reveals that the HOMO is the π bond at –10.3 eV, which is only slightly higher in energy than the lone pair on phosphorus (–10.7 eV).[58] This small energy gap means that electrophiles will sometimes fail to distinguish between the two, as is the case in oxidation and sulfurisation reactions,[59,60] but the prototypical reactivity of these species is at the double bond. According to calculations, the P=C π bond is significantly weaker than the C=C analogue (180 kJ mol^{-1} versus 272 kJ mol^{-1}). This is in complete accord with the earlier discussion of the double bond rule, and makes the P=C double bond very reactive. The stabilisation of phosphaalkenes with respect to oligomerisation can arise from the aforementioned use of sterically encumbering ligands (as in the compounds in Scheme 1.2), conjugation,[61,62] or complexation to a metal centre.[63,64] The latter method is an interesting case, and there are several bonding modes accessible for phosphaalkenes.[65–68] As phosphorus ligands they are relatively poor σ donors and good π acceptors, on account of sp^2 hybridisation of the phosphorus centre. This is in contrast to traditional phosphine ligands, which are generally regarded as good σ donors and poor π acceptors (depending on the substituents on the phosphorus). Coordination complexes of phosphaalkenes have shown promise in homogeneous catalysis, showing that these compounds are more than conceptual curiosities.[69]

1.4.2.2 Phosphaalkynes

The chemistry of phosphaalkynes started in 1961 when Gier detected the parent species of this class of compounds, HC≡P, using IR spectroscopy and mass spectrometry.[70] However the unorthodox synthetic procedure, which involved the decomposition of PH_3 in an electric arc between graphite electrodes, impeded further progress in this field. Fifteen years later, Nixon and Kroto reported an improved synthesis involving the double dehydrohalogenation of RCH_2PCl_2 that corroborated and extended Gier's initial findings, but the products were

still thermally unstable at ambient temperatures.[71] The goal of accessing a phosphaalkyne that was stable under ambient conditions was finally realised by Becker, who synthesised ^{t}BuC≡P in 1981, which was the first isolable compound containing a formal triple bond between carbon and phosphorus (Scheme 1.3).[35]

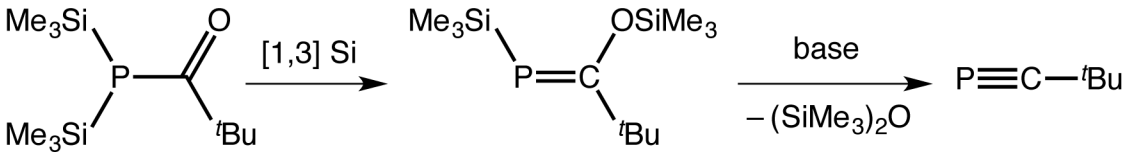

Scheme 1.3: Becker's synthesis of the first isolable phosphaalkyne.[35]

The electronic features of phosphaalkynes are different to those of phosphaalkenes. The P≡C triple bond is typically strongly polarised towards carbon, in contrast with the apolar P=C double bond, and as such protonation of the former with super acids occurs exclusively at carbon.[72] UV photoelectron spectroscopy of ^{t}BuC≡P reveals the HOMO at –9.61 eV corresponding to the π bonds, while the lone pair on phosphorus is significantly lower in energy (–11.44 eV).[73] This suggests that the chemistry of phosphaalkynes will be dominated by reactivity with the π system, and this is indeed borne out experimentally. The cycloaddition chemistry of phosphaalkynes has been thoroughly developed,[47,74] notably the [2+3] cycloadditions with 1,3-dipole compounds such as azides or nitrile oxides as a general route for the formation of heterophospholes.[75]

An intriguing aspect of phosphaalkyne chemistry is the large variety of products derived from oligomerisation reactions. These often lead to complicated cage compounds, but there are some instances where more classical alkyne-like behaviour is observed (Scheme 1.4). Thermally induced tetramerisation leads to a tetraphosphacubane compound,[76] although a more efficient synthesis of these compounds has been developed.[77] A vanadium imido-catalysed cyclic trimerisation yields a 1,3,5-triphosphinine, also known as triphosphabenzene.[78] Studies into the role of the transition metal catalyst led to the

observation of a relatively rare [2+2] cycloaddition product of the phosphaalkyne and the M=N imido double bond.[79]

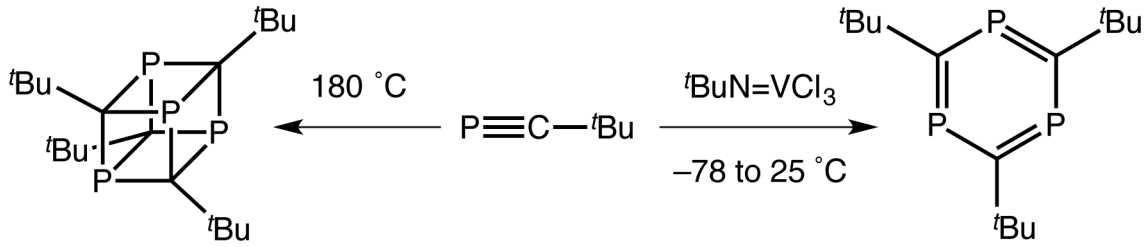

Scheme 1.4: Oligomerisation reactions of *tert*-butylphosphaalkyne.[76,78]

1.4.2.3 Phosphaketenes

The chemistry of phosphaketenes, which can also be regarded as phosphorus analogues of isocyanates, is significantly less well developed than that of the previously discussed low-coordinate phosphorus species. Only two hydrocarbon-substituted phosphaketenes are known, both of which were initially reported by Appel and Paulen. The first to be unequivocally detected was the *tert*-butyl derivative, ^{t}BuP=C=O, but this is unstable as a monomer above –60 ˚C, and rapidly dimerises to give the diphosphetanedione.[80] The use of a bulkier R group, namely the supermesityl group, allowed the isolation of the monomeric species at room temperature.[81] Scheme 1.5 shows the general reaction scheme for both compounds; the *tert*-butyl derivative is synthesised at –90 ˚C, whereas the supermesityl compound is heated to 45 ˚C. Both are obtained via the reaction of the appropriate bis(trimethylsilyl)phosphine with phosgene, resulting in loss of trimethylsilyl chloride to give the intermediate shown. This intermediate is observable spectroscopically at –90 ˚C when R = ^{t}Bu, but is not observed at all when R = Mes* due to the more forcing reaction conditions. Loss of the second equivalent of trimethsilyl chloride affords the desired phosphaketene products.

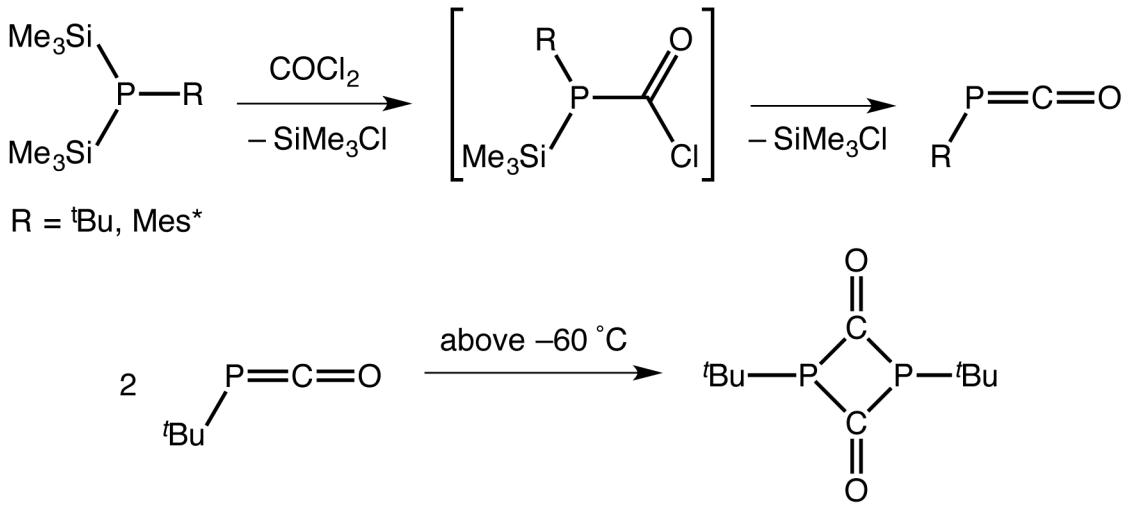

Scheme 1.5: General reaction scheme for *tert*-butyl and supermesityl phosphaketenes (above, conditions not included) and the thermal dimerisation of the *tert*-butyl derivative (below).[80,81]

Ab initio calculations on the parent phosphaketene, HP=C=O, have revealed that protonation occurs exclusively at the phosphorus centre, in contrast to other phosphaallene species.[82] The majority of practical reactivity studies on phosphaketenes, however, have been limited to the supermesityl species. UV photolysis stimulates the loss of carbon monoxide to generate the transient phosphinidene, which is the phospha-organic equivalent of a carbene.[83] This compound is highly reactive, and the phosphorus centre rapidly attacks one of the methyl fragments on the supermesityl group to yield a phosphaindane. The loss of CO can also be effected by a range of transition metal catalysts, and allows the formation of several complexes bearing this phosphinidene moiety.[84–87] The simple methylphosphaketene could be generated in the coordination sphere of tungsten, and its chemistry was recently explored by Mathey.[88] Although the compound itself could not be isolated, both the phosphaketene complex $[W(CO)_5(MePCO)]$ and the decarbonylated methylphosphinidene analogue could be inferred from trapping experiments with alcohols.

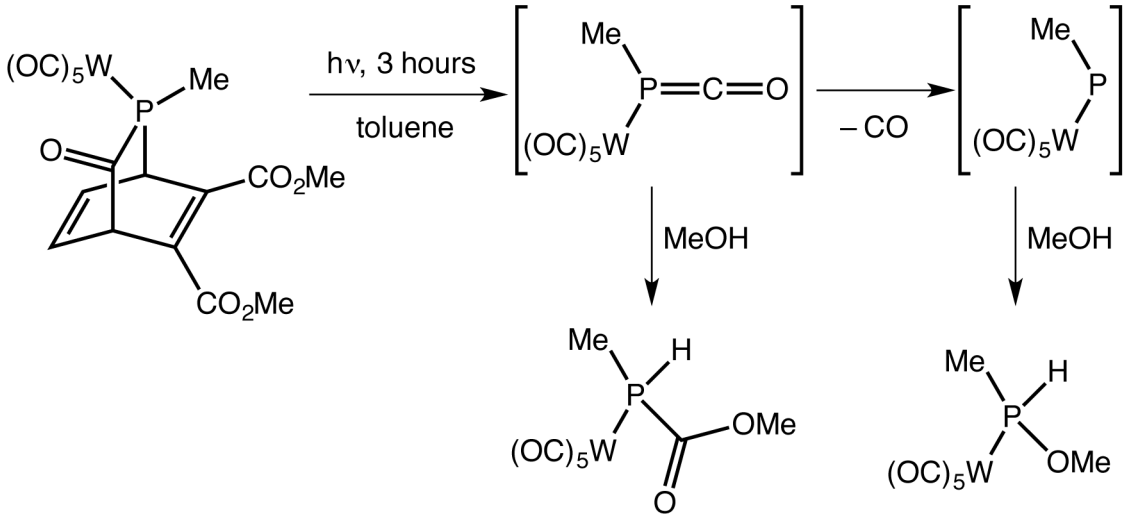

Scheme 1.6: Generation and trapping of transient methylphosphaketene and methylphosphinidene in the coordination sphere of tungsten. Figure adapted from Mao et al.[88]

Phosphaketenes can be stabilised using heteroatoms coordinated to the phosphorus centre, for example in a recently reported phosphanyl phosphaketene.[89] This species is relevant to later work in this chapter and the thesis, and will not be discussed further at this point.

1.5 Sources of phosphorus

1.5.1 Phosphorus trichloride in industry

The vast majority of organophosphorus compounds are industrially synthesised using phosphorus trichloride, PCl_3, as a precursor, generated in turn by the direct chlorination of white phosphorus. Phosphorus trichloride can be functionalised using Grignard or organolithium reagents, or by reaction with halogenated organic compounds under forcing reducing conditions.[90,91] However, PCl_3 is not an ideal reagent for organophosphorus molecules in terms of sustainability and safety due to its inherent corrosiveness, high toxicity and moisture sensitivity. In fact it is a precursor on the list of Schedule 3 substances of the Chemical Weapons Convention, and thus its manufacture is carefully regulated.[92] Moreover, very few of the final products contain a P–Cl bond, so the use of the toxic chlorine gas to activate white phosphorus can be regarded as a necessary yet wasteful step.

For completeness, it should be noted that some industrial processes employ phosphine, PH_3, to prepare a range of phosphorus-containing products, despite the fact that it is a highly toxic and pyrophoric gas.[93–95] Phosphinate esters ($H_2P(O)(OR)$) are also synthesised on a large scale from the alkaline hydrolysis of white phosphorus, but their industrial utility is limited to a single process called electroless plating.[5,96]

1.5.2 Direct activation of white phosphorus

In an effort to circumvent this undesired chlorination step, the direct activation of white phosphorus is an established field that has been researched in earnest since the 1970s, and has led to a range of phosphorus fragments ranging from P_1 to P_{29}.[97] The reactivity of the P_4 tetrahedron is often attributed to the inherently high bond strain energy.[98,99] The major mode of reactivity is the nucleophilic attack of a P–P σ* orbital, although P_4 can also act as an electrophile either through the lone pairs or the σ bonds. This is in addition to redox processes leading to the formation of higher nuclearity polyphosphides such as $[P_{21}]^{3-}$, which can be formed by the reduction of white phosphorus with substoichiometric sodium.[100] It can frequently be difficult to deconvolute these reaction mechanisms, and the combination of nucleophilic, electrophilic and redox pathways operating concurrently is not uncommon (Figure 1.4).

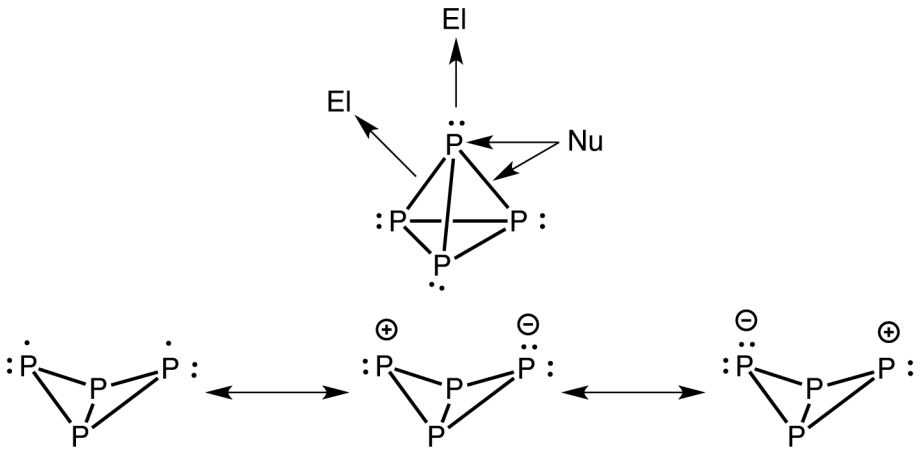

Figure 1.4: General reactivity of white phosphorus, showing nucleophilic and electrophilic sites (above) and radical bond breaking (below). Figure adapted from Scheer et al.[101]

1.5.2.1 Transition metal-mediated activation

Early research into the activation of white phosphorus was carried out almost exclusively with transition metals, which are proficient at the task due to a combination of their coordinative unsaturation, Lewis acidity and availability of d-electrons. This topic has been comprehensively reviewed,[102,103] and representative examples showcasing the diversity of different phosphorus moities are depicted in Scheme 1.7. A brief summary of these compounds and further salient points will be discussed below.

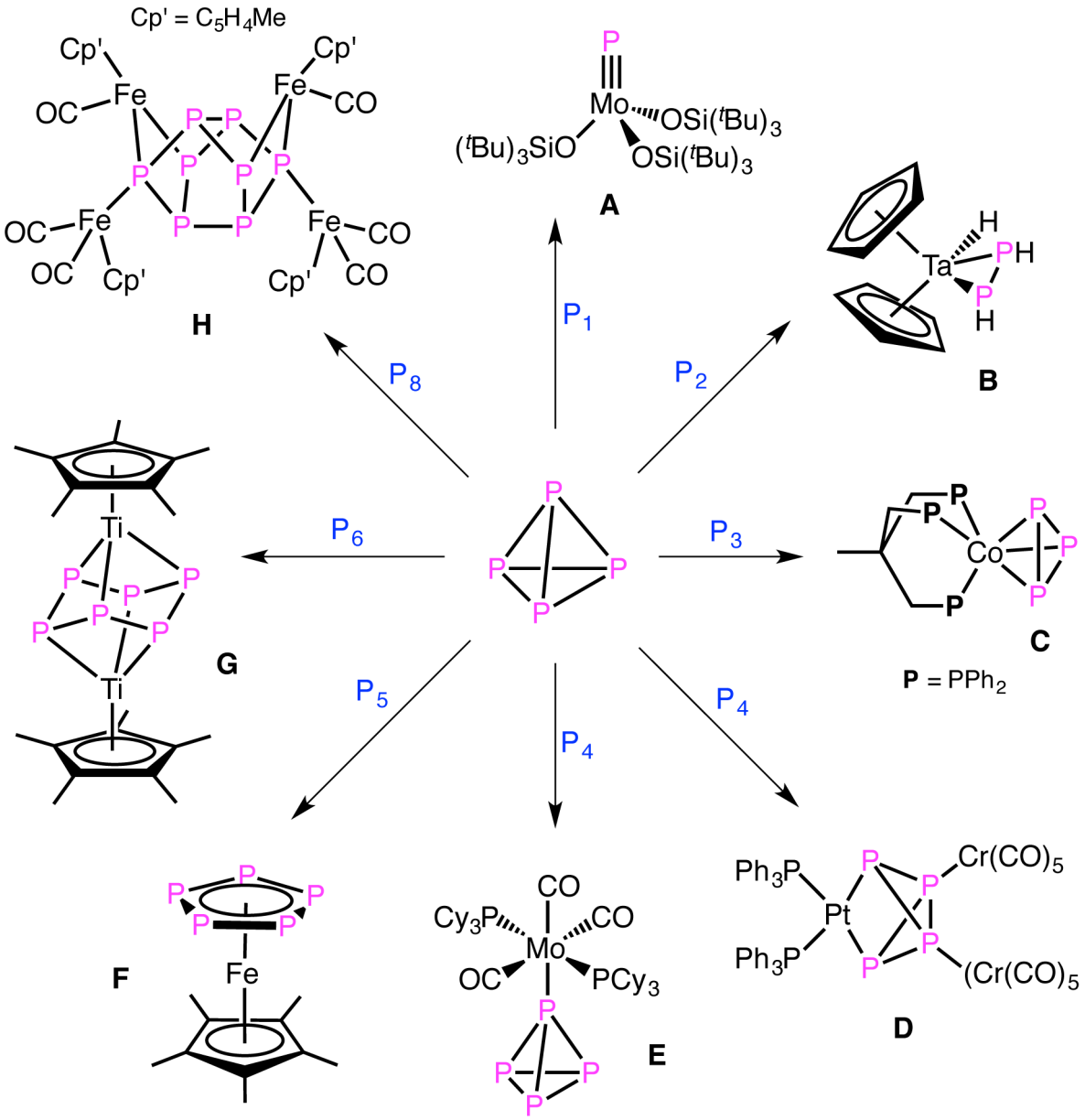

Scheme 1.7: Different P_n fragments derived from the transition metal-mediated activation of white phosphorus. Relevant references are in text.

Compounds **A**–**C** in Scheme 1.7 are the result of degradation of the P_4 cluster to smaller P_n fragments. Terminal monophosphorus ligands are relatively rare and are often found stabilised by group 6 metals, as in the molybdenum complex **A**,[104] although the group of Cummins has also explored the reactivity of an anionic niobium analogue.[105] The symmetrical fragmentation to P_2 moieties typically leads to diphosphorus ligands bridging two metal centres in a μ_2:η^2,η^2 fashion.[106] Examples exist, however, that show cyclopentadienyl-supported transition metal hydride complexes can yield coordinated diphosphene ligands arising from the hydride transfer from the metal to the phosphorus centres, as in **B**.[107] The triphosphorus moiety usually exists as a cyclo-P_3 unit, and can be found bound in either a bridging or terminal manner; an example of the latter is shown in **C**.[108] Despite the abundance of reported reactions, the mechanism for the degradation of white phosphorus is poorly understood, and proposals have only been volunteered in a few cases.[109,110]

White phosphorus can also be activated to a lesser degree, where at least one P–P bond has been broken, but four phosphorus atoms are retained in the product. If only one bond is broken then the familiar butterfly structure is obtained, as seen in **D**.[111] Cleavage of a second bond can yield the cyclo-P_4 ligand,[112] although other motifs are possible.[113,114] Due to the high reactivity of the P_4 cluster, transition metal complexes with an intact P_4 tetrahedron are relatively rare, and an example from Scheer and co-workers is shown in **E**.[115] This complex is thermally unstable in solution above 0 ˚C, but can be isolated and stored as a solid under argon at ambient temperatures. This coordination mode may hint at probable reaction pathways and likely intermediates in many reported activation reactions of white phosphorus in the literature.

Compounds **F**–**H** demonstrate examples of aggregation, where $P_{\geq 5}$ fragments are formed. Such complexes are important in developing a detailed understanding of the structure and

bonding with phosphorus-containing species. **F** is Scherer's pentaphosphaferrocene derivative,[116] which has received significant attention as an inorganic metallocene, and has been exploited by the group of Scheer to form one- or two-dimensional coordination polymers and three-dimensional fullerene-like cages.[117,118] The $[P_5]^-$ ring featured in this species will be examined in more detail later. Both monocyclic and bicyclic P_6 ligands have been isolated when sandwiched between transition metal centres, and are often seen in triple-decker complexes.[119] These P_6 rings are predominantly planar, but one of the few exceptions is **G**, where the chair-like cyclohexaphosphido unit binds in a μ_2:η^3,η^3 fashion.[120] The final compound to be mentioned here is **H**, which is significant as it is the first complex containing the same P_8 subunit that is found in the violet phosphorus allotrope discussed previously.[121]

1.5.2.2 Main group element-mediated activation

Despite the plethora of different P_n fragments arising from the transition metal-mediated activation of white phosphorus, these moieties are rarely converted to useful organophosphorus compounds by subsequent reactions with organic substrates. A possible alternative is the use of highly reactive p-block compounds for similar transformations. This parallel between transition metals and main group elements was highlighted in an excellent and inspiring review article by Power in 2010.[122] The field of main group activation of white phosphorus is a significantly less well-developed topic, but examples are now available from groups 13–17 in the periodic table.[101] This short discussion will focus on the use of carbon-based reagents, as these have the advantage of directly forming P–C bonds during the activation process. This field has been revitalised in recent years by the use of singlet carbene reagents, spearheaded in particular by the pioneering work of Bertrand. The most common of these are the N-heterocyclic carbenes (NHCs), which were first isolated and crystallographically characterised in 1991,[123] and have since found use in wide-ranging

applications from catalysis to the stabilisation of low-coordinate main group fragments.[124,125]

Figure 1.5: Examples of stable singlet carbenes. **I**: NHC (SIPr); **J**: CAAC.

The reaction of SIPr (**I**, Figure 1.5) with white phosphorus leads to the formation of a neutral P_{12} cluster stabilised by two NHC ligands, demonstrating the activation and formation of new P–C bonds.[126] The electronic properties and therefore the reactivity of the carbenic centre can be tuned by changing the NHC for a cyclic (alkyl)(amino)carbene (CAAC). The latter are both more electrophilic and nucleophilic on account of the reduced singlet-triplet gap and the reduced energy of the LUMO.[127] The reaction of three equivalents of the CAAC **J** with white phosphorus in diethyl ether leads to degradation of the P_4 cluster, to afford a mixture of carbene-supported P_2 and activated P_4 fragments, which are shown in Figure 1.6.[18] Aggregation to a P_8 cluster stabilised by four CAAC molecules can be favoured, however, by simply switching the solvent to benzene.[128] This has been rationalised on the basis of the reduced solubility of white phosphorus in diethyl ether; the carbene is therefore present in greater excess and favours the fragmented products.

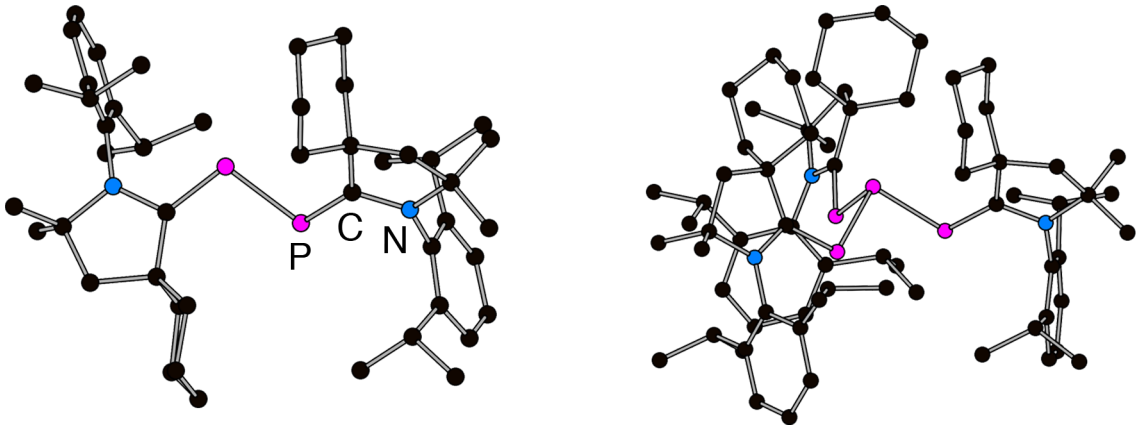

Figure 1.6: Ball and stick models showing the products of the activation of white phosphorus with a CAAC. Hydrogen atoms omitted for clarity.[18]

While the range of transformations of white phosphorus to phosphorus-containing products is extensive, there are still potential drawbacks with its use as the major P atom source in industry. White phosphorus is extremely toxic and pyrophoric, and its infamous role in chemical warfare has been documented for over a century.[129] Synthetically, the reduced reactivity of the remaining P–P bonds after the initial activation of the P_4 tetrahedron means the incorporation of all four phosphorus atoms into useful products can be challenging. Finally, although the diversity of the stoichiometric activation of white phosphorus is impressive, the target of *catalytic* functionalisation has still not been achieved. This has stimulated interest in the use of the other allotropes as alternative phosphorus atom sources.

1.5.3 Red phosphorus

Of the four allotropes of phosphorus, only white phosphorus is pyrophoric. The polymeric chain structures of the other allotropes also make them less toxic on account of their reduced solubility. They are therefore attractive alternative sources of phosphorus, although their chemical activation requires more forcing conditions. There has been relatively little published on the functionalisation chemistry of violet and black phosphorus, although the latter has recently undergone a renaissance in the world of nanomaterials as a

semiconducting phosphorus analogue of graphene.[130–132] Red phosphorus is therefore currently the most feasible replacement as a source of elemental phosphorus in industry.

Red phosphorus has already been employed in the manufacture of matches and in the synthesis of flame-retardants in plastics and aluminium phosphide. A recent report by Peruzzini and co-workers demonstrated the high-pressure reaction of red phosphorus and water under near-UV irradiation to afford a range of oxy-acids and phosphine.[133] The P–P bonds in red phosphorus can be cleaved in super base media, such as potassium hydroxide in DMSO, to afford a range of organic phosphines and phosphine oxides.[134] A more common way of accessing activation chemistry is the chemical reduction with alkali metals to form metal phosphides, M_3P (M = Li, Na, K), often in the presence of an electron-transfer agent such as naphthalene.[135] Due to their high reactivity these species are typically generated and functionalised *in situ*, often via the protonated mono- and dihydrogenphosphides, M_2PH and MPH_2, respectively, affording a diverse range of primary, secondary and tertiary phosphines and phosphine oxides, including chiral derivatives.[136–139] As a simple and representative example, Scheme 1.8 shows the potassium reduction of red phosphorus in liquid ammonia, and the following protonation with a mild acid (*tert*-butanol) to form KPH_2. This reacts with a variety of alkenes and, after quenching the resulting carbanion with another equivalent of *tert*-butanol, yields the corresponding tertiary phosphines.[140] It is important to add the third equivalent of *tert*-butanol after the alkene to prevent formation of phosphine gas.

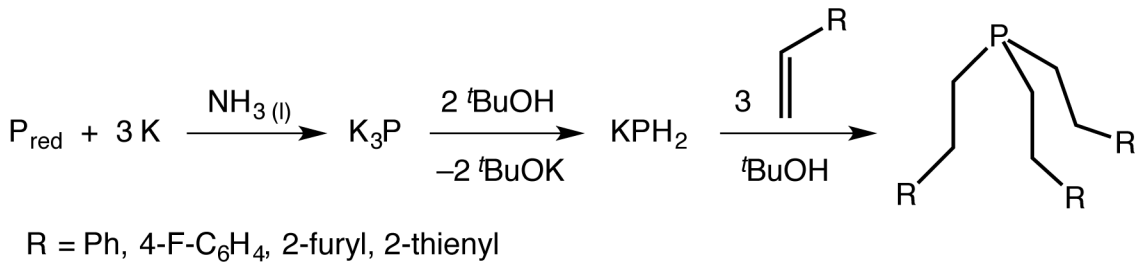

Scheme 1.8: Activation of red phosphorus under reducing conditions to generate a range of phosphines.[140]

This field took a further step forward in 2010 with a report from the group of Grützmacher.[141] The alkali metal dihydrogenphosphides had been established as versatile reagents for several decades, but they always had to be generated *in situ*, and the exact nature of the reagent was unknown. This was overcome with the report of isolable crystals of $[PH_2]^-$ ions encapsulated in an icosahedral cage of sodium cations and *tert*-butoxide anions.[141] The two different clusters, of the form $[Na(dme)_3][Na_{12}(PH_2)(O^tBu)_{12}]$ and $Na_{13}(PH_2)(O^tBu)_{12}$, contain twelve or thirteen sodium ions, respectively, dynamically disordered over the twenty vertices of a dodecahedron. The cluster anion of the former is shown in Figure 1.7. The ^{31}P NMR signals for both species are observable in solution, and there is no evidence of interconversion between the two clusters on the NMR timescale. The $NaPH_2/(NaO^tBu)_x$ aggregates can be used for further chemistry, for example in the formation of surface-modified bis(acyl)phosphine oxides, which have applications as photoinitiators, or in the formation of phosphorus-containing heterocycles.[142,143]

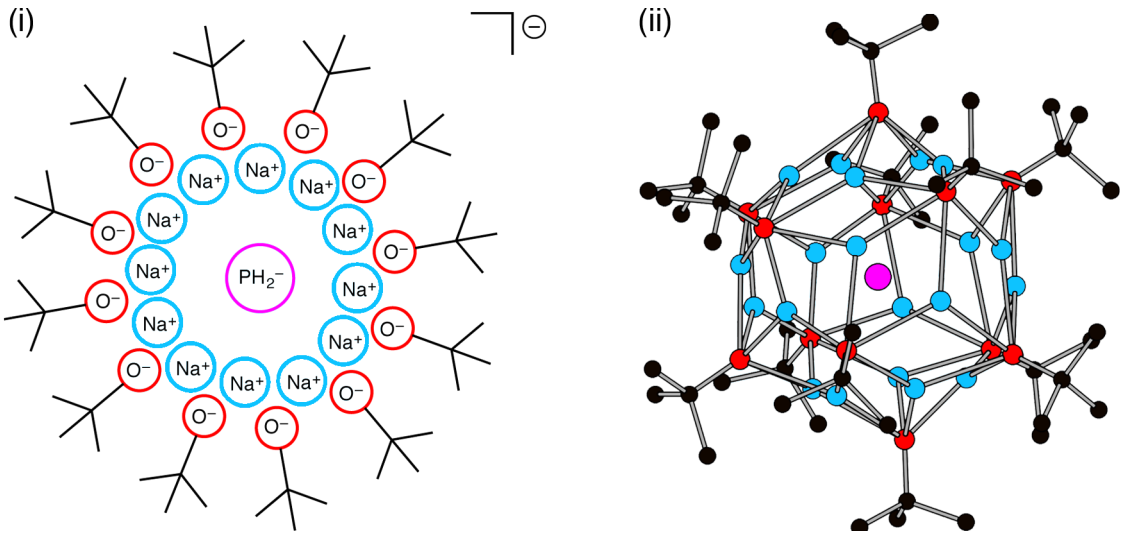

Figure 1.7: (i) A two-dimensional representation and (ii) a ball and stick model of $[Na_{12}(PH_2)(O^tBu)_{12}]^-$. The twelve sodium ions are disordered over the twenty positions shown in light blue. Hydrogen atoms are omitted for clarity.[141]

In addition to the formation of simple phosphides of the form M_3P, the reaction of elemental phosphorus with alkali metals can also lead to a rich range of polyphosphide clusters, with the product dependent on the relative stoichiometries used. A full discussion

of this topic is outside the remit of this thesis, but their chemistry has already been comprehensively studied and reviewed, principally by the groups of Baudler and von Schnering.[144–147] As such, the following discussion will focus exclusively on the trianionic heptaphosphide Zintl cluster, $[P_7]^{3-}$, and its heavier group 15 analogues.

1.6 The $[P_7]^{3-}$ Zintl anion

1.6.1 Introduction

The chemistry of the naked (substituent-free) group 15 Zintl anions has blossomed over the last twenty years, and there are several recent reviews available on the topic.[148–150] Of the vast array of different homoatomic polypnictide clusters known, the family that has received most attention is the trianionic heptapnictide cluster, $[E_7]^{3-}$ (E = P, As, Sb). This is due to their relative ease of synthesis, as the corresponding solid state Zintl phases, A_3E_7 (A = Li–Cs), are readily prepared by heating stoichiometric quantities of the corresponding elements in a furnace. These phases can be dissolved in polar solvents in the presence of cation-sequestering agents to yield the naked clusters in solution.[151,152] The bismuth analogue, $[Bi_7]^{3-}$, which had previously been unattainable due to the lack of an appropriate A_3Bi_7 phase, was recently prepared via a solution-phase method.[153]

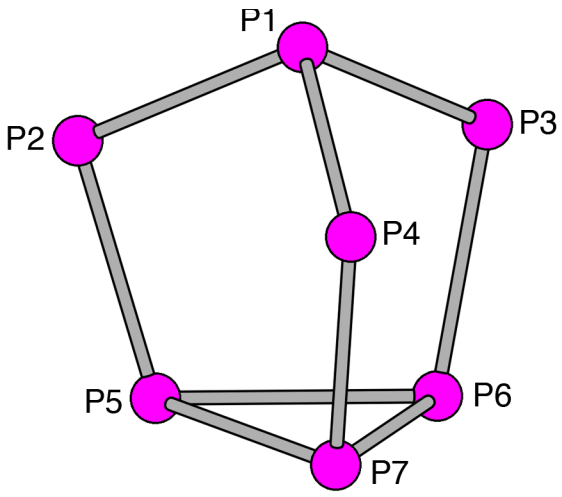

Figure 1.8: Ball and stick representation of $[P_7]^{3-}$.

All of the $[E_7]^{3-}$ clusters are isostructural; they adopt the C_{3v}-symmetric nortricyclane structure in the solid state. The lightest congener is shown in Figure 1.8. These clusters are electron-precise, so all of the bonds can be described by conventional two-centre, two-electron bonds, which is in contrast with some of the group 14 polyanions, where the Wade-Mingos rules need to be invoked to rationalise the bonding.[154,155] There are three unique environments in the $[P_7]^{3-}$ cluster. The apical position (P1) is linked to the basal three-membered ring (P5, P6, P7) by the three bridging atoms (P2, P3, P4). The bridging atoms bear a formal negative charge, making the overall structure isoelectronic with the P_4S_3 cluster.[156]

Despite these three different environments, the ^{31}P NMR spectrum of this species exhibits a single broad resonance at room temperature, which sharpens to a singlet at –119 ppm at 50 °C.[144] The expected spectrum can be obtained at low temperature, showing the three resonances in a 3:3:1 ratio by integration. This is evidence for the fluxionality of this molecule, where all seven phosphorus atoms are rendered equivalent on the NMR timescale. Intriguingly, this behaviour is even mimicked in the solid state.[157] Studies have attributed this to a degenerate Cope-like rearrangement, similar to that found in the organic molecule bullvalene.[158,159] The relative ease of this process is likely due to the combination of the inherent strain in the base of the cluster and the presence of mobile electron pairs on the bridging phosphide vertices. It is reasonable to assume the above discussion holds true for the heavier group 15 analogues as well, but this is significantly more difficult to investigate practically for arsenic or antimony.

The $[E_7]^{3-}$ clusters have two major modes of reactivity: those where the geometry of the cage is retained (coordination and functionalisation reactions), and those where the geometry of the cage is lost (activation reactions). These modes will be discussed in more detail now.

1.6.2 Coordination and functionalisation chemistry

The three pnictide vertices in the $[E_7]^{3-}$ clusters give such species a strongly nucleophilic and basic nature. This allows the synthesis of a series of *exo*-functionalised mono-, di- and tri-substituted cages of the form $[E_7R_x]^{(3-x)-}$ (x = 1–3), and examples are known for organic, main group and transition metal substituents.[150] As the overarching theme of this thesis is the generation of organophosphorus reagents, the select examples below only include those that result in the formation of new P–C bonds.

The use of tetraalkylammonium salts permits the convenient synthesis of a range di-substituted $[P_7R_2]^-$ cages (R = Me, Et, Bu, PCH_2, $EtOCOCH_2$, EtOCOCHMe).[160,161] The neutral tri-substituted $[P_7R_3]$ (R = Me, Et, ^{i}Pr, Bu, ^{i}Bu) clusters can also be prepared by salt metathesis with an appropriate alkyl halide.[162–164] A recent and novel route to P–C bond formation involved the uncatalysed hydrophosphination of the C=N double bonds of carbodiimides and isocyanates using the protonated $[HP_7]^{2-}$ cage (Scheme 1.9).[165–167] The mechanism is not fully understood, but deuterium-labelling studies using $[DP_7]^{2-}$ showed that the hydrogen atom from the phosphide cage is transferred to the nitrogen atom during the course of the reaction.

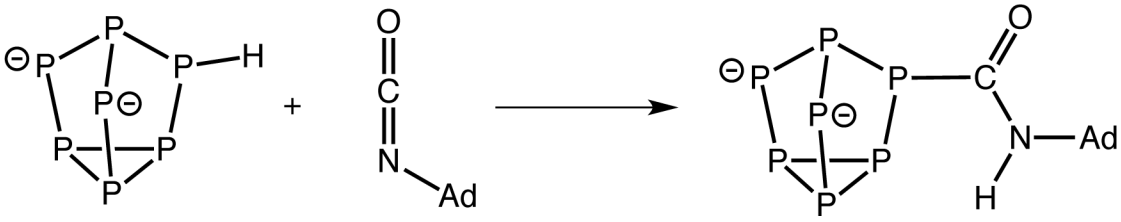

Scheme 1.9: Uncatalysed hydrophosphination of adamantyl isocyanate.[167]

The $[E_7]^{3-}$ clusters also readily coordinate to metal centres. This can occur in three different ways. The cage can bind in an η^1, η^2 or η^4 fashion, where the cage acts as a 2-, 4- or 6-electron donor, respectively, and there are many examples of all three modes in the literature.[148,150] The latter mode arises from the homolytic cleavage of a P–P bond in the

basal ring, which means the geometry of the heptaphosphide moiety changes subtly from the classical nortricyclane structure to a norbornadiene-like structure. An example is shown on the left in Figure 1.9. This $[P_7NiCO]^{3-}$ species was synthesised by the reaction of K_3P_7 with $[Ni(CO)_2(PPh_3)_2]$ in ethylenediamine in the presence of 2,2,2-crypt, and features a nickel centre with eighteen valence electrons, as expected.[168] This reactivity is in stark contrast to the reaction of ethylenediamine solutions of the heavier congener, $[Sb_7]^{3-}$, with the same $[Ni(CO)_2(PPh_3)_2]$ in toluene.[169] Here the product is the $[Sb_7(NiCO)_3]^{3-}$ anion, shown on the right of Figure 1.9, which can be regarded as a ten-vertex cluster formed from the activation of the antimony cage precursor. The electron-deficient polyhedron can be described as a *nido* structure based on the Wade-Mingos rules,[154,155] although it has a different architecture to other known *nido* structures, such as $B_{10}H_{14}$.[10,169]

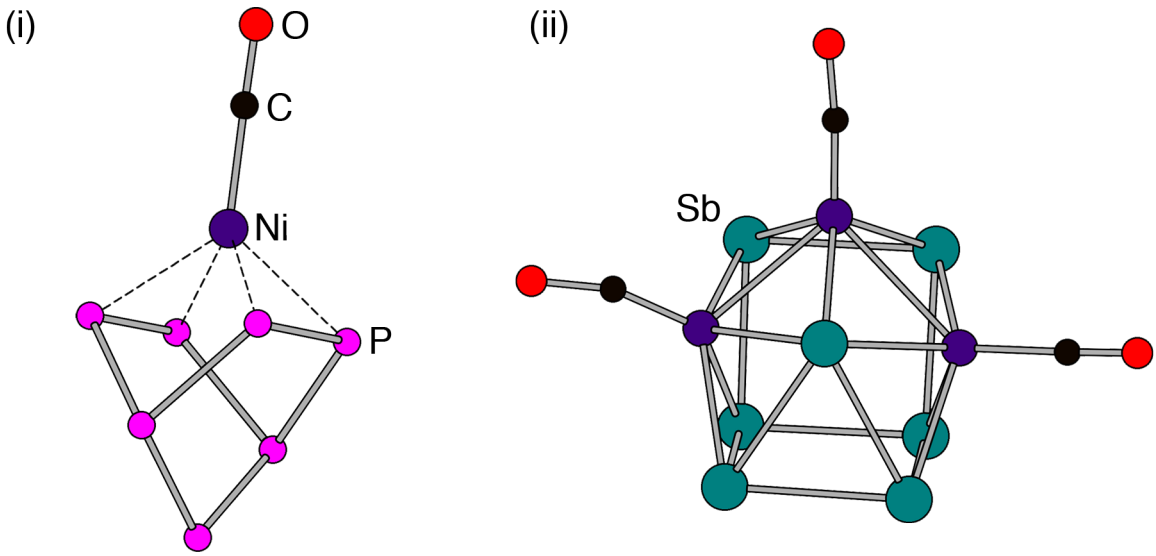

Figure 1.9: Ball and stick models of: (i) $[P_7NiCO]^{3-}$, and (ii) $[Sb_7(NiCO)_3]^{3-}$.[168,169]

This example highlights a key feature of the chemistry of the $[E_7]^{3-}$ clusters. The propensity for activation and fragmentation reactions over simple coordination increases significantly down the group. This can be rationalised by the decreasing E–E bond strength on descending group 15 (Table 1.2).[170] The data provided are for the bond strengths within the E_4 tetrahedra, which can be considered reasonable estimates for the $[E_7]^{3-}$ clusters, as the

first E–E bonds being broken are presumably those in the basal three-membered ring. Either way, the qualitative trends are poignant, and the more facile breaking of the bonds encourages cluster rearrangement for the heavier congeners.

Table 1.2: Bond strengths for E–E bonds within E_4 tetrahedra.[170]

	Bond strength (kJ mol^{-1})
P–P	201
As–As	146
Sb–Sb	121

1.6.3 Activation chemistry

There are a great number of cases of activation of the heavier $[As_7]^{3-}$ and $[Sb_7]^{3-}$ cages, but a real paucity of examples for the lighter analogue. The $[P_7]^{3-}$ cluster can undergo mild oxidative coupling to afford higher nuclearity polyphosphides, such as $[P_{14}]^{4-}$, $[P_{16}]^{2-}$ and $[P_{21}]^{3-}$. Furthermore, the fact that the η^4 coordination mode requires prior cleavage of one of the P–P bonds means that this can be regarded as a mild activation process, although there is no further rearrangement of the cage. I will therefore define activation for the remainder of this discussion as the fragmentation of the $[P_7]^{3-}$ cage into smaller P_n moieties that can be functionalised, or at least have the potential to be functionalised, to useful organophosphorus species. Using this practical definition, there were no examples in the chemical literature of the activation of the $[P_7]^{3-}$ cage when I first joined the Goicoechea group in 2011. Most of the following examples have arisen from research carried out in our group, and I have worked on a number of these projects. A very recent example from a collaboration between the groups of Gudat and Grützmacher will also be presented. These results are presented thematically, and are not necessarily in the chronological order they were first reported.

1.6.3.1 Transition metal-mediated activation

As already mentioned, the reactions of the $[P_7]^{3-}$ cluster with transition metal complexes tend to lead to simple coordination of the cage to the metal centre. However, the reaction of K_3P_7 with the low-valent, low-coordinate $[Co(Mes)_2(PPhEt_2)_2]$ complex led to the first transition metal-mediated activation of the cage. The nuclearity of the cluster (i.e. seven) is maintained in the product, but extensive rearrangement has taken place to yield the $[Co(\eta^5\text{-}P_5)(\eta^2\text{-}P_2H(Mes))]^{2-}$ anion (Figure 1.10).[171] The product contains an $[\eta^5\text{-}P_5]^-$ ring, which has been mentioned before and will be discussed in more detail shortly, and an $\eta^2\text{-}P_2$ fragment, which may be viewed as a diphosphene stabilised by extensive back-donation into the π^* orbital, imbuing significant metallacyclic character on the CoP_2 moiety. It is worth noting that a new P–C bond was formed in the rearrangement, due to migration of one of the mesityl groups from the cobalt centre to a phosphorus atom. The mechanism for this reaction is as yet undetermined.

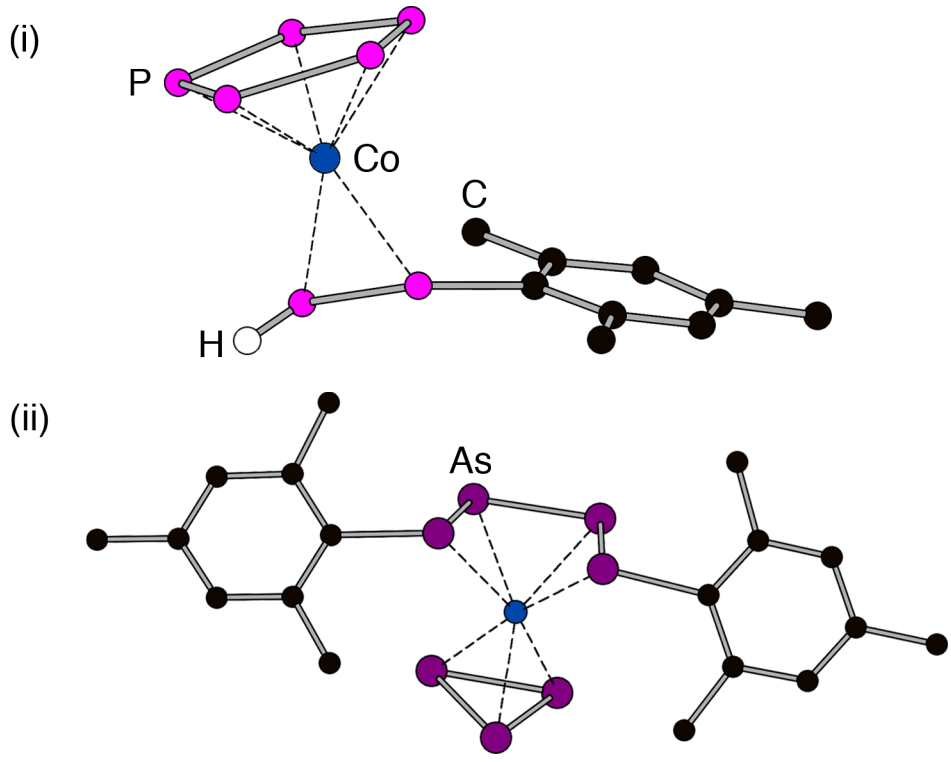

Figure 1.10: Ball and stick diagrams of: (i) $[Co(\eta^5\text{-}P_5)(\eta^2\text{-}P_2H(Mes))]^{2-}$, and (ii) $[Co(\eta^3\text{-}As_3)(\eta^4\text{-}As_4(Mes)_2]^{2-}$. Hydrogen atoms on the mesityl groups omitted for clarity.[171,172]

Curiously, when the similar reaction is carried out with the K_3As_7 congener, activation is once again achieved, but the product is not simply the heavier analogue of the phosphorus complex (Figure 1.10).[172] The nuclearity of the parent cluster is once again retained, but in this case the $[Co(\eta^3\text{-}As_3)(\eta^4\text{-}As_4(Mes)_2]^{2-}$ product contains a three-membered $\eta^3\text{-}As_3$ ring, and a rare example of a group 15 analogue of butadienediide.

These transition metal-mediated activations are interesting examples of the generation and stabilisation of rare group 15 fragments. However, as is the case with the analogous activation of white phosphorus, they do not necessarily represent viable synthetic routes to isolable organophosphorus (or organoarsenic) compounds. Therefore, with this ultimate aim in mind, the remaining examples feature direct activation of the $[P_7]^{3-}$ cluster with organic substrates.

1.6.3.2 Activation with imidazolium salts to afford phosphaalkenes

The activation of the $[P_7]^{3-}$ cluster with a range of imidazolium salts has recently been demonstrated by the groups of Gudat and Grützmacher to yield phosphaalkenes (Scheme 1.10).[173] The heptaphosphide precursor in this instance was generated via a solution phase reduction of red phosphorus using sodium metal and a catalytic amount of naphthalene. This reaction is relatively versatile and works well for both *N*-alkylated and *N*-arylated imidazolium salts, though more forcing conditions are required for the former (heated under reflux for 16 hours, whereas the latter react at 20 ˚C).

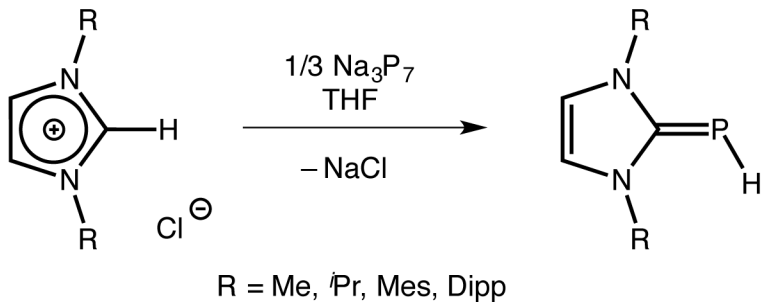

Scheme 1.10: Activation of the $[P_7]^{3-}$ cluster with imidazolium salts to yield phosphaalkenes.[173]

Arguably the liveliest debate in contemporary main group chemistry is the depiction of chemical bonding in certain molecules, and whether or not the use of arrows is a valid representation.[174,175] The products of the above reaction and structurally related compounds have been the subjects of such speculation. The P–C bonding can either be rationalised as that found in an inversely polarised phosphaalkene, with a polarised covalent σ bond and an inversely polarised π bond,[46] or as a dative phosphinidene-NHC adduct (Figure 1.11).[176] The spectroscopic and structural data match that of a recent computational study,[177] and are in complete accordance with the inversely polarised phosphaalkene description (i), although the authors note that the relatively low value for the calculated P–C dissociation energy may suggest some contribution from the phosphinidene resonance (ii). If these products could be subsequently utilised as phosphorus transfer agents then this could open the doors for the generation of new organophosphorus moieties.

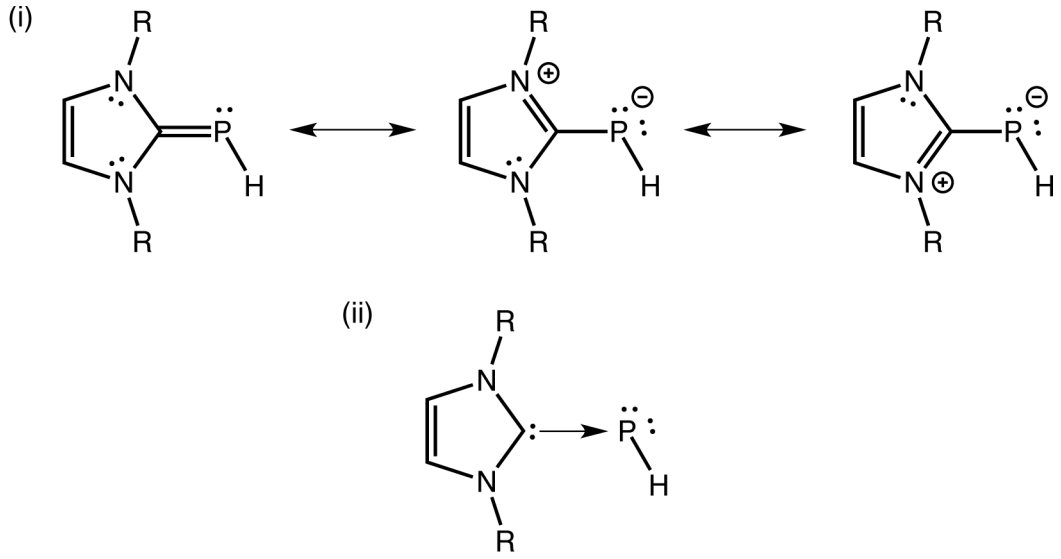

Figure 1.11: Different resonance contributions for (i) inversely polarised phosphaalkenes and (ii) phosphinidene-NHC adduct.

1.6.3.3 Activation with 1,3-butadienes to afford monophospholides

The conceptual stepwise replacement of CH moieties in cyclopentadienide with isolobal P atoms leads to the formation of a family of aromatic phospha-organic anions called

phospholides (or phospholyl anions). Due to the inherent possibility of isomerism within the di- and tri-substituted systems, there are seven members of this group (Figure 1.12), all of which are known, either as the free anions or stabilised in the coordination sphere of a transition metal.[45,178,179] Although this hypothetical replacement of a methine unit with a phosphorus atom is simple on paper, it can often be difficult to realise experimentally, and general synthetic procedures for many of these isomers are either non-existent or only tolerant for certain R groups on the carbon atoms.

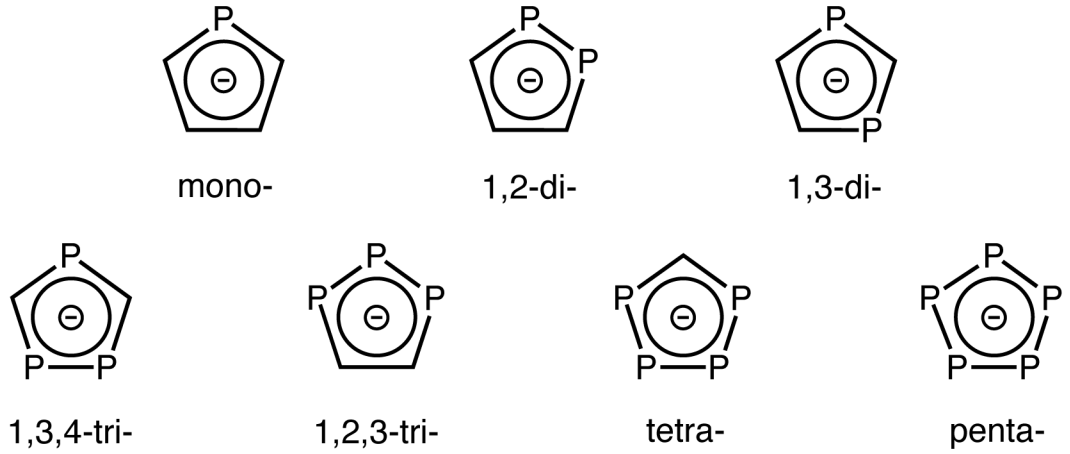

Figure 1.12: The range of possible phospholide anions.

The monophospholides, $[PC_4R_4]^-$, are the most established member of this family, and have the most general routes to their synthesis. The first preparative method by Braye and co-workers involved the alkali metal-induced reductive cleavage of the P–Ph bond in *P*-phenylphospholes, eliminating MPh (M = Li, Na, K) (Scheme 1.11).[180] A radical intermediate has been postulated and observed in some cases.[181] This method is straightforward and has been used to prepare many different monophospholides, but it requires R groups that are tolerant to reducing conditions. Mathey and co-workers subsequently developed an alternative route based on the established [1,5] sigmatropic shift of the phosphorus substituents and subsequent deprotonation to yield α-functionalised phospholides.[182]

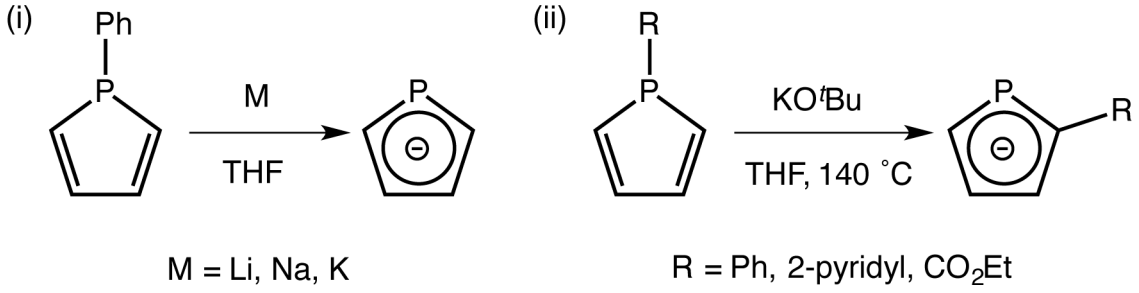

Scheme 1.11: (i) Braye[180] and (ii) Mathey[182] methods for the generation of monophospholides.

We have discovered a completely novel synthetic route to monophospholides based on the activation of the $[P_7]^{3-}$ cluster. This was work carried out jointly with a student that I supervised and has not been published, but a more comprehensive account and additional data can be found in the Masters thesis of David Gillott.[183] The reaction of K_3P_7 with a range of 1,3-butadienes was explored, but only one of these yielded the desired monophospholide product in a somewhat reproducible manner. The prolonged heating of a pyridine solution of $[K(18\text{-crown-6}]_3[P_7]$ and a ten-fold excess of *trans*,*trans*-1,4-diphenyl-1,3-butadiene at 60 ˚C led to a mixture of phosphorus-containing products (Scheme 1.12).

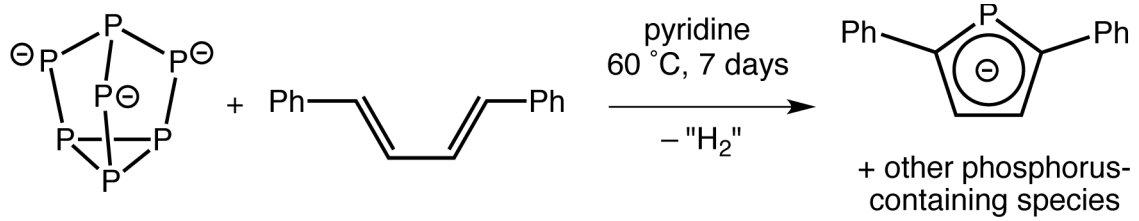

Scheme 1.12: Activation of the $[P_7]^{3-}$ cluster with a 1,3-butadiene to yield 2,5-diphenylmonophospholide and other products.

A pure sample of $[K(18\text{-crown-6})][PC_4Ph_2H_2]$ could be obtained by extraction of the product into diethyl ether and subsequent washings with hexane to remove the excess butadiene starting material. This was demonstrated by the sole presence of a singlet in the ^{31}P NMR spectrum at 82.4 ppm, in accord with a previous report of the lithium salt.[184] The mechanism for this reaction is unknown, but both fragmentation of the cage and loss of two atoms of hydrogen (in the form of dihydrogen or otherwise) are required. Crystals suitable

for single crystal X-ray diffraction were obtained after exchange of the cation-sequestering agent from 18-crown-6 to the three-dimensional analogue, 2,2,2-crypt (Figure 1.13). This anion has been synthesised before,[185] but this is the first time the corresponding cation has been encapsulated to such a degree as to preclude significant cation-anion interactions, and thus arguably the first isolation of the truly "free" anion.

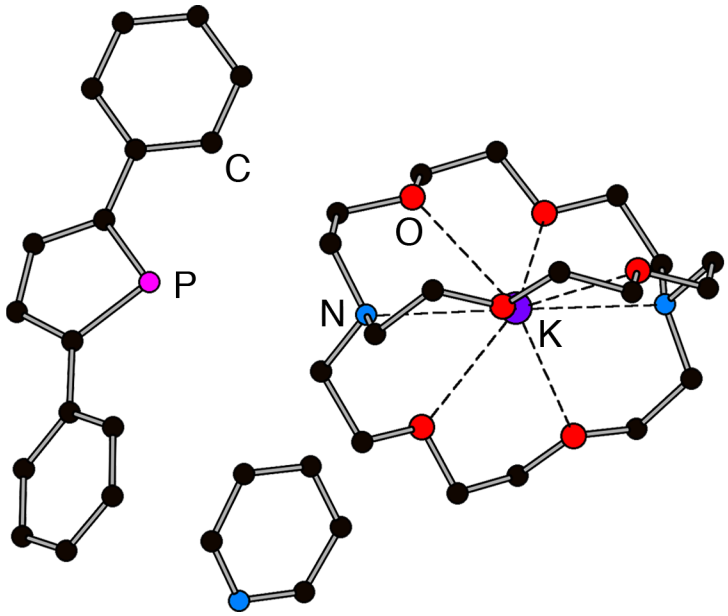

Figure 1.13: Ball and stick model of the asymmetric unit of [K(2,2,2-crypt][$PC_4Ph_2H_2$]·pyridine. Hydrogen atoms omitted for clarity.

The isolobality of monophospholides (and indeed all phospholides in general) with the ubiquitous cyclopentadienide anion allows for some interesting parallels and comparisons regarding coordination to metal centres. As expected, the η^5 coordination mode is common for both species. However, the presence of a radially extended lone pair on the phosphorus atom also opens the possibility of η^1 coordination for the monophospholides without disrupting the aromaticity in the five-membered ring. There are numerous examples of both modes in the literature.[186–188] We sought to corroborate these findings and influence the coordination mode by judicious choice of ligands on a tungsten centre (Scheme 1.13).

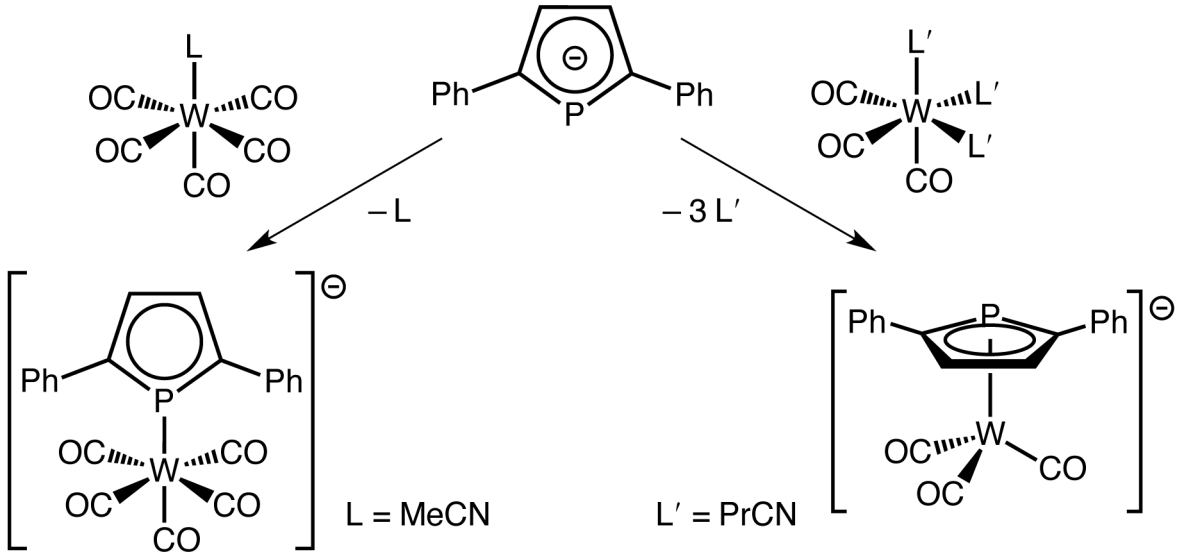

Scheme 1.13: Reaction scheme to target different coordination modes of a monophospholide.

As desired, when only one labile acetonitrile ligand is present the η^1 complex is formed. This was characterised by ^{31}P NMR spectroscopy, which shows a resonance at –29.6 ppm with the characteristic satellites due to coupling to the ^{183}W nucleus (14.3% abundant, I = ½), with a value of $^1J_{P–W}$ = 129 Hz. The η^5 product could be favoured by employing three labile butyronitrile ligands, as the 6-electron donor maintains the 18-valence electron count at tungsten. The ^{31}P NMR spectrum shows a resonance at –24.5 ppm, with much smaller tungsten satellites ($J_{P–W}$ = 10 Hz) due to the decreased interaction between the phosphorus and tungsten centres. This product was also characterised crystallographically (Figure 1.14).

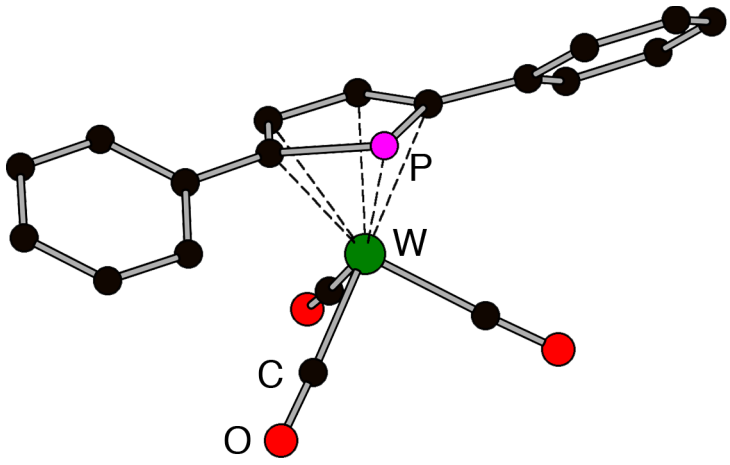

Figure 1.14: Ball and stick model of $[W(CO)_3(\eta^5\text{-}PC_4Ph_2H_2)]^-$. Hydrogen atoms omitted for clarity.

A comparison of the bond metrics between the free and η^5 coordinated monophospholide reveals a slight lengthening of the P–C and C–C bonds in the latter. This is consistent with the back-donation of electron density from the tungsten centre into the π^* orbitals of the monophospholide ring.

The forcing conditions, poor yield, and limited scope of substrate tolerance all mean that this method will not be adopted as a general synthetic method for the generation of monophospholides. However, the underlying reactivity is fascinating, as it shows that the $[P_7]^{3-}$ cluster can be activated to yield a formal "P^-" fragment that can be incorporated into organophosphorus products. The following example will show that the activation of the heptaphosphide cage with unsaturated organic substrates can yield more promising and practically useful results.

1.6.3.4 Activation with alkynes to afford 1,2,3-triphospholides

Of the two possible triphospholides shown in Figure 1.12, the 1,3,4-tri-substituted isomer is significantly more common, and general synthetic routes are well established.[189–192] In contrast, only a handful of 1,2,3-triphospholide derivatives are known, either as free anions or in the coordination sphere of a transition metal.[193–199] Each of these examples were synthesised on a case-by-case basis, and no general synthetic procedure existed prior to this work.

The reaction of the $[P_7]^{3-}$ cluster with acetylene, phenylacetylene and diphenylacetylene leads to the formation of a family of 1,2,3-triphospholides (Scheme 1.14).[200,201] The reactivity was extended to include the activation of the $[As_7]^{3-}$ cluster to yield the first examples of 1,2,3-triarsolides. The mechanism is not known, but the reaction is reminiscent of the 1,3-dipolar cycloaddition between an alkyne and an azide to form a triazole ("click chemistry"), thus the $[E_7]^{3-}$ cages can be viewed as a source of the corresponding $[E_3]^-$ fragment.[202]

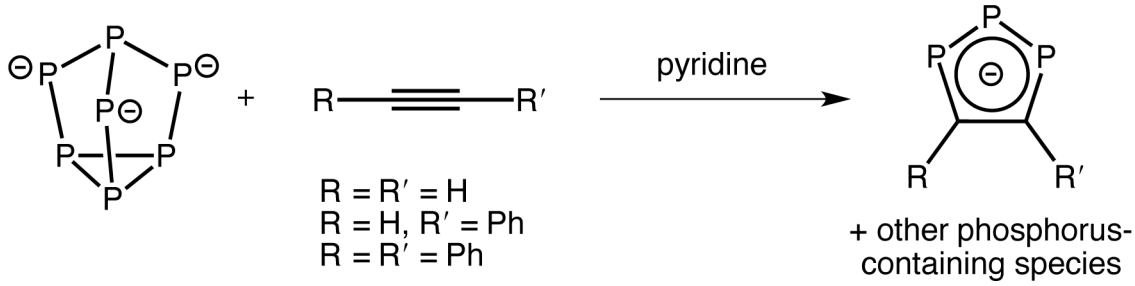

Scheme 1.14: Activation of the $[P_7]^{3-}$ cluster with alkynes to yield 1,2,3-triphospholides and other products.[201]

As this was the first family of isolable and related 1,2,3-tripnictolides, we opted to carry out a study of their ligand properties. The tricarbonyl molybdenum fragment was chosen, as the IR stretching frequency of the carbonyl groups could be used to probe the π accepting properties across the series. The formation of the $[Mo(CO)_3(\eta^5\text{-}L)]^-$ complexes was quantitative by NMR spectroscopy for the six 1,2,3-tripnictolides listed in Table 1.3. Crystal structures for all of these complexes were obtained, except for the asymmetrically substituted triphospholide, $[1,2,3\text{-}P_3C_2PhH]^-$, though most of these exhibited discrete positional disorder of the tripnictolide ligand within the crystal. The major components of the parent tripnictolide complexes (R = R′ = H) are shown in Figure 1.15 as representative examples. The cyclopentadienide complex was synthesised for comparison.

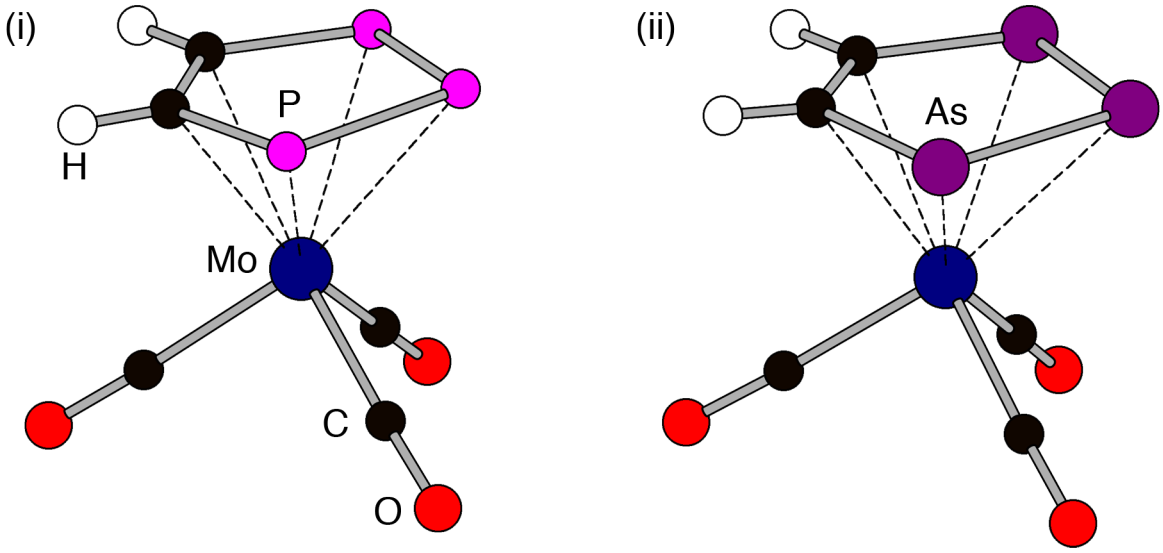

Figure 1.15: Ball and stick models of $[Mo(CO)_3(\eta^5\text{-}E_3C_2H_2)]^-$, (i) E = P, (ii) E = As. In each case, only the major component of the disordered pnictolide ring is shown.[201]

The IR data for the carbonyl stretches (Table 1.3) reveal that the tripnictolides all have very similar π acceptor properties, irrespective of the substituents on the backbone or the identity of the pnictogen atoms.[203,204] They are all significantly stronger π acceptors than the all-carbon analogue, however, as can be seen from the lower stretching frequencies for the latter, which is in accord with previous DFT computational reports.[205,206]

Table 1.3: IR carbonyl stretching frequencies for $[Mo(CO)_3(\eta^5\text{-}L)]^-$ for a range of ligands.

$[\eta^5\text{-}L]^-$	ν_{CO} (cm^{-1})
$[P_3C_2H_2]^-$	1916 (A′), 1834, 1814 (A′ + A″)
$[As_3C_2H_2]^-$	1910 (A′), 1830, 1817 (A′ + A″)
$[P_3C_2PhH]^-$	1925 (A′), 1842, 1828 (A′ + A″)
$[As_3C_2PhH]^-$	1911 (A′), 1828, 1818 (A′ + A″)
$[P_3C_2Ph_2]^-$	1921 (A′), 1842, 1821 (A′ + A″)
$[As_3C_2Ph_2]^-$	1910 (A′), 1836, 1818 (A′ + A″)
$[C_5H_5]^-$	1884 (A_1), 1760 (E)

The generality of this "Zintl method" as a way for preparing 1,2,3-triphospholides via activation of the $[P_7]^{3-}$ cluster, and their arsenic analogues, was tested by incorporating functional groups in the backbone. A number of novel and previously reported derivatives have since been synthesised, and some are shown in Figure 1.16.[150,204,207] This research shows that activation of the heptaphosphide cluster can yield synthetically useful organophosphorus products that are otherwise inaccessible with alternative phosphorus sources.

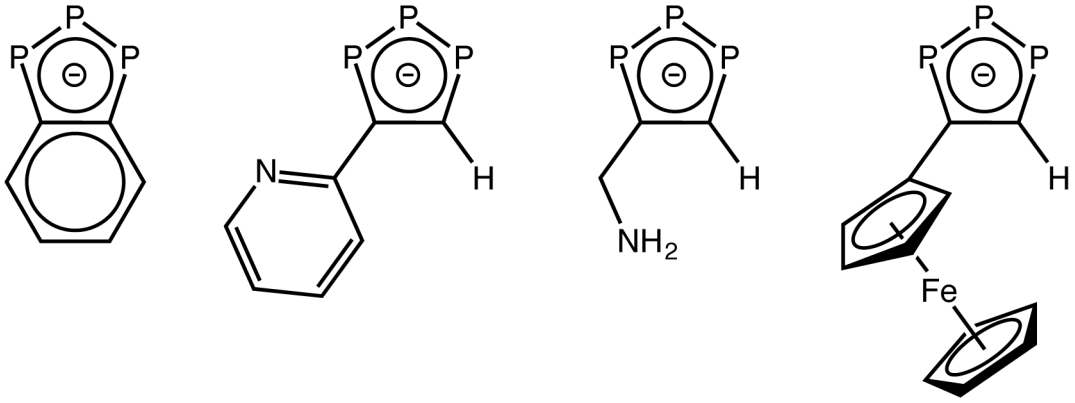

Figure 1.16: Range of 1,2,3-triphospholides with functional groups on backbone. Figure adapted from Turbervill and Goicoechea.[150]

1.6.3.5 Thermal activation to afford pentaphospholide

The final example is the work that was my main focus when I started my DPhil project. It was observed that during several of the previous studies that involved the heating of solutions of the $[P_7]^{3-}$ cluster with a range of unsaturated organic substrates, there would be a side-product in the ^{31}P NMR spectrum with a distinctive downfield resonance between +468 and +472 ppm, depending on the nature of the solvent and the concentration. This was subsequently identified as pentaphospholide, the all-phosphorus analogue of cyclopentadienide shown previously in Figure 1.12.

The free $[P_5]^-$ anion was first observed spectroscopically by Baudler in 1987, by the reduction of white phosphorus with sodium in diglyme, alongside other polyphosphides and phospholides.[193] Although its synthesis was subsequently improved to yield [Na(18-crown-6][P_5] in THF, the solution was still highly air- and moisture-sensitive, and the extensive decomposition to $[P_{16}]^{2-}$ and $[P_{21}]^{3-}$ precluded all attempts to isolate a solid sample of the product.[208] There are a small number of cases where the $[P_5]^-$ ring has been stabilised in the coordination sphere of a transition metal, and fewer still where the resulting complex has been structurally authenticated. The first was Scherer's triple-decker species in 1986 (Figure 1.17).[209] Other notable examples include the aforementioned

pentaphosphaferrocene derivative (**F** in Scheme 1.7),[116,210] and the only homoleptic pentaphospholide sandwich complex, $[Ti(\eta^5\text{-}P_5)_2]^{2-}$, reported by Ellis in 2002.[211]

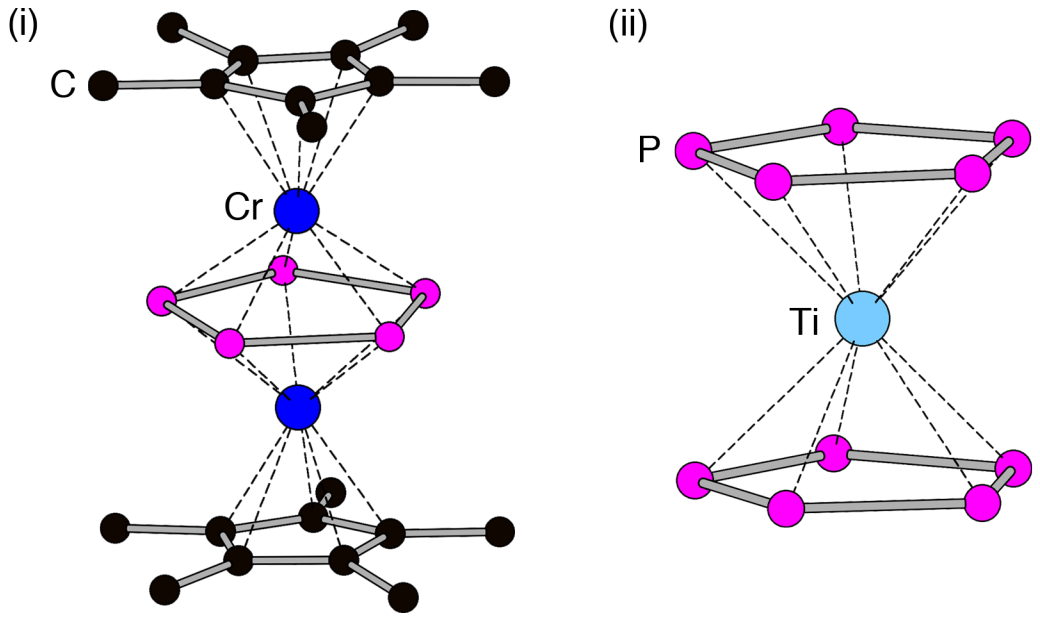

Figure 1.17: Ball and stick models of pentaphospholide rings coordinated to transition metal centres. (i) $[((Cp^*)Cr)_2(\mu_2\text{:}\eta^5,\eta^5\text{-}P_5)]$ by Scherer,[209] and (ii) $[Ti(\eta^5\text{-}P_5)_2]^{2-}$ by Ellis.[211] Hydrogen atoms omitted for clarity.

As control experiments to our earlier observations, the crude K_3P_7 phase and 18-crown-6 (to aid dissolution of the otherwise insoluble Zintl precursor) were refluxed in DMF, but in the absence of any other organic substrates. This led to the clean formation of the pentaphospholide by ^{31}P NMR spectroscopy. This can be considered a relatively mild oxidation of the $[P_7]^{3-}$ cage, which we believe is stimulated by decomposition of the DMF to Me_2NH and CO (a known phenomenon for DMF). The amine acts as the oxidant, being reduced to an amide in the process (Scheme 1.15), and the carbon monoxide is lost under the flow of dinitrogen used during the reaction. This mechanism is based on conjecture, and no experiments to detect the resulting amide were carried out, though a later finding does corroborate the decomposition of the DMF solvent (*vide infra*).

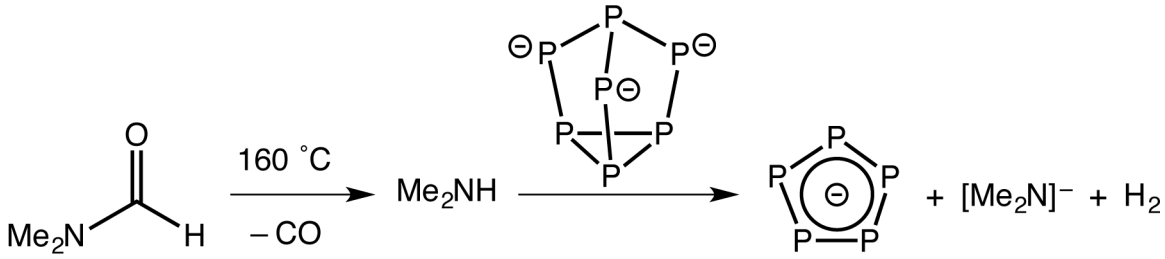

Scheme 1.15: Possible mechanism for the thermal activation of the $[P_7]^{3-}$ cluster in DMF to yield $[P_5]^-$.

The precipitation of this product from THF using diethyl ether allowed the first isolation of a solid sample of the free pentaphospholide, in the form of [K(18-crown-6][P_5], as an orange powder. A crystal suitable for single crystal X-ray diffraction was grown and a good data set was collected. However, the pentaphospholide ring appears to be dynamically disordered, and sits atop a six-fold symmetry axis (presumably driven by the packing of the $[K(18\text{-crown-6})]^+$ moiety), which renders the solution useless for determining metric data or even connectivity within the anion. Nevertheless, the product has been well characterised by NMR spectroscopy, electrospray ionisation mass spectrometry and elemental microanalysis, and supports the notion of having obtained the first isolated and "bottle-able" source of the pentaphospholide anion.

We wanted to demonstrate that this was indeed the case, thus we set out to explore its reactivity towards transition metal complexes. Heating an equimolar solution of [K(18-crown-6)][P_5] and $[W(CO)_3(NCPr)_3]$ in pyridine at 60 ˚C overnight leads to displacement of the labile ligands and the formation of $[K(18\text{-crown-6})][W(CO)_3(\eta^5\text{-}P_5)]$. Single crystals suitable for X-ray diffraction were grown by slow diffusion of hexane into a pyridine/THF solution of the product, revealing the anion to have a piano-stool structure, as expected (Figure 1.18).

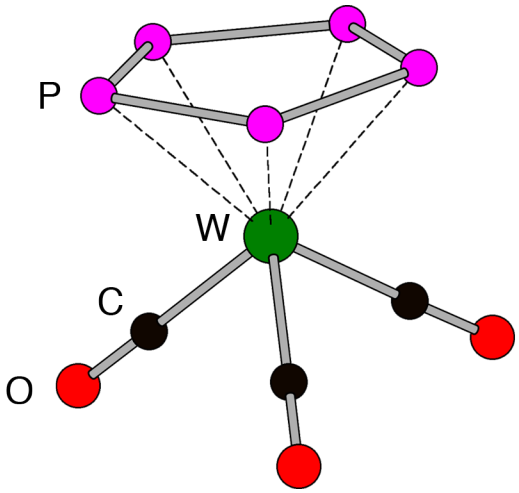

Figure 1.18: Ball and stick model of $[W(CO)_3(\eta^5\text{-}P_5)]^-$.

This reaction can be readily followed using ^{31}P NMR spectroscopy, and quantitative conversion from the free pentaphospholide at +468.0 ppm to the product at +105.9 ppm was observed. The analogous molybdenum half-sandwich complex can be obtained using the $[Mo(CO)_3(NC_5H_5)_3]$ precursor, although no suitable single crystals were obtained. The corresponding ^{31}P NMR chemical shift is observed at +143.6 ppm. Both of these $[M(CO)_3(\eta^5\text{-}P_5)]^-$ (M = Mo, W) anions have been previously reported by the group of Baudler, but their assignment was based solely on IR and NMR spectroscopic data, and were never structurally authenticated.[212] Our data corroborate their findings, and represent the first example of any tungsten complex bearing a pentaphospholide ring that has been crystallographically characterised.

The reactivity of the pentaphospholide ring towards a diverse range of transition metal and main group compounds was explored, both by others and myself, and most of them ultimately resulted in intractable dark precipitates that defied characterisation. This could be due to the formation of extended coordination polymers through the use of the phosphorus lone pairs, or decomposition via redox processes, driven by the large π acceptor ability of $[P_5]^-$. Furthermore, the work-up to isolate the clean [K(18-crown-6)][P_5] is not always

reproducible, and sometimes leads to dark oils where the desired product is contaminated with higher nuclearity polyphosphides.

In a bid to prevent this, I tried to optimise the reaction by varying the solvents and degree of heating, and carried out some reactions in gas-tight NMR tubes to monitor the formation of the pentaphospholide *in situ* by ^{31}P NMR spectroscopy. Under certain conditions, a new side-product started appearing in the ^{31}P NMR spectrum at approximately –390 ppm (depending on the solvent and concentration), over 850 ppm away from the desired product. The side-product only appeared under certain conditions, namely when DMF was used as the solvent and when the traditional reflux was carried out under a reduced flow of dinitrogen or in a closed system, such as a gas-tight NMR tube. It was not until the manual separation of this white impurity from the orange [K(18-crown-6)][P_5] under an inert atmosphere and subsequent recrystallisation that the identity of the impurity was first elucidated. A discussion of this species comprises the final topic of this chapter.

1.7 The 2-phosphaethynolate anion

A single crystal X-ray diffraction study of these crystals yielded the identity of the side-product as [K(18-crown-6)][PCO] (Figure 1.19).[213] The carbon monoxide moiety in this species clearly arises from the thermal decomposition of the DMF solvent, which supports the tentative mechanism outlined previously in Scheme 1.15. The use of DMF as a versatile source of organic synthons, including carbon monoxide and dimethylamine, has been reviewed recently in separate reports from Muzart and Jiao.[214,215]

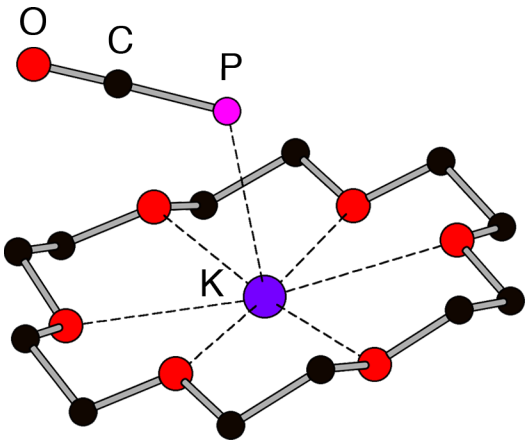

Figure 1.19: Ball and stick model of [K(18-crown-6)][PCO]. Hydrogen atoms omitted for clarity.[213]

This simple low-coordinate phosphorus species is the 2-phosphaethynolate anion, and forms the basis of my DPhil thesis. When I started work on this remarkable anion there were few reports in the chemical literature concerning its structure, properties or reactivity; however, since our first publication in 2013,[213] there has been a flurry of both experimental and computational reports from groups around the world, particularly from ourselves and the group of Grützmacher. The remainder of this brief discussion in the Introduction will be limited to the synthetic procedures and reactivity carried out prior to 2012, and subsequent reports will be discussed alongside my own research where relevant in the following results chapters.

The 2-phosphaethynolate anion was first synthesised as the lithium salt by Becker and co-workers in 1992, by the reaction of lithium bis(trimethylsilyl)phosphide and dimethyl carbonate (Scheme 1.16).[216] This procedure was extended several years later to synthesise the analogous alkaline earth metal salts, however, the products decomposed on isolation and had to be stored in ethereal solvents at low temperatures.[217]

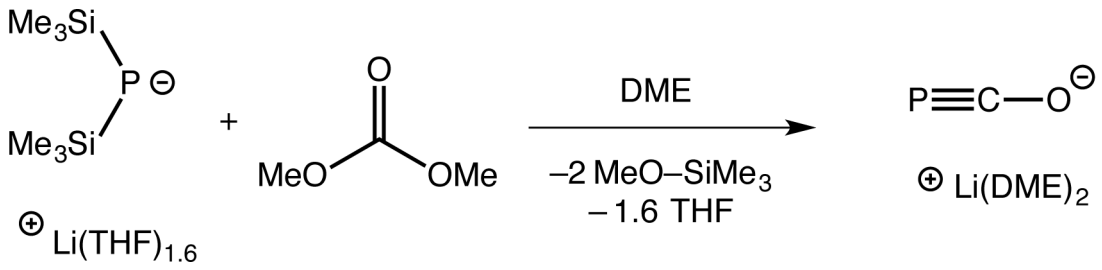

Scheme 1.16: Becker's synthesis of $[Li(dme)_2][PCO]$.[216]

This anion, the phosphorus-containing analogue of cyanate, contains a multiple bond between the phosphorus and carbon atoms, in violation of the double bond rule discussed earlier. Unlike the previous examples, there are no sterically encumbering ligands to kinetically and thermodynamically stabilise this bond. Instead it is the negative charge that plays a key role, as the electrostatic repulsion between neighbouring molecules prevents the classic dimerisation and oligomerisation routes to decomposition. The structure of the anion will be discussed in more detail in the next chapter.

The cycloaddition reaction of [Li][PCO] with an activated alkyne afforded a phosphinine derivative, presumably via a Dewar benzene-like intermediate.[218] The same paper detailed the reaction with relatively mild oxidants such as iodine or sulfur dioxide to yield the oxidative tetramerisation product $[(PCO)_4]^{2-}$ (Scheme 1.17), and betrayed the highly reducing nature of $[PCO]^-$.[218] The transition metal-mediated dimerisation has also been observed using a range of iron complexes (Scheme 1.17).[219]

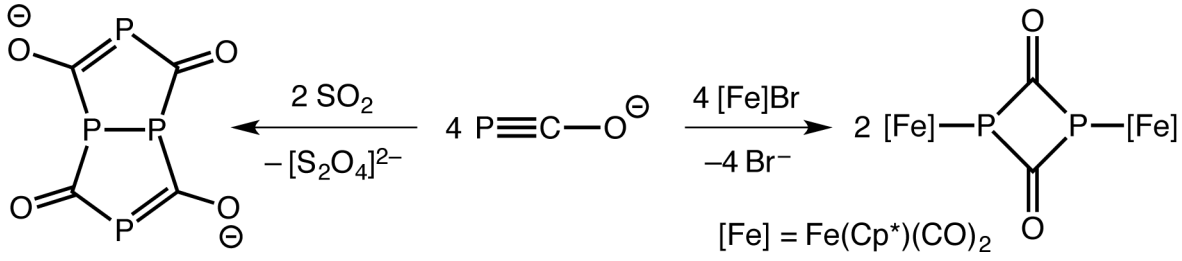

Scheme 1.17: Oxidative tetramerisation[218] and transition metal-mediated dimerisation[219] of $[PCO]^-$.

The heavier group 16 analogue, $[PCS]^-$, could be accessed by reaction of *O*,*O*′-diethylthiocarbonate with lithium bis(trimethylsilyl)phosphide, by analogy with the original synthesis of $[PCO]^-$ in Scheme 1.16.[220] The same product could also be obtained by a direct metathesis reaction of $[PCO]^-$ with carbon disulfide. Both of these reactions had to be carried out at low temperature to avoid decomposition, and no further reactivity of the $[PCS]^-$ anion has been reported.

The limited exploration of the 2-phosphaethynolate anion for the twenty years following its initial discovery can be attributed to its challenging synthesis and the high sensitivity of the lithium salt. Interest in this anion was renewed by simultaneous reports of novel synthetic routes to the sodium salt by the groups of Cummins and Grützmacher in 2011. The former features an elegant bond metathesis reaction of carbon dioxide with a terminal niobium phosphide to afford a niobium oxo complex and an equivalent of $[PCO]^-$ (Scheme 1.18).[221] Crystals of $[Na(DME)_2][PCO]$ were grown from DME and pentane at –30 ˚C, but they were of insufficient quality for a properly refined solution to be obtained.

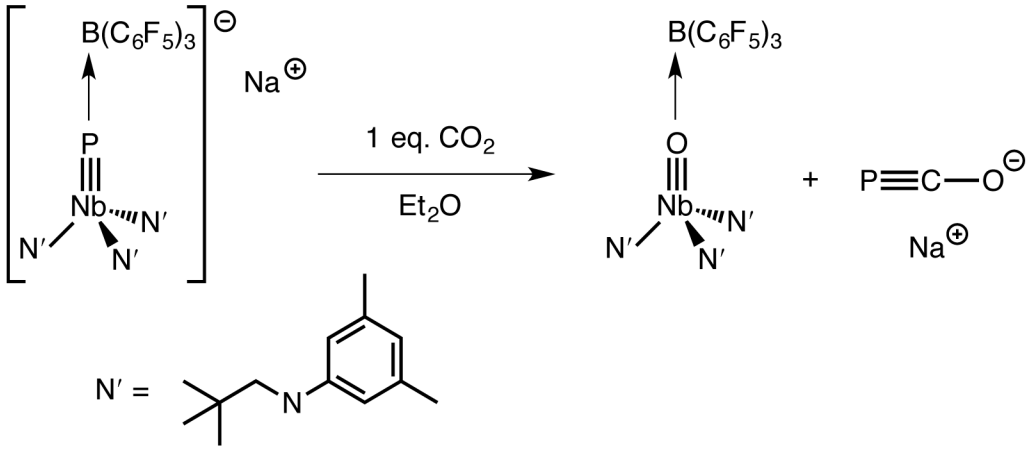

Scheme 1.18: Cummins' synthesis of [Na][PCO].[221]

The same salt was reported by the group of Grützmacher, although the initial aim had been to synthesise the free cyaphide anion, $[P{\equiv}C]^-$, which they had previously stabilised as a

terminal ligand in a ruthenium complex.[222] The reaction of sodium dihydrogen phosphide with a high pressure of carbon monoxide at 80 °C in an autoclave generates the $\{[Na(DME)_2][PCO]\}_2$ dimer alongside small quantities of sodium phosphanylidenemethanolate (shown in Scheme 1.18) and an insoluble orange-brown precipitate.[223] The accompanying thermal decomposition of the $NaPH_2$ meant that even the optimised conditions shown in Scheme 1.19 only yielded $[Na(1,4\text{-dioxane})_{2.5}][PCO]$ in 30% yields after work-up with 1,4-dioxane. The crystal structure of this adduct features a regular three-dimensional network of octahedrally coordinated Na^+ cations bridged by 1,4-dioxane molecules with highly disordered $[PCO]^-$ moieties in the cavities.

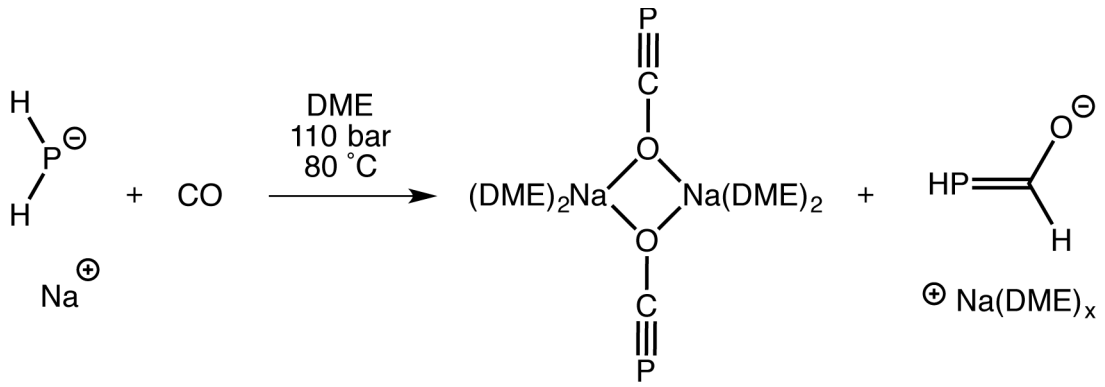

Scheme 1.19: Grützmacher's synthesis of $[Na(dme)_2][PCO]$.[223]

This 1,4-dioxane adduct is surprisingly stable in air for short periods of time. Dissolution in deoxygenated water leads to slow hydrolysis, eventually yielding phosphine gas, sodium phosphinate ($[Na][H_2PO_2]$), sodium hydrogencarbonate, carbon monoxide and an unidentified species bearing a PH_2 group ($\delta(^{31}P)$ = –134 ppm, t, $^1J_{P–H}$ = 217 Hz). This unknown hydrolysis product will be revisited in Chapter 7. The paper concludes briefly with the use of the aforementioned $[NaPH_2]\cdot[NaO^tBu]_x$ clusters with either iron pentacarbonyl or ethylene carbonate as carbon monoxide sources as alternative methods for the preparation of the [Na][PCO] salt.

The only subsequent publication on the reactivity of sodium phosphaethynolate prior to 2013 was demonstrating its ability as a ligand in a transition metal complex. The [Re(triphos)$(CO)_2(\eta^1$-PCO)] complex was readily synthesised by displacement of a labile triflate ligand in [Re(triphos)$(CO)_2$(OTf)], and the cyanate analogue was similarly prepared for comparative purposes (Figure 1.20).[224] The major difference between the two complexes is the coordination mode of the ligands; both appear to bind exclusively though the group 15 atom, but the PCO moiety is bound in a side-on manner while the nitrogen analogue is bound end-on. This was corroborated by computational calculations, and is not merely an effect of crystal packing, however crystallographic disorder in both structures precludes an accurate analysis of bond metric data. IR spectroscopy revealed similar carbonyl stretching frequencies for both species, implying that, despite the profound difference in coordination modes, the two ligands exert similar electronic effects. This will be explored in detail in the next chapter.

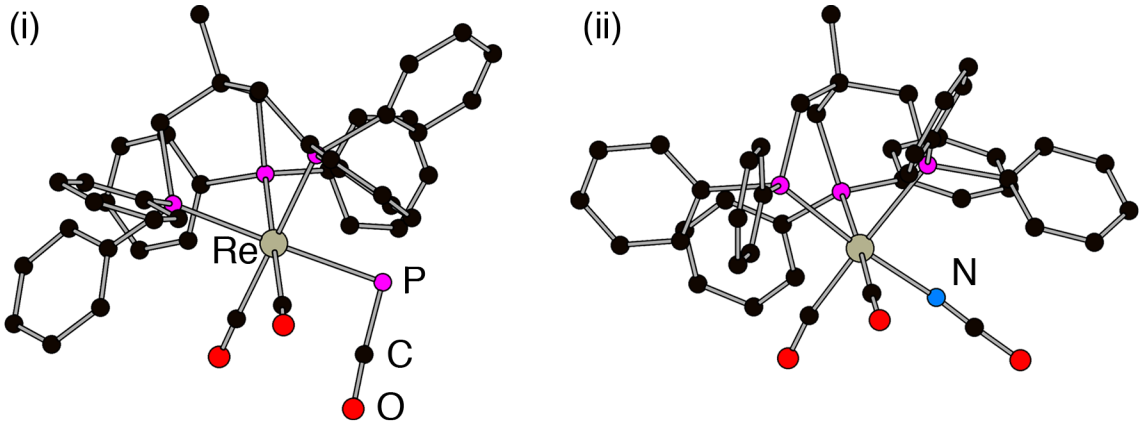

Figure 1.20: Ball and stick models of [Re(triphos)$(CO)_2(\eta^1$-ECO)], (i) E = P, (ii) E = N. Hydrogen atoms omitted for clarity.[224]

1.8 Project aims

At the time of starting this project, there was a dearth of knowledge concerning the 2-phosphaethynolate anion, particularly relative to other low-coordinate phosphorus species such as phosphaalkenes and phosphaalkynes. The sensitivity of the lithium salt made it

difficult to handle and less amenable to further study. The available routes to the sodium salts suffered from either poor atom economy (the stoichiometric use of a bulky niobium complex) or the need for highly forcing conditions (110 bar of CO at 80 ˚C in an autoclave).

We therefore sought to generate a more convenient synthesis via the activation of the $[P_7]^{3-}$ Zintl cluster in order to further study this remarkably versatile anion. This will be outlined in Chapter 2, along with an in-depth study of the ligand properties of the $[ECX]^-$ ligands (E = N, P; X = O, S). Chapter 3 will explore the cycloaddition chemistry of $[PCO]^-$ towards a range of heteroallenes to generate novel phosphorus-containing heterocycles.

Chapter 4 will document the reaction of $[PCO]^-$ with ammonium salts to synthesise phosphinecarboxamide, the phosphorus analogue of urea, and to determine its ability to coordinate to transition metal centres. This will be extended in Chapter 5 to incorporate *N*-functionalised phosphinecarboxamides with a range of different functional groups. The Brønsted acidity, *P*-functionalisation and oxidation chemistry of these species will be discussed in Chapter 6. Finally, preliminary results showing the generality of the reaction of $[PCO]^-$ with other protic nucleophiles will be detailed in Chapter 7, along with concluding remarks and other potential applications for molecules described in this thesis. The experimental details and data for all of the techniques and compounds reported herein can be found in Chapter 8.

1.9 References

(1) Filippelli, G. M. *Elements* **2008**, *4*, 89–95.

(2) Westheimer, F. H. *Science* **1987**, *235*, 1173–1178.

(3) Emsley, J. *The Shocking History of Phosphorus: A Biography of the Devil's Element*; Pan Books: London, 2001.

(4) Weeks, M. E. *J. Chem. Educ.* **1933**, *10*, 302.

(5) Montchamp, J.-L. *Acc. Chem. Res.* **2014**, *47*, 77–87.

(6) Vaccari, D. A. *Sci. Am.* **2009**, *300*, 54–59.

(7) Gilbert, N. *Nature* **2009**, *461*, 716–718.

(8) Elser, J.; Bennett, E. *Nature* **2011**, *478*, 29–31.

(9) Sartorius, C.; von Horn, J.; Tettenborn, F. *Water Environ. Res.* **2012**, *84*, 313–322.

(10) Greenwood, N. N.; Earnshaw, A. *Chemistry of the Elements*; 2nd ed.; Butterworth-Heinemann: Boston, Mass., 1997.

(11) Shriver, D. F.; Atkins, P. W. *Inorganic Chemistry*; 3rd ed.; Oxford University Press: Oxford, 1999.

(12) Shaver, M. P.; Fryzuk, M. D. *Adv. Synth. Catal.* **2003**, *345*, 1061–1076.

(13) Crossland, J. L.; Tyler, D. R. *Coord. Chem. Rev.* **2010**, *254*, 1883–1894.

(14) Simon, A.; Borrmann, H.; Craubner, H. *Phosphorus and Sulfur* **1987**, *30*, 507–510.

(15) Thurn, H.; Krebs, H. *Acta. Cryst. B* **1969**, *25*, 125–135.

(16) Hultgren, R.; Gingrich, N. S.; Warren, B. E. *J. Chem. Phys.* **1935**, *3*, 351–355.

(17) Wang, Y.; Xie, Y.; Wei, P.; King, R. B.; Schaefer III, H. F.; Schleyer, P. v. R.; Robinson, G. H. *J. Am. Chem. Soc.* **2008**, *130*, 14970–14971.

(18) Back, O.; Kuchenbeiser, G.; Donnadieu, B.; Bertrand, G. *Angew. Chem. Int. Ed.* **2009**, *48*, 5530–5533.

(19) Piro, N. A.; Figueroa, J. S.; McKellar, J. T.; Cummins, C. C. *Science* **2006**, *313*, 1276–1279.

(20) Tofan, D.; Cummins, C. C. *Angew. Chem. Int. Ed.* **2010**, *49*, 7516–7518.

(21) Velian, A.; Cummins, C. C. *J. Am. Chem. Soc.* **2012**, *134*, 13978–13981.

(22) Velian, A.; Nava, M.; Temprado, M.; Zhou, Y.; Field, R. W.; Cummins, C. C. *J. Am. Chem. Soc.* **2014**, *136*, 13586–13589.

(23) Velian, A.; Cummins, C. C. *Science* **2015**, *348*, 1001–1004.

(24) Pitzer, K. S. *J. Am. Chem. Soc.* **1948**, *70*, 2140–2145.

(25) Jutzi, P. *Angew. Chem. Int. Ed. Engl.* **1975**, *14*, 232–245.

(26) Sanderson, R. T. *Chemical Bonds and Bond Energy*; Physical Chemistry, a Series of Monographs; 2nd ed.; Academic Press: New York, 1976.

(27) Power, P. P. *Chem. Rev.* **1999**, *99*, 3463–3504.

(28) Fischer, R. C.; Power, P. P. *Chem. Rev.* **2010**, *110*, 3877–3923.

(29) Geng, X.-L.; Ott, S. *Chem. Commun.* **2009**, No. 46, 7206–7208.

(30) Wright, V. A.; Patrick, B. O.; Schneider, C.; Gates, D. P. *J. Am. Chem. Soc.* **2006**, *128*, 8836–8844.

(31) Orthaber, A.; Löfås, H.; Öberg, E.; Grigoriev, A.; Wallner, A.; Jafri, S. H. M.; Santoni, M.-P.; Ahuja, R.; Leifer, K.; Ottosson, H.; Ott, S. *Angew. Chem. Int. Ed.* **2015**, *54*, 10634–10638.

(32) Niecke, E.; Flick, W. *Angew. Chem. Int. Ed. Engl.* **1973**, *12*, 585–586.

(33) Becker, G. *Z. Anorg. Allg. Chem.* **1976**, *423*, 242–254.

(34) Yoshifuji, M.; Shima, I.; Inamoto, N.; Hirotsu, K.; Higuchi, T. *J. Am. Chem. Soc.* **1981**, *103*, 4587–4589.

(35) Becker, G.; Gresser, G.; Uhl, W. *Z. Naturforsch. B* **1981**, *36b*, 16–19.

(36) Tokitoh, N.; Arai, Y.; Okazaki, R.; Nagase, S. *Science* **1997**, *277*, 78–80.

(37) Corriu, R. J. P.; Dutheil, J. P.; Lanneau, G. F. *J. Am. Chem. Soc.* **1984**, *106*, 1060–1065.

(38) van Bochove, M. A.; Swart, M.; Bickelhaupt, F. M. *J. Am. Chem. Soc.* **2006**, *128*, 10738–10744.

(39) Hoffmann, R. *Angew. Chem. Int. Ed. Engl.* **1982**, *21*, 711–724.

(40) Elian, M.; Chen, M. M. L.; Mingos, D. M. P.; Hoffmann, R. *Inorg. Chem.* **1976**, *15*, 1148–1155.

(41) Albright, T. A. *Tetrahedron* **1982**, *38*, 1339–1388.

(42) *Quantities, Units and Symbols in Physical Chemistry*; Royal Society of Chemistry: Cambridge, 2002.

(43) Waluk, J.; Klein, H. P.; Ashe, A. J.; Michl, J. *Organometallics* **1989**, *8*, 2804–2808.

(44) Dillon, K. B.; Mathey, F.; Nixon, J. F. *Phosphorus: The Carbon Copy: From Organophosphorus to Phospha-organic Chemistry*; Wiley: Chichester, 1998.

(45) Mathey, F. *Angew. Chem. Int. Ed.* **2003**, *42*, 1578–1604.

(46) Weber, L. *Eur. J. Inorg. Chem.* **2000**, *2000*, 2425–2441.

(47) Gaumont, A. C.; Denis, J. M. *Chem. Rev.* **1994**, *94*, 1413–1439.

(48) Mathey, F. *Acc. Chem. Res.* **1992**, *25*, 90–96.

(49) Markovski, L. N.; Romanenko, V. D. *Tetrahedron* **1989**, *45*, 6019–6090.

(50) Appel, R.; Laubach, B.; Siray, M. *Tetrahedron Lett.* **1984**, *25*, 4447–4448.

(51) Appel, R.; Fölling, P.; Krieger, L.; Siray, M.; Knoch, F. *Angew. Chem. Int. Ed. Engl.* **1984**, *23*, 970–971.

(52) Appel, R.; Barth, V. *Angew. Chem. Int. Ed. Engl.* **1979**, *18*, 469–470.

(53) Appel, R.; Barth, V.; Halstenberg, M.; Huttner, G.; von Seyerl, J. *Angew. Chem. Int. Ed. Engl.* **1979**, *18*, 872–873.

(54) Issleib, K.; schmidt, H.; Meyer, H. *J. Organomet. Chem.* **1980**, *192*, 33–39.

(55) Klebach, T. C.; Lourens, R.; Bickelhaupt, F. *J. Am. Chem. Soc.* **1978**, *100*, 4886–4888.

(56) Van Der Knaap, T. A.; Klebach, T. C.; Visser, F.; Bickelhaupt, F.; Ros, P.; Baerends, E. J.; Stam, C. H.; Konijn, M. *Tetrahedron* **1984**, *40*, 765–776.

(57) Schoeller, W. W. *J. Chem. Soc., Chem. Commun.* **1985**, 334–335.

(58) Lacombe, S.; Gonbeau, D.; Cabioch, J. L.; Pellerin, B.; Denis, J. M.; Pfister-Guillouzo, G. *J. Am. Chem. Soc.* **1988**, *110*, 6964–6967.

(59) Van der Knaap, T. A.; Klebach, T. C.; Lourens, R.; Vos, M.; Bickelhaupt, F. *J. Am. Chem. Soc.* **1983**, *105*, 4026–4032.

(60) Niecke, E.; Wildbredt, D.-A. *J. Chem. Soc., Chem. Commun.* **1981**, 72–73.

(61) Oehme, H.; Leissring, E.; Meyer, H. *Tetrahedron Lett.* **1980**, *21*, 1141–1144.

(62) Becker, G.; Mundt, O. *Z. Anorg. Allg. Chem.* **1980**, *462*, 130–142.

(63) Deschamps, B.; Mathey, F. *J. Chem. Soc., Chem. Commun.* **1985**, 1010–1012.

(64) Deschamps, B.; Mathey, F. *J. Organomet. Chem.* **1988**, *354*, 83–90.

(65) Klebach, T. C.; Lourens, R.; Bickelhaupt, F.; Stam, C. H.; Van Herk, A. *J. Organomet. Chem.* **1981**, *210*, 211–221.

(66) Lorenz, I.-P.; Pohl, W.; Nöth, H.; Schmidt, M. *J. Organomet. Chem.* **1994**, *475*, 211–221.

(67) Apfel, R.; Casser, C.; Knoch, F. *J. Organomet. Chem.* **1985**, *293*, 213–217.

(68) Knoll, K.; Huttner, G.; Wasiucionek, M.; Zsolnai, L. *Angew. Chem. Int. Ed. Engl.* **1984**, *23*, 739–740.

(69) Weber, L. *Angew. Chem. Int. Ed.* **2002**, *41*, 563–572.

(70) Gier, T. E. *J. Am. Chem. Soc.* **1961**, *83*, 1769–1770.

(71) Hopkinson, M. J.; Kroto, H. W.; Nixon, J. F.; Simmons, N. P. C. *J. Chem. Soc., Chem. Commun.* **1976**, 513–515.

(72) Laali, K. K.; Geissler, B.; Regitz, M.; Houser, J. J. *J. Org. Chem.* **1995**, *60*, 6362–6367.

(73) Laurent, J. C. T. R. B.-S.; King, M. A.; Kroto, H. W.; Nixon, J. F.; Suffolk, R. J. *J. Chem. Soc., Dalton Trans.* **1983**, 755–759.

(74) Regitz, M. *Chem. Rev.* **1990**, *90*, 191–213.

(75) Schmidpeter, A. *Phosphorus-Carbon Heterocyclic Chemistry: The Rise of a New Domain*; Pergamon: Oxford, 2001; pp 363-461.

(76) Wettling, T.; Schneider, J.; Wagner, O.; Kreiter, C. G.; Regitz, M. *Angew. Chem. Int. Ed. Engl.* **1989**, *28*, 1013–1014.

(77) Wettling, T.; Geissler, B.; Schneider, R.; Barth, S.; Binger, P.; Regitz, M. *Angew. Chem. Int. Ed. Engl.* **1992**, *31*, 758–759.

(78) Tabellion, F.; Nachbauer, A.; Leininger, S.; Peters, C.; Preuss, F.; Regitz, M. *Angew. Chem. Int. Ed.* **1998**, *37*, 1233–1235.

(79) Cloke, F. G. N.; Hitchcock, P. B.; Nixon, J. F.; Wilson, D. J.; Mountford, P. *Chem. Commun.* **1999**, 661–662.

(80) Appel, R.; Paulen, W. *Tetrahedron Lett.* **1983**, *24*, 2639–2642.

(81) Appel, R.; Paulen, W. *Angew. Chem. Int. Ed. Engl.* **1983**, *22*, 785–786.

(82) Nguyen, M. T.; Hegarty, A. F.; McGinn, M. A.; Ruelle, P. *J. Chem. Soc., Perkin Trans. 2* **1985**, No. 12, 1991–1997.

(83) Cowley, A. H.; Gabbai, F.; Schluter, R.; Atwood, D. *J. Am. Chem. Soc.* **1992**, *114*, 3142–3144.

(84) Cowley, A. H.; Pellerin, B.; Atwood, J. L.; Bott, S. G. *J. Am. Chem. Soc.* **1990**, *112*, 6734–6735.

(85) David, M.-A.; Paisner, S. N.; Glueck, D. S. *Organometallics* **1995**, *14*, 17–19.

(86) David, M.-A.; Glueck, D. S.; Yap, G. P. A.; Rheingold, A. L. *Organometallics* **1995**, *14*, 4040–4042.

(87) David, M.-A.; Wicht, D. K.; Glueck, D. S.; Yap, G. P. A.; Liable-Sands, L. M.; Rheingold, A. L. *Organometallics* **1997**, *16*, 4768–4770.

(88) Mao, Y.; Wang, Z.; Ganguly, R.; Mathey, F. *Organometallics* **2012**, *31*, 4786–4790.

(89) Li, Z.; Chen, X.; Bergeler, M.; Reiher, M.; Su, C.-Y.; Grützmacher, H. *Dalton Trans.* **2015**, *44*, 6431–6438.

(90) Corbridge, D. E. C. *Phosphorus: Chemistry, Biochemistry and Technology*; CRC Press: Boca Raton, 2013.

(91) Engel, R. *Synthesis of Carbon-Phosphorus Bonds*; 2nd ed.; CRC Press: Boca Raton, 2004.

(92) Schedule 3, C. W. C., Organisation for the Prohibition of Chemical Weapons, last reviewed 2008.

(93) Tanaka, M. *Top. Curr. Chem.* **2004**, *232*, 25–54.

(94) Baillie, C.; Xiao, J. *Curr. Org. Chem.* **2003**, *7*, 477–514.

(95) Trofimov, B. A.; Arbuzova, S. N.; Gusarova, N. K. *Russ. Chem. Rev.* **1999**, *68*, 215–228.

(96) Büchel, K. H.; Moretto, H.-H.; Woditsch, P. *Industrial Inorganic Chemistry*; 2nd ed.; Wiley VCH: New York, 2000; pp 65-101.

(97) Dielmann, F.; Sierka, M.; Virovets, A. V.; Scheer, M. *Angew. Chem. Int. Ed.* **2010**, *49*, 6860–6864.

(98) Schoeller, W. W.; Staemmler, V.; Rademacher, P.; Niecke, E. *Inorg. Chem.* **1986**, *25*, 4382–4385.

(99) Jones, R. O.; Hohl, D. *J. Chem. Phys.* **1990**, *92*, 6710–6721.

(100) Baudler, M.; Düster, D.; Langerbeins, K.; Germeshausen, J. *Angew. Chem. Int. Ed. Engl.* **1984**, *23*, 317–318.

(101) Scheer, M.; Balázs, G.; Seitz, A. *Chem. Rev.* **2010**, *110*, 4236–4256.

(102) Cossairt, B. M.; Piro, N. A.; Cummins, C. C. *Chem. Rev.* **2010**, *110*, 4164–4177.

(103) Caporali, M.; Gonsalvi, L.; Rossin, A.; Peruzzini, M. *Chem. Rev.* **2010**, *110*, 4178–4235.

(104) Kuiper, D. S.; Wolczanski, P. T.; Lobkovsky, E. B.; Cundari, T. R. *J. Am. Chem. Soc.* **2008**, *130*, 12931–12943.

(105) Figueroa, J. S.; Cummins, C. C. *Angew. Chem. Int. Ed.* **2004**, *43*, 984–988.

(106) Scherer, O. J.; Sitzmann, H.; Wolmershäuser, G. *J. Organomet. Chem.* **1984**, *268*, C9–C12.

(107) Etkin, N.; Benson, M. T.; Courtenay, S.; McGlinchey, M. J.; Bain, A. D.; Stephan, D. W. *Organometallics* **1997**, *16*, 3504–3510.

(108) Di Vaira, M.; Ghilardi, C. A.; Midollini, S.; Sacconi, L. *J. Am. Chem. Soc.* **1978**, *100*, 2550–2551.

(109) Ehses, M.; Romerosa, A.; Peruzzini, M. *Top. Curr. Chem.* **2002**, *220*, 107–140.

(110) Stephens, F. H.; Johnson, M. J. A.; Cummins, C. C.; Kryatova, O. P.; Kryatov, S. V.; Rybak-Akimova, E. V.; McDonough, J. E.; Hoff, C. D. *J. Am. Chem. Soc.* **2005**, *127*, 15191–15200.

(111) Scheer, M.; Dargatz, M.; Rufińska, A. *J. Organomet. Chem.* **1992**, *440*, 327–334.

(112) Scherer, O. J.; Vondung, J.; Wolmershäuser, G. *Angew. Chem. Int. Ed. Engl.* **1989**, *28*, 1355–1357.

(113) Hey, E.; Lappert, M. F.; Atwood, J. L.; Bott, S. G. *J. Chem. Soc., Chem. Commun.* **1987**, 597–598.

(114) Chirik, P. J.; Pool, J. A.; Lobkovsky, E. *Angew. Chem. Int. Ed.* **2002**, *41*, 3463–3465.

(115) Gröer, T.; Baum, G.; Scheer, M. *Organometallics* **1998**, *17*, 5916–5919.

(116) Scherer, O. J.; Brück, T. *Angew. Chem. Int. Ed. Engl.* **1987**, *26*, 59–59.

(117) Bai, J.; Virovets, A. V.; Scheer, M. *Angew. Chem. Int. Ed.* **2002**, *41*, 1737–1740.

(118) Bai, J.; Virovets, A. V.; Scheer, M. *Science* **2003**, *300*, 781–783.

(119) Scherer, O. J.; Schwalb, J.; Swarowsky, H.; Wolmershäuser, G.; Kaim, W.; Gross, R. *Chem. Ber.* **1988**, *121*, 443–449.

(120) Scherer, O. J.; Swarowsky, H.; Wolmershäuser, G.; Kaim, W.; Kohlmann, S. *Angew. Chem. Int. Ed. Engl.* **1987**, *26*, 1153–1155.

(121) Barr, M. E.; Adams, B. R.; Weller, R. R.; Dahl, L. F. *J. Am. Chem. Soc.* **1991**, *113*, 3052–3060.

(122) Power, P. P. *Nature* **2010**, *463*, 171–177.

(123) Arduengo, A. J.; Harlow, R. L.; Kline, M. *J. Am. Chem. Soc.* **1991**, *113*, 361–363.

(124) Bourissou, D.; Guerret, O.; Gabbaï, F. P.; Bertrand, G. *Chem. Rev.* **2000**, *100*, 39–92.

(125) Braunschweig, H.; Dewhurst, R. D.; Hammond, K.; Mies, J.; Radacki, K.; Vargas, A. *Science* **2012**, *336*, 1420–1422.

(126) Masuda, J. D.; Schoeller, W. W.; Donnadieu, B.; Bertrand, G. *J. Am. Chem. Soc.* **2007**, *129*, 14180–14181.

(127) Soleilhavoup, M.; Bertrand, G. *Acc. Chem. Res.* **2015**, *48*, 256–266.

(128) Martin, C. D.; Weinstein, C. M.; Moore, C. E.; Rheingold, A. L.; Bertrand, G. *Chem. Commun.* **2013**, *49*, 4486–4488.

(129) MacLeod, I. J.; Rogers, A. P. V. *Yearbook of International Humanitarian Law* **2007**, *10*, 75–97.

(130) Li, L.; Yu, Y.; Ye, G. J.; Ge, Q.; Ou, X.; Wu, H.; Feng, D.; Chen, X. H.; Zhang, Y. *Nature Nanotech.* **2014**, *9*, 372–377.

(131) Ezawa, M. *New J. Phys.* **2014**, *16*, 115004–115016.

(132) Brent, J. R.; Savjani, N.; Lewis, E. A.; Haigh, S. J.; Lewis, D. J.; O'Brien, P. *Chem. Commun.* **2014**, *50*, 13338–13341.

(133) Ceppatelli, M.; Bini, R.; Caporali, M.; Peruzzini, M. *Angew. Chem. Int. Ed.* **2013**, *52*, 2313–2317.

(134) Trofimov, B.; Gusarova, N.; Brandsma, L. *Phosphorus Sulfur Silicon Relat. Elem.* **1996**, *109*, 601–604.

(135) Peterson, D. J. Patent No. 3,397,039; 1967.

(136) Gusarova, N.; Brandsma, L.; Malysheva, S.; Arbuzova, S.; Trofimov, B. *Phosphorus Sulfur Silicon Relat. Elem.* **1996**, *111*, 174–174.

(137) Brandsma, L.; Gusarova, N.; Arbuzova, S.; Trofimov, B. *Phosphorus Sulfur Silicon Relat. Elem.* **1996**, *111*, 175–175.

(138) Müller, G.; Zalibera, M.; Gescheidt, G.; Rosenthal, A.; Santiso-Quinones, G.; Dietliker, K.; Grützmacher, H. *Macromol. Rapid Commun.* **2015**, *36*, 553–557.

(139) Kasák, P.; Arion, V. B.; Widhalm, M. *Tetrahedron Lett.* **2007**, *48*, 5665–5668.

(140) Brandsma, L.; Arbuzova, S.; Lang, R.-J. D.; Gusarova, N.; Trofimov, B. *Phosphorus Sulfur Silicon Relat. Elem.* **1997**, *126*, 125–128.

(141) Podewitz, M.; van Beek, J. D.; Wörle, M.; Ott, T.; Stein, D.; Rüegger, H.; Meier, B. H.; Reiher, M.; Grützmacher, H. *Angew. Chem. Int. Ed.* **2010**, *49*, 7465–7469.

(142) Huber, A.; Kuschel, A.; Ott, T.; Santiso-Quinones, G.; Stein, D.; Bräuer, J.; Kissner, R.; Krumeich, F.; Schönberg, H.; Levalois-Grützmacher, J.; Grützmacher, H. *Angew. Chem. Int. Ed.* **2012**, *51*, 4648–4652.

(143) Stein, D.; Ott, T.; Grützmacher, H. *Z. Anorg. Allg. Chem.* **2009**, *635*, 682–686.

(144) Baudler, M. *Angew. Chem. Int. Ed. Engl.* **1982**, *21*, 492–512.

(145) Baudler, M.; Glinka, K. *Chem. Rev.* **1993**, *93*, 1623–1667.

(146) Baudler, M. *Angew. Chem. Int. Ed. Engl.* **1987**, *26*, 419–441.

(147) von Schnering, H. G.; Hoenle, W. *Chem. Rev.* **1988**, *88*, 243–273.

(148) Scharfe, S.; Kraus, F.; Stegmaier, S.; Schier, A.; Fässler, T. F. *Angew. Chem. Int. Ed.* **2011**, *50*, 3630–3670.

(149) Fässler, T. F. *Struct. Bonding* **2011**, *140*, 91–131.

(150) Turbervill, R. S. P.; Goicoechea, J. M. *Chem. Rev.* **2014**, *114*, 10807–10828.

(151) Corbett, J. D. *Chem. Rev.* **1985**, *85*, 383–397.

(152) Corbett, J. D. *Angew. Chem. Int. Ed.* **2000**, *39*, 670–690.

(153) Perla, L. G.; Oliver, A. G.; Sevov, S. C. *Inorg. Chem.* **2015**, *54*, 872–875.

(154) Wade, K. *Adv. Inorg. Chem. Radiochem.* **1976**, *18*, 1–66.

(155) Mingos, D. M. P. *Acc. Chem. Res.* **1984**, *17*, 311–319.

(156) Leung, Y. C.; Waser, J.; Houten, S. v.; Vos, A.; Wiegers, G. A.; Wiebenga, E. H. *Acta Cryst.* **1957**, *10*, 574–582.

(157) Sen, T.; Poupko, R.; Fleischer, U.; Zimmermann, H.; Luz, Z. *J. Am. Chem. Soc.* **2000**, *122*, 889–896.

(158) Seifert, G.; Jones, R. O. *J. Chem. Phys.* **1992**, *96*, 2951–2952.

(159) Poupko, R.; Zimmermann, H.; Müller, K.; Luz, Z. *J. Am. Chem. Soc.* **1996**, *118*, 7995–8005.

(160) Charles, S.; Fettinger, J. C.; Eichhorn, B. W. *J. Am. Chem. Soc.* **1995**, *117*, 5303–5311.

(161) Mattamana, S. P.; Promprai, K.; Fettinger, J. C.; Eichhorn, B. W. *Inorg. Chem.* **1998**, *37*, 6222–6228.

(162) Baudler, M.; Faber, W.; Hahn, J. *Z. Anorg. Allg. Chem.* **1980**, *469*, 15–21.

(163) Fritz, G.; Hoppe, K. D.; Hönle, W.; Weber, D.; Mujica, C.; Manriquez, V.; Schnering, H. G. v. *J. Organomet. Chem.* **1983**, *249*, 63–80.

(164) Fritz, G.; Schneider, H.-W. *Z. Anorg. Allg. Chem.* **1990**, *584*, 12–20.

(165) Turbervill, R. S. P.; Goicoechea, J. M. *Organometallics* **2012**, *31*, 2452–2462.

(166) Turbervill, R. S. P.; Goicoechea, J. M. *Chem. Commun.* **2012**, *48*, 1470–1472.

(167) Turbervill, R. S. P.; Goicoechea, J. M. *Eur. J. Inorg. Chem.* **2014**, *2014*, 1660–1668.

(168) Charles, S.; Fettinger, J. C.; Bott, S. G.; Eichhorn, B. W. *J. Am. Chem. Soc.* **1996**, *118*, 4713–4714.

(169) Charles, S.; Eichhorn, B. W.; Bott, S. G. *J. Am. Chem. Soc.* **1993**, *115*, 5837–5838.

(170) Huheey, J. E.; Keiter, E. A.; Keiter, R. L. *Inorganic Chemistry: Principles of Structure and Reactivity*; 4th ed.; Harper Collins, 1993; pp A31.

(171) Knapp, C. M.; Westcott, B. H.; Raybould, M. A. C.; McGrady, J. E.; Goicoechea, J. M. *Angew. Chem. Int. Ed.* **2012**, *51*, 9097–9100.

(172) Knapp, C. M.; Westcott, B. H.; Raybould, M. A. C.; McGrady, J. E.; Goicoechea, J. M. *Chem. Commun.* **2012**, *48*, 12183–12185.

(173) Cicač-Hudi, M.; Bender, J.; Schlindwein, S. H.; Bispinghoff, M.; Nieger, M.; Grützmacher, H.; Gudat, D. *Eur. J. Inorg. Chem.* **2016**, *2016*, 649–658.

(174) Himmel, D.; Krossing, I.; Schnepf, A. *Angew. Chem. Int. Ed.* **2014**, *53*, 370–374.

(175) Frenking, G. *Angew. Chem. Int. Ed.* **2014**, *53*, 6040–6046.

(176) Frison, G.; Sevin, A. *J. Organomet. Chem.* **2002**, *643–644*, 105–111.

(177) Kelemen, Z.; Streubel, R.; Nyulászi, L. *RSC Adv.* **2015**, *5*, 41795–41802.

(178) Mathey, F. *Coord. Chem. Rev.* **1994**, *137*, 1–52.

(179) Nixon, J. F. *Coord. Chem. Rev.* **1995**, *145*, 201–258.

(180) Braye, E. H.; Caplier, I.; Saussez, R. *Tetrahedron* **1971**, *27*, 5523–5537.

(181) Thomson, C.; Kilcast, D. *Angew. Chem. Int. Ed. Engl.* **1970**, *9*, 310–311.

(182) Holand, S.; Jeanjean, M.; Mathey, F. *Angew. Chem. Int. Ed. Engl.* **1997**, *36*, 98–100.

(183) Gillott, D. *Masters Thesis: Unsaturated Group 15 Ring Systems and their Reactivity*; St. John's College, University of Oxford, 2014.

(184) Charrier, C.; Mathey, F. *Tetrahedron Lett.* **1987**, *28*, 5025–5028.

(185) Wimmer, K.; Birg, C.; Kretschmer, R.; Al-Shboul, T. M. A.; Görls, H.; Krieck, S.; Westerhausen, M. *Z. Naturforsch. B* **2009**, *64b*, 1360–1368.

(186) Abel, E. W.; Towers, C. *J. Chem. Soc., Dalton Trans.* **1979**, 814–819.

(187) De Lauzon, G.; Deschamps, B.; Fischer, J.; Mathey, F.; Mitschler, A. *J. Am. Chem. Soc.* **1980**, *102*, 994–1000.

(188) Schnitzler, V.; Frank, W.; Ganter, C. *J. Organomet. Chem.* **2008**, *693*, 2610–2614.

(189) Bartsch, R.; Nixon, J. F. *Polyhedron* **1989**, *8*, 2407.

(190) Bartsch, R.; Nixon, J. F. *J. Organomet. Chem.* **1991**, *415*, C15–C18.

(191) Lynam, J. M.; Copsey, M. C.; Green, M.; Jeffery, J. C.; McGrady, J. E.; Russell, C. A.; Slattery, J. M.; Swain, A. C. *Angew. Chem. Int. Ed.* **2003**, *42*, 2778–2782.

(192) Fish, C.; Green, M.; Jeffery, J. C.; Kilby, R. J.; Lynam, J. M.; Russell, C. A.; Willans, C. E. *Organometallics* **2005**, *24*, 5789–5791.

(193) Baudler, M.; Düster, D.; Ouzounis, D. *Z. Anorg. Allg. Chem.* **1987**, *544*, 87–94.

(194) Baudler, M.; Hahn, J. *Z. Naturforsch. B* **1990**, *45b*, 1139–1142.

(195) Maigrot, N.; Sierra, M.; Charrier, C.; Mathey, F. *Bull. Soc. Chim. Fr.* **1994**, *131*, 397–399.

(196) Butts, C. P.; Green, M.; Hooper, T. N.; Kilby, R. J.; McGrady, J. E.; Pantazis, D. A.; Russell, C. A. *Chem. Commun.* **2008**, 856–858.

(197) García, F.; Less, R. J.; Naseri, V.; McPartlin, M.; Rawson, J. M.; Tomas, M. S.; Wright, D. S. *Chem. Commun.* **2008**, 859–861.

(198) Scherer, O. J.; Hilt, T.; Wolmershäuser, G. *Angew. Chem. Int. Ed.* **2000**, *39*, 1425–1427.

(199) Deng, S.; Schwarzmaier, C.; Eichhorn, C.; Scherer, O.; Wolmershäuser, G.; Zabel, M.; Scheer, M. *Chem. Commun.* **2008**, 4064–4066.

(200) Turbervill, R. S. P.; Goicoechea, J. M. *Chem. Commun.* **2012**, *48*, 6100–6102.

(201) Turbervill, R. S. P.; Jupp, A. R.; McCullough, P. S. B.; Ergöçmen, D.; Goicoechea, J. M. *Organometallics* **2013**, *32*, 2234–2244.

(202) Kolb, H. C.; Finn, M. G.; Sharpless, K. B. *Angew. Chem. Int. Ed.* **2001**, *40*, 2004–2021.

(203) Jupp, A. R. *Masters Thesis: Transition Metal-Mediated Activation of Group 15 Zintl Ions*; The Queen's College, University of Oxford, 2012.

(204) Turbervill, R. S. P. *DPhil Thesis: Solution Reactivity Studies of Group 15 Zintl Anions Towards Unsaturated Substrates*; Wadham College, University of Oxford, 2014.

(205) Bartsch, R.; Cloke, F. G. N.; Green, J. C.; Matos, R. M.; Nixon, J. F.; Suffolk, R. J.; Suter, J. L.; Wilson, D. J. *J. Chem. Soc., Dalton Trans.* **2001**, 1013–1022.

(206) Bruce, Ê. D. V.; Rocha, W. R. *Organometallics* **2004**, *23*, 5308–5313.

(207) Turbervill, R. S. P.; Goicoechea, J. M. *Inorg. Chem.* **2013**, *52*, 5527–5534.

(208) Baudler, M.; Akpapoglou, S.; Ouzounis, D.; Wasgestian, F.; Meinigke, B.; Budzikiewicz, H.; Münster, H. *Angew. Chem. Int. Ed. Engl.* **1988**, *27*, 280–281.

(209) Scherer, O. J.; Schwalb, J.; Wolmershäuser, G.; Kaim, W.; Gross, R. *Angew. Chem. Int. Ed. Engl.* **1986**, *25*, 363–364.

(210) Scheer, M.; Gregoriades, L. J.; Virovets, A. V.; Kunz, W.; Neueder, R.; Krossing, I. *Angew. Chem. Int. Ed.* **2006**, *45*, 5689–5693.

(211) Urnėžius, E.; Brennessel, W. W.; Cramer, C. J.; Ellis, J. E.; Schleyer, P. von R. *Science* **2002**, *295*, 832–834.

(212) Baudler, M.; Etzbach, T. *Angew. Chem. Int. Ed. Engl.* **1991**, *30*, 580–582.

(213) Jupp, A. R.; Goicoechea, J. M. *Angew. Chem. Int. Ed.* **2013**, *52*, 10064–10067.

(214) Muzart, J. *Tetrahedron* **2009**, *65*, 8313–8323.

(215) Ding, S.; Jiao, N. *Angew. Chem. Int. Ed.* **2012**, *51*, 9226–9237.

(216) Becker, G.; Schwarz, W.; Seidler, N.; Westerhausen, M. *Z. Anorg. Allg. Chem.* **1992**, *612*, 72–82.

(217) Westerhausen, M.; Schneiderbauer, S.; Piotrowski, H.; Suter, M.; Nöth, H. *J. Organomet. Chem.* **2002**, *643–644*, 189–193.

(218) Becker, G.; Heckmann, G.; Hübler, K.; Schwarz, W. *Z. Anorg. Allg. Chem.* **1995**, *621*, 34–46.

(219) Weber, L.; Torwiehe, B.; Bassmann, G.; Stammler, H.-G.; Neumann, B. *Organometallics* **1996**, *15*, 128–132.

(220) Becker, G.; Hübler, K. *Z. Anorg. Allg. Chem.* **1994**, *620*, 405–417.

(221) Krummenacher, I.; Cummins, C. C. *Polyhedron* **2012**, *32*, 10–13.

(222) Cordaro, J. G.; Stein, D.; Rüegger, H.; Grützmacher, H. *Angew. Chem. Int. Ed.* **2006**, *45*, 6159–6162.

(223) Puschmann, F. F.; Stein, D.; Heift, D.; Hendriksen, C.; Gal, Z. A.; Grützmacher, H.-F.; Grützmacher, H. *Angew. Chem. Int. Ed.* **2011**, *50*, 8420–8423.

(224) Alidori, S.; Heift, D.; Santiso-Quinones, G.; Benkő, Z.; Grützmacher, H.; Caporali, M.; Gonsalvi, L.; Rossin, A.; Peruzzini, M. *Chem. Eur. J.* **2012**, *18*, 14805–14811.

Chapter 2

The 2-phosphaethynolate anion and coordination chemistry of $[ECX]^-$ ligands (E = N, P; X = O, S)

2.1 Introduction and objectives

2.1.1 Previous synthetic procedures of the 2-phosphaethynolate anion, and subsequent reactivity

The 2-phosphaethynolate anion, the phosphorus-containing analogue of the common cyanate anion, has been known since Becker's seminal report in 1992.[1] Very few examples of further reactivity were reported in the ensuing twenty years. The 2-phosphaethynolate anion can undergo metal-mediated dimerisations and oxidative tetramerisations to yield $[P_2C_2O_2]^{2-}$ and $[P_4C_4O_4]^{2-}$, respectively.[2,3] The latter report also details the reaction with an activated alkyne to afford a phosphinine derivative.[3] The lithium salt can also react with carbon disulfide at low temperatures to yield the heavier isoelectronic analogue, $[PCS]^-$.[4] The alkaline earth metal salts, $Ae(PCO)_2$ (Ae = Mg–Ba) were synthesised using an analogous method to the lithium salt.[5] These products were incredibly sensitive and decomposition precluded attempts to isolate solid samples, although a crystal structure of the calcium salt was obtained when three DME co-ligands were employed to enhance the stability of the complex. Interest in this simple anion was revived in 2011, when synthetic procedures of the sodium salt were reported from the groups of Cummins[6] and Grützmacher.[7]

Common to all of the known preparations of the 2-phosphaethynolate anion is the attack of a carbonyl moiety by a phosphide source; the sources of these synthons and the conditions for their reactivity are shown in Table 2.1. All of these procedures suffer from various setbacks. The initial lithium salt was highly sensitive and difficult to handle, which is why the subsequent reactivity was limited to only a handful of examples. The group 2 salts were even more unstable, and could only be stored in ethereal solutions at low temperature. The metathesis reaction of carbon dioxide with a terminal niobium phosphide by Cummins is a very elegant reaction, but the stoichiometric use of the bulky niobium complex renders it

atom inefficient. Grützmacher's first reported synthesis used very forcing conditions, namely 110 bar of carbon monoxide at 80 ˚C in an autoclave. The other two preparations from his group required the prior synthesis of the $[NaPH_2]\cdot[NaO^tBu]_x$ clusters, and were mentioned as curiosities with no indication of whether they could be scaled up to preparative quantities.

Table 2.1: Reagents and conditions for previously known syntheses of the $[PCO]^-$ anion.

Phosphide source	Carbonyl source	Cation	Conditions	Reference
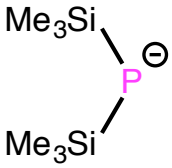	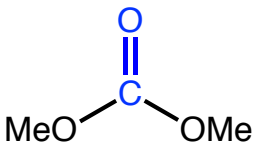	Li^+	DME –20 ˚C	Becker[1]
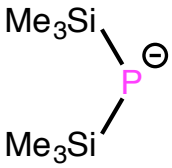	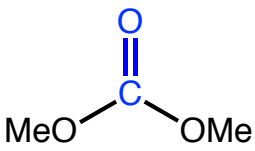	Mg^{2+} Ca^{2+} Sr^{2+} Ba^{2+}	DME –20 ˚C	Westerhausen[5]
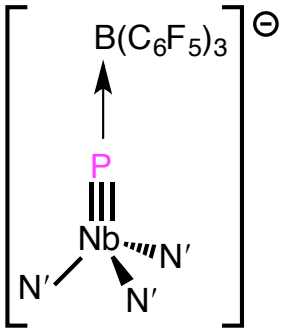		Na^+	1 eq. CO_2 Et_2O 25 ˚C	Cummins[6]
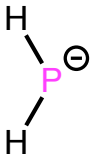	CO	Na^+	DME 110 bar CO 80 ˚C	Grützmacher[7]
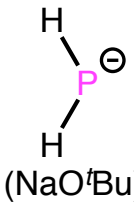	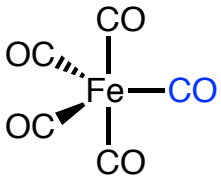	Na^+	THF 25 ˚C	Grützmacher[7]
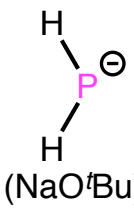	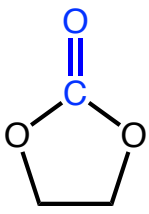	Na^+	DME 25 ˚C	Grützmacher[7]

The only report of the subsequent reactivity of the sodium salt of $[PCO]^-$ before I started research in 2012 was its coordination to a transition metal centre. The [Re(triphos)$(CO)_2(\eta^1$-ECO)] complexes (E = N, P) were readily synthesised by displacement of a labile trifluoromethanesulfonate (triflate, OTf) ligand in [Re(triphos)$(CO)_2$(OTf)] (Figure 2.1).[8] This permitted a brief comparison between cyanate and its heavier phosphorus-containing congener, and found that the two isoelectronic species have profoundly different coordination modes. The PCO moiety is bound in a side-on (bent) manner, with a Re–P–C bond angle of approximately 90˚, whereas the nitrogen analogue is bound end-on and the Re–N–C bond angle approaches 180˚. This was corroborated computationally, and cannot be attributed merely to crystal packing effects; however a crystallographic disorder phenomenon precluded any accurate discussion of bond metric data within these species. The species were probed by IR spectroscopy, which demonstrated that, despite the stark contrast in coordination modes, both $[ECO]^-$ ligands "*...exert indistinguishable effects on the [Re(triphos)$(CO)_2$] fragment*."

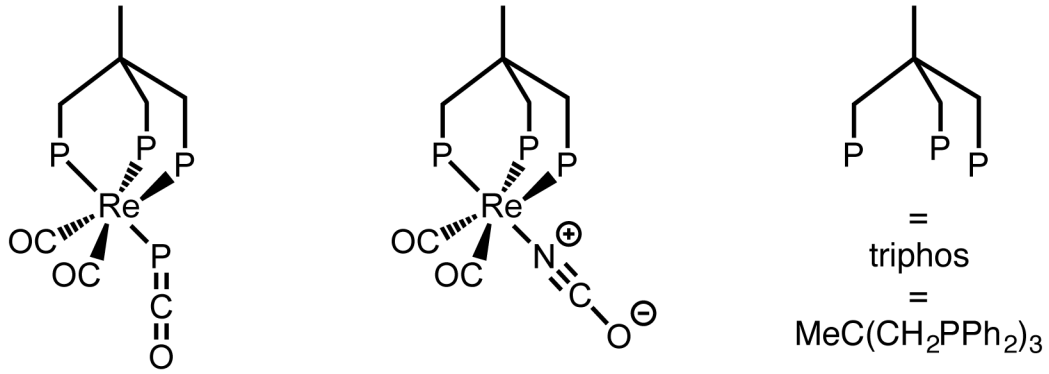

Figure 2.1: [Re(triphos)$(CO)_2(\eta^1$-ECO)] complexes as depicted in publication by Alidori et al.[8]

In my work on the thermal activation of the $[P_7]^{3-}$ cluster to afford the pentaphospholide ring (described in Chapter 1), the appearance of a side-product was observed when the reaction was carried out in DMF in a closed system. This was identified as [K(18-crown-6)][PCO]. This arises from the initial thermal decomposition of the DMF solvent to

dimethylamine and carbon monoxide, and the subsequent attack of the latter by an anionic phosphorus moiety (Scheme 2.1). This serendipitous discovery was the starting point for the work described henceforth in this thesis.

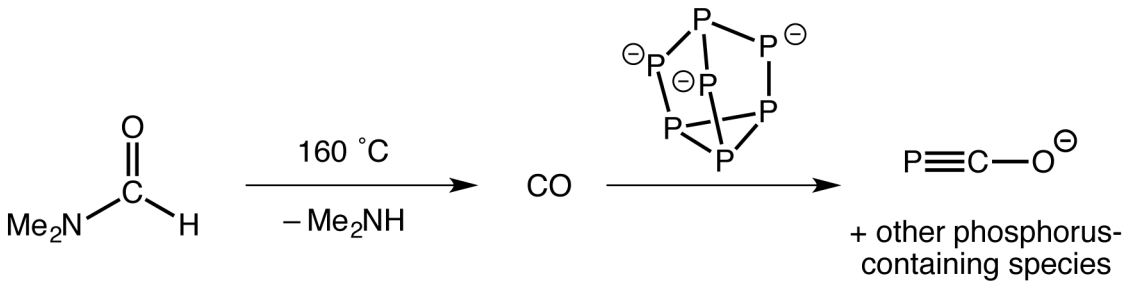

Scheme 2.1: Thermal decomposition of DMF and subsequent reaction with $[P_7]^{3-}$ to yield $[PCO]^-$.

Since our initial report in 2013 there has been a renaissance in the chemistry of the 2-phosphaethynolate anion, spearheaded by our group and that of Grützmacher. There have been numerous reports exploring the practical use of this anion as a precursor to original organophosphorus derivatives,[9,10] phosphorus-containing heterocycles,[11–15] and as a phosphide-transfer agent.[16–18] There are also probes into its ligand properties,[19,20] computational studies,[21–23] and an article highlighting its potential within organic chemistry.[24] These will be brought up and discussed as appropriate over the course of this thesis.

2.1.2 Chapter outline

Ignoring these later developments for the time being, when our research group started working on $[PCO]^-$ the field was very limited. We sought to take advantage of our serendipitous finding that $[PCO]^-$ was formed as a side-product when heating the K_3P_7 Zintl phase in DMF, and expand the known chemistry of this fundamental anion. This chapter will detail our novel and targeted synthesis of the $[K(18\text{-crown-6})]^+$ salt of the 2-phosphaethynolate anion, via a rare activation of the $[P_7]^{3-}$ Zintl cluster. The ligand properties of $[PCO]^-$ will be explored in detail and compared to the isoelectronic analogues,

$[NCO]^-$ and $[NCS]^-$. This study will be extended to incorporate the heavier $[PCS]^-$ anion, which has been synthesised at ambient temperatures for the first time. The chapter will conclude with a brief discussion of the properties of these anions in the coordination sphere of actinides. The species will be abbreviated as $[ECX]^-$ ligands over the course of this discussion, where E will always refer to the group 15 element (N, P) and X is the group 16 element (O, S), as applicable.

2.2 The 2-phosphaethynolate anion, $[PCO]^-$

2.2.1 Synthesis of [K(18-crown-6)][1] (1: $[PCO]^-$)

The generation of small amounts of the 2-phosphaethynolate anion during the thermal activation of the $[P_7]^{3-}$ cluster in DMF prompted us to explore this mode of reactivity further, and target the product in greater yields. This was achieved by circumventing the need for the decomposition of the DMF solvent as a source of the CO moiety, and instead gaseous carbon monoxide was used directly. Heating a DMF solution of K_3P_7 and 18-crown-6 at 150 ˚C under one atmosphere of carbon monoxide for 24 hours afforded [K(18-crown-6)][**1**] (**1**: $[PCO]^-$).[25]

This is in line with the previous reports of the synthesis of **1**, with a formal transfer of a phosphide anion to the carbon atom of CO. In this case, the phosphide vertex is derived from the naked $[P_7]^{3-}$ cluster, and is a rare example of activation of this species to yield an organophosphorus product. This activation is accompanied by the formation of oxidised polyphosphide clusters, namely $[P_{16}]^{2-}$ and $[P_{21}]^{3-}$, which can be readily identified by their characteristic and complex ^{31}P NMR spectroscopic signatures (shown in the lower NMR spectrum of Figure 2.2).[26,27] The reaction can also be carried out at slightly lower temperatures, but this increases the amount of time for full conversion to several days, and

allows the observation of a singlet corresponding to the $[P_5]^-$ ring at +468 ppm in the ^{31}P NMR spectrum during the course of the reaction (Figure 2.2).

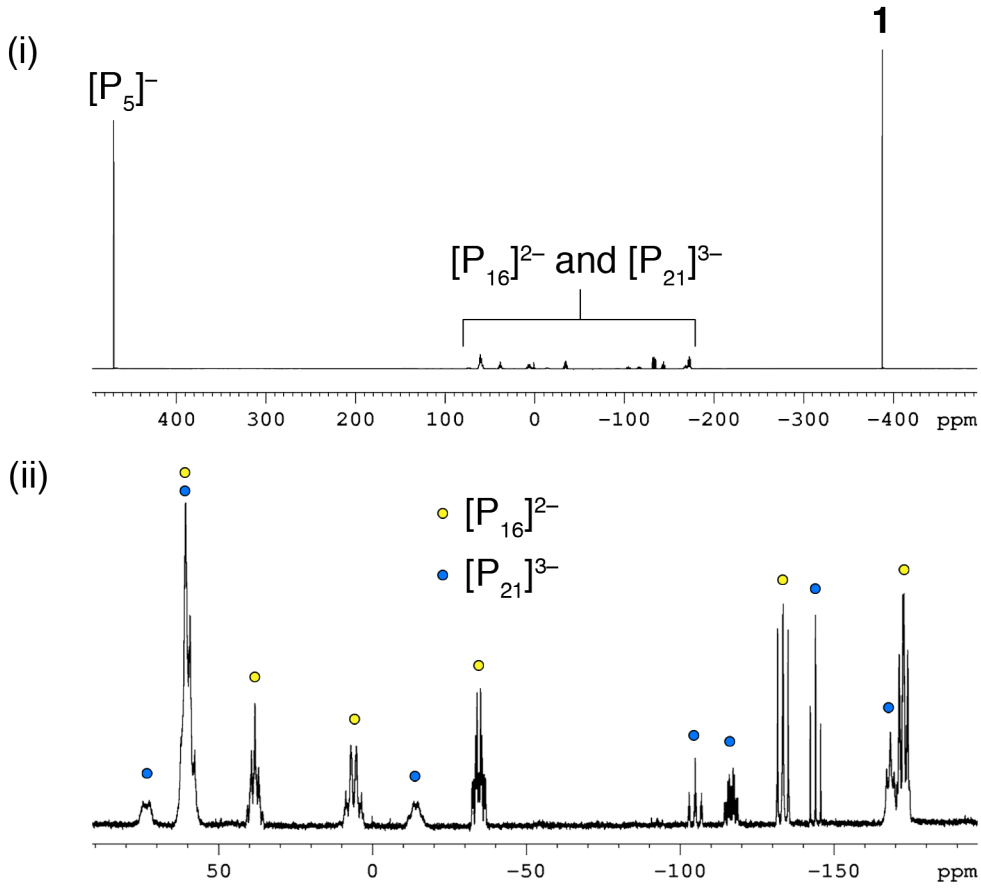

Figure 2.2: ^{31}P NMR spectra of: (i) a DMF solution of K_3P_7, 18-crown-6 and CO heated at 110 ˚C for 24 hours to give **1**, $[P_5]^-$ and polyphosphide resonances; (ii) expanded region to show characteristic $[P_{16}]^{2-}$ and $[P_{21}]^{3-}$ resonances.

The $[P_5]^-$ anion reacts with carbon monoxide and is eventually consumed to afford **1**, $[P_{16}]^{2-}$ and $[P_{21}]^{3-}$ as the only phosphorus-containing species in solution. Due to the fact that the reaction needs to be carried out at elevated temperatures, $[P_5]^-$ formation was always observed during the reaction. It is therefore unclear whether the carbon monoxide reacts with the $[P_7]^{3-}$ cage directly, or whether the reaction only proceeds after the cluster has been thermally fragmented. The overall reaction, however, is unequivocally an activation of the cluster to yield the carbonylated product, **1**, and polyphosphide by-products.

Clean solutions of [K(18-crown-6)][**1**] can be obtained by exploiting the stability of the product in deoxygenated water. The addition of degassed water to the reaction mixture

hydrolyses the other by-products, and the pale yellow solution can be filtered and the volatiles subsequently removed *in vacuo* to afford [K(18-crown-6)][**1**] as an off-white solid in moderate yields (38%). Treating the P^- moiety as the stoichiometrically limiting reagent, and in the absence of other redox processes, the maximum yield available is only 43%. Attempts to increase this yield with the addition of a reducing agent to the reaction mixture, with the aim of converting the oxidised polyphosphide by-products back to $[P_7]^{3-}$ or $[P_5]^-$ in order to react further with CO, were unsuccessful.

2.2.2 Characterisation of [K(18-crown-6)][1]

Single crystals of [K(18-crown-6)][**1**] suitable for X-ray diffraction were obtained by slow diffusion of hexane into a THF solution of the product. The crystal structure solves in the monoclinic space group $P2_1$, and the asymmetric unit is shown in Figure 2.3. The hydrogen atoms on the 18-crown-6 moiety were assigned idealised geometric coordinates after the heavier elements had been refined anisotropically.

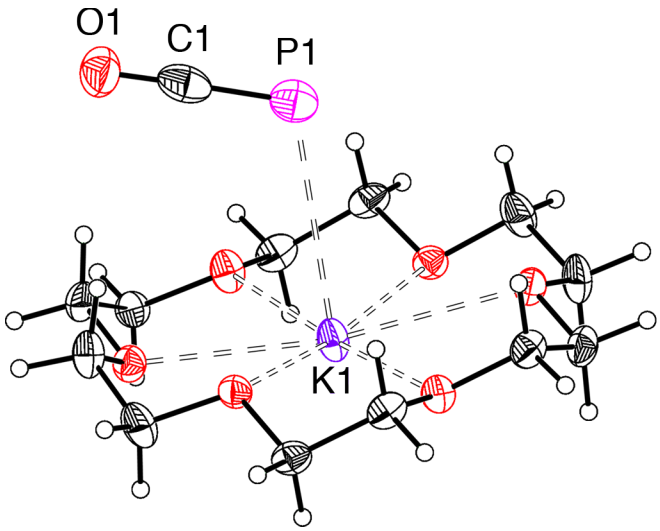

Figure 2.3: Molecular structure of [K(18-crown-6)][**1**]. Anisotropic displacement ellipsoids are set at 50% probability. Hydrogen atoms are shown as spheres of arbitrary radii.

The structure of [K(18-crown-6)][**1**] reveals a linear triatomic anion (P1–C1–O1 bond angle: 178.9(3)°) alongside a $[K(18\text{-crown-6})]^+$ cation. There is a close electrostatic contact between P1 and the K^+ cation (3.383(1) Å), while O1 is in close contact with an adjacent

[K(18-crown-6)]$^+$ moiety (2.901(2) Å). This leads to one-dimensional coordination polymer chains of alternating [K(18-crown-6)]$^+$ cations and [PCO]$^-$ anions propagating through the crystal structure (Figure 2.4).

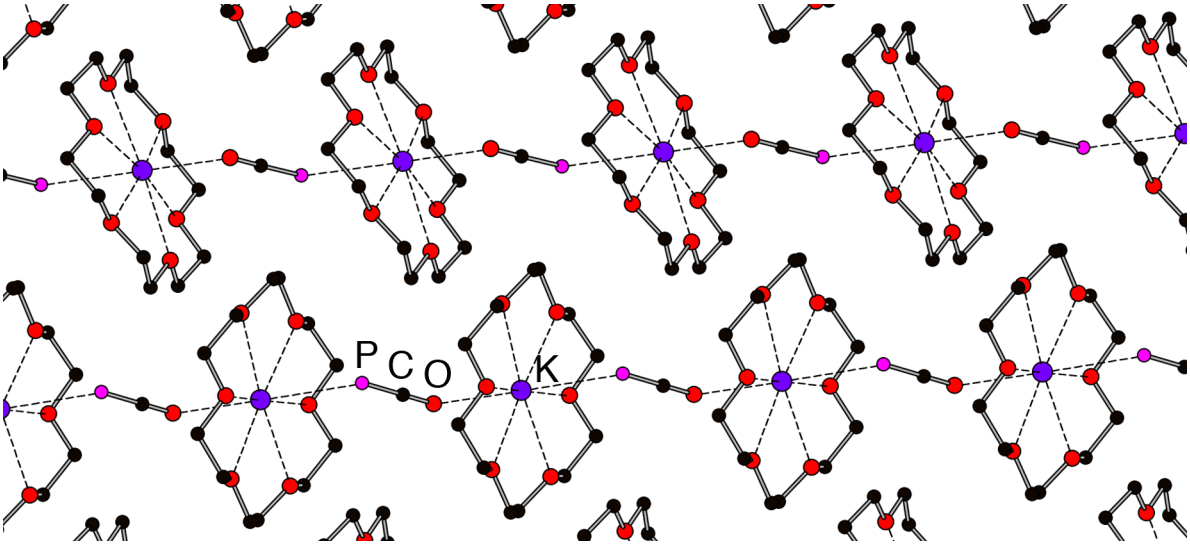

Figure 2.4: Ball and stick model showing one-dimensional coordination polymer chains of [K(18-crown-6)][**1**] within the crystal structure. Hydrogen atoms omitted for clarity.

The P1–C1 bond is very short at 1.579(3) Å, and certainly has significant multiple bond character. Figure 2.5 shows the two resonance structures with the highest weighting for [PCO]$^-$ and the lighter nitrogen analogue, as calculated using natural resonance theory (NRT) analysis by the groups of Grützmacher and Peruzzini.[8] **1** can be considered as an anionic phosphaketene derivative, **α**, or as a phosphaalkyne where the R group is a negatively charged oxygen atom, **β**, and the reality lies somewhere between these two extremes.

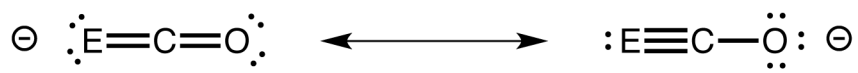

α		**β**
33.5%	E = N	60.0%
40.2%	E = P	51.7%

Figure 2.5: The two major resonance contributions and their respective weights for [NCO]$^-$ and [PCO]$^-$ (B3LYP/6-31+G*). Figure adapted from Alidori et al.[8]

These calculations show that both anions favour the alkyne-like resonance **β**, with a formal E≡C triple bond. This preference is slightly greater for cyanate, however, because of the more efficient overlap of the 2p–2p π orbitals for N and C than the 3p–2p overlap for P and C. This is in accord with the predictions of the double bond rule. Regardless of the exact nature of the P–C multiple bond, the negative charge is fundamental for its stabilisation, as the electrostatic repulsion between anions prevents classical oligomerisation decomposition routes. This also offers a rationale as to why some of the earlier salts of this anion were more sensitive and prone to decomposition than the more recent sodium and potassium salts. Lithium is highly oxophilic, and is well-known to be anomalous within the alkali metals for conferring a significant degree of covalency within its bonding. These two factors indicate a structure that can be described as P≡C–OLi, and there is a diminished negative charge associated with the PCO moiety, which leads to more facile decomposition. For the alkaline earth salts, $Ae(PCO)_2$ (Ae = Mg–Ba), the dicationic charge on the metal necessarily brings two $[PCO]^-$ anions in close contact with each other, and lowers the kinetic and thermodynamic energy barrier to dimerisation and subsequent decomposition. The bond metric data of [K(18-crown-6)][**1**] are in good agreement with those of the previously published and structurally authenticated salts (Table 2.2).

Table 2.2: Comparison of bond metric parameters for crystallographically characterised salts of the 2-phosphaethynolate anion.

	[K(18-crown-6)][**1**]	$[Na(DME)(\mathbf{1})]_2$[7]	$[Li(DME)_2][\mathbf{1}]$[1]	$[Ca(DME)_3][\mathbf{1}]$[5]
P–C (Å)	1.579(3)	1.589(3)/1.575(3)	1.555(3)	1.575(2)
C–O (Å)	1.212(4)	1.203(4)/1.213(4)	1.198(4)	1.199(3)
P–C–O (˚)	178.9(3)	179.3(3)/179.5(4)	178.5(3)	179.2(2)

The only real deviation within this series is Becker's lithium salt, where the P–C bond length is significantly shorter than those of the other structures. This is easily explained by

an extension of the above discussion; the oxophilicity of the hard lithium cation better stabilises resonance **β** from Figure 2.5, and leads to a greater P≡C triple bond character.

The ^{31}P NMR spectrum of [K(18-crown-6)][**1**] features a very upfield shifted and diagnostic singlet resonance between –387 and –397 ppm, depending on the exact nature of the solvent and counter-cation. For example, the [K(18-crown-6]$^+$ salt appears at –388.0 ppm in DMF (Figure 2.6), and at –396.8 ppm in d_8-THF. The ^{13}C{^{1}H} NMR spectrum in d_8-THF reveals a doublet at 170.3 ppm ($^1J_{C–P}$ = 62.0 Hz).

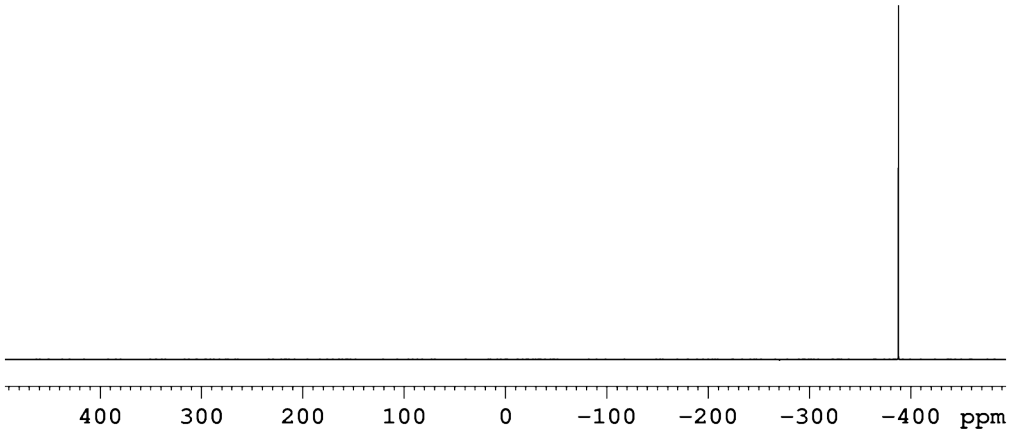

Figure 2.6: ^{31}P NMR spectrum of DMF solution of [K(18-crown-6)][**1**].

An IR spectrum of the solid in a Nujol mull revealed a band at 1730 cm^{-1}, which is the asymmetric stretching mode of **1**. This can be attributed to the C–O stretch, although the P–C and C–O stretching modes exhibit substantial coupling by DFT calculations.[8] The symmetric stretch was obscured by bands arising from the [K(18-crown-6]$^+$ moiety (this was observed at 1247 cm^{-1} for the [Na(1,4-dioxane)$_{2.5}$][PCO] salt).[7]

The anion **1** was too light to be observed in the negative ion mode electrospray ionisation mass spectrometric experiments, as it was below the minimum threshold of the detector. However the cation-paired species {[K(18-crown-6)]$_2$[**1**]}$^+$ could be observed in the positive mode with an *m/z* ratio of 665.7. The compositional purity of the solid was also confirmed by an accurate elemental analysis.

2.3 Ligand properties of the 2-phosphaethynolate, cyanate and thiocyanate anions

Equipped with a multi-gram synthesis of compositionally pure [K(18-crown-6)][**1**], we sought to explore the ligand properties of the 2-phosphaethynolate anion compared to the other isoelectronic pseudohalides: cyanate and thiocyanate. This was achieved by the formation of a series of anionic complexes with the general formula $[W(CO)_5(L)]^-$ (**2**: L = PCO; **3**: L = NCO; **4**: L = NCS).

This choice of the tungsten carbonyl derivatives was based on a number of factors. The $W(CO)_5$ fragment has many spectroscopic handles available through which to probe the ligand properties, including the presence of a well-defined carbonyl group *trans* to the $[ECX]^-$ ligand in question on formation of the complexes. Many reactive species have been trapped and stabilised in the coordination sphere of this moiety in the past, and as a result there are a multitude of $[W(CO)_5(L)]$ complexes in the literature that have been used in experimental and computational studies, allowing a thorough comparison to other systems. Finally, it has already been established that **1** is highly reducing, as evidenced by the reactions with mild oxidants such as I_2 and SO_2 to afford the oxidised tetramer, $[P_4C_4O_4]^{2-}$.[3] This has plagued the simple salt metathesis reactions of **1**, often leading to insoluble red precipitates in previous cases.[8] The low oxidation state tungsten(0) centre is stable to reduction by **1**, and allowed the isolation of the corresponding complex in good yields.

2.3.1 Synthesis of tungsten pentacarbonyl complexes

UV irradiation of a THF solution of [K(18-crown-6)][**1**] and $[W(CO)_6]$ led to the formation of [K(18-crown-6)][**2**] (**2**: $[W(CO)_5(PCO)]^-$), via the initial photolysis of one of the W–CO bonds. However it was difficult to obtain a compositionally pure sample of the product, and there were often small quantities of other unknown phosphorus-containing species present

by ^{31}P NMR spectroscopy. These presumably arise due to subsequent photolysis of [K(18-crown-6)][**2**], and although the careful monitoring of the reaction allowed the extent of these impurities to be minimised, it proved challenging to eradicate them entirely.

The same compound could be obtained cleanly via an alternative route (Scheme 2.2). Trimethylamine *N*-oxide can be employed as a decarbonylation agent with tungsten hexacarbonyl in the presence of acetonitrile to yield the intermediate shown, with the loss of trimethylamine and carbon dioxide. The labile nitrile ligand can be readily displaced by [K(18-crown-6)][**1**] to yield [K(18-crown-6)][**2**]. The displacement of the acetonitrile with $[NCO]^-$ and $[NCS]^-$ leads to the formation of the analogous anionic complexes $[W(CO)_5(NCO)]^-$ (**3**) and $[W(CO)_5(NCS)]^-$ (**4**), respectively.

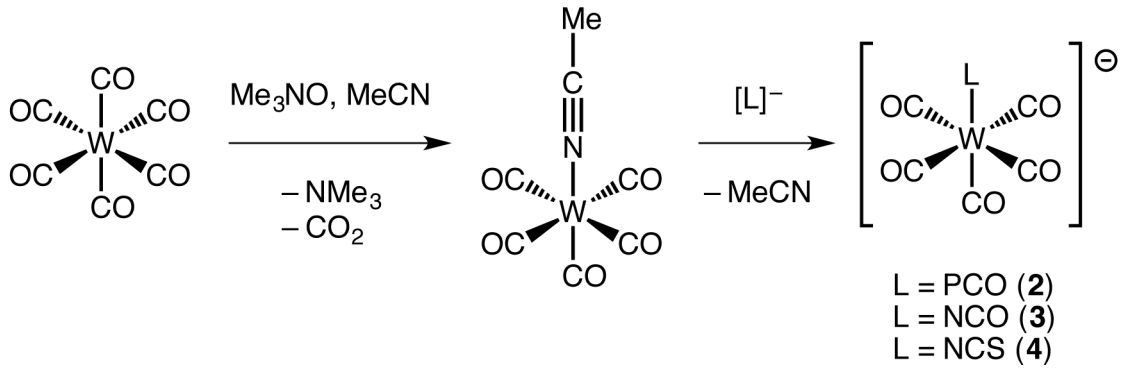

Scheme 2.2: General formation of $[W(CO)_5(ECX)]^-$ complexes.

2.3.2 Single crystal X-ray diffraction study

2.3.2.1 Crystallisation of 2, 3 and 4

Large yellow block-shaped crystals of [K(18-crown-6)][**2**] were grown by slow diffusion of hexane into a THF solution of the product. Crystallographic analysis clearly shows the PCO moiety to be bound through the phosphorus atom in a bent geometry (Figure 2.7). Unfortunately, substitutional disorder causes the PCO moiety to be located over two positions *trans* to each other, with the C2–O2 carbonyl group occupying the other position 50% of the time. Therefore, restraints of the W1–C2 and C2–O2 bond lengths were required

to produce a satisfactory solution. This renders an accurate analysis of the bond metric data futile, especially as the W1–C2 bond length was one of the targeted metrics for comparison to assess the *trans* influence of $[PCO]^-$ as a ligand. This appears reminiscent of the disorder within the [Re(triphos)$(CO)_2(\eta^1$-PCO)] structure published by Peruzzini and Grützmacher.[8]

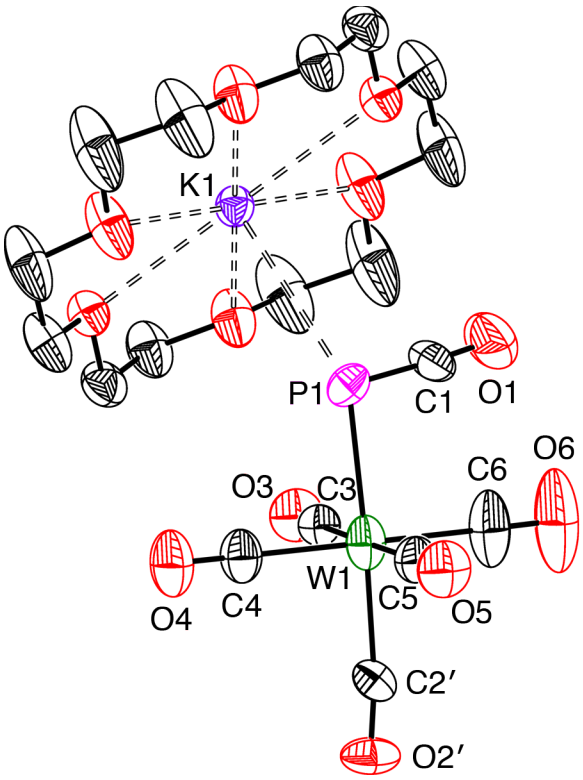

Figure 2.7: Molecular structure of [K(18-crown-6)][**2**]. Anisotropic displacement ellipsoids are set at 50% probability. Hydrogen atoms omitted for clarity. Symmetry element ′: *–x*, 2*–y*, *–z*.

Crystals of [K(18-crown-6)][**3**] and [K(18-crown-6)][**4**] were grown in a similar manner to [K(18-crown-6)][**2**]. Both the cyanate and thiocyanate anions are known to be ambidentate ligands, and can either bind through the nitrogen or the chalcogen atom. The anions **3** and **4** revealed the NCX (X = O, S) moiety to be bound in an end-on manner exclusively through the nitrogen atom when bound to the $W(CO)_5$ fragment in these systems. Both of these anions have been synthesised previously. **3** has long been known, commonly synthesised by the reaction of tungsten hexacarbonyl with an azide salt, but has only been characterised spectroscopically.[28–32] Similarly, IR spectroscopic studies on **4** suggested that the thiocyanate ligand is N-bound, but this was never verified crystallographically.[33,34] The

structures of [K(18-crown-6)][**3**] and [K(18-crown-6)][**4**] are free from any disorder phenomena and offer verification for the previous assertions of the nature of the ligand (Figure 2.8).

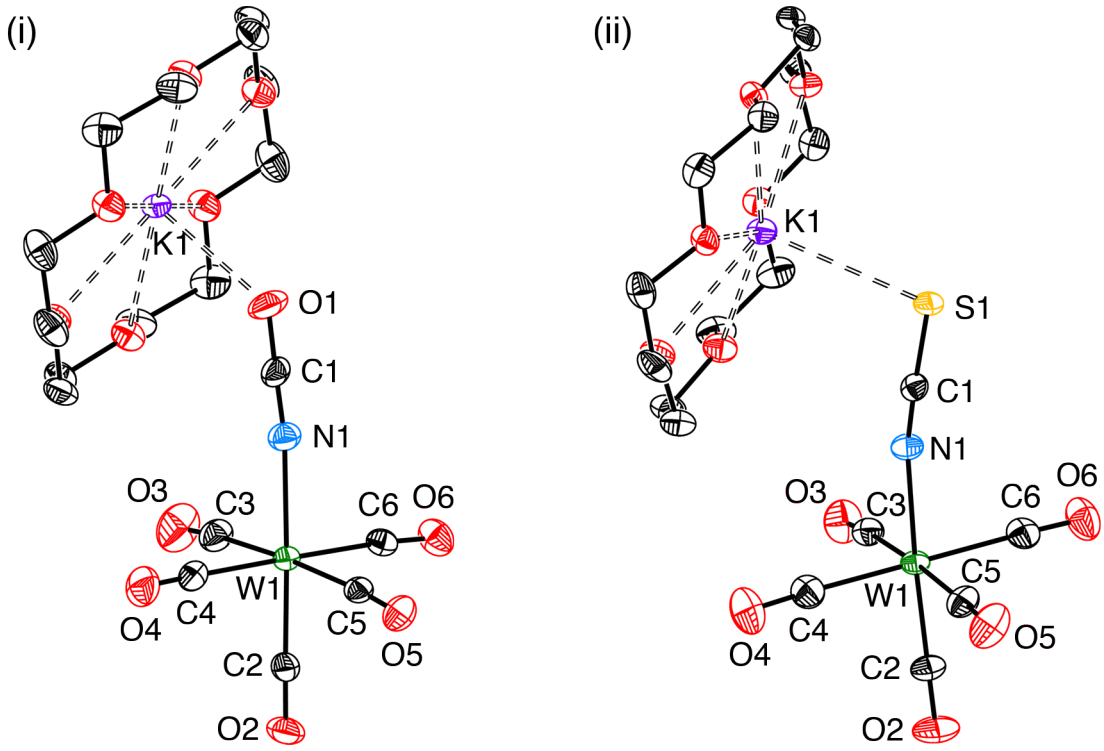

Figure 2.8: Molecular structures of: (i) [K(18-crown-6)][**3**] and (ii) [K(18-crown-6)][**4**]. Anisotropic displacement ellipsoids are set at 50% probability. Hydrogen atoms omitted for clarity.

Although the $[K(18\text{-crown-6})]^+$ salt of **2** revealed the crude nature of the bonding of the $[PCO]^-$ ligand, the disorder precluded the desired detailed analysis of ligand properties. Therefore, alternative counter-cations were used to obtain a better crystallographic solution. An exchange of the potassium-sequestering agent from 18-crown-6 to the three-dimensional cryptand, 2,2,2-crypt, afforded [K(2,2,2-crypt)][**2**]. Single crystals were grown as before, and the X-ray diffraction study yielded a solution free from any disorder (Figure 2.9). The molecular structure shows a very similar anionic moiety of **2** to that found in the $[K(18\text{-crown-6})]^+$ salt, however in this case there is complete separation of the potassium cation due to the more sterically encapsulating sequestering agent.

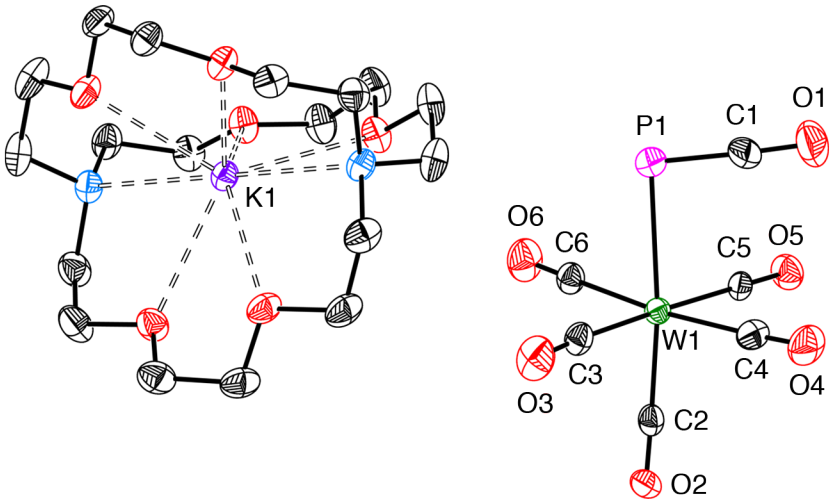

Figure 2.9: Molecular structure of [K(2,2,2-crypt)][**2**]. Anisotropic displacement ellipsoids are set at 50% probability. Hydrogen atoms omitted for clarity.

To enable a more relevant comparison, the cyanate analogue was also synthesised with the cryptand sequestering agent to yield [K(2,2,2-crypt)][**3**] (Figure 2.10). Remarkably, in this case there is a splaying open of the cryptand and a relatively close contact between O1 of the cyanate moiety and the potassium cation (K1–O1 distance 3.080(2) Å).

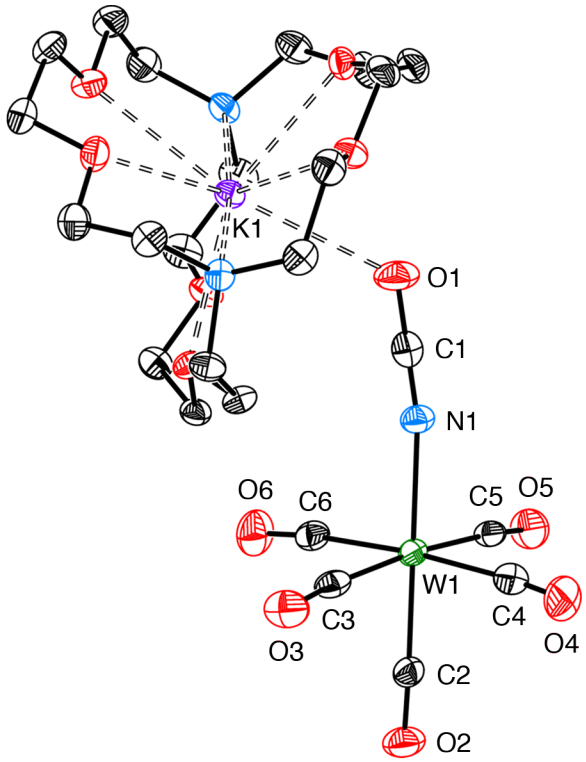

Figure 2.10: Molecular structure of [K(2,2,2-crypt)][**3**]. Anisotropic displacement ellipsoids are set at 50% probability. Hydrogen atoms omitted for clarity.

The potential reasons for this will now be explored, along with a detailed comparison of the bond metric data.

2.3.2.2 Comparison of ECX moieties

The first assessment will focus on the ECX moiety in the crystal structures (Table 2.3).

Table 2.3: Selected crystallographic bond lengths (Å) and bond angles (˚).

	[K(2,2,2-crypt)] [**2**]	[K(18-crown-6)] [**3**]	[K(2,2,2-crypt)] [**3**]	[K(18-crown-6)] [**4**]
W1–E1	2.666(1)	2.183(3)	2.193(2)	2.180(2)
E1–C1	1.616(4)	1.159(4)	1.156(4)	1.157(4)
C1–X1	1.176(5)	1.209(4)	1.221(4)	1.648(3)
K1–X1	N.A.	2.656(3)	3.080(2)	3.200(1)
K2–O2	N.A.	2.756(3)	N.A.	N.A.
W1–E1–C1	94.7(1)	172.9(2)	170.0(2)	169.6(2)
E1–C1–X1	176.8(4)	177.1(3)	179.3(3)	177.4(3)

The first point to note is the obviously contrasting binding modes of the $[PCO]^-$ ligand compared to both the nitrogen-containing species, which was highlighted above. The W1–P1–C1 angle of 94.7(1)˚ reveals the PCO moiety to be bound in a bent fashion, whereas the NCX moieties are all bound in a manner approaching linearity, with W1–N1–C1 bond angles in the range 169.6(2)–172.9(2)˚. This directional bonding of nearly 90˚ for the $[PCO]^-$ ligand immediately hints that the p orbital on phosphorus is significantly involved in the bond to the tungsten centre. This is in agreement with the rhenium structure reported by Peruzzini and Grützmacher, where the remaining lone pair on phosphorus was calculated to have very high s orbital character (68%) by DFT.[8] All of the ECX moieties themselves remain linear after binding, with only minor deviations from 180˚ for the E1–C1–X1 bond angles, as expected.

There are several different resonance structures that could be used to describe the bonding of the ECX moieties within the tungsten pentacarbonyl complexes (Figure 2.11). For **2**, **3** and **4**, which contain the $[ECX]^-$ ligand bound exclusively through the pnictogen atom, only resonances **A** and **B** are relevant.

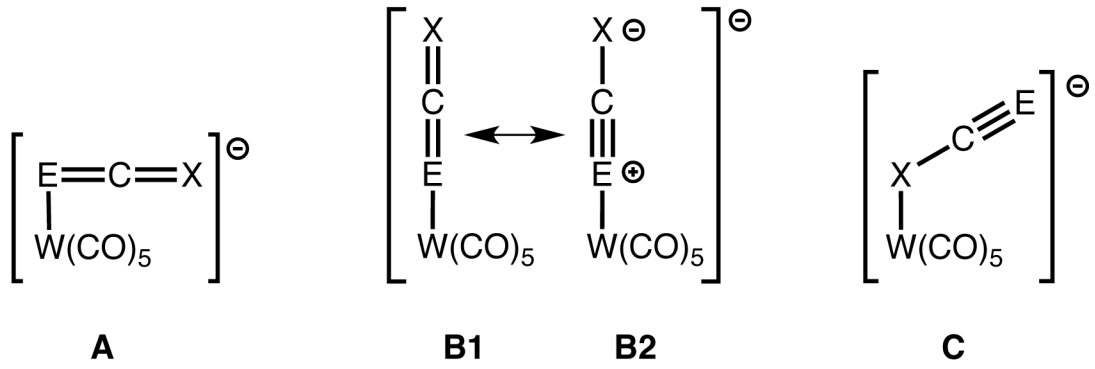

Figure 2.11: Resonance structures for $[ECX]^-$ ligands bound to the $W(CO)_5$ moiety.

The P1–C1 bond length increases from 1.579(3) Å in free [K(18-crown-6)][**1**] to 1.616(4) Å in the coordinated complex [K(2,2,2-crypt)][**2**]. The corresponding C1–O1 bond length decreases from 1.212(4) Å to 1.176(5) Å upon coordination. These bond lengths are consistent with **2** resembling a metallaphosphaketene, **A**, with a formal P=C=O moiety. In contrast, the coordinated cyanate anion in [K(2,2,2-crypt)][**3**] has a markedly longer C1–O1 bond length of 1.221(4) Å and a short N1–C1 bond length of 1.156(4) Å. For reference, the values for the "free" cyanate anion are 1.219(5) Å and 1.128(5) Å, respectively, in $[NMe_4][OCN]$.[35] This is more consistent with **3** having a significant contribution from the zwitterionic structure, **B2**. This can be rationalised by the fact that the multiple bonding between N and C is more favourable than between P and C, based on the more efficient overlap of the p orbitals. These data are in line with the previously mentioned rhenium structures.[8] The N1–C1 bond length within the thiocyanate complex **4** (1.157(4) Å) is statistically similar to those in the cyanate complexes, and thus **B2** seems an apt description of the bonding within this system as well.

The data for the $[K(18\text{-crown-6})]^+$ and $[K(2,2,2\text{-crypt})]^+$ salts of **3** are very similar; in fact the only statistically significant difference between the two salts is the interaction of the anion with the potassium cation. In the former, the two faces of the $[K(18\text{-crown-6})]^+$ ring allow close electrostatic interactions of the potassium with both the O1 of the cyanate moiety and the O2 atom of the *trans* carbonyl group on a neighbouring anion, giving chains of alternating anions and cations throughout the crystal structure. For the $[K(2,2,2\text{-crypt})]^+$ salt, however, the potassium is encapsulated to a much higher degree, and the inherent strain that must be overcome to splay open the 2,2,2-crypt moiety explains the longer K1–O1 contact (3.080(2) Å versus 2.656(3) Å).

The fact that there is a K1–O1 contact in [K(2,2,2-crypt)][**3**] at all merits further consideration, especially considering there is no such interaction in [K(2,2,2-crypt)][**2**]. This may serve as further, albeit somewhat anecdotal, evidence that the resonance **B2** contributes to the bonding within the cyanate complex **3**. The increased negative charge localised on O1 in **B2** would lead to a greater electrostatic interaction with the potassium cation, and this is presumably sufficient to overcome the strain of opening the 2,2,2-crypt moiety. This could also explain the shorter K1–O1 contact (2.656(3) Å) relative to the K2–O2 bond length (2.756(3) Å, as the *trans* carbonyl moiety has a smaller negative charge associated with it, and a weaker ionic bond. For the phosphorus analogue, the resonance **A** for the anion **2** leads to the negative charge being more delocalised over the anion, and less negative charge associated with O1, and thus the interaction with K1 is less favourable and insufficient to open the 2,2,2-crypt.

The W1–P1 bond length in [K(2,2,2-crypt)][**2**] is remarkably long at 2.666(1) Å. For comparison, a search of the Cambridge Structural Database (CSD) for tungsten pentacarbonyl fragments bearing a phosphorus-bound ligand returned a mean W–P bond length of only 2.513 Å.[36] In fact, our value is only slightly shorter than the maximum value

of 2.686(4) Å, found in the tris(*tert*-butyl)phosphine tungsten pentacarbonyl complex, $[W(CO)_5(P^tBu_3)]$.[37] In this latter complex, the long bond length primarily arises from the large steric bulk of the phosphine, which has a Tolman cone angle of 182±2°.[38] In the anion of **2**, however, the steric constraints are relatively insignificant. In this case the long bond length can be attributed to the fact that the bonding is predominantly p orbital based.

2.3.2.3 Comparison of $W(CO)_5$ moieties

The *trans* influence, also known as the structural *trans* effect, is a ground state phenomenon defined as the ability of a ligand L within the linear fragment L–M–L′ to weaken the M–L′ bond.[39] This is not to be confused with the kinetic *trans* effect, which is concerned with the labilisation of the M–L′ bond, and describes the enhancement of the rate of substitution of L′ caused by L.[40] The *trans* influence is most commonly assessed in terms of the length of the metal–ligand bond *trans* to the ligand in question, as derived from crystallographic data. The bond metric data relevant to this discussion are shown in Table 2.4.

Table 2.4: Selected crystallographic bond lengths (Å) related to the $W(CO)_5$ moiety.

	[K(2,2,2-crypt)] [**2**]	[K(18-crown-6)] [**3**]	[K(2,2,2-crypt)] [**3**]	[K(18-crown-6)] [**4**]
W1–C_{trans}[a]	1.969(3)	1.960(3)	1.969(3)	1.966(3)
C–O_{trans}[b]	1.161(4)	1.164(4)	1.155(3)	1.147(5)
W1–C_{cis}[c]	2.057(av)	2.047(av)	2.044(av)	2.046(av)
C–O_{cis}[d]	1.123(av)	1.138(av)	1.140(av)	1.137(av)

[a] W1–C2. [b] C2–O2. [c] Average (av) of W1–C3, W1–C4, W1–C5 and W1–C6. [d] Average (av) of C3–O3, C4–O4, C5–O5 and C6–O6.

The W1–C_{trans} bond length, that is, the bond length *trans* to the ECX moiety, is identical in [K(2,2,2-crypt)][**2**] and [K(2,2,2-crypt)][**3**] at 1.969(3) Å, and within statistical error of the other two complexes. This suggests that the three $[ECX]^-$ ligands have very similar electronic properties; however, these experimental data only give an indication of the net electronic effect, and do not offer insight into the relative weighting of the σ and π effects.

This will be probed later in the chapter. In all cases, the W1–C_{cis} bonds are considerably longer than the W1–C_{trans} bonds, which implies that the $[ECX]^-$ ligands exert a weaker *trans* influence than the CO ligands, as expected.

2.3.3 NMR spectroscopic studies

The $^{13}C\{^1H\}$ NMR spectra for the anions **2**, **3** and **4** all have distinctive resonances attributable to the central C1 carbon atom in the ECX moiety and for the carbonyl groups of the $W(CO)_5$ moiety. The latter in particular is the source of useful information regarding the ligand properties. The identity of the counter-cation, $[K(18\text{-crown-6})]^+$ or $[K(2,2,2\text{-crypt})]^+$, seems largely irrelevant, and so only the former will be discussed, although the relevant data for all species can be found in the Experimental section in Chapter 8. The discussion will start with an analysis of the ^{31}P NMR spectrum of **2**.

2.3.3.1 The ECX moieties

The ^{31}P NMR spectrum of the 2-phosphaethynolate coordination complex, [K(18-crown-6)][**2**], reveals a singlet at δ = –439.3 ppm in d_8-THF, with satellite resonances corresponding to coupling to the ^{183}W nucleus (14.3% abundant, I = ½) (Figure 2.12). This represents an upfield shift of approximately 44 ppm for the $[PCO]^-$ ligand upon coordination to the tungsten centre, relative to the free anion within [K(18-crown-6)][**1**]. The most striking feature of the ^{31}P NMR spectrum of the anion **2** is the magnitude of the ^{183}W satellites, with a one-bond coupling to phosphorus of only 51.9 Hz. Typical $^1J_{P–W}$ coupling constants are significantly larger, and are commonly of the order of 250 Hz. For example, the $[W(CO)_5(P^tBu_3)]$ complex mentioned above has a larger $^1J_{P–W}$ of 228.5 Hz, despite containing a longer P–W bond.[37,41]

The magnitude of a spin–spin coupling constant across one bond is dominated by the Fermi-contact term, which is itself largely dependent on the s character of the bonding hybrids. This is because only s orbitals have a non-zero probability of having electron

density at the nucleus. The low value of the coupling constant in **2** is diagnostic of a bond with little s orbital character, and is therefore a manifestation of the bonding originating largely from a p orbital on phosphorus. Following this argument, a low $^{1}J_{P-W}$ can be perceived as a simple spectroscopic indicator of the side-on bonding mode exhibited by the PCO moiety.

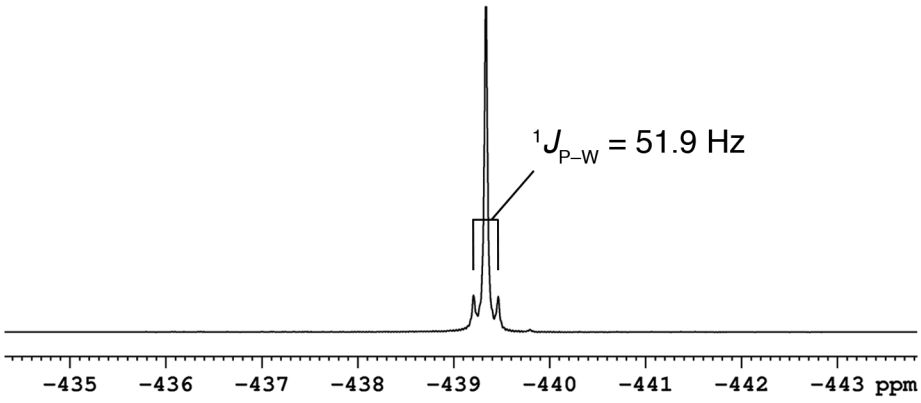

Figure 2.12: ^{31}P NMR spectrum of d_8-THF solution of [K(18-crown-6)][**2**].

The $^{13}C\{^{1}H\}$ NMR spectrum of [K(18-crown-6)][**2**] reveals a doublet at 173.0 ppm with a $^{1}J_{C-P}$ of 94.7 Hz that can be assigned as the carbon atom of the PCO moiety, alongside the tungsten carbonyl resonances that will be discussed shortly. Although it may be tempting to relate the larger coupling constant between carbon and phosphorus in **2** relative to the free anion **1** ($^{1}J_{C-P}$ = 62.0 Hz) to an increase in bond strength, this would go against the data obtained from single crystal X-ray diffraction showing a decrease in the P–C multiple bond character upon coordination. Instead, this can be rationalised by the observation that there is an increase in coupling between two atoms as electron density is removed from the system.[42] This trend can be seen by looking at the increase in $^{1}J_{C-H}$ values during the stepwise replacement of the protons within methane by more electronegative fluorine substituents ($^{1}J_{C-H}$ = 125 Hz (CH_4); 149 Hz (CH_3F); 185 Hz (CH_2F_2); 239 (CHF_3)).[43] Therefore, the larger $^{1}J_{C-P}$ in **2** over **1** can be simply correlated to the decrease in electron density on the phosphorus atom upon coordination to the metal centre.[44]

The $^{13}C\{^1H\}$ NMR spectrum obtained for [K(18-crown-6)][**3**] in d_8-THF shows a singlet resonance at 129.9 ppm attributable to the carbon of the NCO moiety, broadened by quadrupolar coupling to the adjacent ^{14}N nucleus (99.63% abundant, $I = 1$). The analogous NCS resonance in **4** is at 139.6 ppm. These values are consistent with previously reported N-bound cyanate and thiocyanate metal complexes, respectively.[45] At no point during any of the investigations was there any evidence that the $[PCO]^-$, $[NCO]^-$ or $[NCS]^-$ ligands were bound to the tungsten through the group 16 element; all reactions led to quantitative conversion (by NMR spectroscopy) to the pnictogen-bound products.

2.3.3.2 Comparison of $W(CO)_5$ moieties: Introduction

In addition to the crystallographic determination of bond lengths, the *trans* influence can be analysed using the $^{13}C\{^1H\}$ NMR spectroscopic data of the tungsten pentacarbonyl fragment within $[W(CO)_5(L)]$ complexes. Figure 2.13 shows the $^{13}C\{^1H\}$ NMR spectrum of [K(18-crown-6)][**2**], zoomed in to show the coupling within the tungsten carbonyl region. The magnitude of the $^2J_{C-P}$ coupling is larger for the *trans* carbonyl (9.4 Hz) than the *cis* carbonyls (3.7 Hz), as expected. The signs for the coupling constants (positive for *trans* and negative for *cis*) were derived from previously reported double resonance experiments.[46,47]

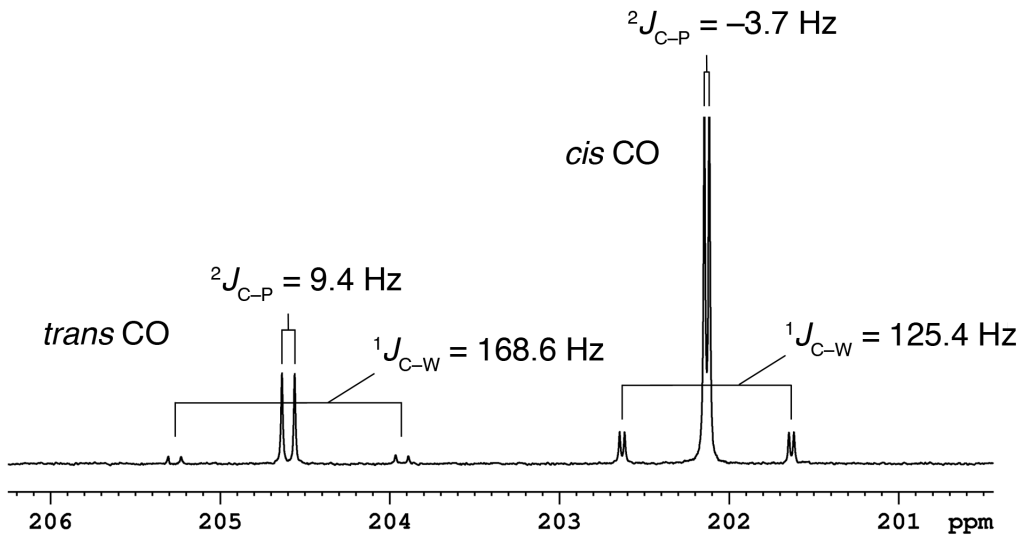

Figure 2.13: $^{13}C\{^1H\}$ NMR spectrum of d_8-THF solution of [K(18-crown-6)][**2**], zoomed in to the tungsten carbonyl region.

More pertinent to the discussion of ligand properties are the coupling constants and chemical shifts of the carbonyls within the tungsten pentacarbonyl fragment. This analysis was inspired by a previous study in 1984 by Buchner and Schenk, in which they compared a large range of mono-substituted tungsten pentacarbonyl complexes using $^{13}C\{^{1}H\}$ NMR data.[34] Table 2.5 shows the coupling constants between tungsten and the *cis* and *trans* carbonyls in the complexes **2**, **3** and **4** synthesised thus far in the chapter, and a few select examples for comparative purposes. The *cis* and *trans* labels are obviously meaningless for the last compound in the table, $[W(CO)_6]$.

Table 2.5: Chemical shifts (ppm) and coupling constants (Hz) derived from $^{13}C\{^{1}H\}$ NMR data of a range of mono-substituted tungsten pentacarbonyl complexes, $[W(CO)_5(L)]$.

		cis CO		*trans* CO	
L	Counter-cation	δ	$^{1}J_{C-W}$	δ	$^{1}J_{C-W}$
$[PCO]^{-}$[a]	$[K(18\text{-crown-6})]^{+}$	202.1	125.4	204.6	168.6
$[PCO]^{-}$[a]	$[K(2,2,2\text{-crypt})]^{+}$	202.2	125.5	204.6	167.8
$[NCO]^{-}$[a]	$[K(18\text{-crown-6})]^{+}$	199.6	127.8	201.7	146.5
$[NCO]^{-}$[a]	$[K(2,2,2\text{-crypt})]^{+}$	199.6	127.7	201.7	146.6
$[NCS]^{-}$[a]	$[K(18\text{-crown-6})]^{+}$	198.8	128.3	201.3	147.7
$[NCS]^{-}$[b]	$[NEt_4]^{+}$	197.5	128.7	201.1	150.0
$[CH_3]^{-}$[c]	$[NEt_4]^{+}$	206.9	124.7	209.1	149.2
PPh_3[b]	N.A.	197.2	125.7	199.0	140.0
$P(OPh)_3$[b]	N.A.	194.0	125.4	196.5	137.7
CO[d]	N.A.	191.0	124.5	191.0	124.5

[a] In d_8-THF (this work). [b] in $CDCl_3$.[34] [c] In CD_2Cl_2.[34] [d] In $CDCl_3$.[48]

The first point to note is how similar the data are for the different salts of a particular anion. The $[K(18\text{-crown-6})]^{+}$ and $[K(2,2,2\text{-crypt})]^{+}$ salts of **2** and **3** vary negligibly, and although the disparity between the $[K(18\text{-crown-6})]^{+}$ salt and the previously synthesised $[NEt_4]^{+}$ salt of **4** is slightly larger, this could also be explained by the change in solvent from d_8-THF to $CDCl_3$. The coupling constant data will be analysed presently, and the chemical shift data will be treated as a separate discussion thereafter.

2.3.3.3 Comparison of $W(CO)_5$ moieties: Coupling constants

The *trans* influence can be analysed by the magnitude of the $^1J_{C–W}$ coupling constant of the carbonyl *trans* to the ECX moiety: the higher this value, the weaker the *trans* influence of the $[ECX]^-$ ligand in question. The strong W–C bond, strengthened by the large π accepting ability of the CO ligand, makes it sensitive to variations in ligand properties, and is thus an ideal probe for this study.[49] This gives an indication of the σ donating ability of a ligand, at least to a first approximation.

If the $[ECX]^-$ ligand *trans* to a carbonyl ligand makes a lesser demand for the tungsten 6s orbital, then a rehybridisation will occur to increase the contribution from this orbital to the W–C_{trans} bond. Perturbation theory by Burdett and Albright has shown that the W–C_{trans} bond will be strengthened if there is an increase in the energy difference between the donor orbitals of the $[ECX]^-$ ligand and the tungsten acceptor orbital, or if there is a decrease in the overlap integral of the W–E bond.[49]

The *trans* coupling constant within [K(18-crown-6)][**2**] is 168.8 Hz, which is significantly higher than those for the two $[NCX]^-$ complexes. This implies that the $[PCO]^-$ ligand exerts a weaker *trans* influence, on account of being a poorer σ donor, than the two nitrogen-containing species. This is most likely another effect of the bonding being primarily through the p orbital on phosphorus, as other the phosphorus-bound ligands in Table 2.5, triphenylphosphine and triphenylphosphite, have significantly lower *trans* $^1J_{C–P}$ values (140.0 and 137.7 Hz, respectively) as they have a greater s contribution to the W–P bonding. Considering the ligands in Table 2.5, this gives a *trans* influence series of:

$$CO >> P(OPh)_3 > PPh_3 > [NCO]^- \approx [CH_3]^- \approx [NCS]^- >> [PCO]^-$$

It is worth noting that this order of ligands differs significantly if the series is instead measured using NMR data from Rh(I) and Pt(II) square planar complexes. For example, the $^1J_{Pt–P}$ data of a series of $[Pt(diphos)(Me)(L)]^{n+}$ complexes suggested that the $[CH_3]^-$ ligand

exerts a substantially larger *trans* influence than CO, in contrast with our order above. This can be rationalised by the fact that an anionic ligand, such as $[CH_3]^-$, will bind more strongly to a cationic Pt(II) fragment than to a neutral tungsten fragment. Furthermore, a strong π acceptor such as CO will bind more strongly to the relatively electron rich tungsten(0) centre, which will in turn increase the σ overlap integral and thus its *trans* influence. It is therefore difficult to completely deconvolute σ and π effects even in this study, but we can say with a degree of confidence that $[PCO]^-$ is a weaker σ donor than the $[NCX]^-$ ligands, certainly within tungsten pentacarbonyl derivatives.

The coupling constants to the *cis* carbonyl groups only vary to a small degree, and are not hugely informative when it comes probing ligand properties. The only point worth noting is that the value is broadly determined by the identity of the atom bonded to tungsten in the ligand in question. All of the N-bound ligands have *cis* $^1J_{C-W}$ values of approximately 128 Hz, whereas the P-bound ligands have slightly lower values of roughly 125 Hz. This is somewhat surprising considering the large fluctuations of the *trans* coupling constants within the phosphorus-containing ligands, for example the *trans* $^1J_{C-W}$ values for $[PCO]^-$ and $P(OPh)_3$ differ by over 30 Hz, but their *cis* coupling constants are identical at 125.4 Hz. This observation is consistent with the previous study by Buchner and Schenk.[34]

2.3.3.4 Comparison of $W(CO)_5$ moieties: Chemical shifts

The chemical shift of the $^{13}C\{^1H\}$ NMR resonances for the carbonyls can also be indicative of the bonding within these complexes, although it is important to consider that the identity of the solvent can have a profound effect on this metric. This factor notwithstanding, good π acceptor ligands will yield $^{13}C\{^1H\}$ NMR chemical shifts that resonate at high field for the carbonyl groups.[34,50] This can be seen by comparing the two extremes in Table 2.5. CO is well-known as a potent π acceptor, and $[W(CO)_6]$ has an accordingly low chemical shift of only 191.0 ppm, whereas the carbonyl chemical shifts are at 206.9 and 209.1 ppm in the

$[W(CO)_5(CH_3)]^-$ complex, as the $[CH_3]^-$ ligand is incapable of acting as a π acceptor. It also shows that triphenylphosphite is a better π acceptor than triphenylphosphine, as the electronegative substituents on the phosphorus on the former lower the energy of the σ* framework (which act as the π acceptor orbitals) and allow a better energy match with the filled d orbitals on tungsten.

By comparing the $[ECX]^-$ ligands then, it is clear that $[PCO]^-$ is a worse π acceptor than the $[NCO]^-$ and $[NCS]^-$ ligands, both of which are again comparable. This finding is in line with the previous results, as the side-on bonding mode of the PCO moiety necessarily means there are fewer antibonding orbitals of the correct symmetry to accept electron density from the tungsten centre. Furthermore, the long W–P bond means that even if these orbitals were accessible, the overlap integral would be relatively low.

By combining the various findings from this NMR spectroscopic study, we can infer that the $[PCO]^-$ ligand is simultaneously a poorer σ donor and a poorer π acceptor than the $[NCX]^-$ analogues. However, these contrasting properties imbue remarkably similar net electronic effects for the three $[ECX]^-$ ligands discussed thus far, which is manifest in the comparable $W–C_{trans}$ bond lengths and the IR spectra (*vide infra*) of their tungsten pentacarbonyl derivatives.

2.4 The 2-phosphathioethynolate anion, $[PCS]^-$

The study was extended to include the heavier group 16 analogue of **1**, the 2-phosphathioethynolate anion, $[PCS]^-$. This species was originally synthesised as the lithium salt by Becker in 1994.[51] One of the reported syntheses was the reaction of lithium bis(trimethyl)phosphide with *O*,*O*′-diethylthiocarbonate, by analogy with the initial preparation of $[PCO]^-$.[1] More interesting from our perspective was an alternative synthesis involving the direct reaction of $[PCO]^-$ with carbon disulfide to afford $[PCS]^-$ and OCS,

presumably via an undetected cyclic intermediate (Scheme 2.3). Both of these procedures required the mixing of reagents at –50 ˚C, and yielded sensitive, pale yellow crystals of $[Li(DME)_3][PCS]$. No reactivity on this anion has been reported since its initial preparation.

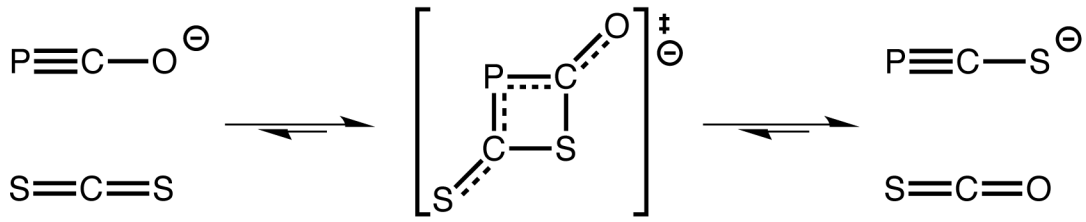

Scheme 2.3: Formation of $[PCS]^-$ via proposed cyclic intermediate.

2.4.1 Synthesis of [K(18-crown-6)][5] (5: $[PCS]^-$)

We reasoned that, by analogy with the recent formation of stable $[PCO]^-$ salts, the formation of an alkali metal salt of $[PCS]^-$ other than that of lithium would make the compound easier to handle and the anion more amenable to further study. As such, the change of cation from lithium to potassium, combined with a judicious choice of solvent, permitted the first ambient-temperature synthesis of the 2-phosphathioethynolate anion.[20]

[K(18-crown-6)][**1**] was dissolved in 1,2-dichlorobenzene (1,2-DCB) in an NMR tube, and one equivalent of CS_2 was added using a microsyringe. The yellow solution immediately turned orange, and ^{31}P NMR spectroscopy revealed a singlet resonance at δ = –118.0 ppm. This is indicative of the clean and quantitative formation of [K(18-crown-6)][**5**] (**5**: $[PCS]^-$), and is consistent with the previously reported lithium salt (δ = –121.3 ppm).[51] These solutions can be stored at room temperature for several weeks without any apparent decomposition.

The same reaction can be carried out in 1,2-difluorobenzene (1,2-DFB), and the solutions show clean formation of [K(18-crown-6)][**5**] by ^{31}P NMR spectroscopy. However, the solution slowly changes colour to a very dark red over the course of a few hours, so it is possible that there are unidentified redox processes involving the solvent occurring in

solution. The colour change aside, the 1,2-DFB solutions are also stable (by ^{31}P NMR spectroscopy) for several weeks, and can be used for further reactivity.

We believe that 1,2-DCB and 1,2-DFB are particularly effective solvents because they are highly polar yet relatively non-coordinating. By comparison, if the same reaction is carried out in THF under otherwise identical conditions, a copious amount of dark precipitate is produced, and only a very weak signal corresponding to **5** is observed in the ^{31}P NMR spectrum after a couple of hours.

2.4.2 Synthesis of [Na(18-crown-6)][5]

Following our report of the relatively facile synthesis of [K(18-crown-6)][**1**], the group of Grützmacher published an altered version of one of their previous synthetic procedures, which permitted the isolation of [Na(1,4-dioxane)*x*][PCO] ($1 < x < 3$) on a much larger scale.[15] The exact value of x depends on how long the product is kept under dynamic vacuum during the final step of its synthesis, but can be readily determined by integrating the inverse gated ^{31}P{^{1}H} NMR spectrum (acquired with a long T_1 relaxation time) against a known quantity of triphenylphosphine. We were therefore interested in exploring whether this product could undergo a similar reaction with carbon disulfide to that described above to yield the first sodium salt of **5**.

The [Na(1,4-dioxane)$_{2.69}$][**1**] starting material was weighed into an NMR tube, as before, and 1,2-DCB was added. In this case however, the starting material is completely insoluble in 1,2-DCB, as evidenced by the undissolved solid in the NMR tube and the silent ^{31}P NMR spectrum. This is presumably due to the stable three-dimensional network of octahedrally coordinated Na^+ cations bridged by 1,4-dioxane units, as described previously.[7] Unsurprisingly, therefore, no reaction is observed at all on addition of the CS_2. However, the addition of one equivalent of 18-crown-6 to the reaction mixture leads to the immediate darkening of the solution, and the formation of **5** by ^{31}P NMR spectroscopy, as indicated by

the presence of a singlet at δ = –119.4 ppm. The 18-crown-6 solubilises the starting material by sequestering the sodium cations and breaking apart the three-dimensional extended network, leading to reactivity that mirrors that seen for the potassium cation previously (Scheme 2.4).

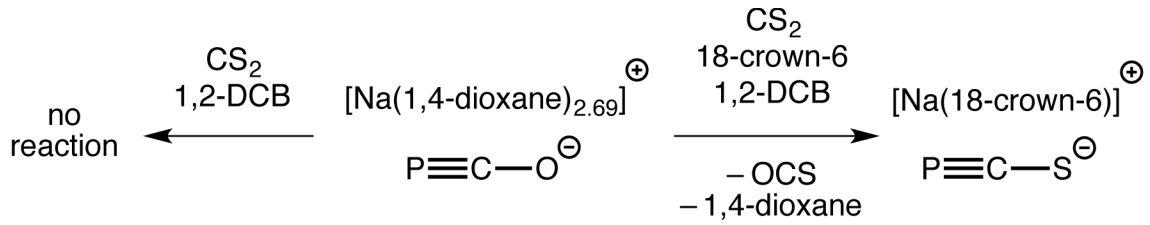

Scheme 2.4: Formation of [Na(18-crown-6)][**5**], highlighting the importance of the sequestering agent.

2.4.3 Characterisation of [K(18-crown-6)][5] and [Na(18-crown-6)][5]

Pale yellow needles of [K(18-crown-6)][**5**] suitable for single crystal X-ray diffraction were obtained by slow diffusion of hexane into a 1,2-DFB solution of the product (Figure 2.14). The structure revealed a linear triatomic anion with close electrostatic interactions to neighbouring $[K(18\text{-crown-6})]^+$ cations through the P1 and S1′ atoms, leading to similar one-dimensional coordination polymers as observed for [K(18-crown-6)][**1**]. However, crystallographic disorder renders the P1 and S1′ atoms indistinguishable, as C1 sits atop an inversion centre. This is a manifestation of the comparable P–C and C–S bond lengths, and the fact that phosphorus and sulfur have similar X-ray scattering factors, on account of being adjacent in the periodic table. This disorder prevents a meaningful discussion of the bond metric data within the anionic moiety.

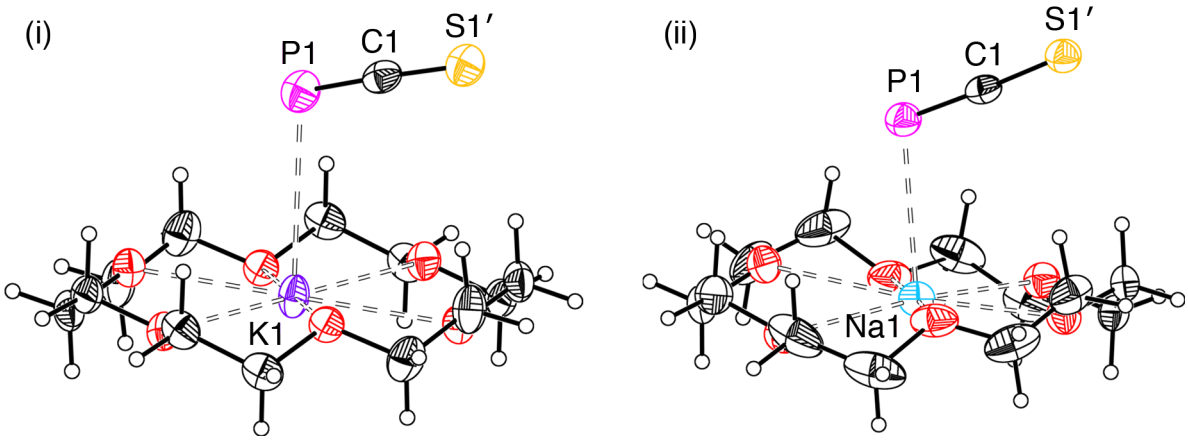

Figure 2.14: Molecular structures of: (i) [K(18-crown-6)][**5**] and (ii) [Na(18-crown-6)][**5**]. Anisotropic displacement ellipsoids are set at 50% probability. Hydrogen atoms are shown as spheres of arbitrary radii. Symmetry element in: (i) ′: 1–*x*, 1–*y*, 1–*z*; (ii) ′: –*x*, –*y*, 1–*z*.

Pale yellow plates of [Na(18-crown-6)][**5**] were obtained by slow diffusion of hexane into a 1,2-DCB solution of the product (Figure 2.14). The structure is very similar to the potassium salt, as expected. There is an analogous P/S disorder preventing bond metric analysis, and once again there are chains of anions and cations, albeit with a slightly different packing motif to that seen in [K(18-crown-6)][**5**]. The only real, although relatively inconsequential, difference is the interaction of the cation with the sequestering agent. The cavity of the 18-crown-6 is well-known to be ideally sized for a potassium cation, and as such the K–O interactions in [K(18-crown-6)][**5**] are within a small range (2.776(1) – 2.821(1) Å) as the cation is approximately situated in the centre of the ring. In [Na(18-crown-6)][**5**], however, the 18-crown-6 ring has to distort slightly to accommodate the smaller sodium cation, and there is a larger discrepancy between Na–O distances (2.683(2) – 2.783(2) Å).

For consistency with the previously discussed $[ECX]^-$ anions and their complexes, the remainder of the characterisation and subsequent discussion of ligand properties will focus solely on the $[K(18\text{-crown-6})]^+$ salt of **5**. The ^{31}P NMR resonance for **5** has been mentioned in passing (δ = –118.0 ppm), and the spectrum is shown in Figure 2.15.

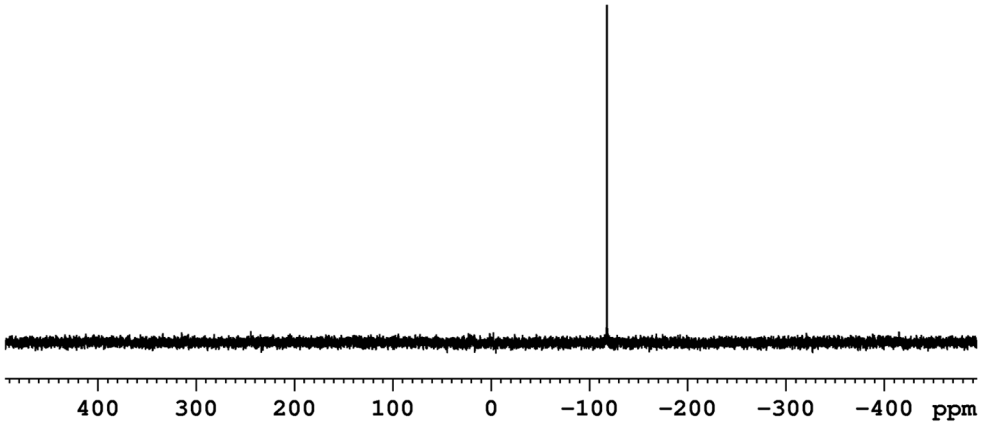

Figure 2.15: ^{31}P NMR spectrum of d_4-1,2-DCB solution of [K(18-crown-6)][**5**].

This chemical shift is remarkably different to that for **1**, despite the similar structure of the two anions. The ^{31}P NMR chemical shifts and the $^{1}J_{C-P}$ coupling constants, measured from the $^{13}C\{^{1}H\}$ NMR spectra, of the anions **1** and **5** are shown in Figure 2.16, along with the data for the di(isopropyl)aminophosphaalkyne.[52,53]

	$P\equiv C-O^{\ominus}$	$P\equiv C-S^{\ominus}$	$P\equiv C-N(^{i}Pr)_2$
$\delta(^{31}P)$ (ppm):	–396.8	–118.0	–99.6
$^{1}J_{C-P}$ (Hz):	62.0	20.7	14.7

Figure 2.16: Comparison of NMR spectroscopic parameters for $[PCO]^-$ (in d_8-THF), $[PCS]^-$ (in d_4-1,2-DCB) and $PCN(^{i}Pr)_2$ (in $CDCl_3$). Data for the latter taken from Grobe at al.[52]

The resonance structures shown in Figure 2.16 are those containing a formal P≡C triple bond (**β** in Figure 2.5), though there are also contributions from the resonance with a formal P=C double bond and the negative charge on the phosphorus atom. This second resonance structure has a reasonable contribution for $[PCO]^-$ (40.2% from the previously discussed calculations), and leads to an upfield chemical shift in the ^{31}P NMR spectrum (–396.8 ppm). The phosphaalkyne, $PCN(^{i}Pr)_2$, although stabilised by the delocalisation of the nitrogen lone pair into the P–C π* orbitals, has a greater contribution from the resonance structure shown, and as such has a downfield shifted ^{31}P chemical shift (–99.6 ppm). On comparison

of the data, it is clear that $[PCS]^-$ more closely resembles the phosphaalkyne than $[PCO]^-$, and has a greater contribution from the resonance shown in Figure 2.16 with a formal P≡C triple bond. Thus, although the disorder in the crystal structures containing **5** prevents a direct comparison of the P–C bond lengths with **1**, the spectroscopic data suggest the P–C bond length is shorter in **5**. This is corroborated by the DFT calculations that will be discussed later. This is also the predicted result based on the weightings of the resonance structures; the $[P=C=O]^-$ phosphaketene resonance structure is going to be more favourable than the $[P=C=S]^-$ analogue due to the better overlap of the 2p–2p orbitals between carbon and oxygen in the former than the 2p–3p orbitals between carbon and sulfur.

The $^1J_{C-P}$ coupling constants are also very similar for $[PCS]^-$ and $PCN(^iPr)_2$, both of which are significantly smaller than the value in $[PCO]^-$. As with the earlier discussion, these data go against the bond strength arguments, where you might expect the shorter bond to have a larger one-bond coupling constant. Instead, this can be explained once again by the electronegativity of the substituent; oxygen is more electronegative than sulfur and nitrogen, and therefore removes more electron density from the P–C system, leading to a larger coupling constant.[44]

2.5 Ligand properties of the 2-phosphathioethynolate anion

We sought to explore the ligand properties of the 2-phosphathioethynolate anion in an analogous manner to the previously discussed $[ECX]^-$ ligands. The reaction of $[W(CO)_5(MeCN)]$ with a 1,2-DFB solution of [K(18-crown-6)][**5**] led to a darkening of the solution, and ^{31}P NMR spectroscopy revealed a mixture of products, as well as unreacted starting material after several days (Figure 2.17).

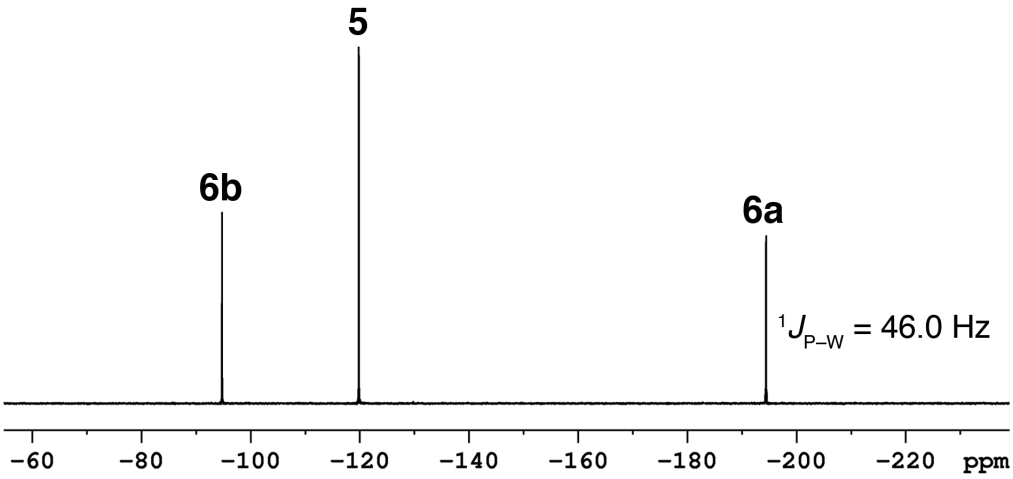

Figure 2.17: ^{31}P NMR spectrum of 1,2-DFB solution of [W(CO)$_5$(MeCN)] and [K(18-crown-6)][**5**], showing concomitant formation of two distinct products, **6a** and **6b**.

The two resonances at –192.6 ppm and –92.9 ppm have been attributed to the phosphorus-bound (**6a**) and sulfur-bound (**6b**) [W(CO)$_5$(PCS)]$^-$ complexes, respectively (Figure 2.18). These are readily distinguishable by the presence of ^{183}W tungsten satellites on the former only. This suggests that, unlike the previous [ECX]$^-$ ligands, **5** can act as an ambidentate ligand, and this will be explored in more detail later. The chemical shifts are also consistent with this assignment; the phosphorus-bound **6a** is upfield relative to free **5**, as with [PCO]$^-$ in **2** relative to **1**, and the downfield shift of **6b** is consistent with another X-bound [PCX]$^-$ complex that will be discussed at the end of the chapter.

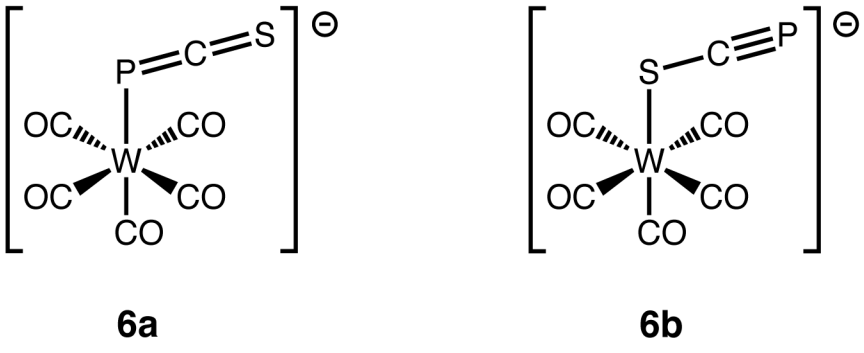

6a **6b**

Figure 2.18: Structures of P-bound and S-bound [(W(CO)$_5$(PCS)]$^-$, **6a** and **6b**.

The value of the $^1J_{P-W}$ coupling constant for **6a** of 46.0 Hz is very low, and of the same magnitude as that found in **2**. By analogy with the PCO moiety, this is good spectroscopic

evidence that the $[PCS]^-$ anion is bound in a side-on manner, predominantly through a p orbital.

Crystals suitable for single crystal X-ray diffraction were grown by slow diffusion of hexane into a 1,2-DFB solution of the reaction mixture containing **5**, **6a** and **6b**. Unfortunately, extensive crystallographic disorder makes the unambiguous assignment of the product challenging, and an analysis of the bond metric data meaningless. The structure certainly contains a PCS moiety coordinated in a bent manner to a tungsten pentacarbonyl centre, and the complex is mono-anionic due to the presence of a $[K(18\text{-crown-6})]^+$ counter-cation, as expected. However, the nature of the coordination to the tungsten centre, i.e. whether the ligand is bound through the phosphorus (**6a**) or the sulfur (**6b**), or indeed a disordered combination of the two, is non-trivial. The final solution has been modelled as sulfur-bound (Figure 2.19), as this gave the lowest R1(all data) value of 2.29%. It is important to note that modelling the structure as phosphorus-bound results in only a small increase of the residual electron density (R1(all data) is 2.36%).

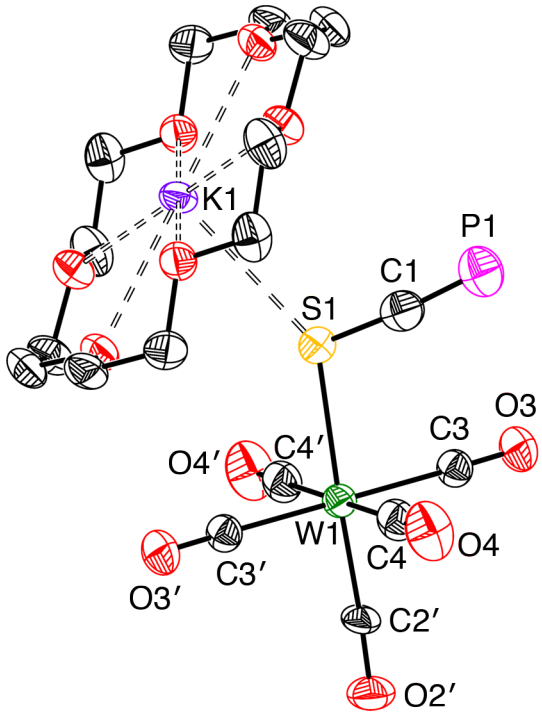

Figure 2.19: Molecular structure of [K(18-crown-6)][**6b**]. Anisotropic displacement ellipsoids are set at 50% probability. Hydrogen atoms omitted for clarity. Symmetry element ′: 1–*x*, –*y*, 1–*z*.

Both **6a** and **6b** are unstable in 1,2-DCB at room temperature over the course of approximately four days, as monitored by ^{31}P NMR spectroscopy. In addition, the displacement of the acetonitrile ligand with [PCS]$^-$ was very slow, as evidenced by the prolonged presence of free **5** in solution, in contrast with the other [ECX]$^-$ ligands, which reacted very quickly. Extensive attempts were made to vary the reaction conditions to improve this reaction. Carrying out the reactions at low temperatures was not a viable option, as this further retarded the already slow coordination of **5**. A range of other tungsten pentacarbonyl precursors were explored, but there was no improvement on the [W(CO)$_5$(MeCN)] used initially. Likewise, photolysis of tungsten hexacarbonyl in the presence of **5** appeared to increase the rate of decomposition. The experiments were further limited by the necessity to use non-coordinating solvents, as this ruled out common precursors such as [W(CO)$_5$(THF)].

These factors meant it was not possible to obtain a compositionally pure sample of either **6a** or **6b**. As such, the detailed experimental exploration of the ligand properties of **5** in an analogous manner to those reported in this chapter so far was not possible. Therefore, a comprehensive computational comparison of all of the [ECX]$^-$ ligands was carried out, with the aim of corroborating the experimental findings so far and further exploring the properties of **5**.

2.6 Computational studies on [ECX]$^-$ ligands

All of the [ECX]$^-$ anions and their complexes with the W(CO)$_5$ moiety were studied computationally using the B3LYP hybrid functional. Figure 2.20 shows: (i) the free [ECX]$^-$ anions; (ii) the E-coordinated [W(CO)$_5$(ECX)]$^-$ complexes; (iii) the X-coordinated [W(CO)$_5$(ECX)]$^-$ complexes; and (iv) the [W(CO)$_5$(PCX)]$^-$ complexes constrained to C_{4v} geometry to model the end-on bonding. Solvent interactions were treated implicitly using a

polarisable continuum model, and were modelled as THF in all cases for consistency. Figure 2.20 shows the optimised geometries of the anions, as determined by the lack of imaginary frequencies during a vibrational analysis, except for the C_{4v}-constrained geometries (iv), each of which displayed two imaginary frequencies (*vide infra*). Several trends emerge from this data that are worth discussing.

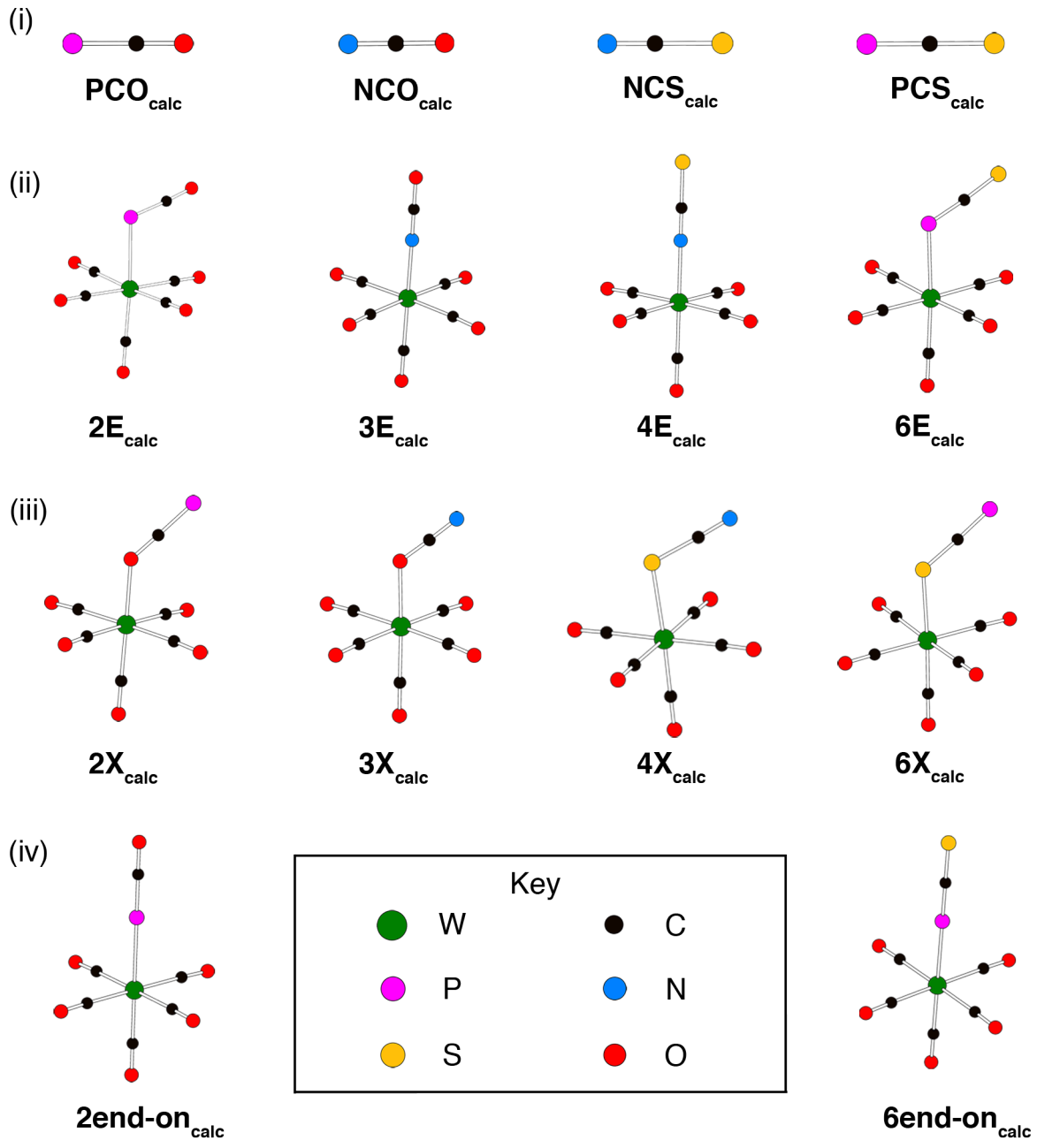

Figure 2.20: Calculated structures of: (i) free $[ECX]^-$ ligands; (ii) E-coordinated $[W(CO)_5(ECX)]^-$ complexes; (iii) X-coordinated $[W(CO)_5(ECX)]^-$ complexes; (iv) $[W(CO)_5(PCX)]^-$ complexes constrained to C_{4v} geometry. Computational details are in text.

2.6.1 Changes to ECX moiety on coordination

The optimised structures and the derived metric data are a good match to the experimentally determined crystallographic data where a comparison was possible. For example, the W–C_{trans} bond lengths for the four E-bound complexes (shown in (ii)) are all within a very small range 1.988–1.998 Å, reinforcing the notion of the similar net electronic effects of the $[ECX]^-$ ligands. Selected bond metrics relating to the ECX moiety for the experimentally relevant anions are shown in Table 2.6.

Table 2.6: Selected computed bond lengths (Å) and angles (˚) for free and coordinated $[ECX]^-$ ligands.

	E–C	C–X	W–E(X)–C[a]
PCO_{calc}	1.622	1.200	
$2E_{calc}$	1.643	1.177	99.4
NCO_{calc}	1.193	1.223	
$3E_{calc}$	1.179	1.207	179.2
NCS_{calc}	1.179	1.658	
$4E_{calc}$	1.169	1.637	179.7
PCS_{calc}	1.594	1.631	
$6E_{calc}$	1.618	1.595	104.0
$6X_{calc}$	1.575	1.653	110.0

[a] The bond angle W–X–C refers to **$6X_{calc}$** only.

The computed structures show that the P–C bond is indeed shorter in free $[PCS]^-$ (1.594 Å) than in free $[PCO]^-$ (1.622 Å), as predicted from the spectroscopic data previously. For both $[PCX]^-$ ligands, phosphorus coordination leads to a lengthening of the P–C bond and a shortening of the C–X bond relative to the free anion. This is consistent with the proposed $[W–P=C=X]^-$ metallaphosphaketene resonance structure (**A** in Figure 2.11).

Nitrogen coordination for the $[NCX]^-$ ligands leads to a slight shortening of the N–C bond and a larger contraction of the C–X bond. This is consistent with the $[W–N=C=X]^-$ resonance (**B1**), although there is certainly some contribution from the zwitterionic

$[W–N^{+}\equiv C–X^{-}]^{-}$ form (**B2**). These data vary slightly from the crystallographic bond metric data for the coordinated $[NCX]^{-}$ complexes, **3** and **4**. In both cases, the crystallographic N–C bond lengths are shorter than their computational analogues, and the C–X bonds are longer. This suggests that the crystallographic structures have a greater contribution from resonance **B2**. This is presumably because the formal negative charge on the X atom can be stabilised by electrostatic interactions with the localized K^{+} cation in the crystal structure, and these interactions are not present in the computationally derived model.

When the PCS moiety is bound through the sulfur atom, the P–C bond shortens and the C–S bond lengthens relative to the free anion. This is consistent with resonance **C**, which contains a formal P≡C triple bond.

2.6.2 Linkage isomerism

Linkage isomerism describes coordination complexes with the same composition but differing connectivity between the ligand and the metal centre. Thiocyanate is a prototypical example of an ambidentate ligand, and is able to bind through the S or N atoms depending on the nature of the metal in question. The ambidenticity of the $[PCO]^{-}$ nucleophile with triorganyl compounds of heavier group 14 elements was probed in a spectroscopic and computational study by the group of Grützmacher in 2014.[54] For example, in the case of the reaction of $[PCO]^{-}$ with $(^{i}Pr)_3SiOTf$, they found that the O-bound species was the kinetic product, but this rearranged to exclusively yield the thermodynamic P-bound product on gentle heating (Scheme 2.5).

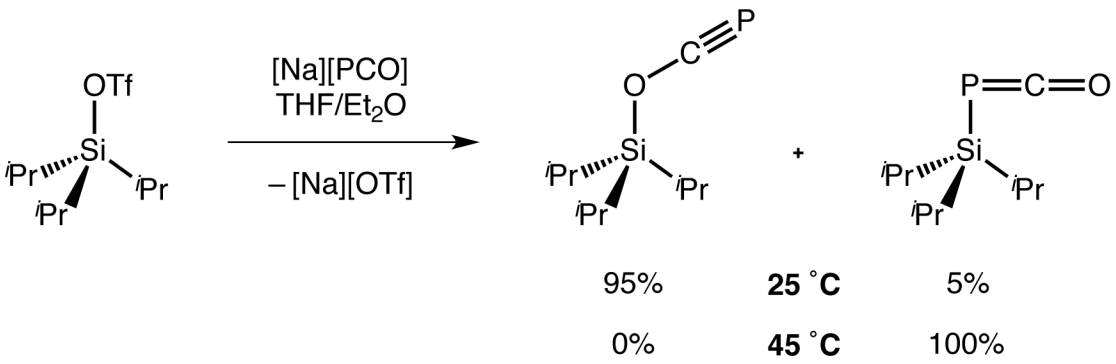

Scheme 2.5: Reaction of $(^{i}Pr)_3SiOTf$ with [Na][PCO].[54]

We computationally probed the possible ambidentate nature of the $[ECX]^-$ ligands within our $[W(CO)_5(ECX)]^-$ complexes, albeit only from a thermodynamic viewpoint. This was achieved by calculating $\Delta E_{linkage}$, which is defined as:

$$\Delta E_{linkage} = E(\text{X-bound}) - E(\text{E-bound})$$

For example, to assess the ambidentate nature of $[PCO]^-$, the difference in energy would be given by (using the notation from Figure 2.20):

$$\Delta E_{linkage}(PCO) = E(\mathbf{2X_{calc}}) - E(\mathbf{2E_{calc}})$$

This value has been calculated for all four $[ECX]^-$ ligands (Table 2.7).

Table 2.7: The difference in energy (in kJ mol^{-1}) between X-bound and E-bound $[ECX]^-$ ligands within $[W(CO)_5(ECX)]^-$, as defined above.

	$\Delta E_{linkage}$
$[PCO]^-$	+47.5
$[NCO]^-$	+54.2
$[NCS]^-$	+31.4
$[PCS]^-$	+3.5

All of these values are positive, which means that all of the ligands preferentially bind through the pnictogen atom. The value for $[PCS]^-$ is very small, however, which implies that there is little preference for coordination through the P or S atom. These results tally perfectly with the experimental observations. There was no evidence during any of the

reactions for any X-bound complexes of $[PCO]^-$, $[NCO]^-$ or $[NCS]^-$, whereas the P-bound and S-bound complexes **6a** and **6b** are both formed in roughly equal quantities by ^{31}P NMR spectroscopy (Figure 2.17).

2.6.3 Side-on versus end-on coordination

The optimised geometries $\mathbf{2E_{calc}}$ and $\mathbf{6E_{calc}}$ both show the PCX moiety to be bound in a side-on manner, with W–P–C bond angles of 99.4˚ and 104.0˚, respectively. To probe the preference for this side-on bonding mode, the energies of the complexes were calculated with the PCX moiety moved to an end-on position and the optimisation constrained to a C_{4v} geometry ($\mathbf{2end\text{-}on_{calc}}$ and $\mathbf{6end\text{-}on_{calc}}$). The optimised geometries each gave two imaginary frequencies, which correspond to two symmetric relaxations to the side-on geometry. This is consistent with the rehybridisation of the phosphorus orbitals to afford the concomitant generation of a lone pair and loss of P–C multiple bond character. The difference in energy between the end-on and side-on binding modes for $[PCO]^-$ and $[PCS]^-$ were calculated as:

$$\Delta E_{\text{geometry}}(\text{PCO}) = E(\mathbf{2end\text{-}on_{calc}}) - E(\mathbf{2E_{calc}}) = +65.9 \text{ kJ mol}^{-1}$$

$$\Delta E_{\text{geometry}}(\text{PCS}) = E(\mathbf{6end\text{-}on_{calc}}) - E(\mathbf{6E_{calc}}) = +38.5 \text{ kJ mol}^{-1}$$

The fact that both values are positive once again shows that the side-on geometry is more thermodynamically favoured, and not merely an effect of crystal packing. The larger $\Delta E_{\text{geometry}}$ for $[PCO]^-$ relative to $[PCS]^-$ shows the former has a greater preference to be bound in a side-on manner, which could also explain why the W–P–C bond angle is slightly smaller in $\mathbf{2E_{calc}}$ (99.4˚) than in $\mathbf{6E_{calc}}$ (104.0˚). This can be rationalised by considering that the side-on bonding mode has a smaller degree of P–C multiple bonding but a larger amount of C–X multiple bonding character relative to the end-on mode, and this C–X multiple bond is less favoured for the PCS moiety than the PCO moiety due to the poorer overlap of the orbitals involved.

2.6.4 Stretching frequency analysis and comparison to IR data

The tungsten pentacarbonyl moiety is an ideal fragment for the assessment of ligand properties using IR spectroscopy. $[W(CO)_5(PR_3)]$ complexes have been extensively used to study the bonding nature of phosphines as a safer alternative to those derived from the toxic $[Ni(CO)_4]$ used by Tolman in his seminal studies.[38,55] The C–O stretching frequencies of the E-bound $[W(CO)_5(ECX)]^-$ complexes have been calculated and compared to the experimental data derived from IR spectroscopy of Nujol mulls of the $[K(18\text{-crown-6})]^+$ salts of **2**, **3** and **4** (Table 2.8). The force constants for the *cis* and *trans* carbonyls have also been derived for both computational and experimental data using the methods and approximations described by Cotton and Kraihanzel.[56] Note *ab initio* harmonic vibrational frequencies are typically larger than the fundamentals obtained experimentally for a variety of reasons,[57] and no correction factors have been applied to these data, but a qualitative comparison of trends between the datasets is still poignant.

Table 2.8: Computed (above) and experimental (below, in italics) C–O stretching frequencies (cm^{-1}) for $W(CO)_5$ moiety within $[W(CO)_5(ECX)]^-$ complexes, and Cotton-Kraihanzel force constants (mdyne $Å^{-1}$).[56]

	$[PCO]^-$	$[NCO]^-$	$[NCS]^-$	$[PCS]^-$
$A_1^{(1)}$	2107	2115	2119	2108
	2047	*2064*	*2065*	
B_1	2000	2003	2010	2006
	1970	*1966*	*1980*	
E	1948	1946	1954	1954
	1917	*1902*	*1906*	
$A_1^{(2)}$	1895	1883	1900	1901
	1858	*1823*	*1851*	
k_1 (*trans*)	14.70	14.52	14.79	14.79
	14.09	*13.60*	*14.03*	
k_2 (*cis*)	16.13	16.15	16.25	16.20
	15.48	*15.41*	*15.46*	

The symmetry labels in Table 2.8 are strictly for $[W(CO)_5(L)]$ structures with C_{4v} symmetry, in which case the B_1 band would not be visible at all in the IR spectrum. In all cases this symmetry is slightly relaxed, although the end-on $[NCX]^-$ complexes are very close. The side-on bonding mode of the $[PCX]^-$ ligands means that they both have C_s symmetry, which lifts the degeneracy of the E band, but the separation is less than 2 cm^{-1}, so an average value is given. The symmetry of the experimental structures is further lowered by the interaction of the $[K(18\text{-crown-6})]^+$ cation with the anion, so the $[W(CO)_5(ECX)]^-$ complexes can never truly be considered in isolation. However, all of the anions correspond to pseudo-C_{4v} symmetry, and have been treated as such in this analysis.

The data in Table 2.8 reveal that all of the $[ECX]^-$ ligands exert comparable effects on the $W(CO)_5$ moiety, despite the significant variations in the binding modes of the ligands. This is exemplified in the values for the $A_1^{(1)}$ band (the symmetric "breathing" mode of the $W(CO)_5$ unit), which is often taken as an indicator to assess the degree of back-bonding into the σ* antibonding orbitals of the carbonyls. This varies by no more than 12 cm^{-1} between the four complexes. The *cis* carbonyl force constants are also very similar across the four complexes, suggesting a comparable net electron density on the tungsten centre.

The *trans* force constant for $[NCO]^-$ is slightly smaller than the other ligands, which possibly corroborates the previous NMR spectroscopic finding that the $[NCO]^-$ ligand exerts a greater *trans* influence than $[PCO]^-$. Caution has to be taken against overanalysing these data, however, as the differences are relatively small. In fact, the k_1 (*trans*) values for the $[NCS]^-$ and $[PCO]^-$ complexes are very similar, whereas the NMR data suggested the NCS moiety would exert a greater *trans* influence. The overarching conclusion from the vibrational study is that the ligands exert comparable net electronic effects on the $W(CO)_5$ moiety, in agreement with the assessment of the aforementioned rhenium complexes.

2.7 Coordination of $[PCO]^-$, $[NCO]^-$ and $[NCS]^-$ to actinides

Having thoroughly explored the properties of the $[ECX]^-$ ligands towards the $W(CO)_5$ fragment both experimentally and computationally, we wanted to determine the behaviour of these ligands within a very different environment. Thus, in a collaboration with the groups of Laurent Maron and John Arnold, the novel tris(amidinate) thorium and uranium complexes of 2-phosphaethynolate, cyanate and thiocyanate were synthesised. The specialised work of synthesising and handling the actinide complexes was carried out by our collaborators, and as such these compounds are not included in the Experimental section of Chapter 8, but full experimental details and supplementary data can be found in the published article.[19]

2.7.1 Synthesis of thorium and uranium complexes

The salt metathesis of the $[An(amid)_3(Cl)]$ precursors (An = Th, U; amid = *N*,*N*′-bis(trimethylsilyl)benzamidinate) with $[Na(1,4\text{-dioxane})_{2.90}][PCO]$ yields the coordinated products $[An(amid)_3(OCP)]$ (An = Th: **Th-OCP**; An = U: **U-OCP**) as block-shaped crystals in 63% and 76% isolated yields, respectively (Scheme 2.6). The $[NCX]^-$ complexes were synthesised analogously using sodium cyanate and potassium thiocyanate to afford the **Th-NCO** (40%), **U-NCO** (63%), **Th-NCS** (65%) and **U-NCS** (80%) products in the isolated yields shown.

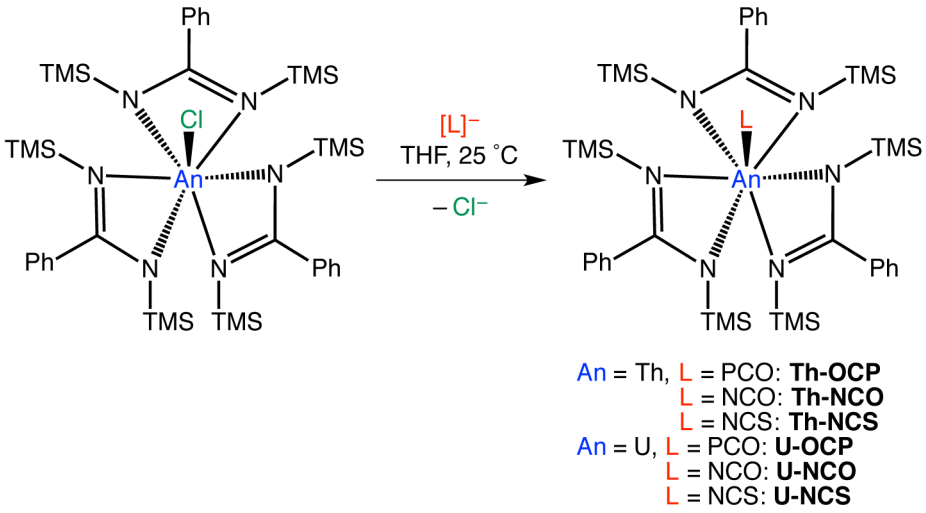

Scheme 2.6: Synthesis of [An(amid)$_3$(ECX)] complexes.

2.7.2 Characterisation of thorium and uranium complexes

The ^{1}H NMR spectra of all of the complexes were consistent with the C_3-symmetric propeller-like arrangement of the amidinate ligands, with the ECX moiety in the axial position. These geometries are confirmed by single crystal X-ray analyses of all six complexes; the solid-state structures of the three uranium species are shown in Figures 2.21 and 2.22. **Th-OCP** crystallised with two independent molecules in the asymmetric unit, one of which featured the PCO moiety disordered over two positions, so the discussion of bond metric data below is for the non-disordered molecule only.

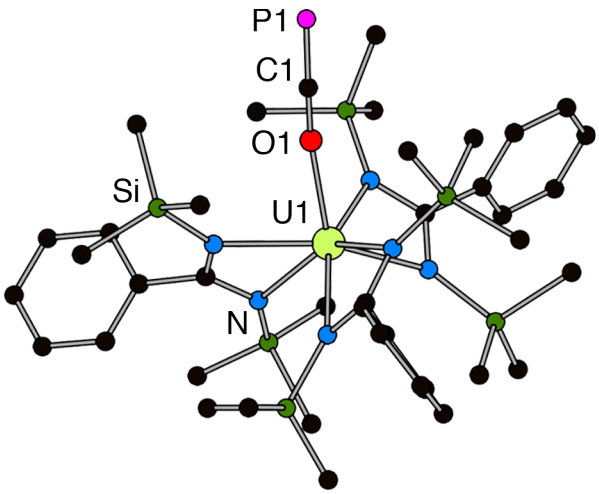

Figure 2.21: Ball and stick diagram of **U-OCP**. All protons are omitted for clarity.

The most striking feature of this series is the fact the $[PCO]^-$ ligand coordinates through the oxygen atom in both **Th-OCP** and **U-OCP**, with An–O1–C1 bond angles of 176.4(3)° and 170.9(3)°, respectively. The U1–O1 bond length in **U-OCP** (2.297(3) Å) is slightly shorter than the analogous Th–O bond length (2.318(2) Å), which is consistent with the slightly larger ionic radium of Th(IV).[58] The P1–C1 and C1–O1 bond lengths (1.576(5) Å and 1.219(6) Å in **U-OCP**; 1.561(4) Å and 1.246(4) Å in **Th-OCP**, respectively) are indicative of a P≡C triple bond and C–O single bond, consistent with An–O–C≡P moiety.

This resonance form is further corroborated by the IR spectroscopic data, as the **Th-OCP** and **U-OCP** compounds feature strong absorption bands at 1683 cm^{-1} and 1685 cm^{-1}, respectively. These values correlate to the C–O stretching vibration, and are lower than that found in [K(18-crown-6)][**1**] (1730 cm^{-1}), which indicates a weakening of the C–O bond on coordination to the actinide centre.

The ^{31}P NMR spectrum shows a downfield chemical shift for the **Th-OCP** at –334 ppm (in C_6D_6) relative to the free anion **1**. This is consistent with the downfield shift due to X-coordination of the PCS moiety in **6b**. The shift is even more pronounced in **U-OCP** due to the paramagnetic nature of the U(IV) centre ($\delta(^{31}P)$ = –285 ppm).

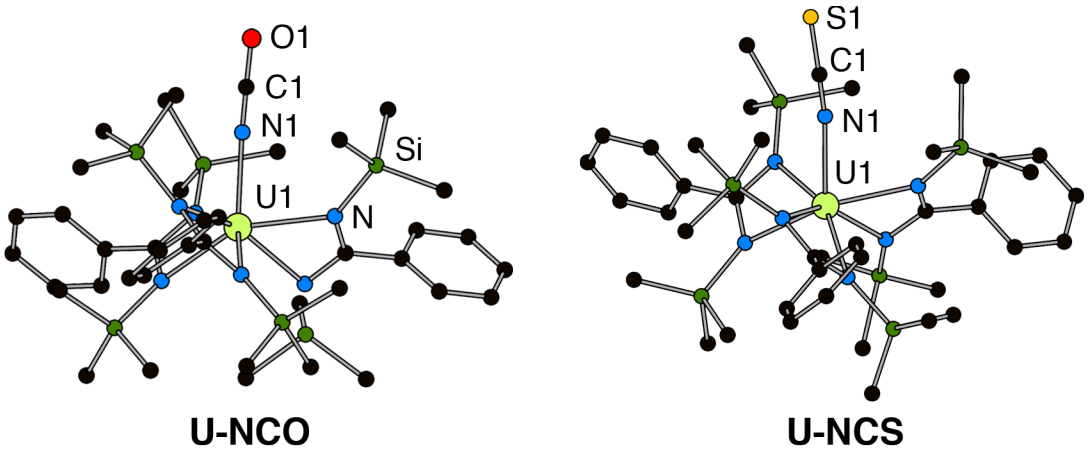

Figure 2.22: Ball and stick diagrams of **U-NCO** and **U-NCS**. All protons are omitted for clarity.

In stark contrast, both NCX moieties coordinate to the uranium and thorium metal centres through the nitrogen atom in a linear fashion (Figure 2.22). The bond metric data are unremarkable, and are consistent with other structurally characterised actinide cyanate[59,60] and thiocyanate[61–63] complexes. The C–N stretching mode derived from IR spectroscopic data (2199 cm^{-1} in **U-NCO**, 2200 cm^{-1} in **Th-NCO**, 2021 cm^{-1} in **U-NCS**, and 2018 cm^{-1} in **U-NCS**) fall within the range for previously reported N-bound cyanate and thiocyanate An(IV) complexes.[59–62] The fact that the $[NCO]^-$ and $[NCS]^-$ ligands bind to the actinide through the nitrogen atom while $[PCO]^-$ binds through the oxygen atom merits further discussion.

2.7.3 Rationale for E versus X binding

This result may initially be surprising. Based on the previous ligand studies of $[PCO]^-$ and $[NCO]^-$ with rhenium[8] and tungsten[20] centres, one might expect both ligands to be bound through the pnictogen atom. On the other hand, based on the oxophilicity of the An(IV) centres, one might expect both ligands to preferentially bind through the oxygen atom. In fact, the observed ligand behaviour can neatly be rationalised by the correlation of the largely ionic nature of bonds to actinides with the partial charges of the ligands (Table 2.9).

Table 2.9: Natural population analysis charges (q) for $[ECO]^-$ ligands. Data from ref.[8]

	$[PCO]^-$	$[NCO]^-$
q(E)	–0.44	–0.81
q(C)	+0.09	+0.56
q(O)	–0.65	–0.75

The terminus (E or X atom) with the greater negative charge is preferentially bound to the actinide, and thus the interaction is charge driven. DFT calculations were performed and the findings matched the experimental observations. The difference in energies between the

conformational isomers of An(amid)$_3$(ECX) were calculated in an analogous manner to the tungsten complexes above:

$$\Delta E_{\text{linkage}} = E(\text{X-bound}) - E(\text{E-bound})$$

The calculated $\Delta E_{\text{linkage}}$ values are shown in Table 2.10. The negative values for both complexes of $[PCO]^-$ demonstrate the preference for binding through the oxygen atom, whereas all of the $[NCX]^-$ complexes have positive values and show preferential coordination through the nitrogen atom, as expected.

Table 2.10: The difference in energy (in kJ mol^{-1}) between X-bound and E-bound $[ECX]^-$ ligands within [An(amid)$_3$(ECX)], as defined above.

Actinide	Ligand	$\Delta E_{\text{linkage}}$
Th	$[PCO]^-$	–32.2
Th	$[NCO]^-$	+56.1
Th	$[NCS]^-$	+73.2
U	$[PCO]^-$	–25.9
U	$[NCO]^-$	+64.4
U	$[NCS]^-$	+81.2

It is surprising that the $\Delta E_{\text{linkage}}$ values for $[PCO]^-$ have a smaller magnitude than those for $[NCO]^-$, as based on the difference in partial charges it would be expected that $[PCO]^-$ would have the greater E/X selectivity. This suggests that the ambidentate character of these anions is rather subtle, and certainly depends on the nature of the metal centre in question, although general trends can be established.

2.7.4 Further reactivity of Th-OCP

Preliminary reactivity investigations of the coordination product **Th-OCP** were carried out. The attempted generation of the $[PCS]^-$ ligand *in situ* was unsuccessful, as **Th-OCP** appears stable with respect to [2+2] cycloaddition chemistry with carbon disulfide. The reaction with a late transition metal complex, however, did show that reactivity at the

terminal C≡P moiety is indeed possible. The treatment of **Th-OCP** with one equivalent of [Ni(COD)$_2$] (COD = 1,5-cyclooctadiene) affords the heterobimetallic adduct [(amid)$_3$Th(μ-η^1(O):η^2(C,P)-OCP)Ni(COD)] (**Th-OCP-Ni(COD)**) shown in Figure 2.23.

The single crystal X-ray diffraction analysis shows the formation of the three-membered nickel phosphametallacycle, resulting from addition of the nickel centre across the P–C bond. This leads to substantial bending of the PCO moiety (O1–C1–P1 bond angle = 148.1(3)˚, Th1–O1–C1 bond angle = 157.5(3)˚), bridging the two metal centres in an unprecedented μ-η^1(O):η^2(C,P) fashion. The P1–C1 bond length in **Th-OCP-Ni(COD)** (1.660(4) Å) is lengthened relative to the **Th-OCP** starting material (1.561(4) Å), due to the donation of electron density from the Ni(0) centre into the P–C π* antibonding orbitals. This value, along with the Ni1–C1 and Ni1–P1 bond lengths (1.895(4) Å and 2.171(2) Å, respectively) compare well with previously reported side-on coordination complexes of phosphaalkynes to nickel.[64,65]

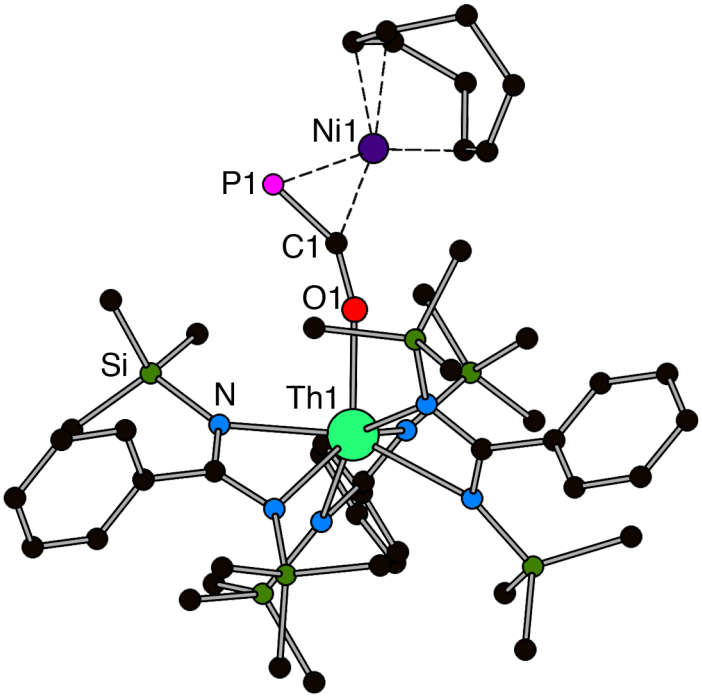

Figure 2.23: Ball and stick diagram of **Th-OCP-Ni(COD)**. All protons are omitted for clarity.

While this is the only product formed during this reaction, NMR spectroscopic studies performed in benzene reveal it is in equilibrium with the starting materials. The ^{31}P NMR chemical shift at $\delta = -7.7$ ppm is indicative of substantial rearrangement of the PCO moiety, and is consistent with the strong deshielding of the phosphorus atom in related η^2 phosphaalkyne derivatives.[64–69]

These preliminary results demonstrate the possibility of further reactivity of coordinated 2-phosphaethynolate complexes to generate novel heteropolymetallic compounds.

2.8 Conclusions

This chapter has described the synthesis and characterisation of the potassium salt of the 2-phosphaethynolate anion **1** from the activation of the $[P_7]^{3-}$ Zintl cluster with carbon monoxide. A detailed ligand study was carried out on the isoelectronic $[PCO]^-$, $[NCO]^-$ and $[NCS]^-$ anions via the synthesis of their coordination compounds with the tungsten pentacarbonyl fragment: **2**, **3** and **4**, respectively. This analysis was initially based on single crystal X-ray diffraction data, and found that all three ligands preferentially bound through the group 15 atom, although the PCO moiety was bound in a side-on manner, while the NCX moieties were bound end-on. The net electronic properties of the three ligands were similar, but an NMR spectroscopic analysis found that this was due to different underlying causes, as $[PCO]^-$ is both a weaker σ donor and π acceptor.

The study was extended to incorporate the first ambient temperature synthesis of the $[PCS]^-$ anion (**5**). The synthesis of the analogous tungsten pentacarbonyl complex found that **5** is an ambidentate ligand, and binds to the tungsten centre through the P or S atom almost indiscriminately, to form the anions **6a** and **6b**, respectively. A computational and IR spectroscopic study probed and corroborated the previous findings of the $[ECX]^-$ anions as a family of ligands.

The reactivity of the $[PCO]^-$, $[NCO]^-$ and $[NCS]^-$ anions were also explored towards thorium and uranium complexes, in a collaboration with the groups of Maron and Arnold. The study found that, in this case, the $[PCO]^-$ anion preferentially binds to the metal centre through the O atom, which polarises the PCO moiety and enhances its phosphaalkyne character, whereas both NCX moieties coordinate via the N atom. This is due to the large ionic nature of the bonding to actinide centres. The preliminary studies of **Th-OCP** with $[Ni(COD)_2]$ showed that the metal-coordinated PCO unit is accessible for further reactivity.

2.9 References

(1) Becker, G.; Schwarz, W.; Seidler, N.; Westerhausen, M. *Z. Anorg. Allg. Chem.* **1992**, *612*, 72–82.

(2) Weber, L.; Torwiehe, B.; Bassmann, G.; Stammler, H.-G.; Neumann, B. *Organometallics* **1996**, *15*, 128–132.

(3) Becker, G.; Heckmann, G.; Hübler, K.; Schwarz, W. *Z. Anorg. Allg. Chem.* **1995**, *621*, 34–46.

(4) Becker, G.; Hübler, K.; Niemeyer, M.; Seidler, N.; Thinus, B. *Z. Anorg. Allg. Chem.* **1996**, *622*, 197–211.

(5) Westerhausen, M.; Schneiderbauer, S.; Piotrowski, H.; Suter, M.; Nöth, H. *J. Organomet. Chem.* **2002**, *643–644*, 189–193.

(6) Krummenacher, I.; Cummins, C. C. *Polyhedron* **2012**, *32*, 10–13.

(7) Puschmann, F. F.; Stein, D.; Heift, D.; Hendriksen, C.; Gal, Z. A.; Grützmacher, H.-F.; Grützmacher, H. *Angew. Chem. Int. Ed.* **2011**, *50*, 8420–8423.

(8) Alidori, S.; Heift, D.; Santiso-Quinones, G.; Benkő, Z.; Grützmacher, H.; Caporali, M.; Gonsalvi, L.; Rossin, A.; Peruzzini, M. *Chem. Eur. J.* **2012**, *18*, 14805–14811.

(9) Jupp, A. R.; Goicoechea, J. M. *J. Am. Chem. Soc.* **2013**, *135*, 19131–19134.

(10) Jupp, A. R.; Trott, G.; Payen de la Garanderie, É.; Holl, J. D. G.; Carmichael, D.; Goicoechea, J. M. *Chem. Eur. J.* **2015**, *21*, 8015–8018.

(11) Robinson, T. P.; Goicoechea, J. M. *Chem. Eur. J.* **2015**, *21*, 5727–5731.

(12) Chen, X.; Alidori, S.; Puschmann, F. F.; Santiso-Quinones, G.; Benkő, Z.; Li, Z.; Becker, G.; Grützmacher, H.-F.; Grützmacher, H. *Angew. Chem. Int. Ed.* **2014**, *53*, 1641–1645.

(13) Heift, D.; Benkő, Z.; Grützmacher, H. *Angew. Chem. Int. Ed.* **2014**, *53*, 6757–6761.

(14) Heift, D.; Benkő, Z.; Grützmacher, H. *Chem. Eur. J.* **2014**, *20*, 11326–11330.

(15) Heift, D.; Benkő, Z.; Grützmacher, H. *Dalton Trans.* **2014**, *43*, 831–840.

(16) Heift, D.; Benkő, Z.; Grützmacher, H.; Jupp, A. R.; Goicoechea, J. M. *Chem. Sci.* **2015**, *6*, 4017–4024.

(17) Robinson, T. P.; Cowley, M. J.; Scheschkewitz, D.; Goicoechea, J. M. *Angew. Chem. Int. Ed.* **2015**, *54*, 683–686.

(18) Tondreau, A. M.; Benkő, Z.; Harmer, J. R.; Grützmacher, H. *Chem. Sci.* **2014**, *5*, 1545–1554.

(19) Camp, C.; Settineri, N.; Lefèvre, J.; Jupp, A. R.; Goicoechea, J. M.; Maron, L.; Arnold, J. *Chem. Sci.* **2015**, *6*, 6379–6384.

(20) Jupp, A. R.; Geeson, M. B.; McGrady, J. E.; Goicoechea, J. M. *Eur. J. Inorg. Chem.* **2016**, *2016*, 639–648.

(21) Lu, Y.; Wang, H.; Xie, Y.; Liu, H.; Schaefer III, H. F. *Inorg. Chem.* **2014**, *53*, 6252–6256.

(22) Lü, W.; Wang, C.; Luo, Q.; Li, Q.; Xie, Y.; King, R. B.; Schaefer III, H. F. *New J. Chem.* **2015**, *39*, 1390–1403.

(23) Liu, L.; Zhu, J.; Zhao, Y. *Chem. Commun.* **2014**, *50*, 11347–11349.

(24) Quan, Z.-J.; Wang, X.-C. *Org. Chem. Front.* **2014**, *1*, 1128–1131.

(25) Jupp, A. R.; Goicoechea, J. M. *Angew. Chem. Int. Ed.* **2013**, *52*, 10064–10067.

(26) Baudler, M.; Düster, D.; Langerbeins, K.; Germeshausen, J. *Angew. Chem. Int. Ed. Engl.* **1984**, *23*, 317–318.

(27) Baudler, M. *Angew. Chem. Int. Ed. Engl.* **1982**, *21*, 492–512.

(28) Beck, W.; Smedal, H. S. *Angew. Chem. Int. Ed. Engl.* **1966**, *5*, 253–253.

(29) Dahlgren, R. M.; Zink, J. I. *J. Am. Chem. Soc.* **1979**, *101*, 1448–1454.

(30) Asali, K. J.; Dobson, G. R. *J. Organomet. Chem.* **1979**, *179*, 169–179.

(31) Herberhold, M.; Ehrenreich, W. *Angew. Chem. Int. Ed. Engl.* **1982**, *21*, 633–633.

(32) Palitzsch, W.; Beyer, C.; Böhme, U.; Rittmeister, B.; Roewer, G. *Eur. J. Inorg. Chem.* **1999**, *1999*, 1813–1820.

(33) Wojcicki, A.; Farona, M. F. *J. Inorg. Nucl. Chem.* **1964**, *26*, 2289–2290.

(34) Buchner, W.; Schenk, W. A. *Inorg. Chem.* **1984**, *23*, 132–137.

(35) Albert, B.; Jansen, M. *Z. Anorg. Allg. Chem.* **1995**, *621*, 464–468.

(36) For 782 crystallographically characterised complexes of tungsten pentacarbonyl bearing a P-bound ligand (CSD version 5.36, June 2015): d(min) = 2.375 Å, d(max) = 2.686 Å, d(mean) = 2.513 Å, Var(d) = 0.002, σ(d) = 0.047 Å, mean deviation = 0.037 Å.

(37) Pickardt, J.; Rösch, L.; Schumann, H. *Z. Anorg. Allg. Chem.* **1976**, *426*, 66–76.

(38) Tolman, C. A. *J. Am. Chem. Soc.* **1970**, *92*, 2956–2965.

(39) Appleton, T. G.; Clark, H. C.; Manzer, L. E. *Coord. Chem. Rev.* **1973**, *10*, 335–422.

(40) Shustorovich, E. M.; Porai-Koshits, M. A.; Buslaev, Y. A. *Coord. Chem. Rev.* **1975**, *17*, 1–98.

(41) Schumann, H.; Kroth, H.-J. *Z. Naturforsch. B* **1977**, *32b*, 768–770.

(42) Paris, S. I. M.; Lemke, F. R.; Sommer, R.; Lönnecke, P.; Hey-Hawkins, E. *J. Organomet. Chem.* **2005**, *690*, 1807–1813.

(43) Gordon, A. J.; Ford, R. A. *The Chemist's Companion: A Handbook of Practical Data, Techniques, and References*; Wiley: New York, 1972.

(44) Kühl, O. *Phosphorus-31 NMR Spectroscopy: A Concise Introduction for the Synthetic Organic and Organometallic Chemist*; Springer-Verlag: Berlin, 2008.

(45) Kargol, J. A.; Crecely, R. W.; Burmeister, J. L. *Inorg. Chem.* **1979**, *18*, 2532–2535.

(46) Colquhoun, I. J.; Grim, S. O.; McFarlane, W.; Mitchell, J. D.; Smith, P. H. *Inorg. Chem.* **1981**, *20*, 2516–2521.

(47) Bertrand, R. D.; Ogilvie, F. B.; Verkade, J. G. *J. Am. Chem. Soc.* **1970**, *92*, 1908–1915.

(48) Köhler, F. H.; Kalder, H. J.; Fischer, E. O. *J. Organomet. Chem.* **1976**, *113*, 11–22.

(49) Burdett, J. K.; Albright, T. A. *Inorg. Chem.* **1979**, *18*, 2112–2120.

(50) Buchner, W.; Schenk, W. A. *J. Magn. Reson.* **1982**, *48*, 148–151.

(51) Becker, G.; Hübler, K. *Z. Anorg. Allg. Chem.* **1994**, *620*, 405–417.

(52) Grobe, J.; Van, D. L.; Lüth, B.; Hegemann, M. *Chem. Ber.* **1990**, *123*, 2317–2320.

(53) Becker, G.; Ditten, G.; Hübler, K.; Merz, K.; Niemeyer, M.; Seidler, N.; Westerhausen, M.; Zheng, Z. *Organosilicon Chem. II* **1996**, 161–187.

(54) Heift, D.; Benkő, Z.; Grützmacher, H. *Dalton Trans.* **2014**, *43*, 5920–5928.

(55) Tolman, C. A. *Chem. Rev.* **1977**, *77*, 313–348.

(56) Cotton, F. A.; Kraihanzel, C. S. *J. Am. Chem. Soc.* **1962**, *84*, 4432–4438.

(57) Scott, A. P.; Radom, L. *J. Phys. Chem.* **1996**, *100*, 16502–16513.

(58) Shannon, R. D. *Acta. Cryst. A* **1976**, *32*, 751–767.

(59) Cleaves, P. A.; King, D. M.; Kefalidis, C. E.; Maron, L.; Tuna, F.; McInnes, E. J. L.; McMaster, J.; Lewis, W.; Blake, A. J.; Liddle, S. T. *Angew. Chem. Int. Ed.* **2014**, *53*, 10412–10415.

(60) Castro-Rodríguez, I.; Nakai, H.; Meyer, K. *Angew. Chem. Int. Ed.* **2006**, *45*, 2389–2392.

(61) Al-Daher, A. G. M.; Bagnall, K. W.; Castellani, C. B.; Benetollo, F.; Bombieri, G. *Inorg. Chim. Acta* **1984**, *95*, 269–277.

(62) Fischer, R. D.; Klähne, E.; Kopf, J. *Z. Naturforsch. B* **1978**, *33b*, 1393–1397.

(63) Bagnall, K. W.; Benetollo, F.; Forsellini, E.; Bombieri, G. *Polyhedron* **1992**, *11*, 1765–1770.

(64) Schaub, T.; Radius, U. *Z. Anorg. Allg. Chem.* **2006**, *632*, 981–984.

(65) Trincado, M.; Rosenthal, A. J.; Vogt, M.; Grützmacher, H. *Eur. J. Inorg. Chem.* **2014**, *2014*, 1599–1604.

(66) Laurent, J. C. T. R. B.-S.; Hitchcock, P. B.; Kroto, H. W.; Nixon, J. F. *J. Chem. Soc., Chem. Commun.* **1981**, 1141–1143.

(67) Binger, P.; Biedenbach, B.; Herrmann, A. T.; Langhauser, F.; Betz, P.; Goddard, R.; Krüger, C. *Chem. Ber.* **1990**, *123*, 1617–1623.

(68) Mansell, S. M.; Green, M.; Russell, C. A. *Dalton Trans.* **2012**, *41*, 14360–14368.

(69) Burrows, A. D.; Dransfeld, A.; Green, M.; Jeffery, J. C.; Jones, C.; Lynam, J. M.; Nguyen, M. T. *Angew. Chem. Int. Ed.* **2001**, *40*, 3221–3224.

Chapter 3
Cycloaddition chemistry of the 2-phosphaethynolate anion

3.1 Introduction and objectives

3.1.1 Heteroallenes

An allene is a compound in which one carbon has two double bonds to two other carbon atoms, with the general formula $R_2C=C=CR_2$. They possess a linear sp hybridised central carbon atom with two separate π bonds, which are necessarily mutually orthogonal and therefore non-conjugated. Simple alkyl-substituted allenes tend to react as nucleophiles, akin to alkenes and alkynes.[1]

The replacement of one or both of the CR_2 groups with an isolobal heteroatom substituent yields a family of compounds called heteroallenes. The heteroallenes relevant to this chapter are ketenes, carbodiimides and isocyanates (shown in Figure 3.1). The presence of electronegative atoms in the terminal positions of these heteroallenes changes the reactivity of these species, and the heteroallenes shown typically act as electrophiles at the central carbon atom.[2]

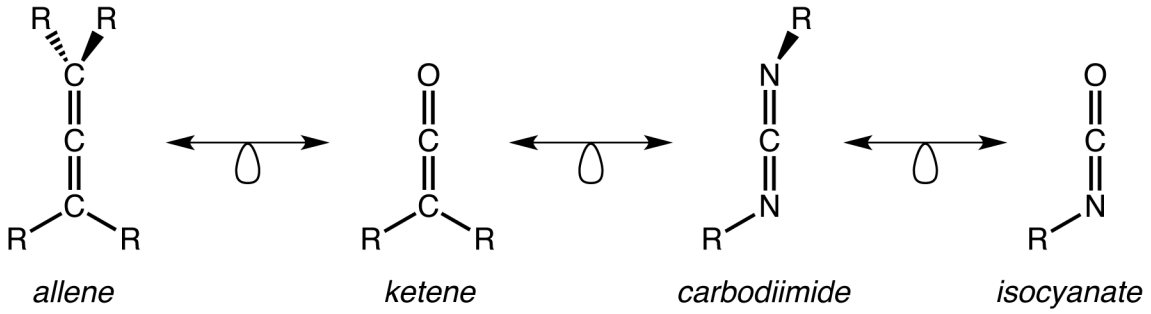

Figure 3.1: The isolobality of allenes and a range of heteroallenes.

3.1.2 [2+2] Cycloadditions

A cycloaddition is defined as a "*reaction in which two or more unsaturated molecules (or parts of the same molecule) combine with the formation of a cyclic adduct in which there is a net reduction of the bond multiplicity*".[3] Cycloadditions can be further specified by the numbers of electrons in each interacting fragment that participates in the transformation of

reactants to products, and are denoted in square brackets. For example, the prototypical Diels-Alder reaction, shown in (i) of Figure 3.2, is a [4+2] cycloaddition.[4]

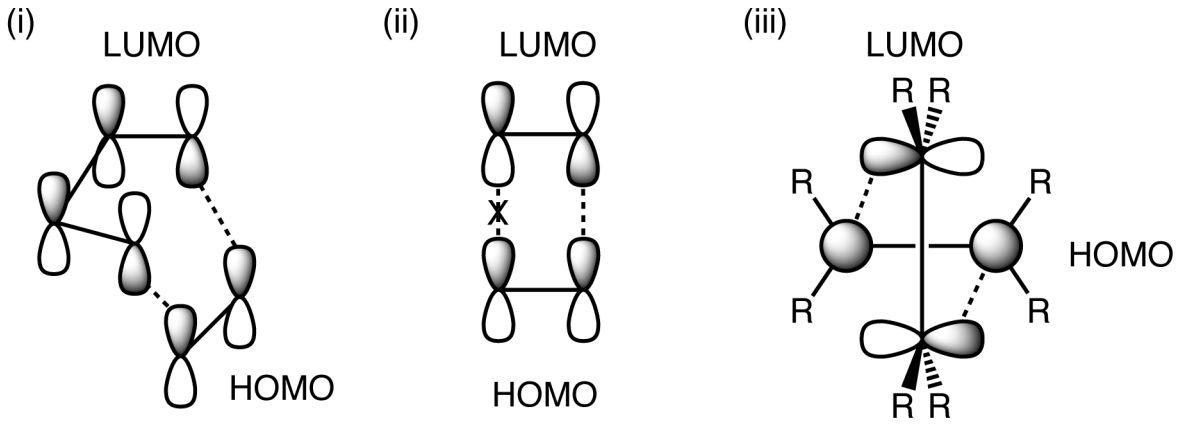

Figure 3.2: Molecular orbital approach showing (under thermal conditions): (i) allowed [4+2] cycloaddition; (ii) forbidden [2+2] cycloaddition; (iii) allowed [2+2] cycloaddition via a crossed transition state.

Concerted cycloadditions are governed by the Woodward-Hoffmann rules.[5,6] Only certain combinations of fragments are allowed, although this differs depending on whether the reaction is carried out thermally or photochemically. For example, the [4+2] cycloaddition in (i) is thermally allowed based on symmetry arguments, whereas the suprafacial [2+2] cycloaddition (ii), for example the interaction of two alkenes to afford a cyclobutane derivative, is formally forbidden under thermal conditions. The latter can, however, be carried out under photochemical conditions. Note the terms *allowed* and *forbidden* are based on the predicted heights of electronic barriers due to the alignment of the relevant orbitals, and as such a formally forbidden reaction may still be possible, but would require significantly more energy to proceed.

It has long been known that ketenes appear to violate the Woodward-Hofmann rules, and can readily undergo thermal [2+2] cycloadditions with alkenes.[7–10] It has been suggested that this is due to a crossed transition state, which allows the correct alignment of the relative orbitals.[11] Diagram (iii) of Figure 3.2 shows the cycloaddition of two alkenes in a crossed transition state, which is unfavourable due to the steric clash of the R substituents of

the two alkenes. It is argued that the analogous transition state for the [2+2] cycloaddition of a ketene and an alkene is more favourable based on sterics, because the $R_2C=C=O$ system only has one R group pointing into the plane of the alkene.

The basis for concertedness in pericyclic reactions is often based on the stereospecific nature of the reactions and products.[6] It has, however, been convincingly argued by Dewar and others that this is not necessarily the case, and that the stereochemical outcomes can be rationalised using non-synchronous and asymmetric transition states, close to biradical or zwitterionic intermediates.[12,13] The [2+2] cycloaddition of ketenes with cyanoketenes has been shown to proceed via a step-wise mechanism, and the independent syntheses of the expected zwitterionic intermediates lead to the same products as the cycloaddition itself.[14]

It is important to note that the IUPAC definition of a cycloaddition does encompass non-concerted step-wise reactions, and is certainly not limited to pericyclic reactions that proceed according to Woodward-Hoffmann theory.[3] Thus a formal [2+2] cycloaddition product may be generated and termed as such, without inferring any assumptions of concertedness on the reaction mechanism.

3.1.3 Cycloaddition chemistry of P–C multiple bonds

The cycloaddition chemistry of P–C multiple bonds in low-coordinate phosphorus compounds is well-established.[15] For example, the P≡C triple bond of phosphaalkynes has been shown to undergo [2+1] cycloadditions with carbenes,[16,17] silylenes,[18,19] germylenes,[20,21] and phosphinidenes.[22] Furthermore, [2+3] cycloadditions of phosphaalkynes with 1,3-dipole compounds such as azides or nitrile oxides have been utilised as a general route for the formation of heterophospholes.[23]

By contrast, [2+2] cycloadditions are possible but relatively rare for phosphaalkynes. The reaction of a Schrock carbene with *tert*-butylphosphaalkyne showed the initial [2+2] cycloaddition product, followed by migration of an alkoxy group from the metal centre to

the phosphorus atom (Scheme 3.1).[24] The same phosphaalkyne can also undergo a [2+2] cycloaddition with a diphosphene, once again followed by a slow isomerisation at room temperature.[25]

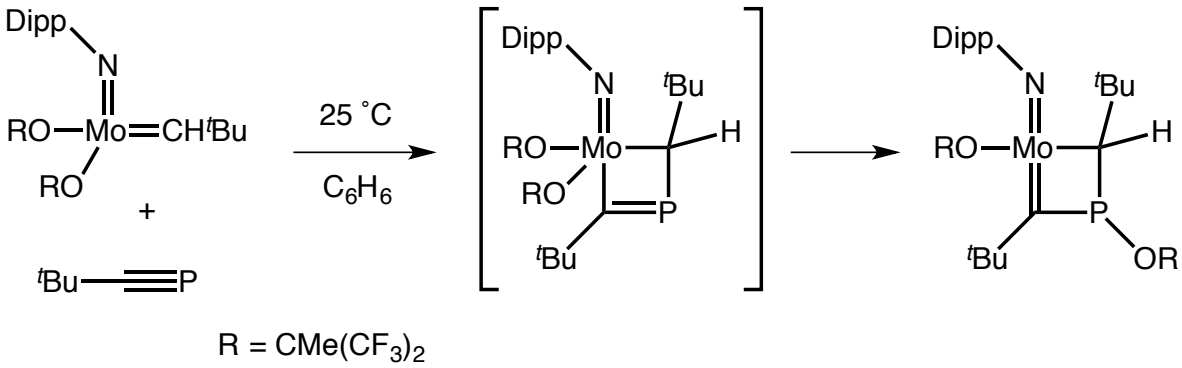

Scheme 3.1: [2+2] Cycloaddition reaction of a phosphaalkyne with a Schrock carbene.[24]

Prior to our discovery of [K(18-crown-6)][**1**],[26] there was very little in the chemical literature on the cycloaddition chemistry of the 2-phosphaethynolate anion. The reaction of $[PCO]^-$ with carbon disulfide is assumed to proceed via a [2+2] cycloaddition followed by a cycloreversion to afford $[PCS]^-$ and OCS, although the proposed intermediate has never been detected (shown previously in Scheme 2.3).[27,28] The only other example was published by Becker in 1995, and is the reaction of the lithium salt of $[PCO]^-$ with two equivalents of an activated alkyne to yield a phosphinine derivative (Scheme 3.2).[29] This reaction presumably proceeds via two [2+2] cycloadditions to afford the undetected Dewar benzene-like intermediate, followed by rearrangement to give the final product shown.

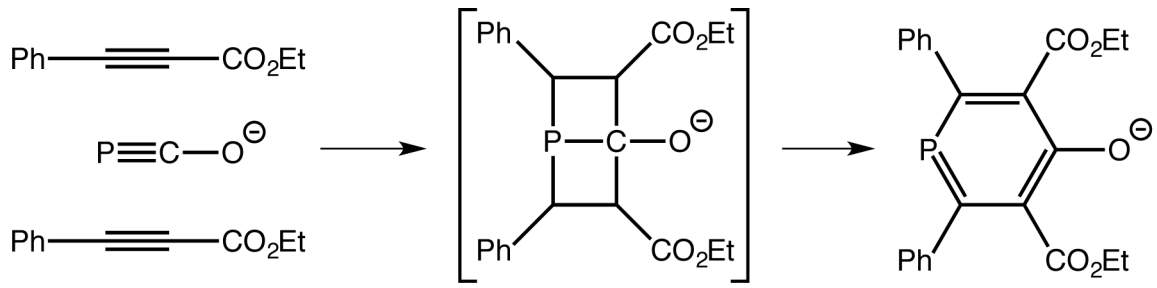

Scheme 3.2: Reaction of $[PCO]^-$ with activated alkyne to give phosphinine derivative.[29]

3.1.4 Chapter outline

These two examples show the potential of the cycloaddition chemistry of the P–C multiple bond of $[PCO]^-$ as a synthetic route to a range of phosphorus-containing heterocycles. Utilising our facile and relatively large-scale preparation of [K(18-crown-6)][**1**], we sought to explore its cycloaddition chemistry with a range of heteroallenes. This chapter will outline the synthesis and characterisation of novel four-membered heterocycles derived from the reactivity of **1** with ketenes and carbodiimides, followed by a brief discussion of mechanistic insights. The study will be extended to incorporate the cycloaddition products derived from isocyanates, which contrast those of the other heteroallenes. This work will be described within the context of a collaborative project with the Grützmacher group.

3.2 Cycloaddition chemistry with ketenes and carbodiimides

3.2.1 Synthesis of [K(18-crown-6)][7] (7: $[P(C(O))_2CPh_2]^-$)

The reaction of [K(18-crown-6)][**1**] with diphenylketene in pyridine led to the generation of [K(18-crown-6)][**7**] (**7**: $[P(C(O))_2CPh_2]^-$) (Scheme 3.3). It was determined by ^{31}P NMR spectroscopic analysis that 1.5 equivalents of the diphenylketene were required for the optimal conversion of **1** into **7** (δ = 165.7 ppm), as small quantities of unidentified phosphorus-containing side-products were also formed during this reaction. These side-products could be separated by washing the product with diethyl ether and cold THF, to afford [K(18-crown-6)][**7**] as a pale orange solid.

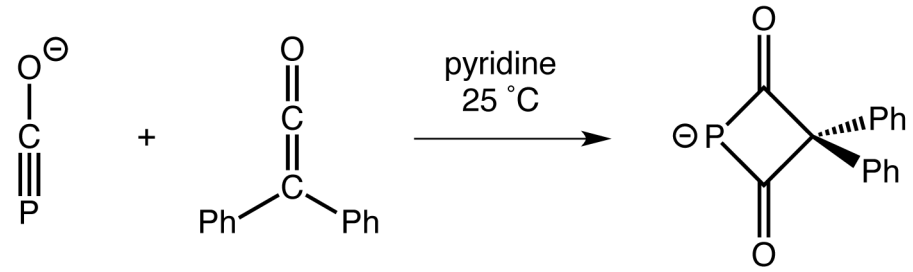

Scheme 3.3: Reaction of **1** with diphenylketene to afford **7**.

3.2.2 Characterisation of [K(18-crown-6)][7]

This product arises from the formal [2+2] cycloaddition of the P–C multiple bond in **1** across the C=C double bond in diphenylketene. There are several resonance structures that could be drawn for the product, and the three with the greatest expected contributions are shown in Figure 3.3. Note due to the C_{2v} symmetry of the anion, resonance forms **7ii** and **7iii** are the same if the anion is considered in isolation, however any asymmetric interaction with the counter-cation would render these resonance forms inequivalent.

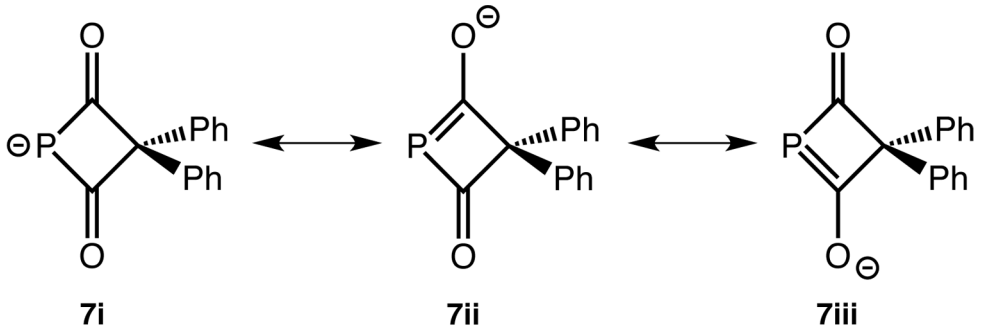

Figure 3.3: Possible resonance structures of **7**.

Crystals of [K(18-crown-6)][**7**] were grown by slow diffusion of hexane into a THF solution of the product. The crystal structure reveals a single crystallographically unique anion with a close electrostatic interaction with the potassium cation through one of the oxygen atoms (Figure 3.4).

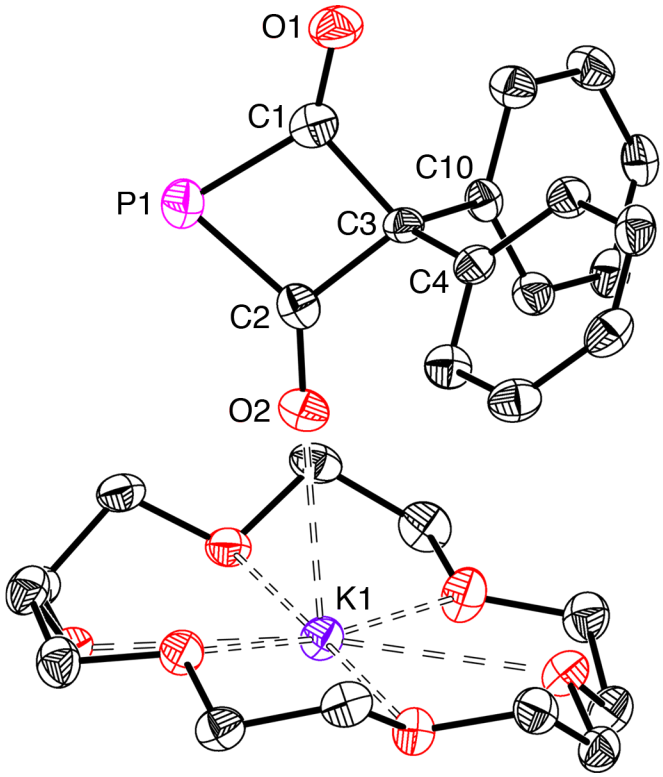

Figure 3.4: Molecular structure of [K(18-crown-6)][**7**]. Anisotropic displacement ellipsoids are set at 50% probability. Hydrogen atoms omitted for clarity.

The central moiety of the anion is a planar four-membered PC_3 ring (maximum deviation from planarity: 0.012 Å) (Figure 3.4). This is consistent with the three resonance structures shown in Figure 3.3. Selected crystallographic bond lengths and bond angles are shown in Table 3.1 (the computed data will be discussed shortly).

Table 3.1: Selected crystallographic and computed bond lengths (Å) and angles (˚) of **7**.

Bond distance (Å)	**7**	**7_{calc}**
P1–C1	1.799(3)	1.807
P1–C2	1.784(2)	1.809
C1–O1	1.228(3)	1.226
C2–O2	1.237(3)	1.226
C3–C1	1.564(3)	1.571
C3–C2	1.562(3)	1.571
C3–C4	1.528(3)	1.521
C3–C10	1.522(3)	1.521
K1–O2	2.667(2)	N.A.

Bond angle (°)		
C1–P1–C2	75.1(2)	75.4
P1–C1–C3	97.8(2)	97.6
P1–C2–C3	98.5(2)	97.5
C1–C3–C2	88.6(2)	89.5

The P1–C1 (1.799(3) Å) and P1–C2 (1.784(2) Å) bond lengths lie in between the sum of single and double bond covalent radii for P and C (1.86 Å and 1.69 Å, respectively).[30,31] The C–O bond distances are comparable to other structurally authenticated ketones. These data suggest that **7i** is the major resonance contribution, but with a small contribution from **7ii** and **7iii**. It is worth noting that the P1–C1 and P1–C2 bond lengths are similar within statistical error, as are the C1–O1 and C2–O2 bond lengths. This is despite the fact that the potassium cation only interacts with O2, and as such it could be rationalised that **7iii** (as drawn, with the negative charge formally localised on the O2 oxygen) would have a greater contribution than **7ii**. The fact that this is not the case, to a statistically significant degree at least, implies that **7ii** and **7iii** both contribute a similar (but small) amount to the bonding model of **7**. The C3–C1 and C3–C2 bond lengths are both longer than the C3–C4 and C3–C10 bond lengths, on account of the ring strain within the molecule. The C1–P1–C2 bond angle (75.1(2)°) is the most acute of the angles within the four-membered ring, as expected based on the long P–C bond lengths.

Density functional theory (DFT) calculations have been carried out and yielded an optimised structure of **7** in excellent agreement with that derived crystallographically, and the data are also included in Table 3.1. The anion is almost perfectly C_{2v} symmetric, as would be expected for the anion in the gas phase with no cation interaction. The P–C bond lengths are slightly longer in $\mathbf{7}_{\mathbf{calc}}$ than **7**, and the C–O bond lengths are slightly shorter. This suggests a slightly enhanced contribution from **7ii** and **7iii** in the crystal structure relative to the computed optimised structure, which can be rationalised by the interaction of

the K^+ cation stabilising the increased negative charge localised on the oxygen atoms in the crystal structure.

7 bears a close resemblance to a five-membered anionic heterocycle synthesised by Liotta and co-workers, which is the phosphorus analogue of the phthalimide anion (Figure 3.5).[32] The authors conclude that the bond metric data within this anion (which are similar to those in **7**) indicate that there is very little delocalisation of the negative charge into the carbonyl groups. As with **7**, the $[K(18\text{-crown-6})]^+$ counter-cation of the this phthalimide analogue interacts with one of the oxygen atoms instead of the localised negative charge on the phosphorus atom.

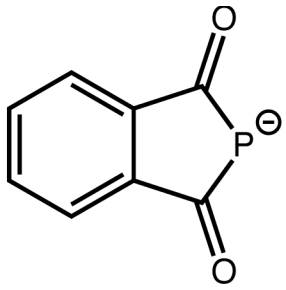

Figure 3.5: Phosphorus analogue of phthalimide anion, synthesised by Liotta and co-workers.[32]

The ^{31}P NMR spectrum of a d_8-THF solution of [K(18-crown-6)][**7**] exhibits a singlet at δ = 165.7 ppm. ^1H NMR spectroscopy shows that the two phenyl groups are equivalent, as expected based on the C_{2v} symmetry of the anion. The $^{13}C\{^1H\}$ NMR spectrum reveals six resonances for the anion, three of which are doublets due to coupling to the phosphorus nucleus (C1 and C2: $^1J_{C-P}$ = 40 Hz; C3: $^2J_{C-P}$ = 16 Hz; C4 and C10: $^3J_{C-P}$ = 5 Hz).

The anion **7** was readily observed in DMF solutions using electrospray ionisation (ESI) mass spectrometric experiments. The negative ion mode revealed the anion at *m/z* = 253.4, and the positive ion mode showed the cation-paired species $\{[K(18\text{-crown-6})]_2[\mathbf{7}]\}^+$ at *m/z* = 859.4. The IR spectrum of [K(18-crown-6)][**7**] showed two strong bands in the carbonyl stretching region at 1598 and 1557 cm^{-1}.

3.2.3 Synthesis of [K(18-crown-6)][8] (8: [PC(O)(CNDipp)NDipp]$^-$)

The change of the identity of the heteroallene from a ketene to carbodiimide resulted in analogous reactivity. The reaction of a pyridine solution of [K(18-crown-6)][**1**] with one equivalent of bis(2,6-diisopropylphenyl)carbodiimide led to the formation of [K(18-crown-6)][**8**] (**8**: [PC(O)(CNDipp)NDipp]$^-$) (Scheme 3.4). Full conversion of **1** to **8** was observed in the ^{31}P NMR spectrum after approximately three hours at room temperature, and there was no indication of any intermediates during this transformation.

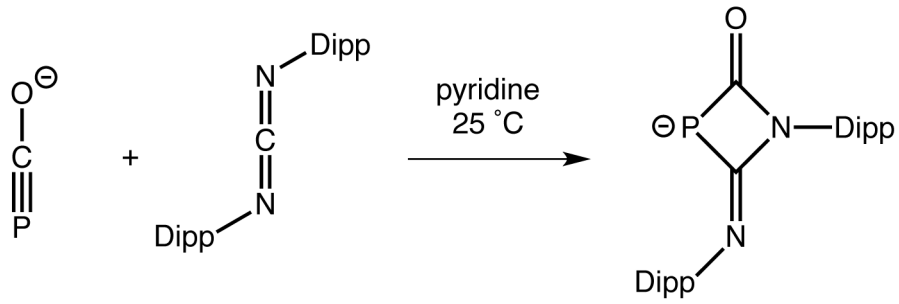

Scheme 3.4: Reaction of **1** with bis(2,6-diisopropylphenyl)carbodiimide to afford **8**.

It is important to note that this adduct formation appears dependent on the identity of the substituents on the carbodiimide. The reaction of **1** with bis(cyclohexyl)carbodiimide showed no evidence of the cycloaddition product under identical conditions. Even after prolonged heating at 60 ˚C, the ^{31}P NMR spectrum showed only unreacted **1** in solution. The possible reasons and implications for this will be discussed shortly.

3.2.4 Characterisation of [K(18-crown-6)][8]

The analogous resonance structures as those proposed for **7** can be invoked for **8**, and are shown in Figure 3.6. In this case the asymmetry of the molecule clearly renders **8ii** and **8iii** distinct.

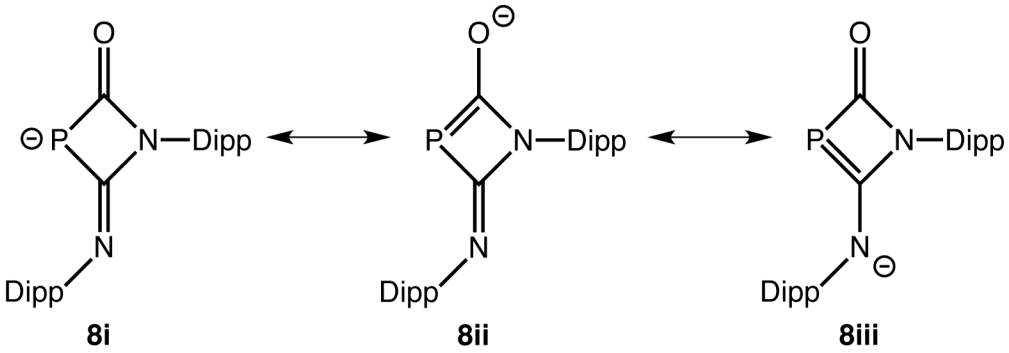

Figure 3.6: Possible resonance structures of **8**.

Crystals of [K(18-crown-6)][**8**] suitable for single crystal X-ray diffraction were grown by slow diffusion of hexane into a THF solution of the product (Figure 3.7).

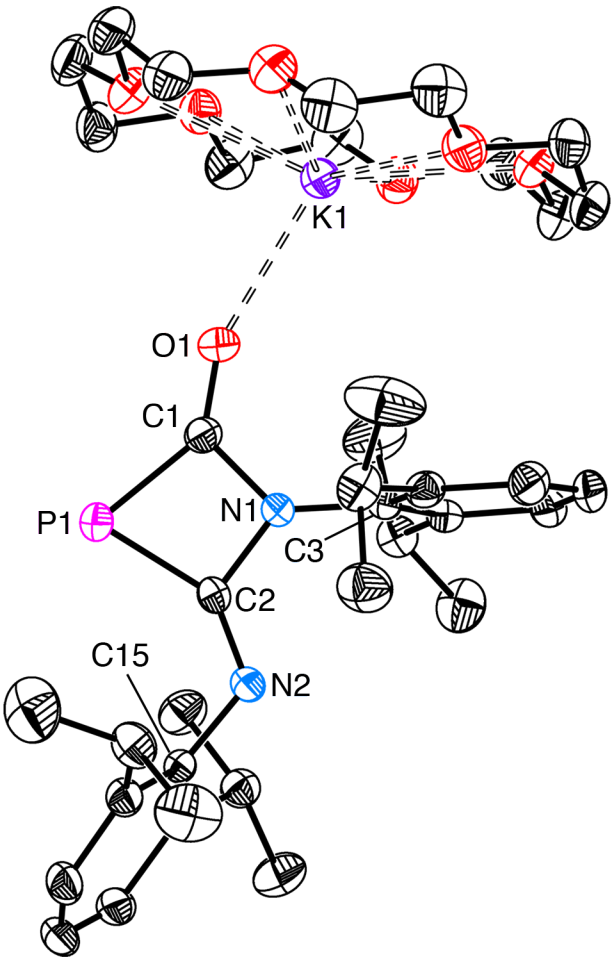

Figure 3.7: Molecular structure of [K(18-crown-6)][**8**]. Anisotropic displacement ellipsoids are set at 50% probability. Only the major component of the disordered 18-crown-6 moiety is shown. Hydrogen atoms omitted for clarity.

By analogy with **7**, the structure of **8** shows a planar four-membered heterocyclic core (maximum deviation from planarity: 0.015 Å). Selected crystallographic bond metric data are shown in Table 3.2, along with the analogous data derived from DFT calculations.

Table 3.2: Selected crystallographic and computed bond lengths (Å) and angles (˚) **8**.

Bond distance (Å)	**8**	**8_{calc}**
P1–C1	1.837(2)	1.848
P1–C2	1.839(2)	1.854
C1–O1	1.226(2)	1.221
C2–N2	1.269(2)	1.270
C1–N1	1.406(2)	1.414
C2–N1	1.417(2)	1.412
N1–C3	1.429(2)	1.421
N2–C15	1.415(2)	1.406
K1–O1	2.655(2)	N.A.
Bond angle (˚)		
C1–P1–C2	71.0(1)	70.8
P1–C1–N1	95.5(1)	95.4
P1–C2–N1	95.1(1)	95.2
C1–N1–C2	98.3(2)	98.7

The P1–C1 (1.837(2) Å) and P1–C2 (1.839(2) Å) bond lengths are identical within statistical error despite the different substituents on the carbon atoms. This implies that resonances **8ii** and **8iii** each contribute a similar amount to the bonding model. These values are approximately 0.04 Å larger than those for **7**, which presumably arises from the increased electron density in the π manifold of the four-membered ring due to the presence of the lone pair on the N1 atom. The C2–N2 bond length (1.269(2) Å) is consistent with a double bond (sum of covalent double bond radii is 1.27 Å),[31] and is significantly shorter than the other C–N bond distances in the structure (1.406(2)–1.429(2) Å). These data are consistent with the bonding being principally described by **8i**, with an even smaller contribution from **8ii** and **8iii** than the analogous resonance structures in **7**. Once again, the

$[K(18\text{-crown-6})]^+$ cation interacts exclusively with the O1 atom in the solid state, and there is no interaction with the localised negative charge on P1. Only the *Z* isomer across the C2–N2 double bond (as shown) is observed in the crystal structure, and no evidence for the *E* isomer was observed in any of the experimental investigations.

The DFT data are a good match to the crystallographic bond metric data. Once again, the P–C bond lengths are slightly longer in $\mathbf{8}_{\mathbf{calc}}$ than **8**, and the C1–O1 bond length is shorter, which is attributed to the increased contribution of **8ii** in the crystal structure due to the interaction of O1 with the K^+ cation.

The ^{31}P NMR spectrum of **8** exhibits a singlet at δ = 18.6 ppm, which is a notable upfield shift relative to **7**. This is consistent with increased electron density on the phosphorus atom in **8**, owing to competition of delocalising the electron density into the C–O π^* orbitals with the N1 lone pair (and thus a relatively greater contribution from resonance **8i**). Two chemically inequivalent Dipp groups could be distinguished in the ^1H and $^{13}C\{^1H\}$ NMR spectra. The $^{13}C\{^1H\}$ NMR spectrum showed two doublet resonances arising from the carbonyl (C1: $^1J_{C–P}$ = 42 Hz) and imine (C2: $^1J_{C–P}$ = 48 Hz) carbons, and two further doublets arising from the three-bond coupling of the phosphorus atom to both *ipso* carbons of the Dipp groups (C3: $^3J_{C–P}$ = 3 Hz; C15: $^3J_{C–P}$ = 3 Hz).

ESI mass spectrometry showed the anion **8** at *m/z* = 421.9 in the negative ion mode, and the cation-paired species $\{[K(18\text{-crown-6})]_2[\mathbf{8}]\}^+$ at *m/z* = 1030.4 in the positive ion mode spectrum.

An IR spectrum of the solid revealed two bands at 1599 and 1579 cm^{-1}, arising from the C=O and C=N stretching modes.

3.2.5 Computational comparison of 7 and 8

As seen in Table 3.2, the DFT computational bond metric data are in excellent agreement with those derived crystallographically. The HOMO for both **7** and **8** are shown in Figure 3.8. Both of these are in accord with the earlier assertion that there is very little donation of the electron density into the C–O or C–N π* antibonding orbitals, as in both **7** and **8** the HOMO is localised principally on the p_y orbital on the phosphorus atom (55.5% and 73.7%, respectively). These values also give a quantitative assessment of the fact that, although the delocalisation is small in both species, there is slightly greater degree of delocalisation in **7** (10.1% O1 p_y, 9.3% O2 p_y) than in **8** (2.7% O1 p_y, 2.9% N2 p_y).

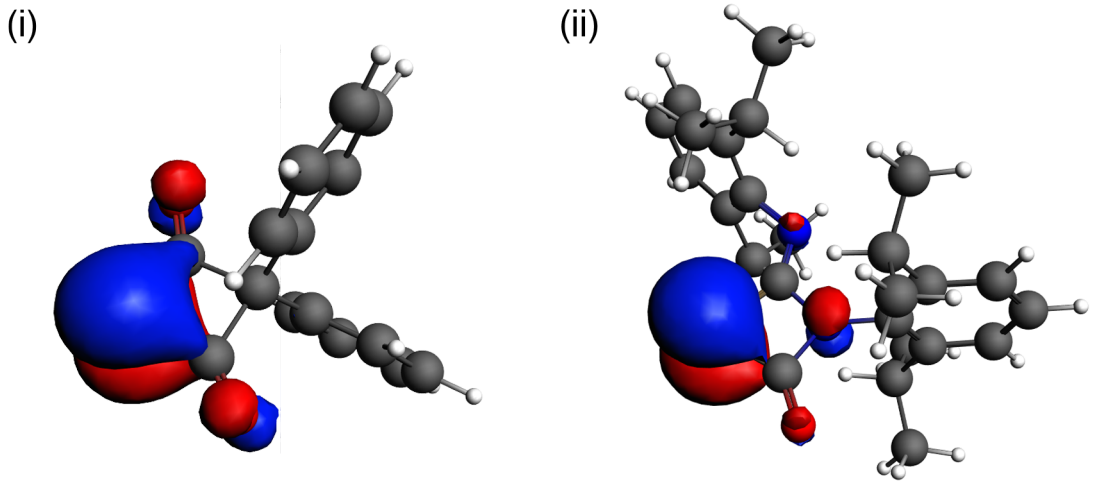

Figure 3.8: Kohn-Sham molecular orbital representations (contour values 0.05 au) of the HOMO of (selected atomic orbital contributions shown in brackets): (i) **7** (55.5% P1 $3p_y$, 10.1% O1 $2p_y$, 9.3% O2 $2p_y$); and (ii) **8** (73.7% P1 $3p_y$, 8.8% N1 $2p_y$, 2.7% O1 $2p_y$, 2.9% N2 $2p_y$). The *y* axis is orthogonal to the plane of the four-membered ring.

3.2.6 Mechanism of [2+2] cycloaddition

Our hypothesis is that both of the cycloadditions reported above are step-wise processes, and do not occur via a concerted mechanism. This would occur via initial nucleophilic attack of the central carbon of the heteroallene moiety by the phosphorus atom of **1**. This is consistent with the fact that **1** preferably acts as a nucleophile via the P atom instead of the O atom, as discussed in Chapter 2. The relatively large bulk of the phenyl and Dipp groups

would sterically encumber the crossed transition states required for concerted reactions in either case. Furthermore, the small amounts of phosphorus-containing side-products formed during the ketene reaction could possibly be the acyclic intermediates, although no attempts were made to verify this experimentally. Finally, the fact that the cycloaddition proceeded rapidly with the carbodiimide bearing aryl substituents to generate **8**, while the analogous reaction with alkyl-substituted carbodiimides was unsuccessful, can be rationalised by the stabilisation of the negative charge in the proposed intermediates of the step-wise mechanism (Scheme 3.5). The σ donating effect of the alkyl substituents would raise the energy of this intermediate, and thus make the reaction less favourable. The stereochemistry of **8** can also be explained, as the reduced bonding character in the C–N bonds allows sufficient rotation to maximise the distance between the two bulky Dipp groups, so that upon cyclisation only the *Z* isomer across the C=N bond is observed.

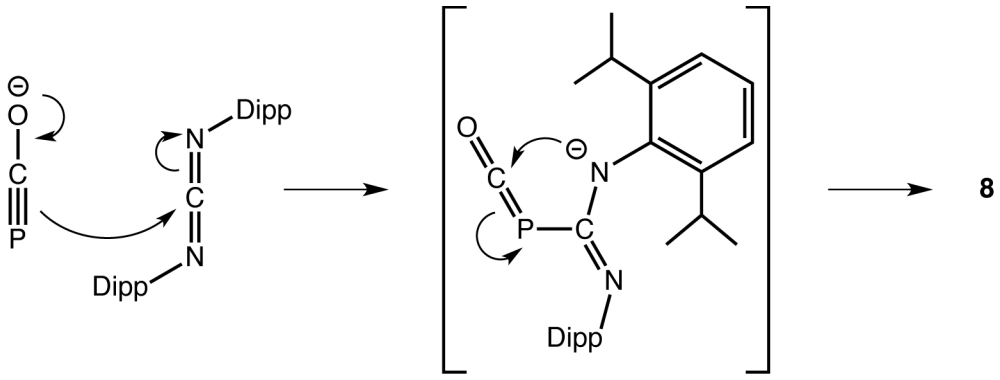

Scheme 3.5: Proposed mechanism for the formation of the [2+2] cycloadduct **8**.

These assertions were confirmed in a subsequent computational paper published in 2014 by Liu, Zhu and Zhao.[33] They employed DFT calculations to probe and corroborate the cycloaddition chemistry of the 2-phosphaethynolate anion with a number of unsaturated bonds, including ketenes and carbodiimides. They found that all attempts to locate a transition state for a concerted [2+2] cycloaddition failed, and that the first step in the reaction was indeed attack of the central carbon of the heteroallene by the phosphorus atom

of $[PCO]^-$. This last finding was also supported by natural population analysis (NPA) showing the partial charges of the relevant atoms.

3.2.7 Subsequently published cycloaddition chemistry

Following our initial publication on the reaction of $[PCO]^-$ with unsaturated substrates to afford phosphorus-containing heterocycles, there have been numerous reports exploiting this mode of reactivity, notably from the research group of Grützmacher.[34–38] The most relevant of these builds directly on the work described above, and is the reaction of the sodium salt of $[PCO]^-$ with a range of carbodiimides (Scheme 3.6).[35] In this case, the reactions all afforded six-membered phosphorus-containing heterocycles and required two equivalents of the carbodiimides. They propose the mechanism proceeds via the four-membered heterocyclic intermediate shown, which is the analogue of **8** with different R groups. They carried out calculations that support this mechanism, but no spectroscopic evidence was obtained for this intermediate with any of the R groups listed.

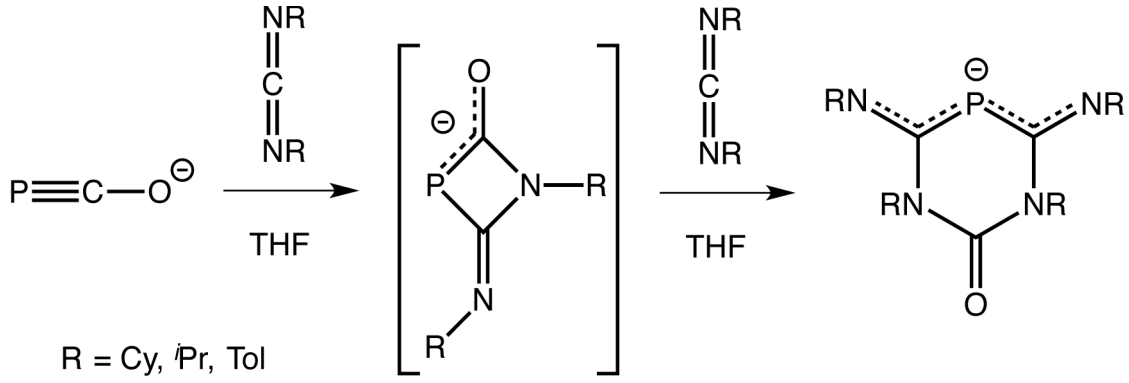

Scheme 3.6: Reaction of $[PCO]^-$ with carbodiimides to afford six-membered heterocycles. Figure adapted from Heift et al.[35]

The two alkyl-substituted carbodiimides used in these reactions (cycloheyxyl and isopropyl) required heating to 80 ˚C before the reaction would proceed, which is in agreement with our observation that there was no reaction between **1** and the bis(cyclohexyl)carbodiimide at 60 ˚C. It is slightly surprising that the four-membered intermediate was not observed during the reaction of $[PCO]^-$ with the carbodiimide bearing the aromatic tolyl substituents, as this

was carried out at room temperature and is similar to our study above. The accompanying DFT calculations (carried out on the methyl derivative for computational ease) show that the six-membered ring is significantly lower in energy than the four-membered intermediate. It is therefore possible in our case that the addition of a second equivalent of the Dipp-substituted carbodiimide to **8** would yield the analogous six-membered ring. This would presumably still be less favourable than the tolyl-substituted case, on account of the enhanced steric demand of the Dipp groups relative to the tolyl groups, and could explain why the four-membered intermediate is not observed in the latter case.

They also published a report describing the reaction of $[PCO]^-$ with carbon dioxide (which is also a heteroallene) at low temperatures, and showed that the carbon dioxide promotes the dimerisation of two molecules of $[PCO]^-$, although this product could not be structurally authenticated.[37]

3.3 Cycloaddition chemistry with isocyanates

The reactivity of [K(18-crown-6)][**1**] with heteroallenes was extended to incorporate isocyanates, RN=C=O.[39] This was carried out at the same time as the ketene and carbodiimide work described in the previous section, and it was initially predicted that the isocyanates would react in an analogous manner. There was no reaction of **1** with (adamantyl)isocyanate at room temperature, which was in accordance with the observed lack of reactivity of **1** with the alkyl-substituted bis(cyclohexyl)carbodiimide. Thus the reaction of **1** with an aryl-substituted isocyanate was expected to afford the anionic four-membered heterocycle shown in Scheme 3.7.

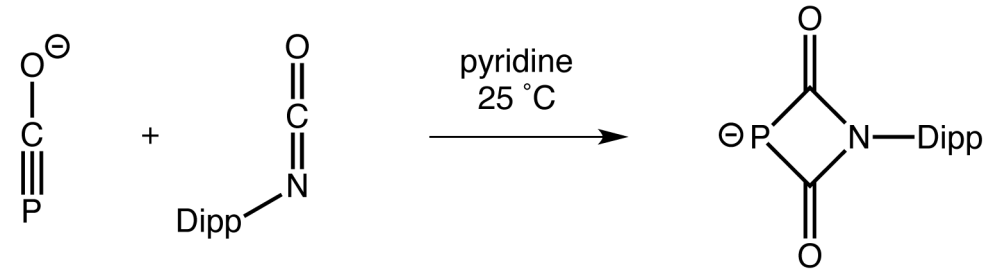

Scheme 3.7: Expected reactivity of **1** with (diisopropylphenyl)isocyanate.

3.3.1 Formation of [K(18-crown-6)][9]

It was quickly shown, however, that this was not the case, and that the isocyanates exhibited a different mode of reactivity to the other heteroallenes. The reaction of [K(18-crown-6)][**1**] with one equivalent of (diisopropylphenyl)isocyanate in pyridine at room temperature showed mostly unreacted **1** in the ^{31}P NMR spectrum, even after several days. When the same reaction was carried out with four equivalents of the isocyanate, ^{31}P NMR spectroscopy revealed that **1** was consumed, and that the major product revealed a singlet at –42.7 ppm, along with a smaller side-product resonating at –36.8 ppm (Figure 3.9). The identity of this side-product will be postulated later in the chapter.

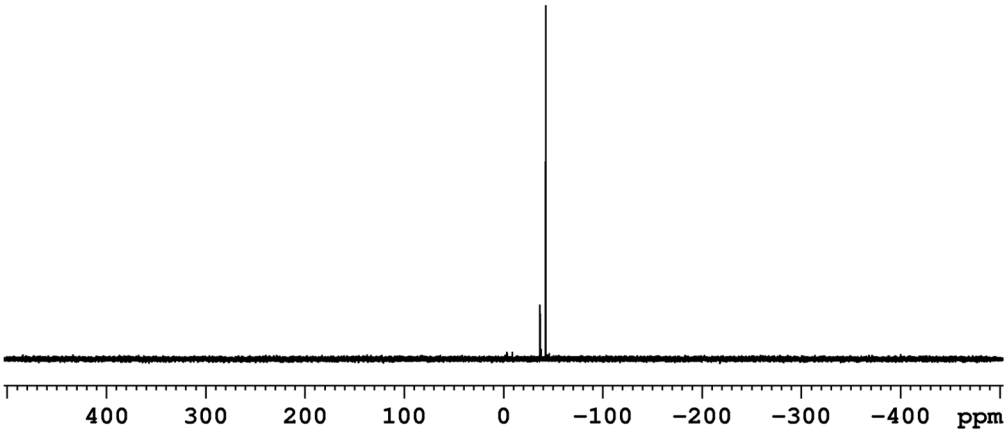

Figure 3.9: ^{31}P NMR spectrum of pyridine solution of [K(18-crown-6)][**1**] and four equivalents of (diisopropylphenyl)isocyanate.

The ^{13}C{^{1}H} NMR spectrum revealed two doublets with small coupling constants at δ = 179.3 ppm ($^{1}J_{C–P}$ = 11 Hz) and δ = 156.8 ppm ($^{2}J_{C–P}$ = 2 Hz), in addition to a host of resonances corresponding to several inequivalent Dipp groups. Single crystals suitable for

X-ray diffraction studies were grown by slow diffusion of hexane into this pyridine solution, and revealed the structure to be the spiro-anion [K(18-crown-6)][**9**] (**9**: $[P\{C(O)N(Dipp)C(O)N(Dipp)\}_2]^-$) shown in Figure 3.10. This product can be viewed as the aggregation of $[PCO]^-$ and four isocyanate molecules, with the loss of an equivalent of carbon monoxide. The chiral molecule crystallised in the non-centrosymmetric space group $P2_1$, but analysis of the Flack parameter, which has a value of 0.306(13), shows that no conclusive comment can be made on the absolute configuration of the molecule in the solid state.[40]

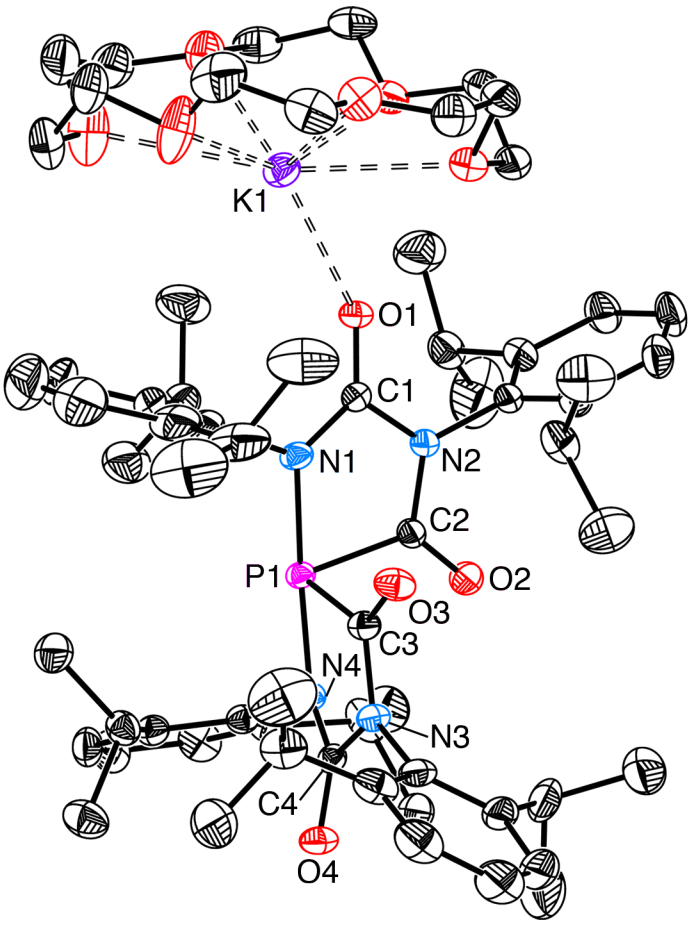

Figure 3.10: Molecular structure of [K(18-crown-6)][**9**]. Anisotropic displacement ellipsoids are set at 50% probability. Hydrogen atoms omitted for clarity.

The structure shows two approximately planar five-membered PN_2C_2 rings fused at the phosphorus centre, with the C2–P1–C3 bond angle of 89.6(2)˚ as an indicator that the planes of the two rings are roughly perpendicular. The N1–P1–N4 bond angle is 176.8(2)˚,

which reveals the linear nature of this moiety and the approximately disphenoidal geometry around phosphorus arising from the presence of a lone pair. The higher electronegativity of the nitrogen atoms relative to the carbon atoms is consistent with the former occupying the apical positions in the trigonal bipyramidal arrangement of electron density. The bond metric data are shown in Table 3.3.

Table 3.3: Selected crystallographic bond lengths (Å) and angles (˚) of the two PN_2C_2 rings within [K(18-crown-6)][**9**].

Bond length (Å)	**Ring 1**	**Bond length (Å)**	**Ring 2**
P1–N1	1.933(3)	P1–N4	1.939(3)
N1–C1	1.340(4)	N4–C4	1.340(4)
C1–O1	1.226(4)	C4–O4	1.233(4)
C1–N2	1.416(4)	C4–N3	1.419(4)
N2–C2	1.385(4)	N3–C3	1.386(4)
C2–O2	1.215(4)	C3–O3	1.206(5)
C2–P1	1.901(3)	C3–P1	1.906(4)
K1–O1	2.747(2)	N.A.	N.A.
Bond angle (˚)	**Ring 1**	**Bond angle (˚)**	**Ring 2**
P1–N1–C1	115.4(2)	P1–N4–C4	113.8(2)
N1–C1–N2	110.2(3)	N4–C4–N3	110.6(3)
C1–N2–C2	118.1(3)	C4–N3–C3	117.8(3)
N2–C2–P1	111.0(2)	N3–C3–P1	110.4(3)
C2–P1–N1	83.2(2)	C3–P1–N4	83.6(2)

The data are ordered to allow direct comparison between the analogous bond lengths and angles between the two PN_2C_2 rings in **9**. All of the metric data are statistically similar between the two rings, with the exception of the P1–N1–C1 and P1–N4–C4 bond angles, which are still very close (115.4(2)˚ and 113.8(2)˚, respectively). A small degree of asymmetry between the two rings might have been expected based on the fact that the potassium cation only interacts with O1, and there is no analogous interaction with the O2

atom. The sum of the internal angles of each of the two five-membered rings are 537.9˚ and 536.2˚, which are close to the expected 540˚ for a perfectly planar system.

All of the P–N and P–C bond lengths within this anion are very long, which is consistent with the small magnitude of the $^{1}J_{C-P}$ and $^{2}J_{C-P}$ coupling constants described earlier (11 Hz and 2 Hz, respectively). The N1–C1 and N4–C4 bond distances are both shorter than those of N2–C2 and N3–C3. These data are consistent with the formulation of the anion as an intramolecular donor–acceptor complex between a phosphenium cation, $[PR_2]^+$, and two terminal imino groups bearing negatively charged oxygen atoms (Figure 3.11). This electronic ground state is corroborated by computational calculations carried out by the Grützmacher group (*vide infra*).

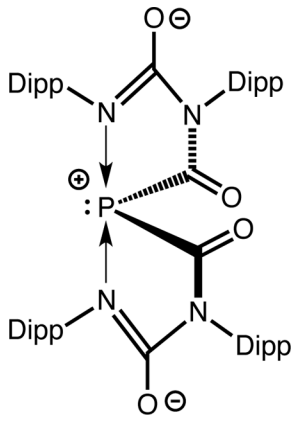

Figure 3.11: Major resonance contribution to the electronic ground state of **9**.

3.3.2 Formation of [K(18-crown-6)][10]

The colourless crystals obtained were isolated and redissolved in pyridine for analysis by ^{31}P NMR spectroscopy, which showed the presence of a new singlet resonance at δ = 120.9 ppm, alongside the same two resonances as before (Figure 3.12).

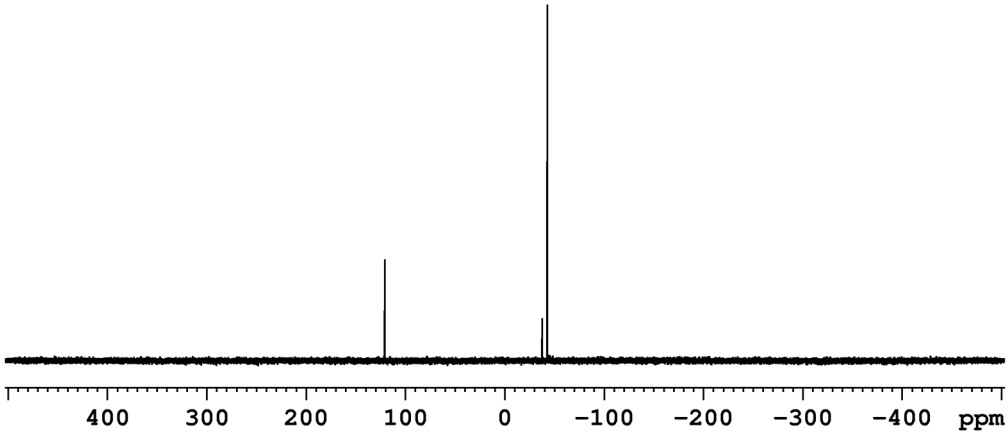

Figure 3.12: ^{31}P NMR spectrum of pyridine solution of [K(18-crown-6)][**9**], showing the growth of a new resonance at δ = 120.9 ppm.

This new resonance at δ = 120.9 ppm always appeared when trying to isolate [K(18-crown-6)][**9**] as a solid sample, whether by rapid precipitation or by slow diffusion of hexane into a solution of the product to promote the growth of crystals. A single crystal X-ray diffraction study identified this new side-product as [K(18-crown-6)][**10**] (**10**: [PC(O)N(Dipp)C(O)N(Dipp)]$^-$), shown in Figure 3.13.

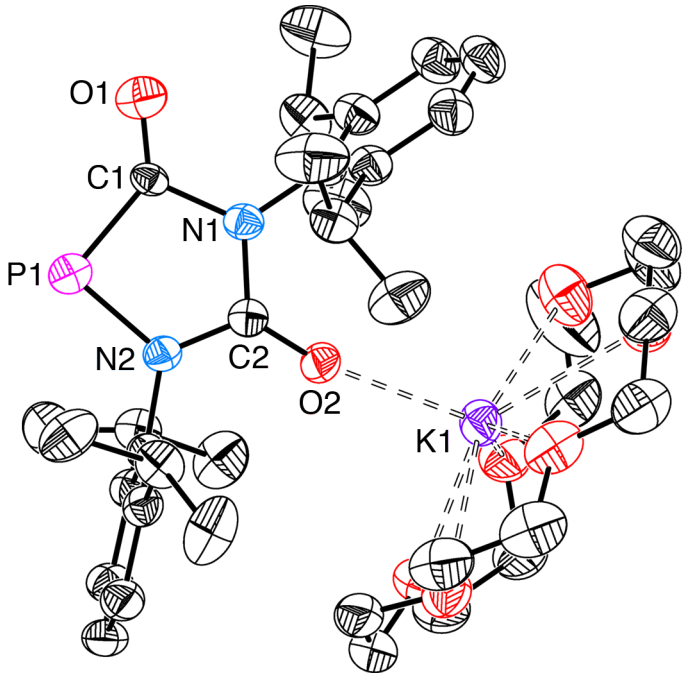

Figure 3.13: Molecular structure of [K(18-crown-6)][**10**]. Anisotropic displacement ellipsoids are set at 50% probability. Only the major component of the disordered 18-crown-6 moiety is shown. Hydrogen atoms omitted for clarity.

The crystal structure shows **10** to be the anionic planar PN_2C_2 ring that is a constituent part of the spiro-anion **9**. The two Dipp substituents are nearly orthogonal to the plane of the five-membered ring, as expected based on sterics, and the $[K(18\text{-crown-6})]^+$ cation interacts solely with the O2 atom. Bond metric data for the anionic moiety are shown in Table 3.4.

Table 3.4: Selected crystallographic bond lengths (Å) and angles (˚) within [K(18-crown-6)][**10**].

Bond distance (Å)	
P1–C1	1.778(2)
C1–O1	1.184(3)
C1–N1	1.501(3)
N1–C2	1.386(3)
C2–O2	1.239(3)
C2–N2	1.348(3)
N2–P1	1.767(2)
K1–O2	2.638(2)
Bond angle (˚)	
P1–C1–N1	105.9(1)
C1–N1–C2	117.0(2)
N1–C2–N2	109.7(2)
C2–N2–P1	116.7(2)
N2–P1–C1	90.7(1)

The P1–C1 bond length (1.778(2) Å) suggests a small amount of multiple bond character and delocalisation of the negative charge into the C1=O1 π^* antibonding orbital, although the C1–O1 bond length is relatively short (1.184(3) Å). The C1–N1 bond length is particularly long (1.501(3) Å), whereas the other C–N bond distances are between the expected values of single and double bonds (C–N: 1.46 Å, C=N: 1.27 Å).[30,31] This is indicative of delocalisation of the lone pairs on N1 and N2 into the C2–O2 π^* orbital, and is substantiated by the elongated C2–O2 bond distance (1.239(3) Å). This resonance would be stabilised by the interaction of O2 with the K^+ cation. The sum of the internal angles of the five-membered ring is 540.0˚, demonstrating the planarity of the system.

Due to the fact that small amounts [K(18-crown-6)][**10**] appeared to be generated during the attempted isolation of [K(18-crown-6)][**9**], and the fact that both species had similar solubilities in laboratory solvents, it was not possible to obtain compositionally pure samples of either product. An ESI mass spectrometric investigation was carried out on a DMF solution containing both products. The negative ion mode showed the anions **9** and **10** at *m/z* values of 843.2 and 437.0, respectively, alongside some other fragments. The positive ion mode spectrum revealed the cation-paired species $\{[K(18\text{-crown-6})]_2[\mathbf{9}]\}^+$ and $\{[K(18\text{-crown-6})]_2[\mathbf{10}]\}^+$ at *m/z* ratios of 1449.4 and 1044.4, respectively.

3.3.3 Mechanism of formation of 9 and 10

It is clear that the anions **9** and **10** differ substantially from **7** and **8**, although they are all derived from the reactions of $[PCO]^-$ with heteroallenes. Despite the apparent order that the products were first observed, it is clear that the five-membered ring **10** is an intermediate on the route to formation of the spiro-anion **9**. Thus the proposed mechanism for the formation of **10** is outlined in Scheme 3.8.

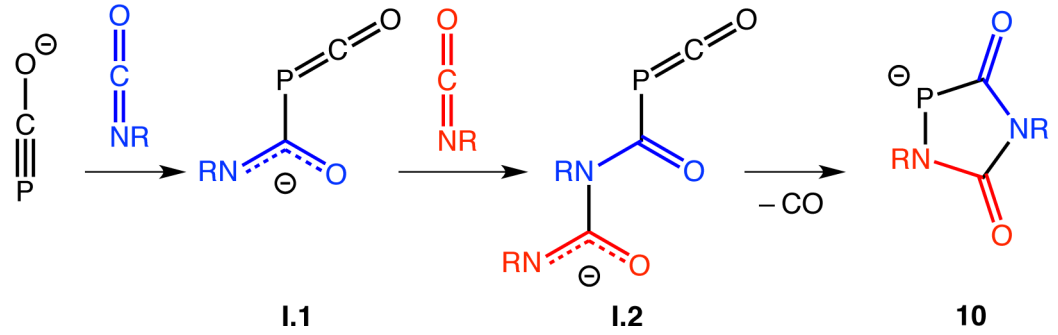

Scheme 3.8: Proposed mechanism of formation of **10**.

The reaction proceeds by nucleophilic attack of the central carbon atom of the isocyanate by the phosphorus atom of **1** to afford the intermediate **I.1**. At this point the nitrogen atom could attack the central carbon of the PCO moiety to yield the four-membered ring, by analogy with the previously discussed formations of **7** and **8**. This appears to not be the case, however, and instead the nitrogen atom attacks the central carbon of a second

isocyanate molecule, to afford intermediate **I.2**. This is followed by intramolecular nucleophilic attack of the di-coordinated nitrogen atom on the phosphorus with extrusion of carbon monoxide to afford the five-membered ring **10**. In the presence of excess isocyanate, the reaction can continue to afford **9** (Scheme 3.9).

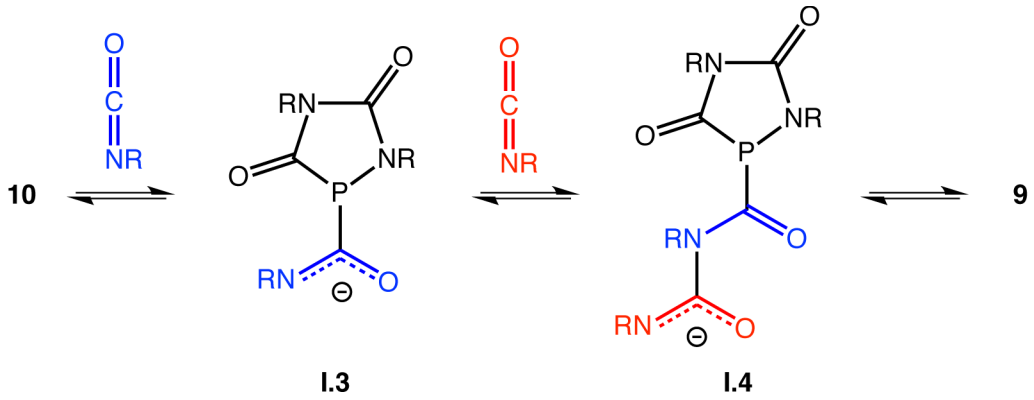

Scheme 3.9: Proposed mechanism of formation of **9**.

The same colour scheme has been used in Schemes 3.8 and 3.9 to highlight the similarity between the reactions and the nature of the intermediates. The principal difference is that the formation of **9** from **10** is presumably reversible, based on the experimental observations. This may stem from the relatively weak binding of the isocyanates with the five-membered ring (as shown by the long P–C and P–N bond lengths in the crystal structure of **9**), and the fact that there is no further loss of carbon monoxide in this mechanism, so **9** can be viewed simply as an adduct of **10** and two isocyanate molecules. The fact that **9** forms at all, and rapidly enough that **10** is not spectroscopically observed as an intermediate in the initial formation of **9**, suggests that the spiro-anion is lower in energy.

3.3.4 $[PCO]^-$ as a source of phosphide, "P^-"

The formation of **10** from **1** and two equivalents of isocyanate represents a very important and promising mode of reactivity of the 2-phosphaethynolate anion. The loss of carbon monoxide in the final step of Scheme 3.8 shows that $[PCO]^-$ can act as a source of the naked phosphide anion "P^-". The ease of handling of **1**, coupled with the potentially facile

cleavage of the P–C bond, whether it be chemically or photolytically, would render $[PCO]^-$ an ideal and versatile synthon as a *masked phosphide* reagent.

This idea has been broached in other studies. Our group, in a collaboration with the group of Scheschkewitz, showed that $[PCO]^-$ can react with cyclotrisilene, an unsaturated silicon-containing three-membered ring bearing bulky 2,4,6-triisopropylphenyl (Tipp) substituents, to cleave the P–C bond and afford the product shown in Scheme 3.10 (i).[41] Photolysis of this compound results in decarbonylation and the incorporation of the phosphide vertex in an anionic Si_3P four-membered heterocycle.

Grützmacher and co-workers have also demonstrated the reaction of $[PCO]^-$ with imidazolium salts to yield the phosphaalkene product shown in Scheme 3.10 (ii).[42] This reaction occurs via the protonation of the $[PCO]^-$ unit to afford a carbene-stabilised HP=C=O moiety, followed by loss of carbon monoxide. This product was already discussed in Chapter 1, where it was synthesised by the reaction of imidazolium salts with $[P_7]^{3-}$ in a collaborative study between Gudat and Grützmacher.[43]

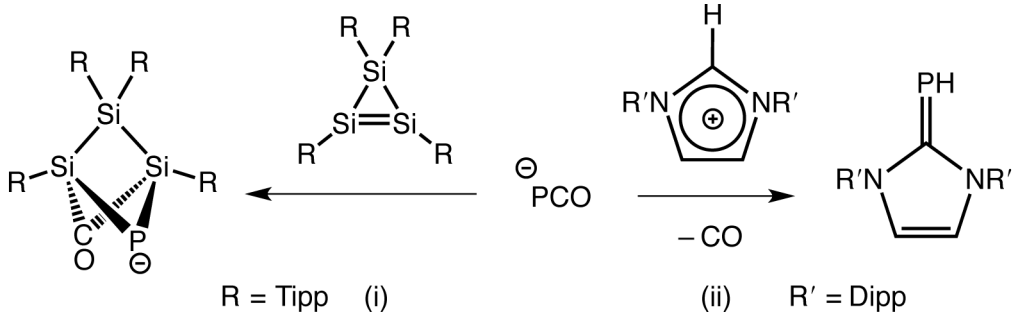

Scheme 3.10: $[PCO]^-$ as a phosphide source with: (i) a cyclotrisilene;[41] and (ii) an imidazolium salt.[42]

3.3.5 Collaboration with the group of Grützmacher

Having carried out the reactions of [K(18-crown-6)][**1**] with isocyanates described above, we became aware that the research group of Grützmacher were working on similar chemistry, and we decided to collaborate on the project.

By direct comparison with our work, they showed that [Na(1,4-dioxane)$_{2.5}$][PCO] reacts with two equivalents of the Dipp-substituted isocyanate to cleanly yield the five-membered ring **10**, which crystallised as the [Na(THF)$_2$]$^+$ salt. In this case the crystal structure shows each Na$^+$ cation coordinates to two THF molecules and two anions (one through O1, the other through O2), to afford a stable linear coordination polymer. Interestingly, they observed no evidence of the spiro-anion **9**, even when a greater excess of the isocyanate was used, which highlights the subtle difference between the [K(18-crown-6)]$^+$ and Na$^+$ salts of **1**.

They extended this study to include other isocyanates with less sterically demanding substituents. The reaction of [Na][**1**] with (phenyl)isocyanate leads to a mixture of products. The major product was characterised as the spiro-anion (**A**) ($\delta(^{31}P)$ = –66.0 ppm, 85%), while the minor product was the anionic six-membered ring (**B**) ($\delta(^{31}P)$ = –16.9 ppm, 15%) shown in Scheme 3.11. The formation of **B** can readily be rationalised by the nucleophilic attack of the anionic nitrogen atom of intermediate **I.2** (Scheme 3.8) at the central carbon of the PCO moiety. It is possible that the Dipp-substituted derivative of **B** is the identity of the previously unknown side-product in our reactions of [K(18-crown-6)][**1**] with the isocyanate that appeared at $\delta(^{31}P)$ = –36.8 ppm, although this product was never isolated in our studies.

Full conversion of **1** was only observed when at least an eight-fold excess of the isocyanate was used, and it was noted that isocyanurate, the cyclic trimer of isocyanate (**C**), also crystallised out of solution. The same reactivity was observed for the aliphatic isocyanates (the cyclohexyl and butyl derivatives), and in both cases the spiro-anion **A** was the major phosphorus-containing product by ^{31}P NMR spectroscopy.

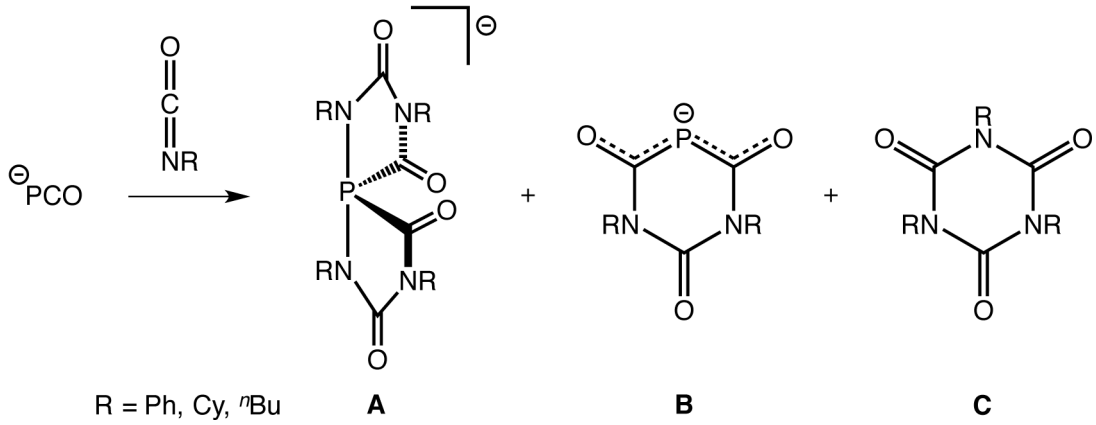

Scheme 3.11: Reaction of $[PCO]^-$ with isocyanates to yield the products labelled as **A**, **B** and **C**, with a range of substituents: Ph, Cy and ^{n}Bu.

The formation of the isocyanurates was interesting, and prompted the idea that the $[PCO]^-$ anion could act as a catalyst for the cyclo-trimerisation of isocyanates. Isocyanurates are industrially relevant materials, and are employed to control the degree of cross-linking and therefore the mechanical and thermal properties of rigid polyurethane foams.[44] Indeed, the addition of a catalytic amount (1 mol%) of [Na][**1**] to (phenyl)isocyanate at room temperature resulted in the formation of triphenyl isocyanurate in a 92% yield. It should be stressed that no other practical investigations of the catalytic activity were carried out, so no catalytic metrics were obtained.

Instead, the Grützmacher group focussed on carrying out a computational assessment of this reaction. The minimum energy reaction pathway (MERP) was calculated for the formation of the products **A** and the five-membered ring, using R = Me for computational simplicity. The data are in good agreement with the description of the mechanism discussed previously in Schemes 3.8 and 3.9. The MERP shows that a greater activation barrier is present for the intramolecular attack of **I.2** (Scheme 3.8) to yield the six-membered ring **B** than the five-membered ring, which is in agreement with the observation that the spiro-anion **A** is always formed in higher yields than **B**.

They also calculated the MERPs for the catalytic trimerisation of (methyl)isocyanate using $[PCO]^-$, the five-membered anionic heterocycle, and the six-membered anionic heterocycle **B** as the catalysts (Scheme 3.12).

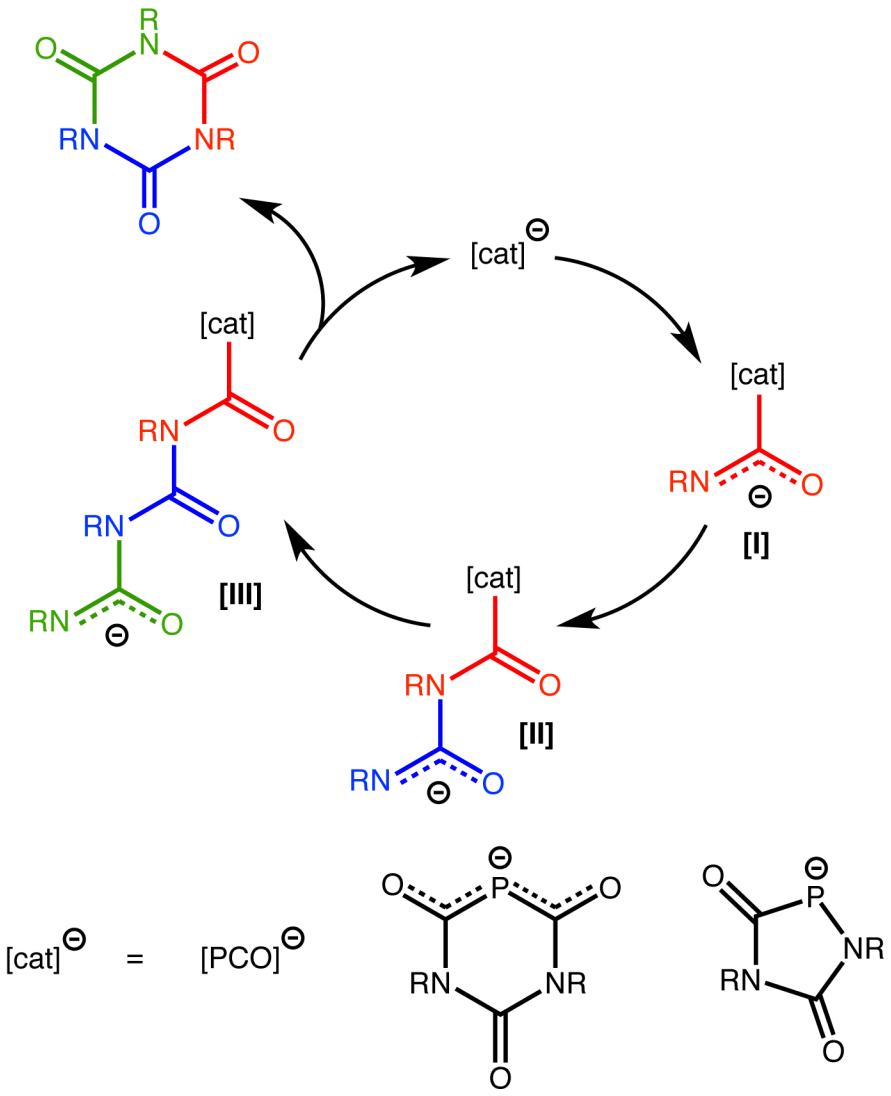

Scheme 3.12: Proposed catalytic cycle for trimerisation of isocyanates.

The calculated MERPs for the three potential catalysts are comparable to those reported for the isocyanate trimerisations catalysed by neutral proazaphosphatranes.[45] The trimerisation of (methyl)isocyanate is strongly thermodynamically favoured by $\Delta H_R = -240.6$ kJ mol^{-1}. All of the catalysts shown appeared capable of catalysing the reaction, although some of the energy barriers were larger when the five-membered ring was considered, indicating this was a less efficient catalyst.

In all cases the phosphorus atom of the anionic catalyst attacks the electrophilic carbon atom of the isocyanate to afford intermediate **[I]**. The sequential reaction with further isocyanate yields intermediates **[II]** and **[III]**, before cyclisation to yield the isocyanurate and regeneration of the catalyst. Note that when the catalyst is $[PCO]^-$, intermediates **[I]** and **[II]** are the same as intermediates **I.1** and **I.2** in Scheme 3.8, and thus in this case **[II]** is the precursor to the five- and six-membered phosphorus-containing heterocycles discussed previously. These species are subsequently considered as alternative possible catalysts. When the catalyst is the five-membered ring, **[II]** can be considered as the open-chain form of the spiro-anion **A**, and a weak binding of the pendant nitrogen atom to the phosphorus atom would result in the formation of the spiro-product.

Thus all of the heterocycles and the spiro-anion mentioned above can be invoked as intermediates or side-products in the cyclic trimerisation of isocyanates by $[PCO]^-$, although the computational study to identify the active catalyst was inconclusive. Unfortunately, due to their similar solubilities, the five- and six-membered anionic rings could not be isolated as compositionally pure samples, so they were not tested independently as catalysts. However, although the exact nature of the catalyst is unclear, the fact that the readily obtained $[PCO]^-$ can be added to a range of isocyanates and result in relatively pure and industrially relevant isocyanurates is of interest and could lead to a range of applications.

3.4 Conclusions

This chapter has described the cycloaddition chemistry of $[PCO]^-$ with a range of heteroallenes. The reactions of [K(18-crown-6)][**1**] with diphenylketene and bis(2,6-diisopropylphenyl)carbodiimide afforded the [2+2] cycloadducts **7** and **8**, respectively.

These novel anions were comprehensively characterised and their electronic ground-state probed experimentally and computationally.

The reaction of [K(18-crown-6)][**1**] with an alternative heteroallene, (2,6-diisopropylphenyl)isocyanate, afforded the spiro-anion **9** and the five-membered heterocycle **10**. These anions can be described as adducts of P^- with four and two isocyanate molecules, respectively, and demonstrate the huge potential of **1** as a phosphide source. A collaboration with the group of Grützmacher then revealed that these products can also be invoked in the catalytic cyclic trimerisation of isocyanates by $[PCO]^-$.

3.5 References

(1) Taylor, D. R. *Chem. Rev.* **1967**, *67*, 317–359.

(2) Smith, M. B. *March's Advanced Organic Chemistry: Reactions, Mechanisms and Structure*; 7th ed.; Wiley: Hoboken, 2013.

(3) *IUPAC. Compendium of Chemical Terminology*; 2nd ed. (the "Gold Book"); compiled by McNaught, A. D. and Wilkinson, A., Blackwell Scientific Publications: Oxford, 1997.

(4) Diels, O.; Alder, K. *Justus Liebigs Ann. Chem.* **1928**, *460*, 98–122.

(5) Hoffmann, R.; Woodward, R. B. *J. Am. Chem. Soc.* **1965**, *87*, 2046–2048.

(6) Woodward, R. B.; Hoffmann, R. *Angew. Chem. Int. Ed. Engl.* **1969**, *8*, 781–853.

(7) Frey, H. M.; Isaacs, N. S. *J. Chem. Soc. B* **1970**, 830–832.

(8) Montaigne, R.; Ghosez, L. *Angew. Chem. Int. Ed. Engl.* **1968**, *7*, 221–221.

(9) Huisgen, R.; Otto, P. *Tetrahedron Lett.* **1968**, *9*, 4491–4495.

(10) Ghosez, L.; Montaigne, R.; Mollet, P. *Tetrahedron Lett.* **1966**, *7*, 135–139.

(11) Rey, M.; Roberts, S.; Dieffenbacher, A.; Dreiding, A. S. *Helv. Chim. Acta* **1970**, *53*, 417–432.

(12) Dewar, M. J. S.; Olivella, S.; Stewart, J. J. P. *J. Am. Chem. Soc.* **1986**, *108*, 5771–5779.

(13) Dewar, M. J. S.; Pierini, A. B. *J. Am. Chem. Soc.* **1984**, *106*, 203–208.

(14) Moore, H. W.; Wilbur, D. S. *J. Org. Chem.* **1980**, *45*, 4483–4491.

(15) Mathey, F. *Angew. Chem. Int. Ed.* **2003**, *42*, 1578–1604.

(16) Wagner, O.; Ehle, M.; Regitz, M. *Angew. Chem. Int. Ed. Engl.* **1989**, *28*, 225–226.

(17) Hahn, F. E.; Wittenbecher, L.; Le Van, D.; Fröhlich, R.; Wibbeling, B. *Angew. Chem. Int. Ed.* **2000**, *39*, 2307–2310.

(18) Schäfer, A.; Weidenbruch, M.; Saak, W.; Pohl, S. *Angew. Chem. Int. Ed. Engl.* **1987**, *26*, 776–777.

(19) Weidenbruch, M.; Olthoff, S.; Peters, K.; Schnering, H. G. von. *Chem. Commun.* **1997**, 1433–1434.

(20) Cowley, A. H.; Hall, S. W.; Nunn, C. M.; Power, J. M. *J. Chem. Soc., Chem. Commun.* **1988**, 753–754.

(21) Meiners, F.; Saak, W.; Weidenbruch, M. *Chem. Commun.* **2001**, 215–216.

(22) Niecke, E.; Streubel, R.; Nieger, M.; Stalke, D. *Angew. Chem. Int. Ed. Engl.* **1989**, *28*, 1673–1674.

(23) Schmidpeter, A. *Phosphorus-Carbon Heterocyclic Chemistry: The Rise of a New Domain*; Pergamon: Oxford, 2001; pp 363-461.

(24) Jamison, G. M.; Saunders, R. S.; Wheeler, D. R.; McClain, M. D.; Loy, D. A.; Ziller, J. W. *Organometallics* **1996**, *15*, 16–18.

(25) Grobe, J.; Van, D. L.; Pohlmeyer, T.; Krebs, B.; Conrad, O.; Dobbert, E.; Weber, L. *Organometallics* **1998**, *17*, 3383–3386.

(26) Jupp, A. R.; Goicoechea, J. M. *Angew. Chem. Int. Ed.* **2013**, *52*, 10064–10067.

(27) Becker, G.; Hübler, K. *Z. Anorg. Allg. Chem.* **1994**, *620*, 405–417.

(28) Jupp, A. R.; Geeson, M. B.; McGrady, J. E.; Goicoechea, J. M. *Eur. J. Inorg. Chem.* **2015**, DOI: 10.1002/ejic.201501075.

(29) Becker, G.; Heckmann, G.; Hübler, K.; Schwarz, W. *Z. Anorg. Allg. Chem.* **1995**, *621*, 34–46.

(30) Pyykkö, P.; Atsumi, M. *Chem. Eur. J.* **2009**, *15*, 186–197.

(31) Pyykkö, P.; Atsumi, M. *Chem. Eur. J.* **2009**, *15*, 12770–12779.

(32) Liotta, C. L.; McLaughlin, M. L.; Van Derveer, D. G.; O'Brien, B. A. *Tetrahedron Lett.* **1984**, *25*, 1665–1668.

(33) Liu, L.; Zhu, J.; Zhao, Y. *Chem. Commun.* **2014**, *50*, 11347–11349.

(34) Chen, X.; Alidori, S.; Puschmann, F. F.; Santiso-Quinones, G.; Benkő, Z.; Li, Z.; Becker, G.; Grützmacher, H.-F.; Grützmacher, H. *Angew. Chem. Int. Ed.* **2014**, *53*, 1641–1645.

(35) Heift, D.; Benkő, Z.; Grützmacher, H. *Angew. Chem. Int. Ed.* **2014**, *53*, 6757–6761.

(36) Heift, D.; Benkő, Z.; Grützmacher, H. *Chem. Eur. J.* **2014**, *20*, 11326–11330.

(37) Heift, D.; Benkő, Z.; Grützmacher, H. *Dalton Trans.* **2014**, *43*, 831–840.

(38) Robinson, T. P.; Goicoechea, J. M. *Chem. Eur. J.* **2015**, *21*, 5727–5731.

(39) Heift, D.; Benkő, Z.; Grützmacher, H.; Jupp, A. R.; Goicoechea, J. M. *Chem. Sci.* **2015**, *6*, 4017–4024.

(40) Flack, H. D. *Acta. Cryst. A* **1983**, *39*, 876–881.

(41) Robinson, T. P.; Cowley, M. J.; Scheschkewitz, D.; Goicoechea, J. M. *Angew. Chem. Int. Ed.* **2015**, *54*, 683–686.

(42) Tondreau, A. M.; Benkő, Z.; Harmer, J. R.; Grützmacher, H. *Chem. Sci.* **2014**, *5*, 1545–1554.

(43) Cicač-Hudi, M.; Bender, J.; Schlindwein, S. H.; Bispinghoff, M.; Nieger, M.; Grützmacher, H.; Gudat, D. *Eur. J. Inorg. Chem.* **2016**, *2016*, 649–658.

(44) Wirpsza, Z. *Polyurethanes: Chemistry, Technology and Applications*; Ellis Horwood: New York, 1993.

(45) Gibb, J. N.; Goodman, J. M. *Org. Biomol. Chem.* **2012**, *11*, 90–97.

Chapter 4
Phosphinecarboxamide and its coordination complexes

4.1 Introduction and objectives

4.1.1 Phosphine chemistry

Phosphines (PR_3) as ligands are ubiquitous in organometallic chemistry for a number of reasons.[1] They are highly tuneable, both electronically and sterically, and are capable of stabilising a wide variety of metal complexes. Phosphines are also very versatile, and a vast range of monodentate, chelating and chiral derivatives have been synthesised as ancillary ligands.[1] These factors, combined with the relative ease of ^{31}P NMR spectroscopy, mean phosphines have long played a central role in organometallic chemistry.

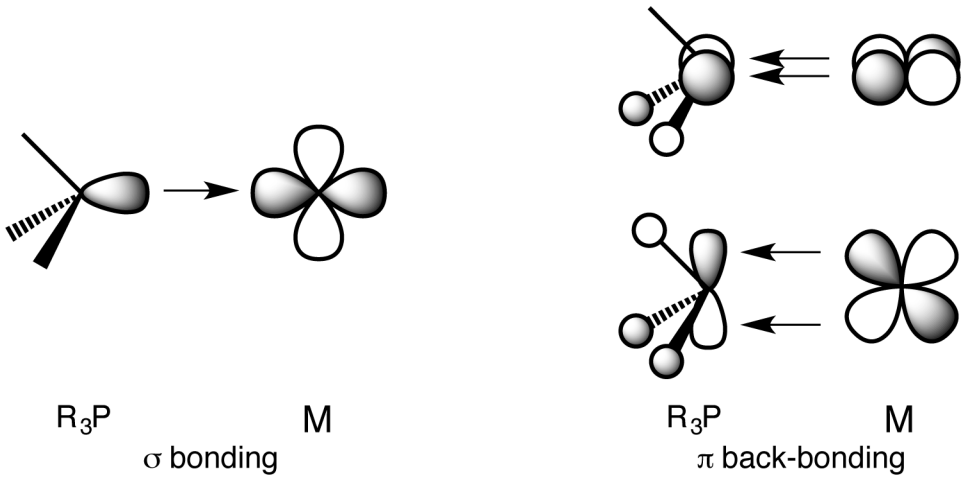

Figure 4.1: Molecular orbitals involved in metal–phosphine bonding interactions.

They can behave as σ donors and π acceptors, in a model similar to the classical metal–carbonyl bonding interaction (Figure 4.1). The orbitals responsible for the π acceptor behaviour were once believed to be the vacant 3d orbitals on the phosphorus, but it has since been shown that this actually arises from donation of electron density into degenerate P–R σ* antibonding orbitals of π symmetry.[2,3]

4.1.2 The Tolman Electronic Parameter

Understanding the stereoelectronic properties and the nature of the phosphine–metal interaction is highly important. Tolman defined the concepts of the cone angle (θ) and the

electronic parameter (ν) as methods of classifying phosphines (later known as the Tolman Cone Angle and the Tolman Electronic Parameter (TEP), respectively).[4,5] The TEP was defined as the A_1 carbonyl stretch of the prototypical $[Ni(CO)_3(PR_3)]$ complex in CH_2Cl_2, and permitted the systematic quantification of the electronic interaction of different phosphine ligands with a metal centre.

Table 4.1: Tolman Electronic Parameter (in cm^{-1}) for selected phosphines. Data from Tolman.[5]

Phosphine	TEP
PMe_3	2064
PPh_3	2069
PF_3	2111

Table 4.1 shows the TEPs for a range of phosphine ligands. Phosphines are poorer π acceptors than CO, so there is increased electron density on the nickel centre in $[Ni(CO)_3(PR_3)]$ relative to the $[Ni(CO)_4]$ complex. This leads to enhanced donation of electron density into the C–O π* antibonding orbitals in the former, and a lower A_1 carbonyl stretch. Arylphosphines tend to be slightly greater π acceptors than alkylphosphines, as is exemplified by the higher TEP for PPh_3 than PMe_3. Phosphines with electronegative substituents are stronger π acceptors, as the σ* orbitals are lower in energy and a better energy match with the d orbitals on the metal. Thus PF_3 has a high TEP value of 2111 cm^{-1}, which makes it a comparable π acceptor ligand to carbon monoxide ($\nu(A_1)$ of $[Ni(CO)_4]$: 2117 cm^{-1}).[5]

There has been controversy surrounding this parameter as an accurate measure of the electronic properties of a phosphine, as the deconvolution of the (often) complementary σ donor and π acceptor contributions to the bonding is difficult.[6–8] This so-called σ/π controversy, and possible alternative measures for quantifying the bonding in metal–phosphine complexes, will be discussed later in the chapter.

4.1.3 Primary phosphine chemistry

Primary phosphines (PH_2R) are typically pyrophoric, miasmic, toxic and extremely air-sensitive. Consequently, they are underemployed as chemical reagents, despite their utility in the fields of macrocycle synthesis,[9] medicinal chemistry,[10] polymer science,[11–13] and asymmetric catalysis.[14–18] On account of this versatility, the generation of more "user-friendly" primary phosphines with reduced sensitivity to air and moisture are highly desirable.

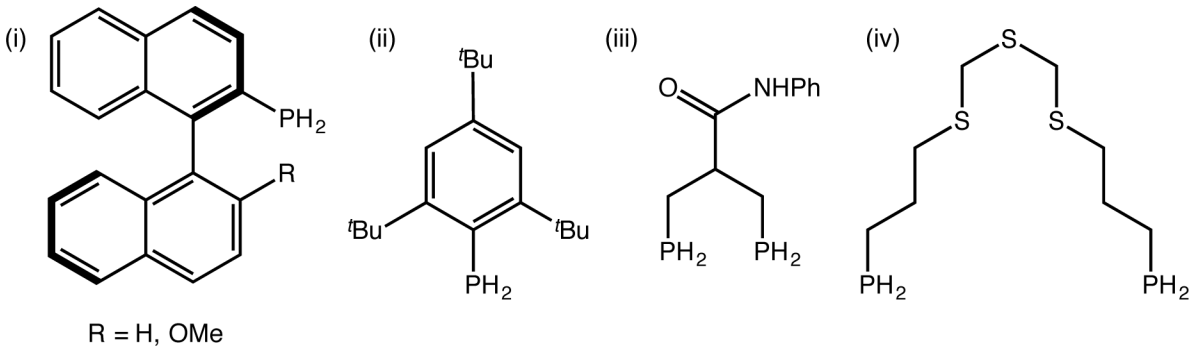

Figure 4.2: Diverse range of air-stable primary phosphines. Figure adapted from Stewart et al.[19]

The number of reported air-stable primary phosphines has grown rapidly in recent years, with strategies typically relying on kinetic stabilisation using bulky substituents and/or the use of substituents that electronically stabilise the phosphine by delocalisation of the lone pair on phosphorus ((i) and (ii) in Figure 4.2).[20,21] In some cases, however, the rationale for the air-stability of the primary phosphine in question is less intuitive (such as (iii) and (iv) in Figure 4.2).[10,22] Higham and co-workers have recently developed a theory based on the absolute energy of the SOMO of the radical cation intermediate as calculated by DFT.[19] If the energy of this SOMO is above the threshold value of –10.0 eV, then the phosphine is predicted to be air-stable; this will be explored in more detail later in the chapter. The predictive powers of this computational method could potentially assist with the design of novel "user-friendly" primary phosphines where the P–H bond is still accessible for further functionalisation.

4.1.4 Wöhler's synthesis of urea

Wöhler's original synthesis of urea in 1828 is a scientific milestone considered by many as the birth of modern organic chemistry.[23–25] At that time in history it was believed that organic molecules possessed a certain *vital force*, and thus that it was not possible for a living organic molecule to be synthesised from purely inorganic precursors.[26] However, Wöhler's unprecedented synthesis of urea from ammonium chloride and silver cyanate served to blur the boundaries between the theretofore disparate scientific disciplines of organic and inorganic chemistry, and it is commonly perceived as the beginning of the demise of the theory of *vitalism*.[26]

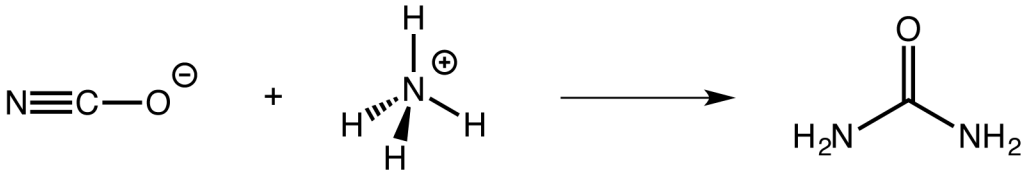

Scheme 4.1: Wöhler's synthesis of urea.

It is worthy of note that this discovery was serendipitous, and Wöhler's initial aim had been to simply obtain the ammonium cyanate salt. He achieved this goal with von Liebig shortly after,[27] although the solid-state structure was not elucidated until 2003, 173 years after the original report.[28,29]

4.1.5 Chapter outline

Wöhler's paradigm-shifting reaction inspired us to explore the possible chemical similarities of the $[PCO]^-$ anion with that of $[NCO]^-$. This chapter will describe the reaction of **1** with ammonium salts to yield phosphinecarboxamide, a phosphorus-containing analogue of urea. This product is a rare example of an air- and moisture-stable primary phosphine, and the structure and electronic properties of this novel and simple molecule will be discussed. The coordination chemistry of this phosphine will be explored within a range of complexes, and the nature of the metal–phosphine interactions probed.

4.2 Phosphinecarboxamide

4.2.1 Original synthesis of $H_2PC(O)NH_2$ (11)

By direct analogy with Wöhler's synthesis of urea, we probed the reactivity of $[PCO]^-$ towards ammonium salts. In a typical reaction, a solid sample of [K(18-crown-6)][**1**] was dissolved in pyridine or THF with an equimolar quantity of $[NH_4][X]$ (X = BF_4, BPh_4) to afford the parent phosphinecarboxamide (or carbamoylphosphine) $H_2PC(O)NH_2$ (**11**) in solution, shown in Scheme 4.2.[30]

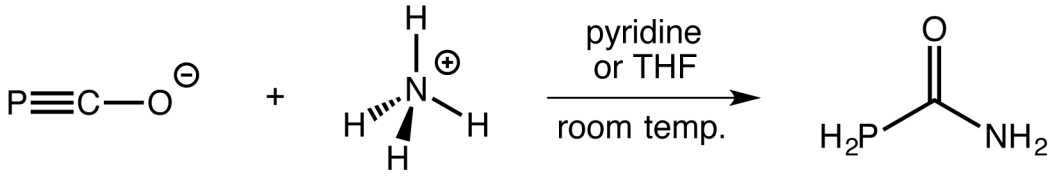

Scheme 4.2: Synthesis of phosphinecarboxamide from $[PCO]^-$ and ammonium salts.[30]

11 is a phosphorus-containing analogue of urea. The mechanism presumably proceeds in an analogous manner to the formation of urea, which has been studied computationally, and is postulated to involve initial protonation of the anion, and the interaction of ammonia with the resulting acid.[31] This topic will be discussed in more detail in the next chapter, where the use of substituted amines to afford *N*-substituted phosphinecarboxamides provides valuable insight into the reaction mechanism.

Despite the simple nature and structure of this fundamental molecule, **11** is unprecedented in the chemical literature. The syntheses of *P*-functionalised phosphinecarboxamides, such as $Ph_2PC(O)NH_2$, were reported in the late 1960s by the reaction of isocyanic acid with secondary phosphines.[32,33] To the best of our knowledge, no attempts were made to synthesise the parent primary phosphine species by the reaction of isocyanic acid with PH_3. More recently, the hydrophosphination of isocyanates with secondary phosphines, catalysed by lanthanum and yttrium complexes, has been shown to afford a range of novel

phosphinecarboxamides ($R_2PC(O)NHR'$: R = Ph, 4-$(MeO)C_6H_4$, 4-MeC_6H_4; R′ = Ph, Cy, Ad, 1-Naph and 4-XC_6H_4 where X is F, Cl, Br, OMe, CF_3).[34] Once again, however, the synthetic scope was limited to the generation of tertiary phosphines.

There is a stark difference in reactivity between primary and tertiary phosphines, and between other moieties where the presence of a hydrogen atom instead an alkyl or aryl R group substantially alters the reactivity and nature of the functional group (such as, for example, aldehydes versus ketones). **11** thus represents a new family of primary phosphines and a new functional group. Intriguingly, the molecule also appears to be remarkably air- and moisture-stable, which is rare for primary phosphines, and the reasons underpinning this will be explored in more detail shortly. We set out to explore the nature of this novel species, and to determine whether it reacts principally as a primary phosphine, as an amide, as a combination of the two, or in a completely different manner altogether. This would reveal which of the following resonance forms contribute most significantly to the bonding in **11** (Figure 4.3).

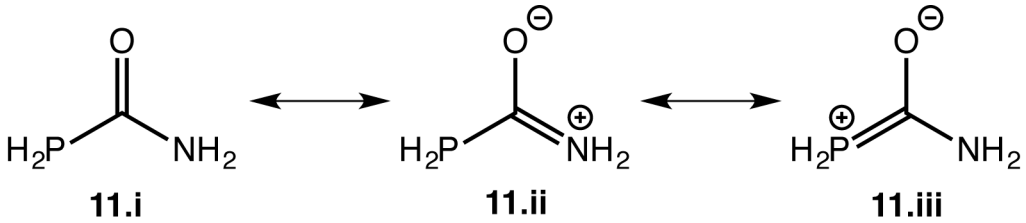

Figure 4.3: Possible resonance forms for **11**.

11 is volatile in solution, so a trap-to-trap distillation under reduced pressure of the pyridine or THF solutions discussed above permitted separation of the [K(18-crown-6)][X] by-product, and afforded a clean solution of **11**. Interestingly, the same reaction could be carried out with $[NH_4][Cl]$, but separation by trap-to-trap distillation was not possible in this case, presumably due to strong hydrogen bonding interactions of the amide protons with the chloride anion. This is consistent with the prominent role of urea-based receptors in anion

binding.[35–38] Due to the poor solubility of ammonium chloride, this reaction was also significantly slower (several days at room temperature) than the ammonium tetrafluoroborate and tetraphenylborate reactions (went to completion in a matter of minutes; the reaction was always complete before the ^{31}P NMR spectrum could be obtained).

4.2.2 NMR spectroscopic analysis

4.2.2.1 Characterisation of 11

The apparent volatility of **11** in solution under reduced pressure, coupled with the fact that the product did not appear to precipitate out of solution with a large range of solvents, even after cooling to –80 ˚C, initially precluded the isolation of **11** as a solid. Therefore we had to heavily rely on extensive NMR spectroscopic characterisation to confirm that our product was indeed the phosphorus analogue of urea, and to gain structural information on this novel species.

The ^{31}P NMR spectrum of a d_5-pyridine solution of **11** shows a triplet of doublets at –134.4 ppm ($^{1}J_{P–H}$ = 209 Hz, $^{3}J_{P–H}$ = 12 Hz), which collapses to a singlet on proton decoupling (Figure 4.4). The ^{1}H NMR spectrum reveals a doublet centred at 3.82 ppm ($^{1}J_{H–P}$ = 209 Hz), which collapses on selected decoupling of the ^{31}P NMR resonance at –134.4 ppm. This resonance corresponds to the two magnetically equivalent protons on the phosphorus, which is consistent with free rotation around the P–C bond.

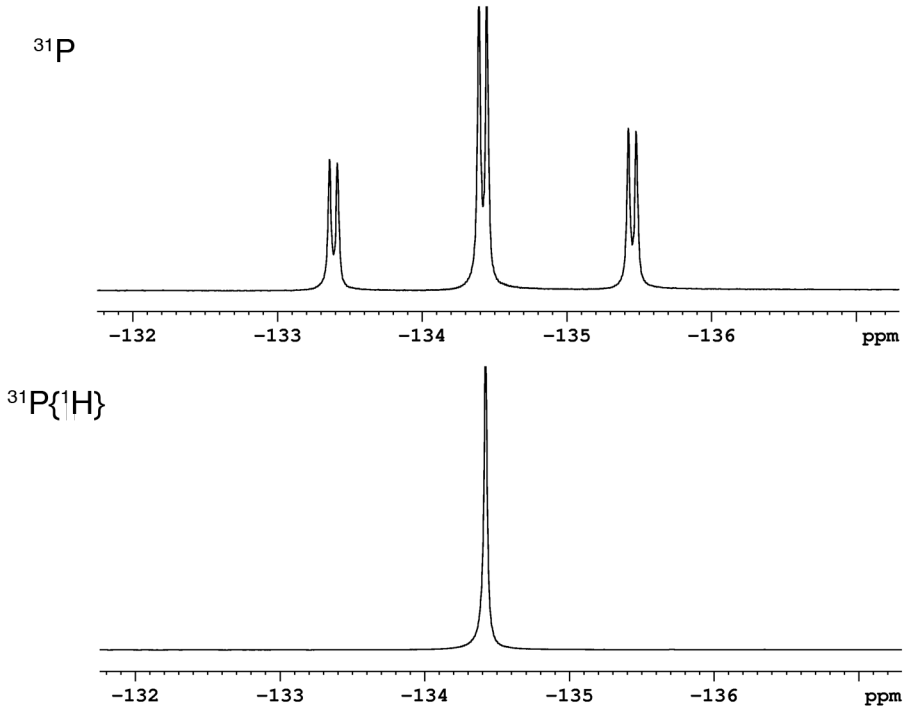

Figure 4.4: ^{31}P and $^{31}P\{^{1}H\}$ NMR spectra of d_5-pyridine solution of **11**.

The room temperature ^{1}H NMR spectrum of **11** reveals two downfield broad resonances at 8.57 ppm and 9.05 ppm, corresponding to two inequivalent amide N–H protons (Figure 4.5). These two resonances coalesce to a singlet at temperatures above 75 ˚C, implying restricted rotation around the C–N bond at room temperature. The prolonged heating of the sample leads to decomposition, principally to PH_3 and isocyanic acid.

The $^{13}C\{^{1}H\}$ NMR spectrum reveals a doublet at 175.8 ppm ($^{1}J_{C-P}$ = 8 Hz). All of the spectroscopic data are consistent with significant contributions from resonances **11.i** and **11.ii**, with marked double bond character in the C–N bond, and a significantly smaller contribution from **11.iii**. The fact that the ^{31}P NMR resonance is only a triplet of doublets (instead of the expected triplet of doublet of doublets) indicates that the $^{3}J_{P-H}$ coupling to the second amide proton is too small to be resolved experimentally.

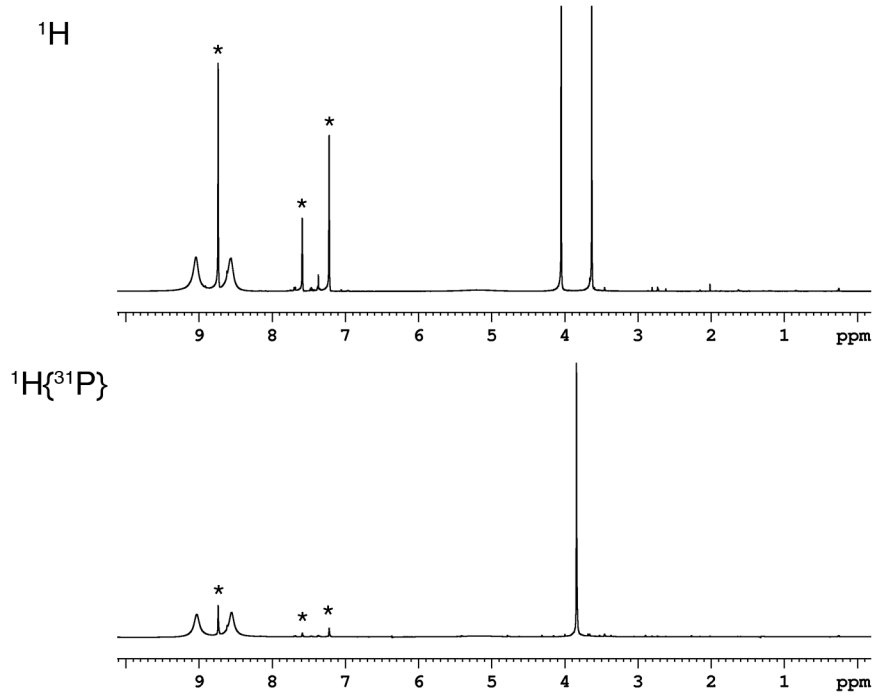

Figure 4.5: ^{1}H and ^{1}H{^{31}P} NMR spectra of d_5-pyridine solution of **11**. Resonances marked with * are due to residual protic solvent.

4.2.2.2 Isotopic labelling studies

These spectroscopic assignments were further corroborated using isotopic labelling studies. The amide proton resonances of **11** are broadened in part due to the coupling with the quadrupolar ^{14}N nucleus (99.63% abundant, I = 1), which can be circumvented by enriching the sample with ^{15}N (I = ½). Thus the reaction of [K(18-crown-6)][**1**] with [^{15}NH$_4$][Cl] afforded H$_2$PC(O)^{15}NH$_2$ (**11-^{15}N**) after several days (again due to the relative insolubility of the chloride salts). This allowed the assignment of the upfield amide resonance to the proton that would be *trans* to the phosphorus across the C=N double bond in **11.ii** (from Figure 4.3), as indicated by the presence of a doublet of doublets (δ = 9.92 ppm; $^1J_{H–N}$ = 85 Hz, $^3J_{H–P}$ = 8 Hz) in the ^{1}H NMR spectrum (Figure 4.6). This resonance is still broadened due to exchange broadening arising from the hindered rotation around the C–N bond, and by hydrogen bonding interactions with the d_5-pridine solvent. This is perhaps why the coupling constant to phosphorus is only measured at 8 Hz (slightly smaller than the $^3J_{P–H}$ = 12 Hz reported for **11** above), although this could also arise from the isotopic enrichment of the

nitrogen atom. The downfield amide resonance appears as a doublet at δ = 8.49 ppm ($^1J_{H–N}$ = 89 Hz). Both of these resonances have shifted significantly downfield relative to the data reported for **11**, but this is simply because the amide protons in **11-^{15}N** are strongly hydrogen bonding to the chloride anion in solution, which was not present in the previously discussed sample. The $^{31}P\{^1H\}$ NMR spectrum of **11-^{15}N** reveals a doublet with a $^2J_{P–N}$ coupling constant of 12 Hz.

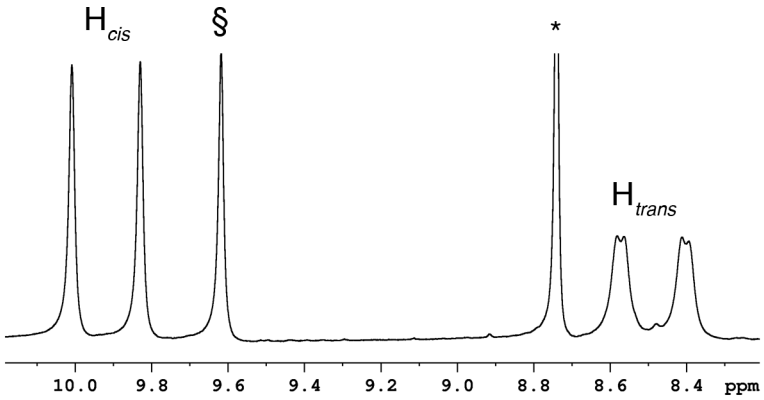

Figure 4.6: ^{1}H NMR spectrum of d_5-pyridine solution of **11-^{15}N**. Resonance marked with * is due to residual protic solvent. Resonance marked with § is an unknown impurity

Deuterium labelling using $[ND_4][Cl]$ afforded primarily $D_2PC(O)ND_2$ (**11-D$_4$**). This was shown by ^{2}H NMR spectroscopy, where the spectrum was analogous to the ^{1}H NMR spectrum of **11**, except for the magnitude of the coupling constant to phosphorus ($^1J_{D–P}$ = 31 Hz) in the former. This is in line with the different gyromagnetic ratios of ^{2}H and ^{1}H ($\gamma_H/\gamma_D \approx 6.5$).[39] This difference in coupling constant is neatly but unintentionally highlighted in the ^{31}P and $^{31}P\{^1H\}$ NMR spectra of this sample (Figure 4.7). Incomplete deuteration of the starting material leads to the observation of PD_2, PHD and PH_2 moieties in solution. The PHD fragment shows significantly greater coupling of the phosphorus nucleus to the hydrogen ($^1J_{P–H}$ = 209 Hz) than to the deuterium ($^1J_{P–D}$ = 31 Hz). Note, due to the fact that deuterium has I = 1, the PD_2 resonance is a quintet with integration 1:2:3:2:1, not the typical binomial 1:4:6:4:1 quintet arising from the coupling of a nucleus to four equivalent I = ½ nuclei.

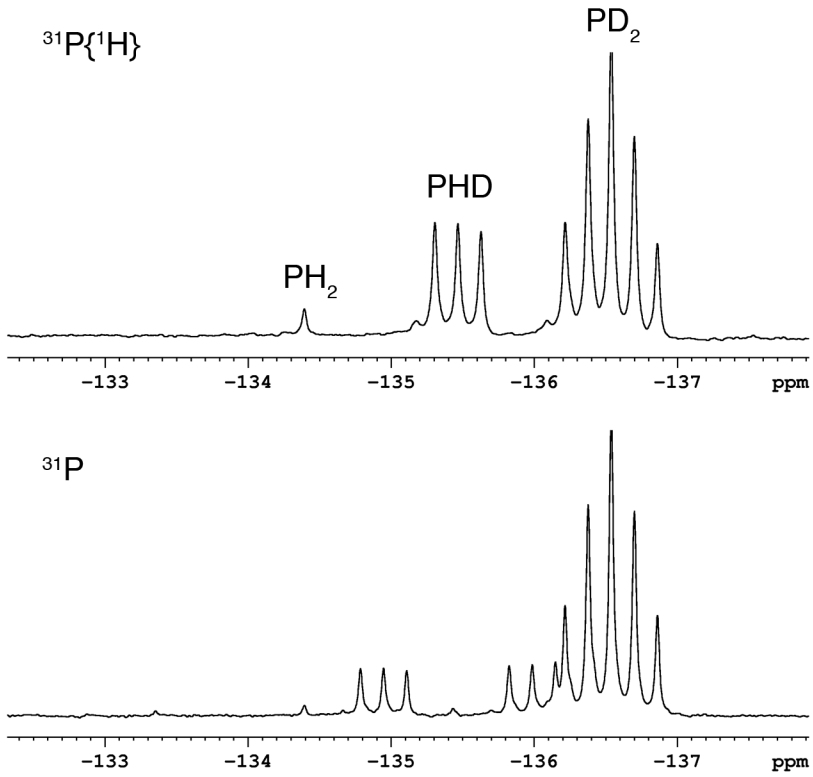

Figure 4.7: $^{31}P\{^{1}H\}$ and ^{31}P NMR spectra of pyridine solution of **11-D$_4$**. PHD and PH_2 moieties arise from incomplete deuteration of the starting material.

4.2.3 Refined synthesis of 11

The initial synthetic procedure of dissolving the ammonium salt and 2-phosphaethynolate anion in THF, pyridine or DMF, followed by a trap-to-trap distillation to separate the salt by-product and afford **11** cleanly in solution was successful, but onerous when it came to further exploring the chemistry of this simple molecule. Not only was it a time-consuming procedure, but it was also clear that a fraction of the desired product was not distilling between the two traps, even after prolonged distillation times and with gentle heating. This meant the subsequent reactions were challenging to carry out in a controlled stoichiometric manner, but also hinted that **11** was less volatile as a solid. These factors prompted the design of a revised and refined synthesis of **11** that would be more amenable for the further study of its chemistry.

This was achieved with the use of liquid ammonia as the solvent. Liquid ammonia was condensed into a round-bottomed flask containing equimolar quantities of [Na(1,4-

dioxane)$_{1.75}$][**1**] and [NH_4][BF_4] at –78 ˚C. This slurry was stirred for one hour, after which the mixture was allowed to slowly warm up to room temperature and all of the ammonia boiled off, yielding a white solid consisting of **11** and [Na(1,4-dioxane)$_x$][BF_4]. The remaining 1,4-dioxane was removed *in vacuo*, with the solid product being cooled to 15 ˚C to help prevent product loss. Sublimation under reduced pressure at 50 ˚C permitted the facile separation of the [Na][BF_4], and yielded **11** as a white crystalline solid in multi-gram quantities. This new method has been crucial in the development of **11** as a useful chemical precursor, because we can now access the compound quickly on a relatively large scale, and can carry out further reactions stoichiometrically without the need for adding external references to determine the quantity of **11** in solution.

4.2.4 Crystallographic and computed structure of 11

Sublimation of **11** under reduced pressure at room temperature afforded colourless crystals suitable for single crystal X-ray diffraction. The product crystallises in the non-standard monoclinic space group $P2_1/n$. The structure is shown in Figure 4.8.

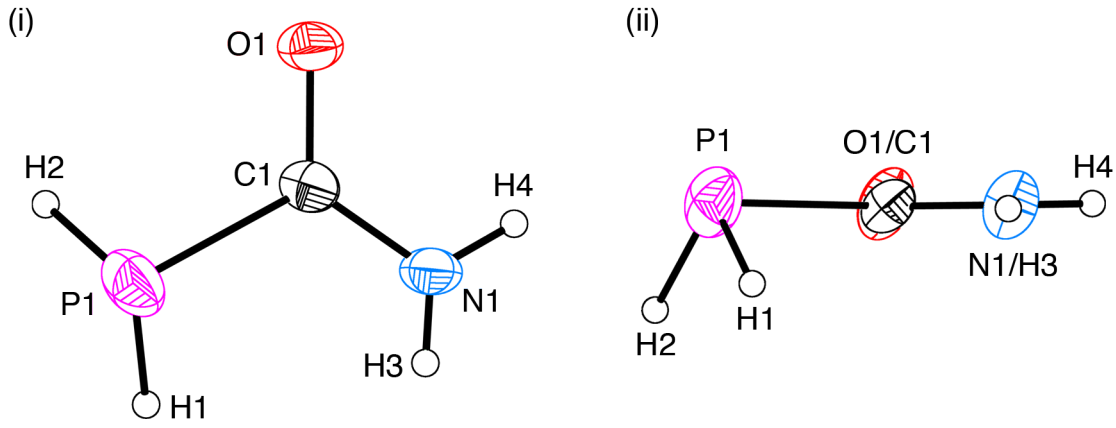

Figure 4.8: (i) Molecular structure of **11**. (ii) The same structure rotated 90˚ to highlight the planarity of the C(O)NH_2 moiety and the pyramidal geometry around P1. Anisotropic displacement ellipsoids are set at 50% probability. Hydrogen atoms are shown as spheres of arbitrary radii.

The hydrogen atoms were located in the difference Fourier map after the heavier atoms had been refined anisotropically. Identifying the locations of hydrogen atoms using X-ray crystallography can often be challenging, on the basis of the very low electron density

around the hydrogen nuclei to scatter the X-rays, and are more reliably located using neutron scattering experiments. In this example, however, the hydrogen atoms were relatively simple to position due to the simple nature of the molecule and the high quality of the data obtained, although the standard deviations on all bond lengths and angles involving hydrogen atoms are relatively large. Table 4.2 shows the crystallographic bond metric data, alongside the analogous data derived computationally that will be discussed shortly.

Table 4.2: Selected crystallographic and computed bond lengths (Å) and angles (˚) in **11**.

Bond distance (Å)	**11**	**11_{calc}**
P1–C1	1.860(2)	1.880
C1–N1	1.326(2)	1.343
C1–O1	1.239(2)	1.230
P1–H1	1.29(2)	1.42
P1–H2	1.36(2)	1.41
N1–H3	0.81(2)	1.01
N1–H4	0.88(2)	1.01
Bond angle (˚)		
P1–C1–O1	118.9(1)	119.6
P1–C1–N1	118.1(1)	117.2
N1–C1–O1	122.9(2)	123.0
C1–P1–H1	98(2)	98
C1–P1–H2	93(1)	94
H1–P1–H2	97(2)	95
C1–N1–H1	120(2)	122
C1–N1–H4	117(2)	120
H3–N1–H4	123(2)	119

The crystallographic structure of **11** shows a pyramidalised geometry around the phosphorus atom (sum of angles without rounding error around P1 is 287˚), whereas the carboxamide moiety is planar (sum of angles around N1 is 360˚). The P1–C1 bond length (1.860(2) Å) is typical of a single bond (sum of single bond covalent radii is 1.86 Å), while

the C1–N1 bond length (1.326(2) Å) possesses significant double bond character (sum of single bond radii is 1.46 Å, sum of double bond radii is 1.27 Å).[40,41] These data are consistent with the spectroscopic data, which predict the large π delocalisation in the carboxamide moiety, but minimal interaction of the phosphorus lone pair with the C–O π* antibonding orbital.

Density functional theory (DFT) calculations support this as well, and in general are in good agreement with the experimental data. The C1–N1 bond length is slightly shorter in $\mathbf{11_{calc}}$ than in **11**, while the C1–O1 bond length is slightly longer. This is presumably due to the fact that the calculations are carried out in the gas phase, while the experimental data is derived from an extended crystal structure where intermolecular hydrogen bonding is present, which would favour the partial negative charge on the oxygen and the partial positive charge on the nitrogen, as in resonance **11.ii** in Figure 4.3. The more obvious difference is the significantly longer N–H and P–H bond distances in $\mathbf{11_{calc}}$ than in **11**. The discrepancy arises from the involvement of the H 1s electron in bonding, which results in a localisation of electron density between the heteroelement and the H atom, and such a notable asymmetric distribution of electron density about the H nucleus is manifested in unrealistically short E−H bonds in structures derived from X-ray data.[42,43]

Inspection of the Kohn-Sham orbitals reveals that the HOMO (Figure 4.9) has significant lone pair character on the phosphorus atom (44.4% P), although the $3p_z$ orbital (where the *z* axis is defined as orthogonal to the $PC(O)NH_2$ plane) also contributes to the other lower-energy π orbitals HOMO−1 and HOMO−2. The HOMO−3 and HOMO−4 are mainly of P−H and P−C σ-bonding character, respectively. The HOMO–5 (Figure 4.9) reveals a very small involvement of the P $3p_z$ orbital (3.9%) with the carboxamide π bonding orbital, which is in agreement with the previous findings. We decided to probe this potentially small

involvement of the phosphorus lone pair and the electronic structure of **11** further, through the means of the barrier to rotation of the amide bond.

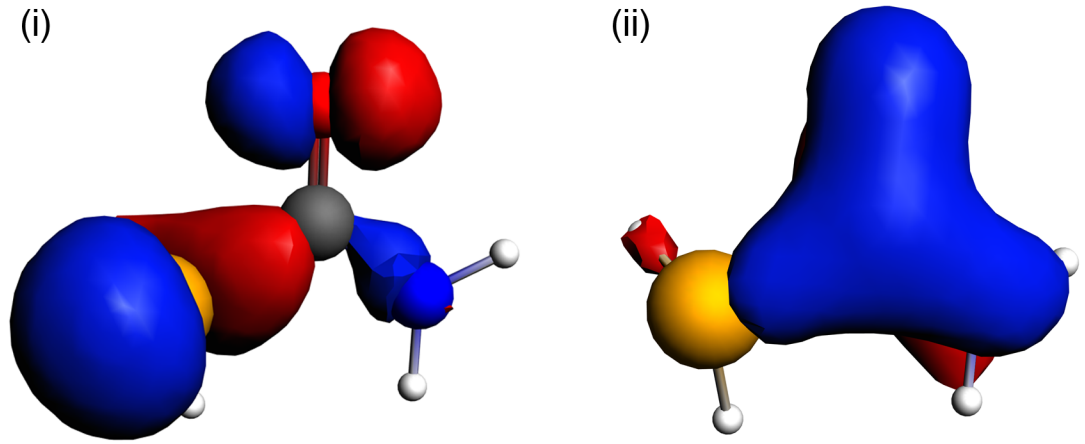

Figure 4.9: Kohn-Sham molecular orbital representations (contour values 0.05 au) of **11** (selected atomic orbital contributions shown in brackets) showing the: (i) HOMO (39.0% O $2p_y$, 23.9% P $3p_z$, 11.9% P $3p_y$); and (ii) HOMO–5 (34.3% C $2p_z$, 30.2% O $2p_z$, 18.0% N $2p_z$, 3.9% P $3p_z$). The *z* axis is orthogonal to the $PC(O)NH_2$ plane, the *x* axis is pointing in the direction of O.

4.2.5 Amide bond rotation

Hindered rotation around the C–N bond due to nitrogen lone pair delocalisation into the C–O π* antibonding orbital is a well-known phenomenon.[44,45] The prototypical example is *N*,*N*-dimethylformamide (DMF), where the hindered rotation yields two distinct methyl resonances in the ^{1}H NMR spectrum.[46,47] This was alluded to earlier in the discussion of the ^{1}H NMR spectrum of **11**, where the two amide protons were inequivalent, which is evidence of contributions from resonance form **11.ii** in Figure 4.3. We decided to probe the height of this barrier to rotation further, both computationally and experimentally, as a means of assessing the electronic structure of **11** and allowing a comparison of **11** with other simple amides.

4.2.5.1 Computationally derived barrier to amide bond rotation

The barrier to C–N bond rotation was calculated at the CCSD/6-311+G(2df,p) level of theory (see Experimental section for further details). As the planar NH_2 moiety in the ground state (**GS**) of **11** is rotated by 90˚, the nitrogen centre can undergo a rehybridisation from sp^2 planar to sp^3 pyramidal.

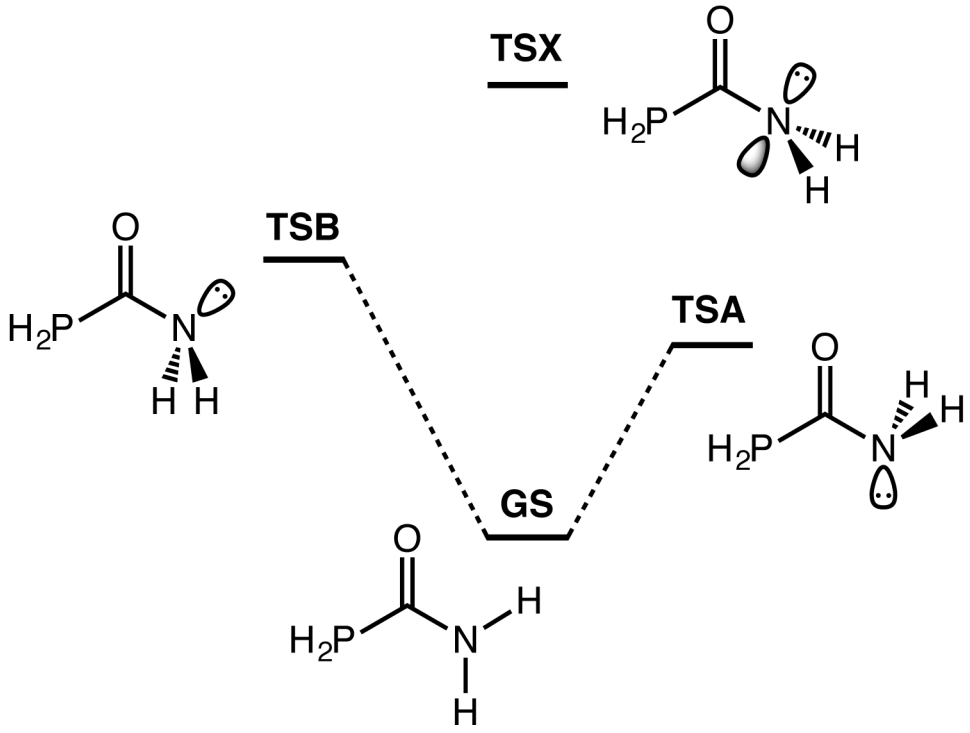

Figure 4.10: A schematic representation of the potential energy surface for C–N bond rotation. $\Delta G^{\ddagger}$ (kJ mol^{-1}): **GS** = 0; **TSA** = 56; **TSB** = 66.

TSA in Figure 4.10 is the result of a 90˚ rotation around the C–N bond leading to a pyramidal amide moiety, and **TSB** is the result of a 90˚ rotation in the opposite direction. The opposite rotations lead to different geometric outcomes for the two transition states, based on the direction of the hydrogen atoms and the lone pair relative to the carbonyl moiety. **TSA** is lower in free energy than **TSB** by 10 kJ mol^{-1}, which presumably arises from the stabilising donation of the nitrogen lone pair into the C–O σ* antibonding orbital. **TSX** is observed as a second order saddle point, in which there is a 90˚ rotation relative to the ground state but no concomitant rehybridisation of the nitrogen centre.

The minimum barrier to C–N bond rotation is therefore 56 kJ mol^{-1}, where **TSA** is the appropriate transition state. This value will shortly be compared to other amides.

4.2.5.2 Experimental barrier to bond rotation: Coalescence temperature method

The barrier to amide bond rotation can also be calculated experimentally using NMR spectroscopy. A variable temperature ^{1}H NMR spectroscopic study of **11** was carried out from 210 K, where the rotation is slow on the NMR timescale, up to 370 K, which is beyond the coalescence temperature of the two resonances, but not necessarily in the fast exchange limit as the resonance is still relatively broad. Note, at these higher temperatures **11** begins to decompose, which is why the study was not performed at higher temperatures. The experiment was carried out in d_7-DMF to allow a more accurate comparison with other amide systems that have been previously carried out in the same solvent.

One of the simpler and best-known procedures to calculate the barrier is via the coalescence temperature method.[39] The rate of exchange, k_c, for two equally populated sites (the two amide protons in this case) at the coalescence temperature, T_c, is given by:

$$k_c = \frac{\pi(\delta\nu)}{\sqrt{2}} \qquad \textbf{(Eq. 4.1)}$$

where δν is the difference in frequency between the two sites in the absence of exchange broadening.[39,48] The chemical shifts of the two amide proton resonances vary as a function of temperature due to the decreasing hydrogen bonding interactions with the solvent at higher temperatures. The two resonances change at slightly different rates, and consequently δν varies as a function of temperature, even when the effects of exchange broadening are ignored. Therefore δν is recorded for several different temperatures in the slow exchange limit (see Figure 4.11), and extrapolation of the line of best fit permits a reasonable estimation of δν at the coalescence temperature.

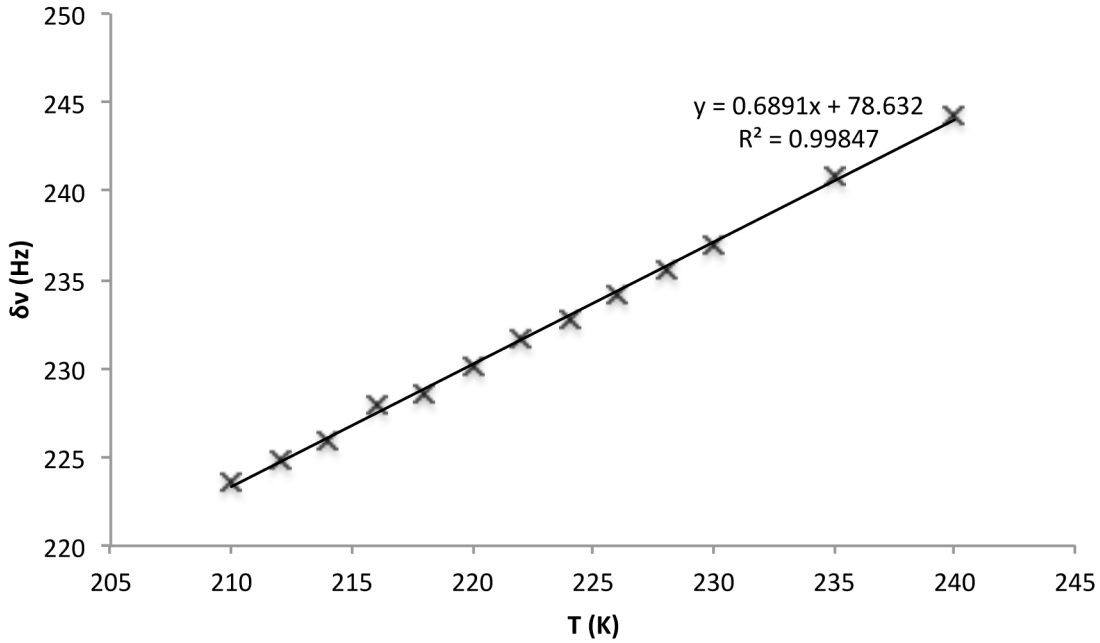

Figure 4.11: Graph plotting δν as a function of temperature in the slow exchange limit.

The gradual broadening of the resonance around the coalescence temperature renders the precise value of T_c challenging to pinpoint. We therefore decided it would more meaningful to state a small range over which coalescence had definitely occurred, in this case 355 to 360 K, and calculate upper and lower bounds of the barrier to rotation. Extrapolation using the equation of the line of best fit from Figure 4.11 gives:

$$\delta\nu\ (T_c = 355\ \text{K}) = 323.3\ \text{Hz}$$

$$\delta\nu\ (T_c = 360\ \text{K}) = 326.7\ \text{Hz}$$

These data can be used in conjunction with the Eyring equation, which defines the rate of reaction as:

$$k = K\frac{k_B T}{h}e^{\frac{-\Delta G^{\ddagger}}{RT}} \qquad \textbf{(Eq. 4.2)}$$

where K is the transmission coefficient (usually taken as unity), k_B is the Boltzmann constant, h is Planck's constant and R is the gas constant.[49,50] A simple rearrangement yields the equation for the free energy of activation, $\Delta G^{\ddagger}$, at the coalescence temperature:

$$\Delta G^{\ddagger} = RT_c ln\left[\frac{k_B T_c}{k_c h}\right] \quad \textbf{(Eq. 4.3)}$$

The values of δν above can be used with Eq. 4.1 to find the appropriate values of k_c, which can then be used with Eq. 4.3 to yield the final barriers to amide rotation (using the coalescence temperature method) as:

$$\Delta G^{\ddagger} (T_c = 355 \text{ K}) = 68.1 \text{ kJ mol}^{-1}$$

$$\Delta G^{\ddagger} (T_c = 360 \text{ K}) = 69.0 \text{ kJ mol}^{-1}$$

This method gives a relatively straightforward calculation of the barrier to rotation, but it relies on several assumptions. The first is that the dependence of temperature on the chemical shift is a linear relationship, and hence the extrapolation of δν at the coalescence temperature from the low temperature regime is valid. This is a reasonable approximation but is unlikely to be precisely correct. Furthermore, it should be noted that the value of $\Delta G^{\ddagger}$ obtained is temperature-dependent, because of the entropy term ($\Delta G^{\ddagger} = \Delta H^{\ddagger} - T\Delta S^{\ddagger}$).[39] Thus a comparison of $\Delta G^{\ddagger}$ values is only reasonable if the entropy of activation is zero, although for similar systems that coalesce at similar temperatures the discrepancy should not be too severe.

4.2.5.3 Experimental barrier to bond rotation: Line shape analysis method

A more accurate method for a kinetic measurement is a complete line shape analysis of the resonances over a range of temperatures, although this necessarily requires a greater expenditure of time and effort. The analysis is based on the change on the shape of the resonances over different exchange limits, and builds on the theoretical foundations established by McConnell in the 1950s.[51] The rate can be calculated by comparison of a theoretical spectrum with that obtained experimentally, and iteratively varying the parameters that determine the shape of the line of the former (one of which is the rate of exchange) until the two correlate well (Figure 4.12).

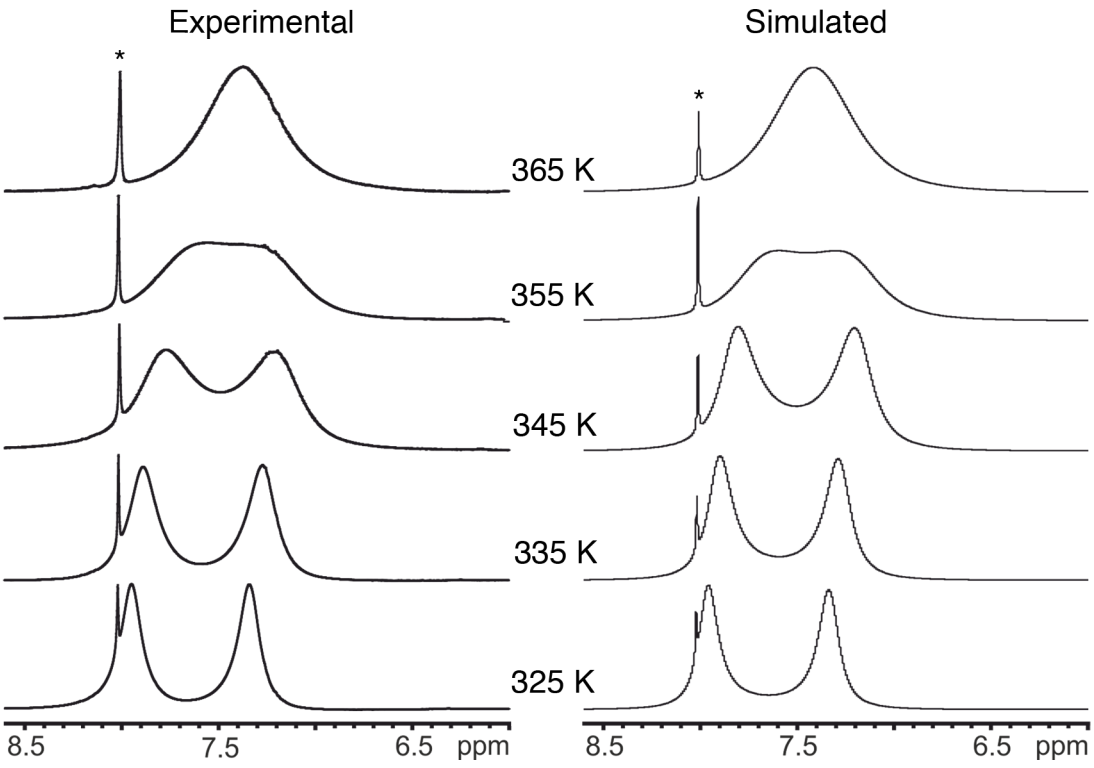

Figure 4.12: Line shape analysis carried out on a d_7-DMF solution of **11** over a range of temperatures. The resonances marked with * are due to the most downfield protic residual in d_7-DMF.

The Eyring equation in Eq. 4.2 can be rewritten following the substitution of $\Delta G^{\ddagger} = \Delta H^{\ddagger} - T\Delta S^{\ddagger}$ to afford the equation in the form:

$$\ln \frac{k}{T} = \frac{-\Delta H^{\ddagger}}{R}\frac{1}{\mathrm{T}} + \ln\left[\frac{k_{\mathrm{B}}}{h}\right] + \frac{\Delta S^{\ddagger}}{R} \qquad \textbf{(Eq. 4.4)}$$

The plotting of the graph of ln[k/T] against 1/T (known as an Eyring plot) for a range of rate constants calculated over different temperatures allows the determination of $\Delta H^{\ddagger}$ (from the gradient) and $\Delta S^{\ddagger}$ (from the y-intercept). This process was carried out by Dr. Nick Rees of the University of Oxford, using the same variable temperature NMR spectroscopic data as above, to give the Eyring plot shown in Figure 4.13.

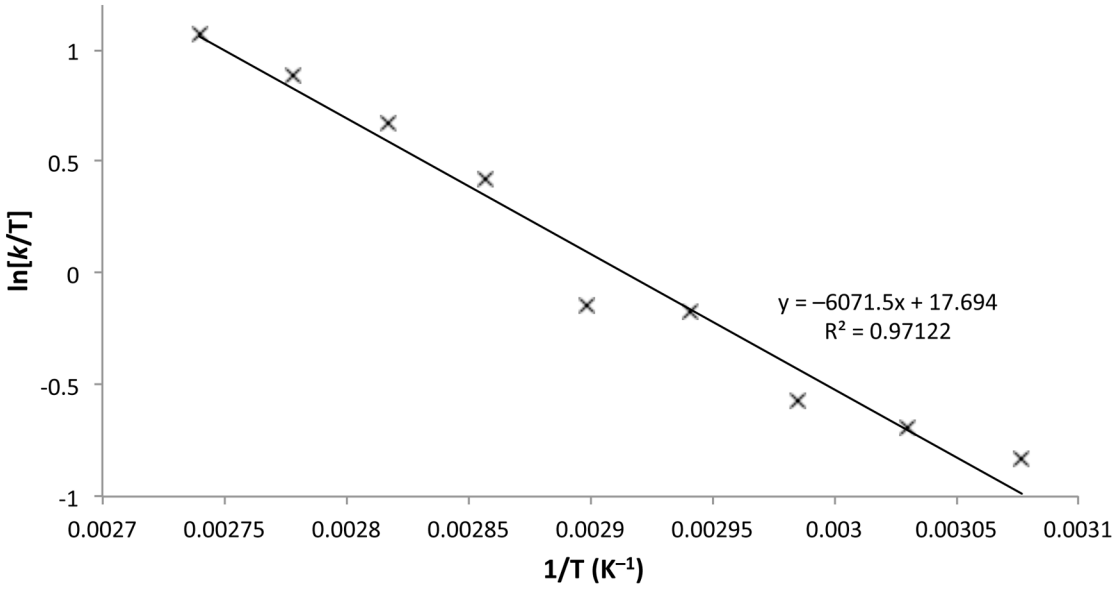

Figure 4.13: Eyring plot derived from line shape analysis of d_7-DMF solution of **11**.

The values for the enthalpy and entropy of activation derived from this plot were:

$$\Delta H^{\ddagger} = 50(3) \text{ kJ mol}^{-1}$$

$$\Delta S^{\ddagger} = 51(10) \text{ J K}^{-1} \text{ mol}^{-1}$$

These values can be used to determine the free energy of activation, which in this case is the barrier to C–N bond rotation, of:

$$\Delta G^{\ddagger} = 66(3) \text{ kJ mol}^{-1} \text{ (at 298 K)}$$

These values have relatively large errors associated with them, which are derived from a regression analysis of the line of best fit. Note that the barrier to amide bond rotation derived from the full line shape analysis is in good agreement with the value obtained from the significantly quicker coalescence temperature method. This shows that the approximations made in the latter method are reasonable, or at least any systematic errors are consistent (and/or cancel out) between the two methods.

4.2.5.4 Comparison of barrier to amide bond rotation with other systems

The C–N bond rotation barriers for selected small amides are reported in Table 4.3. Care has been taken to ensure consistency across the data. Despite the fact that the calculated barriers for all of the amides shown other than phosphinecarboxamide have been previously reported in the chemical literature,[52–55] they were all calculated at different levels of theory, and thus they have been recalculated to allow a more fruitful comparison. The experimental data are all derived from a line shape analysis in DMF as the solvent. The choice of solvent is particularly important in these systems due to the potential of relatively strong hydrogen bonding to the amide protons, which can affect the barriers to rotation.[56] This is why all of the values for the barrier calculated in the gas phase are lower than the experimentally derived values in solution. It is important to note that even with the care taken to ensure consistency, small effects such as concentration of the amide in solution can still lead to discrepancies between the experimental values.

Table 4.3: C–N free energy bond rotation barriers (in kJ mol^{-1}) for selected small amides of the form $H_2NC(O)R$.

Amide	**Urea**	**Phosphine-carboxamide**	**Acetamide**	**Carbamic acid**	**Thiocarbamic acid**
R	NH_2	PH_2	CH_3	OH	SH
Calculated (gas phase)[a]	34	56	58	31	46
Experimental (solution)[b]	47[c]	66	72[d]	-	-

[a] CCSD/6-311+G(2df,p). [b] all derived using line shape analysis in DMF. [c] at 220 K.[57] [d] at 298 K.[56]

The data can be rationalised by considering the three resonance forms in Figure 4.14. These are analogous to the three resonance contributions already considered for **11** when R = PH_2 (in Figure 4.3).

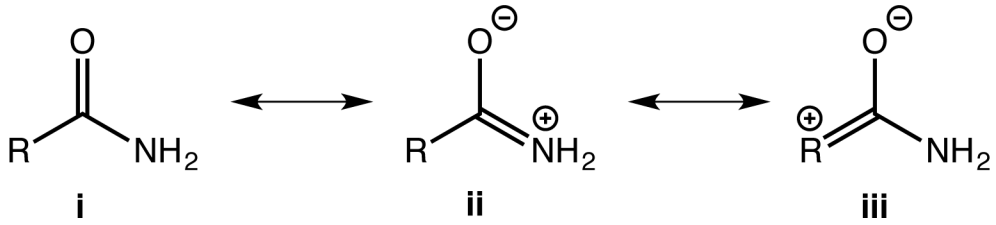

Figure 4.14: Possible resonance forms of amides with different functional groups.

A large contribution from resonance form **iii** blocks donation of electron density from the nitrogen lone pair into the C–O π* orbital, and thus reduces the contribution from **ii** and lowers the amide rotation barrier. Urea has a notably low barrier to amide rotation, which can be attributed to both nitrogen atoms competing for the LP(N) → π*(CO) interaction. The amide rotation barrier is larger in **11** because of the poorer overlap of the phosphorus lone pair with the C–O π* orbital, which leads to a smaller contribution from **iii** and a greater contribution from **ii**. This difference between the second and third period elements is corroborated by the data for carbamic acid and thiocarbamic acid (Table 4.3), where the heavier substituent (SH in this case) has a poorer overlap and thus thiocarbamic acid has a larger amide rotation barrier.

Acetamide, where R = CH_3, possesses no lone pair on the R substituent, and thus **iii** is not accessible, which leads to a relatively large barrier to C–N bond rotation. This value is slightly larger than in phosphinecarboxamide, which may suggest that there is a small contribution from **ii** in the latter (i.e. **11.ii**). This is consistent with the observation that **11** is relatively stable in air, although this is not necessarily an explanation for the phenomenon. The values of **11** and acetamide are actually very close, so the two molecules can be perceived as electronically similar. This is in accord with the formulation of phosphorus as a "carbon copy", as discussed in Chapter 1.

4.2.6 Phosphine inversion

The inversion energy of the phosphine centre in **11** was calculated as a method of gaining further insight into the phosphorus participation in the amide moiety. The transition state of this inversion, **TSC**, has a trigonal planar geometry around the phosphorus (Figure 4.15). This is typical for most phosphines, with PF_3 being a notable exception.[58]

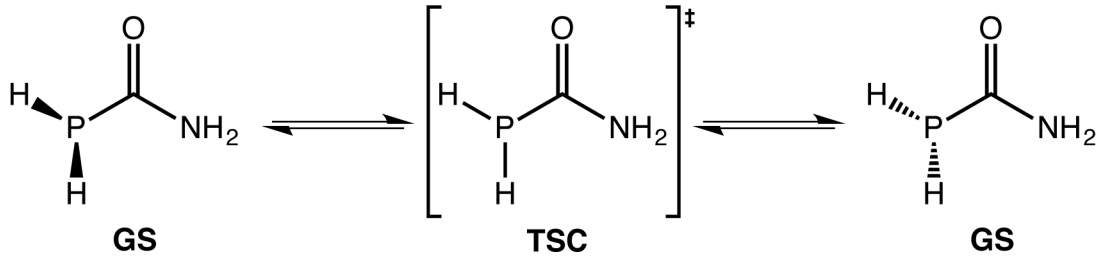

Figure 4.15: Inversion of the phosphine moiety of **11**, via the planar transition state **TSC**. $\Delta G^{\ddagger}$ (kJ mol^{-1}): **GS** = 0; **TSC** = 120.

The P–C bond shortens substantially in **TSC** (1.80 Å) relative to the ground state **GS** (1.88 Å), suggesting a degree of delocalisation of the phosphorus lone pair into the C–O π* antibonding orbital. This would necessarily lead to a decrease in the multiple bonding character of the C–N bond and a decrease in the planarity around the nitrogen atom as measured by the sum of the angles around the nitrogen centre, which is indeed the case (1.37 Å and 350˚ in **TSC** relative to 1.36 Å and 357˚ in **GS**).

The free energy barrier to inversion was calculated at 120 kJ mol^{-1}, which is in good agreement with other phosphines.[59] The inversion barriers have been shown to be dependent on a range of factors, such as sterics, and the electronegativities and conjugation properties of substituents on the phosphorus centre.[60] The value in **11** is slightly lower than that in phosphine (PH_3, 140 kJ mol^{-1}),[61] which is principally due to the delocalisation of the phosphorus lone pair into the carbonyl moiety of the amide unit in **TSC**.

4.2.7 Additional characterisation of 11

An IR spectroscopic investigation of a Nujol mull of **11** revealed a band at 1647 cm^{-1} corresponding to the carbonyl stretching mode (Figure 4.16). This is consistent with other amides, and is lower in energy than the analogous stretching mode found in ketones due to the donation of electron density into the C–O π* antibonding orbital in **11**.[62] The PH_2 stretching modes are at 2320 cm^{-1} and 2334 cm^{-1}, while the NH_2 stretches are at higher wavenumbers (3123 cm^{-1} and 3311 cm^{-1}), due to the lighter mass of the nitrogen atom (and thus the lower reduced mass of the N–H unit). The NH_2 stretching bands are also significantly broader than the PH_2 analogues, on account of intermolecular hydrogen bonding. The NH_2 bending mode and the C–N stretching mode were found at 1585 cm^{-1} and 1134 cm^{-1}, respectively. All of these vibrational modes were identified with the aid of the predicted vibrational modes from DFT calculations, and by discounting the known peaks arising from Nujol.

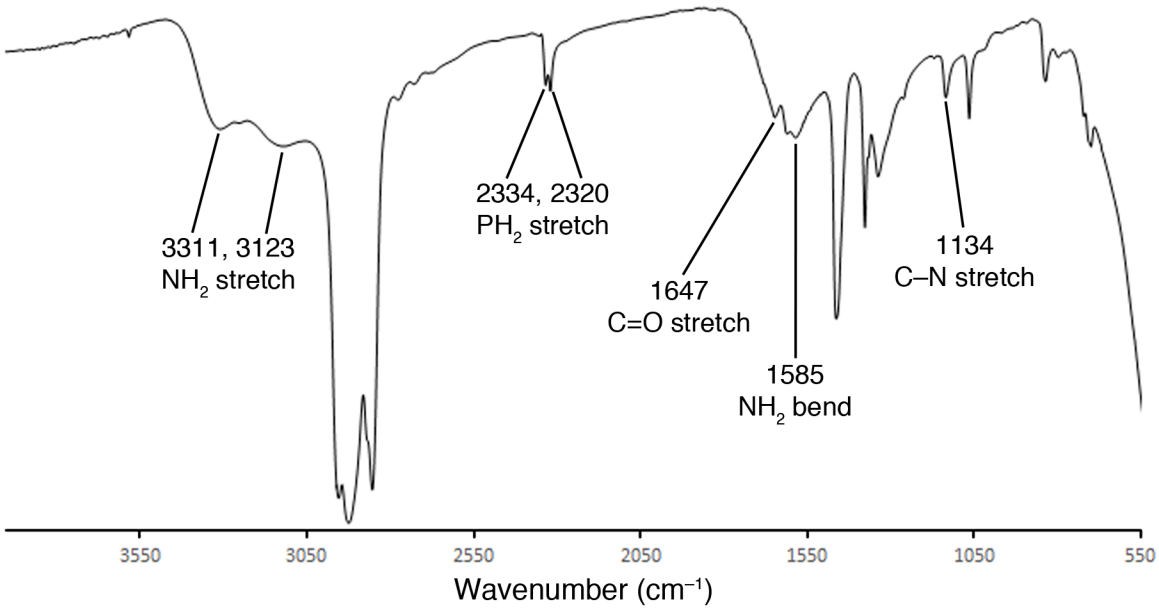

Figure 4.16: IR spectrum of Nujol mull of **11**. Selected vibrational modes of **11** are labelled.

A mass spectrometric study on THF and diethyl ether solutions of **11** revealed that the molecule is very prone to fragmentation, and no molecular ion peak could be found using

electron ionisation (EI, also known as electron impact) or chemical ionisation (CI) techniques. Field ionisation (FI) mass spectrometry is a notably milder technique, and generates the molecular ion by applying a high electric field gradient across the tips of very fine "whiskers", where quantum mechanical tunnelling of an electron leads to ionisation.[63–65] The application of this experiment to **11** yielded a mass envelope with a *m/z* ratio of 77.0027 as the predominant peak, which is a very good match with the calculated monoisotopic mass for **11** of 77.0031 Da.

The compositional purity of **11** was further confirmed using elemental microanalysis, where a very good match between the predicted and experimentally determined values was obtained. The melting point of **11** was determined as 64 ˚C, which is significantly lower than its lighter analogue, urea (133 ˚C), due to the reduced capacity for hydrogen bonding in the former. It is worth noting that although the sample of **11** does become a liquid at this temperature, decomposition (to release PH_3) has also started to occur, so it is not possible to cycle between the solid and liquid phases of **11** in a purely reversible manner.

4.2.8 Air-stability of 11

The reputation of primary phosphines as highly air-sensitive and pyrophoric compounds is merited, particularly those with a low molecular weight and that lack steric encumbrance.[19,20] The decomposition is a highly exothermic reaction, and although the mechanism is not fully understood, it is postulated to occur via a radical cation that then reacts with dioxygen, as shown in Scheme 4.3.[66–68]

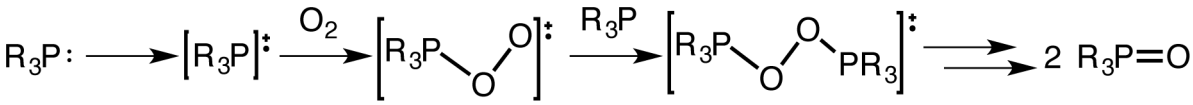

Scheme 4.3: Postulated steps in oxidation of phosphines. Figure adapted from Stewart et al.[19]

11 is remarkably air- and moisture-stable for a primary phosphine. It can be handled as a solid on the bench-top for several hours without noticeable decomposition, although it does

need to be stored under inert conditions to prevent gradual decomposition. **11** is also stable in solution; a d_5-pyridine solution of **11** had a half-life of nine days when exposed to air. It is even stable in water, as evidenced by the clean resonance corresponding to **11** in the ^{31}P NMR spectrum recorded in H_2O. This means that bench-top solvents that have not been laboriously and extensively dried are suitable for use, and makes **11** a very user-friendly primary phosphine.

We were intrigued to identify the underlying cause of this unexpected stability. Most air-stable primary phosphines are stabilised kinetically by large encumbering substituents, which is clearly not the case in **11**.[20] Nor is there extensive π delocalisation of the phosphorus lone pair, as indicated by the long P–C bond length typical of single bonds, the high amide rotation barrier, and the fact that the HOMO has significant lone pair character on the phosphorus atom. This prompted us to employ Higham's method of calculating the absolute energy of the SOMO of the radical cation (specifically the first intermediate in Scheme 4.3) to ascertain whether **11** corroborated this hypothesis.[19]

The structures of the neutral and radical cation (RC) of phosphinecarboxamide were optimised at the B3LYP/6-311+G(d,p) level of theory, corresponding to the level used by Higham and co-workers in their study. The calculated orbital energies are given in Table 4.4, along with those of other selected phosphines for comparison purposes.

Higham's model predicts that a phosphine will be air-stable if the energy of the SOMO is above –10.00 eV. This is the case for PPh_3, which is a well-known air-stable phosphine and has a SOMO energy of –9.50 eV. By this model, the SOMO energy of –13.74 eV suggests that **11** is air-sensitive, which contradicts our experimental observations. However, it is important to note that the concept of air-stability is a continuum, and the fact that **11** does indeed slowly decompose in air, even if it is on the timescale of several days, perhaps

suggests that this model is still valid. **11** is certainly more air-stable than PH_3 and $PMeH_2$, but less stable than PPh_3, and this is consistent with the data below.

Table 4.4: Energies (in eV) of orbital energies of the neutral and radical cation species of selected phosphines.

	Neutral (N)			**Radical cation (RC)**			HOMO(N) – SOMO(RC)[c]
	HOMO	LUMO	Gap[a]	SOMO	LUMO	Gap[b]	
11	–7.13	–0.74	6.39	–13.74	–10.72	3.02	6.61
PH_3	–7.50	0.87	8.37	–15.73	–11.88	3.85	8.23
$PMeH_2$	–6.84	0.92	7.76	–14.33	–10.79	3.54	7.49
PPh_3	–5.75	–0.52	5.23	–9.50	–7.61	1.89	3.75

[a] Energy difference between the HOMO and LUMO of the neutral species. [b] Energy difference between the SOMO and LUMO of the radical cation species. [c] Energy difference between the HOMO of the neutral and SOMO of the radical cation species.

All experimental attempts to generate the radical cation of **11** through chemical oxidation using $[Ph_3C][BF_4]$ and $[NO][BF_4]$ were unsuccessful. For future work, it would be interesting to probe the stability of **11** with respect to electrochemical oxidation.

In conclusion, the major factor of the stability of **11** remains unclear, and all of the previously reported explanations seem to not apply to a significant degree in this system. Due to the fact that there is negligible stabilisation from steric encumbrance of the phosphorus centre, and that the energy of the SOMO is not above the threshold value of –10.00 by Higham's theory, we conclude that the stability presumably does in fact arise from the mixing of the π orbitals of the phosphorus centre and the delocalisation of the HOMO over several atoms in the molecule. This is despite the repeated experimental observations that there is minimal donation of the phosphorus lone pair into the C–O π* antibonding orbital. Although the reasons behind the stability of **11** are not obvious, the fact that it can be used in chemical synthesis without the need for specialist Schlenk-line techniques, coupled with the high reactivity of the P–H bonds for further functionalisation, make it an attractive reagent that warrants further exploration.

4.3 Coordination chemistry of 11

Having synthesised and comprehensively characterised **11**, we were interested in exploring its coordination chemistry. The following section will detail a simple hydrogen-bonded adduct and three metal–phosphine complexes as a means of assessing the ligand properties of the phosphinecarboxamide, and demonstrate that **11** as a functional group can behave both as an amide and a phosphine.

4.3.1 $[(H_2PC(O)NH_2)_2(18\text{-crown-6})]$ (12)

Urea is known to form sufficiently strong hydrogen bonds to denature proteins by displacing water in the solvation shell and reducing the hydrophobic effect critical to maintaining the protein's quaternary structure.[69,70] Furthermore, urea-based receptors have played a key role in recent developments in anion binding and sensing.[35–38] This prompted us to synthesise an adduct in which **11** is coordinated through hydrogen bonds, and to verify that the carboxamide moiety of **11** acts as a typical amide.

This was achieved by the interaction of **11** with 18-crown-6. Slow diffusion of hexane into a THF solution of this mixture afforded colourless crystals suitable for X-ray diffraction. The product is $[(H_2PC(O)NH_2)_2(18\text{-crown-6})]$ (**12**), although the asymmetric unit shows one phosphinecarboxamide moiety coordinated to half of an 18-crown-6 ring. The other half of the molecule is symmetry-generated by the presence of an inversion centre in the centre of the crown ether, and gives an overall structure of the product as that shown in Scheme 4.4.

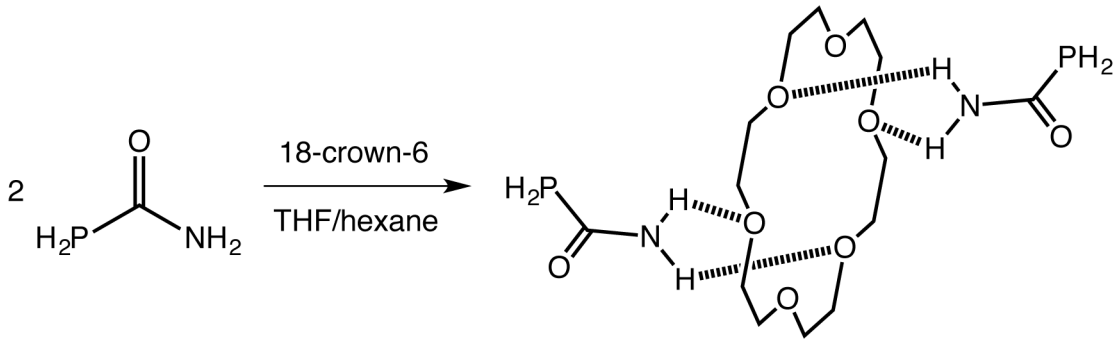

Scheme 4.4: Coordination of two equivalents of **11** to one equivalent of 18-crown 6 to afford the hydrogen-bonded complex **12**.

The crystallographically determined structure is shown in Figure 4.17, which depicts the asymmetric unit with the second half of the 18-crown-6 ring included to show both hydrogen bonding interactions. Thus the crystal structure shown is **12** with the symmetry-generated phosphinecarboxamide moiety omitted for clarity.

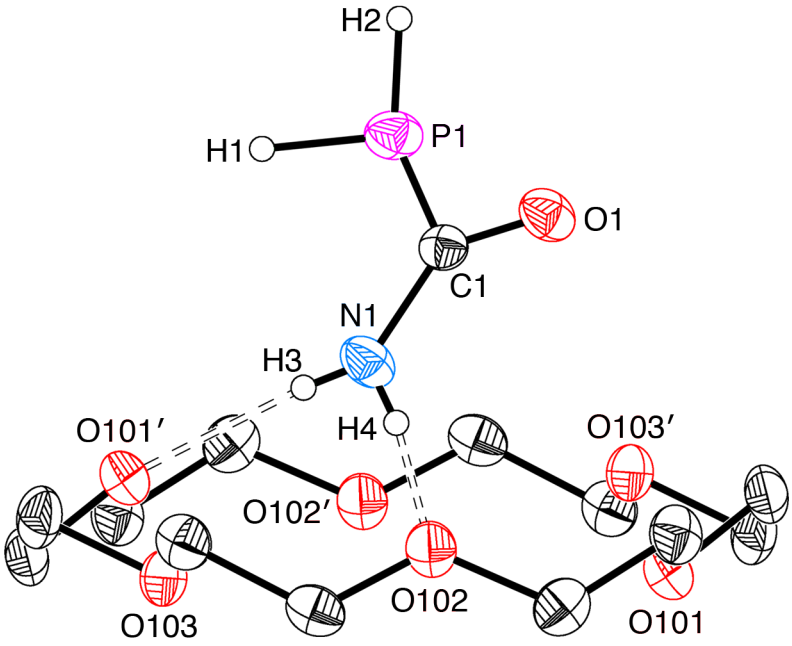

Figure 4.17: Molecular structure of **12**, with the second equivalent of the phosphinecarboxamide moiety omitted for clarity. Anisotropic displacement ellipsoids are set at 50% probability. Hydrogen atoms on the phosphinecarboxamide are shown as spheres of arbitrary radii. Hydrogen atoms on the 18-crown-6 ring omitted for clarity. Symmetry element ′: 1–*x*, 2–*y*, 1–*z*.

There is no evidence in the crystal structure of any significant intermolecular interactions involving the phosphine protons, as expected based on the lower electronegativity value of

phosphorus compared to nitrogen. The bond metric data of **12** are shown in Table 4.5, alongside **11** for comparison purposes.

Table 4.5: Selected crystallographic bond lengths (Å) and angles (˚) of **12** and **11**.

Bond distance (Å)	**12**	**11**
P1–C1	1.865(2)	1.860(2)
C1–N1	1.329(2)	1.326(2)
C1–O1	1.230(2)	1.239(2)
H3–O101′	2.22(2)	N/A
H4–O102	2.09(2)	N/A
Bond angle (˚)		
P1–C1–O1	118.5(1)	118.9(1)
P1–C1–N1	117.3(1)	118.1(1)
N1–C1–O1	124.1(2)	122.9(2)
Sum around P1	289	287
Sum around N1	359	360

All of the bond lengths within the phosphinecarboxamide moiety are same within statistical error for **11** and **12**, and the bond angles are very similar as well. This shows that there is little difference between the two species, which is unsurprising considering the crystal structure for the "free" **11** features intermolecular hydrogen bonding between different phosphinecarboxamide molecules in the crystal structure. The IR data for a solid sample of **12** in a Nujol mull is also similar to those observed for **11** that have already been discussed (see Experimental section for full values).

The NMR spectroscopic data is identical between d_5-pyridine solutions of **11** and **12**, other than the presence of the resonances corresponding to the 18-crown-6 moiety in the ^{1}H and ^{13}C{^{1}H} NMR spectra. This is indicative of the hydrogen bonding interactions present in the solid state being broken by the coordinating solvent. The same is true when d_8-THF is used as the solvent. This suggests that **12** only forms and crystallises out as a solid sample as the hexane slowly diffuses into the THF solution of the mixture of **11** and 18-crown-6.

The formation of **12** shows that the primary phosphinecarboxamide functional group can indeed act as an amide in certain circumstances.

4.3.2 [(*p*-cymene)$RuCl_2(H_2PC(O)NH_2)$] (13)

The spectroscopic and crystallographic evidence discussed earlier suggests that the phosphorus lone pair in **11** is reasonably separated from the carboxamide moiety. This is corroborated by the computed HOMO having considerable phosphorus lone pair character (44.4%). These data suggested that **11** should be able to act as a Lewis base through the phosphorus centre, and coordinate to metal centres in an analogous manner to other phosphines.

It was established that **11** is out-competed in terms of ligation to a metal centre by strongly coordinating solvents such as pyridine; consequently THF and more typically non-coordinating solvents need to be employed. The reaction of two equivalents of **11** with the [{(*p*-cymene)$RuCl_2$}$_2$] dimer (*p*-cymene = 4-isopropyltoluene) in CH_2Cl_2 at room temperature results in the symmetric cleavage of the bridging chloride ligands and formation of the primary phosphine complex, [(*p*-cymene)$RuCl_2(H_2PC(O)NH_2)$] (**13**), as shown in Scheme 4.5. This particular Ru(II) fragment was chosen because analogous complexes of ferrocene-derivatised primary phosphines have previously been synthesised.[71,72] **13** could readily be isolated in good yields (77%) as an orange solid by the addition of diethyl ether to a concentrated CH_2Cl_2 solution of the product.

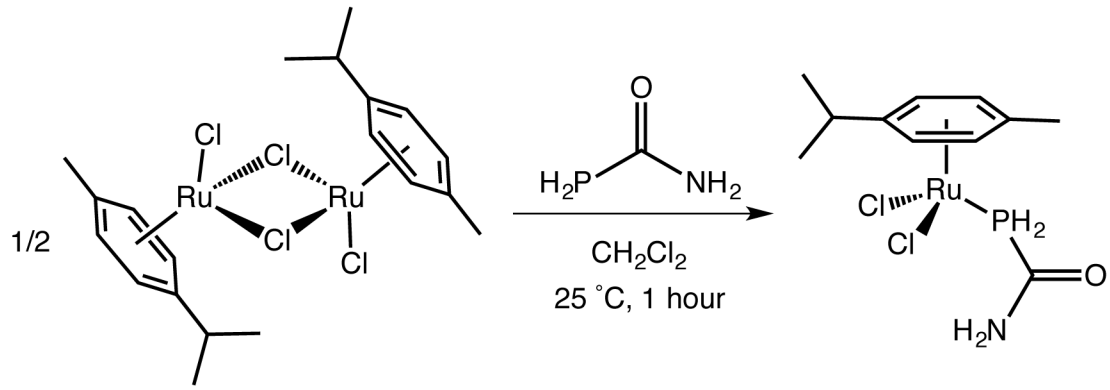

Scheme 4.5: Reaction of half an equivalent of [{(*p*-cymene)$RuCl_2$}$_2$] dimer with **11** to yield **13**.

The ^{31}P NMR spectrum of a CD_2Cl_2 solution of **13** (δ = –35.9 ppm) reveals a downfield shift of 102.1 ppm relative to free **11**, consistent with the reduction of electron density around the phosphorus centre on coordination to a Ru(II) fragment. The resonance remains a triplet of doublets (that collapses to a singlet on proton decoupling), but the coupling to the protons has increased significantly ($^1J_{P–H}$ = 380 Hz and $^3J_{P–H}$ = 25 Hz in **13**, compared to $^1J_{P–H}$ = 209 Hz and $^3J_{P–H}$ = 12 Hz in **11**), which is also characteristic of complex formation. This can be explained by the increase in coupling between two atoms as electron density is removed from the system, as discussed in Chapter 2.[72,73]

An alternative rationalisation arises from the changes in character of the orbitals that occur when a phosphine coordinates to a metal centre, and that the Fermi contact interaction is dependent on the s orbital character of the bond.[39] As a representative example, PH_3 has H–P–H bond angles close to 90˚, so the P–H bonds are high in p orbital character and the lone pair is largely s orbital based.[61,74] Upon coordination, the phosphorus centre goes from three-coordinate to four-coordinate, and effectively "rehybridises" to a more sp^3 tetrahedral geometry. This necessarily leads to an increase in s character in the P–H bonds, and thus an increase in the $^1J_{P–H}$ coupling constant. These ^{31}P NMR data are consistent with the previously reported primary phosphine complexes, [(*p*-cymene)$RuCl_2(H_2PR)$] (R = Fc, δ = –27.6 ppm, $^1J_{P–H}$ = 394 Hz; R = CH_2Fc, δ = –27.7 ppm, $^1J_{P–H}$ = 359 Hz).[71,72]

The ^{1}H NMR spectrum of **13** (Figure 4.18) reveals a large doublet for the phosphine protons ($^{1}J_{H–P}$ = 380 Hz) centred at δ = 5.22 ppm, which collapses to a singlet on decoupling of the ^{31}P nucleus. There are only two aromatic resonances, and the two CH_3 substituents on the isopropyl group are magnetically equivalent and appear as a doublet from coupling to the methine proton ($^{3}J_{H–H}$ = 6.9 Hz) at δ = 1.19 ppm. This methine proton appears as a septet, as expected.

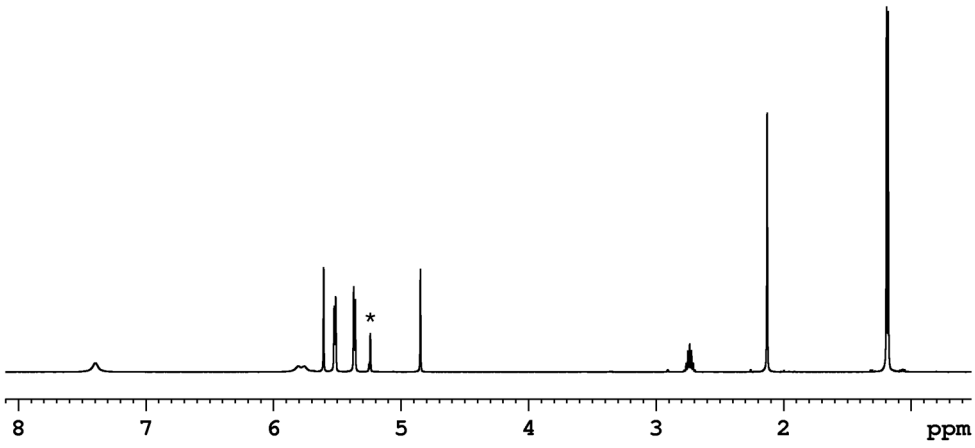

Figure 4.18: ^{1}H NMR spectrum of CD_2Cl_2 solution of **13**. Resonance marked with ***** is due to residual protic solvent.

The ^{13}C{^{1}H} NMR spectrum shows the expected resonances for the *p*-cymene moiety, and the six carbon atoms in the aromatic ring give rise to four distinct resonances that all feature a weak coupling to the phosphorus centre ($J_{C–P}$ is in the range 2.4–4.7 Hz). The phosphinecarboxamide carbon resonance at δ = 167.8 ppm is a doublet with a notably larger coupling constant than in the uncoordinated species ($^{1}J_{C–P}$ = 50 Hz in **13**, $^{1}J_{C–P}$ = 8 Hz in **11**). This is for the same reasons as discussed for the increase in $^{1}J_{P–H}$ coupling constant upon coordination above. The simple nature of the ^{1}H and ^{13}C NMR spectra indicates that the molecule has C_s symmetry.

Despite repeated attempts, no crystals suitable for an X-ray diffraction study were obtained, although the similarity of the NMR spectroscopic data of **13** with those of analogous Ru(II) complexes of other primary phosphines makes us confident of our assignment of the

structure of **13**. The compositional purity of the product was confirmed by elemental microanalysis. An EI mass spectrometric analysis of **13** revealed fragmentation of the complex, and only afforded mass envelopes arising from the *p*-cymene moiety and decomposition thereof.

4.3.3 $[W(CO)_5(H_2PC(O)NH_2)]$ (14)

Having demonstrated that **11** can bind to a metal centre through the lone pair on phosphorus, we sought to synthesise complexes that would allow a comparison of the ligand properties of **11** with other phosphines. The Tolman Electronic Parameter (TEP) was introduced at the start of this chapter, and is defined in terms of the A_1 CO stretching frequency within $[Ni(CO)_3(PR_3)]$ complexes.[4,5] However, the high toxicity of the $[Ni(CO)_4]$ precursor renders the generation of such complexes undesirable, and alternatives have been sought. One such system is the $[W(CO)_5(PR_3)]$ series of complexes, which utilises the same tungsten pentacarbonyl fragment as that employed in Chapter 2.[75,76]

4.3.3.1 Synthesis of 14

The complex $[W(CO)_5(H_2PC(O)NH_2)]$ (**14**) was initially synthesised by photolysis of a THF solution of $[W(CO)_6]$ and **11**, although this led to extensive decomposition of the phosphinecarboxamide and ^{31}P NMR spectroscopy revealed PH_3 as the major product. To avoid the exposure of **11** to photolytic conditions, the weakly coordinated $[W(CO)_5(THF)]$ precursor was generated *in situ* by simple photolysis of $[W(CO)_6]$ in THF. The subsequent addition of **11** resulted in exchange of the substitutionally labile THF ligand and afforded **14** cleanly in solution (Scheme 4.6).[77]

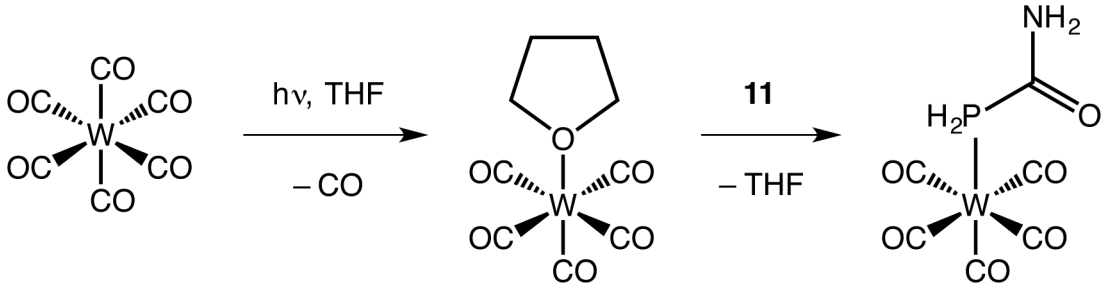

Scheme 4.6: Reaction of $[W(CO)_5(THF)]$ with **11** to afford **14**.

4.3.3.2 Experimental characterisation of 14

The ^{31}P NMR spectrum of a d_8-THF solution of **14** reveals a triplet of doublets centred at $\delta = -103.1$ ppm (Figure 4.19), which represents a downfield shift of 34.9 ppm relative to **11**. This is consistent with donation of the phosphorus lone pair into the vacant orbitals on tungsten.[78] The $^1J_{P-H}$ coupling constant has also increased from 209 Hz in **11** to 347 Hz in **14**, consistent with coordination through the phosphorus lone pair, for the same reasons discussed for **13** above. Coupling to the ^{183}W nucleus (14.3% abundant, $I = ½$) gives rise to tungsten satellites with a coupling constant of $^1J_{P-W} = 216$ Hz (Figure 4.19).

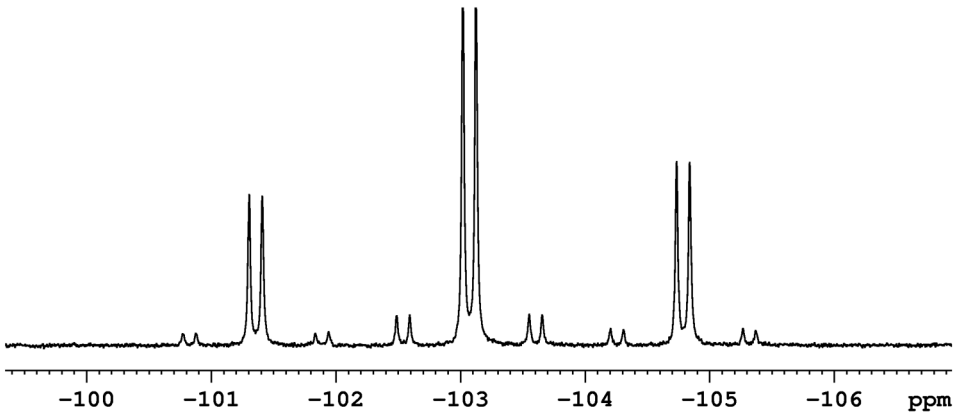

Figure 4.19: ^{31}P NMR spectrum of d_8-THF solution of **14**.

This coupling constant value is identical to that reported for $[W(CO)_5(PH_3)]$ (Table 4.6).[78] The similarity between these values is not surprising, as the magnitude of the coupling constant is known to be highly dependent on the electronegativities of the substituents on

the phosphine.[39] Accordingly, the $^{1}J_{P-W}$ in $[W(CO)_5(PF_3)]$ is significantly larger at 485 Hz.[79] The resonance collapses to a singlet (with tungsten satellites) on proton decoupling.

Table 4.6: $^{1}J_{P-W}$ (in Hz) from ^{31}P NMR spectroscopy, and A_1 carbonyl stretching frequency (in cm^{-1}) from IR spectroscopy, in $[W(CO)_5(PR_3)]$ complexes, with references.

Phosphine	$^{1}J_{P-W}$ (Hz)	A_1 stretch (cm^{-1})
$H_2PC(O)NH_2$	216	2077
PMe_3	220[80]	2071[76]
PH_3	216[78]	2080[81]
PF_3	485[79]	2103[82]

The ^{1}H NMR spectrum shows a doublet from the phosphine protons centred at 5.22 ppm, which collapses to a singlet on ^{31}P decoupling. The $^{13}C\{^{1}H\}$ NMR spectrum reveals a doublet corresponding to the phosphinecarboxamide carbon centre with a coupling constant of $^{1}J_{C-P}$ = 54 Hz (compared to 8 Hz in **11**). There are two resonances corresponding to the *cis* and *trans* carbonyl ligands at 192.5 ppm and 196.2 ppm, respectively.

The solution phase IR spectrum of **14** in THF revealed an A_1 stretching frequency corresponding to the $W(CO)_5$ moiety of 2077 cm^{-1}. Table 4.5 shows the IR spectroscopic data for related $[W(CO)_5(PR_3)]$ complexes. Phosphinecarboxamide shows diminished π acceptor properties compared to PF_3, as expected, and has a similar electronic parameter to phosphine (PH_3).

Surprisingly, removal of the solvent from a solution of **14** under dynamic vacuum resulted in the decomposition of the complex, indicating that the phosphinecarboxamide is only weakly coordinated to the tungsten centre. Despite repeated attempts, the isolation of single crystals for further analysis was not possible, in part due to the high solubility of the species. The lack of structural data prompted us to explore **14** computationally.

4.3.3.3 Computational analysis of W–P interaction

The bonding interaction between the metal centre and the phosphinecarboxamide ligand was probed using DFT calculations. The structure of the $[W(CO)_5(PR_3)]$ complexes (PR_3 = PMe_3, PH_3, **11**, PF_3) were first freely optimised, then single point calculations were carried out on the $W(CO)_5$ and PR_3 fragments in the geometries they adopt in the optimised structure of $[W(CO)_5(PR_3)]$. The two fragments are then brought together again, and the total interaction energy, ΔE_{tot}, gives a measure of the strength of the W–P bond (Table 4.7). The major contribution to this bonding interaction (in addition to steric and dispersion energies) is the orbital interaction energy, ΔE_{oi}, which relates to the stabilisation gained from allowing the electron density to relax through charge transfer from the occupied orbitals of one fragment to the vacant orbitals of the other.

The fragment calculation can also be performed after removing some or all of the virtual (vacant) orbitals on either of the two fragments ($W(CO)_5$ or PR_3). Removing the vacant orbitals on PR_3 effectively blocks transfer of electron density from the metal centre to the π* orbitals of the phosphine (back-bonding). Conversely, if the vacant orbitals on $W(CO)_5$ are removed, σ donation from the PR_3 unit is blocked. Comparison of the interaction energies with and without the subsets of virtual orbitals allows a deconvolution of the σ and π effects of phosphine bonding. For example, when PR_3 = **11**, the difference in orbital energies with and without the vacant orbitals on PR_3 is 86.5 kJ mol^{-1} (–228.5 – (–142.0) kJ mol^{-1}), which equates to a relative π back-bonding contribution of 38% (100×86.5/228.5). Note that the contributions from forward- and back-bonding sum to slightly less than 100%; this is because even in the absence of vacant orbitals on PR_3, the presence of occupied orbitals on this fragment allows the orbitals on $W(CO)_5$ to relax, effectively redistributing electron density between occupied and virtual spaces on the same fragment.[77]

Table 4.7: Interaction energies between PR_3 and $W(CO)_5$ fragments (distance in Å, energies in kJ mol^{-1}).

	PMe_3	**PH_3**	**$H_2PC(O)NH_2$**	**PF_3**
W–P bond length	2.52	2.50	2.50	2.40
ΔE_{tot}	–259.0	–187.0	–211.3	–192.1
ΔE_{oi}	–226.8	–207.5	–228.5	–266.5
ΔE_{oi} (– $W(CO)_5$ virtual)[a]	–90.8	–92.9	–102.5	–147.7
ΔE_{oi} (– PR_3 virtual)[b]	–151.5	–129.3	–142.0	–150.2
Relative importance of σ bonding[c]	60%	55%	55%	45%
Relative importance of π back-bonding[d]	33%	38%	38%	44%

[a] Orbital interaction energies without the vacant orbitals on $W(CO)_5$. [b] Orbital interaction energies without the vacant orbitals on PR_3. [c] Derived from difference with and without vacant orbitals on $W(CO)_5$. [d] Derived from difference with and without vacant orbitals on PR_3.

The PMe_3 ligand has a greater relative contribution from σ bonding, as expected based on the electron-donating ability of alkyl groups, while PF_3 has the greatest contribution from π back-bonding. This is in accordance with the IR spectroscopic data on PF_3, which shows that it is a comparable π acceptor to CO, on account of the electronegative fluorine substituents lowering the energy of the antibonding orbitals (consisting of the P–F σ* orbitals). The phosphinecarboxamide ligand, **11**, has identical σ and π contributions in this complex to those of PH_3, and is consistent with the model that **11** is a moderate σ donor and a moderate π acceptor. This is further corroborated by the similar computed W–P bond lengths in the complexes $[W(CO)_5(PH_3)]$ and **14**.

4.3.4 $[Mo(CO)_4(H_2PC(O)NH_2)_2]$ (15)

Another alternative to the TEP derived from the $[Ni(CO)_4]$ precursor is the $[Mo(CO)_4(PR_3)_2]$ system, which features two phosphine ligands in a *cis* arrangement. This series of complexes is particularly pertinent because of a well-argued report from Anton and Crabtree,[83] which shows that the A_1 carbonyl stretching frequencies in these compounds are

directly related (with an R^2 factor of 0.995) to those in $[Ni(CO)_3(PR_3)]$ by the expression (in units of cm^{-1}):

$$\nu_{Ni} = 0.593\nu_{Mo} + 871 \qquad \textbf{(Eq. 4.5)}$$

This formula allows the stretching frequencies from the molybdenum complexes to be mapped onto Tolman's original work on the extended phosphine family. It is worth noting the molybdenum system spans a greater range of values for the stretching frequencies, and thus potentially has a greater sensitivity than the nickel system.

4.3.4.1 Synthesis of 15

The novel complex $[Mo(CO)_4(H_2PC(O)NH_2)_2]$ (**15**) was synthesised by the reaction of $[Mo(CO)_4(COD)]$ (COD = 1,5-cyclooctadiene) with two equivalents of **11** in non-coordinating solvents such as CH_2Cl_2 (Scheme 4.7).

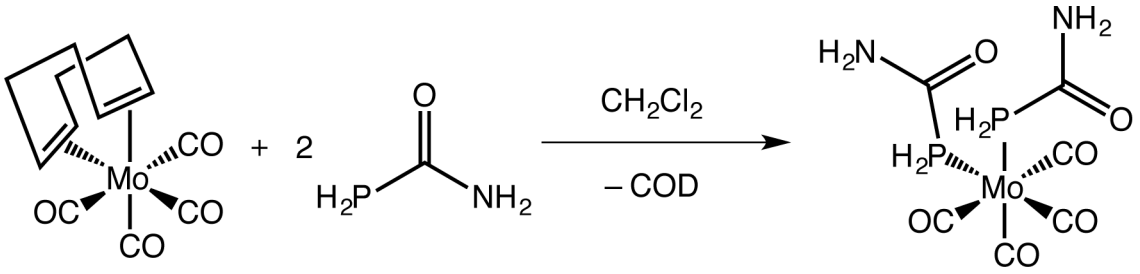

Scheme 4.7: Reaction of $[Mo(CO)_4(COD)]$ with two equivalents of **11** to afford **15**.

15 does not decompose when exposed to dynamic vacuum, and the additional stabilisation relative to **14** presumably arises from the increased propensity for hydrogen bonding in the former.

4.3.4.2 Structural characterisation of 15

Crystals of **15** suitable for single crystal X-ray diffraction were grown from a concentrated CD_2Cl_2 solution (Figure 4.20). The structure shows the two phosphinecarboxamide ligands bound through the phosphorus lone pair in a *cis* arrangement.

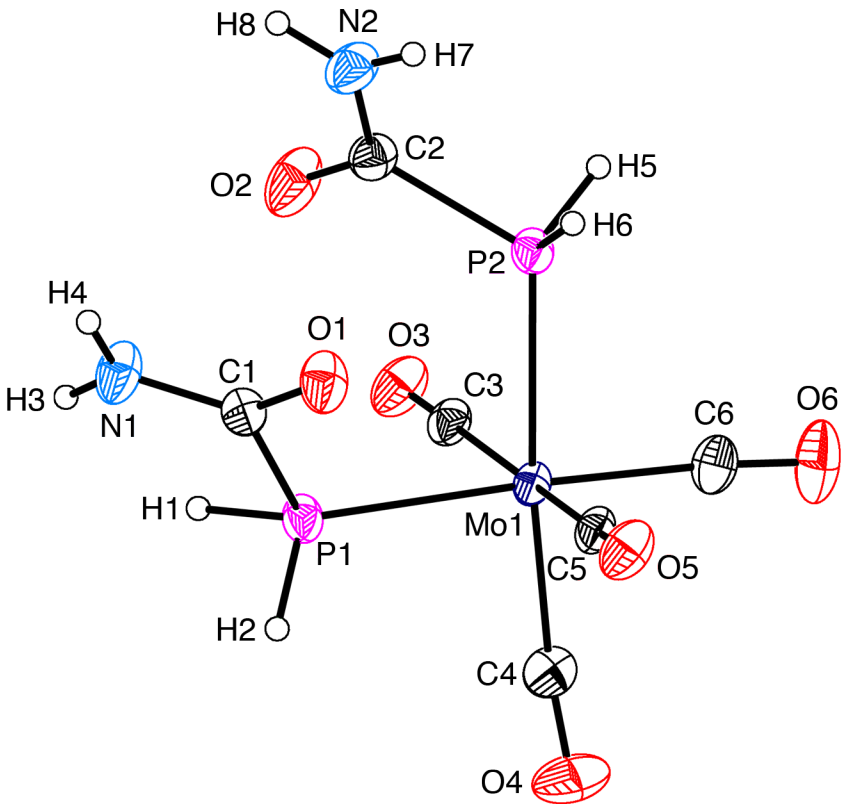

Figure 4.20: Molecular structure of **15**. Anisotropic displacement ellipsoids are set at 50% probability. Hydrogen atoms are shown as spheres of arbitrary radii.

The two phosphinecarboxamide moieties are coplanar, and exhibit intermolecular hydrogen bonding to adjacent molecules in the crystal structure instead of intramolecular hydrogen bonding. Table 4.8 shows the selected bond angles and bond lengths in **15**. All of the relevant bond lengths are statistically identical between both phosphinecarboxamide moieties. The P–C bond lengths (1.870(2) Å and 1.871(2) Å) in the coordinated complex **15** are within the statistical error of the analogous bond length in the free phosphinecarboxamide (**11**: 1.860(2) Å). The bond length might be expected to be elongated in the coordinated complex due to the back-bonding from the filled orbitals on molybdenum into the P–C σ* antibonding orbital, but this effect is mitigated by the simultaneous shortening of the P–C bond arising from donation of the phosphorus lone pair to the metal and the consequent decrease in lone pair/bonding pair repulsions.[2]

Table 4.8: Selected crystallographic bond lengths (Å) and angles (˚) of **15**.

Bond distance (Å)	15	Bond angle (˚)	15
Mo1–P1	2.481(1)	P1–Mo1–P2	91.7(1)
Mo1–P2	2.480(1)	P1–Mo1–C3	86.6(1)
P1–C1	1.870(2)	P1–Mo1–C4	92.5(1)
P2–C2	1.871(2)	P1–Mo1–C5	87.6(1)
C1–O1	1.230(2)	P2–Mo1–C3	89.5(1)
C2–O2	1.226(2)	P2–Mo1–C5	85.3(1)
C1–N1	1.325(2)	P2–Mo1–C6	91.6(1)
C2–N2	1.328(2)	Mo1–P1–C1	117.4(1)
Mo1–C3	2.044(2)	Mo1–P2–C2	118.3(1)
Mo1–C4	1.997(2)	P1–C1–O1	118.0(1)
Mo1–C5	2.041(2)	P2–C2–O2	118.3(1)
Mo1–C6	1.995(2)	P1–C1–N1	118.0(1)
C3–O3	1.140(2)	P2–C2–N2	117.8(1)
C4–O4	1.147(2)	N1–C1–O1	124.0(2)
C5–O5	1.140(2)	N2–C2–O2	123.9(2)
C6–O6	1.148(2)	H1–P1–H2	100(2)
		H5–P2–H6	98(1)

The Mo–P bond distances 2.480(1) Å and 2.481(1) Å are also identical within experimental error. A survey of the chemical literature revealed that short M–P bond distances are typically associated with relatively good π interactions (Mo–P bond distance in $[Mo(CO)_4\{P(OPh)_3\}_2]$ is 2.432(1)/2.436(1) Å),[84] while systems that are strong σ donors and weak or negligible π acceptors have longer Mo–P bonds (2.522(1)/2.522(1) Å in $[Mo(CO)_4(PMe_3)_2]$, 2.649(4)/2.659(4) Å in $[Mo(CO)_4(PCy_3)_2]$).[85,86] In the latter example, the large steric bulk of the PCy_3 group has an influence on the long bond distance. The calculated data for the tungsten species in Table 4.7 agree with the proposition as well, as the W–P bond length in $[W(CO)_5(PF_3)]$ is notably shorter than those of the other species. There are clearly numerous electronic and steric factors that affect the metal–phosphine bond lengths, and caution must be employed when utilising this metric as a measure of

bond strength. In fact, previous studies have noted an inverse relationship between M–PR_3 bond distances and energies.[87]

The Mo–C bond distances vary depending on whether they are *cis* or *trans* to the phosphinecarboxamide fragment. The CO ligands that are *trans* to other carbonyl groups have longer Mo–C bond (2.044(2) Å and 2.041(2) Å) than those that are *trans* to the $H_2PC(O)NH_2$ moieties (1.997(2) Å and 1.995(2) Å). This is consistent with the observation that **11** exerts a weaker *trans* influence than CO, due to the enhanced σ donating and/or π accepting ability of the latter.

4.3.4.3 Spectroscopic characterisation of 15

The ^{31}P NMR spectrum of a CD_2Cl_2 solution of **15** revealed a complex multiplet (Figure 4.21), and the coupling was assigned using calculated coupling constant values followed by a least squares simulation of the spectrum. The two phosphorus atoms are chemically equivalent, as the two environments are related by a C_2 rotation axis. However, P1 (for example, using the labelling from the crystal structure in Figure 4.20) evidently couples to H1 and H2 ($^1J_{P–H}$ = 328 Hz) in a different manner to H5 and H6 ($^3J_{P–H}$ = 9 Hz), and thus P1 and P2 are magnetically inequivalent. This results in the two phosphorus nuclei coupling to each other with a value of $^2J_{P–P}$ = –25 Hz. This resonance is further complicated by coupling to one of the amide protons (H4 in the case of P1, $^3J_{P–H}$ = 18 Hz), while the coupling to the other amide proton is still too weak to resolve, even in the simulated spectrum. The resonance in the $^{31}P\{^1H\}$ NMR spectrum collapses down to a singlet, as in the absence of coupling to the protons the phosphorus atoms become magnetically equivalent, and no longer couple to each other.

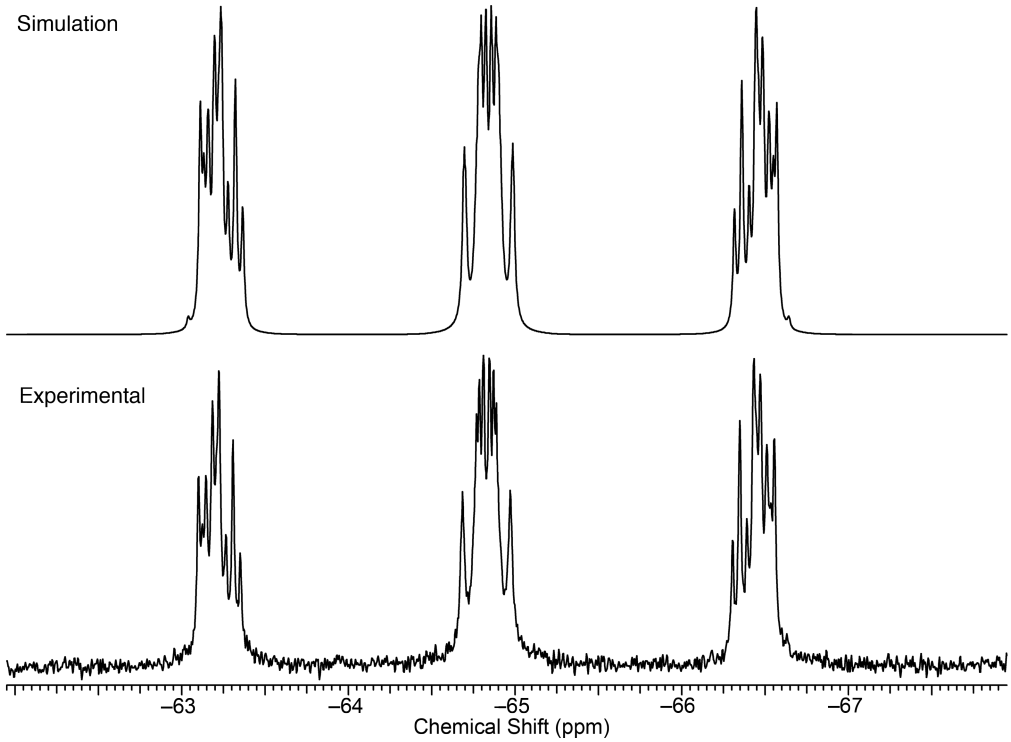

Figure 4.21: ^{31}P NMR spectrum of CD_2Cl_2 of **15**, and the simulated spectrum.

^{1}H NMR spectroscopy reveals two broad resonances at 6.71 ppm and 5.92 ppm arising from the two distinct amide environments. The phosphine protons give rise to a second order multiplet centred at 5.00 ppm ($^{1}J_{H–P}$ = 328 Hz, $^{3}J_{H–P}$ = 9 Hz), which collapses to a singlet on ^{31}P decoupling. The $^{13}C\{^{1}H\}$ NMR spectrum reveals two different signals for the carbonyl resonances bound to the molybdenum centre. The carbonyl *cis* to the phosphinecarboxamide ligand (at δ = 212.1 ppm) is a triplet, arising from coupling to the two equivalent *cis* phosphorus nuclei ($^{2}J_{C–P}$ = 9 Hz). The other is a doublet (at δ = 206.8 ppm), due to coupling to the *trans* phosphorus centre ($^{2}J_{C–P}$ = 19 Hz). No coupling is observed to the *cis* phosphorus in this latter resonance. An additional resonance in the $^{13}C\{^{1}H\}$ NMR spectrum is a doublet at 171.9 ppm arising from the phosphinecarboxamide carbon centres ($^{1}J_{C–P}$ = 43 Hz).

The highest energy absorption in the carbonyl stretching region of the IR spectrum of **15** was observed at 2040 cm^{-1}. Using the equation derived by Anton and Crabtree (Equation 4.5), this corresponds to a TEP of 2081 cm^{-1}. The TEPs of the other phosphines we have

been considering thus far are shown in Table 4.9. Once again, the ligand properties of **11** are remarkably similar to PH_3. This further supports the notion that phosphinecarboxamide is a relatively weak σ donor and π acceptor.

Table 4.9: The TEP of **11** and selected other phosphines. Data from Tolman.[5]

Phosphine	TEP (cm^{-1})
$H_2PC(O)NH_2$	2081
PMe_3	2063
PH_3	2083
PF_3	2111

4.4 Conclusions

This chapter has reported the first synthesis of phosphinecarboxamide, a simple phosphorus analogue of urea, by analogy with Wöhler's historic reaction. This novel moiety has been comprehensively characterised by X-ray crystallography and spectroscopic methods, including various isotopologues. A detailed exploration of the barrier to amide bond rotation was also carried out, both experimentally and computationally, and found that there is minimal involvement of the phosphorus lone pair with the carboxamide moiety. Despite this, **11** is remarkably air-stable, which is a very unusual property of a primary phosphine.

Initial reactivity studies were carried out, and found that **11** can act as an amide (by hydrogen bonding to a crown ether in **12**) and as a phosphine ligand by coordination to a range of metal centres (in **13**, **14** and **15**). The latter two complexes, featuring ligation to W(0) and Mo(0) centres, permitted an analysis of the bonding properties of **11** as a ligand, and found that is a relatively weak σ donor and π acceptor, and is very similar to PH_3. The similarity of **11** and PH_3, coupled with the fact that the former is a solid that can be readily

manipulated in air, mean **11** could find use as a safe and direct replacement for PH_3 in metal complexes that feature this ligand.

4.5 References

(1) Hartwig, J. F. *Organotransition Metal Chemistry: From Bonding to Catalysis*; University Science Books: New York, 2011.

(2) Orpen, A. G.; Connelly, N. G. *Organometallics* **1990**, *9*, 1206–1210.

(3) Gilheany, D. G. *Chem. Rev.* **1994**, *94*, 1339–1374.

(4) Tolman, C. A. *J. Am. Chem. Soc.* **1970**, *92*, 2956–2965.

(5) Tolman, C. A. *Chem. Rev.* **1977**, *77*, 313–348.

(6) Dias, P. B.; de Piedade, M. E. M.; Simões, J. A. M. *Coord. Chem. Rev.* **1994**, *135*, 737–807.

(7) Song, S.; Alyea, E. C. *Comments Inorg. Chem.* **1996**, *18*, 145–164.

(8) Alyea, E. C.; Song, S. *Comments Inorg. Chem.* **1996**, *18*, 189–221.

(9) Kyba, E. P.; Liu, S. T. *Inorg. Chem.* **1985**, *24*, 1613–1616.

(10) Katti, K. V.; Gali, H.; Smith, C. J.; Berning, D. E. *Acc. Chem. Res.* **1999**, *32*, 9–17.

(11) Hooper, T. N.; Huertos, M. A.; Jurca, T.; Pike, S. D.; Weller, A. S.; Manners, I. *Inorg. Chem.* **2014**, *53*, 3716–3729.

(12) Dorn, H.; Singh, R. A.; Massey, J. A.; Nelson, J. M.; Jaska, C. A.; Lough, A. J.; Manners, I. *J. Am. Chem. Soc.* **2000**, *122*, 6669–6678.

(13) Dorn, H.; Singh, R. A.; Massey, J. A.; Lough, A. J.; Manners, I. *Angewandte Chemie International Edition* **1999**, *38*, 3321–3323.

(14) Clark, T.; Landis, C. *Tetrahedron: Asymmetry* **2004**, *15*, 2123–2137.

(15) Hoge, G.; Samas, B. *Tetrahedron: Asymmetry* **2004**, *15*, 2155–2157.

(16) Brauer, D. J.; Kottsieper, K. W.; Roßenbach, S.; Stelzer, O. *Eur. J. Inorg. Chem.* **2003**, *2003*, 1748–1755.

(17) Herrbach, A.; Marinetti, A.; Baudoin, O.; Guénard, D.; Guéritte, F. *J. Org. Chem.* **2003**, *68*, 4897–4905.

(18) Chatterjee, S.; George, M. D.; Salem, G.; Willis, A. C. *J. Chem. Soc., Dalton Trans.* **2001**, 1890–1896.

(19) Stewart, B.; Harriman, A.; Higham, L. J. *Organometallics* **2011**, *30*, 5338–5343.

(20) Fleming, J. T.; Higham, L. J. *Coord. Chem. Rev.* **2015**, *297–298*, 127–145.

(21) Hiney, R. M.; Higham, L. J.; Müller-Bunz, H.; Gilheany, D. G. *Angew. Chem. Int. Ed.* **2006**, *45*, 7248–7251.

(22) Pillarsetty, N.; Raghuraman, K.; Barnes, C. L.; Katti, K. V. *J. Am. Chem. Soc.* **2005**, *127*, 331–336.

(23) Wöhler, F. *Ann. Phys. (Berlin)* **1828**, *87*, 253–256.

(24) Wöhler, F. *Ann. Chim. Phys.* **1828**, *37*, 330–333.

(25) Wöhler, F. *Quart. J. Sci. Lit. Art, Series 2, Part 1, (April-June)* **1828**, 491.

(26) Cohen, P. S.; Cohen, S. M. *J. Chem. Educ.* **1996**, *73*, 883–886.

(27) von Liebig, J.; Wöhler, F. *Ann. Phys. (Berlin)* **1830**, *96*, 369–400.

(28) Dunitz, J. D.; Harris, K. D. M.; Johnston, R. L.; Kariuki, B. M.; MacLean, E. J.; Psallidas, K.; Schweizer, W. B.; Tykwinski, R. R. *J. Am. Chem. Soc.* **1998**, *120*, 13274–13275.

(29) MacLean, E. J.; Harris, K. D. M.; Kariuki, B. M.; Kitchin, S. J.; Tykwinski, R. R.; Swainson, I. P.; Dunitz, J. D. *J. Am. Chem. Soc.* **2003**, *125*, 14449–14451.

(30) Jupp, A. R.; Goicoechea, J. M. *J. Am. Chem. Soc.* **2013**, *135*, 19131–19134.

(31) Tsipis, C. A.; Karipidis, P. A. *J. Am. Chem. Soc.* **2003**, *125*, 2307–2318.

(32) Papp, G. P.; Buckler, S. A. *J. Org. Chem.* **1966**, *31*, 588–589.

(33) Vaughan, L. G.; Lindsey, R. V. *J. Org. Chem.* **1968**, *33*, 3088–3089.

(34) Behrle, A. C.; Schmidt, J. A. R. *Organometallics* **2013**, *32*, 1141–1149.

(35) Li, A.-F.; Wang, J.-H.; Wang, F.; Jiang, Y.-B. *Chem. Soc. Rev.* **2010**, *39*, 3729–3745.

(36) Caltagirone, C.; Gale, P. A. *Chem. Soc. Rev.* **2009**, *38*, 520–563.

(37) Gale, P. A.; García-Garrido, S. E.; Garric, J. *Chem. Soc. Rev.* **2007**, *37*, 151–190.

(38) Gale, P. A. *Acc. Chem. Res.* **2006**, *39*, 465–475.

(39) Günther, H. *NMR Spectroscopy: Basic Principles, Concepts and Applications in Chemistry*; 3rd ed.; Wiley-VCH: Weinheim, 2013.

(40) Pyykkö, P.; Atsumi, M. *Chem. Eur. J.* **2009**, *15*, 186–197.

(41) Pyykkö, P.; Atsumi, M. *Chem. Eur. J.* **2009**, *15*, 12770–12779.

(42) Aldridge, S.; Downs, A. J. *Chem. Rev.* **2001**, *101*, 3305–3366.

(43) Ebsworth, E. A. V.; Rankin, D. W. H.; Cradock, S. *Structural Methods in Inorganic Chemistry*; 2nd ed.; Blackwell Scientific Publications: Oxford, 1991.

(44) Kessler, H. *Angew. Chem. Int. Ed. Engl.* **1970**, *9*, 219–235.

(45) Stewart, W. E.; Siddall, T. H. *Chem. Rev.* **1970**, *70*, 517–551.

(46) Gutowsky, H. S.; Holm, C. H. *J. Chem. Phys.* **1956**, *25*, 1228–1234.

(47) Kowalewski, V. J.; Kowalewski, D. G. de. *J. Chem. Phys.* **1960**, *32*, 1272–1273.

(48) Frank, J. H.; Powder-George, Y. L.; Ramsewak, R. S.; Reynolds, W. F. *Molecules* **2012**, *17*, 7914–7926.

(49) Eyring, H. *J. Chem. Phys.* **1935**, *3*, 107–115.

(50) Evans, M. G.; Polanyi, M. *Trans. Faraday Soc.* **1935**, *31*, 875–894.

(51) McConnell, H. M. *J. Chem. Phys.* **1958**, *28*, 430–431.

(52) Kontoyianni, M.; Phillip Bowen, J. *J. Comput. Chem.* **1992**, *13*, 657–666.

(53) Kemnitz, C. R.; Loewen, M. J. *J. Am. Chem. Soc.* **2007**, *129*, 2521–2528.

(54) Wiberg, K. B.; Rablen, P. R.; Rush, D. J.; Keith, T. A. *J. Am. Chem. Soc.* **1995**, *117*, 4261–4270.

(55) Kaur, D.; Sharma, P.; Bharatam, P. V. *J. Mol. Struct. (Theochem.)* **2005**, *757*, 149–153.

(56) Drakenberg, T. *Tetrahedron Lett.* **1972**, *13*, 1743–1746.

(57) Stilbs, P.; Forsen, S. *J. Phys. Chem.* **1971**, *75*, 1901–1902.

(58) Dixon, D. A.; Arduengo, A. J.; Fukunaga, T. *J. Am. Chem. Soc.* **1986**, *108*, 2461–2462.

(59) Baechler, R. D.; Mislow, K. *J. Am. Chem. Soc.* **1970**, *92*, 3090–3093.

(60) Rauk, A.; Allen, L. C.; Mislow, K. *Angew. Chem. Int. Ed. Engl.* **1970**, *9*, 400–414.

(61) Puzzarini, C. *Theor. Chem. Acc.* **2008**, *120*, 325–336.

(62) Clayden, J.; Greeves, N.; Warren, S.; Wothers, P. *Organic Chemistry*; Oxford University Press: Oxford, 2001.

(63) Beckey, H. D. *Principles of Field Ionization and Field Desorption Mass Spectrometry*; Pergamon Press Ltd.: Oxford, 1977.

(64) Beckey, H. D. *Int. J. Mass Spectrom. Ion Phys.* **1969**, *2*, 500–502.

(65) Beckey, H. D.; Heindrichs, A.; Winkler, H. U. *Int. J. Mass Spectrom. Ion Phys.* **1970**, *3*, A9–A11.

(66) Buckler, S. A. *J. Am. Chem. Soc.* **1962**, *84*, 3093–3097.

(67) Barder, T. E.; Buchwald, S. L. *J. Am. Chem. Soc.* **2007**, *129*, 5096–5101.

(68) Yasui, S.; Tojo, S.; Majima, T. *Org. Biomol. Chem.* **2006**, *4*, 2969–2973.

(69) Zou, Q.; Habermann-Rottinghaus, S. M.; Murphy, K. P. *Proteins* **1998**, *31*, 107–115.

(70) Pace, C. N. *Methods in Enzymology*; Hirs, C. H. W., Timasheff, S. N., Eds; Academic Press: New York, 1986; Vol. 131, pp 266-280.

(71) Goodwin, N. J.; Henderson, W.; Nicholson, B. K.; Fawcett, J.; Russell, D. R. *J. Chem. Soc., Dalton Trans.* **1999**, 1785–1794.

(72) Paris, S. I. M.; Lemke, F. R.; Sommer, R.; Lönnecke, P.; Hey-Hawkins, E. *J. Organomet. Chem.* **2005**, *690*, 1807–1813.

(73) Kühl, O. *Phosphorus-31 NMR Spectroscopy: A Concise Introduction for the Synthetic Organic and Organometallic Chemist*; Springer-Verlag: Berlin, 2008.

(74) Helms, D. A.; Gordy, W. *J. Mol. Spectrosc.* **1977**, *66*, 206–218.

(75) Buchner, W.; Schenk, W. A. *Inorg. Chem.* **1984**, *23*, 132–137.

(76) Davies, M. S.; Pierens, R. K.; Aroney, M. J. *J. Organomet. Chem.* **1993**, *458*, 141–146.

(77) Geeson, M. B.; Jupp, A. R.; McGrady, J. E.; Goicoechea, J. M. *Chem. Commun.* **2014**, *50*, 12281–12284.

(78) Nief, F.; Mercier, F.; Mathey, F. *J. Organomet. Chem.* **1987**, *328*, 349–355.

(79) Mercier, F.; Mathey, F.; Afiong-Akpan, C.; Nixon, J. F. *J. Organomet. Chem.* **1988**, *348*, 361–367.

(80) Wosnick, J. H.; Morin, F. G.; Gilson, D. F. R. *Can. J. Chem.* **1998**, *76*, 1280–1283.

(81) Jeanne, C.; Pince, R.; Poilblanc, R. *Spectrochim. Acta, Part A* **1975**, *31*, 819–838.

(82) Keiter, R. L.; Verkade, J. G. *Inorg. Chem.* **1969**, *8*, 2115–2120.

(83) Anton, D. R.; Crabtree, R. H. *Organometallics* **1983**, *2*, 621–627.

(84) Darensbourg, D. J.; Andreatta, J. R.; Stranahan, S. M.; Reibenspies, J. H. *Organometallics* **2007**, *26*, 6832–6838.

(85) Cotton, F. A.; Darensbourg, D. J.; Klein, S.; Kolthammer, B. W. S. *Inorg. Chem.* **1982**, *21*, 2661–2666.

(86) Watson, M.; Woodward, S.; Conole, G.; Kessler, M.; Sykara, G. *Polyhedron* **1994**, *13*, 2455–2458.

(87) Ernst, R. D.; Freeman, J. W.; Stahl, L.; Wilson, D. R.; Arif, A. M.; Nuber, B.; Ziegler, M. L. *J. Am. Chem. Soc.* **1995**, *117*, 5075–5081.

Chapter 5
N-Functionalised phosphinecarboxamides

5.1 Introduction and objectives

5.1.1 Mechanism for formation of urea

The previous chapter introduced the novel molecule phosphinecarboxamide, a phosphorus-containing analogue of urea, which was synthesised by the reaction of ammonium salts with the 2-phosphaethynolate anion. This preparation is analogous to Wöhler's paradigm-shifting synthesis of urea reported in 1828,[1–3] which has since been extensively studied, both in solution and in the solid state.[4] There was long-standing controversy surrounding the mechanism of this reaction, with various kinetic data purported to support both an ionic mechanism (involving an interaction of $[NH_4]^+$ and $[NCO]^-$, via a hydrogen-bonded complex, as the rate-determining step) and a molecular mechanism (where the nucleophilic attack of ammonia on the carbon atom of the HN=C=O moiety is the rate-determining step).[4–6] The two steps of this reaction are shown in Scheme 5.1.

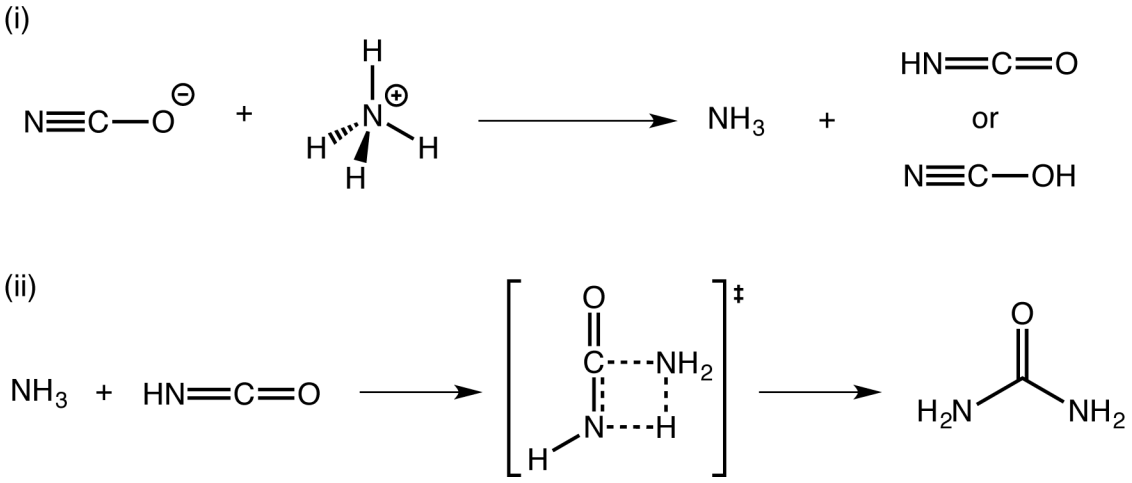

Scheme 5.1: Mechanism for formation of urea: (i) protonation of cyanate followed by (ii) interaction of ammonia with isocyanic acid.

A recent and comprehensive computational study by Tsipis and Karipidis has probed the mechanism using first-principles quantum calculations, and the data support the latter molecular mechanism.[7] The initial protonation of the cyanate anion can yield either cyanic

acid (N≡C–OH) or isocyanic acid (HN=C=O). The latter is energetically more favourable by 118.0 kJ mol^{-1}, and is the "correct" acid required for the subsequent attack by ammonia to yield urea. A four-membered cyclic transition state, shown in Scheme 5.1, is observed when the calculations are carried out in a vacuum. When the reaction was modelled in aqueous solution or in the solid state, it was found that the process was assisted (or autocatalysed) by H_2O or additional NH_3 molecules, through a cooperative hydrogen-transfer mechanism involving six-membered or even eight-membered transition states.

5.1.2 Extension to phosphinecarboxamide

We believe the mechanism for the formation of phosphinecarboxamide is comparable to that of urea. The simple protonation of $[PCO]^-$ at the phosphorus centre yields the parent phosphaketene, HP=C=O. Density functional theory (DFT) calculations suggest that this is more favourable than protonation at the oxygen atom by 80.5 kJ mol^{-1}. This is in good agreement with the calculations carried out by Tondreau et al. where the protonation of the phosphorus atom of $[PCO]^-$ by an imidazolium salt was favoured by 94.1 kJ mol^{-1}.[8]

The parent phosphaketene is inherently unstable, and attempts to observe this molecule by the protonation of $[PCO]^-$ in solution were unsuccessful. The expected doublet was not observed in the ^{31}P NMR spectrum of the product, even when the trifluoromethanesulfonic (triflic) acid was added slowly to a solution of **1** at –78 ˚C and the spectrum was obtained at low temperature. Instead, a bright yellow solid rapidly precipitates out of solution, which proved insoluble in all common laboratory solvents and thus precluded further analysis. The formation of phosphinecarboxamide can thus be viewed as the trapping of the unstable HP=C=O moiety by ammonia via hydroamination of the P=C double bond.

5.1.3 Chapter outline

This notion will be explored by using a range of substituted amines to trap the parent phosphaketene, affording a family of *N*-functionalised phosphinecarboxamides. The

discussion will start with primary amines bearing an array of aliphatic and aromatic substituents. The ligand chemistry of the *N*-cyclohexyl derivative will be briefly explored via the synthesis of a ruthenium complex and the crystallographic characterisation of a subsequent decomposition product. Secondary amines appear to react much more sluggishly to afford *N*,*N*-difunctionalised phosphinecarboxamides in certain cases, although this retardation can be circumvented by employing a heteroatom-substituted secondary amine. These observations can be rationalised by considering the mechanism of formation of the products. The scope of the reaction will finally be probed using amines bearing a range of functional groups to generate more complex phosphinecarboxamides that can undergo further reactivity.

5.2 Simple primary amines

5.2.1 Synthesis of $H_2PC(O)NHR$ (R = Et (16), Cy (17), ^{t}Bu (18), Ph (19))

Building on the synthesis of phosphinecarboxamide documented in the previous chapter, we were keen to explore the scope of this reaction. The small-scale reaction of **1** with simple primary amines RNH_2 (R = Et, Cy, ^{t}Bu, Ph) in the presence of an acid, typically triflic acid or pyridinium triflate, led to the formation of *N*-functionalised phosphinecarboxamides $H_2PC(O)NHR$ (R = Et (**16**), Cy (**17**), ^{t}Bu (**18**), Ph (**19**)), as shown in Scheme 5.2.[9]

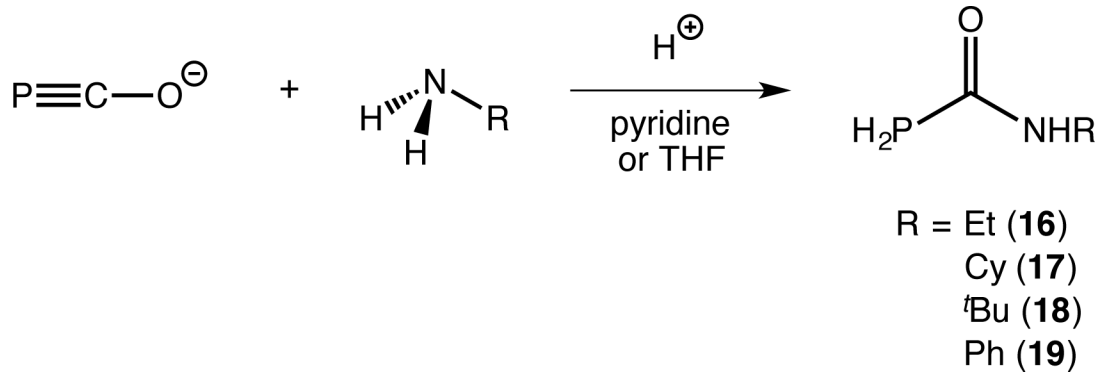

Scheme 5.2: Reaction of **1** with a proton source and a range of primary amines to afford *N*-functionalised phosphinecarboxamides.

It is important to note that the crude reaction mixtures give rise to vastly differing yields of products as monitored by ^{31}P NMR spectroscopy, although this was not measured quantitatively. Thus, while the formation of **16** and **17** in solution were relatively high-yielding, the formation of **18** was accompanied with significant generation of a bright yellow precipitate and only gave rise to a weak resonance in the ^{31}P NMR spectrum. The synthesis of **19** was poorer still, and although the resonance attributable to the product was visible in the $^{31}P\{^{1}H\}$ NMR spectrum, the proton coupled spectrum was too weak to resolve the coupling to the phosphine protons.

The yellow solid side-product is presumably the same as that obtained when an acid is added to **1** in the absence of an amine, and indicates that in these reactions the unstable HPCO intermediate is decomposing. This implies that the nucleophilic attack of the amine on the central carbon atom of this intermediate is too slow for the reaction to occur. Consequently the corresponding phosphinecarboxamide cannot be synthesised (and where possible, isolated) in suitably high yields.

The syntheses of **16**–**19** were originally carried out in gas-tight NMR tubes. [K(18-crown-6)][**1**] and the primary amine were dissolved in either d_8-THF or d_5-pyridine (with no observable reaction), and then the acid was added to the solution. ^{1}H NMR spectroscopy was used to determine whether all of the starting amine had been consumed, and if not then more [K(18-crown-6)][**1**] and acid were added to the mixture. When there was no unreacted amine present in solution, a trap-to-trap distillation at elevated temperatures (typically 50 ˚C) under reduced pressure was used to obtain a clean sample of the product. There did not appear to be any significant amelioration in these reactions when a preformed primary ammonium salt (such as $[EtNH_3][Cl]$) was used instead of adding an acid to a solution containing **1** and the appropriate amine. This supports the theory that the generation of phosphinecarboxamides proceeds via initial protonation of $[PCO]^{-}$.

5.2.2 Refined synthesis of 17

Of these species, the cyclohexyl-substituted phosphinecarboxamide, **17**, is the most readily isolable. The reaction of a pyridine solution of cyclohexylamine with a slight excess of [Na(1,4-dioxane)$_{2.69}$][**1**] and pyridinium triflate at room temperature affords a pale yellow solution. Removal of the volatiles *in vacuo* followed by extraction into toluene allows the facile isolation of **17** as a compositionally pure solid on a multi-gram scale in 77% yields. Note this method was not accessible for the synthesis of the parent phosphinecarboxamide, **11**, due to the relatively high volatility of the latter in solution. On account of the ease of its synthesis, **17** is the focus of the majority of the further reactivity in the next chapter.

5.2.3 Characterisation of 16–19

The spectroscopic data for these new *N*-functionalised phosphinecarboxamides are very similar, and do not differ significantly from those of the parent phosphinecarboxamide, **11**. A summary of selected spectroscopic data is shown in Table 5.1. Due to the very low-yielding synthesis of **19**, only the ^{31}P NMR chemical shift was obtained, and this molecule will not be discussed further.

Table 5.1: Selected spectroscopic data for **16–19**. All data obtained in THF or d_8-THF solvents.

	δ(^{31}P) (ppm)	$^{1}J_{P–H}$ (Hz)	δ(^{13}C) (ppm)	$^{1}J_{C–P}$ (Hz)	ν(CO) (cm^{-1})
16	–136.7	205	171.3	6	1651
17	–135.8	206	170.7	6	1644
18	–134.8	206	171.3	7	1655
19	–130.9	-	-	-	-

The ^{31}P NMR spectra for **16–18** exhibit distinctive triplets from coupling to the two phosphine protons, which collapse to a singlet on proton decoupling. The ^{1}H NMR spectra each show one broad resonance corresponding to the amide proton, and a doublet from the two equivalent phosphine protons, in addition to the expected resonances corresponding to

the appropriate R group. The $^{13}C\{^{1}H\}$ NMR spectra each exhibit the expected doublet arising from the carbonyl moiety with a small coupling constant to the phosphorus nucleus, as well as the R group carbon atoms. As a representative example, the spectra for a d_8-THF solution of **17** are shown in Figure 5.1.

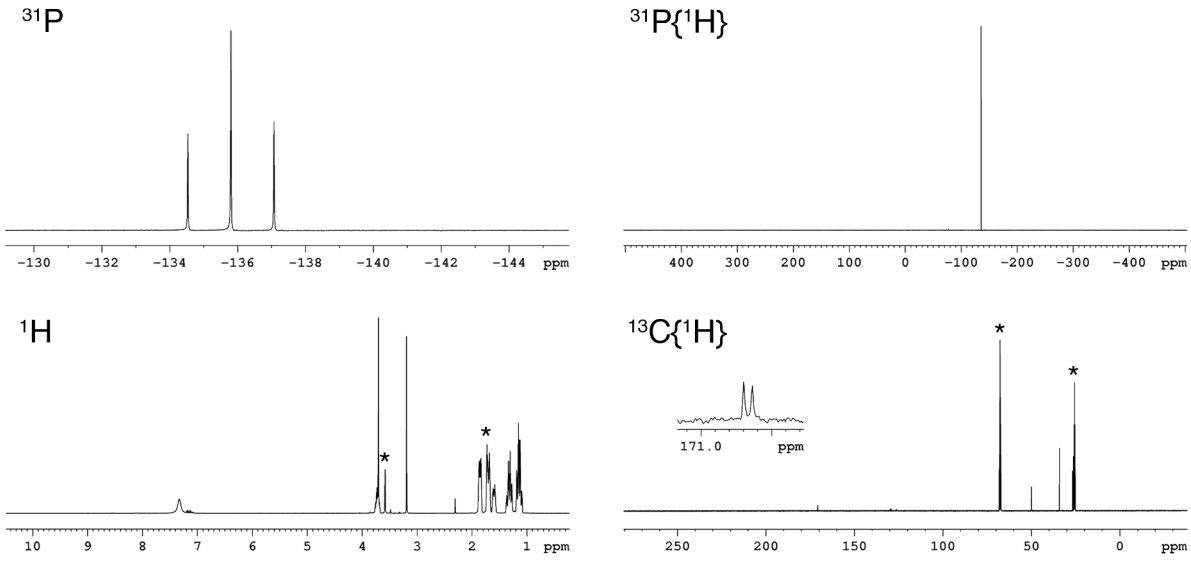

Figure 5.1: Multielement NMR spectra of a d_8-THF solution of **17**. Resonances marked with * are due to solvent resonances. The inset in the $^{13}C\{^{1}H\}$ NMR spectrum shows the doublet resonance of the carbonyl moiety.

The IR spectra of THF solutions of **16**–**18** show distinctive bands due to the carbonyl stretching frequencies. It is evident that the IR and NMR spectroscopic data (highlighted in Table 5.1) do not appear to vary significantly between the different species and thus appear largely independent on the nature of the R group on the nitrogen atom. The solid-state IR spectrum of **17** was also recorded, and it was found that the ν(CO) was lower in energy (1607 cm^{-1}) than that in solution (1644 cm^{-1}). This is not surprising as vibrational spectroscopy is known to be dependent on the phase in which it is recorded. The solid-state stretching frequency of **17** is also notably lower than the parent phosphinecarboxamide, **11**, which has a value of 1647 cm^{-1}. This is due to the inductively donating nature of the cyclohexyl group in **17** relative to a proton, which increases the double bond character of the C–N bond and thus weakens the C–O bond.

17 was further characterised using field ionisation (FI) mass spectrometry, which gave a peak with a *m/z* ratio of 159.0818. This is in excellent agreement with the calculated monoisotopic mass of 159.0813 Da. The compositional purity of **17** was also confirmed by elemental microanalysis.

5.2.4 Ru(II) complexes of 17

Despite repeated attempts, including a range of slow diffusion and sublimation techniques, we were unable to obtain a crystalline sample of **17** suitable for single crystal X-ray diffraction. Thus, in order to obtain structural information corresponding to the cyclohexylphosphinecarboxamide moiety, we sought to synthesise and characterise a complex containing this species.

5.2.4.1 [(*p*-cymene)$RuCl_2(H_2PC(O)NHCy)$] (20)

The similarity between the spectroscopic data of **11** and **17** suggested that the latter could form an analogous complex to that discussed in the previous chapter. Indeed, the reaction of **17** with half an equivalent of the [{(*p*-cymene)$RuCl_2$}$_2$] dimer in CH_2Cl_2 resulted in cleavage of the bridging chloride ligands and afforded the expected primary phosphine complex [(*p*-cymene)$RuCl_2(H_2PC(O)NHCy)$] (**20**), as shown in Scheme 5.3.

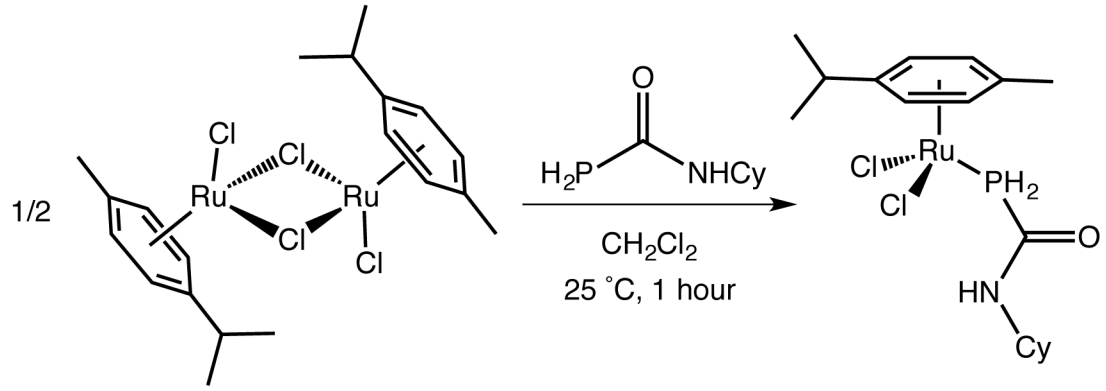

Scheme 5.3: Reaction of half an equivalent of [{(*p*-cymene)$RuCl_2$}$_2$] dimer with **17** to yield **20**.

Orange blocks of **20** suitable for single crystal X-ray diffraction were grown by the slow diffusion of hexane into a THF solution of the product (Figure 5.2). This structure offers further evidence for the proposed structure of **13** in the previous chapter, which was based principally on spectroscopic data.

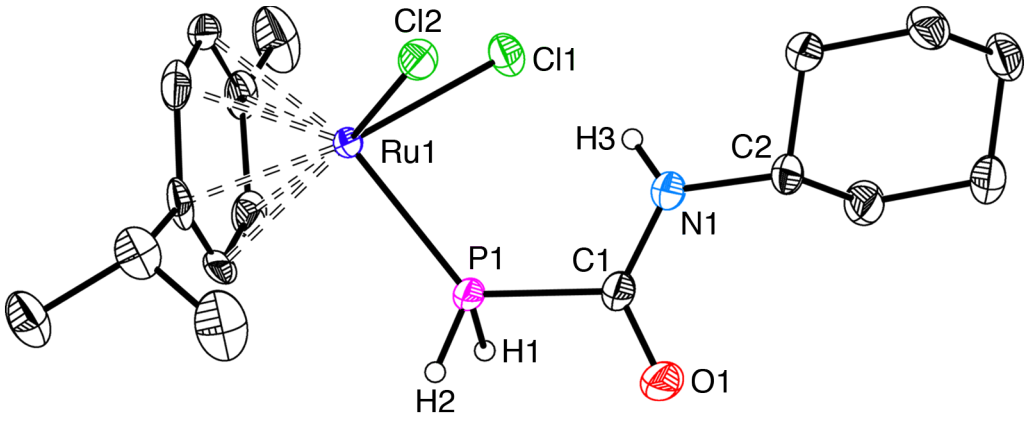

Figure 5.2: Molecular structure of **20**. Anisotropic displacement ellipsoids are set at 50% probability. Heteroatom-bound hydrogen atoms are shown as spheres of arbitrary radii, other hydrogen atoms omitted for clarity.

This complex shows that the lone pair on the phosphorus atom is available for donation into the vacant orbitals on the ruthenium centre, as expected based on the findings from the coordination chemistry of the parent phosphinecarboxamide. This suggests that the work in the previous chapter is relatively general, and can be applied to the substituted species discussed henceforth. The bond metric data are shown in Table 5.2.

The bond lengths of the phosphinecarboxamide moiety in **20** (P1–C1: 1.878(3) Å, C1–O1: 1.227(4) Å, C1–N1: 1.323(4) Å) are closely related to those in **11** (P1–C1: 1.860(2) Å, C1–O1: 1.230(2) Å, C1–N1: 1.329(2) Å).[10] A slight lengthening of the P–C bond distance may be expected on complexation based on back-donation of electron density into the P–C and P–H σ* orbitals, although this is typically mitigated by the decrease in lone pair/bonding pair repulsions as the lone pair on phosphorus is coordinated to the ruthenium centre.[11] Therefore, the metric data in **20** can be considered a good estimate for what would be expected in **17**. The C1–N1 bond length is significantly shorter than N1–C2, which is due to

the double bond character of the amide bond arising from donation of the nitrogen lone pair into the C–O π* antibonding orbital. The Ru1–P1 bond length (2.318(1) Å) is consistent with the previously reported primary phosphine complexes, [(*p*-cymene)$RuCl_2(H_2PR)$] (R = Fc, Ru–P = 2.312(2) Å; R = CH_2Fc, Ru–P = 2.310(1) Å).[12]

Table 5.2: Selected crystallographic bond lengths (Å) and angles (°) of **20**.

Bond distance (Å)	20	Bond angle (°)	20
P1–C1	1.878(3)	P1–C1–O1	117.8(2)
C1–O1	1.227(4)	P1–C1–N1	116.7(2)
C1–N1	1.323(4)	N1–C1–O1	125.5(3)
N1–C2	1.461(4)	Ru1–P1–C1	127.8(1)
P1–H1	1.28(4)	C1–P1–H1	98(2)
P1–H2	1.24(4)	C1–P1–H2	97(2)
N1–H3	0.80(4)	H1–P1–H2	99(3)
Ru1–P1	2.318(1)	C1–N1–C2	123.8(3)
Ru1–Cl1	2.412(1)	C1–N1–H3	116(3)
Ru1–Cl2	2.413(1)	C2–N1–H3	120(3)
		P1–Ru1–Cl1	85.4(1)
		P1–Ru1–Cl2	88.8(1)

Upon formation of **20**, there is a significant downfield shift of the ^{31}P NMR resonance to –36.9 ppm, and an increase in the $^1J_{P–H}$ coupling constant to 376 Hz ($^1J_{P–H}$ = 206 Hz in **17**). This is entirely analogous to the formation of **13** from **11**, and will not be discussed again here (see previous chapter). The ^1H and $^{13}C\{^1H\}$ NMR spectra are also similar to **13**, with the addition of the resonances attributable to the cyclohexyl group. These appear in the ^1H NMR spectrum at 3.77 ppm (the methine proton) and in the range 1.14–1.85 ppm (the methylene protons), as shown Figure 5.3.

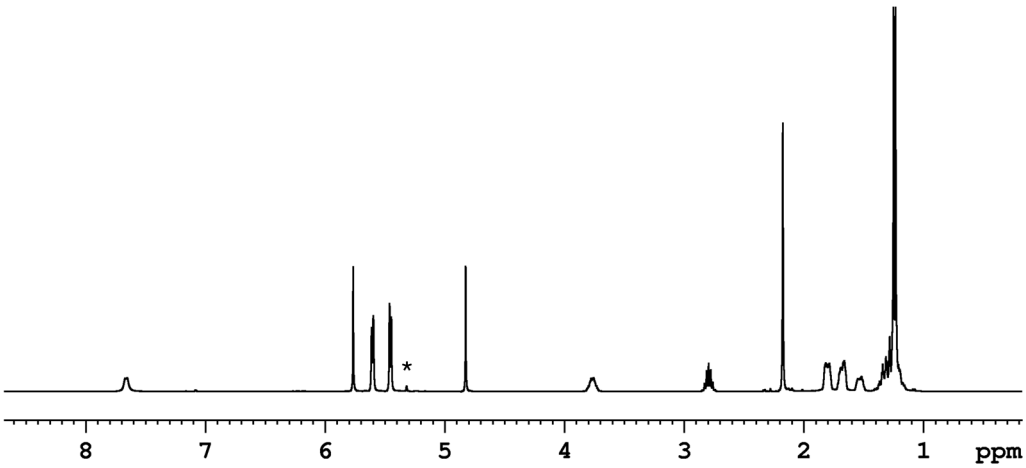

Figure 5.3: ^{1}H NMR spectrum of CD_2Cl_2 solution of **20**. Resonance marked with * is due to residual protic solvent.

5.2.4.2 [(*p*-cymene)$_2$Ru$_2$Cl$_2$(μ-Cl)(μ-PHC(O)NHCy)] (21)

The compositional purity of **20** was confirmed by elemental microanalysis, and appeared to be indefinitely stable when stored under an inert atmosphere. However, **20** appeared to slowly decompose in solution to give a mixture of products, some of which precipitated out of solution. One of these products was identified with the aid of single crystal X-ray diffraction. The product, [(*p*-cymene)$_2$Ru$_2$Cl$_2$(μ-Cl)(μ-PHC(O)NHCy)] (**21**), corresponds to that in the following reaction scheme, and features a phosphido ligand bridging two ruthenium centres (Scheme 5.4). The crystal structure is shown in Figure 5.4.

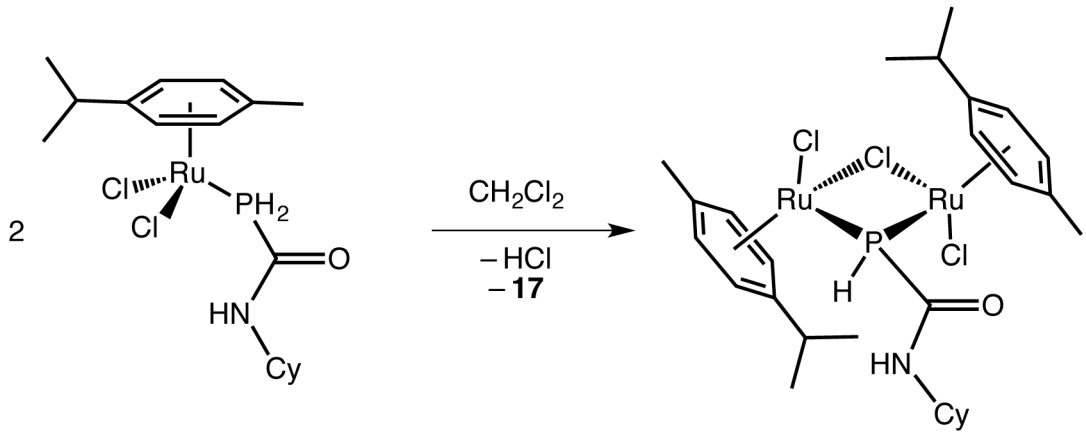

Scheme 5.4: Decomposition of **20** to afford **21**.

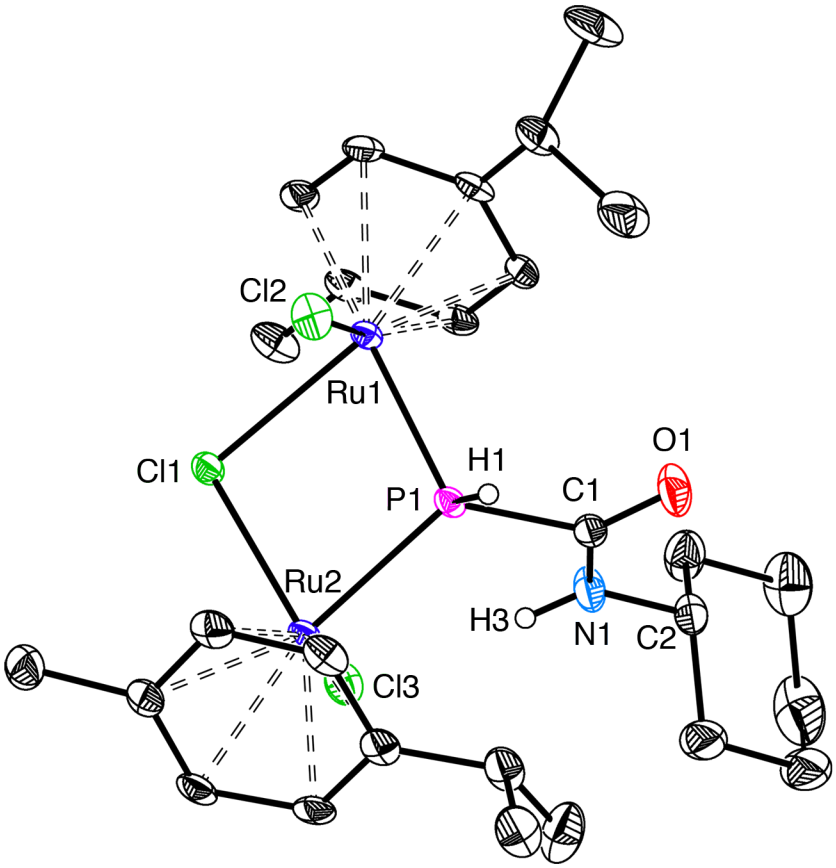

Figure 5.4: Molecular structure of **21**. Anisotropic displacement ellipsoids are set at 50% probability. Heteroatom-bound hydrogen atoms are shown as spheres of arbitrary radii, other hydrogen atoms omitted for clarity.

Although the mechanism of this decomposition was not explored further, a proposal can be volunteered. The P–H bonds of primary and secondary phosphines are known to weaken on coordination to a metal centre.[12] This is demonstrated in the literature by the generation of bridging phosphido and phosphinidene species in some systems when trying to incorporate neutral primary or secondary phosphine ligands.[13–15] Thus the first step could be the cleavage of one of the P–H bonds, driven by the loss of HCl. The phosphide centre subsequently displaces the weakly bound phosphinecarboxamide moiety of a second molecule of **20**, resulting in liberation of an equivalent of **17**. We know the neutral phosphinecarboxamide is relatively weakly coordinated to the Ru(II) centre because it is outcompeted by solvents such as pyridine. A simple rearrangement where one of the

terminal chloride ligands becomes a bridging ligand to maintain an 18 valence electron count on both metal centres affords the observed product **21**.

The bond metric data for **21** are reported in Table 5.3.

Table 5.3: Selected crystallographic bond lengths (Å) and angles (˚) of **21**.

Bond distance (Å)	21	Bond angle (˚)	21
P1–C1	1.875(2)	P1–C1–O1	118.2(2)
C1–O1	1.227(3)	P1–C1–N1	117.6(2)
C1–N1	1.329(3)	N1–C1–O1	125.1(2)
N1–C2	1.467(3)	Ru1–P1–C1	113.4(1)
P1–Ru1	2.337(1)	Ru2–P1–C1	121.8(1)
P1–Ru2	2.339(1)	Ru1–P1–Ru2	104.5(1)
Ru1–Cl1	2.470(1)	P1–Ru1–Cl1	78.8(1)
Ru2–Cl1	2.453(1)	P1–Ru2–Cl1	79.1(1)
Ru1–Cl2	2.402(1)	Ru1–Cl1–Ru2	97.4(1)
Ru2–Cl3	2.417(1)	P1–Ru1–Cl2	83.7(1)
		P1–Ru2–Cl3	92.1(1)

Surprisingly, despite the fact the phosphinecarboxamide moiety has been deprotonated and is formally a phosphido ligand in **21**, the bond lengths within this fragment (P1–C1, C1–O1 and N1–O1) and the associated bond angles are statistically the same in **20** and **21**. The P1–Ru1 and P1–Ru2 bond distances in **21** are very similar (2.337(1) Å and 2.339(1) Å, respectively), and are both longer than the Ru1–P1 bond length in **20** (2.318(1) Å). The bridging chloride ligand is asymmetrically disposed between the two ruthenium centres, as indicated by the shorter Ru2–Cl1 bond length (2.453(1) Å) compared to Ru1–Cl1 (2.470(1) Å). As expected, both of these bond distances to the bridging chloride ligand are significantly longer than the Ru–Cl distances to the terminal chlorides.

This crystal structure of **21** was somewhat serendipitous, and is likely one of a number of decomposition products of **20**. For this reason, it was not possible to obtain supplementary

characterisation data for **21**. However, the monitoring of a CD_2Cl_2 solution of **20** as it slowly decomposed permitted the assignment of a weak resonance in the ^{31}P NMR spectrum attributable to **21**, which is a doublet at 80.1 ppm with a large $^1J_{P-H}$ coupling constant of 415 Hz. This resonance collapses to a singlet on proton decoupling. Although **21** was not isolated, it gives an insight into a novel decomposition product of a ruthenium half-sandwich complex bearing a primary phosphine. Another product with a similar molecular architecture will be discussed in Chapter 7.

5.3 Secondary amines

We sought to extend the scope of the synthesis of *N*-functionalised phosphinecarboxamides to incorporate secondary amines, R_2NH, with the same R groups as above (R = Et, Cy, ^{t}Bu, Ph) to allow a direct comparison. It became apparent that the reactions with secondary amines were more sluggish than the primary amine counterparts, and often failed to afford the desired products.

5.3.1 $H_2PC(O)NEt_2$ (22)

While the reaction of **1** with an acid and Et_2NH afforded the corresponding *N*,*N*-difunctionalised phosphinecarboxamide, $H_2PC(O)NEt_2$ (**22**), in reasonable yields (Scheme 5.5), the analogous reaction with Cy_2NH was accompanied by extensive decomposition of the parent phosphaketene. The analogous reaction with diphenylamine did not yield any of the desired product at all by ^{31}P NMR spectroscopy. The reaction was not attempted with $^t Bu_2NH$ because neither the amine nor the ammonium salt are commercially available (due to the unfavourable steric hindrance of the two bulky substituents). The synthesis of the amine has been reported, but the procedure was judged too laborious to generate a starting material for a reaction that was expected not to work efficiently.[16]

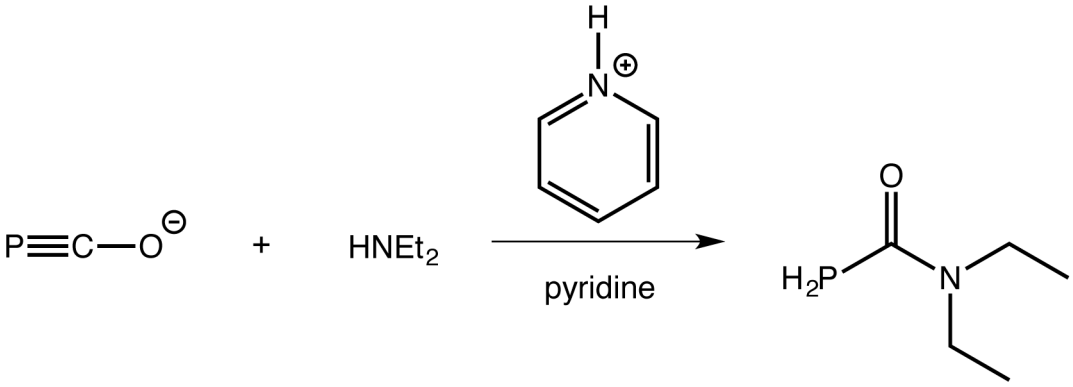

Scheme 5.5: Reaction of **1** with pyridinium triflate and diethylamine to afford **22**.

22 was synthesised in solution and purified by a trap-to-trap distillation, and was characterised spectroscopically. The ^{31}P NMR spectrum reveals a distinctive triplet at –125.4 ppm ($^{1}J_{P–H}$ = 218 Hz), which collapses to a singlet on proton decoupling. The ^{1}H NMR spectrum (Figure 5.5) exhibits a doublet centred at 3.86 ppm attributable to the two phosphine protons, which collapses to a singlet on phosphorus decoupling. The two ethyl groups are chemically inequivalent due to the hindered rotation around the amide bond, and as such there are two distinct methylene resonances that appear as quartets at 3.13 ppm and 3.34 ppm, and two overlapping triplets for the methyl protons at 1.00 ppm and 1.02 ppm (see Figure 5.5).

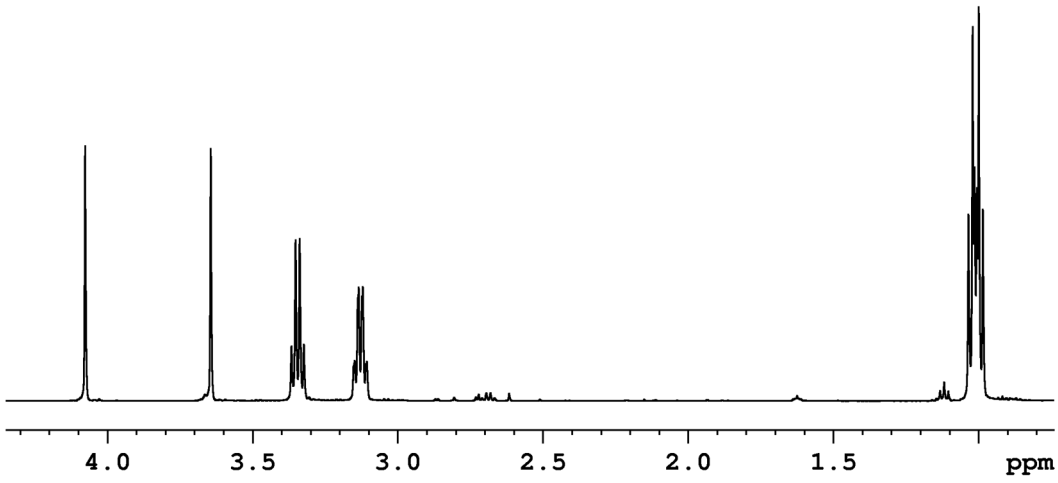

Figure 5.5: ^{1}H NMR spectrum of d_5-pyridine solution of **22**.

The $^{13}C\{^{1}H\}$ NMR spectrum shows the doublet for the carbonyl moiety at 172.9 ppm ($^{1}J_{C-P}$ = 8 Hz), and confirms the chemical inequivalence of the ethyl groups with four distinct resonances.

The solution phase IR spectrum of **22** in d_8-THF reveals a carbonyl stretching band at 1618 cm^{-1}, which is notably lower in energy than the values for the mono-*N*-functionalised phosphinecarboxamides discussed earlier (values in Table 5.1). This is due to the presence of an extra inductively donating alkyl group in **22**, which increases the double bond character of the amide bond and weakens the C–O bond.

5.3.2 Mechanistic implications

These observations (summarised in Table 5.4) can be rationalised based on the current hypothesis for the mechanism.

Table 5.4: Qualitative summary of the formation of primary and secondary *N*-functionalised phosphinecarboxamides.

R	$H_2PC(O)NHR$	$H_2PC(O)NR_2$
Et	high yield (**16**)	reasonable yield (**22**)
Cy	high yield (**17**)	low yield
^{t}Bu	low yield (**18**)	-
Ph	very low yield (**19**)	no reaction

For the reaction to proceed successfully, the amine is required to attack the unstable HPCO parent phosphaketene before the latter decomposes. A key factor is the nucleophilicity of the amine; delocalisation of the nitrogen lone pair of aniline into the aromatic ring diminishes its nucleophilicity, and results in a low yielding reaction relative to the alkyl-substituted amines. This is clearly not the only factor though, because a *tert*-butyl group is more inductively donating than an ethyl group, and so the formation of **18** should be more favourable than **16**, whereas in fact the opposite is true. This suggests that sterics also play a role, as the *tert*-butyl group is significantly more bulky than the ethyl group, and thus it may

be more difficult for the $^{t}BuNH_2$ amine to align in the appropriate manner with the HPCO moiety to form the necessary four-membered transition state discussed previously.

This steric argument can also be used to explain why secondary amines react at a slower rate than their primary amine analogues, as Cy_2NH should be more nucleophilic than $CyNH_2$, yet the former is substantially more bulky and thus leads to an inefficient reaction. Another factor can be rationalised by considering the fact that there are twice as many N–H bonds present in a primary amine than in a secondary amine. Thus, there is a statistically greater chance of obtaining the correct alignment of the N–H bond with the P–C bond to form the four-membered transition state and yield the desired phosphinecarboxamide product for a primary amine. It should be noted that no migration of any group other than a proton to the phosphorus was observed in any of these reactions, and the reaction of the HPCO intermediate with a tertiary amine afforded only decomposition.

5.3.3 The alpha effect and $H_2PC(O)NMe(OMe)$ (23)

We sought to verify these postulations by designing a method by which we could generate a *N*,*N*-difunctionalised phosphinecarboxamide in good yields. The number of N–H bonds in a secondary amine is evidently fixed at one, so this parameter cannot be tailored. To overcome this, we endeavoured to increase the nucleophilicity of the nitrogen lone pair while minimising the steric constraints of the R groups on the amine.

This was achieved by exploiting the alpha effect, which is the enhancement of nucleophilicity of a molecule due to the presence of an adjacent atom with a lone pair of electrons.[17–19] The effect is well established, but the physical origin of the phenomenon is still debated, with possible explanations arising from destabilisation of the ground state of the nucleophile, stabilisation of the transition state, product stability, and solvent effects.[20] A more recent computational paper has described a correlation between the alpha effect and

the deformation energy, which is the energy required to bring the reactants together in the transition state.[21]

Bearing this in mind, we chose the *N*,*O*-dimethylhydroxylamine as a suitable reagent, as the secondary amine has an alpha oxygen atom, small R groups, and the hydrochloride salt is readily available (Scheme 5.6).

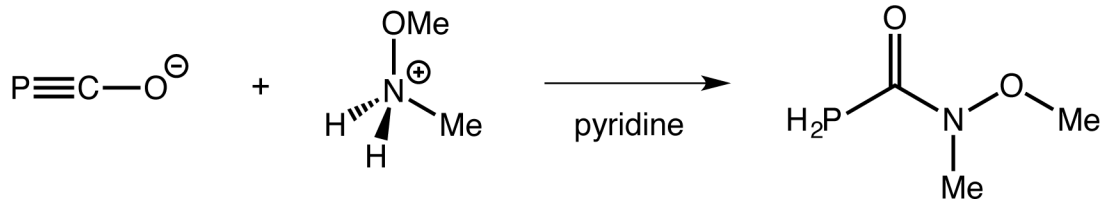

Scheme 5.6: Reaction of **1** with $[H_2NMe(OMe)]^+$ to afford **23**.

1 reacts rapidly with the $[H_2NMe(OMe)][Cl]$ salt in pyridine at room temperature to yield $H_2PC(O)NMe(OMe)$ (**23**) quantitatively by ^{31}P NMR spectroscopy, with no yellow precipitate arising from decomposition. A trap-to-trap distillation under reduced pressure afforded a clean solution of **23**.

The NMR spectroscopic data are unremarkable, and are similar to those discussed previously. The ^{31}P NMR spectrum of a d_5-pyridine solution of **23** reveals the expected triplet at –125.6 ppm ($^1J_{P–H}$ = 219 Hz), and the ^1H NMR spectrum shows the corresponding doublet for the phosphine protons centred at 3.81 ppm. The *O*-methyl protons resonate at a lower field (3.55 ppm) relative to the *N*-methyl protons (3.10 ppm), due to the greater electronegativity of the oxygen atom. Similarly, the $^{13}C\{^1H\}$ NMR spectrum shows the resonance for the methoxy carbon atom at 62.0 ppm, which is downfield relative to the other methyl group at 32.3 ppm. The carbonyl resonance is observed at 164.4 ppm, however the observed signal was too weak to resolve the one-bond coupling to the phosphorus atom.

23 is a novel phosphino-derivative of a Weinreb amide, which are a class of compounds with the general formula RC(O)NMe(OMe).[22] These species are commonly used in organic

synthesis to make carbon–carbon bonds and generate ketones and aldehydes, via the reaction of the Weinreb amide with an organometallic reagent (Scheme 5.7).[23–25]

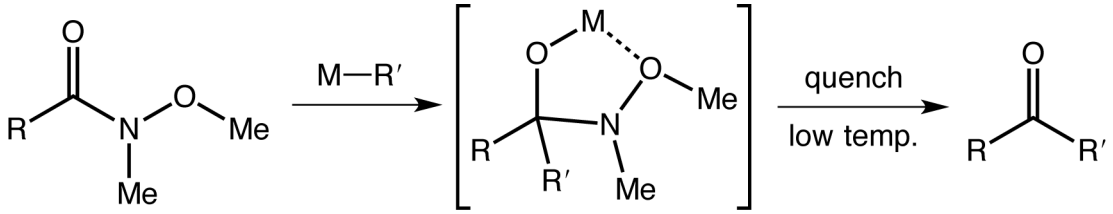

Scheme 5.7: Reaction of a Weinreb amide with an organometallic reagent (M–R′) to give a chelation-stabilised intermediate, which can be quenched at low temperatures to afford ketones or aldehydes.[22]

This application would not be possible with **23**, as the Grignard or organolithium reagent would preferentially react with the acidic protons on the phosphorus instead acting as a nucleophile and attacking the carbonyl group. The tertiary phosphine system ($R_2PC(O)NMe(OMe)$, where $R \neq H$) would have a greater chance of success, and could be employed to synthesise a range of acyl-bearing phosphines. The deprotonation chemistry of **23** will be described in the next chapter.

This section has shown that *N*,*N*-difunctionalised phosphinecarboxamides are accessible, although in general they are produced in a less efficient manner than those derived from primary amines. This can be circumvented, however, by taking advantage of the alpha effect to boost the nucleophilicity of the amine, and produce molecules such as **23** in good yields.

5.4 Functionalised amines

Having established the scope and mechanistic implications of the reactions that yield phosphinecarboxamides, we decided to explore the synthesis of such molecules with further functionality. Some of these products were synthesised with potential applications in mind, and will be discussed in this final section of the chapter.

5.4.1 Amino acids

Having carried out the majority of the above reactions by adding a proton source to $[PCO]^-$ in the presence of an amine, we reasoned it would be easier if the acid and the amine group were present on the same molecule. An exceptionally common class of compounds that fit this criterion are amino acids.

5.4.1.1 [K(18-crown-6)][24] (24: $[H_2PC(O)NHCHMeCO_2]^-$)

One of the simplest amino acids is alanine, where the side-chain is a methyl group. The amino acid can protonate the $[PCO]^-$ and then react via the amine group to form the appropriate phosphinecarboxamide. The reaction scheme is shown in Scheme 5.8. The reaction of [K(18-crown-6)][**1**] with L-alanine can be carried out in water or in a mixture of water and pyridine, to give quantitative formation of [K(18-crown-6)][**24**] (**24**: $[H_2PC(O)NHCHMeCO_2]^-$) by ^{31}P NMR spectroscopy.

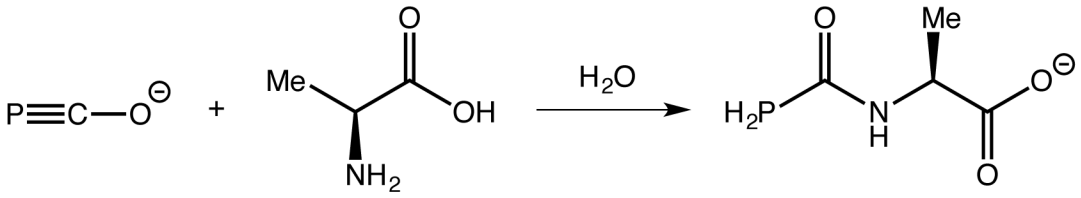

Scheme 5.8: Reaction of **1** with L-alanine to afford **24**.

It can be argued that this reaction is no different from the previous reactions using a preformed ammonium salt (such as in the synthesis of **23**), especially as the amino acid likely exists in its zwitterionic form in water. This is undoubtedly correct, but one difference here is that there are no by-products in this reaction, as the product is a salt. Furthermore, the fact that the amino acid starting material is chiral and enantiopure means that the product generated is a chiral phosphinecarboxamide. The product can be isolated as a solid by simply removing the solvent *in vacuo*. Crystals suitable for single crystal X-ray

diffraction were grown by slow diffusion of hexane into a 50/50 water/pyridine solution of the product (Figure 5.6).

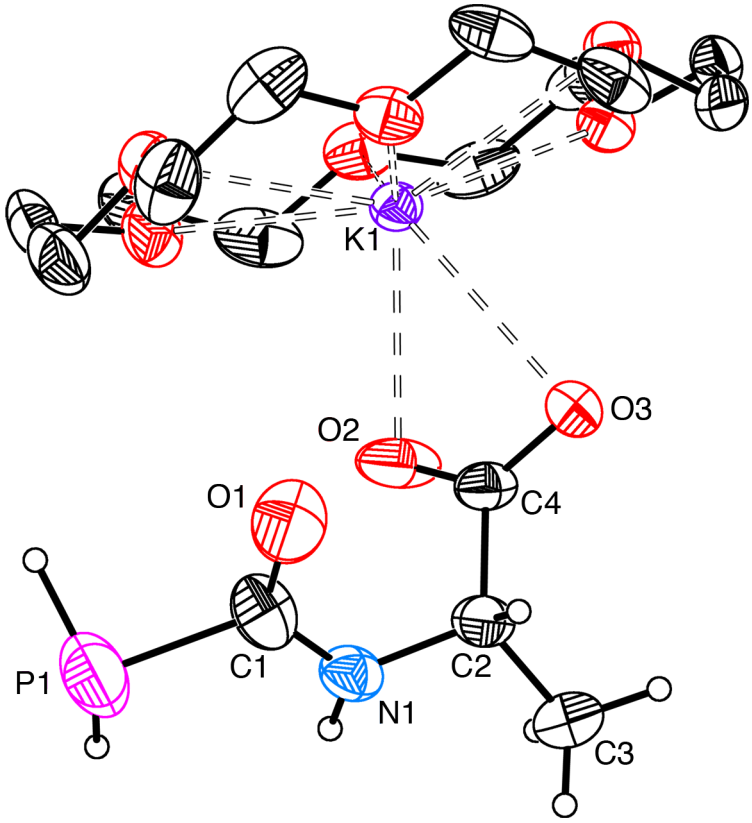

Figure 5.6: Molecular structure of [K(18-crown-6)][**24**]. Note this is one of four such species in the asymmetric unit. Anisotropic displacement ellipsoids are set at 50% probability. Hydrogen atoms on the anion are shown as spheres of arbitrary radii; those on the 18-crown-6 ring are omitted for clarity.

The product crystallised with four distinct molecules of [K(18-crown-6)][**24**] in the asymmetric unit (space group $P2_1$). In all cases the anion is coordinated to a potassium ion through both oxygen centres of the carboxylate group, as shown in Figure 5.6. The phosphine protons had to be restrained (in terms of the phosphorus–proton and proton–proton distances) to yield a satisfactory solution on refinement. The bond metric data for the four different molecules are shown in Table 5.5.

Table 5.5: Bond distances (Å) and angles (˚) for the four distinct molecules of [K(18-crown-6)][**24**] in the asymmetric unit.

Bond distance (Å)	**24a**	**24b**	**24c**	**24d**
P1–C1	1.846(5)	1.853(6)	1.872(5)	1.876(5)
C1–O1	1.205(7)	1.234(7)	1.225(6)	1.220(6)
C1–N1	1.349(7)	1.330(7)	1.335(6)	1.330(6)
N1–C2	1.452(6)	1.463(6)	1.456(5)	1.449(6)
C2–C3	1.527(7)	1.525(6)	1.524(6)	1.509(6)
C2–C4	1.536(6)	1.548(6)	1.543(6)	1.534(6)
C4–O2	1.270(6)	1.264(6)	1.258(5)	1.264(5)
C4–O3	1.238(5)	1.247(5)	1.248(6)	1.248(5)
K1–O2	2.628(4)	2.660(4)	2.725(4)	2.668(3)
K1–O3	2.909(3)	2.886(3)	2.790(4)	2.776(3)
Bond angle (˚)				
P1–C1–O1	117.6(4)	117.9(4)	117.7(4)	118.0(4)
P1–C1–N1	117.5(4)	117.3(4)	116.5(4)	116.5(4)
N1–C1–O1	124.9(5)	124.9(5)	125.6(4)	125.4(5)
C2–C4–O2	117.2(4)	114.9(4)	118.6(4)	118.4(4)
C2–C4–O3	117.8(4)	119.9(4)	115.5(4)	116.6(4)
O2–C4–O3	125.0(4)	125.2(4)	126.0(4)	125.0(4)
K1–O2–C4	97.2(3)	97.0(3)	93.0(3)	93.6(3)
K1–O3–C4	84.9(3)	86.9(3)	90.2(3)	89.0(2)

The bond length data for the four different anions in the asymmetric unit (**24a**–**24d**) are all the same within statistical error, due to the large standard deviations associated with each measurement. For example, the P1–C1 bond lengths for **24a** and **24d** may initially appear different at 1.846(5) Å and 1.876(5) Å, respectively, but the large errors mean they are not statistically different to 3σ (three times the standard deviation). The only discernible difference between the four [K(18-crown-6)][**24**] moieties is the exact nature of the interaction between the cation and the carboxylate group. To take the extreme cases, **24a** interacts in the most asymmetric manner, with a difference of 0.281 Å between the K1–O2 and K1–O3 bond distances and a difference of 12.3˚ between the K1–O2–C4 and K1–O3–

C4 bond angles, whereas the same values for **24c** are 0.065 Å and 2.8˚, respectively, as the cation interacts almost symmetrically with the two oxygen centres. This large discrepancy presumably arises because the interaction is principally electrostatic, and is thus more influenced by the effects of crystal packing.

Taking all four datasets as a whole, the average picture of the anion **24** in the solid state matches that of the previously characterised phosphinecarboxamides. The P1–C1 bond length is indicative of a single bond, and C1–N1 has multiple bond character. The latter is shorter than the N1–C2 bond length, which is purely a single bond. The sum of the bond angles around C1 and C4 are each approximately 360˚, and indicative of both being sp^2 hybridised, as expected.

[K(18-crown-6)][**24**] was also characterised by NMR spectroscopy. The stereogenic centre in **24** renders the two phosphine protons diastereotopic and thus magnetically inequivalent. This is shown in the ^{1}H NMR spectrum (Figure 5.7), in which multiplets arising from each phosphorus-bound proton are observable. Simulation of the spectrum confirmed the assignment, and the shape of the resonance is due to each proton coupling to the phosphorus atom with a large coupling constant ($^1J_{H–P}$ = 205 Hz) and to the other phosphine proton with a smaller coupling constant ($^2J_{H–H}$ = 11 Hz). The second order nature is due to the small difference in chemical shift between the two proton resonances, which are centred at 3.69 ppm and 3.72 ppm (a difference of only 12 Hz on a 400 MHz spectrometer, as was used in this experiment).

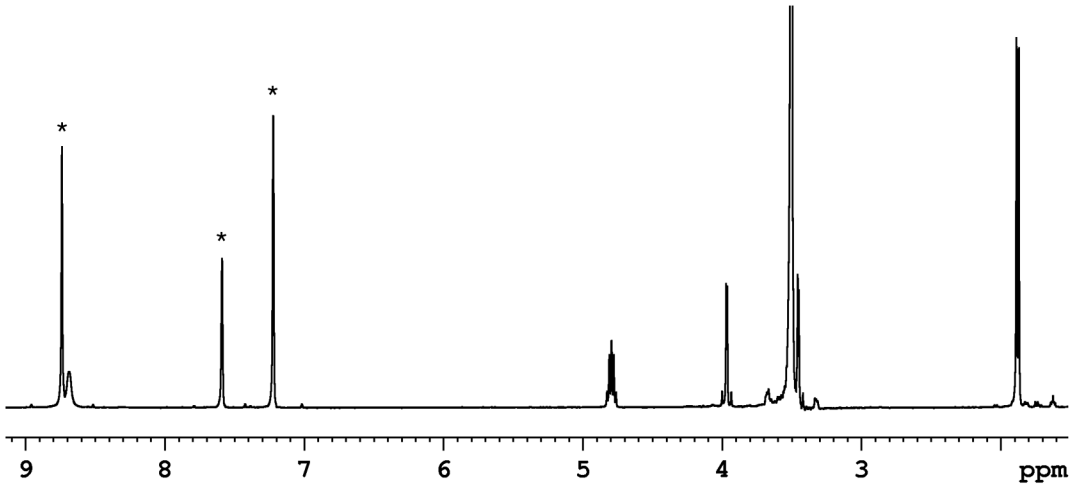

Figure 5.7: ^{1}H NMR spectrum of d_5-pyridine solution of [K(18-crown-6)][**24**]. Resonances marked with ***** are due to residual protic solvent.

The methine proton appears as a virtual quintet at 4.79 ppm. This is actually a doublet of quartets arising from three-bond couplings to the methyl protons and the amide proton with the same magnitude ($^{3}J_{H–H}$ = 7 Hz). This assignment was confirmed using a ^{1}H–^{1}H COSY experiment. The methyl protons appear as a doublet at 1.87 ppm due to this coupling, but the amide resonance at 8.68 ppm appears only as a broad singlet, and the coupling to the methine proton cannot be resolved. The other resonance in the ^{1}H NMR spectrum is the very large signal at 3.50 ppm from the 24 equivalent protons on the 18-crown-6 sequestering agent, and is so strong that the ^{13}C satellites (1.1% abundant, I = ½) are readily observable in Figure 5.7.

The fact that each proton couples to the phosphorus with the same coupling constant leads to the observation of a triplet in the ^{31}P NMR spectrum, although this is more correctly assigned as an overlapping doublet of doublets to yield a virtual triplet. This resonance collapses to a singlet on proton decoupling. The ^{13}C{^{1}H} NMR spectrum is entirely consistent with such a molecule, and the carboxamide carbon appears as a doublet ($^{1}J_{C–P}$ = 5 Hz).

The salt was also characterised by electrospray ionisation (ESI) mass spectrometry. Although the negative ion mode experiment did not reveal a mass envelope corresponding to **24** as a distinct anion, the ion-paired species $\{K[\mathbf{24}]_2\}^-$ was observable at *m/z* = 334.6.

The synthesis of **24** opens the doors for the reaction of **1** with the vast range of amino acids. The wide variety of side-chains that are found on readily accessible amino acids, such as the thiol group on cysteine, means that these reactions could be a simple way of further exploring the functional group tolerance of the formation of the phosphinecarboxamide moiety, particularly as the syntheses of these species can be carried out in water on the bench-top.

5.4.2 Chelating bis(phosphinecarboxamides)

A logical extension of the reaction to yield *N*-functionalised phosphinecarboxamides was to carry out the reaction with two or more amine centres that are linked by bridging groups, to afford larger and potentially chelating molecules with multiple phosphinecarboxamide moieties. There are endless possibilities for the identity of the spacer, but we can use the background work carried out at the start of this chapter to predict whether the product is likely to be formed in reasonable yields.

Arguably the simplest bridge would be an alkyl spacer, such as **A** in Figure 5.8, and this reaction should occur relatively efficiently, by analogy with the formation of **16**. A more rigid spacer would be beneficial in the design of a chelating ligand by helping to spatially direct the phosphinecarboxamide moieties. However, using an aromatic spacer directly bonded to the nitrogen centres, such as **B**, would diminish the nucleophilicity of the amines and lead to a poorly yielding reaction (by analogy with **19**). This could theoretically be overcome by using a rigid aromatic spacer but with one or more methylene groups between the phenyl ring and the nitrogen centres, as in **C**.

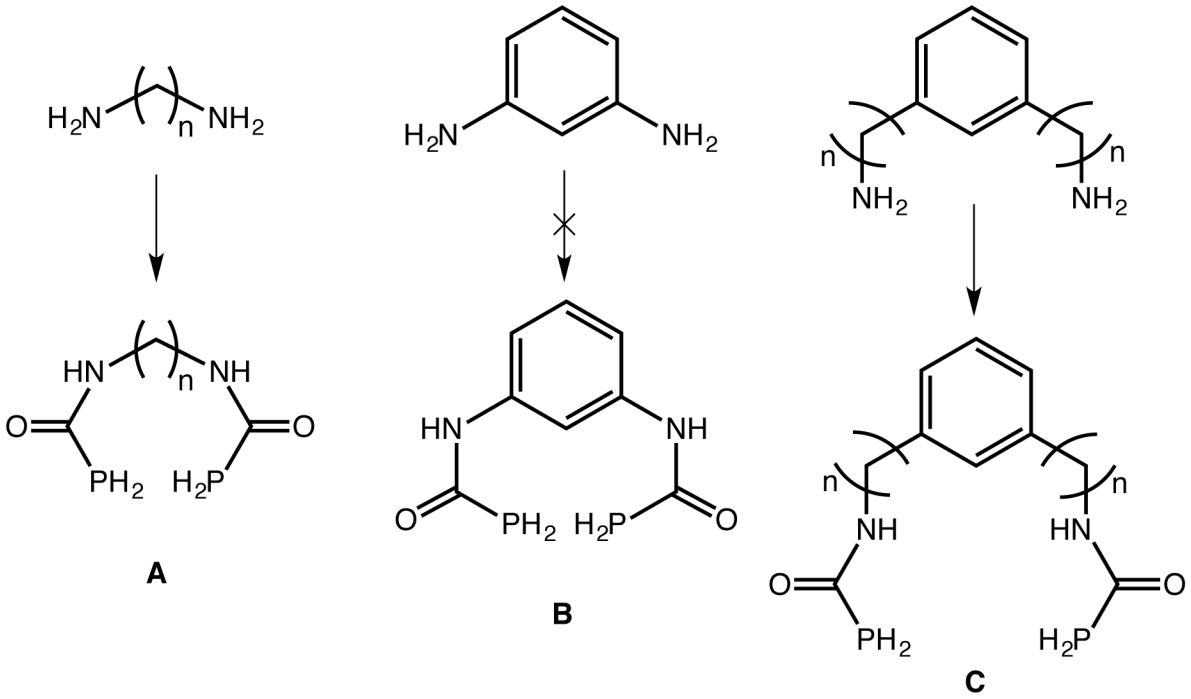

Figure 5.8: Possible chelating bis(phosphinecarboxamide) molecules. For **A** and **C**, n > 1.

5.4.2.1 $H_2PC(O)NHC_2H_4NHC(O)PH_2$ (25)

As a proof of concept, we synthesised the bis(phosphinecarboxamide) molecule with an ethylene linker (the variant of **A** where n = 2). This is derived from the reaction of ethylenediamine with two equivalents of **1** and pyridinium triflate (Scheme 5.9), although an excess of the latter reagents was required to ensure full consumption of the amine starting material.

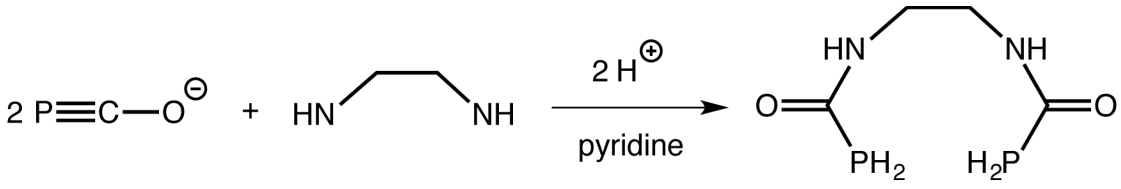

Scheme 5.9: Reaction of two equivalents of **1** and two equivalents of pyridinium triflate with one equivalent of ethylenediamine to afford **25**.

The volatiles were removed under reduced pressure, and the product was extracted into 1,4-dioxane. ^{19}F NMR spectroscopy showed that a small quantity of the [Na][OTf] by-product was also present, so the mixture was recrystallized in hot THF to yield a compositionally

pure sample of **25**, as demonstrated by multielement NMR spectroscopy and elemental microanalysis. Colourless crystals of **25** suitable for single crystal X-ray diffraction were grown by slow diffusion of hexane into a pyridine solution of the product (Figure 5.9).

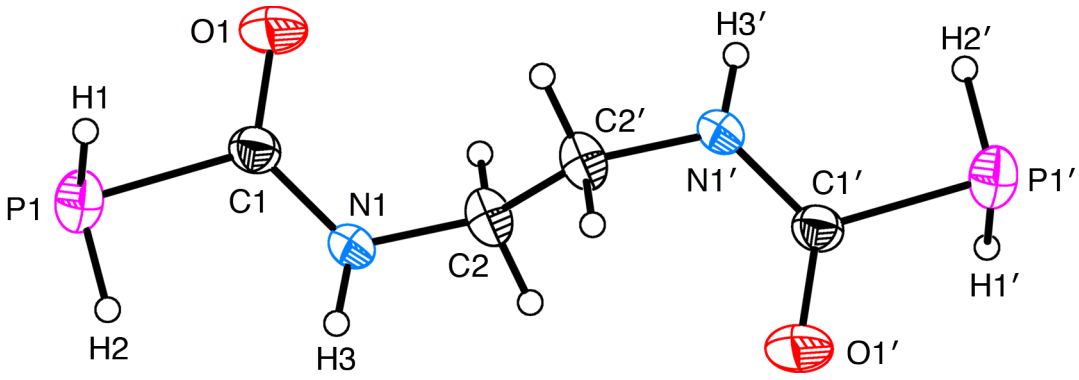

Figure 5.9: Molecular structure of **25**. Anisotropic displacement ellipsoids are set at 50% probability. Hydrogen atoms are shown as spheres of arbitrary radii.
Symmetry operation ′: *–x*, *–y*, 1*–z*.

The solid-state structure of **25** shows the molecule to be extended in a chain-like conformation, instead of the pincer-like conformation drawn in Scheme 5.8. This is due to intermolecular hydrogen bonding between the oxygen centres and the amide-bound protons of adjacent molecules, leading to extended chains throughout the structure. The asymmetric unit is in fact only half of the molecule, with the second half generated by an inversion centre halfway along the C2–C2′ bond. The bond metric data are shown in Table 5.6.

Table 5.6: Selected crystallographic bond lengths (Å) and angles (˚) of **25**.

Bond distance (Å)	**25**	**Bond angle (˚)**	**25**
P1–C1	1.863(2)	P1–C1–O1	118.4(1)
C1–O1	1.228(2)	P1–C1–N1	118.5(1)
C1–N1	1.326(2)	N1–C1–O1	123.1(2)
N1–C2	1.455(2)	Sum around P1	287
C2–C2′	1.519(2)	Sum around N1	360

All of the data are consistent with the previous structural data for phosphinecarboxamides. For example, the P1–C1, C1–O1 and C1–N1 bond lengths are all the same as those for the parent phosphinecarboxamide, **11**, within statistical error. Obviously the metric data for the two phosphinecarboxamide moieties within **25** are identical, as they are related by the inversion centre. The two carboxamide fragments are coplanar, and slightly offset due to the ethylene bridge, which allows for efficient packing and intermolecular hydrogen bonding in the solid state.

The product was also well characterised by NMR spectroscopy. The occurrence of only one triplet resonance at –132.7 ppm ($^{1}J_{P–H}$ = 208 Hz) in the ^{31}P NMR spectrum of a d_5-pyridine solution of **25** revealed the two phosphorus centres to be equivalent, as expected. In addition to the presence of the distinctive amide and phosphine protons, the ^{1}H NMR spectrum shows the ethylene protons are chemically equivalent but magnetically inequivalent, as they couple to the different amide protons in different manners, and thus appear as a multiplet. This is corroborated by the ^{13}C{^{1}H} NMR spectrum, which shows just one resonance for the bridging carbon atoms at 40.8 ppm, as well as the doublet for the carbonyl group at 173.6 ppm ($^{1}J_{C–P}$ = 7 Hz). The IR spectrum of a solid sample of **25** in a Nujol mull revealed a carbonyl stretching band at 1598 cm^{-1}.

A chemical ionisation (CI) mass spectrometric investigation of **25**, using ammonia as the carrier gas, showed the mass envelopes corresponding to $[M+H]^+$ and $[M+NH_4]^+$ at *m/z* ratios of 181.0284 and 198.0545, respectively. These are consistent with the predicted monoisotopic masses for these species, which are 181.0296 and 198.0561 Da, respectively. In addition to these peaks, a large number of others that arise from fragmentation of the molecular ion are observable (Figure 5.10). Some of these are easily identifiable, such as the phosphonium cation $[PH_4]^+$ and the protonated ethylenediamine $[C_2H_9N_2]^+$. There are also some evident pairs of peaks that are separated by approximately 17 Da (the mass of

ammonia), which arise from the same fragment being associated with either a proton or an ammonium cation (as in $[M+H]^+$ and $[M+NH_4]^+$).

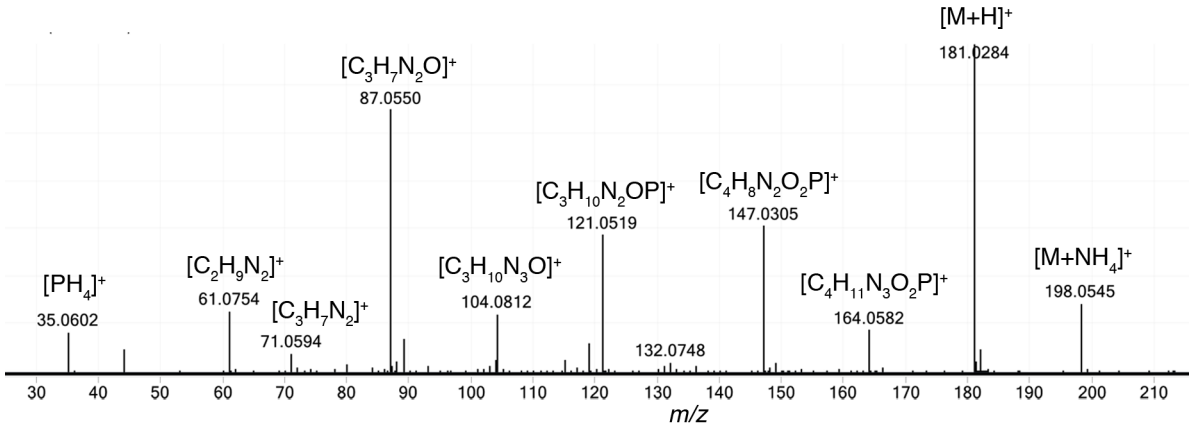

Figure 5.10: CI mass spectrum of **25** (with NH_3 as the carrier gas). M corresponds to **25** ($C_4H_{10}N_2O_2P_2$).

25 was synthesised to show that bis(phosphinecarboxamides) are accessible. Unfortunately, in this particular instance the yield was low due to the relatively inefficient purification of the product, and this prevented further reactivity studies on this molecule. However, the synthetic procedure could almost certainly be optimised, and it would be interesting to explore this compound as a chelating ligand. A range of spacers could be used to design bidentate systems with certain properties, such as preferentially *trans*-spanning ligands. Furthermore, more exotic amine precursors, such as spermidine and spermine (Figure 5.11), could be used to generate tridentate and tetradentate chelating ligands, respectively.

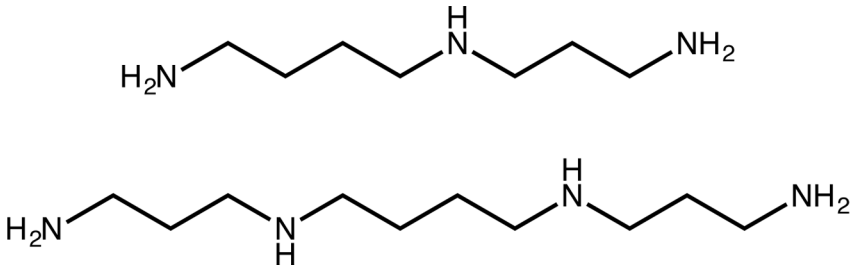

Figure 5.11: Polyamines: spermidine (above) and spermine (below).

The "internal" amines are secondary amines, and thus would react to give the internal phosphinecarboxamide moieties more slowly, but given that **22** was successfully synthesised it should still be possible. The difference in rates of reaction could actually be exploited to generate chelating molecules with terminal phosphinecarboxamides and internal amines. This topic merits further exploration.

5.4.3 Phosphorus-containing polymers

Since the discovery of polyphosphazenes as inorganic analogues of rubber in the late 19th century,[26] phosphorus-containing polymers have been the subject of extensive research, due to their numerous technological applications.[27] They are employed in industry as dispersants and corrosion-inhibiting agents due to their aptitude to bind metals;[28,29] they have medical applications in dentistry, regenerative medicine and drug delivery;[30] and are widely used as flame-retardants due to their ability to efficiently form a char, which acts as a protective coating to starve the fire of oxygen.[31,32]

Our initial target was to generate phosphorus-containing polymers via a condensation reaction of phosphinecarboxamide with formaldehyde (Scheme 5.10), by analogy with the synthesis of the common thermosetting resin, urea-formaldehyde.

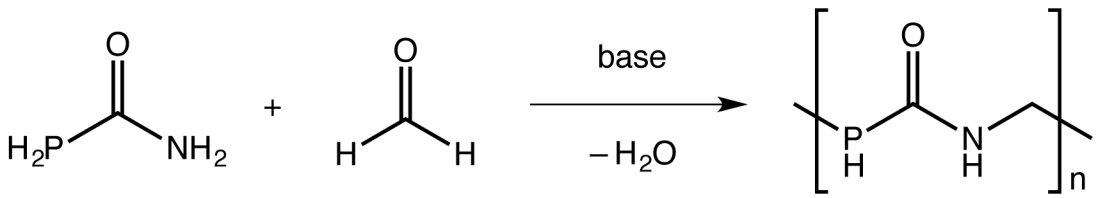

Scheme 5.10: Targeted condensation polymerisation of phosphinecarboxamide with formaldehyde to afford a phosphorus-containing analogue of urea-formaldehyde.

This was initially attempted by heating paraformaldehyde and **11**, where the solvent could also act as the base required to promote the reaction. Paraformaldehyde is not very soluble, and the heating was designed to crack the polymer and afford discrete units of

formaldehyde, which could subsequently react with **11**. However, this method led primarily to thermal decomposition of the phosphinecarboxamide.

The procedure was altered so that the paraformaldehyde was heated to generate the formaldehyde, and this was passed as a gas through a pyridine solution of **11** at room temperature. A white solid did precipitate out of solution, as hoped, but this was simply the recombination of the formaldehyde to generate paraformaldehyde. ^{31}P NMR spectroscopy of the resulting solution suggested that there was a small amount of at least one novel phosphorus-containing product, but the sharpness of the resonance hinted that this was not attributable to the desired polymer.

5.4.3.1 $H_2PC(O)NH(C_9H_9)$ (26)

We therefore designed an alternative methodology for incorporating phosphinecarboxamides into phosphorus-containing polymers, by appending a functionality that is known to polymerise to a phosphinecarboxamide group. This was achieved by the reaction of [Na(1,4-dioxane)$_{2.69}$][**1**] with a primary ammonium chloride salt bearing a styrene moiety to afford $H_2PC(O)NH(C_9H_9)$ (**26**), as shown in Scheme 5.11.

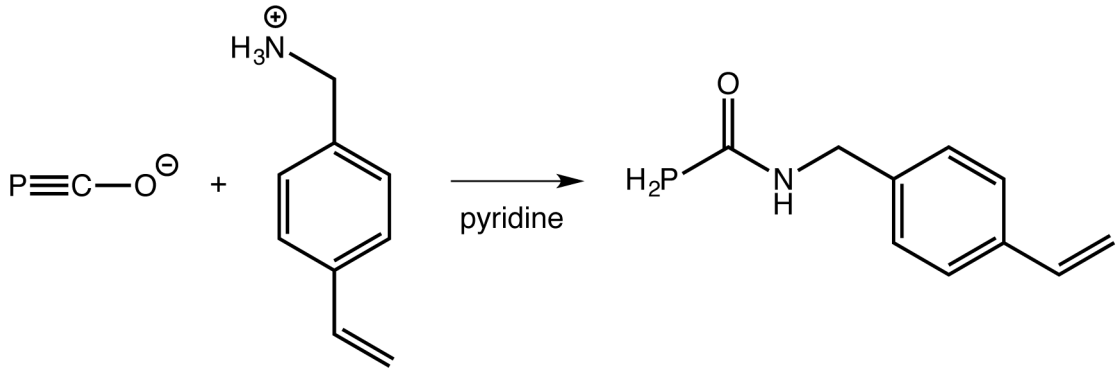

Scheme 5.11: Reaction of **1** with (4-vinylphenyl)methanaminium chloride to afford **26**.

The volatiles were removed under reduced pressure affording an off-white solid. Extraction in THF and removal of the solvent afforded a white solid of compositionally pure **26** in a 90% yield with respect to phosphorus. The starting material was synthesised by reacting the

corresponding alkyl halide with potassium phthalimide, followed by hydrazinolysis to yield the primary amine (Scheme 5.12), which was subsequently worked up with hydrochloric acid to give the salt.[33]

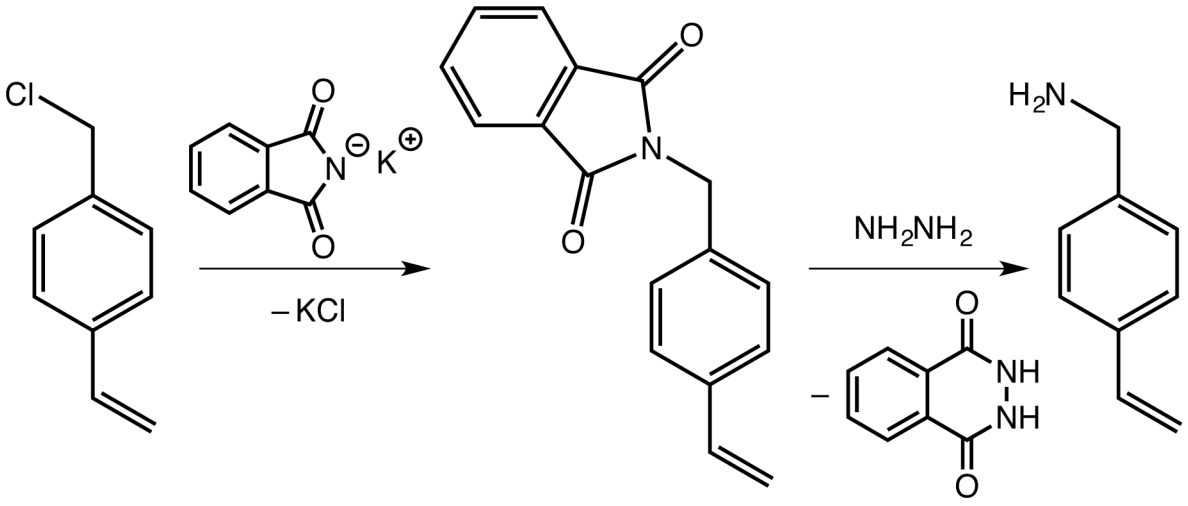

Scheme 5.12: Gabriel synthesis to generate the required primary alkyl amine.

A d_8-THF solution of **26** was characterised using NMR spectroscopy. The ^{31}P NMR spectrum shows the distinctive triplet at –136.1 ppm ($^1J_{P–H}$ = 206 Hz), which collapses to a singlet on proton decoupling. The ^{1}H and ^{13}C{^{1}H} NMR spectra are unremarkable, and are entirely consistent with the formation of **26** (all of the data are listed in the Experimental in Chapter 8). The IR spectrum of a Nujol mull of **26** revealed a carbonyl stretching band at 1610 cm^{-1}, which is similar to the previously discussed *N*-functionalised phosphinecarboxamides (1607 cm^{-1} for **17**, 1598 cm^{-1} for **25**).

Crystals of **26** were grown and used for a single crystal diffraction experiment. Unfortunately the crystals were too weakly diffracting for a publishable dataset to be obtained, but the solution did support the connectivity of the molecule. The white solid was also characterised by FI mass spectrometry, and **26** was observed at *m/z* = 193.0654, which is a good match with the calculated monoisotopic mass of 193.0657 Da. The compositional purity of **26** was confirmed by elemental microanalysis.

26 is readily soluble in THF, and the aforementioned NMR spectroscopy was carried out in this solvent. However, if a THF solution of **26** is stored in daylight under an inert atmosphere for extended periods of time then copious amounts of white solid are produced, which will not redissolve in the solvent. Furthermore, if the freshly prepared solid sample of **26** is stored in light for a period of time, then, although there is no obvious change in appearance, this sample will not dissolve in THF. We believe this is due to the spontaneous light-induced polymerisation of **26**, presumably across the double bond of the styrene moiety (Scheme 5.13).

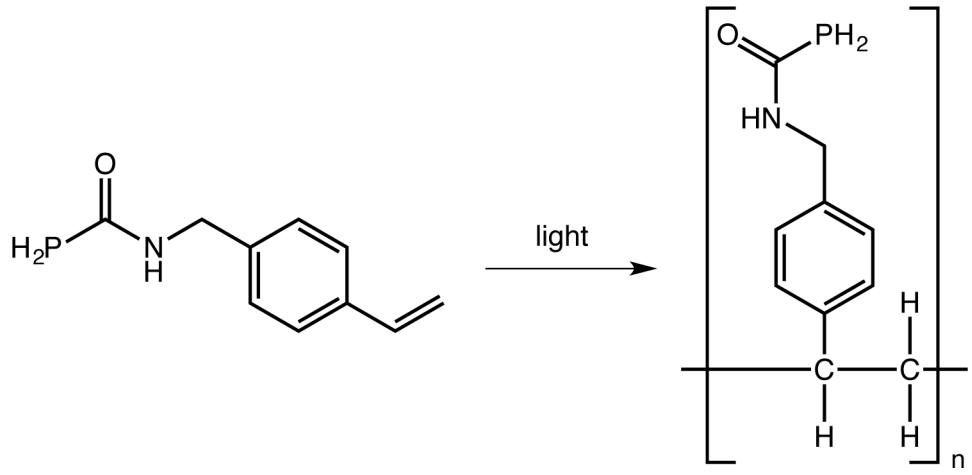

Scheme 5.13: Proposed polymerisation of **26** to yield phosphinecarboxamide-derivatised polystyrene.

The product has not been further characterised thus far, as we have not been able to find a solvent that dissolves the sample to any great extent, including water and acetone, even at elevated temperatures. We are planning to run solid-state ^{31}P NMR spectroscopy in the near future, in order to confirm that the phosphorus atoms are still incorporated in the product, and that there has been no cleavage of the phosphinecarboxamide moiety during polymerisation. This would also reveal if the polymerisation reaction is as simple as shown in Scheme 5.13, or if there are alternative competing pathways from hydrophosphination reactions. If these studies prove fruitful then we are planning to collaborate with a research

group with known specialty in the topic of synthesising and characterising phosphorus-containing polymers.

The facile polymerisation of **26** can be suppressed by storing the solid under an inert atmosphere in the dark. This permits the monomer to be synthesised and stored in bulk, and therefore the subsequent polymerisation process can be targeted in a more controlled manner. This will include copolymerising **26** with other monomers to obtain a range of polymers that have different mechanical, optical or thermal properties. For example, the copolymer of styrene and acrylonitrile affords a resin that has a significantly greater thermal resistance than the polymer of styrene alone.[34] Research is on-going in this area.

5.5 Conclusions

This chapter has extended the work on the parent phosphinecarboxamide discussed in the previous chapter to incorporate *N*-functionalised phosphinecarboxamides. The synthetic scope of the reaction was established using simple primary and secondary amines, and most of the resulting products (**16**–**19**, **22**) have been characterised spectroscopically. It was found that the reactions with secondary amines are significantly more sluggish, due to the steric bulk of the amine and the reduced number of N–H bonds present to adopt the correct alignment in the postulated four-membered transition state. This can be overcome, however, by utilising the alpha effect to boost the nucleophilicity of the amine.

The synthesis of the cyclohexylphosphinecarboxamide, **17**, was optimised, and this product can now be obtained in multi-gram quantities with a 77% yield. The ability of this species to coordinate to a metal centre was examined briefly, and resulted in the formation of the ruthenium half-sandwich, **20**. A novel decomposition route of this type of species was discovered, leading to a bimetallic system with a bridging phosphido ligand, **21**, which was structurally characterised. The reactivity of **17** will be explored in the next chapter.

Building on the basic principles gleaned from the reactions with simple primary and secondary amines, we sought to synthesise more exotic phosphinecarboxamide-containing species. The reaction of [K(18-crown-6)][**1**] with L-alanine afforded the salt [K(18-crown-6)][**24**], which features a chiral anion. Polyamines can be used to generate molecular frameworks featuring multiple phosphinecarboxamide moieties, which can possibly be utilised as chelating ligands. As a proof of concept, **25** was synthesised from ethylenediamine. Finally, in a bid to use these functional groups as a novel way to generate industrially applicable phosphorus-containing polymers, the phosphinecarboxamide bearing a styrene moiety was synthesised (**26**). These last three species, **24**–**26**, are representative examples of three separate avenues of research that could derive from phosphinecarboxamide chemistry, and all would be worth exploring in the future.

5.6 References

(1) Wöhler, F. *Ann. Phys. (Berlin)* **1828**, *87*, 253–256.

(2) Wöhler, F. *Ann. Chim. Phys.* **1828**, *37*, 330–333.

(3) Wöhler, F. *Quart. J. Sci. Lit. Art, Series 2, Part 1, (April-June)* **1828**, 491.

(4) Shorter, J. *Chem. Soc. Rev.* **1978**, *7*, 1–14.

(5) ten Hoor, M. J. *J. Chem. Educ.* **1996**, *73*, 42–45.

(6) Frost, A. A.; Pearson, R. G. *Kinetics and Mechanism*; 2nd ed.; Wiley: New York, 1961.

(7) Tsipis, C. A.; Karipidis, P. A. *J. Am. Chem. Soc.* **2003**, *125*, 2307–2318.

(8) Tondreau, A. M.; Benkő, Z.; Harmer, J. R.; Grützmacher, H. *Chem. Sci.* **2014**, *5*, 1545–1554.

(9) Jupp, A. R.; Trott, G.; Payen de la Garanderie, É.; Holl, J. D. G.; Carmichael, D.; Goicoechea, J. M. *Chem. Eur. J.* **2015**, *21*, 8015–8018.

(10) Jupp, A. R.; Goicoechea, J. M. *J. Am. Chem. Soc.* **2013**, *135*, 19131–19134.

(11) Orpen, A. G.; Connelly, N. G. *Organometallics* **1990**, *9*, 1206–1210.

(12) Paris, S. I. M.; Lemke, F. R.; Sommer, R.; Lönnecke, P.; Hey-Hawkins, E. *J. Organomet. Chem.* **2005**, *690*, 1807–1813.

(13) Goodwin, N. J.; Henderson, W.; Nicholson, B. K.; Fawcett, J.; Russell, D. R. *J. Chem. Soc., Dalton Trans.* **1999**, 1785–1794.

(14) Wells, R. L.; Rahbarnoohi, H.; Glaser, P. B.; Liable-Sands, L. M.; Rheingold, A. L. *Organometallics* **1996**, *15*, 3204–3209.

(15) Carty, A. J.; Hartstock, F.; Taylor, N. J. *Inorg. Chem.* **1982**, *21*, 1349–1354.

(16) Corey, E. J.; Gross, A. W. *Tetrahedron Lett.* **1984**, *25*, 491–494.

(17) Jencks, W. P.; Carriuolo, J. *J. Am. Chem. Soc.* **1960**, *82*, 1778–1786.

(18) Jencks, W. P.; Carriuolo, J. *J. Am. Chem. Soc.* **1960**, *82*, 675–681.

(19) Edwards, J. O.; Pearson, R. G. *J. Am. Chem. Soc.* **1962**, *84*, 16–24.

(20) Fina, N. J.; Edwards, J. O. *Int. J. Chem. Kinet.* **1973**, *5*, 1–26.

(21) Ren, Y.; Yamataka, H. *J. Org. Chem.* **2007**, *72*, 5660–5667.

(22) Nahm, S.; Weinreb, S. M. *Tetrahedron Lett.* **1981**, *22*, 3815–3818.

(23) Paek, S.-M.; Seo, S.-Y.; Kim, S.-H.; Jung, J.-W.; Lee, Y.-S.; Jung, J.-K.; Suh, Y.-G. *Org. Lett.* **2005**, *7*, 3159–3162.

(24) Barbazanges, M.; Meyer, C.; Cossy, J. *Org. Lett.* **2008**, *10*, 4489–4492.

(25) Shimizu, T.; Satoh, T.; Murakoshi, K.; Sodeoka, M. *Org. Lett.* **2005**, *7*, 5573–5576.

(26) Allcock, H. R. *Chemistry and Applications of Polyphosphazenes*; Wiley: Hoboken, 2003.

(27) Popa, A.; Weder, C.; Monge, S.; Tang, B. Z.; Abd-El-Aziz, A. S.; Craig, S.; Dong, J.; Masuda, T. *Phosphorus-Based Polymers: From Synthesis to Applications*; David, G., Ed.; Royal Society of Chemistry: Cambridge, UK, 2014.

(28) Matczak-Jon, E.; Videnova-Adrabińska, V. *Coord. Chem. Rev.* **2005**, *249*, 2458–2488.

(29) Herrera Taboada, L.; Guzmann, M.; Neubecker, K.; Goethlich, A. *PCT Int. Appl.* **2008**, WO 2008077829 A1 20080703.

(30) Monge, S.; Canniccioni, B.; Graillot, A.; Robin, J.-J. *Biomacromolecules* **2011**, *12*, 1973–1982.

(31) Chang, S.; Sachinvala, N. D.; Sawhney, P.; Parikh, D. V.; Jarrett, W.; Grimm, C. *Polym. Adv. Technol.* **2007**, *18*, 611–619.

(32) Singh, H.; Jain, A. K. *J. Appl. Polym. Sci.* **2009**, *111*, 1115–1143.

(33) Bertini, V.; Alfei, S.; Pocci, M.; Lucchesini, F.; Picci, N.; Iemma, F. *Tetrahedron* **2004**, *60*, 11407–11414.

(34) Harper, C. A.; Magazine, "Modern Plastics." *Modern Plastics Handbook*; McGraw-Hill Publishing Co.: New York, 2000.

Chapter 6
Deprotonation, *P*-functionalisation and oxidation chemistry of phosphinecarboxamides

6.1 Introduction and objectives

6.1.1 Photoinitiators

Photoinitiators are compounds that generate reactive species, typically radicals, upon exposure to UV or visible radiation. They are key components in photopolymers that allow the production of resins and coatings with high control and variety in the process parameters.[1] These have industrial applications in a wide range of areas, including laser imaging, microlithography, microelectronics, optics, holography, medicine and nanotechnology.[2] Among the most studied classes of photoinitiator are the bis(acyl) phosphine oxides (BAPOs), such as $PhP(O)\{C(O)Mes\}_2$, which is traded commercially under the name of Irgacure® 819 (Scheme 6.1).[3–8]

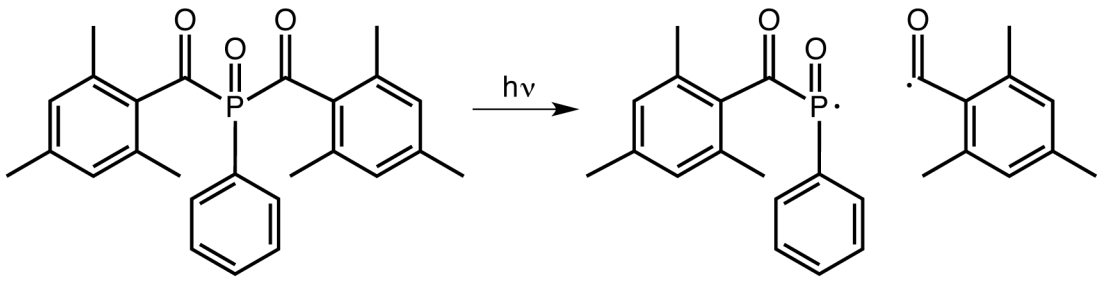

Irgacure® 819

Scheme 6.1: Photolysis of a commercially available BAPO to generate stabilised radicals.

BAPOs offer several advantages over other photoinitiators.[9–11] Photolysis affords multiple radicals, and the phosphinoyl radical is approximately 1000 times more reactive than the acyl radicals. Furthermore, BAPOs absorb light in the visible region, but the cleavage products are transparent, so relatively thick clear coatings can be used that permit a high curing depth. They also have appreciable thermal stability and can be easily stored.

Although these properties mean BAPOs are widely used in industry, very few derivatives have been synthesised.[12] A recent report from the research group of Grützmacher has

described the synthesis of a range of *P*-functionalised BAPOs that offer the possibility of surface modification (Scheme 6.2).[9]

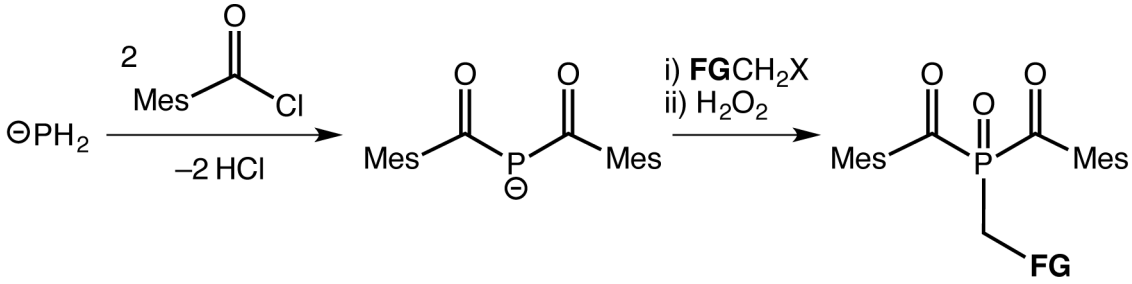

Scheme 6.2: Synthesis of a range of BAPOs with varying functional groups (**FG**). Figure adapted from Huber et al.[9]

The products are derived from the reaction of sodium dihydrogen phosphide with mesitoyl chloride to afford the phosphide intermediate shown. Alkylation and subsequent oxidation affords the BAPO products in a relatively facile manner. These species do indeed act as photoinitiators, and allow the synthesis of photoactive polymers and surfaces. The work in this chapter will be building towards the generation of similar systems bearing carbamoyl groups.

6.1.2 Chapter outline

This chapter will explore the fundamental chemistry of phosphinecarboxamides, and establish their versatility as chemical building blocks. This will commence with the deprotonation of a selection of the *N*-functionalised phosphinecarboxamides discussed in the previous chapter, to afford a range of stable phosphides.[13] Subsequently, the two distinct phosphides derived from the *N*-cyclohexyl phosphinecarboxamide, which differ in the number of carbamoyl groups bound to the phosphorus atom, will be *P*-functionalised with simple electrophiles. Finally, the oxidation chemistry of a range of phosphinecarboxamides will be discussed, to yield a variety of phosphinic acids, phosphinates and phosphine oxides. A number of these species bear strong structural resemblances to known photoinitiators.

6.2 Deprotonation chemistry

The characterisation of a number of the *N*-functionalised phosphinecarboxamides discussed in the previous chapter was limited to solution-based techniques, such as NMR spectroscopy and solution phase IR spectroscopy, which was due to their volatility under reduced pressure. We reasoned that there were two relatively simple ways of isolating and further characterising these species as solids. The first is coordination of the phosphinecarboxamides to metal centres, and this has already been explored in previous chapters. The second was to generate a salt of the product, either by protonation or deprotonation, which could be then be readily isolated by precipitation or removal of the solvent *in vacuo*. This study would also provide further information on the fundamental chemistry of the phosphinecarboxamide moiety, and allow us to ascertain whether it acts primarily as an amide, a phosphine, a combination of the two, or as a new functional group entirely.

It was determined that the parent phosphinecarboxamide, **11**, rapidly decomposes under basic conditions at room temperature to yield PH_3 and $[NCO]^-$, and this will be discussed later in the chapter (see Scheme 6.11). In sharp contrast, **11** is very stable with respect to acidic conditions, with no sign of any decomposition by ^{31}P NMR spectroscopy. In fact, there was no observable reaction of **11** and Brookhart's acid ($[H(OEt_2)_2][BAr^F_4]$, a strong acid that has been used to generate and stabilise highly electrophilic species).[14] Instead, the "free" proton slowly attacks the fluorine atoms and leads to decomposition of the anion.

The study progressed, therefore, from the parent species to the *N*-functionalised phosphinecarboxamides. The Brønsted basicity of these species is unlikely to vary to any great degree, and so we focussed on obtaining salts derived from deprotonation. It was rationalised that the *N*-functionalised phosphinecarboxamides should be more stable with

respect to basic conditions than **11**, because the same decomposition pathway to generate PH_3 is not accessible for the former.

In all of the following cases, the deprotonation was carried out with potassium bis(trimethylsilyl)amide (KHMDS – pictured in Scheme 6.3), which is a strong non-nucleophilic base. The cations have not been included in the reaction schemes for clarity, and the species are stable in solution with the "naked" potassium counter-cation, and can be used as such for further reactivity. The products described herein were all isolated as the $[K(18\text{-crown-6})]^+$ salts, as this was found to aid the growth of single crystals.

6.2.1 [K(18-crown-6)][27] (27: $[HPC(O)NEt_2]^-$)

The simplest case was envisaged to be the deprotonation of **22**, as the two alkyl substituents on the nitrogen centre limit the number of acidic sites in the molecule. Thus, the addition of one equivalent of KHMDS and 18-crown-6 to a d_8-THF solution of **22** resulted in the clean deprotonation of one of the phosphine protons, and the formation of a stable phosphide anion (Scheme 6.3).

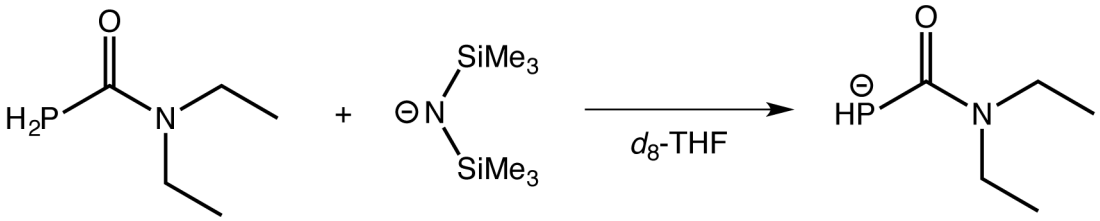

Scheme 6.3: Deprotonation of **22** with KHMDS to afford **27**.

This is apparent from the ^{31}P NMR spectrum, where the triplet at –125.4 ppm ($^1J_{P–H}$ = 218 Hz) arising from **22** has disappeared and been replaced by a doublet at –93.2 ppm ($^1J_{P–H}$ = 154 Hz), as shown in Figure 6.1. The decrease in the $^1J_{P–H}$ coupling constant on deprotonation is due to the increased electron density on phosphorus, and is consistent with the simple series: $[PH_4]^+$ ($^1J_{P–H}$ = 547 Hz), PH_3 ($^1J_{P–H}$ = 189 Hz), $[PH_2]^-$ ($^1J_{P–H}$ = 139 Hz).[15] The doublet collapses to a singlet on proton decoupling. The ^1H NMR spectrum revealed a

doublet for the phosphide proton centred at 1.60 ppm, which is upfield shifted relative to the PH_2 group in **22** (centred at 3.86 ppm).

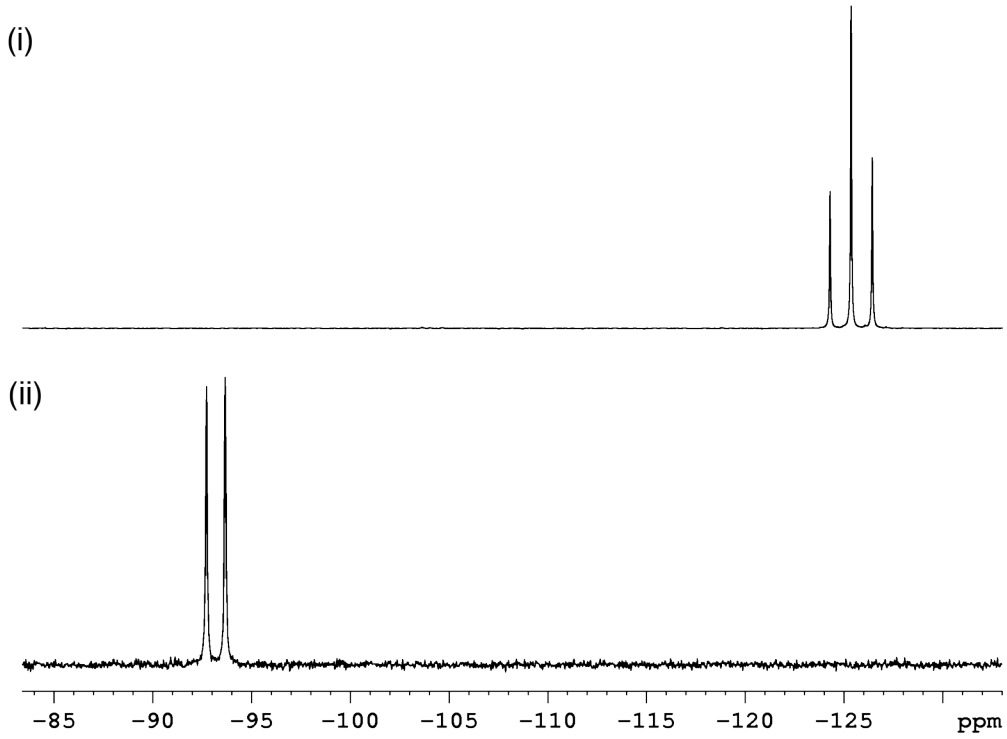

Figure 6.1: ^{31}P NMR spectra of d_8-THF solutions of (i) **22** and (ii) [K(18-crown-6)][**27**].

Crystals of [K(18-crown-6)][**27**]·0.5(1,4-dioxane) were grown by slow diffusion of hexane into the d_8-THF solution of the product, and a single crystal X-ray diffraction study was carried out (Figure 6.2). There is half a molecule of 1,4-dioxane in the asymmetric unit, and is presumably present due to the [Na(1,4-dioxane)$_{1.75}$][**1**] starting material used to generate **22**. This solvent molecule has been omitted from the structure shown in Figure 6.2 for clarity.

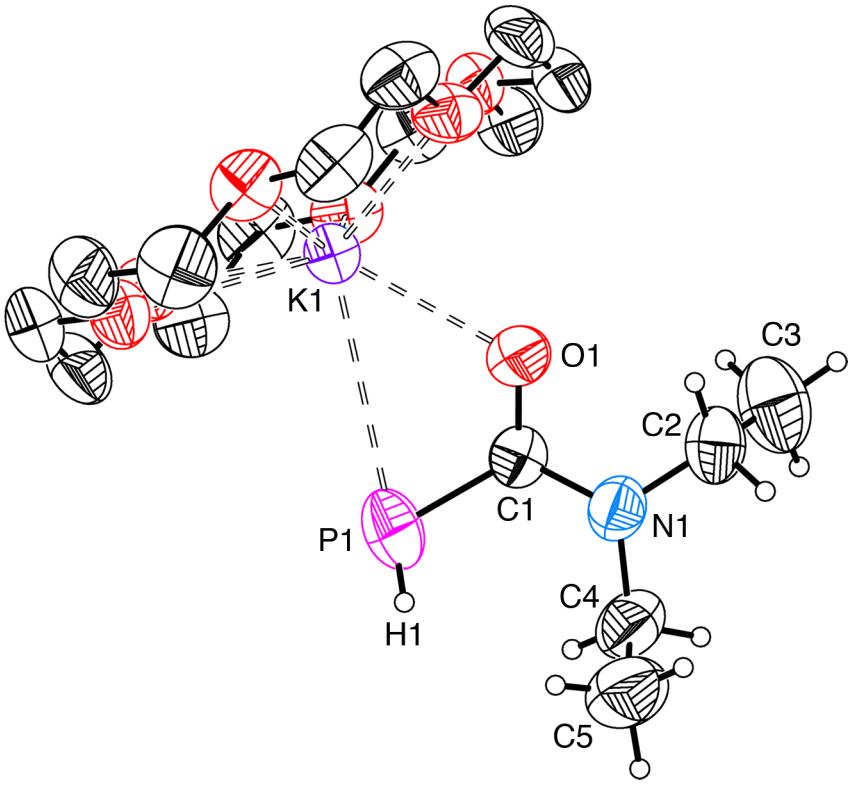

Figure 6.2: Molecular structure of [K(18-crown-6)][**27**]. Anisotropic displacement ellipsoids are set at 50% probability. Hydrogen atoms on the anion are shown as spheres of arbitrary radii; those on the 18-crown-6 ring are omitted for clarity.

The $[K(18\text{-crown-6})]^+$ cation is interacting with both the P1 and O1 atoms. This is evidence for the delocalisation of the negative charge from the phosphorus centre into the carbonyl group. The bond metric data are shown in Table 6.1.

Table 6.1: Selected crystallographic bond lengths (Å) and angles (˚) of [K(18-crown-6)][**27**].

Bond distance (Å)	**27**	**Bond angle (˚)**	**27**
P1–C1	1.790(2)	P1–C1–O1	120.4(2)
C1–O1	1.246(3)	P1–C1–N1	122.5(2)
C1–N1	1.374(3)	N1–C1–O1	117.1(2)
N1–C2	1.474(3)	C1–N1–C2	119.4(2)
N1–C4	1.457(4)	C1–N1–C4	123.1(2)
K1–O1	2.651(2)	C2–N1–C4	117.5(2)
K1–P1	3.538(2)	K1–O1–C1	119.0(2)
		K1–P1–C1	71.9(1)

No crystal structure of **22** was obtained, due to its volatility in solution, but a valid comparison of **27** can be carried out with the neutral parent phosphinecarboxamide, **11**. The P1–C1 bond length (1.790(2) Å) in **27** is significantly shorter than the analogous bond length in **11** (1.860(2) Å), while both the C1–O1 and C1–N1 bonds are elongated in the former (1.246(3) Å and 1.374(3) Å in **27**, 1.230(2) Å and 1.329(2) Å in **11**, respectively). This is consistent with the increase of multiple bond character of the P1–C1 bond on deprotonation, and the concomitant reduction of multiple bond character of C1–O1 and C1–N1. This is due to the donation of the electron density on phosphorus into the C–O π* antibonding orbital, which outcompetes the donation from the nitrogen lone pair in the neutral species.

The phosphide is stable with respect to electrospray ionisation (ESI) mass spectrometry, and **27** can be observed in the negative ion mode at *m/z* = 132.0. The cation-paired species, $\{[K(18\text{-crown-6})]_2[\mathbf{27}]\}^+$, is also observable in the positive ion mode at *m/z* = 737.6.

6.2.2 [K(18-crown-6)][28] (28: [HPC(O)NHCy]⁻)

The synthesis and isolation of [K(18-crown-6)][**27**] has shown that stable phosphides based on the phosphinecarboxamide architecture are viable. We wanted to extend this study to utilise the cyclohexyl-substituted phosphinecarboxamide, **17**, as we can produce this cleanly in multi-gram quantities in good yields. It would also be interesting on a fundamental level to determine whether deprotonation occurs at the phosphorus or nitrogen centre, and cogent arguments can be made for either site. The addition of one equivalent of KHMDS to a solution of **17** in fact led to clean deprotonation at the phosphorus centre, with no evidence of proton loss at the carboxamide moiety (Scheme 6.4).

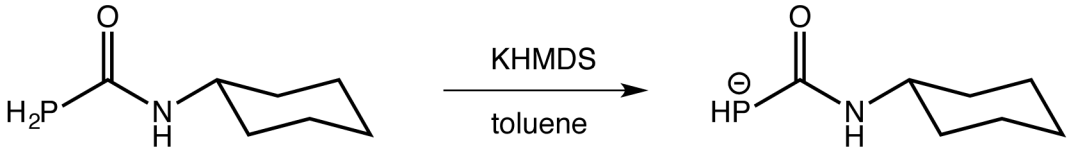

Scheme 6.4: Deprotonation of **17** with one equivalent of KHMDS to afford **28**.

This was evidenced by the formation of a doublet in the ^{31}P NMR spectrum at –97.3 ppm ($^{1}J_{P-H}$ = 148 Hz), which collapses to a singlet on proton decoupling, by analogy with the spectroscopic data for **27**. Crystals of [K(18-crown-6)][**28**] suitable for single crystal X-ray diffraction were grown by slow diffusion of hexane into a THF solution of the product (Figure 6.3).

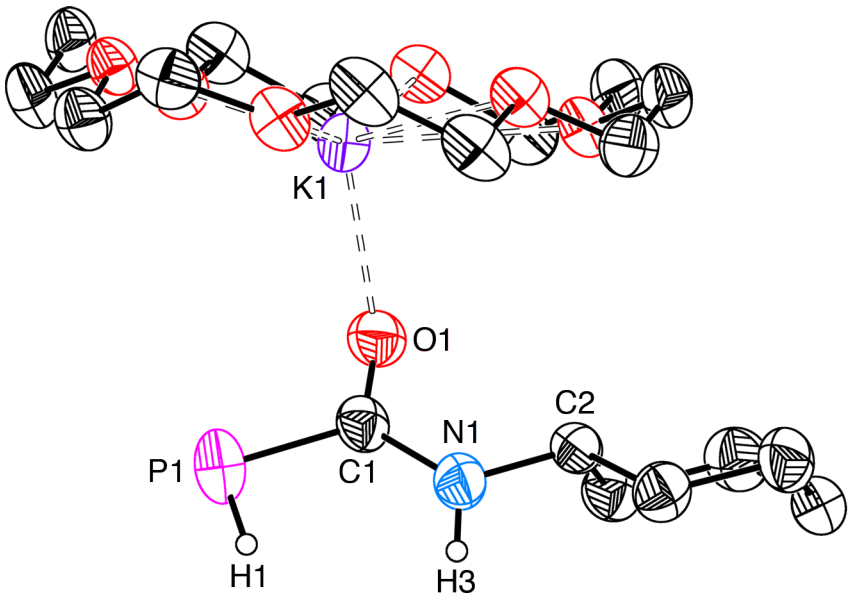

Figure 6.3: Molecular structure of [K(18-crown-6)][**28**]. Anisotropic displacement ellipsoids are set at 50% probability. Heteroatom-bound hydrogen atoms are shown as spheres of arbitrary radii, other hydrogen atoms omitted for clarity.

The molecular structure corroborates the inferences from NMR spectroscopy, and shows that the amide proton is still present, and that there is only one proton on the phosphorus centre. Density functional theory (DFT) calculations were carried out to probe this reaction. The geometry-optimised structures of **28**, with the H1 proton in a *cis* or *trans* position relative to O1, and the product derived from deprotonation of the amide proton (**amide-28**),

were calculated.[13] The bond metric data for all of these structures are shown in Table 6.2, in addition to the total bonding energies for the three computed species.

Table 6.2: Bond distances (Å) and angles (˚) for the crystallographic and computed structures of **28** (*cis* and *trans* with respect to the P–C bond), and the computed structure of **amide-28**. The total bonding energies (kJ mol^{-1}) of the computed structures are also shown.

Bond distance (Å)	**28**	***trans*-28$_{calc}$**	***cis*-28$_{calc}$**	**amide-28$_{calc}$**
P1–C1	1.791(2)	1.823	1.831	1.908
P1–H1	1.00(3)	1.43	1.42	1.42
P1–H2	N.A.	N.A.	N.A.	1.42
C1–O1	1.260(3)	1.255	1.252	1.267
C1–N1	1.371(3)	1.374	1.378	1.306
N1–C2	1.454(3)	1.458	1.457	1.462
N1–H3	0.83(3)	1.01	1.01	N.A.
K1–O1	2.572(2)	N.A.	N.A.	N.A.
Bond angle (˚)				
P1–C1–O1	120.8(2)	120.9	126.3	119.5
P1–C1–N1	121.0(2)	119.8	114.4	110.1
N1–C1–O1	118.2(2)	119.3	119.2	130.4
K1–O1–C1	112.2(2)	N.A.	N.A.	N.A.
Total bonding energy (kJ mol^{-1})		–14680.85	–14678.86	–14651.84

The data for the core phosphinecarboxamide moiety are very similar to those discussed previously in **27**. The P1–C1 bond length (1.791(2) Å) is significantly shorter than in the $H_2P(CO)NHCy$ moiety of the ruthenium complex **20** (1.878(3) Å), consistent with the increase in multiple bond character on deprotonation. An additional manifestation of the delocalised structure is the largely planar nature of the HPC(O)NH core of the molecule (deviation from planarity: 0.0876 Å). Unlike the structure of [K(18-crown-6)][**27**], in this case the K1 cation only interacts with the O1 atom, and not P1. This is likely an effect of crystal packing. The fact that the cation is only interacting with one of the atoms bearing

partial negative charge in [K(18-crown-6)][**28**] is compensated with a shorter K1–O1 interaction (2.572(2) Å, compared to 2.651(2) Å in [K(18-crown-6)][**27**]).

Although it might appear counterintuitive that deprotonation occurs at the less polarised of the E–H bonds (E = N, P), the total bonding energies of the computed structures reveal that the resulting phosphide is 29.0 kJ mol^{-1} more stable than **amide-28**. The computed geometry of ***trans*-28** is only 2.0 kJ mol^{-1} lower in energy than ***cis*-28**, which is too small to make any conclusions about the stability of one over the other (although it is worth noting that the crystal structure obtained does show the molecule in a *trans* conformation). Inspection of the Kohn-Sham frontier orbitals revealed that the HOMO is predominantly P–C π bonding in character, and antibonding with respect to the carbonyl group (Figure 6.4). An analysis of Hirshfeld charges indicated a relatively even distribution of negative charge over P1 and O1 (–0.502 and –0.444, respectively).

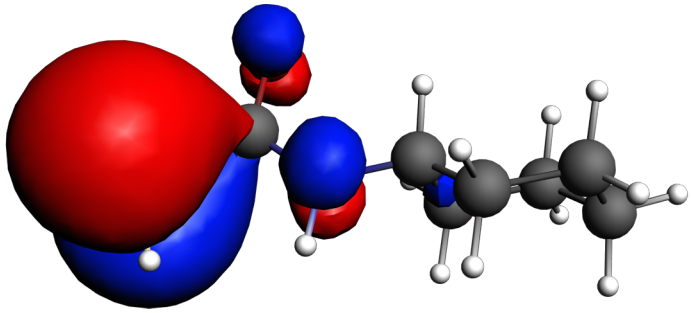

Figure 6.4: Kohn-Sham molecular orbital representation (contour values 0.03 au) of the HOMO of **28**, with selected atomic orbital contributions: 75.7% P1 $3p_z$, 5.3% N1 $2p_z$, 4.3% O1 $2p_z$. The *z* axis is orthogonal to the HPC(O)NH plane.

The ^{1}H NMR spectrum of [K(18-crown-6)][**28**] shows a doublet corresponding to the phosphide proton centred at 2.86 ppm ($^{1}J_{H–P}$ = 148 Hz) and a broad resonance at 5.94 ppm for the amide proton, in addition to the cyclohexyl resonances. The $^{13}C\{^{1}H\}$ NMR spectrum reveals a doublet for the central carbon atom at 202.9 ppm with a coupling constant of $^{1}J_{C–P}$ = 59 Hz. This is significantly larger than the analogous coupling constant in **17** ($^{1}J_{C–P}$ = 6 Hz), and is consistent with the increase in s orbital character of the P–C bond due to

rehybridisation of the phosphorus centre from sp^3 to sp^2 on deprotonation. The remaining resonances are due to the cyclohexyl group and the 18-crown-6 sequestering agent.

The compositional purity of the isolated [K(18-crown-6)][**28**] was confirmed by elemental microanalysis. The salt was also subjected to ESI mass spectrometry, and although the anion was not observed in the negative ion mode, the mass envelope corresponding to the cation-paired species $\{[K(18\text{-crown-6})]_2[\mathbf{28}]\}^+$ was observed at *m/z* = 765.0. An IR spectroscopic investigation of a Nujol mull of [K(18-crown-6)][**28**] revealed the carbonyl stretching band at 1538 cm^{-1}. This is notably lower in energy than that recorded for **17** (1607 cm^{-1}), and is further evidence of the weakening of the C–O bond on deprotonation.

6.2.3 [K(18-crown-6)][29] (29: $[P\{C(O)NHCy\}_2]^-$)

Interestingly, deprotonation of **17** with half an equivalent of KHMDS gave rise to a different phosphide anion, **29** (Scheme 6.5). This product arises from the deprotonation of half of the molecules of **17** to afford **28**, as above, which then acts as a nucleophile and attacks the remaining molecules of **17**. The resulting intermediate was not detected by any experimental methods, and quickly rearranges to afford **29** and phosphine gas, PH_3.

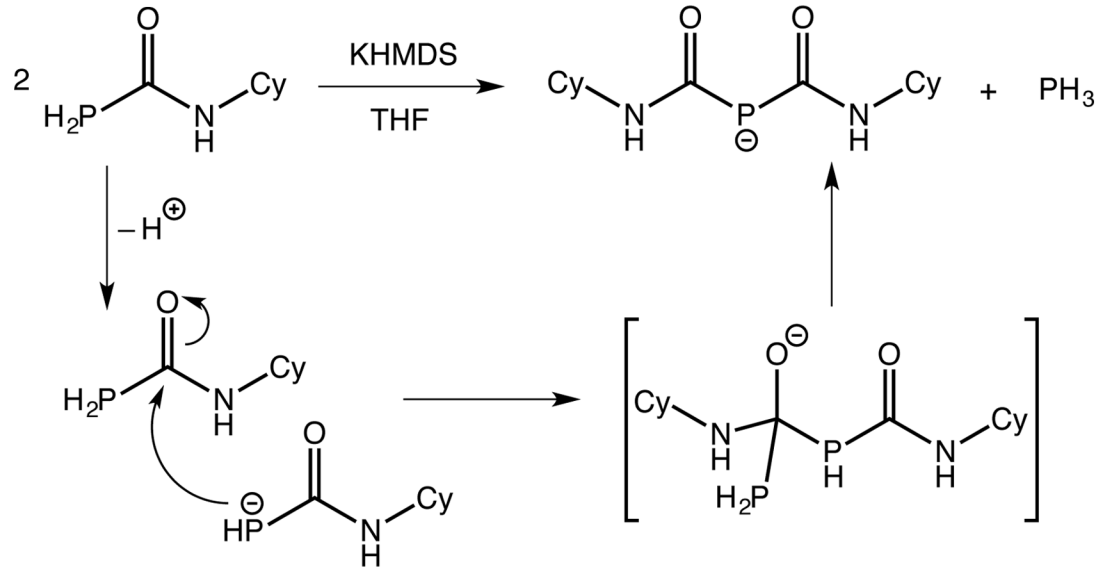

Scheme 6.5: Deprotonation of **17** with half an equivalent of KHMDS to afford **29**, and the postulated mechanism involving an undetected intermediate.

29 is a novel phosphorus-containing anionic analogue of biuret ($HN\{CONH_2\}_2$), which is obtained through the condensation of urea.[16] **29** also bears a structural resemblance to the anionic intermediate discussed at the start of this chapter ($[P\{C(O)Mes\}_2]^-$, shown in Scheme 6.2),[9] and the closely related methyl analogue, $[P\{C(O)Me\}_2]^-$, published by Becker and co-workers in 1996.[17] It is worth noting that both of these species were generated using different synthetic protocols, and that to the best of our knowledge, the mode of reactivity exhibited in the synthesis of **29** is an unprecedented method for the generation of stabilised phosphides.

Crystals of [K(18-crown-6)][**29**] suitable for single crystal X-ray diffraction were grown by slow diffusion of hexane into a THF solution of the product (Figure 6.5).

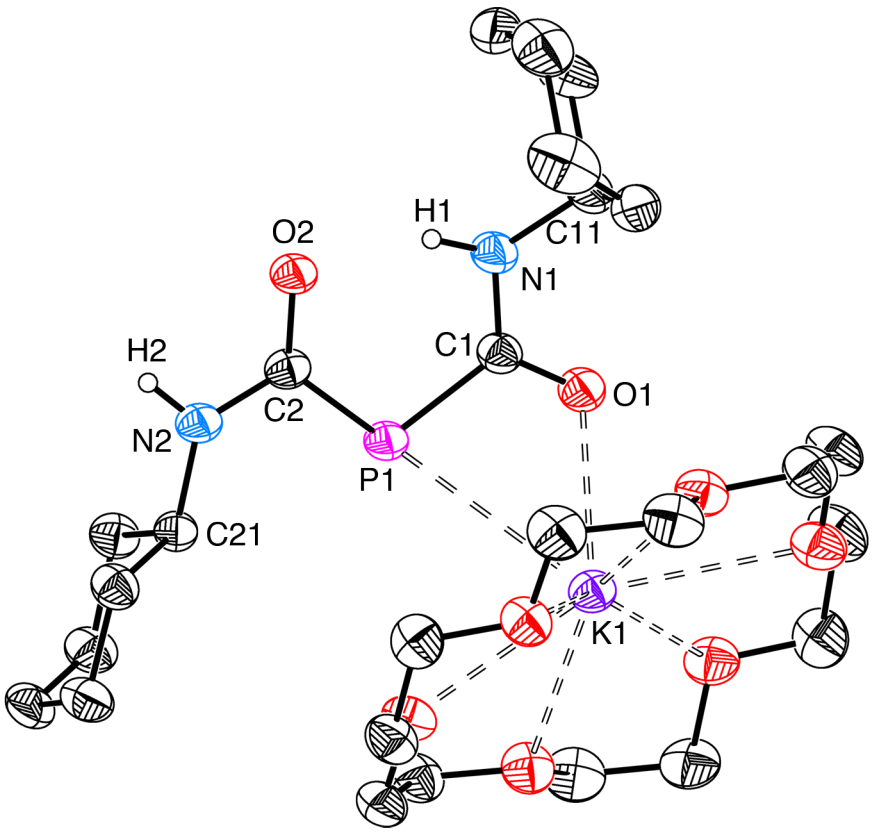

Figure 6.5: Molecular structure of [K(18-crown-6)][**29**]. Anisotropic displacement ellipsoids are set at 50% probability. Heteroatom-bound hydrogen atoms are shown as spheres of arbitrary radii, other hydrogen atoms omitted for clarity.

The structure of the anion revealed an intramolecular hydrogen bonding interaction between one of the amide protons and a carbonyl oxygen atom (H1 and O2, respectively) with a distance of 1.88(4) Å. A computational study on the possible conformations of **29** revealed that this structure is the most stable by 21.5 kJ mol^{-1}.[13] The bond metric data for the crystal structure and the geometry-optimised structure as determined by DFT calculations are shown in Table 6.3.

Table 6.3: Bond distances (Å) and angles (˚) for the crystallographic and computed structures of **29**.

Bond distance (Å)	**29**	**29_{calc}**
P1–C1	1.825(2)	1.848
P1–C2	1.827(2)	1.841
C1–O1	1.250(3)	1.255
C2–O2	1.266(3)	1.261
C1–N1	1.357(3)	1.348
C2–N2	1.359(3)	1.367
N1–C11	1.457(3)	1.461
N2–C21	1.459(3)	1.458
K1–O1	2.726(2)	N.A.
K1–P1	3.262(1)	N.A.
Bond angle (˚)		
P1–C1–O1	116.8(2)	116.4
P1–C2–O2	126.2(2)	126.1
P1–C1–N1	121.3(2)	121.7
P1–C2–N2	116.0(2)	117.2
N1–C1–O1	121.8(2)	121.9
N2–C2–O2	117.8(2)	116.7
K1–O1–C1	104.7(2)	N.A.
K1–P1–C1	74.2(1)	N.A.

As would be expected, there is less delocalisation of the negative charge into each of the two carboxamide moieties than in **28**. Thus, the P1–C1 and P1–C2 bond lengths (1.825(2) and 1.827(2) Å, respectively) are in between the values for the analogous P1–C1 bond

lengths in the neutral phosphinecarboxamide **17** (as measured in the ruthenium complex, **20**, 1.878(3) Å) and the mono(carbamoyl)-substituted phosphide **28** (1.791(2) Å). Accordingly, the C–O and C–N interatomic distances are also shorter in **29** than in **28**, but longer than those in **17**. Despite the asymmetric conformation of **29**, the bond lengths are statistically similar between the two halves of the anion. However, the bond angles in the two carboxamide moieties do differ appreciably (for example Δ(P–C–O) = 9.4˚), as expected based on the slight strain induced in forming the six-membered ring necessary for the intramolecular hydrogen bonding interaction.

The ^{31}P NMR spectrum of [K(18-crown-6)][**29**] reveals a broad singlet at –29.2 ppm. Interestingly, the asymmetric conformation observed in the solid state is not borne out in solution. The NMR spectroscopic data clearly indicate free rotation about the P–C bonds, as the two carboxamide moieties are chemically equivalent. This can be seen in the ^{1}H NMR spectrum (Figure 6.6), where there is only one resonance for the two methine protons at 4.41 ppm. The dynamic hydrogen bonding of the amide protons broaden this resonance to such an extent that it is initially difficult to observe, although close inspection after zooming in on the baseline reveals the signal to be overlapping with the most downfield solvent resonance at 8.74 ppm.

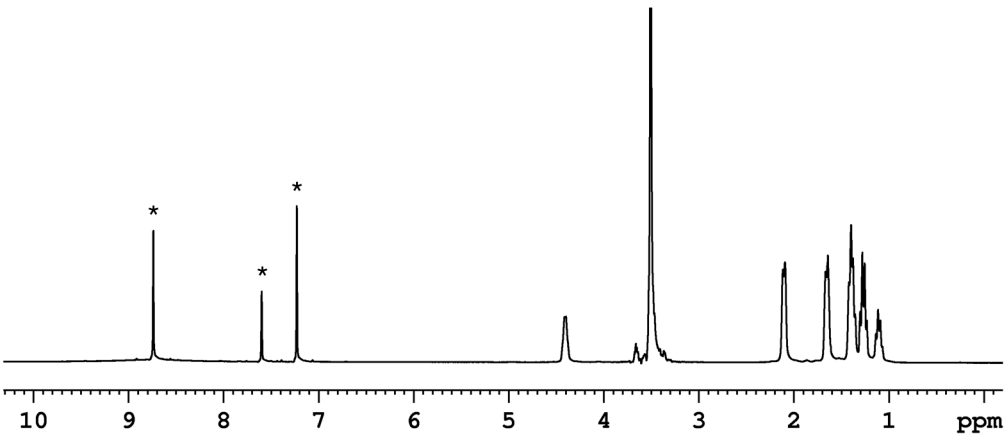

Figure 6.6: ^{1}H NMR spectrum of d_5-pyridine solution of [K(18-crown-6)][**29**]. Resonances marked with ***** are due to residual protic solvent.

The $^{13}C\{^{1}H\}$ NMR spectrum confirms the chemical equivalence of the cyclohexyl groups, and shows a doublet for the C1/C2 carbonyl atoms ($^{1}J_{C-P}$ = 55 Hz), with a similar magnitude coupling constant to that in **28** ($^{1}J_{C-P}$ = 59 Hz).

An assessment of the Kohn-Sham orbitals reveals the HOMO to be delocalised over the phosphorus atom and the two carboxamide moieties (Figure 6.7), by analogy with the HOMO of **28**. The Hirshfeld charges also show the distribution of the negative charge over P1 (–0.304) and the two carbonyl oxygen atoms (O1: –0.441; O2: –0.364), as expected.

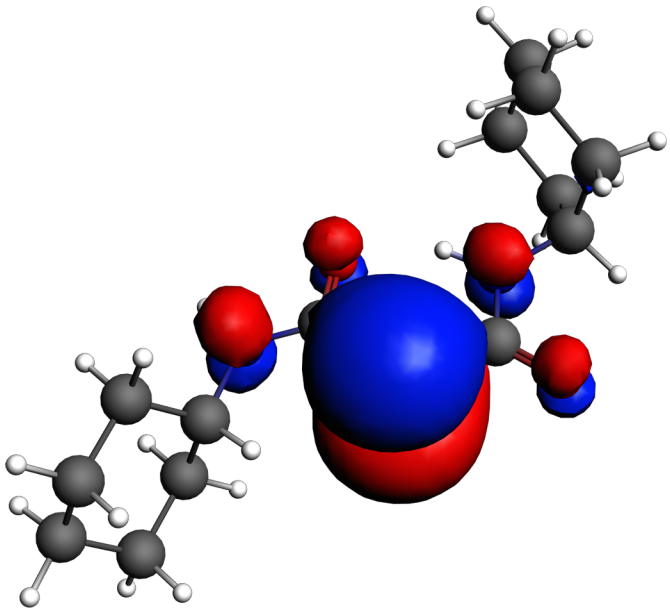

Figure 6.7: Kohn-Sham molecular orbital representation (contour values 0.03 au) of the HOMO of **29**, with selected atomic orbital contributions: 70.2% P1 $3p_z$, 5.6% N2 $2p_z$, 4.4% N1 $2p_z$, 3.3% O1 $2p_z$, 3.2% O2 $2p_z$. The *z* axis is orthogonal to the P{C(O)NH}$_2$ plane.

An ESI mass spectroscopic investigation of [K(18-crown-6)][**29**] shows the anion at *m/z* = 283.1, and the cation-paired species {[K(18-crown-6)]$_2$[**29**]} at *m/z* = 890.3. The IR spectrum of a Nujol mull of [K(18-crown-6)][**29**] showed the bands arising from the carbonyl stretching modes at 1560 cm^{-1} and 1537 cm^{-1}, which is in between the values recorded for **17** and [K(18-crown-6)][**28**]. Note that the two carboxamide moieties, and hence the carbonyl groups, will be inequivalent in the IR spectrum due to intramolecular hydrogen bonding and the significantly shorter timescale of the IR experiment relative to

NMR spectroscopy. The compositional purity of a solid sample of isolated [K(18-crown-6)][**29**] was confirmed by elemental microanalysis.

6.2.4 [K(18-crown-6)][30] (30: [P{C(O)NHMe}$_2$]$^-$)

The final example of deprotonation to be discussed is that of **23**, the phosphinecarboxamide derived from the heteroatom-substituted secondary amine, HNMe(OMe). A pale yellow pyridine solution of **23** was generated by the reaction of [Na(1,4-dioxane)][**1**] and [H_2NMe(OMe)][Cl]. To this one equivalent of KHMDS and 18-crown-6 was added, which resulted in the formation of an orange solution. A small aliquot was taken and used for ^{31}P NMR spectroscopic analysis. The spectrum was weak (poor signal-to-noise), but three distinct resonances could be identified. There was a doublet at –100.8 ppm ($^1J_{P–H}$ = 145 Hz, collapsed to a singlet on proton decoupling), a broad singlet at –26.7 ppm and a sharper singlet at 18.8 ppm. The product corresponding to the latter resonance remains unidentified, but the first two are reminiscent of the spectroscopic data obtained for the mono- and bis(carbamoyl) phosphides discussed thus far in the chapter, respectively.

The volatiles were removed under reduced pressure, and the products were extracted into THF, to separate them from the NaCl by-product from the initial synthesis of **23**. Slow diffusion of hexane into this THF solution afforded crystals suitable for single crystal X-ray diffraction (Figure 6.8), and correspond to the product in the reaction shown in Scheme 6.6.

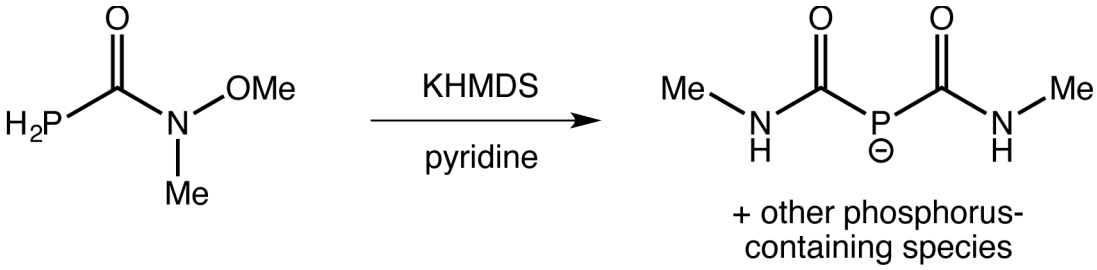

Scheme 6.6: Deprotonation of **23** with KHMDS to afford **30** and other phosphorus-containing products.

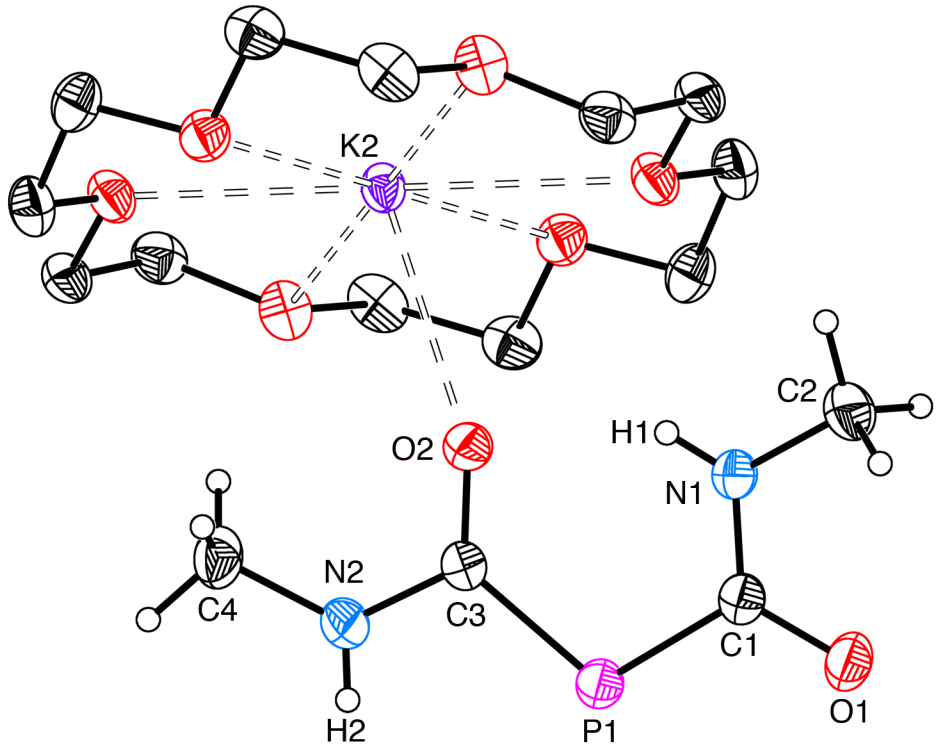

Figure 6.8: Molecular structure of [K(18-crown-6)][**30**]. Anisotropic displacement ellipsoids are set at 50% probability. Hydrogen atoms on the anion are shown as spheres of arbitrary radii; those on the 18-crown-6 ring are omitted for clarity.

The crystal structure reveals a bis(carbamoyl) phosphide, but surprisingly the methoxy groups appear to have been replaced by protons, to give the product [K(18-crown-6)][**30**] (**30**: $[P\{C(O)NHMe\}_2]^-$). This was rationalised with reference to a report on the reactivity of *N*-methoxy-*N*-methyl amides with strongly basic reagents by Graham and Scholz.[18] The base deprotonates one of the methoxy protons, and the resulting anion rapidly rearranges to extrude formaldehyde and afford the (phosphinoylcarbonyl)amide intermediate (Scheme 6.7). This isomerises to afford the mono(carbamoyl) phosphide derivative, which is consistent with the previous studies showing the enhanced acidity of the phosphine protons relative to the amide protons in these systems. This species presumably gives rise to the doublet in the ^{31}P NMR spectrum at –100.8 ppm. This mono(carbamoyl) phosphide acts as a nucleophile and attacks an equivalent of the $H_2PC(O)NHMe$ phosphinecarboxamide (which is presumably present as a transient species in solution due to the mono(carbamoyl) phosphide accepting a proton), via an analogous mechanism to the formation of **29**.

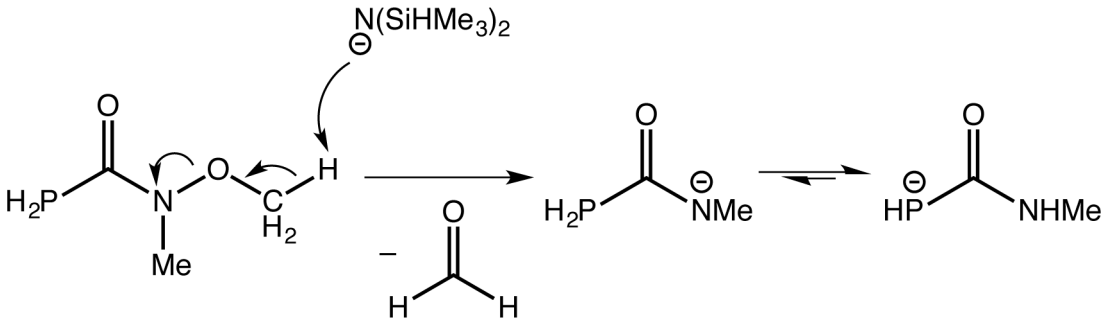

Scheme 6.7: Deprotonation of the methoxy proton of **23** with loss of formaldehyde to afford the mono(carbamoyl) phosphide, $[HPC(O)NHMe]^-$.

The solid-state structure of [K(18-crown-6)][**30**] shows the anion coordinated to two distinct potassium environments, K1 and K2 (interacting with O1 and O2, respectively), both of which are situated on inversion centres. This leads to chains of coordination polymers propagating through the structure. The asymmetric unit shows each potassium ion with only half of an 18-crown-6 moiety around it, as the complete ring for each is symmetry-generated by the inversion centres. One of the 18-crown-6 rings (the one not shown in Figure 6.8, sequestering K1) displays rotational disorder. The bond metric data are shown in Table 6.4.

Table 6.4: Selected crystallographic bond lengths (Å) and angles (˚) of [K(18-crown-6)][**30**].

Bond distance (Å)	**30**	**Bond angle (˚)**	**30**
P1–C1	1.810(2)	P1–C1–O1	117.3(2)
P1–C3	1.824(2)	P1–C3–O2	128.9(2)
C1–O1	1.251(2)	P1–C1–N1	122.4(2)
C3–O2	1.249(2)	P1–C3–N2	111.3(2)
C1–N1	1.350(2)	N1–C1–O1	120.3(2)
C3–N2	1.368(2)	N2–C3–O2	119.8(2)
N1–C2	1.447(2)	C1–P1–C3	104.7(1)
N2–C4	1.442(3)	K1–O1–C1	158.1(2)
K1–O1	2.624(2)	K2–O2–C3	144.4(2)
K2–O2	2.832(2)		

The structure shows the same conformation as **29**, with an intramolecular hydrogen bonding interaction. In this case, however, there are statistically significant differences between the two carboxamide moieties due to this asymmetry, but they are still broadly similar (for example, P1–C1: 1.810(2) Å; P1–C3: 1.824(2) Å). The bond metric data are comparable to those reported for **29**, and shall not be discussed further.

This section has described the synthesis of a number of mono- and bis(carbamoyl) phosphides that are stabilised by delocalisation of the negative charge into the carboxamide moieties. Further work by another member of the Goicoechea group has shown that deprotonation of *N*-propargyl phosphinecarboxamides also occurs at the phosphorus centre, and subsequent intramolecular cyclisation reactions lead to the formation of novel five- and six-membered phosphorus-containing heterocycles.[19] The remainder of this chapter will focus almost exclusively on the two cyclohexyl derivatives, **28** and **29**, as these can be synthesised cleanly on a reasonable scale and allow a comparison between the two systems.

6.3 *P*-Functionalisation chemistry

The phosphides described above are useful precursors for the generation of *P*-functionalised phosphinecarboxamides. We sought to test this by reacting **28** and **29** with simple electrophiles to yield a series of novel secondary and tertiary phosphines bearing carbamoyl moieties.

6.3.1 *P*-Functionalisation of 28

6.3.1.1 Synthesis of RHPC(O)NHCy (R = Me (31), Bn (32))

The protonation of **28** trivially returns the neutral phosphinecarboxamide, **17**. The reactions of **28** with the simple electrophiles iodomethane and benzyl bromide afford the novel *P*-functionalised phosphinecarboxamides, **31** and **32**, respectively (Scheme 6.8).

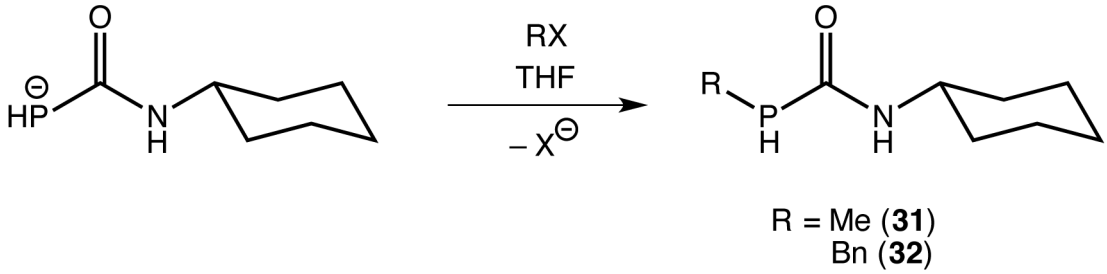

Scheme 6.8: Functionalisation of **28** with iodomethane and benzyl bromide to afford **31** and **32**.

This was initially carried out by adding the electrophile to a solution of [K(18-crown-6)][**28**], and these reactions proceeded in a quantitative manner by NMR spectroscopy. However, it proved challenging to isolate the products cleanly from the [K(18-crown-6)][X] by-products, due to the increased solubility of the latter in relatively non-polar solvents on account of the 18-crown-6 sequestering agent.

A synthetic protocol was therefore employed, which avoided the use of 18-crown-6, to allow the isolation of clean samples of **31** and **32**. Due to the apparent instability of [K][**28**] as a solid, this was achieved by carrying out the step-wise reaction in solution. One equivalent of KHMDS was added to a THF solution of **17** and stirred for three hours, affording [K][**28**] in solution (as confirmed by ^{31}P NMR spectroscopy). To this the appropriate electrophile was added, and led to the rapid precipitation of the [K][X] by-product. The solution was subsequently filtered and the volatiles (including $HN(SiMe_3)_2$) removed under reduced pressure to yield the desired product as a white solid. This simple one-pot method allows the isolation of a range of novel secondary phosphines bearing carbamoyl functionalities.

6.3.1.2 Characterisation of 31 and 32

Crystals of **31** and **32** were obtained, and subjected to a single crystal X-ray diffraction study (Figure 6.9). Unfortunately the residual electron density in the solution of **32** is

unacceptably high (R1(all data) = 12.00%), which is due to a combination of twinning in the crystal and diffuse scattering during the experiment.

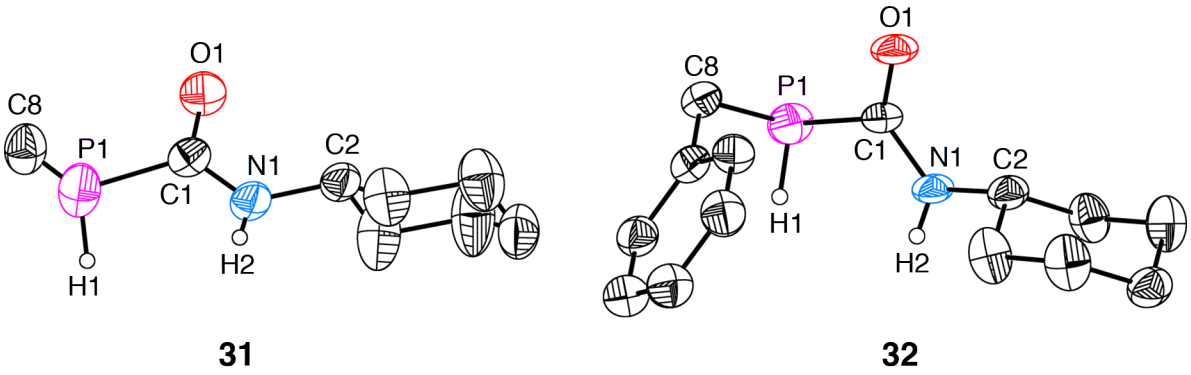

Figure 6.9: Molecular structures of **31** and **32**. Anisotropic displacement ellipsoids are set at 50% probability. Heteroatom-bound hydrogen atoms are shown as spheres of arbitrary radii, other hydrogen atoms omitted for clarity.

Therefore the X-ray structure of **32** is sufficient to confirm connectivity in the molecule, but caution should be employed when analysing the bond metric data. This is evident in the large standard deviations in the data for **32** shown in Table 6.5. The crystal structure of **31** is notably better, and the metric data for this compound are also shown in Table 6.5.

Table 6.5: Bond distances (Å) and angles (°) of **31** and **32**.

Bond distance (Å)	**31**	**32**
P1–C1	1.863(3)	1.851(6)
C1–O1	1.239(3)	1.224(7)
C1–N1	1.323(3)	1.345(7)
P1–C8	1.824(3)	1.854(7)
N1–C2	1.462(4)	1.463(7)
Bond angle (°)		
P1–C1–O1	121.0(2)	118.7(4)
P1–C1–N1	116.3(2)	117.1(4)
N1–C1–O1	122.5(3)	124.1(5)
sum around P1	285	N.A.[a]
sum around N1	359	N.A.[a]

[a] H1 and H2 positions were constrained in the solution of **32**, so an analysis of bond angles around P1 and N1 is meaningless in this molecule.

The bond lengths in **31** are very similar to those of the primary phosphines discussed previously, such as the parent phosphinecarboxamide, **11**, and the *N*-cyclohexyl derivative **17** (as characterised in **20**). The P1–C1 bond length in **31** is 1.863(3) Å, which is longer than that in the phosphide precursor **28** (1.791(2) Å), and similar to **17** (1.878(3) Å). This reveals that there is minimal donation of the phosphorus lone pair into the C–O π* antibonding orbital in the neutral phosphinecarboxamides, and functionalising the phosphorus centre with an alkyl group does not appear to affect this. Accordingly, the C1–O1 and C1–N1 bond lengths are shorter than in **28**.

The P1–C8 bond length (1.824(3) Å) is shorter than the P1–C1 bond length (1.863(3) Å), despite the fact that both are single bonds. This has been attributed to the stabilisation gained from negative hyperconjugation, which arises from donation of electron density from the lone pairs on O1 into the P1–C1 σ* antibonding orbital, lengthening this bond. This interaction is not possible in the P1–C8 bond. The same interaction can occur into the C1–N1 σ* orbital, but the expected bond lengthening is outweighed by the donation of the nitrogen lone pair into the C1–O1 π* orbital that shortens the C1–N1 bond.

NMR spectroscopy of a d_5-pyridine solution of **31** is consistent with methylation at phosphorus. The ^{31}P NMR spectrum reveals a doublet of quartets centred at –81.5 ppm ($^1J_{P–H}$ = 207 Hz, $^2J_{P–H}$ = 3 Hz), which collapses to a singlet on proton decoupling. The methyl group was also observed in the ^{1}H NMR spectrum as a doublet of doublets ($^2J_{H–P}$ = 3 Hz, $^3J_{H–H}$ = 8 Hz) at 1.37 ppm, in addition to the phosphine proton at 4.06 ppm, the amide proton at 8.85 ppm, and the cyclohexyl resonances. The ^{13}C{^{1}H} NMR spectrum revealed a doublet from the methyl carbon at 1.8 ppm, which has a slightly smaller coupling constant to the phosphorus ($^1J_{C–P}$ = 8 Hz) than the central carbonyl carbon ($^1J_{C–P}$ = 11 Hz). This is because the carbon is sp^3 hybridised in the former and sp^2 in the latter, and thus the P1–C1 bond has greater s character.

The NMR spectra of **32** are slightly more complex, but are also entirely consistent with functionalisation at phosphorus. The two methylene protons from the benzyl group are diastereotopic, and thus appear as second order multiplets at different chemical shifts (3.50 ppm and 3.30 ppm) in the ^{1}H NMR spectrum (Figure 6.10, including inset). The magnetically inequivalent methylene protons also result in the phosphine proton resonance being a second order multiplet ($^{1}J_{H–P}$ = 206 Hz, $^{3}J_{H–H}$ = 8 Hz, $^{3}J_{H–H}$ = 5 Hz).

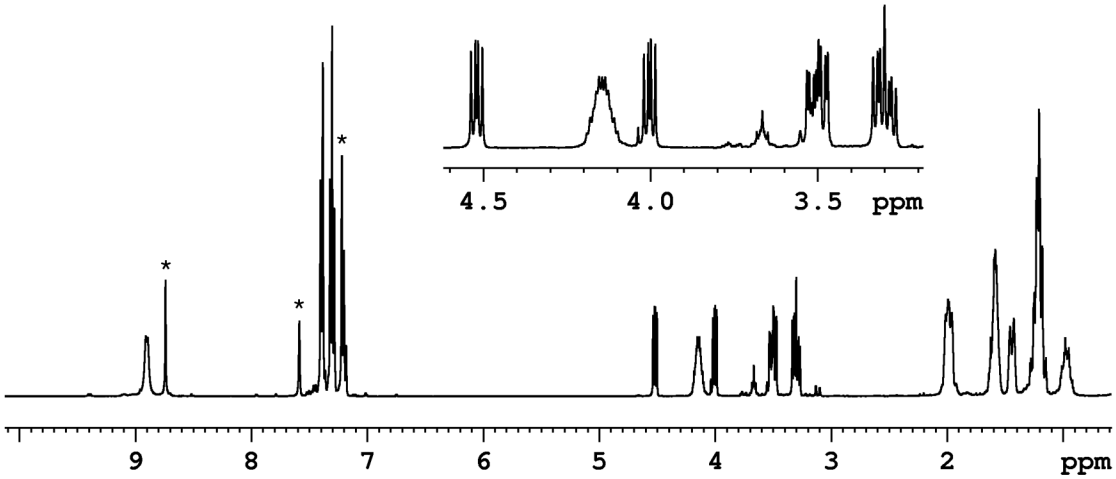

Figure 6.10: ^{1}H NMR spectrum of d_5-pyridine solution of **32**. Inset shows the zoomed region displaying the second order multiplets from the phosphine, methine and methylene protons. Resonances marked with * are due to residual protic solvent.

The ^{31}P NMR spectrum of **32** shows a doublet of doublets at –48.7 ppm ($^{1}J_{P–H}$ = 206 Hz, $^{2}J_{P–H}$ = 8 Hz). The coupling to the second methylene proton is not resolved. The ^{13}C{^{1}H} NMR spectrum reveals the methylene carbon to be coupled to the phosphorus centre ($^{1}J_{C–P}$ = 11 Hz), with a smaller coupling constant than the carbonyl carbon ($^{1}J_{C–P}$ = 13 Hz), by analogy with **31**. There is some surprisingly long-range coupling of some of the carbons in the phenyl ring to the phosphorus centre, and the *para*-carbon even exhibits an observable five-bond coupling ($^{5}J_{C–P}$ = 2 Hz).

31 and **32** were further characterised by field ionisation (FI) mass spectrometry, and mass envelopes were observed at *m/z* = 173.0971 and 249.1280, which are good matches with the predicted monoisotopic masses of 173.0970 and 249.1283 Da, respectively. IR spectra of

the two compounds as Nujol mulls revealed carbonyl stretching bands at 1605 cm^{-1} (**31**) and 1599 cm^{-1} (**32**), which are comparable to that observed in **17** (1607 cm^{-1}), as expected.

6.3.2 *P*-Functionalisation of 29

6.3.2.1 Synthesis of $RP\{C(O)NHCy\}_2$ (R = H (33), Me (34), Bn (35))

The functionalisation chemistry study was continued with the bis(carbamoyl) phosphide, **29**. As with **28**, the reactions could be carried out by adding the electrophile to a solution of the isolated [K(18-crown-6)][**29**], but the by-products were difficult to separate. Thus an analogous one-pot procedure to that described in the previous section was employed, but using only half an equivalent of KHMDS to generate [K][**29**] in solution before the addition of the electrophile. The PH_3 by-product was removed under reduced pressure along with $HN(SiMe_3)_2$ in the final step.

The use of this synthetic protocol with pyridinium trifluoromethanesulfonate (triflate), iodomethane and benzyl bromide permitted the generation of the *P*-protonated (**33**), *P*-methylated (**34**) and *P*-benzylated (**35**) bis(carbamoyl) phosphines, as shown in Scheme 6.9.

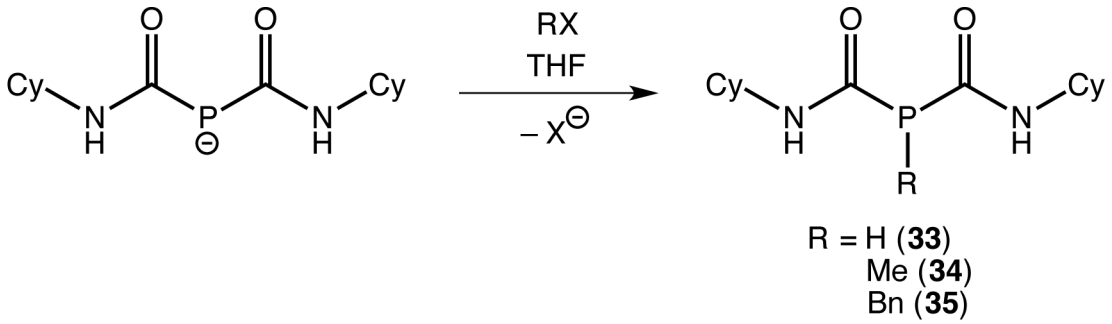

Scheme 6.9: Functionalisation of **29** with pyridinium triflate, iodomethane and benzyl bromide to afford **33**, **34** and **35**, respectively.

6.3.2.2 Characterisation of 33–35

Despite repeated attempts, no single crystals of **33**–**35** could be grown, so these species were primarily characterised by means of NMR spectroscopy. In all cases the data are consistent with functionalisation at the phosphorus centre, and there is no evidence of the

electrophile being attacked by either of the oxygen atoms. The two carboxamide moieties are equivalent by ^{1}H and $^{13}C\{^{1}H\}$ NMR spectroscopy for all three species, despite the potential for intramolecular hydrogen bonding.

33 is the first phosphorus-containing analogue of biuret, and a secondary phosphine bearing two carbamoyl moieties. The ^{31}P NMR spectrum shows a doublet at –74.9 ppm ($^{1}J_{P–H}$ = 235 Hz), shown in Figure 6.11, which appears as a singlet in the $^{31}P\{^{1}H\}$ NMR spectrum. The ^{1}H NMR spectrum reveals a doublet arising from the phosphine proton at 4.95 ppm, in addition to those arising from the chemically equivalent amide moieties. The carbonyl $^{13}C\{^{1}H\}$ NMR resonance was recorded at 172.9 ppm ($^{1}J_{C–P}$ = 12 Hz).

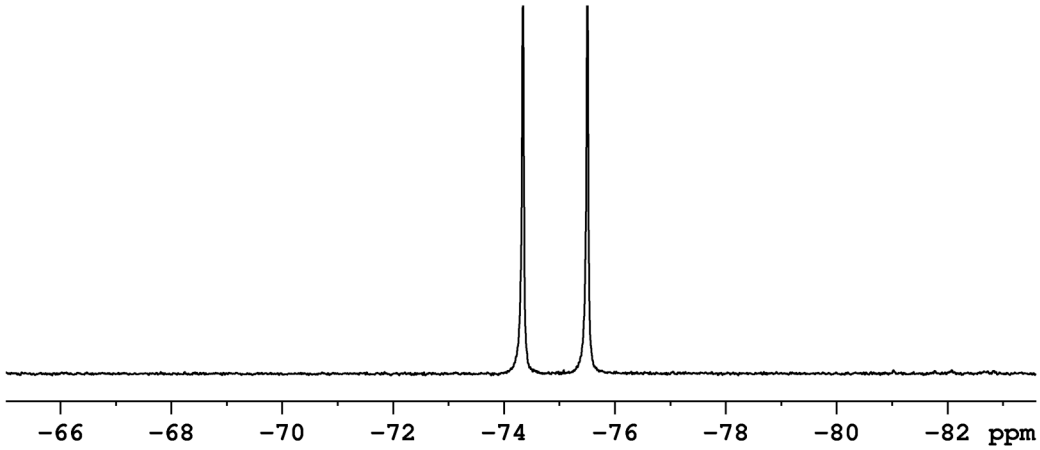

Figure 6.11: ^{31}P NMR spectrum of d_5-pyridine solution of **33**.

The ^{31}P NMR spectra of **34** and **35** reveal broadened resonances that sharpen on proton decoupling, but the expected $^{2}J_{P–H}$ coupling constants for the expected quartet and triplet resonances, respectively, are too small to resolve. The coupling constants can be identified in the respective ^{1}H NMR spectra, however, by the doublets attributable to the methyl group in **34** (at 1.81 ppm; $^{2}J_{H–P}$ = 2 Hz) and the methylene group in **35** (at 3.76 ppm; $^{2}J_{H–P}$ = 2 Hz). It is worth noting that the methylene protons are magnetically equivalent in **35**, unlike the diastereotopic protons in **32**, due to the two equivalent carbamoyl groups bound to the phosphorus centre in the former. *P*-Functionalisation in **34** and **35** is corroborated by the

$^{13}C\{^{1}H\}$ NMR resonances for the methyl and methylene carbons, at 7.2 ppm ($^{1}J_{C–P}$ = 12 Hz) and 31.1 ppm ($^{1}J_{C–P}$ = 17 Hz), respectively. Some of the carbon atoms in the phenyl ring of **35** show long-range coupling to the phosphorus centre, by analogy with **32**.

The three molecules were also characterised by FI mass spectrometry. The molecular ion peaks could be identified at *m/z* = 284.1637 (**33**), 298.1801 (**34**) and 374.2085 (**35**). The $[M+H]^{+}$ peaks were observable for all three species as well, which is not common for FI mass spectrometry, and potentially indicates the formation of hydrogen-bonded dimers during the ionisation process. Fragmentation of the molecules was also observed, leading to a peak with an *m/z* value in the range 125.0839–125.0877 in all three cases, and further fragments at *m/z* = 159.0789 (from **33**), 173.1010 (from **34**), and 249.1269 (from **35**). These have been attributed to a McLafferty-type rearrangement, where a keto-group undergoes β-cleavage with the gain of a γ-hydrogen atom.[20]

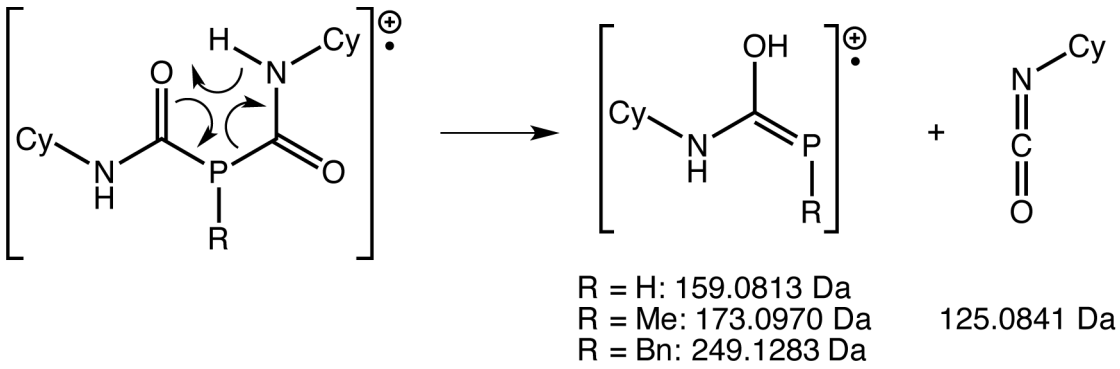

Scheme 6.10: Postulated McLafferty rearrangement of **33**, **34** and **35** to afford the radical cations shown. The calculated monoisotopic masses for the fragments are also given.

This gives rise to the radical cations with the monoisotopic masses shown in Scheme 6.10, which are a good match to the values listed above. Of course, the same rearrangement can afford the CyNCO moiety as the radical cation and the RP(OH)NHCy moiety as the neutral fragment, in which case a mass envelope near 125.0841 Da would be observed in the mass spectrum, and this is indeed the case for these species.

IR spectroscopy was also carried out on compounds **33**–**35** in Nujol mulls. One strong carbonyl stretching band was observed for each compound, at 1639 cm^{-1} (**33** and **35**) and 1633 cm^{-1} (**34**). A second weaker band was observable for **33** and **35**, at 1613 cm^{-1} and 1614 cm^{-1}, respectively. The second expected band for **34** in the same region was not observed in its IR spectrum. This may be indicative of a difference in the solid-state structure of **34** compared to **33** and **35**, although there is no intuitive reason why this might be the case, and crystal data would be required to corroborate this assertion. The three compounds are certainly similar in solution, as shown by the NMR spectroscopic data above.

6.3.3 *P*-Functionalisation of the parent phosphinecarboxamide

This thesis has so far detailed the synthesis of the parent phosphinecarboxamide (**11**), a range of phosphinecarboxamides that are functionalised only at nitrogen (**16**–**19**, **22**–**26**), and a range that are functionalised both at phosphorus and nitrogen (**31**–**35**). We endeavoured to complete the set and synthesise a phosphinecarboxamide that is functionalised only at phosphorus, and thus still has two amide protons present in the molecule.

As mentioned earlier in this chapter, the deprotonation of **11** results in the rapid formation of PH_3 and $[NCO]^-$, as evidenced by the presence of a quartet in the ^{31}P NMR spectrum at –240.1 ppm ($^1J_{P–H}$ = 288 Hz), and a broad singlet in the $^{13}C\{^1H\}$ NMR spectrum at 129.4 ppm, respectively (Scheme 6.11). This remains the case when the base is added at low temperature, and the solution is allowed to slowly warm up to room temperature over a number of hours.

The unstable phosphide was therefore trapped before it could decompose. This was achieved by adding the KHMDS to a solution of **11** and benzyl bromide at –78 ˚C. The base is non-nucleophilic, and therefore preferentially deprotonates **11** instead of attacking the

benzyl bromide. The phosphide subsequently acts as the nucleophile and attacks the benzyl bromide to afford **36** and an equivalent of KBr, which precipitates out of solution (Scheme 6.11).

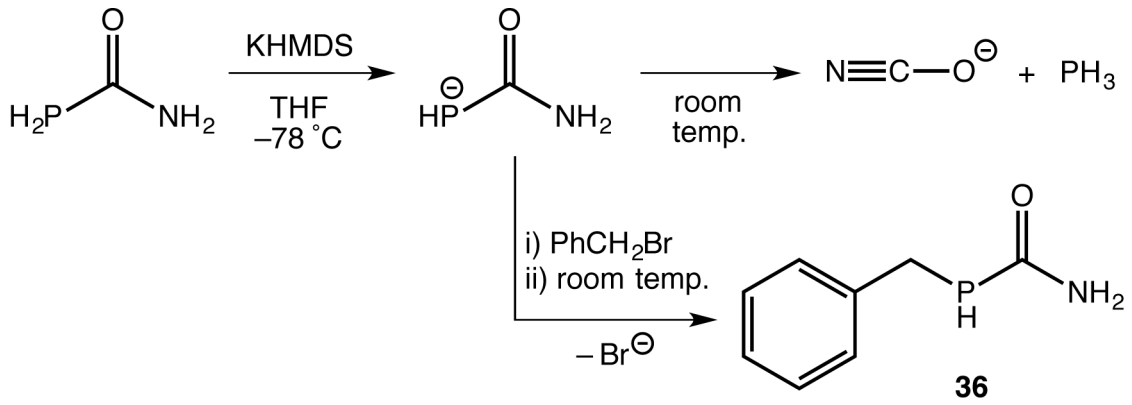

Scheme 6.11: Deprotonation of **11** with KHMDS to afford the phosphide shown, which is unstable at room temperature. The trapping of this species with benzyl bromide at low temperature affords the *P*-functionalised phosphinecarboxamide, **36**.

The NMR spectra of **36** are consistent with benzylation at phosphorus, and are consistent with the phosphinecarboxamides discussed thus far. The methylene protons are diastereotopic, and give rise to complex second order multiplets at 3.03 ppm and 3.22 ppm in the ^{1}H NMR spectrum (Figure 6.12), by analogy with **32**. The phosphine proton is also a second order multiplet, due to coupling to the phosphorus centre ($^{1}J_{H–P}$ = 205 Hz) and the two inequivalent methylene protons ($^{3}J_{H–H}$ = 6 Hz, $^{3}J_{H–H}$ = 7 Hz). The amide protons are reminiscent of those in **11**, with two distinct broad resonances at 6.80 ppm and 7.05 ppm due to hindered rotation around the C–N bond. The more downfield of these resonances overlaps with the aromatic resonances from the phenyl group.

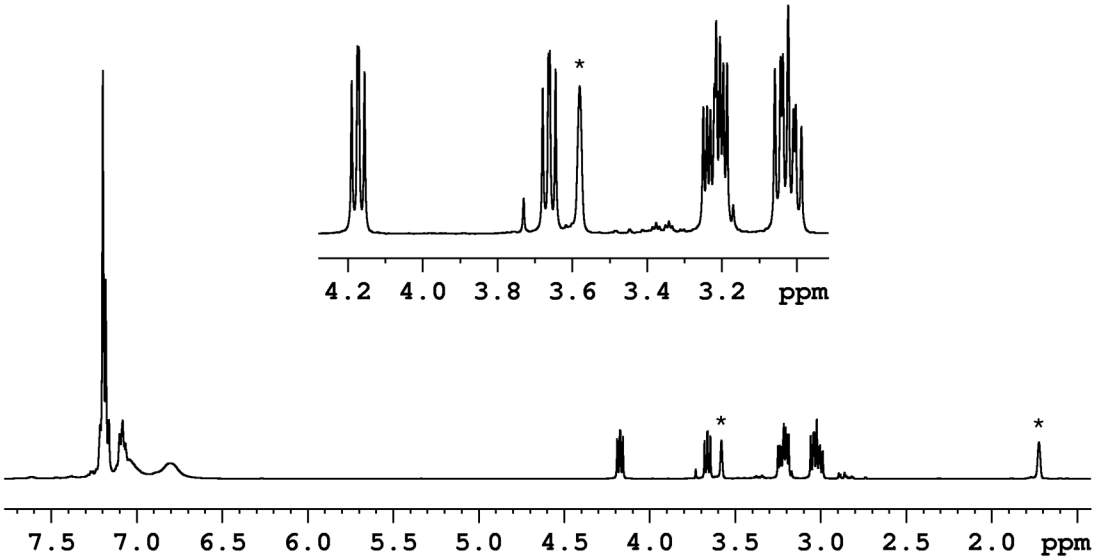

Figure 6.12: ^{1}H NMR spectrum of d_8-THF solution of **36**. Inset shows the zoomed region displaying the second order multiplets from the phosphine and methylene protons. Resonances marked with * are due to residual protic solvent.

The ^{31}P NMR spectrum shows a multiplet centred at –55.5 ppm, due to coupling to the phosphine proton ($^{1}J_{P–H}$ = 205 Hz) and the two methylene protons. The $^{13}C\{^{1}H\}$ NMR spectrum reveals two doublets attributable to the methylene carbon at 26.4 ppm ($^{1}J_{C–P}$ = 11 Hz) and the carbonyl carbon at 178.6 ppm ($^{1}J_{C–P}$ = 14 Hz). These are in addition to the resonances from the phenyl ring, some of which exhibit long-range coupling to the phosphorus, by analogy with the previously discussed *P*-benzylated systems **32** and **35**.

The FI mass spectrum of **36** revealed the molecular ion peak at *m/z* = 167.0499, which is a very good match with the calculated monoisotopic mass of 167.0500 Da.

6.4 Oxidation chemistry

This section will explore the oxidation chemistry of a number of the phosphinecarboxamide molecules described heretofore, including a range of primary, secondary and tertiary phosphines. In all of the following cases an aqueous hydrogen peroxide solution was employed as the oxidising agent. The fact that phosphinecarboxamides can readily be used

in reactions without the need to exclude water further emphasises the "user-friendly" nature of these phosphines.

6.4.1 Synthesis of phosphinic acid derivatives

Phosphinic acids have the general formula $R_2P(O)(OH)$. They are valuable synthetic targets, as some have biologically active properties. For example, CGP36742 is a relatively simple phosphinic acid with butyl and aminopropyl substituents. It was the first orally active $GABA_B$ antagonist (it blocks the γ-aminobutyric acids receptors), and has been shown to block baclofen-induced neuronal depression in rats.[21,22]

We therefore sought to synthesise a range of carbamoyl-bearing phosphinic acids from a selection of the primary and secondary phosphines discussed so far.

6.4.1.1 Oxidation of 17 to afford HP(O)(OH)C(O)NHCy (37)

The oxidation of primary phosphines, H_2PR, was investigated by Buckler and Epstein in 1962.[23] They found that in most cases, the primary phosphine oxide, $H_2P(O)R$, that is formed is unstable with respect to disproportionation, and results in the formation of the original primary phosphine and a phosphinic acid HP(O)(OH)R. The rate at which this happens is dependent on the R group. For example, the cyanoethyl derivative (R = CH_2CH_2CN) disproportionates completely within one hour, whereas the ^{n}octyl phosphine oxide (R = C_8H_{17}) is stable at room temperature for several months.

The oxidation of **17** with one equivalent of hydrogen peroxide gave rise to half an equivalent of the phosphinic acid HP(O)(OH)C(O)NHCy (**37**), while half of **17** remained unreacted (Scheme 6.12). The addition of a second equivalent of hydrogen peroxide led to the full formation of **37**.

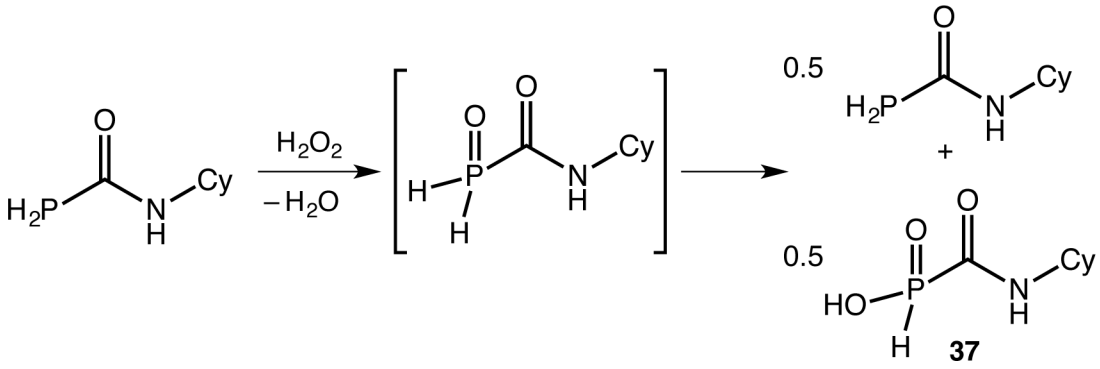

Scheme 6.12: Oxidation of **17** via an undetected intermediate to afford **37**.

The reaction was monitored by ^{31}P NMR spectroscopy, and no evidence of the primary phosphine oxide intermediate was observed, which implies that it rapidly disproportionates under the conditions used. **37** gives rise to a doublet in the ^{31}P NMR spectrum at 5.8 ppm with a coupling constant of $^{1}J_{P–H}$ = 527 Hz. This is significantly larger than the coupling constant in **17** ($^{1}J_{P–H}$ = 206 Hz) due to the fact that the phosphorus centre has been oxidised to the +5 oxidation state in the former, and thus has reduced electron density around the phosphorus centre and a shorter P–H bond length.[15]

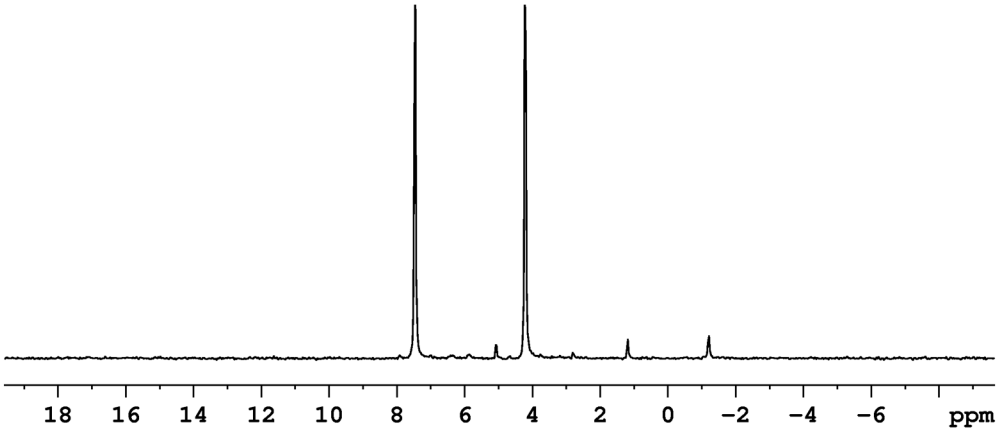

Figure 6.13: ^{31}P NMR spectrum of d_5-pyridine solution of **37**. Two small impurities are also present: a singlet at –1.2 ppm and a doublet centred at 3.1 ppm ($^{1}J_{P–H}$ = 626 Hz), as determined by comparison with the ^{31}P{^{1}H} NMR spectrum.

The same coupling constant was observed in the ^{1}H NMR spectrum for the proton bound to the phosphorus centre at 7.85 ppm ($^{1}J_{H–P}$ = 527 Hz). A notably larger coupling constant for the carbonyl carbon was also resolved in the ^{13}C{^{1}H} NMR spectrum, where a doublet was

observed at 175.2 ppm with a coupling constant of $^{1}J_{C-P}$ = 149 Hz (compared to $^{1}J_{C-P}$ = 6 Hz for **17**). The *N*-bound carbon of the cyclohexyl ring also appeared as a doublet due to coupling to the phosphorus centre ($^{3}J_{C-P}$ = 5 Hz). The acidic proton bound to the oxygen could not be observed in the ^{1}H NMR spectrum, presumably due to deprotonation or broadening arising from strong hydrogen bonding interactions with the d_5-pyridine solvent.

The formation of **37** was typically accompanied by small amounts of impurities, as determined by ^{31}P NMR spectroscopy (Figure 6.13). One of these is a singlet at –1.2 ppm, which we believe is derived from further oxidation of **37** to afford the phosphonic acid derivative (Scheme 6.13).[24]

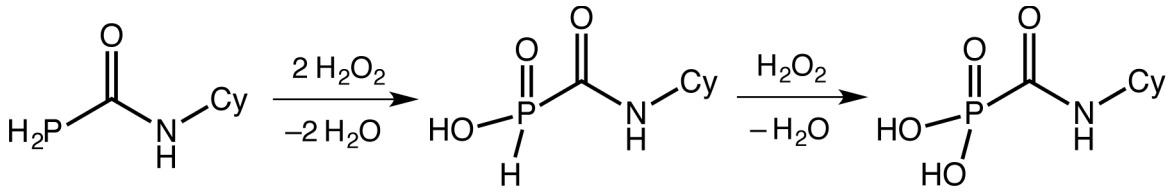

Scheme 6.13: Oxidation of the primary phosphine **17** to generate the phosphinic acid **37** and ultimately the phosphonic acid derivative shown.

The facile formation of **37** does show that the phosphorus centre of phosphinecarboxamides is readily oxidised. However, **37** is a viscous oily substance, which makes it difficult to manipulate for further reactivity. For this reason, and due to the persistent presence of impurities, we sought to generate alternative carbamoyl-bearing phosphinic acids.

6.4.1.2 Oxidation of 31 and 32 to afford MeP(O)(OH)C(O)NHCy (38) and BnP(O)(OH)C(O)NHCy (39)

We reasoned that the oxidation of the *P*-functionalised phosphinecarboxamides would proceed more cleanly, as this would mitigate the problem of over-oxidation of the phosphorus centre. The reactions of **31** and **32** with two equivalents of hydrogen peroxide afforded the phosphinic acid derivatives MeP(O)(OH)C(O)NHCy (**38**) and BnP(O)(OH)C(O)NHCy (**39**), respectively (Scheme 6.14).

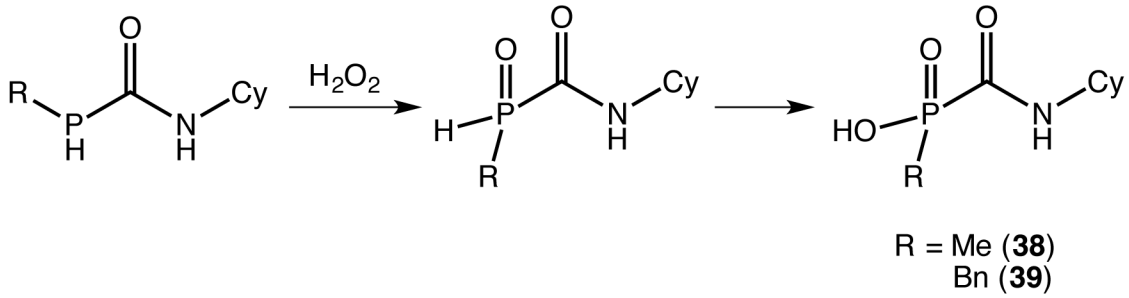

Scheme 6.14: Oxidation of **31** and **32** with two equivalents of hydrogen peroxide to afford **38** and **39**, via the phosphine oxide intermediate.

Unlike during the oxidation of **17**, in these reactions the phosphine oxide intermediates are observable by ^{31}P NMR spectroscopy. The decreased rate of disproportionation is due to the increased steric bulk around the phosphorus centre. Figure 6.14 shows the ^{31}P NMR spectrum of the reaction of **32** and two equivalents of hydrogen peroxide. The larger resonance at 20.7 ppm is the triplet ($^{2}J_{P–H}$ = 17 Hz) from **39**, but clearly visible as well is the doublet of triplets centred at 17.4 ppm ($^{1}J_{P–H}$ = 485 Hz, $^{2}J_{P–H}$ = 15 Hz) arising from the HBnP(O)C(O)NHCy secondary phosphine oxide intermediate.

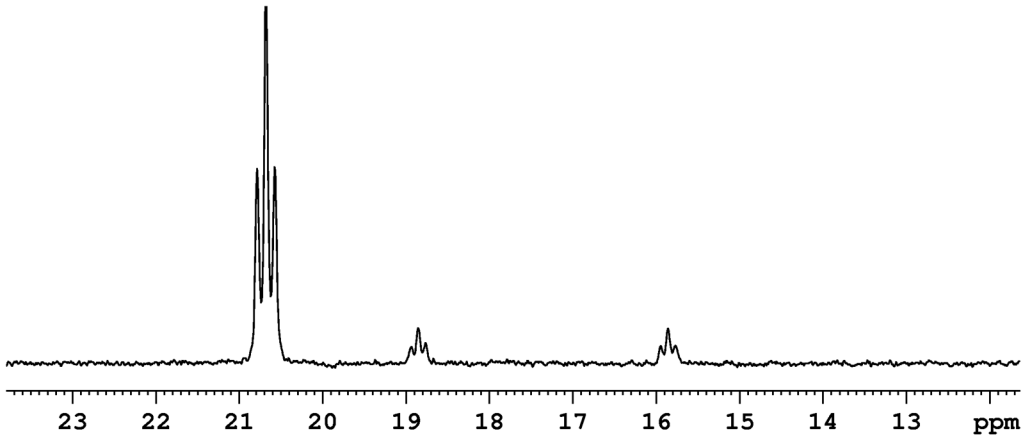

Figure 6.14: ^{31}P NMR spectrum of d_5-pyridine solution of **32** and hydrogen peroxide, with resonances due to **39** and the phosphine oxide intermediate.

The ^{31}P NMR spectrum of **38** reveals a quartet at 23.5 ppm with a notably larger coupling constant ($^{2}J_{P–H}$ = 14 Hz) than that observed in **31**, due to the increase in oxidation state of the phosphorus. This resonance collapses to a singlet on proton decoupling. The same coupling of the methyl protons to the phosphorus was observed in the ^{1}H NMR spectrum,

with a doublet at 1.85 ppm ($^2J_{H–P}$ = 14 Hz). The carbonyl and methyl resonances were observed as doublets in the $^{13}C\{^1H\}$ NMR spectrum at 174.0 ppm ($^1J_{C–P}$ = 150 Hz) and 15.3 ppm ($^1J_{C–P}$ = 96 Hz), respectively.

The intense triplet in the ^{31}P NMR spectrum of **39** (Figure 6.14) suggests that the two methylene protons are magnetically equivalent in this molecule (unlike in **32**), and this is corroborated by the ^1H NMR spectrum showing a single doublet resonance at 3.68 ppm ($^2J_{H–P}$ = 17 Hz). This suggests that the two oxygen atoms bound to the phosphorus are equivalent on the NMR timescale, which indicates fast proton exchange between the P=O and P–OH sites. It may be that the proton is actually bound to the d_5-pyridine solvent, to afford the pyridinium salt of **39**, but there was no evidence of the expected resonance attributable to the nitrogen-bound proton of the pyridinium cation. The $^{13}C\{^1H\}$ NMR spectrum revealed doublet resonances at 174.1 ppm ($^1J_{C–P}$ = 147 Hz) and 38.1 ppm ($^1J_{C–P}$ = 87 Hz), corresponding to the carbonyl and methylene carbons, respectively. By analogy with the aforementioned *P*-benzylated systems (**32**, **35** and **36**), there is long-range coupling of the phenyl carbons to the phosphorus, but they are slightly larger in **39** than in the previous P(III) systems, as expected.

Secondary phosphine oxides have received recent attention due to their use as air- and moisture-stable pre-ligands in certain active catalytic systems.[25,26] Their enhanced thermal stability is achieved by the use of bulky R groups. Thus it should be possible to generate *P*-functionalised phosphinecarboxamides with sterically encumbering groups bound to the phosphorus, which on oxidation afford secondary phosphine oxides that are stable with respect to disproportionation. These could then be explored within the context of ligands for catalysis, to see if there is any benefit in having a carbamoyl group bound to the phosphorus centre. For example, a substrate could interact via hydrogen bonding with the amide proton,

which could lower the energy of it binding to the metal in question, or be used to direct the substrate in a certain orientation (particularly if a chiral phosphinecarboxamide was used).[27]

6.4.2 Synthesis of phosphinate derivatives

Phosphinates are the salts of phosphinic acids, with the general formula $[R_2P(O)_2]^-$, and can potentially be used to generate phosphinate esters ($R_2P(O)(OR)$). The latter have been explored as alternatives to PCl_3 in the synthesis of organophosphorus compounds, principally by the group of Montchamp.[28] The phosphinic acids **37**–**39** were characterised primarily by NMR spectroscopy, and all attempts to grow single crystals suitable for X-ray diffraction were unsuccessful. We reasoned that the formation of ionic salts would be more amenable to the growth of single crystals, and allow the structural authentication of these products.

6.4.2.1 Deprotonation of 39 to afford $[BnP(O)_2C(O)NHCy]^-$ (40)

The reaction of **39** with equimolar quantities of KHMDS and 18-crown-6 in THF affords the expected deprotonation product, $[BnP(O)_2C(O)NHCy]^-$ (**40**), as shown in Scheme 6.15.

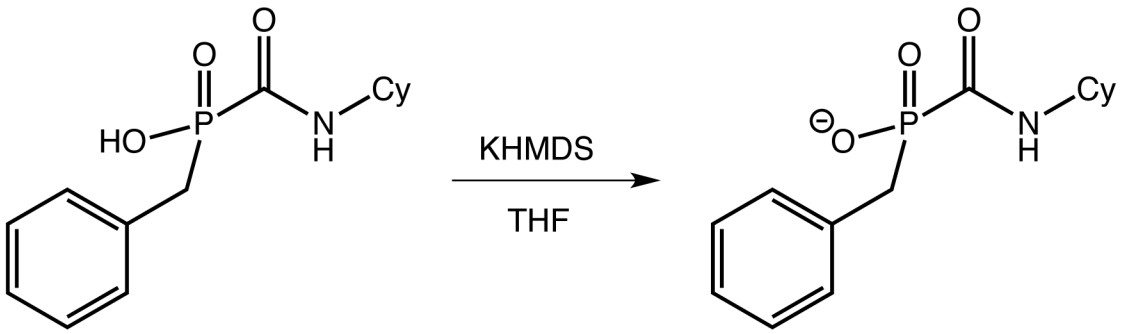

Scheme 6.15: Deprotonation of **39** with KHMDS to afford **40**.

Single crystals suitable for X-ray diffraction were grown by slow diffusion of hexane into a THF solution of the product (Figure 6.15). This structure is good evidence that the postulated oxidation products **38** and **39** are correct, where the phosphorus centre has been doubly oxidised to give the phosphinic acids.

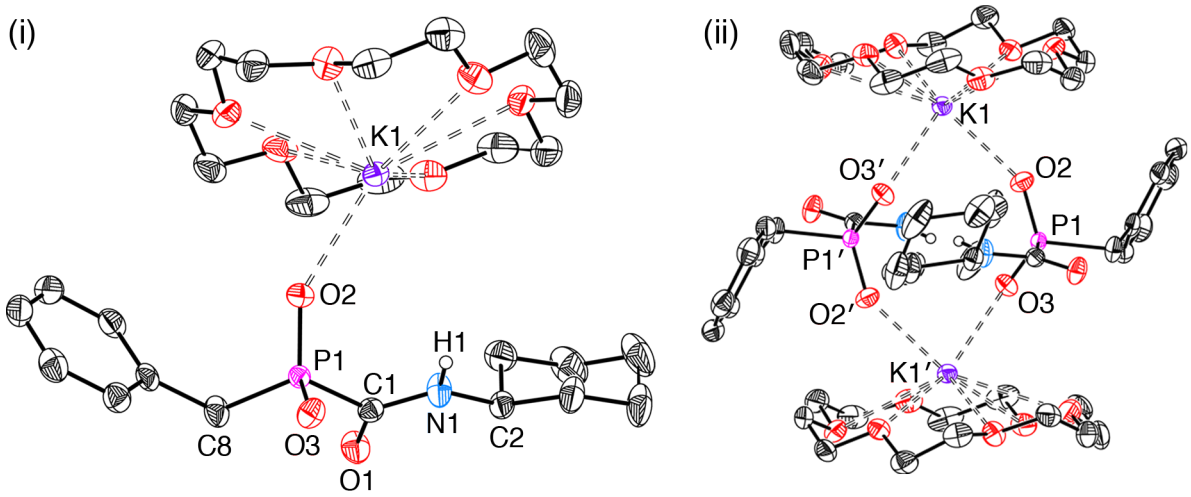

Figure 6.15: (i) Molecular structure of [K(18-crown-6)][**40**]; (ii) the dimeric structure found in the solid state due to inversion centre. Anisotropic displacement ellipsoids are set at 50% probability. Nitrogen-bound hydrogen atoms are shown as spheres of arbitrary radii, other hydrogen atoms omitted for clarity. Symmetry element ′: 2–*x*, –*y*, 1–*z*.

The diffraction study reveals the asymmetric unit to be [K(18-crown-6)][**40**]·0.5(hexane). The presence of an inversion centre generates a dimeric structure (Figure 6.15 (ii)), where the two phosphorus-bound oxygen atoms (O2 and O3) each interact with a different potassium cation, leading to the eight-membered ring shown. The bond metric data are shown in Table 6.6.

Table 6.6: Selected bond lengths (Å) and angles (˚) of [K(18-crown-6)][**40**].

Bond distance (Å)	**40**	**Bond angle (˚)**	**40**
P1–C1	1.872(2)	P1–C1–O1	122.2(1)
C1–O1	1.234(2)	P1–C1–N1	114.5(1)
C1–N1	1.341(2)	N1–C1–O1	123.3(1)
P1–C8	1.829(2)	O2–P1–O3	118.4(1)
P1–O2	1.490(1)	O2–P1–C1	107.2(1)
P1–O3	1.498(1)	O3–P1–C1	108.6(1)
N1–C2	1.460(2)	C1–P1–C8	100.7(1)
K1–O2	2.651(1)	K1–O2–P1	146.8(1)
K1′–O3	2.739(1)	K1′–O3–P1	128.6(1)

The phosphorus atom is in a distorted tetrahedral environment, with a slightly larger O2–P1–O3 bond angle (118.4(1)˚, compared to approximately 109.5˚ in a perfect tetrahedron) due to the electrostatic repulsion of the two oxygen centres. The two P–O bond lengths are similar, and consistent with the delocalisation of the negative charge over both oxygen atoms. The crystal data for the non-oxidised phosphinecarboxamide **32** were unsatisfactory, so a good comparison of the bond metric data cannot be made between **32** and **40**. It is worth noting, however, that the P1–C1 bond length in **40** is long at 1.872(2) Å, especially considering the oxidation from P(III) to P(V) is usually accompanied with a contraction of the bond lengths to phosphorus. We believe this is not the case here due to repulsion of partial positive charges on both P1 and C1, as both are bound to more electronegative elements (oxygen and nitrogen).

The NMR spectra of a d_5-pyridine solution of [K(18-crown-6)][**40**] are similar to those obtained for **39**. In fact they are so similar that it may actually be evidence of the fact that the d_5-pyridine solution of **39** actually exists as [HNC_5D_5][**40**], although as previously stated, the *N*-bound proton in the pyridinium cation could not be observed in the ^{1}H NMR spectrum. The two methylene protons of **40** are equivalent, and give rise to a triplet in the ^{31}P NMR spectrum at 16.3 ppm ($^2J_{P–H}$ = 17 Hz). The methylene group also affords a doublet in the ^{1}H NMR spectrum at 3.54 ppm ($^2J_{H–P}$ = 17 Hz), and a doublet in the $^{13}C\{^1H\}$ NMR spectrum at 40.2 ppm ($^1J_{C–P}$ = 83 Hz). The carbonyl carbon resonates at 178.5 ppm ($^1J_{C–P}$ = 138 Hz), and the phenyl carbons all exhibit long-range coupling to the phosphorus centre as well.

The composition of [K(18-crown-6)][**40**] was further tested by ESI mass spectrometry. The anion was observed in the negative ion mode spectrum at *m/z* = 279.7, and the positive ion mode revealed two different cation-paired species, $\{[K_2(18\text{-crown-6})][\mathbf{40}]\}^+$ and $\{[K(18\text{-crown-6})]_2[\mathbf{40}]\}^+$, at *m/z* = 622.6 and 886.8, respectively.

6.4.2.2 Oxidation of 29 to afford $[P(O)_2\{C(O)NHCy\}_2]^-$ (41)

We subsequently wanted to extend the study and synthesise the bis(carbamoyl) phosphinate $[P(O)_2\{C(O)NHCy\}_2]^-$ (**41**). This molecule could presumably be synthesised following a similar protocol to **40**, thus oxidation of the secondary phosphine, **33**, to afford the phosphinic acid, followed by deprotonation with a base. However, we rationalised that a more efficient synthesis of **41** could be achieved by the direct oxidation of the phosphide, **29**. This reaction worked cleanly, and the addition of excess hydrogen peroxide to a THF solution of [K(18-crown-6)][**29**] gave rise to [K(18-crown-6)][**41**], as shown in Scheme 6.16.

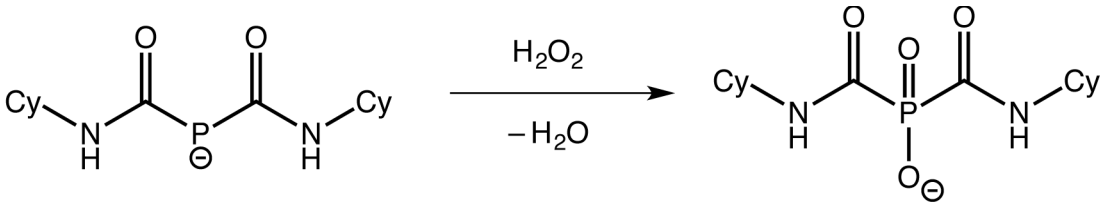

Scheme 6.16: Oxidation of **29** to afford **41**.

A clean sample of [K(18-crown-6)][**41**] could be obtained by removal of the volatiles under reduced pressure. Single crystals of [K(18-crown-6)][**41**]·THF were grown by slow diffusion of hexane into a THF solution of the product (Figure 6.16). There is one molecule of disordered THF in the asymmetric unit, which has been omitted from Figure 6.16 for clarity.

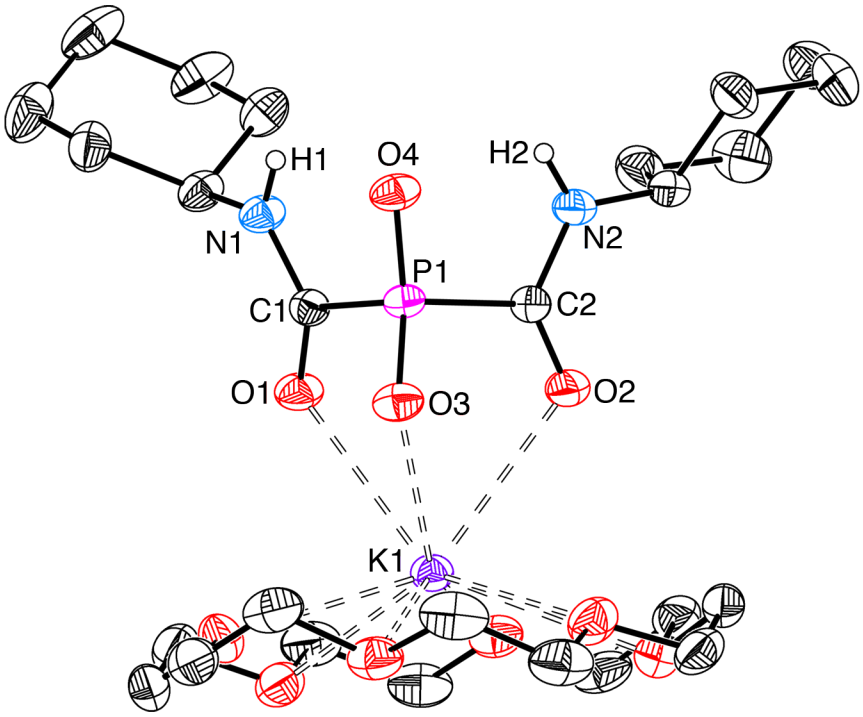

Figure 6.16: Molecular structure of [K(18-crown-6)][**41**]. Anisotropic displacement ellipsoids are set at 50% probability. Nitrogen-bound hydrogen atoms are shown as spheres of arbitrary radii, other hydrogen atoms omitted for clarity.

Interestingly, the structure of the anion shows the two carbonyl substituents to be on the same face of the molecule. This differs from the previous solid-state structures of the bis(carbamoyl) phosphides (**29** and **30**), which both contained a six-membered ring arising from an intramolecular hydrogen bonding interaction of one of the amide protons with the carbonyl group of the other carboxamide moiety. We believe **41** has a different conformation due to the favourable interaction of three oxygen atoms bearing partial negative charges (O1, O2 and O3) with the potassium cation. The bond metric data are shown in Table 6.7.

The negative charge in **41** is clearly no longer located on the phosphorus centre, as it was in the phosphide precursor (**29**), and thus there is no longer any multiple bond character to the P–C bonds. This results in a lengthening of these bonds from 1.826(av) Å in **29** to 1.866(av) Å in **41**. The latter are similar to the analogous P1–C1 bond length in **40**.

Table 6.7: Selected crystallographic bond lengths (Å) and angles (˚) of [K(18-crown-6)][**41**].

Bond distance (Å)	41	Bond angle (˚)	41
P1–C1	1.866(2)	P1–C1–O1	120.7(1)
P1–C2	1.865(2)	P1–C2–O2	122.4(1)
C1–O1	1.241(2)	P1–C1–N1	113.7(2)
C2–O2	1.234(2)	P1–C2–N2	113.7(1)
C1–N1	1.336(2)	N1–C1–O1	125.5(2)
C2–N2	1.340(2)	N2–C2–O2	123.9(2)
P1–O3	1.487(1)	O3–P1–O4	122.8(1)
P1–O4	1.494(1)	C1–P1–C2	96.9(1)
N1–C11	1.458(2)	C1–P1–O3	109.9(1)
N2–C21	1.454(2)	C1–P1–O4	108.2(1)
K1–O1	3.073(2)	C2–P1–O3	108.1(1)
K1–O2	2.925(2)	C2–P1–O4	108.9(1)
K1–O3	2.706(1)	K1–O1–C1	110.2(1)
		K1–O2–C2	115.6(1)
		K1–O3–P1	109.8(1)

The two carboxamide moieties are very similar, with minimal deviation in the bond lengths and bond angles between the two halves of the anion. The P1–O3 and P1–O4 bond lengths are also comparable, and are indicative of delocalisation of the negative charge over both oxygen centres, despite the fact that only O3 is interacting with the potassium cation. The bond angles around the phosphorus are again indicative of a distorted tetrahedral environment, with the same increase in O3–P1–O4 bond angle (122.8(1)˚) relative to a perfect tetrahedron as that seen in **40**. The carboxamide moieties remain planar around the central carbon atoms (sum of angles around C1 = 359.9˚, around C2 = 360.0˚).

The ^{31}P NMR spectrum of [K(18-crown-6)][**41**] in d_5-pyridine revealed a singlet at –1.8 ppm (Figure 6.17). The ^{1}H and ^{13}C{^{1}H} NMR spectra showed the expected resonances for the amide protons and the cyclohexyl groups. The ^{13}C{^{1}H} NMR resonance attributable to

the two equivalent carbonyl carbons was observed as a doublet at 176.9 ppm ($^1J_{C-P}$ = 141 Hz).

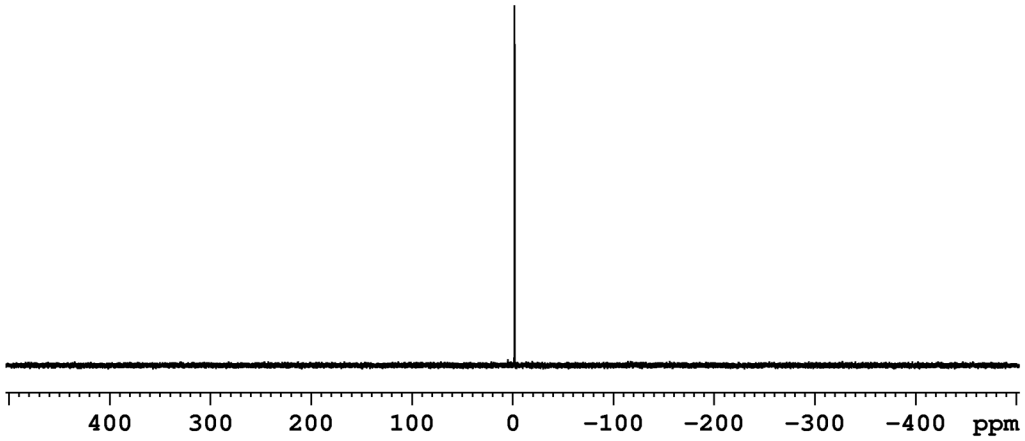

Figure 6.17: ^{31}P NMR spectrum of a d_5-pyridine solution of [K(18-crown-6)][**41**].

An ESI mass spectroscopic study of [K(18-crown-6)][**41**] revealed a mass envelope corresponding to **41** in the negative ion mode at *m/z* = 314.9. The positive ion mode showed two distinct cation-paired species, $\{[K_2(18\text{-crown-6})][\mathbf{41}]\}^+$ and $\{[K(18\text{-crown-6})]_2[\mathbf{41}]\}^+$, at *m/z* = 657.7 and 921.9, respectively, by analogy with the mass spectrum of **40**.

An independent study from the group of Grützmacher has synthesised a similar anion, a phosphinate bearing two acyl groups, which was published recently.[29] They initially synthesised the bis(mesitoyl) phosphide in an analogous manner to that mentioned at the start of this chapter and shown in Scheme 6.2.[9] Interestingly, the protonation of the bis(acyl) phosphide with acetic acid gave rise to the enol tautomer (Scheme 6.17), in stark contrast with the protonation of **29** to afford a secondary phosphine. This phosphaenol has been previously reported by the group of Becker.[30]

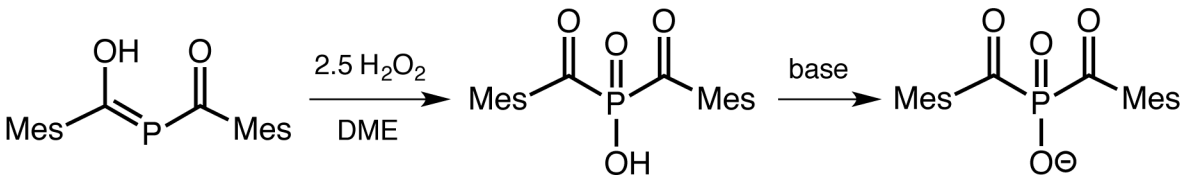

Scheme 6.17: Oxidation of phosphaenol to afford phosphinic acid, and subsequent deprotonation to afford a bis(acyl) phosphinate. Figure adapted from Müller et al.[29]

The oxidation of the phosphaenol with a slight excess of hydrogen peroxide generates the phosphinic acid. This species can be deprotonated with a range of nitrogen-containing bases or $NaHCO_3$ to afford the bis(mesitoyl) phosphinate product. Note, this differs from **41** only by the substitution of acyl groups with carbamoyl groups. The bond metric data of the central $\{P(O)_2(CO)_2\}$ core of this anion, crystallised as the imidazolium salt, is comparable to that of **41**.

The group has gone on to show that the sodium salt of the bis(acyl) phosphinate is soluble and stable in water, and can be utilised as an initiating agent for the surfactant-free emulsion polymerisation of styrene to afford monodisperse and spherical nanoparticles.[29] Based on this research, it would be interesting to explore the possible applications of **41**, and ascertain whether the substitution of the acyl groups for carbamoyl groups affects the properties of this initiation process. Furthermore, building on our research on the formation of **41**, it may be possible to synthesise the bis(acyl) phosphinate more efficiently by the direct oxidation of the bis(acyl) phosphide with hydrogen peroxide, and therefore remove two steps from their synthetic protocol. These compounds are certainly worthy of further exploration.

6.4.3 Synthesis of phosphine oxides

The final section in the oxidation chemistry of phosphinecarboxamides is also the simplest, by design, and involves the oxidation of the *P*-functionalised bis(carbamoyl) species, **34** and **35**. These are tertiary phosphines, and thus the reactions of these molecules with hydrogen peroxide trivially afford the phosphine oxides, $MeP(O)\{C(O)NHCy\}_2$ (**42**) and $BnP(O)\{C(O)NHCy\}_2$ (**43**), respectively (Scheme 6.18). The products were isolated as solids by removal of the volatiles under reduced pressure.

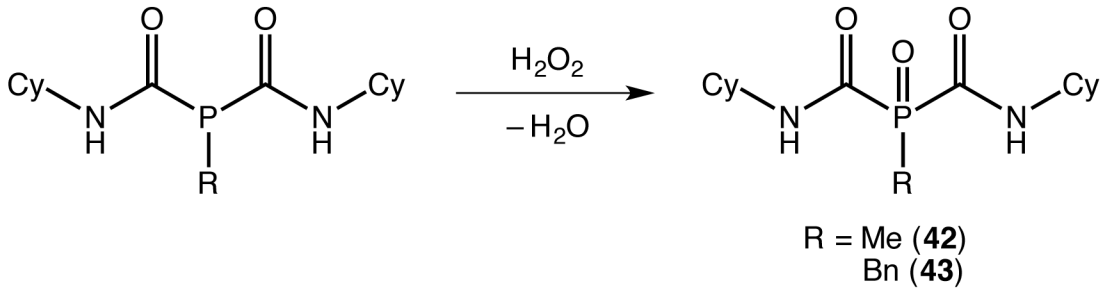

Scheme 6.18: The oxidation of **34** and **35** with hydrogen peroxide to afford **42** and **43**, respectively.

42 and **43** were the initial target molecules mentioned at the start of this chapter, as they bear a strong structural resemblance to bis(acyl) phosphine oxides (BAPOs). They constitute a novel (yet irrefutably related) class of compounds that could act as potential photoinitiators, and will henceforth be abbreviated as BCPOs (bis(carbamoyl) phosphine oxides). Single crystals of both BCPOs were grown by slow diffusion of hexane into THF solutions of the respective products (Figure 6.18).

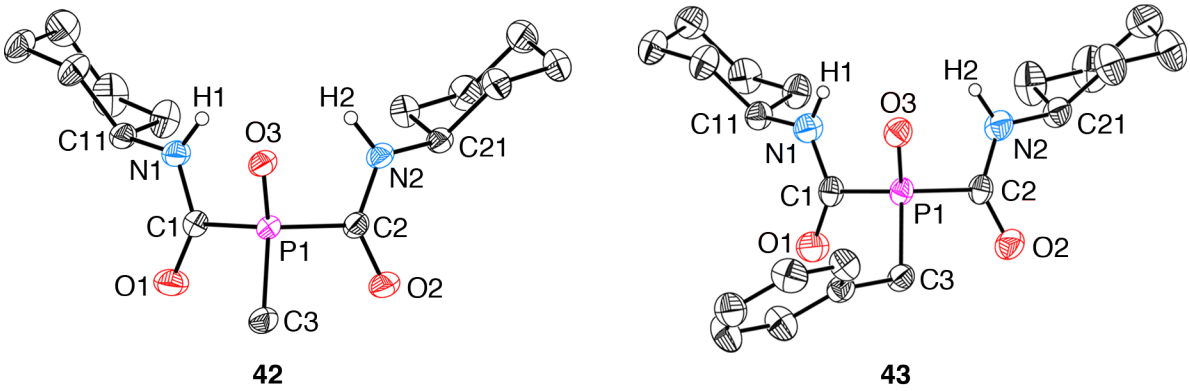

Figure 6.18: Molecular structures of **42** and **43**. Anisotropic displacement ellipsoids are set at 50% probability. Nitrogen-bound hydrogen atoms are shown as spheres of arbitrary radii, other hydrogen atoms omitted for clarity.

42 and **43** are isostructural, and both feature the carbamoyl groups pointing in the same direction, with no intramolecular hydrogen bonding. This is because both species crystallise as dimers in the solid state, with the amide protons H1 and H2 hydrogen bonding to the O3 atom of a neighbouring molecule. The bond metric data for both molecules are shown in Table 6.8.

Table 6.8: Bond distances (Å) and angles (˚) of **42** and **43**.

Bond distance (Å)	**42**	**43**
P1–C1	1.861(2)	1.870(2)
P1–C2	1.863(2)	1.871(2)
C1–O1	1.225(2)	1.221(3)
C2–O2	1.228(2)	1.224(3)
C1–N1	1.332(2)	1.329(3)
C2–N2	1.330(2)	1.333(3)
N1–C11	1.462(2)	1.466(3)
N2–C21	1.465(2)	1.470(3)
P1–C3	1.780(2)	1.797(2)
P1–O3	1.496(2)	1.489(2)
Bond angle (˚)		
P1–C1–O1	120.0(2)	119.1(2)
P1–C2–O2	119.6(2)	119.2(2)
P1–C1–N1	113.5(2)	113.9(2)
P1–C2–N2	113.9(2)	113.9(2)
N1–C1–O1	126.5(2)	127.1(2)
N2–C–O2	126.5(2)	126.9(2)

The bond lengths and bond angles for the carboxamide moieties are similar within each molecule, and between the two different molecules as well. The bond distance between phosphorus and the methyl carbon (P1–C3 in **42**: (1.780(2) Å) is notably shorter than that in the *P*-methylated phosphinecarboxamide **31** (P1–C8: 1.824(3) Å). This is due to the oxidation of the phosphorus from P(III) to P(V). Note, by analogy with the previous oxidation products, the bond distances between the phosphorus and the carbamoyl carbons do not appear to contract on oxidation (1.862(av) Å in **42**, 1.863(3) Å in **31**), due to the partial positive charges on both phosphorus and carbon in the oxidised species. The bond lengths and angles around P1 in the BCPOs are consistent with the analogous data for the structurally authenticated BAPOs.[9,10]

The ^{31}P NMR spectrum of **42** exhibits a quartet at 18.1 ppm ($^{2}J_{P–H}$ = 14 Hz), shown in Figure 6.19, which collapses to a singlet on proton decoupling. This two-bond coupling is also observable by ^{1}H NMR spectroscopy, as the methyl protons appear as a doublet at 2.16 ppm. The methyl and carbonyl carbons resonate at 11.6 ppm ($^{1}J_{C–P}$ = 68 Hz) and 169.1 ppm ($^{1}J_{C–P}$ = 108 Hz), respectively, in the ^{13}C{^{1}H} NMR spectrum. These one-bond carbon–phosphorus coupling constants have smaller magnitudes than the respective coupling constants in **37**–**41**, because in the latter molecules the phosphorus atoms are bonded to an extra electron-withdrawing oxygen atom.[15]

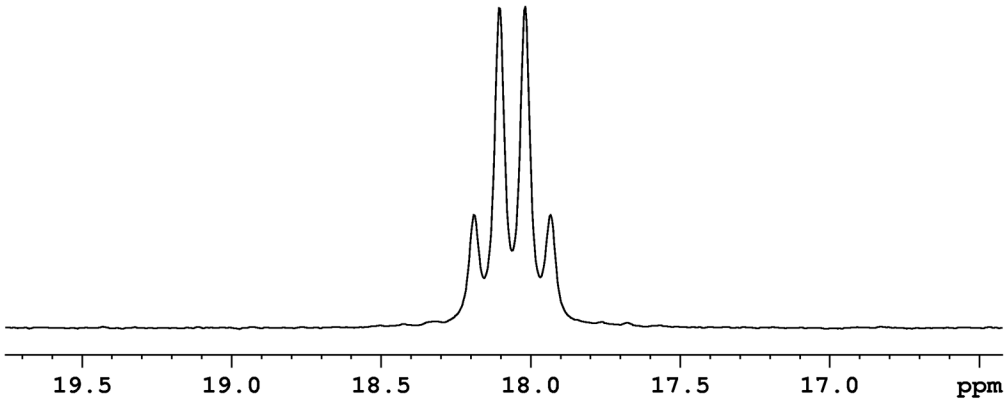

Figure 6.19: ^{31}P NMR spectrum of d_5-pyridine solution of **42**.

The NMR data for **43** is unsurprisingly very similar, with a resonance in the ^{31}P NMR spectrum at 17.2 ppm, which is a triplet due to coupling to the two equivalent methylene protons ($^{2}J_{P–H}$ = 15). The ^{1}H NMR spectrum exhibits a doublet for these methylene protons at 4.12 ppm ($^{2}J_{H–P}$ = 15), in addition to the expected amide, cyclohexyl and phenyl resonances. The methylene and carbonyl carbon resonances appear at 33.4 ppm ($^{1}J_{C–P}$ = 59 Hz) and 168.1 ppm ($^{1}J_{C–P}$ = 104 Hz) in the ^{13}C{^{1}H} NMR spectrum, respectively.

42 was submitted for FI mass spectrometric analysis. The molecular ion peak was observed at *m/z* = 314.1746, which is consistent with the predicted monoisotopic mass of 314.1759 Da. There was also evidence of a similar McLafferty rearrangement as that described previously for the compounds **33**–**35**, and shown in Scheme 6.10. This gave rise to peaks

corresponding to the fragments $[CONCy]^+$ at *m/z* = 125.0848 and $[MePOCOHNHCy]^+$ at *m/z* = 189.0875.

Having synthesised the target BCPOs, we carried out very crude initial reactivity studies on these potential photoinitiators, and tested them against the industry standard BAPO, Irgacure® 819 (shown in Scheme 6.1). This was achieved by mixing 0.1 mol% of the photoinitiator with a monomer, trimethylolpropane triacrylate (TMPTA, shown in Scheme 6.19), in open test tubes, and subjecting the samples to UV light. TMPTA is a trifunctional monomer used in the manufacture of plastics, adhesives and inks, and is useful for its low volatility and fast curing speeds.

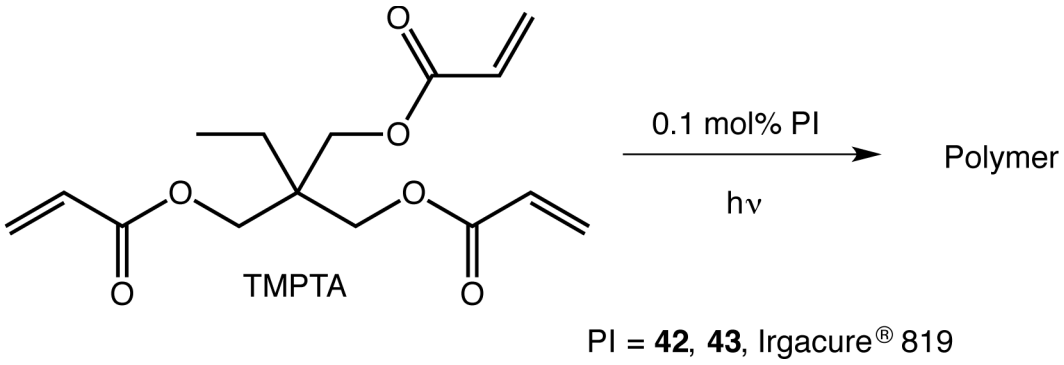

Scheme 6.19: Polymerisation of the monomer, TMPTA, in the presence of a photoinitiator (PI) and UV light.

The polymerisation with Irgacure® 819 as the photoinitiator proceeded in under 30 seconds, giving a soft transparent polymer, as expected. Unfortunately, under the conditions used, there was no evidence that **42** or **43** acted as photoinitiators. A hard and brittle polymer was formed after UV irradiation of the monomer in the presence of **42** and **43** for 20 minutes, but a control experiment (where no photoinitiator was used) showed that this was due to thermally induced polymerisation of the monomer, as the lamp used in the experiment heated the sample significantly over the timeframe of the experiment.

This suggests that BCPOs are not as effective as BAPOs as photoinitiators. However, further studies need to be done to better compare the systems before BCPOs can be

disregarded completely. The samples of **42** and **43** were the crude solid obtained after removing the solvent under reduced pressure after the reaction had taken place, and no further measures were taken to purify these species. Although they appear relatively clean by NMR spectroscopy, an elemental microanalysis of **43** gave an unsatisfactory match (the percentage of carbon was measured at 63.17%, compared to the calculated value of 64.60%). This small quantity of impurities may be quenching the radicals before they interact with the monomer. Therefore, the experiments need to be repeated with samples of **42** and **43** that have been further purified by recrystallisation techniques or column chromatography.

Furthermore, in addition to the two acyl groups, Irgacure® 819 has a phenyl group bound to the phosphorus centre. This is going to be more adept at stabilising the phosphinoyl radicals produced on photolysis than the methyl or benzyl groups in **42** and **43**, respectively. Thus a more fair comparison of the ability of a carbamoyl group relative to an acyl group as a substituent in a photoinitiator would be to synthesise and repeat the test with the *P*-phenyl BCPO. This topic will be further explored in our research group.

6.5 Conclusions

This chapter has explored the versatility of phosphinecarboxamides as chemical precursors to a range of different compounds. The Brønsted acidity of these species was explored, and it was found that the phosphorus-bound protons are more acidic than the amide protons. The architecture of the deprotonated product can be altered by varying the stoichiometry of the base, to afford mono- (**27**, **28**) and bis(carbamoyl) (**29**, **30**) phosphides that can be isolated and are stabilised by delocalisation of the negative charge into the carboxamide moieties.

The subsequent functionalisation of the phosphides **28** and **29** permits a simple synthetic protocol into the formation of *P*-functionalised phosphinecarboxamides (**31**, **32**, **34**, **35**).

The protonation of **29** gives rise to the bis(carbamoyl) phosphine **33**, which is a secondary phosphine and the first phosphorus-containing analogue of biuret. Although the parent phosphinecarboxamide, **11**, is unstable with respect to basic conditions at room temperature, *P*-functionalisation can still be achieved by adding the base to **11** at low temperature in the presence of the electrophile, such as benzyl bromide to afford **36**.

Selected phosphinecarboxamide derivatives were oxidised with hydrogen peroxide to yield a number of phosphinic acids (**37**–**39**), phosphinates (**40**, **41**) and phosphine oxides (**42**, **43**). Some of these products have potential as photoinitiators for radical polymerisation, and research is on-going in this area.

6.6 References

(1) Dietliker, K.; Jung, T.; Benkhoff, J.; Kura, H.; Matsumoto, A.; Oka, H.; Hristova, D.; Gescheidt, G.; Rist, G. *Macromol. Symp.* **2004**, *217*, 77–98.

(2) Fouassier, J.-P.; Lalevée, J. *Photoinitiators for Polymer Synthesis: Scope, Reactivity and Efficiency*; Wiley VCH: Weinheim, Germany, 2012.

(3) Griesser, M.; Neshchadin, D.; Dietliker, K.; Moszner, N.; Liska, R.; Gescheidt, G. *Angew. Chem. Int. Ed.* **2009**, *48*, 9359–9361.

(4) Kolczak, U.; Rist, G.; Dietliker, K.; Wirz, J. *J. Am. Chem. Soc.* **1996**, *118*, 6477–6489.

(5) Sluggett, G. W.; Turro, C.; George, M. W.; Koptyug, I. V.; Turro, N. J. *J. Am. Chem. Soc.* **1995**, *117*, 5148–5153.

(6) Jockusch, S.; Koptyug, I. V.; McGarry, P. F.; Sluggett, G. W.; Turro, N. J.; Watkins, D. M. *J. Am. Chem. Soc.* **1997**, *119*, 11495–11501.

(7) Jockusch, S.; Turro, N. J. *J. Am. Chem. Soc.* **1998**, *120*, 11773–11777.

(8) Shergill, R.; Haberler, M.; Vink, C. B.; Patten, H. V.; Woodward, J. R. *Phys. Chem. Chem. Phys.* **2009**, *11*, 7248–7256.

(9) Huber, A.; Kuschel, A.; Ott, T.; Santiso-Quinones, G.; Stein, D.; Bräuer, J.; Kissner, R.; Krumeich, F.; Schönberg, H.; Levalois-Grützmacher, J.; Grützmacher, H. *Angew. Chem. Int. Ed.* **2012**, *51*, 4648–4652.

(10) Grützmacher, H.; Geier, J.; Stein, D.; Ott, T.; Schönberg, H.; Sommerlade, R. H.; Boulmaaz, S.; Wolf, J.-P.; Murer, P.; Ulrich, T. *Chimia* **2008**, *62*, 18–22.

(11) Murer, P.; Wolf, J.-P.; Burkhardt, S.; Grützmacher, H.; Stein, D.; Dietliker, K. *PCT Int. Appl.* **2006**, WO 200656541 A1 20060601.

(12) Ullrich, G.; Ganster, B.; Salz, U.; Moszner, N.; Liska, R. *J. Polym. Sci. Part A* **2006**, *44*, 1686–1700.

(13) Jupp, A. R.; Trott, G.; Payen de la Garanderie, É.; Holl, J. D. G.; Carmichael, D.; Goicoechea, J. M. *Chem. Eur. J.* **2015**, *21*, 8015–8018.

(14) Brookhart, M.; Grant, B.; Volpe, A. F. *Organometallics* **1992**, *11*, 3920–3922.

(15) Kühl, O. *Phosphorus-31 NMR Spectroscopy: A Concise Introduction for the Synthetic Organic and Organometallic Chemist*; Springer-Verlag: Berlin, 2008.

(16) Wiedemann, G. *Ann. Phys.* **1848**, *150*, 67–84.

(17) Becker, G.; Hübler, K.; Niemeyer, M.; Seidler, N.; Thinus, B. *Z. Anorg. Allg. Chem.* **1996**, *622*, 197–211.

(18) Graham, S. L.; Scholz, T. H. *Tetrahedron Lett.* **1990**, *31*, 6269–6272.

(19) Robinson, T. P.; Goicoechea, J. M. *Chem. Eur. J.* **2015**, *21*, 5727–5731.

(20) McLafferty, F. W. *Anal. Chem.* **1959**, *31*, 82–87.

(21) Mondadori, C.; Jaekel, J.; Preiswerk, G. *Behav. Neural Biol.* **1993**, *60*, 62–68.

(22) Nyitrai, G.; Kékesi, K. A.; Emri, Z.; Szárics, E.; Juhász, G.; Kardos, J. *Eur. J. Pharmacol.* **2003**, *478*, 111–119.

(23) Buckler, S. A.; Epstein, M. *Tetrahedron* **1962**, *18*, 1221–1230.

(24) Fleming, J. T.; Higham, L. J. *Coord. Chem. Rev.* **2015**, *297–298*, 127–145.

(25) Shaikh, T. M.; Weng, C.-M.; Hong, F.-E. *Coord. Chem. Rev.* **2012**, *256*, 771–803.

(26) Chang, Y.-Y.; Hong, F.-E. *Tetrahedron* **2013**, *69*, 2327–2335.

(27) Taylor, M. S.; Jacobsen, E. N. *Angew. Chem. Int. Ed.* **2006**, *45*, 1520–1543.

(28) Montchamp, J.-L. *Acc. Chem. Res.* **2014**, *47*, 77–87.

(29) Müller, G.; Zalibera, M.; Gescheidt, G.; Rosenthal, A.; Santiso-Quinones, G.; Dietliker, K.; Grützmacher, H. *Macromol. Rapid Commun.* **2015**, *36*, 553–557.

(30) Becker, G.; Becker, W.; Schmidt, M.; Schwarz, W.; Westerhausen, M. *Z. Anorg. Allg. Chem.* **1991**, *605*, 7–23.

Chapter 7
Concluding remarks and future work

7.1 Conclusions

This thesis has reported a novel synthesis of the 2-phosphaethynolate anion, $[PCO]^-$, via a rare activation reaction of the heptaphosphide Zintl cluster, $[P_7]^{3-}$. The $[K(18\text{-crown-}6)]^+$ salt was synthesised in suitably high quantities to permit the systematic exploration of the chemistry of this remarkable anion.

The ligand properties of $[PCO]^-$ were studied and compared to its isoelectronic counterparts, $[NCO]^-$ and $[NCS]^-$. It was found that all three anions exhibit similar net electronic effects on a transition metal fragment, although the bonding modes vary significantly between the phosphorus- and nitrogen-containing anions. The study was extended to incorporate the first ambient-temperature synthesis of $[PCS]^-$, and found that this anion can act as an ambidentate ligand, although the resulting complexes are more prone to decomposition.

The reactive nature of the P–C multiple bond in $[PCO]^-$ was exploited to afford a range of cycloaddition products from the reactions with heteroallenes. Aryl-substituted ketenes and carbodiimides both react to yield [2+2] cycloaddition products, featuring novel four-membered phosphorus-containing heterocycles. The reactions with isocyanates gave rise to five-membered heterocycles and spiro-phosphoranides, and a collaborative research project with the group of Grützmacher found that these products could be invoked as intermediates in the catalytic trimerisation of isocyanates.

By analogy with Wöhler's paradigm-shifting synthesis of urea, the reaction of $[PCO]^-$ with ammonium salts gave rise to phosphinecarboxamide, $H_2PC(O)NH_2$. This simple and novel functional group is a relatively air- and moisture-stable primary phosphine, and its electronic ground state was probed using experimental and computational methods. A

number of transition metal complexes of $H_2PC(O)NH_2$ were synthesised, and revealed that phosphinecarboxamide has similar σ and π effects to phosphine, PH_3.

The scope of the protonation of $[PCO]^-$ was investigated, and it was demonstrated that certain substituted amines and ammonium salts could be used to afford *N*-functionalised phosphinecarboxamides, which gave mechanistic insight into the formation of these species. After establishing the basic mode of reactivity, amines with pendant functional groups were employed to synthesise phosphinecarboxamides capable of post-synthetic modification.

Finally, the fundamental reactivity of phosphinecarboxamides was investigated. Deprotonation studies found that the phosphine protons are more acidic than the amine proton(s), and gave rise to stable and isolable phosphides. These anions could be reacted with simple electrophiles to generate *P*-functionalised phosphinecarboxamides. The subsequent oxidation of these species gave rise to a range of carbamoyl-bearing phosphinic acid, phosphinate and phosphine oxide derivatives.

7.2 Future work and preliminary results

7.2.1 Applications for phosphinecarboxamides

Combining the work on phosphinecarboxamides, we have discovered a facile synthetic protocol to generate primary, secondary and tertiary phosphines bearing one or two carbamoyl groups. There are many avenues of research concerning these compounds that would be worth pursuing further. A number of these have been highlighted over the course of the thesis, and involve trying to transform these academic curiosities into real-world applications. The synthesis of the bis(phosphinecarboxamide) species, **25**, underscores the possibility of generating bespoke phosphines with certain properties, such as preferentially *trans*-spanning ligands or chelating tripodal ligands (Section 5.4.2). The styrene-

functionalised phosphinecarboxamide, **26**, will be further explored as a monomer for the synthesis of phosphorus-containing polymers (Section 5.4.3). Lastly, the bis(carbamoyl) phosphinate, **41**, and the bis(carbamoyl) phosphine oxides, **42** and **43**, will be investigated as potential photoinitiators for radical polymerisation, as well as structurally related derivatives with different R groups (Sections 6.4.2 and 6.4.3).

In addition to these ideas, it would also be interesting to study the extent of the parallels between the parent phosphinecarboxamide, **11**, and phosphine, PH_3. Our research so far has revealed that the two are electronically very similar, certainly in terms of their ligand properties. However, **11** is a relatively air- and moisture-stable solid, and is clearly far easier to handle than the pyrophoric and toxic gas, phosphine, and thus **11** could potentially be used as a user-friendly substitute in current procedures or compounds that involve the use of the latter.

7.2.2 Extension to other carbonyl-bearing phosphines

A more fundamental area of research that would be interesting to pursue is the generality of the protonation of $[PCO]^-$ in the presence of different nucleophiles (X–H) to afford carbonyl-bearing phosphines (Scheme 7.1). The reactions with amines (X = NR_2 in Scheme 7.1) have been thoroughly explored over the course of this thesis to synthesise a range of phosphinecarboxamides, but we believe other protic nucleophiles should be capable of a similar reaction.

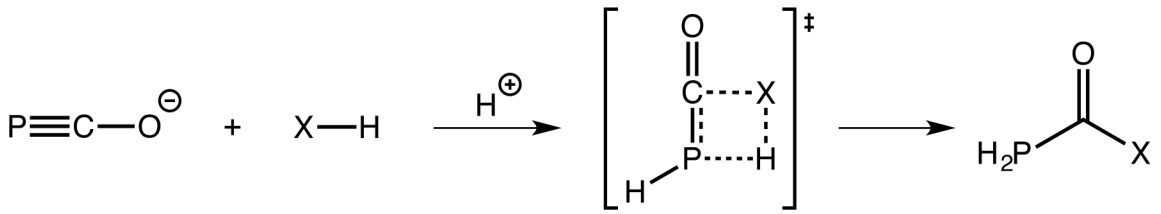

Scheme 7.1: Reaction of $[PCO]^-$ and an acid in the presence of protic nucleophiles to afford carbonyl-bearing primary phosphines. X could represent, for example, NR_2, PR_2, OR^- and OR.

We have carried out some preliminary work in this area, and the most salient results will be briefly reported here. A logical extension from amines is the use of the valence isoelectronic phosphines (X = PR_2), to afford bis(phosphorus) analogues of urea ($H_2PC(O)PR_2$). However, when the reaction with diethylphosphine (X = PEt_2) was carried out, it was found that the product was unstable at room temperature. Thus low-temperature NMR spectroscopic studies need to be carried out in the future to determine the identity of this species; it may also be possible to stabilise the product in the coordination sphere of a metal, and obtain structural authentication and further characterisation in this manner.

The protonation of $[PCO]^-$ in water leads to rapid decomposition. This is unsurprising considering that the phosphinecarboxylic acid product (X = OH) is known to be unstable, although it has previously been trapped and crystallised on a transition metal fragment.[1] We believe the heretofore unidentified hydrolysis product of $[PCO]^-$, as reported by Puschmann et al. ($\delta(^{31}P)$ = 134 ppm, t, $^1J_{P-H}$ = 217 Hz),[2] is the phosphinecarboxylate salt (X = O^-). Its spectroscopic data are strikingly similar to those of the phosphinecarboxamides, although unfortunately we have been unable to structurally characterise and verify this product.

We have had more success when using alcohols as the nucleophile in these reactions (X = OR). The addition of an ethanol solution of HCl to a stirring ethanol solution of [Na(1,4-dioxane)$_{2.90}$][PCO] gave rise to two different products in the ^{31}P NMR spectrum: a triplet at –138.0 ppm ($^1J_{P-H}$ = 217 Hz), and a doublet at –61.9 ppm ($^1J_{P-H}$ = 241 Hz). These have been attributed to $H_2PC(O)OEt$ (**44**) and $HP\{C(O)OEt\}_2$ (**45**), shown in Figure 7.1. We believe the latter is formed in an acid-catalysed reaction of two molecules of **44**, with loss of PH_3, although this needs to be probed further. The analogous reaction of $[PCO]^-$ with triflic acid in *tert*-butanol afforded a triplet in the ^{31}P NMR spectrum at –132.3 ($^1J_{P-H}$ = 214 Hz), which has been assigned as $H_2PC(O)O^tBu$ (**47**), also shown in Figure 7.1.

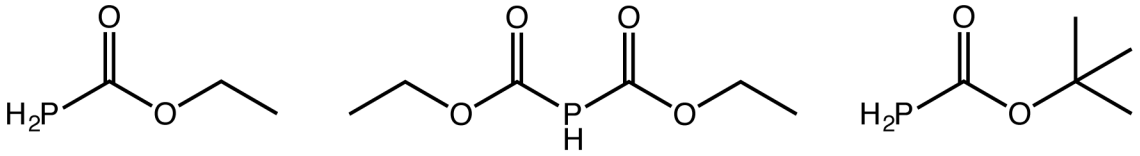

44 **45** **47**

Figure 7.1: Structures of **44**, **45** and **47**.

47 has been previously reported by the group of Becker, but was synthesised by a circuitous low-temperature route starting from bis(trimethylsilyl)phosphine.[3] Furthermore, the product was reported to be unstable, which we do not find via our simple synthesis. Similar species to **45** with different alkyl substituents have also been reported by Becker and co-workers.[4,5] In all cases, the reported spectroscopic data are consistent with those obtained in our systems. It is also interesting to note the similarity of the ^{31}P NMR data for **44** and **47** with the phosphinecarboxamides reported in this thesis, and likewise for **45** and the bis(carbamoyl)phosphine, **33**. Thus, both the chemical shift and $^{1}J_{P–H}$ coupling constants of the ^{31}P NMR resonances appear largely independent of the identity of the X fragment from Scheme 7.1, and are dominated by the $H_2PC(O)$ and $HP\{C(O)\}_2$ fragments, respectively.

We have obtained structural authentication for products derived from **45** and **47**. The addition of the [{(*p*-cymene)$RuCl_2$}$_2$] dimer to the ethanol solution of **44** and **45** gave a mixture of products by ^{31}P NMR spectroscopy, but single crystals grew slowly from the solution, and were characterised as [(*p*-cymene)$_2Ru_2Cl_2$(μ-Cl)(μ-P{C(O)OEt}$_2$)] (**46**). This contains a phosphido ligand bridging two ruthenium centres, and is analogous to the previously discussed product, **21**. This strongly suggests the prior formation of the [(*p*-cymene)$RuCl_2$(PH{C(O)OEt}$_2$)] complex, by analogy with the formation and subsequent decomposition of **20**. The deprotonation of **47** with potassium *tert*-butoxide in the presence of 18-crown-6 gave rise to single crystals of [K(18-crown-6)][**48**] (**48**: $[HPC(O)O^tBu]^-$). Both of these crystal structures are shown in Figure 7.2. Additional characterisation and

synthetic details for compounds **44**–**48** are provided in the Experimental section in Chapter 8.

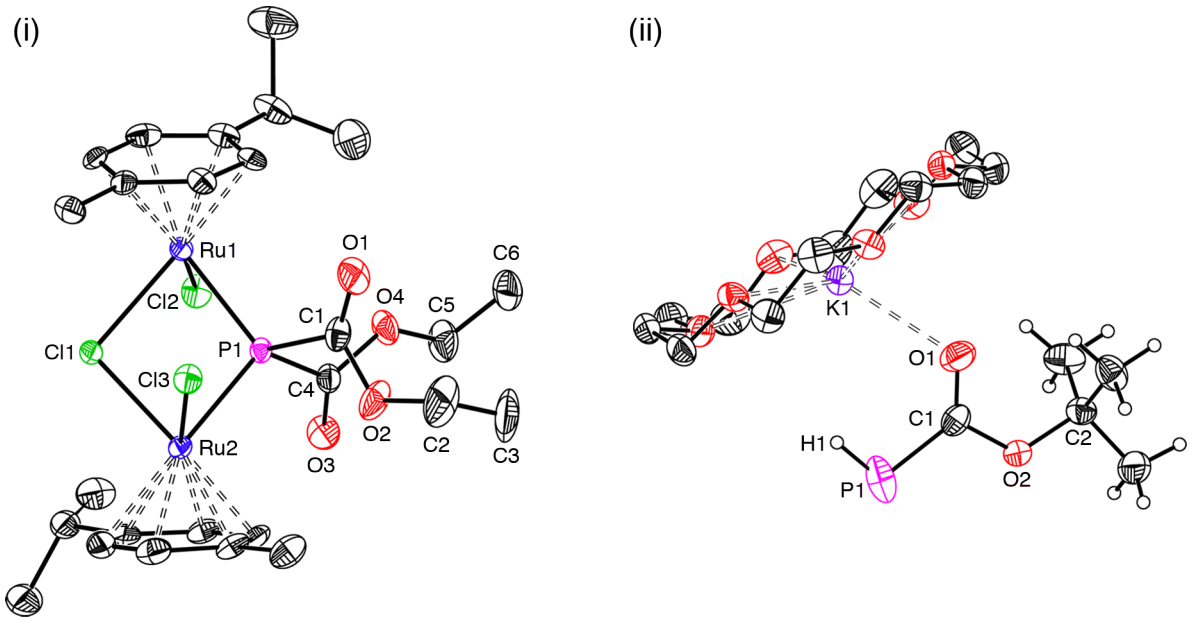

Figure 7.2: Molecular structures of: (i) **46** and (ii) [K(18-crown-6)][**48**]. Anisotropic displacement ellipsoids are set at 50% probability. Hydrogen atoms on the anion **48** are shown as spheres of arbitrary radii, all other hydrogen atoms are omitted for clarity.

It is worth noting that the reactions with alcohols do not proceed as efficiently as those with the primary amines, presumably due to the reduced number of X–H bonds required to generate the transition state in Figure 7.1. This is particularly true for the formation of **47**, where only a weak signal in the ^{31}P NMR spectrum is observed, which is consistent with the relatively poor formation of the *N*-*tert*-butylphosphinecarboxamide, **18**. Furthermore, the synthesis of the ethyl derivatives needs to be improved to target either **44** or **45** cleanly, instead of an intractable mixture of the two products. Finally, it has proved challenging to separate the desired products from the alcohol solutions in which they were synthesised. These are all hurdles that need to be overcome before this chemistry can become as useful and applicable as the phosphinecarboxamide chemistry. However, the research is very much in its infancy, and the preliminary evidence accrued so far does at least hint that the

reactions to afford carbonyl-bearing phosphines from the protonation of $[PCO]^-$ can become more general.

7.3 References

(1) Diemert, K.; Hahn, T.; Kuchen, W.; Mootz, D.; Poll, W.; Tommes, P. *Z. Naturforsch. B* **1995**, *50b*, 209–212.

(2) Puschmann, F. F.; Stein, D.; Heift, D.; Hendriksen, C.; Gal, Z. A.; Grützmacher, H.-F.; Grützmacher, H. *Angew. Chem. Int. Ed.* **2011**, *50*, 8420–8423.

(3) Becker, G.; Rössler, M.; Uhl, W. *Z. Anorg. Allg. Chem.* **1981**, *473*, 7–19.

(4) Becker, G.; Rössler, M.; Uhl, G. *Z. Anorg. Allg. Chem.* **1982**, *495*, 73–88.

(5) Becker, G.; Hübler, K.; Niemeyer, M.; Seidler, N.; Thinus, B. *Z. Anorg. Allg. Chem.* **1996**, *622*, 197–211.

Chapter 8
Experimental

8.1 General synthetic considerations

All reactions and product manipulations were carried out under an inert atmosphere of argon or dinitrogen using standard Schlenk or glovebox techniques (MBraun UNILab glovebox maintained at <0.1 ppm O_2 and <0.1 ppm H_2O) unless otherwise noted.

Tetrahydrofuran (THF; Fisher, HPLC grade) and 1,4-dioxane (Alfa Aesar, 99+%, stab. 5–10 ppm BHT) were distilled from a sodium/benzophenone mixture. Pyridine (Alfa Aesar, 99+%), 1,2-dichlorobenzene (1,2-DCB; Sigma Aldrich, anhydrous 99%) and 1,2-difluorobenzene (1,2-DFB; Fluorochem, 98%) were distilled from CaH_2. Acetonitrile (MeCN; Sigma Aldrich, CHROMASOLV® gradient grade for HPLC, ≥99.9%), *N*,*N*-dimethylformamide (DMF; Rathburn, peptide synthesis grade), dichloromethane (CH_2Cl_2, DCM; Sigma Aldrich, HPLC grade), 1,2-dimethoxyethane (DME; Sigma Aldrich, anhydrous, 99.5%), hexane (Sigma Aldrich, HPLC grade), diethyl ether (Et_2O; Fisher, pesticide residue grade), pentane (Sigma Aldrich, HPLC grade) and toluene (Sigma Aldrich, HPLC grade) were purified using an MBraun SPS-800 solvent system. d_8-THF (Eurisotop, >99.5%), d_5-pyridine (Eurisotop, >99.5%), d_7-DMF (Apollo Scientific, >99.5%), CD_2Cl_2 (Eurisotop, >99.5%) and $CDCl_3$ (Aldrich, 99.8%) were dried over CaH_2, vacuum distilled, and degassed before use. d_4-1,2-Dichlorobenzene (d_4-1,2-DCB; Alfa Aesar, 99% (isotopic)) was dried over activated 3 Å molecular sieves and degassed before use. All dry solvents were stored under argon in gas-tight ampoules. Additionally, THF, 1,4-dioxane, pyridine, 1,2-DCB, 1,2-DFB, DCM, hexane, Et_2O, pentane and toluene were stored over activated 3 Å molecular sieves. Deionised water was obtained from a Millipore Milli-Q machine.

The suppliers and purification procedures for commercially available chemicals are detailed in Table 8.1.

Table 8.1: Supplier and purification procedures for commercially available chemicals.

Reagent	Supplier	Purity	Purification
Potassium	Strem	99.95%	Used as received
Phosphorus	Sigma Aldrich	99.99%	Dried under vacuum
Sodium	Acros Organics	99.8%, oiled sticks	Washed with hexane, dried under vacuum
18-crown-6	Alfa Aesar	99%	Dried under vacuum with heating
2,2,2-crypt	VWR	99%	Dried under vacuum
CO	CK Gas	Unspecified	Used as received
Naphthalene	Sigma Aldrich	99+%	Sublimed under vacuum
$[W(CO)_6]$	Strem	99%	Sublimed under vacuum
$Me_3NO{\cdot}2H_2O$	Alfa Aesar	98+%	Used as received
KOCN	Sigma Aldrich	96%	Used as received
KSCN	Sigma Aldrich	≥99%	Used as received
CS_2	Sigma Aldrich	Anhydrous ≥99%	Used as received
DippNCO	Aldrich	98%	Used as received
$[NH_4][BF_4]$	Aldrich	≥97%	Dried under vacuum
$[NH_4][BPh_4]$	Sigma Aldrich	99%	Dried under vacuum
$[NH_4][Cl]$	Sigma	≥99.5%	Dried under vacuum
$[^{15}NH_4][Cl]$	Cambridge Isotope Laboratories, Inc.	^{15}N 99%	Dried under vacuum
NH_3	BOC	Anhydrous	Used as received
D_2O	Apollo	>99.92 atom % D	Used as received
$[\{(p\text{-cymene})RuCl_2\}_2]$	Johnson Matthey	Unspecified	Used as received
$[Mo(CO)_6]$	Acros Organics	98%	Sublimed under vacuum
1,5-Cyclooctadiene	Sigma Aldrich	99%	Dried over 3 Å molecular sieves
$[EtNH_3][Cl]$	Alfa Aesar	98+%	Dried under vacuum
H_2NCy	Alfa Aesar	98+%	Dried over CaH_2, vacuum distilled and degassed
H_2N^tBu	Sigma Aldrich	98%	Dried over CaH_2, vacuum distilled and degassed
H_2NPh	Sigma Aldrich	99.5+%	Dried over CaH_2, vacuum distilled and degassed
$HNEt_2$	Sigma Aldrich	99+%	Dried over CaH_2, vacuum

			distilled and degassed
$[H_2NMe(OMe)][Cl]$	Sigma Aldrich	98%	Recrystallised from ethanol, dried under vacuum
L-alanine	Alfa Aesar	99%	Dried under vacuum
Ethylenediamine	Alrich	99%	Refluxed over Na, distilled
Pyridinium triflate	Alfa Aesar	97%	Used as received
Triflic acid	Alfa Aesar	98+%	Degassed
(1-Chloromethyl)-4-vinylbenzene	Aldrich	90%	Used as received
Potassium phthalimide	Acros Organics	99%	Used as received
Hydrazine hydrate	Alfa Aesar	98+%	Used as received
HCl (aq. soln.)	Fisher	S.G. 1.18 (37%)	Used as received
KHMDS	Sigma Aldrich	95%	Used as received
Benzyl bromide	Aldrich	98%	Used as received
Iodomethane	Sigma Aldrich	99.5%	Used as received
H_2O_2 (aq. soln.)	Alfa Aesar	35% w/w	Used as received
HCl (EtOH soln.)	Fluka	~1.25 M	Used as received
EtOH	Sigma Aldrich	Absolute ≥99.8%	Refluxed over Mg/I_2, distilled
^{t}BuOH	Alfa Aesar	99%	Refluxed over Mg/I_2, distilled
KO^{t}Bu	Aldrich	≥98%	Used as received

The binary Zintl phase K_3P_7 was synthesised according to a previously reported synthetic procedure from a stoichiometric mixture of the elements heated to 600 ˚C for 72 hours in sealed niobium tubes.[1] The niobium vessels were sealed in silica ampoules under vacuum prior to heating in order to avoid oxidation of the metal at the high reaction temperatures.

$[Na(1,4\text{-dioxane})_x][\mathbf{1}]$ (x = 1.75–2.90),[2] $[W(CO)_5(MeCN)]$,[3] $[Mo(CO)_4(COD)]$,[4] bis(2,6-diisopropylphenyl)carbodiimide ($C(NDipp)_2$)[5] and (4-vinylphenyl)methanaminium chloride[6] were prepared according to literature procedures and stored at ambient temperatures in an inert atmosphere glovebox. Diphenylketene (Ph_2CCO)[7] and Brookhart's

acid ($[H(OEt_2)_2][BAr^F{}_4]$)[8] were prepared according to literature procedures and stored at –25 ˚C in an inert atmosphere glovebox.

8.2 Syntheses of compounds

8.2.1 Chapter 2 – The 2-phosphaethynolate anion and coordination chemistry of $[ECX]^-$ ligands (E = N, P; X = O, S)

8.2.1.1 [K(18-crown-6)][1] (1: $[PCO]^-$)

K_3P_7 (0.60 g, 1.80 mmol) and 18-crown-6 (1.42 g, 5.40 mmol) were weighed into a gas-tight ampoule (approx. volume 350 mL) and DMF (30 mL) was added to form a dark green/brown slurry. The ampoule was subsequently degassed and sealed under CO (1 atm). The reaction mixture was heated to 150 ˚C with stirring for 24 hours. The resulting dark red solution was filtered and the DMF removed *in vacuo*. The dark residue was extracted with degassed water and filtered. Solvent was removed from the filtrate and the remaining solid was washed with cold THF (0 ˚C, 3 × 2 mL) to yield a white solid (0.74 g, 38% yield by K). Colourless crystals suitable for single crystal X-ray diffraction were grown by slow diffusion of hexane (20 mL) into a THF (5 mL) solution of the product. ^{1}H NMR (500.0 MHz, d_8-THF): δ (ppm) 3.65 (s; 18-crown-6). ^{31}P{^{1}H} NMR (202.4 MHz, d_8-THF): δ (ppm) –396.8 (s). ^{13}C{^{1}H} NMR (125.8 MHz, d_8-THF): δ (ppm) 170.3 (d, $^1J_{C–P}$ = 62.0 Hz; P*C*O$^-$), 71.3 (s; 18-crown-6). ESI-MS (+ve ion mode, DMF): *m/z* = 665.7 {[K(18-crown-6)]$_2$[PCO]}$^+$. IR (cm^{-1}, Nujol mull): 1770 (ν(asym.)), ν(sym.) obscured by bands arising from 18-crown-6. Anal. Calcd for $C_{13}H_{24}KO_7P$: C, 43.09; H, 6.68. Found: C, 43.18; H, 6.67.

8.2.1.2 [K(18-crown-6)][2] (2: $[W(CO)_5(PCO)]^-$)

[K(18-crown-6)][**1**] (170 mg, 0.469 mmol) was added as a solid to a stirring yellow THF solution (30 mL) of $[W(CO)_5(MeCN)]$ (259 mg, 0.710 mmol). The solution darkened to an orange colour over the course of 30 minutes, then the volatiles were removed *in vacuo* affording an oily yellow/orange solid. This was washed with toluene (3 × 5 mL), then dried *in vacuo* to afford a yellow/orange solid of compositionally pure [K(18-crown-6)][**2**] (161 mg, yield 50% wrt. P). Orange crystals suitable for single crystal X-ray diffraction were grown by slow diffusion of hexane into a THF solution of [K(18-crown-6)][**2**]. ^{1}H NMR (500.0 MHz, d_8-THF): δ (ppm) 3.63 (s; 18-crown-6). ^{31}P NMR (202.4 MHz, d_8-THF): δ (ppm) –439.3 (s, sat. $^{1}J_{P–W}$ = 51.9 Hz). ^{13}C{^{1}H} NMR (125.8 MHz, d_8-THF): δ (ppm) 204.6 (d, $^{2}J_{C–P}$ = 9.4 Hz, sat. $^{1}J_{C–W}$ = 168.6 Hz; *trans*-*C*O), 202.1 (d, $^{2}J_{C–P}$ = –3.7 Hz, sat. $^{1}J_{C–W}$ = 125.4 Hz; *cis*-*C*O), 173.0 (d, $^{1}J_{C–P}$ = 94.7 Hz; P*C*O), 71.3 (s; 18-crown-6). IR (cm^{-1}, Nujol mull): ν(CO) 2047 (w, A_1), 1970 (vw, B_1), 1917 (s, E), 1835 (m, A_1); ν(PCO) 1835 (m, asym.). Anal. Calcd for $C_{18}H_{24}KPO_{12}W$: C, 31.50; H, 3.53. Found: C, 31.13; H, 3.53.

8.2.1.3 [K(2,2,2-crypt)][2]

[K(18-crown-6)][**1**] (288 mg, 0.796 mmol) was added as a solid to a stirring yellow THF solution (30 mL) of $[W(CO)_5(MeCN)]$ (290 mg, 0.796 mmol). After 20 minutes of stirring, 2,2,2-crypt (300 mg, 0.796 mmol) was added as a solid. The solution was left to stir for another 30 minutes, then the volatiles were removed *in vacuo* to leave an oily orange solid. This was washed with toluene (1 × 10 mL) and pentane (2 × 10 mL), then dried *in vacuo* to afford an orange solid (467 mg) of [K(18-crown-6)][**2**], but also a small amount of uncoordinated **1** as evidenced by ^{31}P NMR spectroscopy. The solid was redissolved in THF (10 mL), and $[W(CO)_5(MeCN)]$ (25 mg) was added and stirred for 30 minutes. An orange solid was obtained as before, this time of compositionally pure [K(2,2,2-crypt][**2**], but with a reduced yield due to the extensive washing. (220 mg, yield 28% wrt. P). Orange crystals

suitable for single crystal X-ray diffraction were grown by slow diffusion of hexane into a THF solution of [K(18-crown-6)][**2**]. ^{1}H NMR (500.0 MHz, d_8-THF): δ (ppm) 3.62 (s; 2,2,2-crypt), 3.58 (t, $^{3}J_{H–H}$ = 5 Hz; 2,2,2-crypt), 2.59 (t, $^{3}J_{H–H}$ = 5 Hz; 2,2,2-crypt). ^{31}P NMR (202.4 MHz, d_8-THF): δ (ppm) –441.0 (s, sat. $^{1}J_{P–W}$ = 51.8 Hz). ^{13}C{^{1}H} NMR (125.8 MHz, d_8-THF): δ (ppm) 204.6 (d, $^{2}J_{C–P}$ = 9.4 Hz, sat. $^{1}J_{C–W}$ = 167.8 Hz; *trans*-*C*O), 202.2 (d, $^{2}J_{C–P}$ = –3.7 Hz, sat. $^{1}J_{C–W}$ = 125.5 Hz; *cis*-*C*O), 173.0 (d, $^{1}J_{C–P}$ = 94.9 Hz; P*C*O), 71.5 (s; 2,2,2-crypt), 68.7 (s; 2,2,2-crypt), 55.1 (s; 2,2,2-crypt). IR (cm^{-1}, Nujol mull): ν(CO) 2052 (w, A_1), 1960 (vw, B_1), 1906 (s, E), 1850 (m, A_1); ν(PCO) 1841 (m, asym.). Anal. Calcd for $C_{24}H_{36}KN_2PO_{12}W$: C, 36.10; H, 4.54; N, 3.51. Found: C, 36.03; H, 4.50; N, 3.90.

8.2.1.4 [K(18-crown-6)][3] (3: [W(CO)$_5$(NCO)]$^-$)

[W(CO)$_6$] (20 mg, 0.0568 mmol), KOCN (4.6 mg, 0.0568 mmol) and 18-crown-6 (15.0 mg, 0.0568 mmol) were weighed into a small gas-tight ampoule and dissolved in THF (5 mL) to give a colourless solution. This was degassed once using the freeze-pump-thaw method. The solution was then stirred under a mercury lamp (150 W) for two hours. The bright yellow solution was then transferred to a small Schlenk tube and concentrated *in vacuo* down to 2 mL. Slow diffusion of hexane into this solution yielded yellow crystals suitable for single crystal X-ray diffraction. The crystals of [K(18-crown-6)][**3**] were subsequently isolated and dried *in vacuo* (28.2 mg, 74% crystalline yield). ^{1}H NMR (500.0 MHz, d_8-THF): δ (ppm) 3.63 (s; 18-crown-6). ^{13}C{^{1}H} NMR (125.8 MHz, d_8-THF): δ (ppm) 201.7 (s, sat. $^{1}J_{C–W}$ = 146.5 Hz; *trans*-*C*O), 199.6 (s, sat. $^{1}J_{C–W}$ = 127.8 Hz; *cis*-*C*O), 129.9 (br; N*C*O), 71.3 (s; 18-crown-6). IR (cm^{-1}, Nujol mull): ν(CO) 2064 (w, A_1), 1966 (vw, B_1), 1902 (s, E), 1823 (m, A_1); ν(NCO) 2241 (m, asym.). Anal. Calcd for $C_{18}H_{24}KNO_{12}W$: C, 32.30; H, 3.61; N, 2.09. Found: C, 32.13; H, 3.58; N, 2.32.

8.2.1.5 [K(2,2,2-crypt)][3]

$[W(CO)_5(MeCN)]$ (300 mg, 0.822 mmol), KOCN (44.5 mg, 0.548 mmol) and 2,2,2-crypt (206.4 mg, 0.548 mmol) were dissolved in THF (30 mL) and stirred for one hour to give a yellow/brown solution. Volatiles were removed *in vacuo* to give a yellow/brown solid. This was washed with toluene (3 × 10 mL) to afford a yellow solid (320 mg, yield 75%). Yellow crystals suitable for single crystal X-ray diffraction were grown by slow diffusion of hexane into a THF solution of [K(2,2,2-crypt)][**3**]. ^{1}H NMR (500.0 MHz, d_8-THF): δ (ppm) 3.61 (s; 2,2,2-crypt), 3.56 (t, $^{3}J_{H–H}$ = 5 Hz; 2,2,2-crypt), 2.58 (t, $^{3}J_{H–H}$ = 5 Hz; 2,2,2-crypt). $^{13}C\{^{1}H\}$ NMR (125.8 MHz, d_8-THF): δ (ppm) 201.7 (s, sat. $^{1}J_{C–W}$ = 146.6 Hz; *trans*-*C*O), 199.6 (s, sat. $^{1}J_{C–W}$ = 127.7 Hz; *cis*-*C*O), 130.2 (br; N*C*O), 71.5 (s; 2,2,2-crypt), 68.7 (s; 2,2,2-crypt), 55.1 (s; 2,2,2-crypt). IR (cm^{-1}, Nujol mull): ν(CO) 2062 (w, A_1), 1965 (vw, B_1), 1912 (s, E), 1831 (m, A_1); ν(NCO) 2240 (m, asym.). Anal. Calcd for $C_{24}H_{36}KN_3O_{12}W$: C, 36.89; H, 4.64; N, 5.38. Found: C, 36.93; H, 4.53; N, 5.38.

8.2.1.6 [K(18-crown-6)][4] (4: $[W(CO)_5(NCS)]^-$)

$[W(CO)_5(MeCN)]$ (308 mg, 0.844 mmol), KSCN (86 mg, 0.844 mmol) and 18-crown-6 (234 mg, 0.844 mmol) were stirred in THF (30 mL) and stirred for one hour to give a yellow solution with undissolved white solid. EtOH (30 mL) was added, and this gave the desired yellow solution with no precipitate. This was left to stir for one further hour at room temperature. Volatiles were removed *in vacuo* to give a yellow solid. This was washed with toluene (1 × 20 mL) to afford a yellow solid (396 mg, yield 65%). Yellow crystals suitable for single crystal X-ray diffraction were grown by slow diffusion of hexane into a THF solution of [K(18-crown-6)][**4**]. ^{1}H NMR (500.0 MHz, d_8-THF): δ (ppm) 3.65 (s; 18-crown-6). $^{13}C\{^{1}H\}$ NMR (125.8 MHz, d_8-THF): δ (ppm) 201.3 (s, sat. $^{1}J_{C–W}$ = 147.7 Hz; *trans*-*C*O), 198.8 (s, sat. $^{1}J_{C–W}$ = 128.3 Hz; *cis*-*C*O), 139.6 (br; N*C*S), 71.4 (s; 18-crown-6). IR (cm^{-1}, Nujol mull): ν(CO) 2065 (w, A_1), 1980 (vw, B_1), 1906 (s, E), 1851 (m, A_1); ν(NCS)

2106 (m, asym.). Anal. Calcd for $C_{18}H_{24}KNO_{11}SW$: C, 31.54; H, 3.53; N, 2.04. Found: C, 31.50; H, 3.54; N, 2.02.

8.2.1.7 [K(18-crown-6)][5] (5: [PCS]$^-$)

[K(18-crown-6)][**1**] (30 mg, 0.083 mmol) was dissolved in 1,2-DCB (5 mL) to give a yellow solution. CS_2 (5 μL, 0.083 mmol) was added via a microsyringe and stirred for 30 minutes to give an orange solution. The volatiles were removed *in vacuo* to yield an orange solid. This was redissolved in 1,2-DCB (2 mL) and the volatiles subsequently removed *in vacuo* again to yield a free-flowing orange solid (31.2 mg, 99% yield). Crystals suitable for single crystal X-ray diffraction were grown by slow diffusion of hexane into a 1,2-DFB solution of [K(18-crown-6)][**5**]. ^{1}H NMR (499.9 MHz, d_4-1,2-DCB): δ (ppm) 3.40 (s; 18-crown-6). ^{31}P NMR (202.4 MHz, d_4-1,2-DCB): δ (ppm) –118.0 (s). ^{13}C{^{1}H} NMR (125.8 MHz, d_4-1,2-DCB): δ (ppm) 191.3 (d, $^1J_{C–P}$ = 20.7 Hz; P*C*S), 70.2 (s; 18-crown-6). Anal. Calcd. for $C_{13}H_{24}KO_6PS$: C, 41.26; H, 6.39. Found: C, 40.67; H, 6.18.

8.2.1.8 [Na(18-crown-6)][5]

[Na(dioxane)$_{2.69}$][PCO] (100 mg, 0.313 mmol) and 18-crown-6 (82.9 mg, 0.313 mmol) were dissolved in 1,2-DCB (5 mL) to give a yellow solution. CS_2 (19 μL, 0.313 mmol) was added via a microsyringe and stirred overnight to give an orange solution. ^{31}P NMR spectroscopy of a 0.5 mL aliquot showed quantitative conversion to [Na(18-crown-6)][PCS]. The volatiles were removed *in vacuo* to yield an orange solid. The solid was redissolved in 1,2-DCB (5 mL) and used to obtain crystals suitable for single crystal X-ray diffraction, which were grown by slow diffusion of hexane into the 1,2-DCB solution of [K(18-crown-6)][PCS] in a fridge at 4 °C. ^{31}P NMR (202.4 MHz, 1,2-DCB, 298 K): δ (ppm) –119.4 (s).

8.2.1.9 [K(18-crown-6)][6] (6a: [W(CO)$_5$(PCS)]$^-$; 6b: [W(CO)$_5$(SCP)]$^-$)

A 1,2-DFB solution (30 mL) of [K(18-crown-6)][**5**] (209 mg, 0.552 mol) was added to a stirring yellow 1,2-DFB solution (20 mL) of [W(CO)$_5$(MeCN)] (201 mg, 0.552 mmol) at 0 ˚C and slowly allowed to warm up to room temperature. The solution went dark over the course of an hour. The reaction was monitored by ^{31}P NMR spectroscopy, and showed the growth of two new resonances in addition to that of free **5**, which have been attributed to P-bound **6a** and S-bound **6b**. After four days at room temperature there were no signals in the ^{31}P NMR spectrum. Single crystals were grown by slow diffusion of hexane into a 1,2-DFB solution of a mixture of [K(18-crown-6)][**6a**] and [K(18-crown-6)][**6b**], but the crystals exhibited extensive crystallographic disorder, which precluded detailed analysis. ^{31}P NMR (202.4 MHz, 1,2-DFB): δ (ppm) –92.9 (s; **6b**), –192.6 (s, sat. $^1J_{P–W}$ = 46.0 Hz; **6a**).

8.2.2 Chapter 3 – Cycloaddition chemistry of the 2-phosphaethynolate anion

8.2.2.1 [K(18-crown-6)][7] (7: [P(C(O))$_2$CPh$_2$]$^-$)

[K(18-crown-6)][**1**] (300 mg, 0.828 mmol) was dissolved in pyridine (5 mL) giving rise to an orange solution. Diphenylketene (Ph$_2$CCO, 145 μL, 0.828 mmol) was added, after which the reaction mixture darkened immediately. The mixture was left stirring overnight. Another half an equivalent of Ph$_2$CCO (73 μL, 0.424 mmol) was added the following morning and the mixture left stirring for an additional hour. The solvent was subsequently removed under a dynamic vacuum and the remaining orange oil washed with diethyl ether (3 × 5 mL), affording a pale orange solid. This was further washed with cold THF (0 ˚C, 3 × 2 mL) to yield a pale orange solid. Crystals suitable for single crystal X-ray diffraction were grown from slow diffusion of hexane (20 mL) into a THF (5 mL) solution of [K(18-crown-6)][**7**]. ^{1}H NMR (500.0 MHz, d_8-THF): δ (ppm) 7.55 (m, 4H; *ortho*-Ph), 7.08 (m, 4H; *meta*-Ph), 6.97 (m, 2H; *para*-Ph), 3.56 (s, 24H; 18-crown-6). ^{31}P{^{1}H} NMR (202.4 MHz, d_8-

THF): δ (ppm) 165.7 (s). $^{13}C\{^{1}H\}$ NMR (125.8 MHz, d_8-THF): δ (ppm) 225.1 (d, $^{1}J_{C–P}$ = 40 Hz; *C*O), 145.3 (d, $^{3}J_{C–P}$ = 5 Hz; *ipso*-Ph), 128.5 (s; Ph), 127.8 (s; Ph), 125.4 (s; Ph), 95.7 (d, $^{2}J_{C–P}$ = 16 Hz; *C*Ph_2), 71.2 (s; 18-crown-6). ESI-MS (−ve ion mode, DMF): *m/z* = 253.4 $[P(C(O))_2CPh_2]^-$. ESI-MS (+ve ion mode, DMF): *m/z* = 859.4 $\{[K(18\text{-crown-}6)]_2[P(C(O))_2CPh_2]\}^+$. IR ($cm^{-1}$, Nujol mull): ν(CO) 1598, 1557. Anal. Calcd for $C_{27}H_{34}KO_8P$: C, 58.26; H, 6.16. Found: C, 57.56; H, 6.01.

8.2.2.2 [K(18-crown-6)][8] (8: [PC(O)(CNDipp)NDipp]$^-$)

[K(18-crown-6)][**1**] (34 mg, 0.094 mmol) and $C(NDipp)_2$ (34 mg, 0.094 mmol) were dissolved in d_5-pyridine (0.5 mL) in an air-tight NMR tube to form a yellow solution. The reaction was monitored by ^{31}P NMR spectroscopy. After four hours all of the $[PCO]^-$ had been consumed and the solution had turned orange. The reaction mixture was transferred to a Schlenk tube, and hexane (10 mL) added to precipitate out a yellow solid. The colourless solution was removed by filtration and the remaining solid was dried under vacuum (41.4 mg, 61% yield). Crystals suitable for single crystal X-ray diffraction were grown from slow diffusion of hexane (20 mL) into a THF (5 mL) solution of [K(18-crown-6)][**8**]. ^{1}H NMR (500.0 MHz, d_8-THF): δ (ppm) 7.09 (t, $^{3}J_{H–H}$ = 8 Hz, 1H; *para*-Dipp), 7.03 (d, $^{3}J_{H–H}$ = 8 Hz, 2H; *meta*-Dipp), 6.86 (t, $^{3}J_{H–H}$ = 8 Hz, 2H; *meta*-Dipp), 6.71 (t, $^{3}J_{H–H}$ = 8 Hz, 1H; *para*-Dipp), 3.63 (sept, $^{3}J_{H–H}$ = 7 Hz, 2H; C*H*$(CH_3)_2$), 3.57 (sept, $^{3}J_{H–H}$ = 7 Hz, 2H; C*H*$(CH_3)_2$), 3.53 (s, 24H; 18-crown-6), 1.26 (d, $^{3}J_{H–H}$ = 7 Hz, 6H; CH(C*H*$_3)_2$), 1.22 (d, $^{3}J_{H–H}$ = 7 Hz, 6H; CH(C*H*$_3)_2$), 1.17 (br d, 12H; two sets of overlapping CH(C*H*$_3)_2$ doublets). $^{31}P\{^{1}H\}$ NMR (202.4 MHz, d_8-THF): δ (ppm) 18.6 (s). $^{13}C\{^{1}H\}$ NMR (125.8 MHz, d_8-THF): δ (ppm) 196.6 (d, $^{1}J_{C–P}$ = 42 Hz; *C*=O), 178.2 (d, $^{1}J_{C–P}$ = 48 Hz; C=N), 149.0 (d, $^{3}J_{C–P}$ = 3 Hz; *ipso*-Dipp), 148.8 (s; Dipp), 138.7 (s; Dipp), 133.2 (d, $^{3}J_{C–P}$ = 3 Hz; *ipso*-Dipp), 125.5 (s; Dipp), 120.9 (s; Dipp), 120.5 (s; Dipp), 119.7 (s; Dipp), 69.2 (s; 18-crown-6), 27.8 (s; *C*H$(CH_3)_2$), 26.4 (s; *C*H$(CH_3)_2$), 23.4 (s; CH(*C*H$_3)_2$), 23.0 (br s; overlapping CH(*C*H$_3)_2$), 22.4 (s;

CH(CH$_3$)$_2$). ESI-MS (−ve ion mode, DMF): *m/z* 421.9 [PC(O)(CNDipp)NDipp]$^-$. ESI-MS (+ve ion mode, DMF): *m/z* 1030.4 {[K(18-crown-6)]$_2$[PC(O)(CNDipp)NDipp]}$^+$. IR (cm^{-1}, Nujol mull): ν(CO) 1599, ν(CN) 1579. Anal. Calcd for $C_{38}H_{58}KN_2O_7P$: C, 62.96; H, 8.06; N, 3.86. Found: C, 61.61; H, 7.68; N, 4.32.

8.2.2.3 [K(18-crown-6)][9] (9: [P{C(O)N(Dipp)C(O)N(Dipp)}$_2$]$^-$)

2,6-Diisopropylphenyl isocyanate (200 μL, 0.936 mmol) was added to a stirring pyridine solution (10 mL) of [K(18-crown-6)][**1**] (84.8 mg, 0.234 mmol). We previously determined that an excess of isocyanate was required for the reaction to go to completion. The pale yellow solution was left stirring at room temperature, and gradually turned a dark orange colour overnight. The solution was analysed, and showed relatively clean formation of the spirophosphoranide [K(18-crown)][**9**] by ^{31}P NMR spectroscopy. Crystals suitable for single crystal X-ray diffraction were obtained by slow diffusion of hexane (20 mL) into a pyridine solution (5 mL) of [K(18-crown-6)][**9**]. ^{31}P{^{1}H} NMR (202.4 MHz, d_5-pyridine): δ (ppm) –42.7 (s; **9**). ^{13}C{^{1}H} NMR (125.7 MHz, d_5-pyridine): δ (ppm) 179.3 (d, $^1J_{C–P}$ = 11 Hz; PC(O)), 156.8 (d, $^2J_{C–P}$ = 2 Hz; PC(O)NC(O)), other resonances were ambiguous due to presence of other species. ESI-MS (–ve ion mode, DMF): *m/z* = 843.2 [P{C(O)N(Dipp)C(O)N(Dipp)}$_2$]$^-$. ESI-MS (+ve ion mode, DMF): *m/z* = 1449.4 {[K(18-crown-6)]$_2$[[P{C(O)N(Dipp)C(O)N(Dipp)}$_2$]}$^+$.

8.2.2.4 [K(18-crown-6)][10] (10: [PC(O)N(Dipp)C(O)N(Dipp)]$^-$)

The volume of the orange pyridine solution from [K(18-crown-6)][**9**] was reduced from 10 mL to 2 mL *in vacuo*, then diethyl ether (10 mL) was added to precipitate out an off-white solid. Electrospray ionisation mass spectrometry of a DMF solution and ^{31}P NMR spectroscopic analysis of a THF solution of this solid showed the presence of the five-membered ring [K(18-crown-6)][**10**] (approx. 20%) in addition to [K(18-crown-6)][**9**] (approx. 80%). Crystals suitable for single crystal X-ray diffraction were obtained by slow

diffusion of hexane (20 mL) into a pyridine solution (5 mL) of the reaction mixture. $^{31}P\{^{1}H\}$ NMR (202.4 MHz, THF): δ (ppm) 120.9 (s; **10**), –42.7 (s; **9**). ESI-MS (–ve ion mode, DMF): *m/z* = 409.3 $[PC(O)N(Dipp)N(Dipp)]^{-}$, 437.0 $[PC(O)N(Dipp)C(O)N(Dipp)]^{-}$, 913.2 $\{K[PC(O)N(Dipp)C(O)N(Dipp)]_2\}^{-}$. ESI-MS (+ve ion mode, DMF): *m/z* = 1044.4 $\{[K(18\text{-crown-}6)]_2[PC(O)N(Dipp)C(O)N(Dipp)]\}^{+}$.

8.2.3 Chapter 4 – Phosphinecarboxamide and its coordination complexes

8.2.3.1 $H_2PC(O)NH_2$ (11)

$[Na(1,4\text{-dioxane})_{1.75}][\mathbf{1}]$ (12.75 g, 54.0 mmol) and $[NH_4][BF_4]$ (5.66 g, 54.0 mmol) were added to a Schlenk flask in an inert atmosphere glovebox. Ammonia (approx. 50 mL) was condensed into the flask at –78 °C and the resulting pale yellow solution was stirred for one hour, after which it was allowed to slowly warm to room temperature under a flow of argon over the course of two hours. 1,4-Dioxane was removed from the solid under dynamic vacuum at 15 °C to minimise product loss. **11** was isolated as colourless crystals by sublimation, at 2×10^{-2} mbar and 50 °C. Isolated crystalline yield 1.55 g (37%). Crystals suitable for single crystal X-ray diffraction were grown by sublimation. Melting point: 64 °C. ^{1}H NMR (500.0 MHz, d_5-pyridine): δ (ppm) 9.05 (br s, 1H; N*H*H), 8.57 (br s, 1H; NH*H*), 3.82 (d, 2H, $^{1}J_{H-P}$ = 209 Hz; PH_2). $^{1}H\{^{31}P\}$ NMR (500.0 MHz, d_5-pyridine): δ (ppm) 3.82 (s, 2H; PH_2), the other resonances unchanged. ^{31}P NMR (202.4 MHz, d_5-pyridine): δ (ppm) –134.4 (td, $^{1}J_{P-H}$ = 209 Hz, $^{3}J_{P-H}$ = 12 Hz). $^{31}P\{^{1}H\}$ NMR (202.4 MHz, d_5-pyridine): δ (ppm) –134.4 (s). $^{13}C\{^{1}H\}$ NMR (125.7 MHz, d_5-pyridine): δ (ppm) 175.8 (d, $^{1}J_{C-P}$ = 8 Hz). FI-MS: Calcd: *m/z* = 77.0031. Found: *m/z* = 77.0027. IR (cm^{-1}, Nujol mull): ν 1134 (C–N stretch), 1585 (NH_2 bending), 1647 (C=O stretch), 2320 and 2334 (PH_2 stretch), 3123 and 3311 (NH_2 stretch). Anal. Calcd for CH_4NOP: C, 15.54; H, 5.24; N, 18.19. Found: C, 15.63; H, 5.22; N, 18.21.

8.2.3.2 $D_2PC(O)ND_2$ (11-D_4)

[K(18-crown-6)][**1**] (30 mg, 0.08 mmol) and [ND_4][Cl] (4.8 mg, 0.08 mmol) were dissolved in pyridine (0.5 mL) in a gas-tight NMR tube. A combination of PD_2, PHD and PH_2 groups can be seen in the ^{31}P NMR spectra due to incomplete deuteration of the starting material [ND_4][Cl]. ^{2}H NMR (76.7 MHz, pyridine): δ (ppm) 9.56 (br s; N*D*), 8.48 (br s; N*D*), 3.99 (d, $^{1}J_{D–P}$ = 31 Hz; P*D*$_2$). ^{31}P{^{1}H} NMR (202.4 MHz, pyridine): δ (ppm) –134.4 (s; *P*H_2), –135.5 (t, $^{1}J_{P–D}$ = 31 Hz; *P*HD), –136.5 (quint, $^{1}J_{P–D}$ = 31 Hz; *P*D_2). ^{31}P NMR (202.4 MHz, pyridine): δ (ppm) –134.4 (t, $^{1}J_{P–H}$ = 211 Hz; *P*H_2), –135.5 (dt, $^{1}J_{P–H}$ = 209 Hz, $^{1}J_{P–D}$ = 31 Hz; *P*HD), –136.5 (quint, $^{1}J_{P–D}$ = 31 Hz; *P*D_2).

8.2.3.3 $H_2PC(O)^{15}NH_2$ (11-^{15}N)

[K(18-crown-6)][**1**] (30 mg, 0.08 mmol) and [$^{15}NH_4$][Cl] (4.5 mg, 0.08 mmol) were dissolved in d_5-pyridine (0.5 mL) in a gas-tight NMR tube. ^{1}H NMR (500.0 MHz, d_5-pyridine): δ (ppm) 9.92 (d, 1H, $^{1}J_{H–N}$ = 89 Hz; N*H*H), 8.49 (dd, 1H, $^{1}J_{H–N}$ = 85 Hz, $^{3}J_{H–P}$ = 8 Hz; NH*H*), 4.06 (d, 2H, $^{1}J_{H–P}$ = 209 Hz; P*H*$_2$). ^{31}P{^{1}H} NMR (202.4 MHz, d_5-pyridine): δ (ppm) −135.0 (d, $^{2}J_{P–N}$ = 12 Hz).

8.2.3.4 [$(H_2PC(O)NH_2)_2$(18-crown-6)] (12)

[K(18-crown-6)][**1**] (120 mg, 0.330 mmol) and [NH_4][BPh_4] (112 mg, 0.330 mmol) were stirred in d_5-pyridine (0.5 mL) for 10 minutes in a gas-tight ampoule, yielding a pale yellow suspension. Trap-to-trap distillation afforded a colourless solution of **11** in d_5-pyridine. Crystals of **12** suitable for single crystal X-ray diffraction were grown by slow diffusion of hexane (20 mL) into a THF solution (0.5 mL) containing **11** and half of an equivalent of 18-crown-6. Crystalline yield 29 mg (42%). NMR data same as **11**, with the addition of resonances corresponding to 18-crown-6 at 3.66 ppm and 70.3 ppm in the ^{1}H and ^{13}C{^{1}H} NMR spectra, respectively. IR (cm^{-1}, Nujol mull): ν 1104 (C–N stretch), 1607 (NH_2

bending), 1650 (C=O stretch), 2302 and 2353 (PH_2 stretch), 3318 and 3406 (NH_2 stretch). Anal. Calcd for $C_7H_{16}NO_4P$: C, 40.19; H, 7.71; N, 6.70. Found: C, 40.76; H, 7.71; N, 6.62.

8.2.3.5 [(*p*-cymene)$RuCl_2(H_2PC(O)NH_2)$] (13)

A CH_2Cl_2 solution (15 mL) of **11** (26.4 mg, 0.343 mmol) was added to a stirring CH_2Cl_2 solution (15 mL) of [{(*p*-cymene)$RuCl_2$}$_2$] (105 mg, 0.171 mmol) and stirred for one hour. The orange solution was concentrated down to 10 mL *in vacuo*, followed by addition of an excess of diethyl ether (80 mL) to yield an orange precipitate. The solution was filtered off and the remaining solid dried *in vacuo*. Yield 101 mg (77%). No crystals suitable for single crystal X-ray diffraction could be grown despite repeated attempts. ^{1}H NMR (499.9 MHz, CD_2Cl_2): δ (ppm) 7.66 (br s, 1H; N*H*), 5.78 (br d, $^3J_{H–P}$ = 24.5 Hz, 1H; N*H*), 5.52 (d, $^3J_{H–H}$ = 5.6 Hz, 2H; H_{ar}), 5.37 (d, $^3J_{H–H}$ = 6.0 Hz, 2H; H_{ar}), 5.22 (d, $^1J_{H–P}$ = 380 Hz, 2H; PH_2), 2.74 (sept, $^3J_{H–H}$ = 6.9 Hz, 1H; CH(CH_3)$_2$), 2.13 (s, 3H; $C_{ar}CH_3$), 1.19 (d, $^3J_{H–H}$ = 6.9 Hz, 6H; CH(CH_3)$_2$). ^{1}H{^{31}P} NMR (499.9 MHz, CD_2Cl_2): δ (ppm) 5.78 (br s, 1H; N*H*), 5.22 (s, 2H; PH_2), other resonances unchanged. ^{31}P NMR (162.0 MHz, CD_2Cl_2): δ (ppm) –35.9 (td, $^1J_{P–H}$ = 380 Hz, $^3J_{P–H}$ = 24.5 Hz). ^{31}P{^{1}H} NMR (162.0 MHz, CD_2Cl_2): δ (ppm) –35.9 (s). ^{13}C{^{1}H} NMR (125.7 MHz, CD_2Cl_2): δ (ppm) 167.8 (d, $^1J_{C–P}$ = 50 Hz; H_2PC(O)), 107.9 (d, $J_{C–P}$ = 2.4 Hz; CH(CH_3)$_2C_{ar}$), 103.2 (d, $J_{C–P}$ = 2.6 Hz; CH_3C_{ar}), 87.2 (d, $J_{C–P}$ = 4.7 Hz; HC_{ar}), 87.0 (d, $J_{C–P}$ = 3.6 Hz; HC_{ar}), 31.6 (s; *C*H(CH_3)$_2$), 22.5 (s; CH(*C*H_3)$_2$), 18.9 (s; $C_{ar}CH_3$). EI-MS: Parent peak not observed (*m/z* = 382.9547), only *p*-cymene and fragmentation thereof; *m/z* = 134.1050 $(C_{10}H_{14})^+$, 119.0718 $(C_9H_{11})^+$, 91.0505 $(C_7H_7)^+$. Anal. Calcd for $C_{11}H_{18}Cl_2NOPRu$: C, 34.48; H, 4.73; N, 3.66. Found: C, 34.41; H, 4.75; N 3.76.

8.2.3.6 $[W(CO)_5(H_2PC(O)NH_2)]$ (14)

$[W(CO)_6]$ (32 mg, 0.090 mmol) was dissolved in d_8-THF (1 mL) and transferred to an ampoule equipped with a gas-tight tap. The ampoule was degassed via the freeze-pump-

thaw method. The solution was stirred under a mercury lamp (150 W) for one hour to afford a bright yellow solution. The atmosphere was replaced with argon, and the solution cooled to –78 °C to precipitate unreacted [$W(CO)_6$]. The bright yellow solution was transferred to an NMR tube containing a solid sample of **11** (7 mg, 0.090 mmol) and monitored by NMR spectroscopy. The THF solution of **14** is unstable with respect to reduced pressure, so isolation of a solid was not possible. All attempts to grow crystals suitable for single crystal X-ray diffraction were unsuccessful. ^{1}H NMR (500.0 MHz, d_8-THF): δ (ppm) 7.63 (br, 1H; N*H*), 7.40 (m, 1H; N*H*), 5.22 (d, $^{1}J_{H–P}$ = 347 Hz, 2H; PH_2). ^{31}P NMR (202.4 MHz, d_8-THF): δ (ppm) –103.1 (td, $^{1}J_{P–H}$ = 347, $^{3}J_{P–H}$ = 21 Hz, sat. $^{1}J_{P–W}$ = 216 Hz). ^{31}P{^{1}H} NMR (202.4 MHz, d_8-THF): δ (ppm) –103.1 (s, sat. $^{1}J_{P–W}$ = 216 Hz). ^{13}C{^{1}H} NMR (125.8 MHz, d_8-THF): δ (ppm) 196.2 (d, $^{2}J_{C–P}$ = 7 Hz, sat. $^{1}J_{C–W}$ = 126 Hz; *trans*-*C*O), 192.5 (s, no coupling to *cis*-P observed, sat. $^{1}J_{C–W}$ = 127 Hz; *cis*-*C*O), 168.4 (d, $^{1}J_{C–P}$ = 54 Hz; H_2PC(O)NH_2). IR (cm^{-1}, THF solution): ν(CO) 2077, 1968, 1926, 1882, 1645 (CO of H_2P(CO)NH_2).

8.2.3.7 [$Mo(CO)_4(H_2PC(O)NH_2)_2$] (15)

11 (100 mg, 1.30 mmol) and [$Mo(CO)_4$(COD)] (205 mg, 0.65 mmol) were dissolved in DCM (3 mL) and transferred to an ampoule equipped with a gas-tight tap. The solution was stirred overnight to afford a pale yellow precipitate and a red oil. The pale precipitate was dissolved in a further 10 mL of DCM and separated from the red oil by filtration. The pale yellow filtrate was washed with DCM (3 × 5 mL) to remove COD and dried under dynamic vacuum for a further four hours to afford a pale yellow powder. Yield 63 mg (17.4%). ^{1}H NMR (500.0 MHz, CD_2Cl_2): δ (ppm) 6.71 (br, 2H; N*H*), 5.92 (br d, 2H; N*H*), 5.00 (m, $^{1}J_{H–P}$ = 328 Hz, $^{3}J_{H–P}$ = 9 Hz, 4H; PH_2). ^{1}H{^{31}P} NMR (500.0 MHz, CD_2Cl_2): δ (ppm) 5.00 (s, 2H; PH_2), other resonances unchanged. ^{31}P NMR (202.4 MHz, CD_2Cl_2): δ (ppm) –64.9 (m, $^{1}J_{P–H}$ = 328 Hz, $^{2}J_{P–P}$ = –25 Hz, $^{3}J_{P–H}$ = 18 Hz, $^{3}J_{P–H}$ = 9 Hz). ^{31}P{^{1}H} NMR (202.4 MHz, CD_2Cl_2): δ (ppm) –64.9 (s). ^{13}C{^{1}H} NMR (125.8 MHz, CD_2Cl_2): δ (ppm) 212.1 (d, $^{2}J_{C–P}$ =

19 Hz, no coupling to *cis*-P observed; *trans*-*C*O), 206.8 (t, $^{2}J_{C–P}$ = 9 Hz; *cis*-*C*O), 171.9 (d, $^{1}J_{C–P}$ = 43 Hz; $H_2PC(O)NH_2$). IR (cm^{-1}, Nujol mull): ν(CO) 2040, 1930, 1866, 1639 (CO of $H_2PC(O)NH_2$). Anal. Calcd for $C_6H_8MoN_2O_6P_2$: C, 19.90; H, 2.23; N, 7.74. Found: C, 20.12; H, 2.38; N, 7.48.

8.2.4 Chapter 5 – *N*-Functionalised phosphinecarboxamides

8.2.4.1 $H_2PC(O)NHEt$ (16)

[K(18-crown-6)][**1**] (20 mg, 0.06 mmol) and [$EtNH_3$][Cl] (5 mg, 0.06 mmol) were dissolved in d_8-THF (0.5 mL) in a gas-tight NMR tube. The crude reaction mixture was monitored by ^{1}H and ^{31}P NMR spectroscopy to ensure full conversion of the ammonium salt to **16**. The solution was distilled using a trap-to-trap distillation at 50 °C under reduced pressure to give **16** in solution. ^{1}H NMR (499.9 MHz, d_8-THF): δ (ppm) 7.47 (br, 1H; N*H*), 3.45 (d, $^{1}J_{H–P}$ = 205 Hz, 2H; PH_2), 3.19 (m, 2H; CH_2), 1.07 (t, $^{3}J_{H–H}$ = 7 Hz, 3H; CH_3). ^{1}H{^{31}P} NMR (499.9 MHz, d_8-THF): δ (ppm) 3.45 (s, 2H; PH_2), other resonances unchanged. ^{31}P NMR (202.4 MHz, d_8-THF): δ (ppm) –136.7 (t, $^{1}J_{P–H}$ = 205 Hz). ^{31}P{^{1}H} NMR (202.4 MHz, d_8-THF): δ (ppm) –136.7 (s). ^{13}C{^{1}H} NMR (125.8 MHz, d_8-THF): δ (ppm) 171.3 (d, $^{1}J_{C–P}$ = 6 Hz; H_2PC(O)), 35.4 (s; CH_2), 15.3 (s; CH_3). IR (cm^{-1}, d_8-THF): ν(CO) 1651.

8.2.4.2 $H_2PC(O)NHCy$ (17)

A pyridine solution (100 mL) of [$Na(1,4\text{-dioxane})_{2.69}$][**1**] (7.42 g, 23.3 mmol) was added to a stirring pyridine solution (100 mL) of H_2NCy (1.67 mL, 14.5 mmol) and pyridinium triflate (5.00 g, 21.8 mmol). Volatiles were removed *in vacuo* and **17** extracted in toluene (100 mL). Solvent was removed under a dynamic vacuum to yield **17** as an off-white powder (1.40 g). A second toluene extraction (100 mL) yielded a further 380 mg of product. Combined yield 1.78 g (77% wrt. amine). ^{1}H NMR (499.9 MHz, d_8-THF): δ (ppm) 7.33 (br,

1H; N*H*), 3.72 (m, 1H; NC*H*), 3.44 (d, $^{1}J_{H–P}$ = 206 Hz, 2H; PH_2), 1.08–1.89 (10H; Cy). $^{1}H\{^{31}P\}$ NMR (499.9 MHz, d_8-THF): δ (ppm) 3.44 (s, 2H; PH_2), other resonances unchanged. ^{31}P NMR (202.4 MHz, d_8-THF): δ (ppm) –135.8 (t, $^{1}J_{P–H}$ = 206 Hz). $^{31}P\{^{1}H\}$ NMR (202.4 MHz, d_8-THF): δ (ppm) –135.8 (s). $^{13}C\{^{1}H\}$ NMR (125.8 MHz, d_8-THF): δ (ppm) 170.7 (d, $^{1}J_{C–P}$ = 6 Hz; H_2PC(O)), 49.9 (s; NCH), 34.1 (s; Cy), 26.7 (s; Cy), 26.2 (s; Cy). FI-MS: Calcd: *m/z* = 159.0813. Found: *m/z* = 159.0818. M+H also observed at 160.0930. IR (cm^{-1}, THF): ν(CO) 1644. IR (cm^{-1}, Nujol mull): ν(CO) 1607. Anal. Calcd for $C_7H_{14}NOP$: C, 52.82; H, 8.87; N, 8.80. Found: C, 52.12; H, 8.65; N, 8.51.

8.2.4.3 $H_2PC(O)NH^tBu$ (18)

[K(18-crown-6)][**1**] (51 mg, 0.14 mmol) and H_2N^tBu (6 μL, 0.06 mmol) were dissolved in d_8-THF (0.5 mL) in a gas-tight NMR tube. HOTf (10 μL, 0.11 mmol) was added in 2 μL portions and the reaction monitored by NMR spectroscopy until all the free amine had been consumed. The solution was transferred *via* trap-to-trap distillation at room temperature under reduced pressure to give a solution of **18**. ^{1}H NMR (400.1 MHz, d_8-THF): δ (ppm) 7.05 (br, 1H; N*H*), 3.44 (d, $^{1}J_{H–P}$ = 206 Hz, 2H; PH_2), 1.30 (s, 9H; C(CH_3)$_3$). $^{1}H\{^{31}P\}$ NMR (499.9 MHz, d_8-THF): δ (ppm) 3.44 (s, 2H; PH_2), other resonances unchanged. ^{31}P NMR (162.0 MHz, d_8-THF): δ (ppm) –134.8 (t, $^{1}J_{P–H}$ = 206 Hz). $^{31}P\{^{1}H\}$ NMR (162.0 MHz, d_8-THF): δ (ppm) –134.8 (s). $^{13}C\{^{1}H\}$ NMR (100.6 MHz, d_8-THF): δ (ppm) 171.3 (d, $^{1}J_{C–P}$ = 7 Hz; H_2PC(O)), 53.3 (s; *C*(CH$_3$)$_3$), 29.2 (s; C(*C*H$_3$)$_3$). IR (cm^{-1}, d_8-THF): ν(CO) 1655.

8.2.4.4 $H_2PC(O)NHPh$ (19)

[K(18-crown-6)][**1**] (40 mg, 0.110 mmol), H_2NPh (5 μL, 0.048 mmol) and pyridinium triflate (22.9 mg, 0.100 mmol) were dissolved in d_5-pyridine (0.5 mL) in a gas-tight NMR tube. The reaction was monitored by ^{1}H and ^{31}P NMR spectroscopy until all the $[PCO]^-$ starting material had been consumed. Extensive decomposition was observed. Volatiles were removed *in vacuo*, and the solid was redissolved in THF. $^{31}P\{^{1}H\}$ NMR (162.0 MHz,

THF): δ (ppm) –130.9 (s). The resonance was too weak to observe any coupling in the ^{31}P NMR spectrum.

8.2.4.5 [(*p*-cymene)RuCl$_2$(H$_2$PC(O)NHCy)] (20)

[{(*p*-cymene)RuCl$_2$}$_2$] (38 mg, 0.06 mmol) was added as a solid to a CH_2Cl_2 solution (3 mL) of **17** (20 mg, 0.13 mmol) and stirred for one hour. The solvent was removed *in vacuo* to yield an orange solid. Orange blocks suitable for single crystal X-ray diffraction were grown by slow diffusion of hexane into a THF solution of **20**. ^{1}H NMR (400.1 MHz, CD_2Cl_2): δ (ppm) 7.66 (br d, $^3J_{H–H}$ = 6 Hz, 1H; N*H*), 5.60 (d, $^3J_{H–H}$ = 6 Hz, 2H; H_{ar}), 5.45 (d, $^3J_{H–H}$ = 6 Hz, 2H; H_{ar}), 5.30 (d, $^1J_{H–P}$ = 376 Hz, 2H; PH_2), 3.77 (m, 1H; NC*H*), 2.79 (sept, $^3J_{H–H}$ = 7 Hz, 1H; C*H*(CH$_3$)$_2$), 2.17 (s, 3H; C$_{ar}$CH_3), 1.24 (d, $^3J_{H–H}$ = 7 Hz, 6H; CH(CH_3)$_2$), 1.14–1.85 (10H; Cy). ^{31}P NMR (202.4 MHz, CD_2Cl_2): δ (ppm) –36.9 (t, $^1J_{P–H}$ = 376 Hz). ^{31}P{^{1}H} NMR (202.4 MHz, CD_2Cl_2): δ (ppm) –36.9 (s). ^{13}C{^{1}H} NMR (100.6 MHz, CD_2Cl_2): δ (ppm) 163.9 (d, $^1J_{C–P}$ = 52 Hz; H$_2$P*C*(O)), 107.4 (d, $J_{C–P}$ = 2.0 Hz; C_{ar}CH(CH$_3$)$_2$), 102.8 (d, $J_{C–P}$ = 2.3 Hz; C_{ar}CH$_3$), 87.2 (d, $J_{C–P}$ = 4.7 Hz; HC_{ar}), 87.0 (d, $J_{C–P}$ = 3.6 Hz; H*C*ar), 50.2 (d, $^3J_{C–P}$ = 4.1 Hz; N*C*H), 32.8 (s; Cy), 31.5 (s; *C*H(CH$_3$)$_2$), 25.9 (s; Cy), 24.9 (s; Cy), 22.5 (s; CH(*C*H$_3$)$_2$), 18.9 (s; *C*H$_3$). EI-MS: parent peak not observed, only *p*-cymene and fragmentation thereof: *m/z* = 134.1020 $(C_{10}H_{14})^+$, 119.0684 $(C_9H_{11})^+$, 91.0476 $(C_7H_7)^+$. Anal. Calcd for $C_{17}H_{28}Cl_2NOPRu$: C, 43.88; H, 6.07; N 3.01. Found: C, 43.69; H, 6.00; N 3.08.

8.2.4.6 [(*p*-cymene)$_2$Ru$_2$Cl$_2$(μ-Cl)(μ-PHC(O)NHCy)] (21)

Orange crystals of **21** suitable for single crystal X-ray diffraction were obtained as a minor side-product during the crystallisation process of **20**. They could not be isolated cleanly, but reveal a possible decomposition route of **20**. ^{31}P NMR (161.2 MHz, CD_2Cl_2): δ (ppm) 80.1 (d, $^1J_{P–H}$ = 415 Hz). ^{31}P{^{1}H} NMR (161.2 MHz, CD_2Cl_2): δ (ppm) 80.1 (s).

8.2.4.7 $H_2PC(O)NEt_2$ (22)

[K(18-crown-6)][**1**] (36 mg, 0.10 mmol), $NHEt_2$ (5 μL, 0.05 mmol) and pyridinium triflate (23 mg, 0.10 mmol) were dissolved in d_5-pyridine (0.5 mL) in a gas-tight NMR tube and monitored by NMR spectroscopy until the reaction had gone to completion. The solution was distilled at room temperature under reduced pressure to give **22** in solution. ^{1}H NMR (499.9 MHz, d_5-pyridine): δ (ppm) 3.86 (d, $^1J_{H–P}$ = 218 Hz, 2H; PH_2), 3.34 (q, $^3J_{H–H}$ = 7 Hz, 2H; CH_2), 3.13 (qd, $^3J_{H–H}$ = 7 Hz, $^4J_{H–P}$ = 2 Hz, 2H; CH_2), 1.02 (t, $^3J_{H–H}$ = 7 Hz, 3H; CH_3), 1.00 (t, $^3J_{H–H}$ = 7 Hz, 3H; CH_3). ^{1}H{^{31}P} NMR (499.9 MHz, d_5-pyridine): δ (ppm) 3.86 (s, 2H; PH_2), 3.13 (q, $^3J_{H–H}$ = 7 Hz, 2H; CH_2), other resonances unchanged. ^{31}P NMR (202.4 MHz, d_5-pyridine): δ (ppm) –125.4 (t, $^1J_{P–H}$ = 218 Hz). ^{31}P{^{1}H} NMR (202.4 MHz, d_5-pyridine): δ (ppm) –125.4 (s). ^{13}C{^{1}H} NMR (125.8 MHz, d_5-pyridine): δ (ppm) 172.9 (d, $^1J_{C–P}$ = 8 Hz; H_2PC(O)), 44.6 (d, $^3J_{C–P}$ = 10 Hz; CH$_2$), 40.2 (s; CH$_2$), 14.7 (s; CH$_3$), 13.7 (s; CH$_3$). IR (cm^{-1}, d_8-THF): ν(CO) 1618.

8.2.4.8 $H_2PC(O)NMe(OMe)$ (23)

[K(18-crown-6)][**1**] (35.5 mg, 0.101 mmol) and [H_2NMe(OMe)][Cl] (9.8 mg, 0.101 mmol) were dissolved in d_5-pyridine (0.5 mL) in a gas-tight NMR tube and monitored by NMR spectroscopy until the reaction had gone to completion. The solution was distilled at room temperature under reduced pressure to give **23** in solution. ^{1}H NMR (400.2 MHz, d_5-pyridine): δ (ppm) 3.81 (d, $^1J_{H–P}$ = 219 Hz, 2H; PH_2), 3.55 (s, 3H; OCH_3), 3.10 (s, 3H; NCH_3). ^{31}P NMR (162.0 MHz, d_5-pyridine): δ (ppm) –125.6 (t, $^1J_{P–H}$ = 219 Hz). ^{31}P{^{1}H} NMR (162.0 MHz, d_5-pyridine): δ (ppm) –125.6 (s). ^{13}C{^{1}H} NMR (100.6 MHz, d_5-pyridine): δ (ppm) 164.4 (s, very weak - should be a doublet with a small coupling constant; H_2PC(O)), 62.0 (s; OCH_3), 32.3 (s; NCH_3).

8.2.4.9 [K(18-crown-6)][24] (24: $[H_2PC(O)NHCHMeCO_2]^-$)

[K(18-crown-6][**1**] (20.3 mg, 0.0561 mmol) and L-alanine (5.0 mg, 0.0561 mmol) were weighed into a gas-tight NMR tube and pyridine (0.4 mL) was added to give a pale yellow solution and undissolved white solid. To aid the dissolution of the amino acid, deionised water (0.4 mL) was added and the mixture was sonicated for 30 minutes. The reaction was monitored by ^{31}P NMR spectroscopy, and was shown to go to completion after 24 hours. The pale yellow solution was transferred to a small Schlenk tube, and the volatiles were removed *in vacuo* to afford a yellow oily solid. Single crystals of [K(18-crown-6)][**24**] suitable for single crystal X-ray diffraction were obtained by slow diffusion of hexane (20 mL) into a solution of the product in a 50/50 mix of pyridine/THF (5 mL). The off-white microcrystalline solid was subsequently isolated (9 mg, 36% crystalline yield). The reaction could also be carried out only in deionised water. ^1H NMR (499.9 MHz, d_5-pyridine): δ (ppm) 8.68 (br, 1H; N*H*), 4.79 (dq, virtual quint, $^3J_{H–H}$ = 7 Hz, 1H; NC*H*(CH_3)), 3.72 (m, $^1J_{H–P}$ = 205 Hz, $^2J_{H–H}$ = 11 Hz, 1H; P*H*H), 3.69 (m, $^1J_{H–P}$ = 205 Hz, $^2J_{H–H}$ = 11 Hz, 1H; PH*H*), 3.50 (s, 24H; 18-crown-6), 1.87 (d, $^3J_{H–H}$ = 7 Hz, 3H; NCH(C*H*$_3$)). $^1H\{^{31}P\}$ NMR (499.9 MHz, d_5-pyridine): δ (ppm) 3.72 (m, $^2J_{H–H}$ = 11 Hz), 3.69 (m, $^2J_{H–H}$ = 11 Hz), other resonances unchanged. ^{31}P NMR (162.0 MHz, d_5-pyridine): δ (ppm) –131.4 (dd, virtual triplet, $^1J_{P–H}$ = 205 Hz). $^{31}P\{^1H\}$ NMR (162.0 MHz, d_5-pyridine): δ (ppm) –131.4 (s). $^{13}C\{^1H\}$ NMR (100.6 MHz, d_5-pyridine): δ (ppm) 175.9 (s; *C*O_2^-), 171.0 (d, $^1J_{C–P}$ = 5 Hz; P*C*(O)), 70.7 (s; 18-crown-6), 53.1 (s; N*C*H(CH_3)), 20.8 (s; NCH(*C*H$_3$)). ESI-MS (–ve ion mode, DMF): *m/z* = 334.6 $\{K[H_2PC(O)NHCHMeCO_2]_2\}^-$.

8.2.4.10 $H_2PC(O)NHC_2H_4NHC(O)PH_2$ (25)

A pyridine solution (15 mL) of $[Na(1,4\text{-dioxane})_{2.69}]$[**1**] (1.00 g, 3.13 mmol) was added drop-wise to a pyridine solution (20 mL) of ethylenediamine (105 µl, 1.565 µL) and pyridinium triflate (710 mg, 3.13 mmol). The pale yellow solution turned slightly cloudy

after a few minutes. An aliquot (0.5 mL) was taken and analysed by ^{31}P NMR spectroscopy. This showed that the reaction had not yet gone to completion, so further [Na(1,4-dioxane)$_{2.69}$][**1**] (100 mg, 0.313 mmol) and pyridinium triflate (71 mg, 0.313 mmol) was added. ^{31}P NMR spectroscopy on a new aliquot showed the reaction was complete. Volatiles were removed *in vacuo*, and the product extracted with 1,4-dioxane (30 mL). ^{19}F NMR spectroscopy revealed that a small amount of [Na][OTf] was present, so the volatiles were removed *in vacuo* again, and the resulting white solid was recrystallised from hot THF. This gave a compositionally pure sample microcrystalline of **25**, albeit in a low yield. Colourless crystals suitable for single crystal X-ray diffraction were grown by slow diffusion of hexane (20 mL) into a pyridine solution (5 mL) of the product. ^{1}H NMR (400.2 MHz, d_5-pyridine): δ (ppm) 9.53 (br, 2H; N*H*), 3.73 (d, $^{1}J_{H–P}$ = 208 Hz, 4H; PH_2), 3.69 (m, 4H; NCH_2). ^{31}P NMR (162.0 MHz, d_5-pyridine): δ (ppm) –132.7 (t, $^{1}J_{P–H}$ = 208 Hz). ^{31}P{^{1}H} NMR (162.0 MHz, d_5-pyridine): δ (ppm) –132.7 (s). ^{13}C{^{1}H} NMR (100.6 MHz, d_5-pyridine): δ (ppm) 173.6 (d, $^{1}J_{C–P}$ = 7 Hz; P*C*(O)), 40.8 (s; N*C*H$_2$). CI-MS (NH_3): *m/z* = 181.0284 ([$C_4H_{11}N_2O_2P_2$]$^+$; [M+H]$^+$), 198.0545 ([$C_4H_{14}N_3O_2P_2$]$^+$; [M+NH_4]$^+$); the following fragments were also observed: 164.0582 ([$C_4H_{11}N_3O_2P$]$^+$), 147.0305 ([$C_4H_8N_2O_2P$]$^+$), 121.0519 ([$C_3H_{10}N_2OP$]$^+$), 104.0812 ([$C_3H_{10}N_3O$]$^+$), 87.0550 ([$C_3H_7N_2O$]$^+$), 71.0594 ([$C_3H_7N_2$]$^+$), 61.0754 ([$C_2H_9N_2$]$^+$), 35.0602 ([H_4P]$^+$). IR (cm^{-1}, Nujol mull): ν(CO) 1598. Anal. Calcd for $C_{10}H_{12}NOP$: C, 26.68; H, 5.60; N, 15.56. Found: C, 26.56; H, 5.60; N, 15.48.

8.2.4.11 $H_2PC(O)NH(C_9H_9)$ (26)

[Na(1,4-dioxane)$_{2.69}$][**1**] (500 mg, 1.567 mmol) and (4-vinylphenyl)methanaminium chloride (293 mg, 1.724 mmol) were stirred in pyridine (20 mL) overnight. The slightly pink solution was pumped down under reduced pressure to give an off-white solid. The product was extracted and filtered in THF (1 × 20 mL, 1 × 10 mL). Volatiles were removed

in vacuo to afford a white solid (271 mg, 90% yield wrt. P) of spectroscopically pure styrene-functionalised phosphinecarboxamide, **26**. The white solid was kept in a foil-wrapped vial in the glovebox freezer to prevent undesired polymerisation reactions during storage. ^{1}H NMR (400.2 MHz, d_8-THF): δ (ppm) 7.99 (br, 1H; N*H*), 7.20–7.38 (m, 4H; C*H*$_{Ar}$), 6.69 (dd, $^{3}J_{H–H(trans)}$ = 17.6 Hz, $^{3}J_{H–H(cis)}$ = 10.9 Hz, 1H; C*H*=CH$_2$), 5.73 (dd, $^{3}J_{H–H(trans)}$ = 17.6 Hz, $^{2}J_{H–H(gem)}$ = 0.7 Hz, 1H; CH=C*H*H (*trans* to proton)), 5.17 (dd, $^{3}J_{H–H(cis)}$ = 10.9 Hz, $^{2}J_{H–H(gem)}$ = 0.7 Hz, 1H; CH=CH*H* (*cis* to proton)), 4.35 (d, $^{3}J_{H–H}$ = 5.7 Hz, 2H; NC*H*$_2$), 3.53 (d, $^{1}J_{H–P}$ = 206 Hz, 2H; P*H*$_2$). ^{31}P NMR (162.0 MHz, d_8-THF): δ (ppm) –136.1 (t, $^{1}J_{P–H}$ = 206 Hz). ^{31}P{^{1}H} (162.0 MHz, d_8-THF): δ (ppm) –136.1 (s). ^{13}C{^{1}H} (100.6 MHz, d_8-THF): δ (ppm) 172.0 (d, $^{1}J_{C–P}$ = 6.8 Hz; P*C*(O)), 139.9 (s; *C*$_{Ar}$), 137.8 (s; *C*H=CH$_2$), 137.7 (s; *C*$_{Ar}$), 129.0 (s; *C*$_{Ar}$), 127.2 (s; *C*$_{Ar}$), 113.8 (s; CH=*C*H$_2$), 44.1 (s; NCH$_2$). FI-MS: Calcd: *m/z* = 193.0657. Found: *m/z* = 193.0654. IR (cm^{-1}, Nujol mull): ν(CO) 1610. Anal. Calcd for $C_{10}H_{12}NOP$: C, 62.17; H, 6.26; N, 7.25. Found: C, 62.08; H, 6.29; N, 7.08.

8.2.5 Chapter 6 – Deprotonation, *P*-functionalisation and oxidation chemistry of phosphinecarboxamides

8.2.5.1 [K(18-crown-6)][27] (27: [HPC(O)NEt$_2$]$^-$)

[Na(1,4-dioxane)$_{1.75}$][**1**] (60 mg, 0.254 mmol) and [H$_2$NEt$_2$][Cl] (23.2 mg, 0.212 mmol) were dissolved in d$_8$-THF (0.5 mL) in a gas-tight NMR tube, and the reaction was monitored by ^{31}P NMR spectroscopy until it had gone to completion. The solution of **22** was obtained by a trap-to-trap distillation under reduced pressure at room temperature. KHMDS (33.9 mg, 0.170 mmol) and 18-crown-6 (39.2 mg, 0.170 mmol) were added and the solution stirred. This solution was layered with hexane (10 mL) to yield colourless crystals of [K(18-crown-6)][**27**]·0.5(1,4-dioxane) suitable for single crystal X-ray diffraction. ^{1}H NMR (400.1 MHz, d_8-THF): δ (ppm) 3.62 (s; overlapping 18-crown-6 and

1,4-dioxane), 3.36 (q, $^{3}J_{H–H}$ = 7 Hz, 4H; C*H*$_2$), 1.60 (1, $^{1}J_{H–P}$ = 154 Hz, 1H; P*H*), 1.03 (t, $^{3}J_{H–H}$ = 7 Hz, 6H; C*H*$_3$). ^{31}P NMR (162.0 MHz, d_8-THF): δ (ppm) –93.2 (d, $^{1}J_{P–H}$ = 154 Hz). ^{31}P{^{1}H} NMR (162.0 MHz, d_8-THF): δ (ppm) –93.2 (s). ESI-MS (–ve ion mode, DMF): *m/z* = 132.0 [HPC(O)NEt$_2$]$^-$. ESI-MS (+ve ion mode, DMF): *m/z* = 737.6 {[K(18-crown-6)]$_2$[HPC(O)NEt$_2$]}$^+$.

8.2.5.2 [K(18-crown-6)][28] (28: [HPC(O)NHCy]$^-$)

A toluene solution (100 mL) of **17** (200 mg, 1.26 mmol) was added to a stirring toluene solution (30 mL) of KHMDS (251 mg, 1.26 mmol). The solution turned pale yellow and the reaction mixture was left to stir overnight. 18-crown-6 (332 mg, 1.26 mmol) was then added to the solution and stirred for a further two hours before the volatiles were removed *in vacuo* to afford [K(18-crown-6)][**28**] as a pale yellow powder (393 mg, 68% yield). Single crystals were grown by slow diffusion of hexane (20 mL) into a THF (5 mL) solution of the product and analysed using single crystal X-ray diffraction. ^{1}H NMR (499.9 MHz, d_5-pyridine): δ (ppm) 5.94 (br, 1H; N*H*), 4.17 (m, 1H; NC*H*), 3.53 (s, 24H; 18-crown-6), 2.86 (d, $^{1}J_{H–P}$ = 148 Hz, 1H; P*H*) 1.02–2.20 (10H; Cy). ^{31}P NMR (202.4 MHz, d_5-pyridine): δ (ppm) –97.3 (d, $^{1}J_{P–H}$ = 148 Hz). ^{31}P{^{1}H} NMR (202.4 MHz, d_5-pyridine): δ (ppm) –97.3 (s). ^{13}C{^{1}H} NMR (125.7 MHz, d_5-pyridine): δ (ppm) 202.9 (d, $^{1}J_{C–P}$ = 59 Hz; P*C*(O)), 70.8 (s; 18-crown-6), 49.7 (s; N*C*H), 35.3 (s; Cy), 35.0 (s; Cy), 26.8 (s; Cy), 26.3 (s; Cy) 25.9 (s; Cy). ESI-MS (+ve ion mode, DMF): *m/z* = 765.0 {[K(18-crown-6)]$_2$[HPC(O)NHCy]}$^+$. IR (cm^{-1}, Nujol mull): ν(CO) 1538. Anal. Calcd for $C_{19}H_{37}KNO_7P$: C, 49.44; H, 8.08; N, 3.04. Found: C, 49.20; H, 8.06; N, 3.37.

8.2.5.3 [K(18-crown-6)][29] (29: [P{C(O)NHCy}$_2$]$^-$)

A THF solution (50 mL) of KHMDS (76 mg, 0.38 mmol) and 18-crown-6 (100 mg, 0.38 mmol) was slowly added to a stirring THF solution (10 mL) of **17** (120 mg, 0.76 mmol) at –78 ˚C. The reaction mixture was left to warm up to room temperature over two hours to

yield a pale yellow solution. Volatiles were removed *in vacuo* to yield an off-white solid (102 mg, 46% yield). Crystals suitable for single crystal X-ray diffraction were grown by slow diffusion of hexane (20 mL) into a THF solution (5 mL) of [K(18-crown-6)][**29**]. ^{1}H NMR (500.3 MHz, d_5-pyridine): δ (ppm) 8.72 (br, overlapping with solvent resonance; N*H*), 4.41 (m, 2H; NC*H*), 3.50 (s, 24H; 18-crown-6), 1.04–2.17 (m, 20H; Cy). ^{31}P NMR (162.0 MHz, d_5-pyridine): δ (ppm) –29.2 (br s). ^{13}C{^{1}H} NMR (125.8 MHz, d_5-pyridine): δ (ppm) 197.4 (d, $^{1}J_{C–P}$ = 55 Hz; P(*C*O)$_2$), 70.8 (s; 18-crown-6), 48.0 (s; N*C*H), 34.9 (s; Cy), 26.8 (s; Cy), 25.9 (s; Cy). ESI-MS (–ve ion mode, DMF): *m/z* = 283.1 [P{C(O)NHCy}$_2$]$^-$. ESI-MS (+ve ion mode, DMF): *m/z* = 890.3 {[K(18-crown-6)]$_2$[P{C(O)NHCy}$_2$]}$^+$. IR (cm^{-1}, Nujol mull): ν(CO) 1560, 1537. Anal. Calcd for $C_{26}H_{48}KN_2O_8P$: C, 53.22; H, 8.25; N, 4.77. Found: C, 53.02; H, 8.29; N, 4.73.

8.2.5.4 [K(18-crown-6)][30] (30: [P{C(O)NHMe}$_2$]$^-$)

[H$_2$NMe(OMe)][Cl] (14.4 mg, 0.148 mmol) was added to a stirring pyridine solution (2 mL) of [Na(1,4-dioxane)$_{2.69}$][**1**] (47.1 mg, 0.148 mmol) in the glovebox to give a pale yellow solution. KHMDS (29.5 mg, 0.148 mmol) and 18-crown-6 (39.0 mg, 0.148 mmol) were added to the mixture affording an orange solution. 0.5 mL was decanted to a gas-tight NMR tube for ^{31}P NMR spectroscopic analysis; the spectrum was very weak but the following resonances were present. ^{31}P NMR (162.0 MHz, pyridine): δ (ppm) 18.8 (s), –26.7 (br s), –100.8 (d, $^{1}J_{P–H}$ = 145 Hz). ^{31}P{^{1}H} NMR (162.0 MHz, pyridine): δ (ppm) –100.8 (s), other resonances unchanged. The contents of the NMR tube were recombined with the original solution and the volatiles removed *in vacuo* to yield an orange microcrystalline solid. THF (5 mL) was added to give a pale orange solution and a white solid (NaCl). This was filtered to a thin gas-tight ampoule, and hexane (20 mL) carefully layered on top. Crystals of [K(18-crown-6][**30**] were obtained after slow diffusion of the hexane into the THF fraction.

8.2.5.5 MeHPC(O)NHCy (31)

A THF solution (10 mL) of **17** (128 mg, 0.803 mmol) was added to a stirring THF solution (10 mL) of KHMDS (160 mg, 0.803 mmol) at –78 ˚C. The solution turned pale yellow and was left to stir for three hours while warming to room temperature. Iodomethane (50 μL, 0.803 mmol) was added via a microsyringe to immediately afford a white precipitate (KI) and a colourless solution. The solution was filtered to a Schlenk tube and the volatiles removed *in vacuo* to yield a white solid (101 mg, 73%). Single crystals of **31** were grown by slow evaporation of a THF solution of the product. Alternatively, the product could be obtained by addition of iodomethane (3 μL, 0.05 mmol) to a d_8-THF solution (0.5 mL) of [K(18-crown-6)][**28**] (22.2 mg, 0.05 mmol) in a gas-tight NMR tube to give a colourless solution and a white precipitate. The solution contained a clean sample of **31** and [K(18-crown-6)][I], but complete separation of this by-product proved more difficult. ^{1}H NMR (499.9 MHz, d_5-pyridine): δ (ppm) 8.85 (br, 1H; N*H*), 4.16 (m, 1H; NC*H*), 4.06 (dq, $^{1}J_{H–P}$ = 207 Hz, $^{3}J_{H–H}$ = 8 Hz, 1H; P*H*), 1.37 (dd, $^{2}J_{H–P}$ = 3 Hz, $^{3}J_{H–H}$ = 8 Hz, 3H; C*H*$_3$), 0.80–2.10 (m, 10H; Cy). ^{1}H{^{31}P} NMR (499.9 MHz, d_5-pyridine): δ (ppm) 4.06 (q, $^{3}J_{H–H}$ = 8 Hz, 1H; P*H*), 1.37 (d, $^{3}J_{H–H}$ = 8 Hz, 3H; C*H*$_3$), other resonances unchanged. ^{31}P NMR (162.0 MHz, d_5-pyridine): δ (ppm) –81.5 (dq, $^{1}J_{P–H}$ = 207 Hz, $^{2}J_{P–H}$ = 3 Hz). ^{31}P{^{1}H} NMR (162.0 MHz, d_5-pyridine): δ (ppm) –81.5 (s). ^{13}C{^{1}H} NMR (125.7 MHz, d_5-pyridine): δ (ppm) 176.9 (d, $^{1}J_{C–P}$ = 11 Hz; P*C*(O)), 49.8 (s; N*C*H), 34.0 (s; Cy), 33.9 (s; Cy), 26.3 (s; Cy), 25.9 (s; Cy, two resonances overlapping), 1.8 (d, $^{1}J_{C–P}$ = 8 Hz; P*C*H$_3$). FI-MS: Calcd: *m/z* = 173.0970. Found: *m/z* = 173.0971. IR (cm^{-1}, Nujol mull): ν(CO) 1605. Anal. Calcd for $C_8H_{16}NOP$: C, 55.48; H, 9.31; N, 8.09. Found: C, 54.50; H, 9.02; N, 7.13.

8.2.5.6 BnHPC(O)NHCy (32)

A THF solution (10 mL) of **17** (100 mg, 0.628 mmol) was added to a stirring THF solution (10 mL) of KHMDS (125 mg, 0.628 mmol) at –78 ˚C. The solution turned pale yellow and

was left to stir for three hours while warming to room temperature. Benzyl bromide (75 μL, 0.628 mmol) was added via a microsyringe to immediately afford a white precipitate (KBr) and a colourless solution. The solution was filtered to a Schlenk tube and the volatiles removed *in vacuo* to yield a white solid (119 mg, 48%). Single crystals of **32** were grown by slow diffusion of hexane (20 mL) into a THF (5 mL) solution of the product. ^{1}H NMR (499.9 MHz, d_5-pyridine): δ (ppm) 8.90 (br, 1H; N*H*), 7.40 (m, 2H; *ortho*-Ph), 7.30 (m, 2H; *meta*-Ph), 7.20 (m, 1H; *para*-Ph), 4.26 (ddd, $^{1}J_{H–P}$ = 206 Hz, $^{3}J_{H–H}$ = 8 Hz, $^{3}J_{H–H}$ = 5 Hz, 1H; P*H*), 4.15 (m, 1H; NC*H*), 3.50 (m, 1H; PC*H*H), 3.30 (m, 1H; PCH*H*), 0.88–2.07 (m, 10H; Cy). ^{1}H{^{31}P} NMR (499.9 MHz, d_5-pyridine): δ (ppm) 4.26 (dd, $^{3}J_{H–H}$ = 8 Hz, $^{3}J_{H–H}$ = 5 Hz, 1H; P*H*), 3.50 (simplified m, 1H; PC*H*H), 3.30 (simplified m, 1H; PCH*H*), other resonances unchanged. ^{31}P NMR (162.0 MHz, d_5-pyridine): δ (ppm) –48.7 (dd, $^{1}J_{P–H}$ = 206 Hz, $^{2}J_{P–H}$ = 8 Hz, coupling to other CH proton not observed). ^{31}P{^{1}H} NMR (162.0 MHz, d_5-pyridine): δ (ppm) –48.7 (s). ^{13}C{^{1}H} NMR (125.7 MHz, d_5-pyridine): δ (ppm) 175.5 (d, $^{1}J_{C–P}$ = 13 Hz; P*C*(O)), 141.9 (s; *ipso*-Ph), 129.4 (d, $^{4}J_{C–P}$ = 2 Hz; *meta*-Ph), 129.3 (d, $^{3}J_{C–P}$ = 4 Hz; *ortho*-Ph), 126.7 (d, $^{5}J_{C–P}$ = 2 Hz; *para*-Ph), 49.8 (s; N*C*H), 34.0 (s; Cy), 33.7 (s; Cy), 26.7 (d, $^{1}J_{C–P}$ = 11 Hz; P*C*H$_2$), 26.2 (s; Cy), 25.9 (s; Cy, two resonances overlapping). FI-MS: Calcd: *m/z* = 249.1283. Found: *m/z* = 249.1280. IR (cm^{-1}, Nujol mull): ν(CO) 1599.

8.2.5.7 HP{C(O)NHCy}$_2$ (33)

A THF solution (10 mL) of KHMDS (37.6 mg, 0.188 mmol) was added to a stirring THF solution (10 mL) of **17** (60 mg, 0.377 mmol) at –78 ˚C, and the pale yellow solution was left stirring for two days at room temperature. A THF solution (5 mL) of pyridinium triflate (43.2 mg, 0.188 mmol) was added to the stirring solution to immediately give a white precipitate (KOTf). The colourless solution was filtered to a Schlenk tube and the volatiles removed *in vacuo* to yield a colourless oily substance. A white solid could be obtained by trituration with pentane (20 mL). Alternatively, pyridinium triflate (7 mg, 0.03 mmol) was

added as a solid to a d_5-pyridine solution (0.5 mL) of [K(18-crown-6)][**29**] (19 mg, 0.03 mmol) in a gas-tight NMR tube to give a pale yellow solution containing **33** and [K(18-crown-6)][OTf], though separation of this by-product proved more difficult. ^{1}H NMR (499.9 MHz, d_5-pyridine): δ (ppm) 9.37 (br, 2H; N*H*), 4.95 (d, $^1J_{H–P}$ = 235 Hz, 1H; P*H*), 4.12 (m, 2H; NC*H*), 0.95–2.05 (m, 20H; Cy). ^{1}H{^{31}P} NMR (499.9 MHz, d_5-pyridine): δ (ppm) 4.95 (s, 1H; P*H*), other resonances unchanged. ^{31}P NMR (162.0 MHz, d_5-pyridine): δ (ppm) –74.9 (d, $^1J_{P–H}$ = 235 Hz). ^{31}P{^{1}H} NMR (162.0 MHz, d_5-pyridine): δ (ppm) –74.9 (s). ^{13}C{^{1}H} NMR (125.7 MHz, d_5-pyridine): δ (ppm) 172.9 (d, $^1J_{C–P}$ = 12 Hz; P*C*(O)), 49.7 (s; N*C*H), 33.4 (s; Cy), 26.1 (s; Cy), 25.4 (s, Cy). FI-MS: Calcd: *m/z* = 284.1654. Found: *m/z* = 284.1637. Also observe [CONCy]$^+$ at 125.0839 and [HPCOHNHCy]$^+$ at 159.0789 (both derived from McLafferty rearrangement), [M+H]$^+$ at 285.1724, and [M+HCONCy]$^+$ at 410.2477. This is consistent with formation of H-bonded dimers prior to or during the ionisation process. IR (cm^{-1}, Nujol mull): ν(CO) 1639, 1613.

8.2.5.8 MeP{C(O)NHCy}$_2$ (34)

A THF solution (10 mL) of KHMDS (37.6 mg, 0.188 mmol) was added to a stirring THF solution (10 mL) of **17** (60 mg, 0.377 mmol) at –78 ˚C, and the pale yellow solution was left stirring for two days at room temperature. Iodomethane (12 μL, 0.188 mmol) was added via a 25 μL microsyringe to the stirring solution to immediately give a white precipitate (KI). The colourless solution was filtered to a Schlenk tube and the volatiles removed *in vacuo* to yield a colourless oily substance, from which a white solid could be obtained by trituration with pentane (20 mL). Yield 25 mg (45%). Alternatively, the product could be obtained by addition of iodomethane (2 μL, 0.03 mmol) to a d_5-pyridine solution (0.5 mL) of [K(18-crown-6)][**29**] (18 mg, 0.03 mmol) in a gas-tight NMR tube to give a pale yellow solution. The solution contained a clean sample of **34** and [K(18-crown-6)][I], but separation of this by-product proved more difficult. ^{1}H NMR (499.9 MHz, d_5-pyridine): δ

(ppm) 8.88 (br, 2H; N*H*), 4.14 (m, 2H; NC*H*), 1.81 (d, $^{2}J_{H-P}$ = 2 Hz, 3H; PCH_3), 0.95–2.02 (m, 20H; Cy). $^{1}H\{^{31}P\}$ NMR (499.9 MHz, d_5-pyridine): δ (ppm) 1.81 (s, 3H; CH_3), other resonances unchanged. ^{31}P NMR (162.0 MHz, d_5-pyridine): δ (ppm) –31.1 (q, $^{2}J_{P-H}$ = 2 Hz). $^{31}P\{^{1}H\}$ NMR (162.0 MHz, d_5-pyridine): δ (ppm) –31.1 (s). $^{13}C\{^{1}H\}$ NMR (100.6 MHz, d_5-pyridine): δ (ppm) 177.0 (d, $^{1}J_{C-P}$ = 16 Hz; P*C*(O)), 49.7 (s; N*C*H), 33.5 (s; Cy), 26.2 (s; Cy), 25.6 (s, Cy), 7.2 (d, $^{1}J_{C-P}$ = 12 Hz; P*C*H_3). FI-MS: Calcd: *m/z* = 298.1810. Found: *m/z* = 298.1801. Also observe $[CONCy]^+$ at 125.0877 and $[MePCOHNHCy]^+$ at 173.1010 (both derived from McLafferty rearrangement), and $[M+H]^+$ at 299.1879. IR (cm^{-1}, Nujol mull): ν(CO) 1633, unable to observe second expected band.

8.2.5.9 BnP{C(O)NHCy}$_2$ (35)

A THF solution (10 mL) of KHMDS (217.2 mg, 2.18 mmol) was added to a stirring THF solution (10 mL) of **17** (347 mg, 2.18 mmol) at –78 ˚C, and the pale yellow solution was left stirring for two days at room temperature. Benzyl bromide (130 μL, 2.18 mmol) was added to the stirring solution to immediately give a white precipitate (KBr). The colourless solution was filtered to a Schlenk tube and the volatiles removed *in vacuo* to yield a colourless oily substance. A white solid could be obtained by trituration with pentane (30 mL). Yield 337 mg (83%). ^{1}H NMR (499.9 MHz, d_5-pyridine): δ (ppm) 9.10 (br, 2H; N*H*), 7.51 (m, 2H; *ortho*-Ph), 7.37 (m, 2H; *meta*-Ph), 7.25 (m, 1H; *para*-Ph), 4.12 (m, 2H; NC*H*), 3.76 (d, $^{2}J_{H-P}$ = 2 Hz, 2H; PCH_2), 0.98–2.00 (m, 20H; Cy). $^{1}H\{^{31}P\}$ NMR (499.9 MHz, d_5-pyridine K): δ (ppm) 3.76 (s, 2H; PCH_2), other resonances unchanged. ^{31}P NMR (162.0 MHz, d_5-pyridine): δ (ppm) –11.4 (br s, unable to resolve small coupling). $^{31}P\{^{1}H\}$ NMR (162.0 MHz, d_5-pyridine): δ (ppm) –11.4 (sharp s). $^{13}C\{^{1}H\}$ NMR (100.6 MHz, d_5-pyridine): δ (ppm) 175.2 (d, $^{1}J_{C-P}$ = 19 Hz; P*C*(O)), 139.0 (s; *ipso*-Ph), 130.0 (d, $^{3}J_{C-P}$ = 4 Hz; *ortho*-Ph), 129.2 (s; *meta*-Ph), 127.1 (d, $^{5}J_{C-P}$ = 2 Hz; *para*-Ph), 49.5 (s; N*C*H), 33.5 (s; Cy), 33.4 (s; Cy), 31.1 (d, $^{1}J_{C-P}$ = 17 Hz; P*C*H_2), 26.2 (s; Cy), 25.5 (s; Cy), 25.4 (s; Cy). FI-

MS: Calcd: *m/z* = 374.2123. Found: *m/z* = 374.2085. Also observe $[CONCy]^+$ at 125.0865 and $[BnPCOHNHCy]^+$ at 249.1269 (both derived from McLafferty rearrangement), and $[M+H]^+$ at 375.2139. IR (cm^{-1}, Nujol mull): ν(CO) 1639, 1614.

8.2.5.10 $BnHPC(O)NH_2$ (36)

A THF solution (10 mL) of **11** (50 mg, 0.649 mmol) and benzyl bromide (77 μL, 0.649 mmol) was cooled to –78 ˚C. To this a THF solution (50 mL) of KHMDS (129.5 mg, 0.649 mmol) was added drop-wise, instantly generating white precipitate. The white suspension was allowed to warm to room temperature over the course of two hours. The colourless solution was filtered to a Schlenk tube leaving behind KBr. The solvent was removed *in vacuo* yielding a white microcrystalline solid (79 mg, 73 yield). ^1H NMR (499.9 MHz, d_8-THF): δ (ppm) 7.20 (m, 2H; Ph), 7.18 (m, 2H; Ph), 7.08 (m, 1H; *para*-Ph), 7.05 (br, 1H; N*H*H), 6.80 (br s, 1H; NH*H*), 3.92 (ddd, $^1J_{H–P}$ = 205 Hz, $^3J_{H–H}$ = 6 Hz, $^3J_{H–H}$ = 7 Hz, 1H; P*H*), 3.22 (m, 1H; PC*H*H), 3.03 (m, 1H; PCH*H*). $^1H\{^{31}P\}$ NMR (499.9 MHz, d_8-THF): δ (ppm) 3.92 (dd, $^3J_{H–H}$ = 6 Hz, $^3J_{H–H}$ = 7 Hz, 1H; P*H*), 3.22 (simplified m, 1H; PC*H*H), 3.03 (simplified m, 1H; PCH*H*), other resonances unchanged. ^{31}P NMR (202.4 MHz, d_8-THF): δ (ppm) –55.5 (br d, $^1J_{P–H}$ = 205 Hz, unable to resolve coupling to CH_2 protons). $^{31}P\{^1H\}$ NMR (202.4 MHz, d_8-THF): δ (ppm) –55.5 (s). $^{13}C\{^1H\}$ NMR (125.7 MHz, d_8-THF): δ (ppm) 178.6 (d, $^1J_{C–P}$ = 14 Hz; P*C*(O)), 141.9 (s; *ipso*-Ph), 129.3 (overlapping s, *ortho*-Ph and *meta*-Ph), 126.6 (d, $^5J_{C–P}$ = 2 Hz; *para*-Ph), 26.4 (d, $^1J_{C–P}$ = 11 Hz; P*C*H_2). FI-MS: Calcd: *m/z* = 167.0500. Found: *m/z* = 167.0499.

8.2.5.11 HP(O)(OH)C(O)NHCy (37)

An aqueous hydrogen peroxide solution (152 μL, 1.57 mmol) was added drop-wise to a stirring THF solution (20 mL) of **17** (100 mg, 0.628 mmol) affording a colourless solution. After three hours of stirring at room temperature, the volatiles were removed *in vacuo* to yield **37** as a colourless oily substance. The product remained an oil even after trituration

with pentane (20 mL). ^{1}H NMR (499.9 MHz, d_5-pyridine): δ (ppm) 9.07 (br, 1H; N*H*), 7.85 (d, $^{1}J_{H–P}$ = 527 Hz, 1H; P*H*), 4.14 (m, 1H; NC*H*), 0.93–2.04 (m, 10H; Cy). ^{31}P NMR (162.0 MHz, d_5-pyridine): δ (ppm) 5.8 (d, $^{1}J_{P–H}$ = 527 Hz). ^{31}P{^{1}H} NMR (162.0 MHz, d_5-pyridine): δ (ppm) 5.8 (s). ^{13}C{^{1}H} NMR (100.6 MHz, d_5-pyridine): δ (ppm) 175.2 (d, $^{1}J_{C–P}$ = 149 Hz; P*C*(O)), 48.8 (d, $^{3}J_{C–P}$ = 5 Hz; N*C*H), 33.6 (s; Cy), 26.3 (s; Cy), 25.9 (s; Cy). IR (cm^{-1}, Nujol mull): ν(CO) 1647; ν(P=O) 1260.

8.2.5.12 MeP(O)(OH)C(O)NHCy (38)

An aqueous hydrogen peroxide solution (28 μL, 0.290 mmol) was added drop-wise to a stirring THF solution (5 mL) of **31** (20.1 mg, 0.116 mmol) yielding a colourless solution. After three hours of stirring at room temperature, the volatiles were removed *in vacuo* to afford **38** as a colourless oily substance. A white solid was obtained after trituration with pentane (20 mL). Yield 20.4 mg (86%). ^{1}H NMR (499.9 MHz, d_5-pyridine): δ (ppm) 8.66 (br, 1H; N*H*), 4.11 (m, 1H; NC*H*), 1.85 (d, $^{2}J_{H–P}$ = 14 Hz, 3H; CH_3), 0.95–1.94 (m, 10H; Cy). ^{1}H{^{31}P} NMR (499.94 MHz, d_5-pyridine): δ (ppm) 1.85 (s, 3H; CH_3), other resonances unchanged. ^{31}P NMR (162.0 MHz, d_5-pyridine): δ (ppm) 23.5 (q, $^{2}J_{P–H}$ = 14 Hz). ^{31}P{^{1}H} NMR (162.0 MHz, d_5-pyridine): δ (ppm) 23.5 (s). ^{13}C{^{1}H} NMR (100.6 MHz, d_5-pyridine): δ (ppm) 174.0 (d, $^{1}J_{C–P}$ = 150 Hz; P*C*(O)), 48.7 (d, $^{3}J_{C–P}$ = 5 Hz; N*C*H), 33.4 (s; Cy), 26.2 (s; Cy), 25.8 (s; Cy), 15.3 (d, $^{1}J_{C–P}$ = 96 Hz; P*C*H$_3$). IR (cm^{-1}, Nujol mull): ν(CO) 1625; ν(P=O) 1260.

8.2.5.13 BnP(O)(OH)C(O)NHCy (39)

An aqueous hydrogen peroxide solution (38.7 μL, 0.403 mmol) was added drop-wise to a stirring THF solution (20 mL) of **32** (40.1 mg, 0.161 mmol) to give a colourless solution. After three hours of stirring at room temperature, the volatiles were removed *in vacuo* yielding **39** as a colourless oily substance. A white solid was obtained after trituration with pentane (20 mL). Yield 38.0 mg (84%). ^{1}H NMR (499.9 MHz, d_5-pyridine): δ (ppm) 8.32

(br s, 1H; N*H*), 7.66 (m, 2H; *ortho*-Ph), 7.27 (m, 2H; *meta*-Ph), 7.16 (m, 1H; *para*-Ph), 4.05 (m, 1H; NC*H*), 3.68 (d, $^{2}J_{H-P}$ = 17 Hz, 2H; CH_2P), 0.87–1.86 (m, 10H; Cy). $^{1}H\{^{31}P\}$ NMR (499.9 MHz, d_5-pyridine): δ (ppm) 3.68 (s, 2H; CH_2P), other resonances unchanged. ^{31}P NMR (162.0 MHz, d_5-pyridine): δ (ppm) 20.7 (t, $^{2}J_{P-H}$ = 17 Hz; CH_2P). $^{31}P\{^{1}H\}$ NMR (162.0 MHz, d_5-pyridine): δ (ppm) 20.7 (s; CH_2P). $^{13}C\{^{1}H\}$ NMR (100.6 MHz, d_5-pyridine): δ (ppm) 174.1 (d, $^{1}J_{C-P}$ = 147 Hz; 135.7 (d, $^{2}J_{C-P}$ = 7 Hz; *ipso*-Ph), 131.3 (d, $^{3}J_{C-P}$ = 5 Hz; *ortho*-Ph), 129.0 (d, $^{4}J_{C-P}$ = 3 Hz; *meta*-Ph), 126.7 (d, $^{5}J_{C-P}$ = 3 Hz; *para*-Ph), P*C*(O)), 48.6 (d, $^{3}J_{C-P}$ = 5 Hz; N*C*H), 38.1 (d, $^{1}J_{C-P}$ = 87 Hz; P*C*H_2), 33.3 (s; Cy), 26.2 (s; Cy), 25.7 (s; Cy). IR (cm^{-1}, Nujol mull): ν(CO) 1627; ν(P=O) 1260.

8.2.5.14 [K(18-crown-6)][40] (40: $[BnP(O)_2C(O)NHCy]^-$)

KHMDS (19.9 mg, 0.997 mmol) and 18-crown-6 (26.4 mg, 0.997 mmol) were added as solids to a stirring THF solution (10 mL) of **39** (28.0 mg, 0.997 mmol). The solution remained colourless after the addition and the reaction mixture was left to stir for ten minutes. The volatiles were removed *in vacuo* to afford [K(18-crown-6)][**40**] as a white solid. Single crystals of [K(18-crown-6)][**40**]·0.5(hexane) were grown by slow diffusion of hexane (20 mL) into a THF (5 mL) solution of the product and analysed using single crystal X-ray diffraction. ^{1}H NMR (499.9 MHz, d_5-pyridine): δ (ppm) 7.75 (m, 2H; *ortho*-Ph), 7.64 (br s, 1H; N*H*), 7.32 (m, 2H; *meta*-Ph), 7.19 (m, 1H; *para*-Ph), 3.93 (m, 1H; NC*H*), 3.56 (s, 24H; 18-crown-6), 3.54 (d, $^{2}J_{H-P}$ = 17 Hz, 2H; CH_2P), 0.80–1.75 (m, 10H; Cy). ^{31}P NMR (162.0 MHz, d_5-pyridine): δ (ppm) 16.3 (t, $^{2}J_{P-H}$ = 17 Hz). $^{31}P\{^{1}H\}$ NMR (162.0 MHz, d_5-pyridine): δ (ppm) 16.3 (s). $^{13}C\{^{1}H\}$ NMR (100.6 MHz, d_5-pyridine): δ (ppm) 178.5 (d, $^{1}J_{C-P}$ = 138 Hz; P*C*(O)), 139.2 (d, $^{2}J_{C-P}$ = 6 Hz; *ipso*-Ph), 131.1 (d, $^{3}J_{C-P}$ = 5 Hz; *ortho*-Ph), 128.5 (d, $^{4}J_{C-P}$ = 2 Hz; *meta*-Ph), 125.5 (d, $^{5}J_{C-P}$ = 3 Hz; *para*-Ph), 70.7 (s; 18-crown-6), 47.4 (d, $^{3}J_{C-P}$ = 5 Hz; N*C*H), 40.2 (d, $^{1}J_{C-P}$ = 83 Hz; P*C*H_2), 33.4 (s; Cy), 26.2 (s; Cy), 25.5 (s; Cy). ESI-MS (–ve ion mode, DMF): *m/z* = 279.7 $[BnP(O)_2C(O)NHCy]^-$. ESI-MS (+ve

ion mode, DMF): *m/z* = 622.6 {[K_2(18-crown-6)][$BnP(O)_2C(O)NHCy$]}$^+$, 886.8 {[K(18-crown-6)]$_2$[$BnP(O)_2C(O)NHCy$]}$^+$. IR (cm^{-1}, Nujol mull): ν(CO) 1613; ν(P=O) 1260.

8.2.5.15 [K(18-crown-6)][41] (41: [$P(O)_2${C(O)NHCy}$_2$]$^-$)

An aqueous hydrogen peroxide solution (12.5 μL, 0.128 mmol) was added to a gas-tight NMR tube containing a d_5-pyridine solution (0.5 mL) of [K(18-crown-6)][**29**] (15.0 mg, 0.0256 mmol). A colourless solution of [K(18-crown-6)][**41**] formed. Single crystals of [K(18-crown-6)][**41**]·THF were grown by slow diffusion of hexane (20 mL) into a THF (5 mL) solution of the product and analysed using single crystal X-ray diffraction. ^{1}H NMR (499.9 MHz, d_5-pyridine): δ (ppm) 8.16 (br, 2H; N*H*), 3.98 (m, 2H; NC*H*), 3.60 (s, 24H; 18-crown-6), 0.90–1.85 (m, 20H; Cy). ^{31}P NMR (162.0 MHz, d_5-pyridine): δ (ppm) –1.8 (s). ^{13}C{^{1}H} NMR (125.7 MHz, d_5-pyridine): δ (ppm) 176.9 (d, $^1J_{C–P}$ = 141 Hz; P*C*(O)), 70.7 (s; 18-crown-6), 48.1 (d, $^3J_{C–P}$ = 5 Hz; N*C*H), 33.4 (s; Cy), 26.2 (s; Cy), 25.5 (s; Cy). ESI-MS (–ve ion mode, DMF): *m/z* = 314.9 [$P(O)_2${C(O)NHCy}$_2$]$^-$. ESI-MS (+ve ion mode, DMF): *m/z* = 657.7 {[K_2(18-crown-6)][$P(O)_2${C(O)NHCy}$_2$]}$^+$, 921.9 {[K(18-crown-6)]$_2$[$P(O)_2${C(O)NHCy}$_2$]}$^+$. IR (cm^{-1}, Nujol mull): ν(CO) 1633; ν(P=O) 1260. Anal. Calcd for $C_{26}H_{48}KN_2O_{10}P$: C, 50.47; H, 7.82; N, 4.53. Found: C, 51.19; H, 7.56; N, 4.48.

8.2.5.16 MeP(O){C(O)NHCy}$_2$ (42)

An aqueous hydrogen peroxide solution (120 μL, 1.24 mmol) was added drop-wise to a stirring THF solution (20 mL) of **34** (246 mg, 0.825 mmol) to give a pale orange solution. After two hours of stirring at room temperature, the volatiles were removed *in vacuo* to yield **42** as an off-white solid. Single crystals were grown by slow diffusion of hexane (20 mL) into a THF (5 mL) solution of the product and analysed using single crystal X-ray diffraction. ^{1}H NMR (499.9 MHz, d_5-pyridine): δ (ppm) 9.10 (br, 2H; N*H*), 4.07 (m, 2H; NC*H*), 2.16 (d, $^2J_{P–H}$ = 14 Hz, 3H; CH_3), 0.92–1.96 (m, 20H; Cy). ^{1}H{^{31}P} NMR (499.9 MHz, d_5-pyridine): δ (ppm) 2.16 (s, 3H; CH_3), other resonances unchanged. ^{31}P NMR

(162.0 MHz, d_5-pyridine): δ (ppm) 18.1 (q, $^2J_{P–H}$ = 14 Hz). $^{31}P\{^1H\}$ NMR (161.98 MHz, d_5-pyridine): δ (ppm) 18.1 (s). $^{13}C\{^1H\}$ NMR (100.6 MHz, d_5-pyridine): δ (ppm) 169.1 (d, $^1J_{C–P}$ = 108 Hz; P*C*(O)), 49.8 (d, $^3J_{C–P}$ = 5 Hz; N*C*H), 33.1 (s; Cy), 26.0 (s; Cy), 25.6 (s; Cy), 11.6 (d, $^1J_{C–P}$ = 68 Hz; P*C*H_3). FI-MS: Calcd: *m/z* = 314.1759. Found: *m/z* = 314.1746. Also observe $[CONCy]^+$ at 125.0848 and $[MePOCOHNHCy]^+$ at 189.0875 (both derived from McLafferty rearrangement). IR (cm^{-1}, Nujol mull): ν(CO) 1663, other expected band not observed; ν(P=O) 1147.

8.2.5.17 BnP(O){C(O)NHCy}$_2$ (43)

An aqueous hydrogen peroxide solution (126 μL, 1.30 mmol) was added drop-wise to a stirring THF solution (20 mL) of **35** (325 mg, 0.868 mmol) affording a colourless solution. After two hours of stirring at room temperature, the volatiles were removed *in vacuo* to yield **43** as a white solid (300 mg, 89% yield). Single crystals were grown by slow diffusion of hexane (20 mL) into a THF (5 mL) solution of the product and analysed using single crystal X-ray diffraction. ^1H NMR (499.9 MHz, d_5-pyridine): δ (ppm) 9.00 (br, 2H; N*H*), 7.56 (m, 2H; *ortho*-Ph), 7.33 (m, 2H; *meta*-Ph), 7.27 (m, 1H; *para*-Ph), 4.03 (m, 2H; NC*H*), 4.12 (d, $^2J_{H–P}$ = 15 Hz, 2H; PCH_2), 0.87–1.84 (m, 20H; Cy). $^1H\{^{31}P\}$ NMR (499.9 MHz, d_5-pyridine): δ (ppm) 4.12 (s, 2H; PCH_2), other resonances unchanged. ^{31}P NMR (162.0 MHz, d_5-pyridine): δ (ppm) 17.2 (t, $^2J_{P–H}$ = 15 Hz). $^{31}P\{^1H\}$ NMR (162.0 MHz, d_5-pyridine): δ (ppm) 17.2 (s). $^{13}C\{^1H\}$ NMR (100.6 MHz, d_5-pyridine): δ (ppm) 168.1 (d, $^1J_{C–P}$ = 104 Hz; P*C*(O)), 131.8 (d, $^2J_{C–P}$ = 8 Hz; *ipso*-Ph), 131.2 (d, $^3J_{C–P}$ = 4 Hz; *ortho*-Ph), 129.4 (d, $^4J_{C–P}$ = 3 Hz; *meta*-Ph), 127.9 (d, $^5J_{C–P}$ = 3 Hz; *para*-Ph), 49.8 (d, $^3J_{C–P}$ = 4 Hz; N*C*H), 33.4 (d, $^1J_{C–P}$ = 59 Hz; P*C*H_2), 33.0 (s; Cy), 32.9 (s; Cy), 26.0 (s; Cy), 25.6 (s; Cy), 25.5 (s; Cy). IR (cm^{-1}, Nujol mull): ν(CO) 1661, 1641; ν(P=O) 1160. Anal. Calcd for $C_{21}H_{31}N_2O_3P$: C, 64.60; H, 8.00; N, 7.18. Found: C, 63.17; H, 7.92; N, 7.15.

8.2.6 Chapter 7 – Concluding remarks and future work

8.2.6.1 $H_2PC(O)OEt$ (44) and $HP\{C(O)OEt\}_2$ (45)

HCl in EtOH (0.5 mL, 0.625 mmol) was diluted in EtOH (3 mL). This was added drop-wise to a stirring EtOH solution (3 mL) of [Na(1,4-dioxane)$_{2.90}$][**1**] (211 mg, 0.625 mmol). The solution turned pale yellow and slightly cloudy, and was left stirring overnight. This was transferred to a fritted H-cell, and a trap-to-trap distillation under reduced pressure afforded a colourless solution. ^{31}P NMR spectroscopy revealed a mixture of products, **44** and **45**. This experiment has been repeated several times and the ratio of the two products has varied substantially (% of **44** by integration during different experiments: i. 94%; ii. 50%; iii. 13%); the reason behind this large range in product distribution is still unclear. ^{31}P NMR (162.0 MHz, EtOH): δ (ppm) –61.9 (d, $^1J_{P–H}$ = 241 Hz; **45**), –138.0 (t, $^1J_{P–H}$ = 217 Hz; **44**). $^{31}P\{^1H\}$ NMR (162.0 MHz, EtOH): δ (ppm) –61.9 (s; **45**), –138 (s; **44**).

8.2.6.2 [(*p*-cymene)$_2$Ru$_2$Cl$_2$(μ-Cl)(μ-P{C(O)OEt}$_2$)] (46)

To a gas-tight NMR tube containing an EtOH solution (0.5 mL) of **44** and **45** (iii. above, 13% **44**) was added [{(*p*-cymene)RuCl$_2$}$_2$] (3 mg, 5 μmol). This orange solution initially gave a range of products by ^{31}P NMR, but after two days orange blocks of **46** suitable for single crystal X-ray diffraction had grown. The pale orange solution was decanted off, the crystals dried *in vacuo*, and then redissolved in $CDCl_3$ to give a spectroscopically clean sample of **46**. ^{1}H NMR (499.9 MHz, $CDCl_3$): δ (ppm) 5.86 (d, $^3J_{H–H}$ = 6 Hz, 2H; H_{ar}), 5.83 (d, $^3J_{H–H}$ = 6 Hz, 2H; H_{ar}), 5.60 (d, $^3J_{H–H}$ = 6 Hz, 2H; H_{ar}), 5.54 (d, $^3J_{H–H}$ = 6 Hz, 2H; H_{ar}), 4.40 (m, $^2J_{H–H}$ = 12 Hz, $^3J_{H–H}$ = 7 Hz, 2H; OC*H*HCH$_3$), 4.19 (m, $^2J_{H–H}$ = 12 Hz, $^3J_{H–H}$ = 7 Hz, 2H; OCH*H*CH$_3$), 2.62 (sept, $^3J_{H–H}$ = 7 Hz, 2H; C*H*(CH$_3$)$_2$), 1.93 (s, 6H; C$_{ar}$C*H*$_3$), 1.33 (t, $^3J_{H–H}$ = 7 Hz, 6H; OCH$_2$C*H*$_3$), 1.23 (d, $^3J_{H–H}$ = 7 Hz, 6H; CH(C*H*$_3$)$_2$), 1.12 (d, $^3J_{H–H}$ = 7 Hz, 6H; CH(C*H*$_3$)$_2$). ^{31}P NMR (202.4 MHz, $CDCl_3$): δ (ppm) 25.9 (s). $^{13}C\{^1H\}$ NMR (125.7 MHz, $CDCl_3$): δ (ppm) 174.6 (d, $^1J_{C–P}$ = 52 Hz; P*C*(O)), 103.5 (s; C_{ar}), 92.6 (s; C_{ar}), 90.0 (s;

C_{ar}), 87.0 (s; C_{ar}), 85.5 (s; C_{ar}), 84.0 (s; C_{ar}), 61.9 (s; OCH_2CH_3), 30.4 (s; $CH(CH_3)_2$), 22.4 (s; $CH(CH_3)_2$), 22.2 (s; $CH(CH_3)_2$), 18.8 (s; CH_3), 14.7 (s; OCH_2CH_3).

8.2.6.3 $H_2PC(O)O^tBu$ (47)

Triflic acid (50 μL, 0.563 mmol) was added drop-wise to a ^{t}BuOH solution (10 mL) of [Na(1,4-dioxane)$_{2.90}$][**1**] (190 mg, 0.563 mmol). The solution turned a darker yellow and deposited copious amounts of yellow solid. An aliquot (0.5 mL) was analysed by ^{31}P NMR spectroscopy and revealed a weak resonance attributable to **47**. Trap-to-trap distillation in a fritted H-cell under reduced pressure yielded a colourless ^{t}BuOH solution of **47**. This solution was used in the synthesis of [K(18-crown-6)][**48**]. The volatility of **47** precluded its isolation. ^{31}P NMR (162.0 MHz, ^{t}BuOH): δ (ppm) –132.3 (t, $^1J_{P–H}$ = 214 Hz). ^{31}P{^{1}H} NMR (162.0 MHz, ^{t}BuOH): δ (ppm) –132.3 (s).

8.2.6.4 [K(18-crown-6)][48] (48: $[HPC(O)O^tBu]^-$)

KO^tBu (2.9 mg, 0.023 mmol) and 18-crown-6 (6.5 mg, 0.023 mmol) were added to the colourless ^{t}BuOH solution of **47** mentioned above. An aliquot (0.5 mL) was analysed by ^{31}P NMR spectroscopy and revealed a weak resonance attributable to **48**. This was recombined with the original solution and the volatiles removed *in vacuo* to yield a yellow oily residue. This was dissolved in d_5-pyridine for the spectroscopic analysis detailed below. Subsequently, this solution was transferred to a thin gas-tight ampoule and carefully layered with hexane (10 mL). Slow diffusion of hexane into the d_5-pyridine solution of the product yielded crystals of [K(18-crown-6)][**48**] suitable for single crystal X-ray diffraction. ^{1}H NMR (400.2 MHz, d_5-pyridine): δ (ppm) 3.07 (d, $^1J_{H–P}$ = 154 Hz, 1H; P*H*), 1.74 (s, 9H; $C(CH_3)_3$). ^{31}P NMR (162.0 MHz, d_5-pyridine): δ (ppm) –100.0 (br s, coupling to H not resolved). ^{31}P{^{1}H} NMR (162.0 MHz, d_5-pyridine): δ (ppm) –100.0 (br s).

8.3 Characterisation techniques

8.3.1 Single crystal X-ray diffraction

Single-crystal X-ray diffraction data were collected using either an Oxford Diffraction Supernova dual-source diffractometer equipped with a 135 mm Atlas CCD area detector or an Enraf-Nonius kappa-CCD diffractometer equipped with a 95 mm CCD area detector. Crystals were selected under Paratone-N oil, mounted on micromount loops, and quench-cooled using an Oxford Cryosystems open flow N_2 cooling device. Data were collected at 150 K using mirror monochromated Cu Kα radiation (λ = 1.5418 Å; Oxford Diffraction Supernova) or graphite-monochromated Mo Kα radiation (λ = 0.71073 Å; Enraf-Nonius kappa-CCD). Data collected on the Oxford Diffraction Supernova diffractometer were processed using the CrysAlisPro package, including unit cell parameter refinement and interframe scaling (which was carried out using SCALE3 ABSPACK within CrysAlisPro).[9] Equivalent reflections were merged, and diffraction patterns processed with the CrysAlisPro suite. For data collected on the Enraf-Nonius kappa-CCD, diffractometer equivalent reflections were merged and the diffraction patterns processed with the DENZO and SCALEPACK programs.[10] Structures were subsequently solved using direct methods or using the charge flipping algorithm as implemented in the program SUPERFLIP[11] and refined on F^2 using the SHELXL 97-2 package.[12–14] Tables of selected data collection and refinement parameters are provided in Appendix A.

8.3.2 NMR spectroscopy

Samples were made up inside an inert atmosphere glovebox in NMR tubes fitted with a gas-tight valve. ^{1}H, $^{13}C\{^{1}H\}$ and ^{31}P NMR spectra were recorded at 500.0, 125.8 and 202.4 MHz, respectively, on a Bruker AVIII 500 MHz NMR spectrometer or a Bruker AVII 500 MHz NMR spectrometer (equipped with a dedicated ^{13}C cryoprobe); or at 400.0, 100.6 and

162.0 MHz, respectively, on a Bruker AVIII 400 MHz NMR spectrometer. ^{1}H and $^{13}C\{^{1}H\}$ spectra are reported relative to $Si(CH_3)_4$ (δ_H = 0 ppm, δ_C = 0 ppm) and referenced to the most downfield residual solvent resonances where possible (d_8-THF: δ_H = 3.58 ppm, δ_C = 67.57 ppm; d_5-pyridine: δ_H = 8.74 ppm, δ_C = 150.35 ppm; d_4-1,2-DCB: δ_H = 6.93 ppm, δ_C = 132.39 ppm; d_7-DMF: δ_H = 8.03 ppm, δ_C = 163.15 ppm; CD_2Cl_2: δ_H = 5.32 ppm, δ_C = 54.00 ppm; $CDCl_3$: δ_H = 7.24 ppm, δ_C = 77.23 ppm). ^{31}P spectra were externally referenced to 85% H_3PO_4 (δ_P = 0 ppm). All spectra were obtained at 25 °C unless otherwise specified. Spectral simulations were carried out using the gNMR v5.0 program.[15] The simulation of **15** was carried out by Dr. Rob Turbervill. Data were processed using the Bruker TopSpin 3.1 program.

8.3.3 Mass spectrometry

Electrospray ionisation mass spectrometry (ESI-MS) data in negative and positive ion mode were obtained from THF or DMF solutions (10–20 μM) on a Waters LCT Time of Flight mass spectrometer with a Z-spray source (150 ˚C source temperature, 200 ˚C desolvation temperature, 25 V cone voltage and capillary voltages of 2.4 kV (negative ion mode) and 3.2 kV (positive ion mode)). Samples were made up inside an inert atmosphere glovebox and rapidly transferred to the spectrometer in a gas-tight syringe. Samples were injected directly using a 1 mL SGE syringe and syringe pump at a rate of 10 μL min^{-1}.

Electron ionisation mass spectrometry (EI-MS) and field ionisation mass spectrometry (FI-MS) were carried out by Colin Sparrow of the University of Oxford. Samples were submitted as solids and spectra were obtained using a Waters GCT Time of Flight mass spectrometer with a temperature-programmed solids probe inlet.

Chemical ionisation mass spectrometry (CI-MS) was also carried out by Colin Sparrow using an Agilent 7200 Accurate Mass QTof GCMS, with the SIM heated solid probe inlet

attached. The sample was vaporized directly into the source and does not go through the GC part of the instrument. Ammonia was used as the reagent gas in the CI source.

8.3.4 IR spectroscopy

IR data were recorded in THF solutions or as solid samples in Nujol mulls. Both were prepared inside an inert atmosphere glovebox and the samples placed in airtight holders prior to data collection. Spectra were recorded on a Thermo Scientific iS5 FT-IR spectrometer in absorbance mode.

8.3.5 Elemental analysis

CHN elemental microanalyses were carried out by Elemental Microanalysis Ltd., Devon. Samples were submitted in Pyrex ampoules sealed under vacuum. All values are given as percentages.

8.3.6 Computational details

All calculations were performed by Michael Geeson or Prof. Jose Goicoechea using either the Gaussian09[16] or Amsterdam Density Functional 2013.01 (ADF)[17,18] software packages. Unless otherwise specified, geometries were fully optimised without imposing any symmetry constraints (C_1 symmetry). Stationary points were characterised by analysis of their vibrational frequencies, with minima and transition states having exactly zero and one imaginary frequencies, respectively. All quantum chemical results were visualised using the Chemcraft 1.7[19] software or ADF GUI.[20]

A range of different functionals, basis sets and other parameters have been used, depending on the molecule in question. Explicit computational details for published compounds can be found in the following references:

- **1**–**6**[21]
- **1**, **7**, **8**[22]

- **9**, **10**[23]
- **11**[24]
- **14**, **15**[25]
- **17**, **28**, **29**[26]

Calculations on the barriers to C–N bond rotation and phosphine inversion of **11** were carried out by Michael Geeson using Gaussian09.[16] The calculations used a coupled cluster[27,28] using both single and double substitutions from the Hartree-Fock determinant (CCSD).[29–32] The basis set used was 6-311+G(2df,p).[33]

8.4 References

(1) Santandrea, R. P.; Mensing, C.; von Schnering, H. G. *Thermochim. Acta* **1986**, *98*, 301–311.

(2) Heift, D.; Benkő, Z.; Grützmacher, H. *Dalton Trans.* **2014**, *43*, 831–840.

(3) Nief, F.; Mercier, F.; Mathey, F. *J. Organomet. Chem.* **1987**, *328*, 349–355.

(4) Tekkaya, A.; Kayran, C.; Ozkar, S.; Kreiter, C. G. *Inorg. Chem.* **1994**, *33*, 2439–2443.

(5) Findlater, M.; Hill, N. J.; Cowley, A. H. *Dalton Trans.* **2008**, No. 33, 4419–4423.

(6) Bertini, V.; Alfei, S.; Pocci, M.; Lucchesini, F.; Picci, N.; Iemma, F. *Tetrahedron* **2004**, *60*, 11407–11414.

(7) Taggi, A. E.; Hafez, A. M.; Wack, H.; Young, B.; Ferraris, D.; Lectka, T. *J. Am. Chem. Soc.* **2002**, *124*, 6626–6635.

(8) Brookhart, M.; Grant, B.; Volpe, A. F. *Organometallics* **1992**, *11*, 3920–3922.

(9) *CrysAlisPro*; Agilent Technologies.

(10) Otwinowksi, Z.; Minor, W. *Macromol. Crystallogr. Part A* **1997**, *Volume 276*, 307–326.

(11) Palatinus, L.; Chapius, G. *J. Appl. Cryst.* **2007**, *40*, 786–790.

(12) Sheldrick, G. M. *SHELX97, Programs for Crystal Structure Analysis (Release 97-2)*; University of Göttingen: Göttingen, Germany, 1998.

(13) Sheldrick, G. M. *Acta. Cryst. A* **1990**, *46*, 467–473.

(14) Sheldrick, G. M. *Acta. Cryst. A* **2008**, *64*, 112–122.

(15) Budzelaar, P. H. M. *gNMR v5.0*; Ivorysoft, 1995.

(16) Frisch, M. J.; Trucks, G. W.; Schlegel, H. B.; Scuseria, G. E.; Robb, M. A.; Cheeseman, J. R.; Scalmani, G.; Barone, V.; Mennucci, B.; Petersson, G. A.; Nakatsuji, H.; Caricato, M.; Li, X.; Hratchian, H. P.; Izmaylov, A. F.; Bloino, J.; Zheng, G.; Sonnenberg, J. L.; Hada, M.; Ehara, M.; Toyota, K.; Fukuda, R.; Hasegawa, J.; Ishida, M.; Nakajima, T.; Honda, Y.; Kitao, O.; Nakai, H.; Vreven, T.; Montgomery, J. A., Jr.; Peralta, J. E.; Ogliaro, F.; Bearpark, M.; Heyd, J. J.; Brothers, E.; Kudin, K. N.; Staroverov, V. N.; Kobayashi, R.; Normand, J.; Raghavachari, K.; Rendell, A.; Burant, J. C.; Iyengar, S. S.; Tomasi, J.; Cossi, M.; Rega, N.; Millam, J. M.; Klene, M.; Knox, J. E.; Cross, J. B.; Bakken, V.; Adamo, C.; Jaramillo, J.; Gomperts, R.; Stratmann, R. E.; Yazyev, O.; Austin, A. J.; Cammi, R.; Pomelli, C.; Ochterski, J. W.; Martin, R. L.; Morokuma, K.; Zakrzewski, V. G.; Voth, G. A.; Salvador, P.; Dannenberg, J. J.; Dapprich, S.; Daniels, A. D.; Farkas, Ö.; Foresman, J. B.; Ortiz, J. V.; Cioslowski, J.; Fox, D. J. *Gaussian 09, Revision A.02*; Gaussian, Inc., Wallingford CT, 2009.

(17) te Velde, G.; Bickelhaupt, F. M.; Baerends, E. J.; Fonseca Guerra, C.; van Gisbergen, S. J. A.; Snijders, J. G.; Ziegler, T. *J. Comput. Chem.* **2001**, *22*, 931–967.

(18) Guerra, C. F.; Snijders, J. G.; Velde, G. te; Baerends, E. J. *Theor. Chem. Acc.* **1998**, *99*, 391–403.

(19) Zhurko, G. A. *ChemCraft v1.7 (build 382)*; www.chemcraftprog.com.

(20) *ADF GUI 2013*; ADF: Amsterdam, The Netherlands, www.scm.com.

(21) Jupp, A. R.; Geeson, M. B.; McGrady, J. E.; Goicoechea, J. M. *Eur. J. Inorg. Chem.* **2016**, *2016*, 639–648.

(22) Jupp, A. R.; Goicoechea, J. M. *Angew. Chem. Int. Ed.* **2013**, *52*, 10064–10067.

(23) Heift, D.; Benkő, Z.; Grützmacher, H.; Jupp, A. R.; Goicoechea, J. M. *Chem. Sci.* **2015**, *6*, 4017–4024.

(24) Jupp, A. R.; Goicoechea, J. M. *J. Am. Chem. Soc.* **2013**, *135*, 19131–19134.

(25) Geeson, M. B.; Jupp, A. R.; McGrady, J. E.; Goicoechea, J. M. *Chem. Commun.* **2014**, *50*, 12281–12284.

(26) Jupp, A. R.; Trott, G.; Payen de la Garanderie, É.; Holl, J. D. G.; Carmichael, D.; Goicoechea, J. M. *Chem. Eur. J.* **2015**, *21*, 8015–8018.

(27) Pople, J. A.; Krishnan, R.; Schlegel, H. B.; Binkley, J. S. *Int. J. Quantum Chem.* **1978**, *14*, 545–560.

(28) Bartlett, R. J.; Purvis, G. D. *Int. J. Quantum Chem.* **1978**, *14*, 561–581.

(29) Čížek, J. In *Advances in Chemical Physics*; LeFebvre, R., Moser, C., Eds.; John Wiley & Sons, Inc., 1969; Vol. 14, pp 35–89.

(30) Purvis III, G. D.; Bartlett, R. J. *J. Chem. Phys.* **1982**, *76*, 1910–1918.

(31) Scuseria, G. E.; Janssen, C. L.; Schaefer III, H. F. *J. Chem. Phys.* **1988**, *89*, 7382–7387.

(32) Scuseria, G. E.; Schaefer III, H. F. *J. Chem. Phys.* **1989**, *90*, 3700–3703.

(33) McLean, A. D.; Chandler, G. S. *J. Chem. Phys.* **1980**, *72*, 5639–5648.

Appendix A
Collection and refinement parameters for X-ray data

compound	[K(18-crown-6)][**1**]	[K(18-crown-6)][**2**]	[K(2,2,2-crypt)][**2**]	[K(18-crown-6)][**3**]	[K(2,2,2-crypt)][**3**]
formula	$C_{13}H_{24}KO_7P$	$C_{18}H_{24}KO_{12}PW$	$C_{24}H_{36}KN_2O_{12}PW$	$C_{18}H_{24}KNO_{12}W$	$C_{24}H_{36}KN_3O_{12}W$
Fw (g mol^{-1})	362.39	686.29	798.47	669.13	781.51
crystal system	monoclinic	orthorhombic	monoclinic	triclinic	orthorhombic
space group	$P2_1$	*Pnma*	$P2_1/n$	$P\bar{1}$	*Pbca*
a (Å)	7.7085(1)	16.6552(3)	13.1403(3)	7.2580(1)	12.7102(1)
b (Å)	14.2796(2)	20.3310(6)	17.5555(3)	12.0980(1)	17.6300(2)
c (Å)	8.1433(1)	7.5377(2)	14.9051(3)	15.5600(2)	27.3657(3)
α (°)	90	90	90	108.514(1)	90
β (°)	98.749(1)	90	112.770(2)	92.654(1)	90
γ (°)	90	90	90	103.000(1)	90
V (Å^3)	885.94(2)	2552.39(11)	3170.41(12)	1252.07(3)	6132.13(11)
Z	2	4	4	2	8
radiation, λ (Å)	Cu K_α, 1.54178	Cu K_α, 1.54178	Cu K_α, 1.54178	Mo K_α, 0.71073	Mo K_α, 0.71073
T (K)	150(2)	150(2)	150(2)	150(2)	150(2)
ρ_{calc} (g cm^{-3})	1.358	1.786	1.673	1.775	1.693
μ (mm^{-1})	3.746	10.948	8.927	4.837	3.966
reflns collected	7639	25987	18145	10259	12985
independent reflns	3250	2742	6574	5725	6993
parameters	199	181	370	301	370
R(int)	0.0179	0.0383	0.0344	0.0249	0.0278
R1/wR2, $I \geq 2\sigma_I$ (%)	3.61/9.45	3.25/7.47	2.56/5.93	2.35/5.67	2.70/5.18
R1/wR2, all data (%)	3.63/9.48	3.79/7.94	3.27/6.33	2.51/5.75	5.17/5.76
GOF	1.039	1.046	1.039	1.129	1.020
Flack parameter	0.494(14)	–	–	–	–
A	0.0485	0.0258	0.0308	0.0277	0.0251
B	0.7114	8.2758	0	0.6490	0.6587

R1 = $\Sigma||F_o| - |F_c||]/\Sigma|F_o|$; wR2 = $\{[\Sigma w[(F_o)^2 - (F_c)^2]^2]/[\Sigma w(F_o^2)^2]\}^{1/2}$; $w = [\sigma^2(F_o)^2 + (AP)^2 + BP]^{-1}$, where $P = [(F_o)^2 + 2(F_c)^2]/3$ and the A and B values are listed in the bottom two rows of the table.

compound	[K(18-crown-6)][**4**]	[K(18-crown-6)][**5**]	[Na(18-crown-6)][**5**]	[K(18-crown-6)][**6**]	[K(18-crown-6)][**7**]
formula	$C_{18}H_{24}KNO_{11}SW$	$C_{13}H_{24}KO_6PS$	$C_{13}H_{24}NaO_6PS$	$C_{18}H_{24}KO_{11}PSW$	$C_{27}H_{34}KO_8P$
Fw (g mol^{-1})	685.39	378.45	362.34	702.35	556.61
crystal system	monoclinic	monoclinic	monoclinic	triclinic	triclinic
space group	$P2_1/c$	$P2_1/c$	$C2/c$	$P\bar{1}$	$P\bar{1}$
a (Å)	13.9771(6)	8.4746(4)	12.8436(5)	7.3100(4)	9.1513(3)
b (Å)	8.5055(3)	14.1974(5)	11.0973(3)	10.0817(7)	9.9730(3)
c (Å)	21.5917(8)	7.8369(3)	13.9006(6)	10.4691(6)	15.9030(6)
α (°)	90	90	90	64.684(6)	108.130(1)
β (°)	101.447(3)	99.006(4)	113.950(5)	81.946(5)	99.210(1)
γ (°)	90	90	90	70.122(6)	99.390(1)
V (Å^3)	2515.81(17)	931.29(7)	1810.66(13)	655.88(8)	1326.01(8)
Z	4	2	4	1	2
radiation, λ (Å)	Cu K_α, 1.54178	Cu K_α, 1.54178	Cu K_α, 1.54178	Cu K_α, 1.54178	Mo K_α, 0.71073
T (K)	150(2)	150(2)	150(2)	150(2)	150(2)
ρ_{calc} (g cm^{-3})	1.810	1.350	1.329	1.778	1.394
μ (mm^{-1})	11.260	4.565	2.872	11.363	0.309
reflns collected	12227	8122	10968	5392	21772
independent reflns	5227	1939	1897	2693	5996
parameters	298	106	105	175	334
R(int)	0.0343	0.0264	0.0307	0.0351	0.0878
R1/wR2, $I \geq 2\sigma_I$ (%)	3.51/9.29	2.93/7.67	3.00/8.17	2.29/5.71	4.85/9.45
R1/wR2, all data (%)	3.61/9.44	3.48/8.07	3.34/8.50	2.29/5.71	10.51/11.22
GOF	1.042	1.022	1.065	1.066	1.010
Flack parameter	–	–	–	–	–
A	0.0721	0.0473	0.0441	0.0362	0.0419
B	0.7106	0.1174	0.8881	0	0.1288

R1 = $[\Sigma||F_o| - |F_c||]/\Sigma|F_o|$; wR2 = $\{[\Sigma w[(F_o)^2 - (F_c)^2]^2]/[\Sigma w(F_o^2)^2]\}^{1/2}$; w = $[\sigma^2(F_o)^2 + (AP)^2 + BP]^{-1}$, where P = $[(F_o)^2 + 2(F_c)^2]/3$ and the A and B values are listed in the bottom two rows of the table.

compound	[K(18-crown-6)][**8**]	[K(18-crown-6)][**9**]	[K(18-crown-6)][**10**]	**11**	**12**
formula	$C_{38}H_{58}KN_2O_7P$	$C_{64}H_{92}KN_4O_{10}P$	$C_{38}H_{58}KN_2O_8P$	CH_4NOP	$C_7H_{16}NO_4P$
Fw (g mol^{-1})	724.93	1147.48	740.93	77.02	209.18
crystal system	triclinic	monoclinic	monoclinic	monoclinic	triclinic
space group	*P*–1	$P2_1$	$P2_1/n$	$P2_1/n$	*P*–1
a (Å)	10.9160(1)	13.2330(3)	10.7457(2)	5.6030(2)	8.4093(2)
b (Å)	12.1145(2)	19.9093(4)	17.6496(3)	8.2629(3)	8.6581(3)
c (Å)	16.9926(3)	13.5733(3)	21.5074(3)	8.2125(4)	8.7267(3)
α (°)	86.656(1)	90	90	90	105.959(1)
β (°)	89.992(1)	115.271(3)	99.870(1)	96.534(4)	114.847(2)
γ (°)	64.785(1)	90	90	90	96.574(1)
V (Å^3)	2028.80(5)	3233.79(14)	4018.66(12)	377.74(3)	534.73(3)
Z	2	2	4	4	2
radiation, λ (Å)	Mo K_α, 0.71073	Cu K_α, 1.54178	Cu K_α, 1.54178	Cu K_α, 1.54178	Mo K_α, 0.71073
T (K)	150(2)	150(2)	150(2)	150(2)	150(2)
ρ_{calc} (g cm^{-3})	1.187	1.178	1.225	1.354	1.299
μ (mm^{-1})	0.217	1.412	1.942	4.712	0.243
reflns collected	33320	19203	87300	6483	6640
independent reflns	9201	11186	8414	788	2418
parameters	442	760	479	53	182
R(int)	0.0374	0.0416	0.0508	0.0278	0.0248
R1/wR2, $I \geq 2\sigma_I$ (%)	4.39/11.25	4.58/10.96	6.27/18.22	2.24/6.03	3.21/7.81
R1/wR2, all data (%)	6.50/12.36	5.50/11.68	6.63/18.59	2.49/6.22	4.16/8.21
GOF	1.019	1.025	1.036	1.067	1.046
Flack parameter	–	0.306(13)	–	–	–
A	0.0563	0.0540	0.0992	0.0339	0.0354
B	0.9320	0.6914	3.8426	0.0999	0.1120

R1 = $[\Sigma||F_o| - |F_c||]/\Sigma|F_o|$; wR2 = $\{[\Sigma w[(F_o)^2 - (F_c)^2]^2]/[\Sigma w(F_o^2)^2]\}^{1/2}$; $w = [\sigma^2(F_o)^2 + (AP)^2 + BP]^{-1}$, where $P = [(F_o)^2 + 2(F_c)^2]/3$ and the A and B values are listed in the bottom two rows of the table.

compound	**15**	**20**	**21**	[K(18-crown-6)][**24**]	**25**
formula	$C_6H_8MoN_2O_6P_2$	$C_{17}H_{28}Cl_2NOPRu$	$C_{27}H_{41}Cl_3NOPRu_2$	$C_{16}H_{31}KNO_9P$	$C_4H_{10}N_2O_2P_2$
Fw (g mol^{-1})	362.02	465.34	735.07	451.49	180.08
crystal system	monoclinic	monoclinic	monoclinic	monoclinic	monoclinic
space group	$P2_1/n$	$P2_1/n$	$P2_1/n$	$P2_1$	$P2_1/n$
a (Å)	7.1284(2)	12.6503(2)	10.0859(2)	8.6146(2)	7.1091(2)
b (Å)	9.7853(2)	11.8975(1)	15.2040(2)	29.8779(5)	4.9133(1)
c (Å)	18.2084(5)	13.0798(2)	19.6345(3)	17.5654(3)	12.5171(3)
α (°)	90	90	90	90	90
β (°)	94.130(2)	97.945(1)	100.061(2)	99.466(2)	92.067(2)
γ (°)	90	90	90	90	90
V (Å^3)	1266.80(6)	1949.70(5)	2964.57(9)	4459.53(15)	436.927(18)
Z	4	4	4	8	2
radiation, λ (Å)	Cu K_α, 1.54178	Cu K_α, 1.54178	Cu K_α, 1.54178	Cu K_α, 1.54178	Cu K_α, 1.54178
T (K)	150(2)	150(2)	150(2)	150(2)	150(2)
ρ_{calc} (g cm^{-3})	1.898	1.585	1.647	1.345	1.369
μ (mm^{-1})	11.075	9.824	11.406	3.166	4.156
reflns collected	25541	10687	15880	26764	3760
independent reflns	2649	3885	6148	13248	896
parameters	190	220	324	1036	66
R(int)	0.0316	0.0274	0.0233	0.0463	0.0148
R1/wR2, $I \geq 2\sigma_I$ (%)	1.87/5.07	2.99/7.59	2.61/6.70	4.21/11.04	2.38/6.17
R1/wR2, all data (%)	1.93/5.12	3.13/7.72	2.74/6.81	4.69/11.37	2.42/6.20
GOF	1.073	1.031	1.061	1.017	1.134
Flack parameter	–	–	–	–0.008(8)	–
A	0.0314	0.0425	0.0425	0.0724	0.0327
B	0.4676	2.6866	1.4833	0	0.1084

R1 = $[\Sigma||F_o| - |F_c||]/\Sigma|F_o|$; wR2 = $\{[\Sigma w[(F_o)^2 - (F_c)^2]^2]/[\Sigma w(F_o^2)^2]\}^{1/2}$; w = $[\sigma^2(F_o)^2 + (AP)^2 + BP]^{-1}$, where P = $[(F_o)^2 + 2(F_c)^2]/3$ and the A and B values are listed in the bottom two rows of the table.

compound	[K(18-crown-6)][**27**]·0.5(1,4-dioxane)	[K(18-crown-6)][**28**]	[K(18-crown-6)][**29**]	[K(18-crown-6)][**30**]	**31**
formula	$C_{19}H_{39}KNO_8P$	$C_{19}H_{37}KNO_7P$	$C_{26}H_{48}K_2NO_8P$	$C_{16}H_{32}KN_2O_8P$	$C_8H_{16}NOP$
Fw (g mol^{-1})	479.58	461.57	586.73	450.50	173.19
crystal system	monoclinic	monoclinic	monoclinic	triclinic	monoclinic
space group	$P2_1/n$	$P2_1$	$I2/a$	$P\bar{1}$	$P2_1/c$
a (Å)	8.8174(3)	8.7166(2)	26.594(3)	7.2757(3)	10.6789(8)
b (Å)	21.8046(6)	14.4487(4)	8.7621(8)	9.6900(3)	10.2465(8)
c (Å)	14.1307(4)	9.9967(3)	28.905(6)	15.8225(6)	9.6873(7)
α (°)	90	90	90	97.975(3)	90
β (°)	106.927(3)	101.815(3)	113.490(11)	91.485(4)	108.621(8)
γ (°)	90	90	90	94.447(3)	90
V (Å^3)	2599.07(14)	1232.35(6)	6177.3(16)	1100.64(7)	1004.51(14)
Z	4	2	8	2	4
radiation, λ (Å)	Cu K_α, 1.54178	Cu K_α, 1.54178	Cu K_α, 1.54178	Cu K_α, 1.54178	Cu K_α, 1.54178
T (K)	150(2)	150(2)	150(2)	150(2)	150(2)
ρ_{calc} (g cm^{-3})	1.226	1.244	1.262	1.359	1.145
μ (mm^{-1})	2.712	2.810	2.386	3.183	2.026
reflns collected	41059	10504	17344	9873	4500
independent reflns	5415	4910	6357	4514	1852
parameters	277	271	346	340	108
R(int)	0.0431	0.0325	0.0543	0.0195	0.0297
R1/wR2, $I \geq 2\sigma_I$ (%)	5.59/16.25	4.05/11.26	5.58/14.36	4.13/11.18	5.95/13.42
R1/wR2, all data (%)	6.02/16.79	4.25/11.61	7.08/15.81	4.41/11.45	7.23/14.22
GOF	1.069	0.992	1.054	1.063	1.093
Flack parameter	–	0.520(10)	–	–	–
A	0.0862	0.0823	0.0885	0.0625	0.0404
B	1.0773	0.1729	0.1309	0.6384	1.0609

$R1 = [\Sigma||F_o| - |F_c||]/\Sigma|F_o|$; $wR2 = \{[\Sigma w[(F_o)^2 - (F_c)^2]^2]/[\Sigma w(F_o^2)^2]\}^{1/2}$; $w = [\sigma^2(F_o)^2 + (AP)^2 + BP]^{-1}$, where $P = [(F_o)^2 + 2(F_c)^2]/3$ and the A and B values are listed in the bottom two rows of the table.

compound	**32**	[K(18-crown-6)][**40**]·0.5(hexane)	[K(18-crown-6)][**41**]·0.5(THF)	**42**	**43**
formula	$C_{14}H_{20}NOP$	$C_{29}H_{50}KNO_9P$	$C_{28}H_{52}KN_2O_{10.5}P$	$C_{15}H_{27}N_2O_3P$	$C_{21}H_{31}N_2O_3P$
Fw (g mol^{-1})	249.29	626.77	654.78	314.35	390.45
crystal system	monoclinic	triclinic	triclinic	monoclinic	triclinic
space group	*C*2/*c*	*P*–1	*P*–1	$P2_1/n$	*P*–1
a (Å)	22.2702(8)	11.7275(4)	11.2718(5)	12.0007(4)	8.6666(4)
b (Å)	5.0170(1)	12.5470(4)	13.5806(5)	8.7165(3)	10.7866(6)
c (Å)	27.1725(8)	13.1109(4)	13.8026(7)	16.3218(6)	11.9433(7)
α (°)	90	103.251(3)	61.621(4)	90	84.179(4)
β (°)	115.226(4)	98.105(3)	68.538(4)	98.286(3)	79.506(4)
γ (°)	90	115.801(3)	71.904(4)	90	75.174(4)
V (Å^3)	2746.41(15)	1625.59(10)	1705.77(15)	1689.50(10)	1059.51(10)
Z	8	2	2	4	2
radiation, λ (Å)	Cu K_α, 1.54178	Cu K_α, 1.54178	Cu K_α, 1.54178	Cu K_α, 1.54178	Cu K_α, 1.54178
T (K)	150(2)	150(2)	150(2)	150(2)	150(2)
ρ_{calc} (g cm^{-3})	1.206	1.280	1.275	1.236	1.224
μ (mm^{-1})	1.640	2.317	2.271	1.540	1.330
reflns collected	13811	26917	16601	8496	9463
independent reflns	2861	6763	7021	3496	4346
parameters	155	374	414	199	244
R(int)	0.050	0.0214	0.0265	0.0339	0.0381
R1/wR2, $I \geq 2\sigma_I$ (%)	11.34/47.06	2.85/7.77	3.40/8.39	3.70/9.23	4.88/13.77
R1/wR2, all data (%)	12.00/47.37	2.94/7.87	4.12/8.93	4.87/10.08	6.07/14.68
GOF	0.9962	1.061	1.038	1.047	1.085
Flack parameter	–	–	–	–	–
A	0.20	0.0428	0.0432	0.0528	0.0759
B	0	0.4295	0.2835	0.1289	0.3803

$R1 = [\Sigma||F_o| - |F_c||]/\Sigma|F_o|$; $wR2 = \{[\Sigma w[(F_o)^2 - (F_c)^2]^2]/[\Sigma w(F_o^2)^2]\}^{1/2}$; $w = [\sigma^2(F_o)^2 + (AP)^2 + BP]^{-1}$, where $P = [(F_o)^2 + 2(F_c)^2]/3$ and the A and B values are listed in the bottom two rows of the table.

compound	**46**	[K(18-crown-6)][**48**]
formula	$C_{26}H_{38}Cl_3O_4PRu_2$	$C_{17}H_{34}KO_8P$
Fw (g mol^{-1})	754.02	436.51
crystal system	monoclinic	orthorhombic
space group	$P2_1$	$P2_12_12_1$
a (Å)	11.8546(2)	8.8860(2)
b (Å)	21.0957(3)	15.8440(3)
c (Å)	12.0589(2)	16.1657(3)
α (°)	90	90
β (°)	90.015(1)	90
γ (°)	90	90
V (Å^3)	3015.70(8)	2275.97(8)
Z	4	4
radiation, λ (Å)	Cu K_α, 1.54178	Cu K_α, 1.54178
T (K)	150(2)	150(2)
ρ_{calc} (g cm^{-3})	1.661	1.274
μ (mm^{-1})	11.298	3.034
reflns collected	50991	12107
independent reflns	12521	4658
parameters	649	248
R(int)	0.0917	0.0277
R1/wR2, $I \geq 2\sigma_I$ (%)	5.52/14.86	2.89/7.23
R1/wR2, all data (%)	5.55/14.91	3.11/7.38
GOF	0.970	1.042
Flack parameter	0.496(7)	-0.010(6)
A	0.1193	0.0356
B	8.3197	0.2939

R1 = $[\Sigma||F_o| - |F_c||]/\Sigma|F_o|$; wR2 = $\{[\Sigma w[(F_o)^2 - (F_c)^2]^2]/[\Sigma w(F_o^2)^2]\}^{1/2}$; w = $[\sigma^2(F_o)^2 + (AP)^2 + BP]^{-1}$, where P = $[(F_o)^2 + 2(F_c)^2]/3$ and the A and B values are listed in the bottom two rows of the table.

Appendix B
Publications

1) “Synthesis and Characterization of Free and Coordinated 1,2,3-Tripnictolide Anions” Turbervill, R. S. P.; Jupp, A. R.; McCullough, P. S. B.; Ergöçmen, D., Goicoechea, J. M. *Organometallics*, **2013**, *32*, 2234–2244.

2) “The 2-Phosphaethynolate Anion: A Convenient Synthesis and [2+2] Cycloaddition Chemistry” Jupp, A. R.; Goicoechea, J. M. *Angew. Chem. Int. Ed.*, **2013**, *52*, 10064–10067.

3) “Phosphinecarboxamide: A Phosphorus-Containing Analogue of Urea and Stable Primary Phosphine” Jupp, A. R.; Goicoechea, J. M. *J. Am. Chem. Soc.*, **2013**, *135*, 19131–19134.

4) “On the Coordination Chemistry of Phosphinecarboxamide: Assessing Ligand Basicity” Geeson, M. B.; Jupp, A. R.; McGrady, J. E.; Goicoechea, J. M. *Chem. Commun.*, **2014**, *50*, 12281–12284.

5) “Exploiting the Brønsted Acidity of Phosphinecarboxamides for the Synthesis of New Phosphides and Phosphines” Jupp, A. R.; Trott, G.; Payen de la Garanderie, É.; Holl, J. D. G.; Carmichael, D.; Goicoechea, J. M. *Chem. Eur. J.*, **2015**, *21*, 8015–8018.

6) “Cyclo-oligomerization of Isocyanates with $Na(PH_2)$ or Na(OCP) as “P^-” Anion Sources” Heift, D.; Benkő, Z.; Grützmacher, H.; Jupp, A. R.; Goicoechea, J. M. *Chem. Sci.*, **2015**, *6*, 4017–4024.

7) “Uranium and Thorium Complexes of the Phosphaethynolate Ion” Camp, C.; Settineri, N.; Lefèvre, J.; Jupp, A. R.; Goicoechea, J. M.; Maron, L.; Arnold, J. *Chem. Sci.*, **2015**, *6*, 6379–6384.

8) “Ambient-Temperature Synthesis of 2-Phosphathioethynolate, PCS^-, and the Ligand Properties of ECX^- (E = N, P; X = O, S)” Jupp, A. R.; Geeson, M. B.; McGrady, J. E.; Goicoechea, J. M. *Eur. J. Inorg. Chem.*, **2016**, *2016*, 639–648.